December 2025

The Impact of Sea Level Rise on Salinity Intrusion in the Delaware River Estuary

Technical Report No. 2025 - 6

Managing, Protecting and Improving
the Water Resources of the
Delaware River Basin since 1961

Delaware River Basin Commission
DELAWARE • NEW JERSEY
PENNSYLVANIA • NEW YORK
UNITED STATES OF AMERICA

This page is intentionally left blank.

The Impact of Sea Level Rise on Salinity Intrusion in the Delaware River Estuary

DRBC Report No: 2025-6

Prepared by Fanghui Chen, Ph.D., P.E., Amy L. Shallcross, P.E., and Robert S. Nicholson

DELAWARE RIVER BASIN COMMISSION

25 COSEY ROAD, WEST TRENTON, NEW JERSEY, 08628

KRISTEN BOWMAN KAVANAGH, EXECUTIVE DIRECTOR

Suggested Citation

Chen, F., Shallcross, A., and Nicholson, R. (2025). *The Impact of Sea Level Rise on Salinity Intrusion in the Delaware River Estuary*. (DRBC Report No: 2025-6). West Trenton, New Jersey. Delaware River Basin Commission
https://www.nj.gov/drbc/library/documents/SLR_WaterResourceImpactsDec2025.pdf.

Acknowledgements

The Delaware River Basin Commission (DRBC) staff are grateful to the following national renowned experts for their engagement, valuable guidance on methodology and modeling approach, and insightful technical advice for this project: Dr. Carl Cerco from USACE (retired); Dr. Bob Chant from Rutgers University, Professor in the Department of Marine and Coastal Sciences; Dr. Hugo Rodriguez, who is a former senior water resources & coastal engineer from GHD[1]; and Dr. Gaurav Savant from USACE-ERDC-CHL[2], Rivers and Estuarine Engineering Branch. All four have extensive experience in the fields of oceanography and estuary environmental hydrodynamics modeling and were engaged to provide external technical review of this report. We also acknowledge the guidance from members of DRBC's Advisory Committee on Climate Change about the use of sea level rise projections and their review and input on the draft report.

The project was developed, performed, and documented by Dr. Fanghui Chen, P.E., and Amy L. Shallcross, P.E., of the DRBC Water Resource Operations branch. The draft report was reviewed by former DRBC Executive Director Steven J. Tambini, and edited by Robert S. Nicholson, retired hydrologist formerly of U.S. Geological Survey. Development of this scientific modeling study would not have been possible without the contributions of Dr. Li Zheng, Dr. Joseph Fogarty, and others at the DRBC who provided guidance and support.

Disclaimers

This report and the model results presented are intended solely for the purposes described in the report. They do not constitute a rule, regulation or guidance and have no legal effect. This work was funded in part by the U.S. Fish and Wildlife Service (FWS) through the National Fish and Wildlife Foundation's (NFWF) Delaware Watershed Conservation Fund (DWCF), grant number 75117. The views and conclusions contained in this document are those of the authors and should not be interpreted as representing the opinions or policies of the U.S. Government or the National Fish and Wildlife Foundation and its funding sources. Mention of trade names or commercial products does not constitute their endorsement by the U.S. Government, or the National Fish and Wildlife Foundation or its funding sources.

[1] GHD is a global hydrology and hydrodynamics consulting firm.

[2] USACE-ERDC-CHL: US Army Corps of Engineers, Engineer Research and Development Center (ERDC), Coastal and Hydraulics Laboratory (CHL),

Authorization

The work herein was conducted in accordance with Article 3 Sections 3.6.c and 3.6.f of the Delaware River Basin Compact (Pub. L. No. 87-328, 75 Stat. 688) and approved in DRBC's Water Resources Program for FY2025-2028[3]. Section 3.6.c authorizes the DRBC to conduct and sponsor research on the water resources of the Basin and plan for their use, conservation, management, development, and protection. The results of this study may be used to inform policy, planning, and future policy decisions by the Commission related to the allocation, diversion and releases of water resources as referenced in Sections 3.3.a of the Compact and associated flow and drought management sections of the Delaware River Basin Water Code (18 CFR Part 410).

[3] https://www.nj.gov/drbc/library/documents/WRPFY26-28.pdf

Executive Summary

The purpose of this study is to evaluate how sea level rise will impact salinity intrusion in the Delaware River Estuary. A three-dimensional hydrodynamic and salinity model (SM3D) (Chen, F. et al., 2025)[4] was used to evaluate the hydrodynamics and salinity with increased sea levels, a range of freshwater inflows, and conceptual management actions. In addition, sensitivity tests with SM3D were performed to assess different model assumptions, such as model domain, boundary conditions and non-ocean related salinity. Although sea level rise (SLR) poses many significant threats related to tidal flooding, local flooding, storm surge, and habitat, the results summarized herein are focused on the impacts related to salinity intrusion from the ocean due to sea level rise. The results summarized in this report may be used to: support other Delaware River Basin Commission (DRBC) Basin-wide planning studies; inform DRBC drought and flow management plans and policy; and inform other DRBC and external studies of salinity intrusion into water resources in the Delaware River Estuary.

Introduction

The Delaware River Estuary (Estuary) includes Delaware Bay and the portion of the River influenced by the tide from Trenton, NJ, to the Atlantic Ocean. Potential impacts to the Estuary from SLR are of concern to water resource managers and water users. In addition to exacerbating tidal flooding and storm surge, the additional ocean water entering the mouth of the Estuary resulting from SLR is likely to increase salinity in portions of the Estuary. Salinity can affect the suitability of the water for use, with or without treatment, for multiple purposes including drinking water.

Salinity intrusion in the Estuary is tracked using an indicator known as the salt front. The salt front is defined as the location of the seven-day moving average 250 mg/L chloride concentration (7-day moving average [dma] isochlor). The 250 mg/L chloride concentration is based on a National Secondary Drinking Water Regulation.

Using an analytical approach that includes published projections of SLR and three-dimensional hydrodynamic modeling, potential SLR impacts to salinity intrusion were simulated with historical flows and SLR and shown to be substantial under some future conditions. The sensitivity of simulation results to specific features of model configuration was evaluated, and results of this evaluation indicate that the calibrated model is appropriate for simulating the effects of sea level rise on salinity in the Estuary.

[4] The development and calibration of this model is documented separately.

This technical report presents simulated changes in salinity in the Estuary due to SLR and the location of the salt front during low flow periods. The report presents the modeling study and evaluation of the impacts of SLR-driven salinity intrusion to related flow and drought management plans that are designed to protect water intakes and other uses. Water is withdrawn from intakes in the Estuary for drinking water (with treatment), thermoelectric power generation, refineries, and other commercial and industrial uses. The Estuary is a source of drinking water for the Philadelphia Water Department (PA), Lower Bucks County (PA), Aqua Pennsylvania (PA), Burlington City (NJ), and New Jersey American Water Company (serving three counties in southern NJ), which collectively provide water to approximately 1.37 million people. Higher salinity can also cause corrosion to infrastructure and equipment, affect the quality of products, or require additional treatment, which is energy intensive and cost prohibitive. The objectives of the DRBC flow and drought management plans (Water Code 18 CFR Part 410, Sections 2.5.3–2.5.6) are the preservation of regional storage and salinity management in the Estuary to protect drinking water supplies and other uses, including power generation, industry, irrigation, mining, out-of-Basin diversion, aquatic life and fish consumption, and recreation use, among others.

The locations of water-supply intakes and other points of interest are designated by “River Mile” (RM), the distance between the mouth of the Bay and the point of interest. Accordingly, the mouth of the Bay is defined as RM 0 and the head of tide at Trenton, NJ, is at RM 133. The salt front is normally[5] located between RM 67 and RM 76, but during low-flow conditions it moves farther upstream. The Philadelphia Water Department and the New Jersey American Water Company both have drinking water intakes at RM 110. All other drinking water intakes are located farther upstream away from the ocean. The intakes of many other surface water withdrawals for uses other than drinking water are located farther downstream. During periods of low flow or drought, freshwater is purposefully released from upstream reservoirs in the Basin to repel salinity in the Estuary. During the drought of record in the 1960s, before present drought management plans were established, the salt front was as far upstream as RM 100 (the location of the Benjamin Franklin Bridge), approximately 10 miles downstream from the major drinking water intakes[6].

[5] “Normally”, or the normal range, refers to the range of the range of median monthly salt front location based on the period of record from 1998 to 2013. Up-to-date information regarding the salt front are available at https://drbc.net/Sky/hydro/saltfront.html, and https://www.nj.gov/drbc/programs/flow/salt-front.html

[6] The most upstream observed location of the salt front is RM 102, which was derived from the maximum high tide chloride concentrations measured at the Ben Franklin Bridge (RM 100) and Bridesburg, NJ (106), as reported in multiple annual reports of Office of the Delaware River Master. No information is available about when the concentrations were measured or if they were measured on the same day and same tide. The salt front, the 7-day moving average 250 mg/L chloride concentration, is calculated using paired daily specific conductance data. During the 1960s drought, the maximum salt front location reached RM 100.4 on November 26, 1964.

Since 1983 when the DRBC drought management plans were adopted, the farthest upstream location of the salt front was River Mile 90 in 2016 and 2024 (near the confluence with the Schuylkill River at RM 92.5).

Analytical Approach

DRBC developed a three-dimensional hydrodynamic and salinity model (referred to as "SM3D") as a tool to study the impact of SLR on salinity in the Delaware River Estuary. The focus of this study is to examine how the forces driving salinity intrusion will change with sea level rise and to evaluate: 1) changes in the salinity regime in response to SLR; 2) the extent of salinity intrusion as it relates to the protection of public drinking water supplies; 3) the extent of salinity intrusion in comparison with existing DRBC water quality standards; 4) the relative frequency of salinity intrusion under SLR for key locations; 5) the effect of different model configurations on simulation results; 6) the sensitivity of the results to other potential conditions that may affect salinity intrusion; and 7) the effectiveness of conceptual management actions for reducing impacts of salinity intrusion.

SM3D simulations were performed with a baseline sea level (e.g., 0 m or "no SLR"), referenced to year 2000 sea levels, and five incremental SLR projections (0.3 m, 0.5 m, 0.8 m, 1.0 m, and 1.6 m), which were based on multiple published projections of SLR. The projections are for sea level where the Delaware Bay meets the Atlantic Ocean at Lewes, DE. The probability of 1.0 m SLR is 1.5 percent by the year 2060 but may be 50 percent by year 2100. The probability of 1.6 m SLR by the year 2100 is low.

A representative low-flow condition (represented by July–October 2002 flows) was used to characterize SLR impacts to salinity and to evaluate the sensitivity of results to assumptions used for modeling SLR. Results of additional simulations, representing a wide range of flow conditions over multiple years, including the drought of record, were used to characterize the relative frequency of impacts and to demonstrate how salinity changes seasonally and over a range freshwater flow regimes.

Impacts of Sea Level Rise on Salinity

Simulation results were used to determine changes in the tidal surface water elevation and salinity structure, the spatial and longitudinal salinity, and the upstream extent of salinity intrusion resulting from SLR (Section 4). The maximum salt front location is indicative of the most upstream extent of salinity intrusion in a given year. In addition to the salt front, other indicators of salinity intrusion are the 30-dma chloride concentration in relation to a 180 mg/L standard at RM 98 (Camden, NJ) and salinity, used to describe the salt content of saltier waters, such as the Lower Estuary or Bay. The salt front, chloride, and salinity indicators were all evaluated using simulation results.

With SLR, the predicted upstream water level and tidal amplitude increase in the upper portion of the Estuary. Sea level rise increases the pressure and density of seawater at the mouth of the Bay, causing an increase in the movement of saltwater into the Bay. Scenario simulations indicate that in Delaware Bay, vertical salinity stratification is enhanced due to an increased influx of saltier, denser water moving landward near the bottom, driven by sea level rise. This stratification is particularly pronounced during neap tides and when there is relatively low flow from upstream areas.

Simulations of 10 years of annual flows that represent a range of flow conditions were used to characterize how salinity is impacted by sea level rise. Results of a simulation with the low flows of 1965, the current drought management program, and 1.0 m SLR, show that under these conditions, the maximum salt front location is RM 100.4, as far upstream as it was during the mid-1960s drought of record and less than 10 miles from public drinking water intakes at RM 110. With 1.6 m SLR, the simulated salt front location reaches RM 104.7, within six miles of the drinking water intakes. The normal range of the salt front location also shifts upstream with SLR; with 1.6 m SLR, the upper end of the normal range (25^{th}–75^{th} percentile) of the salt front is at RM 84.1. Results also demonstrate that with 1.0 m SLR, the 30-dma chloride concentration equals or exceeds the 180 mg/L standard at RM 98 (Camden) 3.2 percent of the time under the current drought management program. With 1.6 m SLR, chlorides exceed the water quality standard 7.5 percent of the time (and in four of the 10 representative years simulated). The largest changes in daily depth-averaged salinity occur between the Delaware Memorial Bridge (RM 69) and Chester, PA (RM 83.6). With 0.5 m, 1.0 m, and 1.6 m SLR, the largest increases are 0.6, 1.2, and 2.0 psu respectively.

Model Sensitivity Testing

The effects of changes in specific features of model configuration on simulated salinity intrusion were tested (Section 5), including: (1) extent of marsh area, which may become enlarged with

sea level rise; (2) bottom roughness in marshes, which impacts energy loss as the tide moves upstream; (3) extent of permanent marsh inundation resulting from shoreline retreat and bank erosion; and (4) navigation channel bathymetry.

Marsh areas affect the volume of water moving in and out of the Estuary by providing additional space for water to spread out, which also increases the volume of the tidal prism. A larger modeled marsh area was found to lessen simulated salinity intrusion. With up to 1.6 m SLR during a representative dry season, a larger marsh area results in a maximum salt front location up to 2.6 miles farther downstream. The results demonstrate that preserving marsh areas is beneficial for reducing salinity intrusion.

The effect of possible changes in the type, density, and submergence of marsh vegetation with SLR were evaluated with sensitivity tests of the bottom roughness factor used in simulations. Variations in the roughness factor did not materially affect the simulated upstream extent of the salt front. The simulated salt front was only marginally affected by the modeled representation of the extent of permanent marsh inundation resulting from shoreline retreat and bank erosion. The model does not predict how marsh extent, bottom roughness, shorelines, or erosion will be affected by sea level rise.

Changes in the depth and width of an estuary resulting from natural processes and human activities, such as dredging, can affect salinity intrusion. The Federal Navigation Channel (FNC) is maintained by the United States Army Corps of Engineers (USACE) and is periodically dredged—to a depth of 40 ft in 1940, and most recently to a depth of 45 ft. Simulations were performed to compare the salinity intrusion with SLR for both 40- and 45-ft channel depths. Results of simulations without SLR indicate that the maximum salt front location is 2.4 miles farther upstream with the deeper channel. With up to 1.6 m SLR, the simulated salt front is up to 2.4 miles farther upstream with the deeper channel. Results show that the bathymetry of the FNC influences salinity intrusion. However, the simulated incremental change in salt front location with increasing sea level rise is similar for either the 40- or 45-ft channel.

These results show that the calibrated SM3D model is conservative with respect to the protection of public drinking water supplies and that the model is appropriate for use in analyzing the impacts of SLR on salinity intrusion in the Delaware Estuary.

Analysis of Other Potential Conditions

Other conditions that may affect salinity intrusion along with sea level rise were also evaluated, including increased salinity from non-tidal and point sources, increased drought severity, and increased ocean temperature (which affects density-driven circulation). Simulations were performed to assess the effect of these conditions on model results (Section 6).

Simulation results indicate that if the non-tidal tributary salinity is doubled as projected by the year 2060, the maximum salt front location is up to 0.9 miles farther upstream. Model results were not sensitive to the representation of point-source salinity as either variable by month or constant. Sea level rise has a much larger impact on the simulated salt front location and chloride concentrations than increases in salinity from non-tidal sources.

A hypothetical extreme drought scenario, worse than the drought of record, was formulated using a series of minimum monthly historical flows, adjusted to reflect the current-day flow objective of 2,500 cfs. Simulations with flows representing this scenario indicate that during such an event, even with no sea level rise, the maximum salt front is as far upstream as RM 96.9, within 4 miles of its maximum location in the 1960s, when no flow objective was in place. With 0.5 m and 1.0 m SLR, the simulated maximum salt front locations with a more severe drought are at RM 100.3 and RM 103.6, respectively. With 1.6 m SLR, the maximum salt front location is at RM 108.1, within 2 miles of the drinking water intakes. Although unlikely, a more severe drought than the drought of record would represent a major management concern for drinking water utilities and other water users. At RM 98 (Camden), the maximum 30-dma chloride concentration exceeded the 180 mg/L water quality standard for all values of sea level rise, including the baseline (approximately 6 percent time of exceedance), under a more severe drought condition.

As the ocean temperature rises, the absorbed heat lowers the density of the ocean water, which decreases the pressure forcing at the ocean boundary, reducing salinity intrusion. A sensitivity analysis was conducted to determine the effect of increased ocean temperature on salinity intrusion. Results show that a 1°C increase in ocean boundary temperature has only a marginal impact on the maximum salt front location; the resulting salt front is less than 0.5 mile farther downstream.

Conceptual Analysis of Management Actions for Salinity Repulsion

Simulations were performed to evaluate alternative reservoir release schemes to repel salinity (Section 7). The first set of simulations was used to demonstrate the effectiveness of the 2,500 cfs Trenton Flow Objective under projected SLR conditions. The second set was designed to test the benefit and efficiency of a pulse release (a temporary sustained increase in flow). For these sets of simulations, the additional water to meet the flow objective or the pulse release is represented as additional flow at Trenton. The third set of simulations was performed to determine if the location where reservoir releases for flow objectives enter the Estuary (e.g., from the Delaware or Schuylkill River) changes the effectiveness of repelling salinity than only increasing the flow.

Without SLR, the benefit of the 2,500 cfs Trenton Flow Objective (TFO) is to keep the maximum salt front 3.3 miles farther downstream than without TFO. With SLR, the benefits of the flow

objective are to keep the salt front 4.1–4.3 miles farther downstream and to keep it below RM 105. Simulation results show that although the flow objective can be an effective management concept for salinity repulsion, a flow objective of 2,500 cfs may not be adequate for maintaining the existing water quality standard for chloride at RM 98 (Camden) with sea level rise of 0.5 m or more.

Another conceptual management option is to use pulse releases in addition to TFO. Simulations with pulses of 500 and 1,000 cfs were performed to determine if a short-term increase in flow with a pulse of water, rather than a higher flow objective, could be used to reduce the impacts of SLR-driven salinity intrusion. A short-term pulse with a trigger (in addition to TFO), rather than a constant higher flow objective, saves water. With 0 m SLR, the 500 and 1,000 cfs pulses kept the salt front 1.1 and 2.3 miles farther downstream, respectively. With 1.0 m SLR, the simulated pulses kept the maximum salt front location 1.9 and 3.3 miles farther downstream, respectively. With 1.6 m SLR, the simulated pulses kept the salt front 1.6 and 3.2 miles farther downstream, respectively. Both the 500 cfs and 1,000 cfs pulses were successful at repelling the salinity intrusion to below RM 100 for as much as 1 m SLR. Results show that the effect of the pulse is temporary and persists for almost two months after the termination of the pulse, possibly longer. The extent to which a pulse keeps the salt front downstream is affected by multiple factors, including (1) the base flow to which the pulse is added, and (2) the salt front location prior to the pulse.

Flow for salinity repulsion is currently supplied by reservoirs in either the non-tidal Delaware or Schuylkill River watersheds. Simulations were performed to determine the relative efficiencies of water releases from these respective watersheds. If the salt front is more than a few miles above the Schuylkill River confluence, then additional water from the non-tidal Delaware River is more efficient in repelling it than additional water entering from the Schuylkill River. Augmenting with Schuylkill River flow is more effective than augmenting with Delaware River flow during periods when the salt front is below or near the confluence of the Schuylkill and Delaware Rivers. The impact of the additional water is influenced by the volume of water in the River, the mixing zone created by the freshwater plume near the Schuylkill River, and the location of the salt front in relation to the Delaware-Schuylkill confluence.

Key Results

Sea level rise (SLR) increases tidal water levels throughout the Delaware Estuary, amplifying tidal elevations upstream to Trenton and increase salinity throughout the Estuary. Higher sea levels enhance salinity stratification, spread more saltwater across shallow areas, and transport saltwater farther upstream. Under drought conditions, especially the 1965 drought of record, SLR significantly increases both the maximum location of the salt front maximum location and the

percent of time the chloride standard is exceeded at Camden (RM 98). The greatest increases in the maximum depth-averaged salinity occur between the Delaware Memorial Bridge (RM 69) and Chester (RM 83.6) with sea level rise.

Under the 1965 drought of record hydrologic conditions, and with a 2,500 cfs Trenton Flow Objective, the simulated maximum salt front location migrates farther upstream by 1.6 miles, 2.6 miles, 4.7 miles, 6.2 miles, and 10.5 miles with 0.3 m, 0.5 m, 0.8 m, 1.0 m and 1.6 m of SLR, respectively, compared to the baseline (0 m SLR) scenario. Although the salt front remains below RM 105, SLR was shown to be a potential future threat to the drinking water intakes at RM 110.

Model sensitivity tests show that including more marsh area and simulating the marsh inundation yields less salinity intrusion and changes in marsh roughness, shoreline retreat, and bank erosion have minimal effect on the maximum location of the salt front. A deeper FNC increases upstream salinity intrusion by approximately 2.4 miles, regardless of SLR. Changes in the location of the salt front due to SLR alone are similar regardless of deepening the channel bathymetry[7], but farther upstream for the 45-ft FNC. Other factors, such as increased tributary salinity, more severe droughts, and rising ocean temperatures, produce smaller but measurable differences. Alternately, a more extreme drought presents substantial risks even without SLR.

Simulations of flow management alternatives indicate that the Trenton Flow Objective (2,500 cfs) helps hold the salt front downstream but may no longer maintain chloride standards when SLR exceeds 0.5 m. Additional pulse releases are beneficial. However, their impact diminishes quickly and is not sufficient to address SLR. Reservoir releases entering the Estuary from the non-tidal Delaware River, rather than the Schuylkill River, are more effective when the salt front is above their confluence.

A more detailed summary is presented in Section 8.

Potential Future Work

Results from this study and other on-going work may be used to scope additional studies, define alternatives and scenarios to be simulated, and refine model assumptions relevant to planning for SLR. SM3D can also be used to evaluate flow and drought management options and resources

[7] The model results indicate that the differences in the maximum salt front location due to the change in channel bathymetry (40 to 45 ft) by itself are similar, approximately 2 to 2.4 miles, regardless of the value of sea level rise. For instance, with 0 m SLR the difference is 2.4 miles compared the 45-ft channel with the 40-ft channel cases, and with 1.0 m SLR the difference is 2.2 miles compared the 45-ft channel with the 40-ft channel cases. The change in the maximum salt front location due to sea level rise, by itself, is similar for both channel depths for each value of SLR. For example, with 1.0 m SLR, the difference in maximum salt front location increased by 5.8 miles with 40-ft channel, and 5.6 miles with the 45-ft channel.

to assess the Basin's resiliency to drought and drought conditions. The next steps for SM3D and its continued use include:

- Continued engagement with the Advisory Committee on Climate Change (ACCC), Basin states, and stakeholders about model assumptions for planning studies and other projects;
- Simulation of climate-impacted flows and SLR on salinity;
- Evaluation of flow and drought management programs and their effects on, and utilization of, Basin resources; and
- Periodic refinement of the model based on new data and other information.

Refinement of SM3D with new data when available is needed to maintain an up-to-date tool for investigating the impacts of climate change on Basin resources. For example, some of the parameters needed by the model are those for which little or no information was available prior to and during model development and calibration, including the flow at USGS gage in the Chesapeake and Delaware Canal[8], and the latest 2022–2023 bathymetry survey data near the C&D Canel confluence with the Delaware River, which was obtained later during the study. With the incorporation of the new information into the model during the project demonstrates that the model is a "living" model and will be refined and improved in the future. Communicating the limitations of model results and developing agreement about the assumptions used for different analyses are important for establishing a common foundation for decision makers.

The impacts of climate change (increased temperature and precipitation) on flows and reservoir operations are currently being evaluated; changes in the natural variability, seasonality and magnitude of freshwater flows will continue to be important considerations for flow and drought management. SM3D may also be used with projected flows and output from water supply planning models to evaluate the performance of proposed flow and drought management programs for simulated drought events. Those results, along with other Basin-wide planning and evaluation efforts, may be used to assess Basin vulnerability to drought and climate change and to plan for the water resources that will be needed in the future to continue meeting the water resource goals of the Basin.

[8] C And D Canal NR Delaware City, DE - USGS-01482695 was established in November 2019, and valid flow data were reported from 2020 to present.

List of Acronyms

ACCC	Advisory Committee on Climate Change
ADCP	Acoustic Doppler Current Profiler
CFR	Code of Federal Regulations
cfs	cubic feet per second
cm/s	centimeter per second
C&D Canal	Chesapeake and Delaware Canal
DE	Delaware
DNREC	Delaware Department of Natural Resources and Environmental Control
DRB	Delaware River Basin
DRBC	Delaware River Basin Commission
DR	Delaware River
DRB	Delaware River Basin
#-dma	#-day moving average
DNREC	Delaware Department of Natural Resources and Environmental Control
EFDC	Environmental Fluid Dynamics Code
EPA	U.S. Environmental Protection Agency
FEMA	Federal Emergency Management Agency
FNC	Federal Navigation Channel
ft	feet
GMSL	Global Mean Sea Level
In	inches
km	kilometers
MD	Maryland
m	meters

mi	miles
mm	millimeters
MG	million gallons
mg/L	milligrams per Liter
MHHW	mean higher high water
MLLW	mean lower low water
MSL	mean sea level
NASA	National Aeronautics and Space Administration
NCDC	NOAA's National Climatic Data Center
NJ	New Jersey
NJAW	New Jersey American Water
NJSTAP	New Jersey Science and Technical Advisory Panel
NOAA	National Oceanic and Atmospheric Administration
NTDE	National Tidal Datum Epoch
NY	New York
PA	Pennsylvania
PS	point source
psu	practical salinity units
PWD	Philadelphia Water Department
RM	River Mile
RMSE	root mean square error
RSLR	Relative Sea Level Rise
SF	Salt Front (also refers to Salt Front River Mile)
SK	Schuylkill River
SLR	sea level rise

SM3D	Three-dimensional salinity model developed for this project with EFDC and Grid v2.1, includes marsh area limited to what floods currently and infrequently
SM3D+M	Three-dimensional salinity model developed for this project with EFDC and Grid v4.1, which includes additional marsh areas not currently flooded.
TEFO	Trenton Equivalent Flow Objective
TFO (or FO)	Trenton Flow Objective, or the Flow Objective
ubRMSD	unbiased root mean square difference
USGS	U.S. Geological Survey
USACE	U.S. Army Corps of Engineers
WASP	Water Quality Analysis Simulation Program
WOA	NOAA Ocean Climate Lab's Product World Ocean Atlas Database
WSE	water surface elevation

Table of Contents

List of Figures

List of Tables

List of Appendices

1. INTRODUCTION

An estuary occurs where the water from larger rivers mixes with water from the ocean. In parts of an estuary where freshwater and seawater combine, the water becomes brackish[9] (not fresh, but not as salty as the ocean). Tides push salt water into an estuary, while flow from the upstream river pushes freshwater out into the ocean. The salinity of the water throughout an estuary is not uniform. Generally, water in the upper reaches of an estuary does not routinely mix with higher salinity ocean water and is acceptable for use as a source for public drinking water (after reasonable treatment) and as process and/or cooling water at thermoelectric power generators, refineries, and industrial and manufacturing facilities. The salinity of water is also a factor that can affect the habitat of aquatic life.

The salinity at various points in the Delaware River Estuary ("the Estuary") is a significant concern to water resource managers. Reservoirs have been developed in the Basin to augment flows into the Estuary to manage salinity intrusion during periods of drought. During the worst drought on record in the 1960s, salinity levels became unacceptably high in the Upper Estuary, damaging industrial infrastructure and threatening drinking water sources. In response and after detailed studies, the Delaware River Basin Commission ("the Commission" or DRBC) developed a comprehensive drought management program, adopted in 1983, that has been effectively used since then to manage salinity. The drought management program considers consumptive water use, available storage, and reservoir releases and uses drought-defining criteria to manage salinity while concurrently preserving regional storage to protect drinking water supplies. The drought management program established a flow rate objective in the Delaware River at Trenton, NJ, to maintain adequate freshwater flows into the Estuary. Details about the drought management program are available on DRBC's website and are codified as federal regulation in the Delaware River Basin Water Code.

Sea levels are rising globally and locally due to climate change and vertical land movement (subsidence). Rising sea levels result in more ocean water entering the Estuary and more frequent occurrences of higher salinity water moving farther upstream (also known as salinity intrusion). With these changes, the evaluation of potential impacts resulting from sea level rise on salinity intrusion, of the effectiveness of related flow and drought management plans and protections, and of other water resources impacts is warranted. The results presented in this technical report will be used to: support DRBC Basin-wide planning studies; inform DRBC drought

[9] Brackish water is a mix of fresh and saltwater with a salinity between freshwater and seawater, the salinity may range from 0.5 to 30 psu. The break between "fresh" and "brackish" may vary among water users. For example, the freshwater limit for agricultural irrigation could be 0.2 psu.

and flow management plans and policy; and inform other DRBC and external evaluations of the impacts of salinity intrusion to water resources in the Delaware River Estuary.

1.1 The Delaware River Basin and the Delaware River Estuary

The Delaware River ("the River"), located in the densely populated corridor of the northeastern U.S., forms interstate boundaries between New York, Pennsylvania, New Jersey, and Delaware (**Figure 1.1-1**). The Delaware River is approximately 330 miles long, from its headwaters in New York to its confluence with the Atlantic Ocean. The area drained by the Delaware River ("the Basin" or Delaware River Basin [DRB]) is 13,539 square miles, including the 782 square miles covered by Delaware Bay. The Delaware River begins where the East and West Branches of the Delaware River meet at Hancock, NY, in the forested, western slopes of the Catskill Mountains. The River ends in the Atlantic Coastal Plain at the mouth of Delaware Bay where it meets the Atlantic Ocean. The Delaware River is the longest un-dammed river east of the Mississippi River, although dams are present on some tributaries. The Delaware River Estuary includes Delaware Bay and the portion of the Delaware River influenced by the tide. The mouth of the Bay is defined as River Mile (RM) 0 and the head of tide at Trenton, NJ, is at RM 133[10].

[10] The DRBC River Mile system is available at https://www.nj.gov/drbc/basin/river-mileage-sys.html. Users may download a pdf map or kmz file that can be shown in Google Earth.

Figure 1.1-1. Delaware River Estuary and Bay.

1.2 Water Resource Uses in the Delaware River Estuary

The waters from the Delaware River Estuary are withdrawn and used for multiple purposes including: public drinking water (after reasonable treatment), irrigation, industry (process water and/or cooling towers), and thermoelectric power generation. Of the 130 surface water withdrawals located within approximately 0.7 miles of the Delaware River Estuary, ten are for public water supply[11], nine are for irrigation, 33 are for industry, and 75 are for thermoelectric power generation. **Figure 1.2-1** shows the locations of water withdrawals from the Estuary.

Based on data from 2020, the total daily average of all surface water withdrawals from the Estuary is approximately 3.57 billion gallons per day. As shown on **Figure 1.2-2**, 84 percent of water withdrawn from the Estuary is for thermoelectric power generation, 5 percent is for public water supply, and 11 percent is for industrial purposes. Only 67.8 million gallons (MG) per day (2.2 percent) of the total water withdrawn from the Estuary is used consumptively (water withdrawn and evaporated or removed and not returned to the Basin). As shown on **Figure 1.2-3**, of the total consumptive use, 25 percent is for public water supply, less than 1 percent is for irrigation and other uses, 16 percent is for industrial uses and 58 percent is for thermoelectric power generation.

[11] Public water supplies include the Philadelphia Water Department, New Jersey American Water, Lower Bucks County Joint Municipal Authority, Aqua Pennsylvania, and Burlington City.

Figure 1.2-1. Locations of surface water withdrawals in the Delaware River Estuary

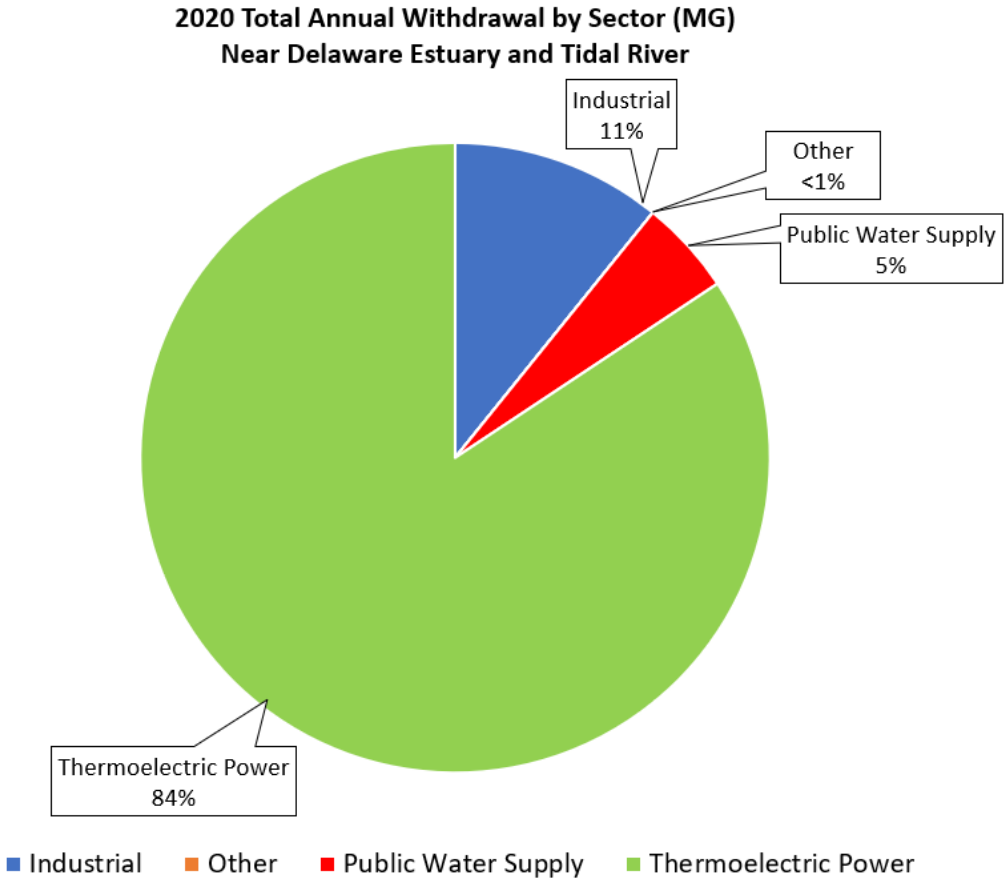

Sector	Water Withdrawal (MG)	Percent of All Withdrawals
Industrial	141,100	11%
Public Water Supply	63,700	5%
Thermoelectric Power	1,101,000	84%
Other	120	<1%
Total	**1,305,920**	

Figure 1.2-2. Surface Water Withdrawals from the Delaware River Estuary by Sector

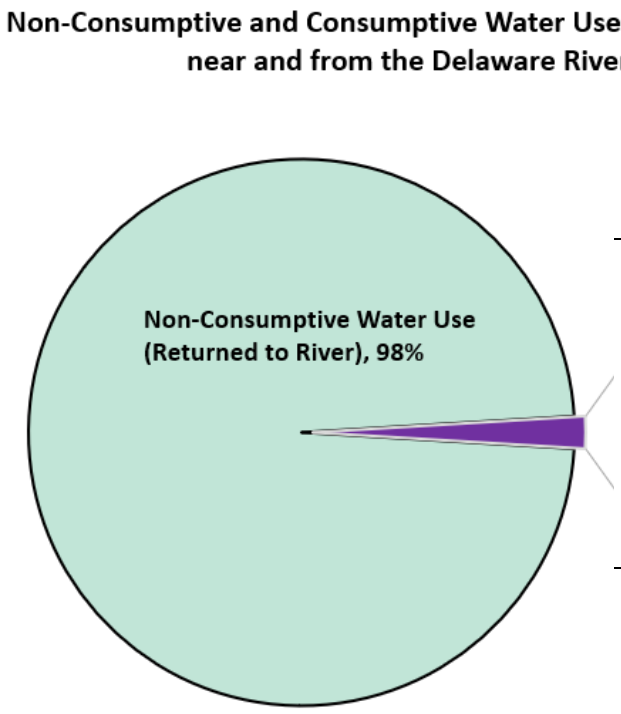

Sector	Consumptive Use (MG)	Percent of Consumptive Use
Industrial	3,900	16%
Public Water Supply	6,300	25%
Thermoelectric Power	14,500	58%
Other	120	<1%
Total	**24,820**	

Figure 1.2-3. Consumptive water use from the Delaware River Estuary by sector.

As noted in the Delaware River Basin Water Code, agricultural (irrigation), industrial, and public water supplies (after reasonable treatment) are to be protected except where natural salinity precludes such uses. The Water Code also notes that other uses of Basin water that apply to the Estuary include habitat for fish and other aquatic life; recreation; navigation; and waste assimilation. This report provides estimates of the impacts of sea level rise and salinity intrusion for evaluations of the existing drought management plans and specifically for the Commission's efforts to protect public drinking water sources.

1.3 Measurement of Salinity Intrusion

Salinity intrusion is the movement of saline water from the ocean into an estuary and its advance upstream. Salinity is a measurement of the salt content in water. In this report, salinity intrusion is measured in one of three ways depending upon the water resource impacts being evaluated:

- The "**salt front**" (SF) location is expressed as a River Mile that represents the position of the 7-day moving average (dma) 250 mg/L isochor[12]. This chloride concentration is

[12] Isochlor: An imaginary line connecting all locations with the same chloride concentration or chlorinity.

equivalent to a salinity of 0.45 practical salinity units (psu). The significance of the 250 mg/L chloride value is based on a secondary drinking water standard that is used as a guideline to assist public water systems in managing their drinking water for aesthetic considerations, such as taste, color, and odor.

- **Chloride concentration** is expressed in mg/L. Chloride concentration is used to describe the salt content of fresher waters, such as the Upper Estuary. Chloride concentrations are determined by in-stream measurements of specific conductance and converted to chloride concentration with a relationship developed by USGS (1970)[13]. The DRBC water quality standard for salinity management is a maximum 30-dma chloride concentration of 180 mg/L at RM 98 (Camden).
- **Salinity** is expressed in psu. Salinity is used to describe the salt content of saltier waters, such as the Lower Estuary or Bay. Different methods are commonly used to determine salinity. These methods are described in Appendix C.

The salinity structure in an estuary is formed by two competing forcings: a) river flow from upstream, which tends to drive saltwater seaward; and b) tidal forcing and gravitational circulation, which tend to drive saltwater landward. The mechanisms that drive salinity transport in an estuary include density-driven estuary exchange flow, turbulent mixing from shear and tidal oscillations,

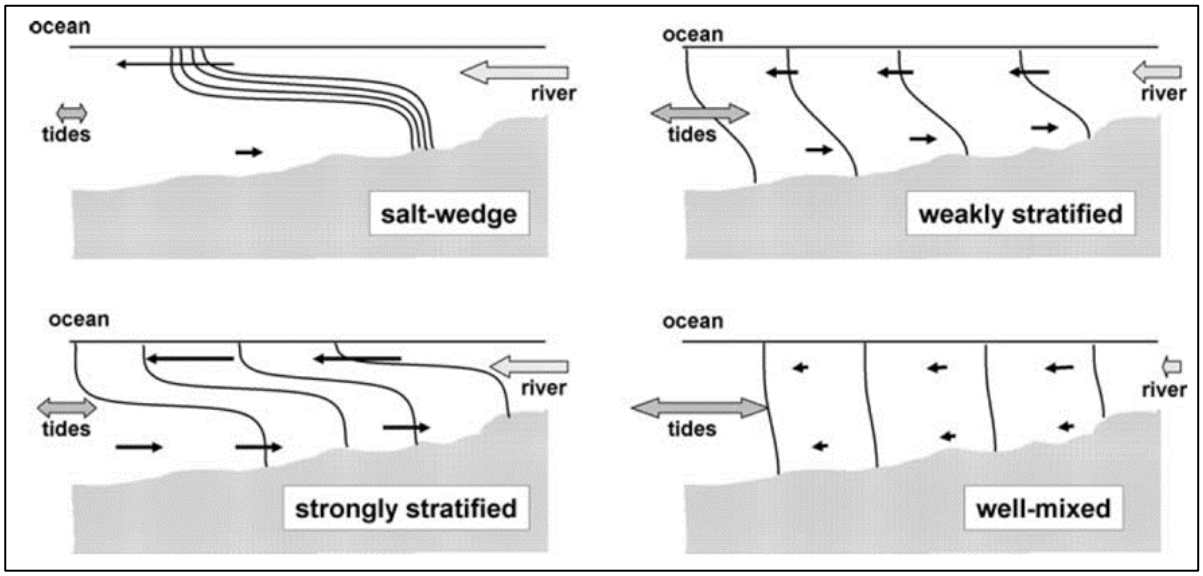

Figure 1.3-1. Classification of estuaries based on vertical structure of salinity (from Valle-Levinson (2009).

[13] Paulson, R.W. A graphical summary of specific conductance data for the Delaware River Estuary correlated with Delaware River flow at Trenton, New Jersey, 1970. 10.3133/ofr70260, USGS Publications Warehouse, http://pubs.er.usgs.gov/publication/ofr70260

and meteorological forcings such as precipitation, evaporation, and wind. **Figure 1.3-1** shows the classification of estuary mixing based on the vertical structure of salinity (Valle-Levinson, 2009). Estuary exchange flow is explained in more detail in Appendix B.

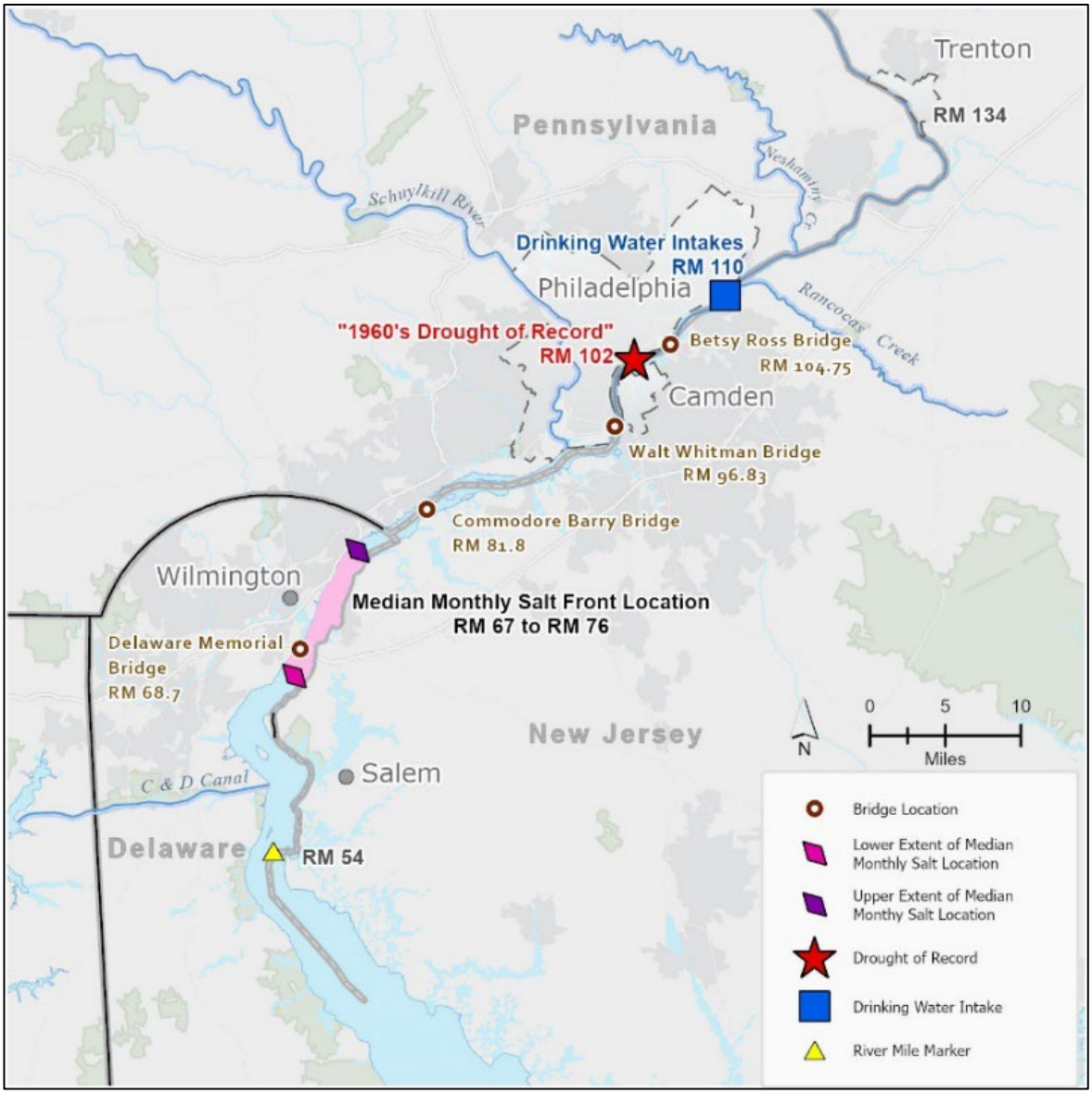

Figure 1.3-2. Median monthly location of the salt front.

Downstream of Marcus Hook, PA (RM 79), the Delaware River Estuary is considered partially mixed or “weakly stratified.” Vertical stratification is most prominent near the mouth of the Bay. The tidally averaged surface and bottom salinities typically differ by less than 10 psu near Ship John Shoal at RM 37 (Aristizabal and Chant, 2014). Upstream of Marcus Hook, PA, the salinity

is generally considered to be relatively uniform and "well mixed" based on the longitudinal vertical structure of the salinity.

The location of the salt front is calculated using real-time specific conductance measurements from U.S. Geological Survey (USGS) water quality monitors, a regression equation developed by USGS in the 1970s relating specific conductance and chlorides, and linear-logarithmic interpolation of the location between the water quality monitoring stations (Zheng et al., 2024). The monitoring stations used to calculate the location of the salt front are distributed along the Estuary from RM 54.1 to RM 100.1 and are described in Appendix C.3. The normal range of the salt front (RM 67 to RM 76) is near the Delaware Memorial Bridge (RM 68.75) and the City of Wilmington, DE (RM 70.5), shown in **Figure 1.3-2**. The lower end of the normal range is near Hoppemense Creek (RM 66.54) near Pennsville, NJ, and the upper end is near Oldman's Creek (RM 76.97) in Swedesboro, NJ (not shown).

1.4 Water Resource Concerns

The purpose of this report is to evaluate the effects of sea level rise in the Delaware River Estuary and the impacts of ocean salinity intrusion on certain Estuary water resources and users. Specifically, the report:

- Reviews published projections of sea level rise (SLR) prepared by government sources through 2100;
- Develops a set of SLR scenarios based upon a range of water resource planning assumptions for 2060 and 2100;
- Evaluates how SLR affects salinity distribution and vertical stratification;
- Estimates changes in Estuary salinity profiles from SLR;
- Evaluates salinity intrusion as it relates to the protection of public drinking water supplies at RM 110 based upon the estimated maximum location of the salt front with a range of SLR scenarios;
- Estimates the extent of future salinity intrusion in comparison with existing DRBC water quality standards;
- Approximates the relative frequency of salinity intrusion under SLR for key locations;
- Assesses the effect of different model configurations on simulation results;
- Analyzes the sensitivity of results to other potential conditions that may affect salinity intrusion; and

- Analyzes certain conceptual management actions for reducing impacts of salinity intrusion.

1.4.1 Protection of Public Drinking Water Intakes

Two major public drinking water intakes located at approximately RM 110 are potentially vulnerable to salinity intrusion. Additional public drinking water intakes in the Delaware River Estuary are above RM 110. Protection of the two intakes at RM 110 also provides protection for the drinking intakes farther upstream.

The Philadelphia Water Department (PWD) Samuel S. Baxter Water Treatment Plant and intake are located on the Delaware River in the Torresdale section of northeast Philadelphia. The Baxter Water Treatment plant serves about 58 percent of the city's water needs (Philadelphia Water Department, 2023). The New Jersey American Water Company (NJAW) has a public drinking water intake located on the Delaware River in Cinnaminson, NJ, across the River from the Baxter intake. Source water from the intake is sent to the NJAW Delaware River Regional Water Treatment Plant in Delran, NJ, treated, and is then provided to several public drinking water systems in three counties in southern New Jersey. Both water treatment plants at RM 110 are considered to have "conventional" treatment and have not been designed to remove salt from water.

Source water with persistent high chloride concentrations can lead to a variety of impacts. Increased salinity can result in corrosion in both the treatment plant and distribution system, potentially causing the pipes to leach lead and copper, both of which are contaminants of concern for human health. In addition, the accompanying increase in sodium can increase the risk of negative health impacts to sensitive customers, such as dialysis patients and those on sodium-restricted diets.

Salinity-related water quality criteria established to protect drinking water intakes were first adopted by the DRBC in 1967. At that time, PWD had the only water intake at RM 110. The standard established in 1967 was an instantaneous chloride concentration of 250 mg/L at the mouth of the Schuylkill River (RM 92.5). During the drought of record in the 1960s, the maximum salt front location was RM 100.4 and occurred in November 1964. In 1983, when the Basin drought management program was adopted, the Commission changed its water quality criteria from the instantaneous chloride concentration at RM 92.5 to a maximum 30-dma chloride concentration of 180 mg/L at RM 98[14] (Camden), which was shown through modeling to be

14 DRBC water quality regulation https://www.nj.gov/drbc/library/documents/WQregs.pdf (see page 97 for Zone 3, C.12).

protective of the river-adjacent well fields being used at that time for public water supply by the City of Camden, NJ. The modeling also showed that the criteria were also protective of the PWD drinking water intake near RM 110.

The highest calculated SF location occurred in 1964 at RM 100[15]. Since then, and with the benefit of the drought management plan, the highest SF locations were just below RM 91 in 2016, 2024, and 2025 (**Figure 1.4-1**).

1.4.2 Other Estuary Water Withdrawals and Uses

Unlike public drinking water intakes, intakes for other water users are located throughout the Estuary, and each user has their own unique water resource and water quality needs related to

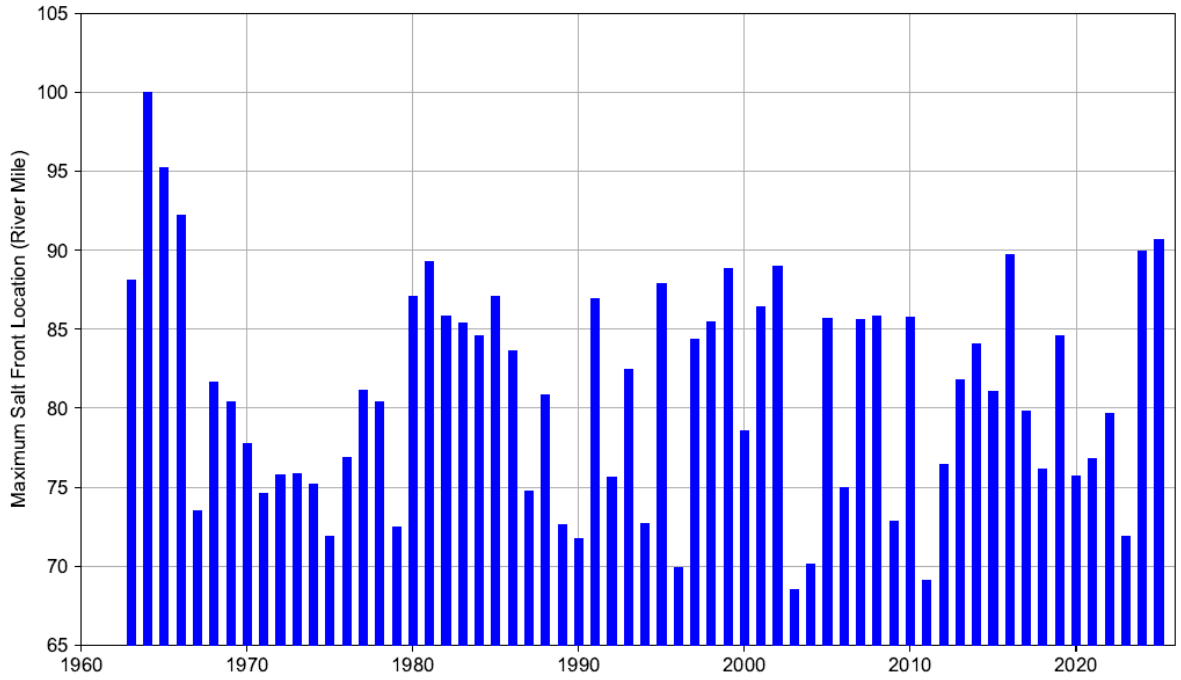

Figure 1.4-1. Historical annual maximum salt front locations from 1963 to 2025.

Data source: DRBC, https://drbc.net/Sky/hydro/SaltFrontHistoricData.txt

[15] The maximum SF location in the observed record of RM 100 occurred on November 26, 1964. Although 1965 is considered a more severe drought year, the salt front was only as far upstream as RM 96. The flows in 1965 from January through September were significantly lower than those of 1964, leading into the critical fall period for upstream movement of the salt front. In 1964 the flows were similar in September and significantly lower than those of 1965 for October through December. For both 1964 and 1965, the instantaneous maximum chloride concentration at RM 100 peaked at 340 mg/L, but at Bridesburg (RM 106) they were 174 and 127 mg/L in 1964 and 1965, respectively. For the 7-day average concentration, a stronger tide and lower flows during November of 1964 resulted in the transport of more salt water past RM 100, than in 1965.

its purpose. While salinity can cause process and corrosion issues and lead to advanced treatment needs and additional costs, it is not within the scope of this study to examine the impacts to agricultural, industrial, or thermoelectric water users in the Estuary.

The Delaware River Estuary is divided into several water quality management and assessment ones as shown on **Figure 1.1-1.** Zone 6 is Delaware Bay, which has higher salinity throughout its extent. SLR is expected to impact salinity in Zones 2, 3, 4 and 5 and, therefore, salinity intrusion was evaluated at locations within these zones. The results could aid water users in determining potential future impacts, if any.

Although the objective of this study is the evaluation of sea level rise and salinity intrusion impacts for the protection of public drinking water supplies. The Delaware River Estuary also provides waste assimilation services and habitat for a large variety of aquatic life species, and these uses could also be impacted by increased salinity intrusion. Defining a suitable habitat can be specific to each species and vary for different life stages. Habitat suitability depends on multiple water quality parameters including salinity, dissolved oxygen, type of sediment and/or substrate, velocity and current, temperature, the presence of other species, food sources, and vegetation, among others. While sea level rise and salinity intrusion have the potential to impact habitat in the Estuary, as well as recreational and commercial fisheries, evaluation and assessment of impacts to these resources is beyond the scope, and not the intent, of this study.

1.5 Results and Indicators

Three metrics are used in this report to evaluate potential impacts to drinking water sources for future SLR scenarios. One metric is the maximum location of the salt front. As shown on **Figure 1.4-1,** the maximum salt front location has not been above RM 91 since 1966 but has been near or slightly above RM 90 in 2016, 2024, and 2025. With implementation of drought management plans that include flow augmentation, the salt front has remained at or below RM 90. The salt front location is also referenced in relation to three landmarks: RM 92.5—the confluence of the Delaware and Schuylkill Rivers; RM 100—its most upstream location during the drought of the 1960s; and RM 110, the location of drinking water intakes for PWD and NJAW.

The second metric is the 30-day moving average chloride concentration at RM 98 (Camden) which is located 12 miles downstream from the drinking water intakes. The water quality criteria (called a “stream quality objective” in DRBC Water Quality Regulations) of a maximum chloride concentration of 180 mg/L at RM 98 was determined to provide adequate protection of drinking water intakes in the Estuary at RM 110 and upstream. The standard was negotiated by the parties to the 1954 Supreme Court Decree, during the development of the drought management plan adopted in the Delaware River Basin Water Code (18 CFR Part 410). The justification for the standard is described in the Interstate Water Management Recommendations of the Parties to

the U.S. Supreme Court Decree of 1954 to the DRBC, also known as the Good Faith Recommendations. Some of the other recommendations from the Good Faith Agreement related to salinity protection were also incorporated by the Commission into the DRB Water Code in 1983.

Salinity is the third metric and is used to describe the salt content of saltier water, such as occurs in the Lower Estuary or Bay. Although salinity is not used to evaluate adherence to water quality standards, it is a useful metric for relating water quality to various uses.

Results used to evaluate the severity of salinity intrusion are presented in tables and graphs as the simulated maximum location of the salt front for future sea level rise, the simulated maximum 30-dma chloride concentration at RM 98 (Camden), and salinity at selected locations. Additional details are presented in the Appendix G through L.

This report also presents overall changes in salinity and the frequency of salinity intrusion at eight locations in Estuary Zones 2 to 5. Changes in salinity and the relative frequency of intrusion due to SLR at these locations can help inform water users as they evaluate potential impacts of SLR.

2. SEA LEVEL RISE

2.1 BACKGROUND

Figure 2.1-1 presents a conceptual mixing diagram of the Estuary generally representing the gradient of salt water from the ocean (left) and fresh water from the land (right). The box on the top represents the Estuary under current sea level conditions. The box on the bottom represents the Estuary at a future higher sea level. The arrows within the boxes represent the relative magnitude of the influence that ocean and fresh water have on salinity. At higher sea levels, the force of the ocean pushing salt water upstream becomes larger while the force of freshwater pushing salt water downstream remains the same, as indicated by the size of the arrows. With the larger ocean force resulting from continued sea level rise, the upstream movement of the salt front in the mixing zone is more likely to extend farther upstream, especially during dry weather conditions when less fresh water from the land is available to push salt water downstream.

Sea level rise (SLR) is the change in the ocean water surface elevation in relation to a datum, which results from both global and local processes. Observations of sea levels, averaged over the globe, (referred to as global mean sea level, or GMSL) demonstrate an increasing trend since the 1900s. Based on analyses of satellite observations summarized in the National Aeronautics and Space Administration's (NASA's) Integrated Multi-Mission Ocean Altimeter Data for Climate Research (Beckley, et al., 2022), GMSL has risen by 104 mm (4.09 in) since 1993, and its average rate of change is 3.4 (+/- 0.4) mm/year or 1.34 in/decade as of October 26, 2022. A detailed literature review of SLR and its causes is presented in Appendix A.

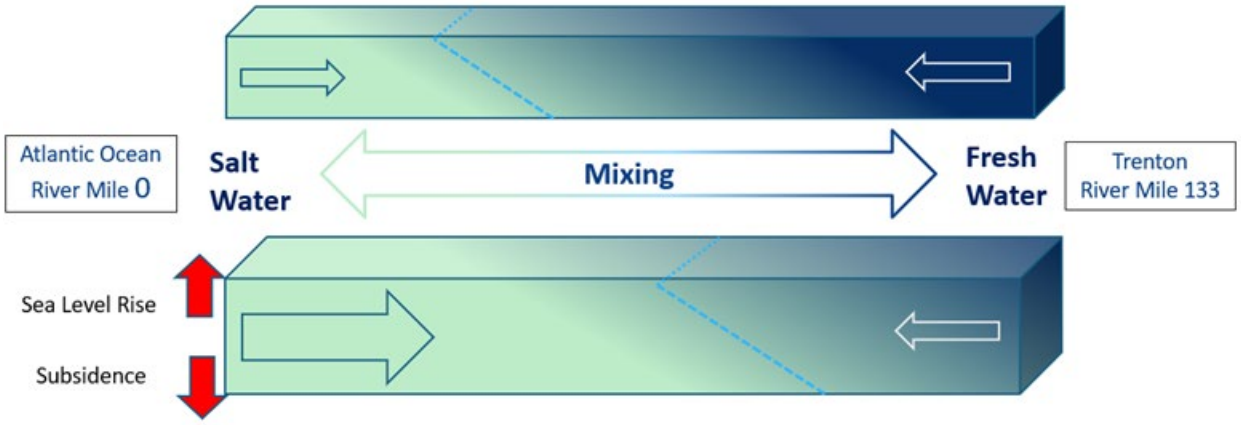

Figure 2.1-1. Conceptual diagram of salt water and fresh water mixing in the Estuary and the effect of sea level rise on the position of the salt front.

2.2 Historical Sea Level Rise

The Delaware River Estuary has experienced sea level rise throughout the 20th century. Historical rates of sea level rise were calculated using monthly averages of mean tide elevations for the period of record at six National Oceanic and Atmospheric Admiration (NOAA) tide gages located in and just outside the Basin (**Figure 2.1-1**). These six tide gages were included in the evaluation since they are located within the model domain or were used to develop model inputs and boundary conditions. The periods of record ranged from 50 to 122 years, and the rates of sea level rise ranged from 3.07 mm/yr to 4.85 mm/yr **Table 2.2-1**[16]). Locations of the six tide gage stations are shown in **Figure 2.2-1**. As an example, and as shown on **Figure 2.2-2**, at the Lewes, DE, tide gage, the rate of increase in sea level was 3.63 mm/year (1.4 in/decade) from 1919 to 2022, which equates to 0.373 m (1.22 ft) of sea level rise over the 103-year period of record.

Table 2.2-1. Observed local sea level rise rates and confidence intervals for selected NOAA tide stations.

NOAA Station	Station Name	Period of Record	Number of Years	Linear Trend and 95% Confidence Interval (mm/yr)
8534720	Atlantic City, NJ	1911 - 2022	111	4.17 +/- 0.14
8536110	Cape May, NJ	1965 - 2022	57	4.85 +/- 0.44
8557380	Lewes, DE	1919 - 2022	103	3.63 +/- 0.22
8545240	Philadelphia, PA	1900 - 2022	122	3.07 +/- 0.18
8551910	Reedy Point, DE	1956 - 2022	66	3.75 +/- 0.42
8573927	Chesapeake City, MD	1972 - 2022	50	4.20 +/- 0.60

Note: Stations are listed approximately from north to south. Source: NOAA Tides and Currents Sea Level Trends website, https://tidesandcurrents.noaa.gov/sltrends/sltrends.html

16 The linear rates are based on the data available for the period of record for a given station. Rates are significantly influenced by the lengths of the period of record, which are not consistent among stations. Therefore, direct comparison of the SLR rate among these stations is not appropriate. The purpose of this table is not to compare SLR rate at different locations, but rather to show that all these locations have experienced SLR for the past 50 to 100 years.

Figure 2.2-1. Locations of NOAA tide stations and USGS gages.

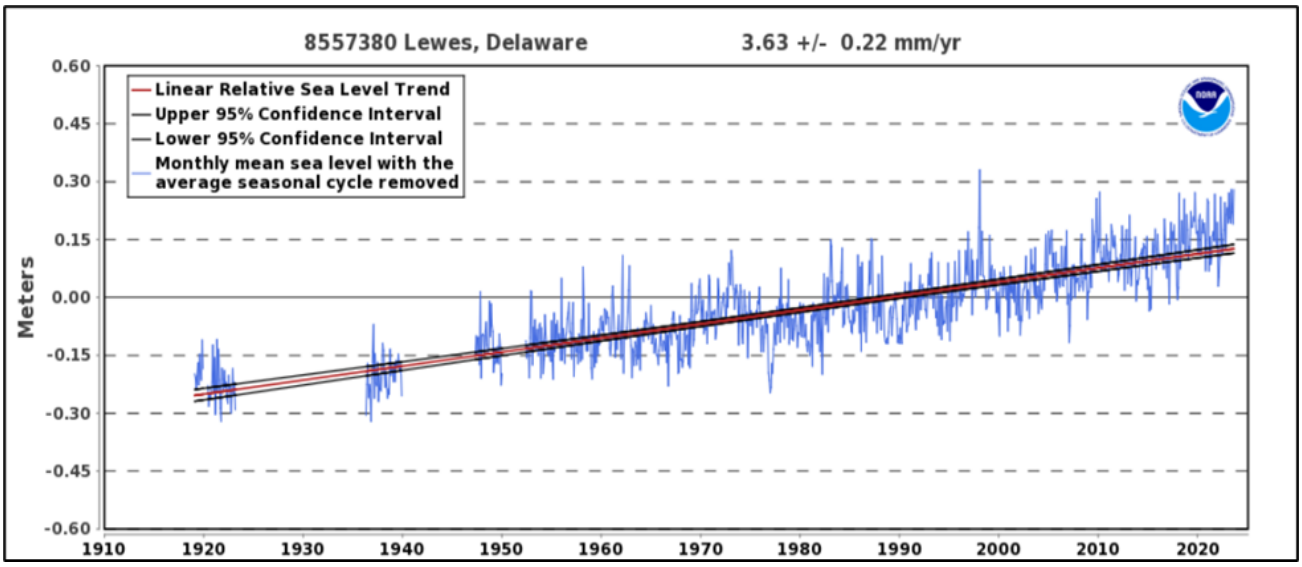

Figure 2.2-2. Relative sea level trend 1919–2022 at Lewes, DE.

Tidal datums are calculated using a 19-year tidal cycle, called an epoch. The current National Tidal Datum Epoch (NTDE), determined by NOAA, is 1983 through 2001 (centered at 1992), and is also referred to as NTDE1992 (NOAA is in the process of updating to the 2002–2020 epoch, which will be released in 2026[17]). In this study, the 19-year epoch from 1991 to 2009 was used as the tidal datum and referenced to the year 2000 to be consistent with other studies in the Basin (NOAA, 2017; NJSTAP, 2019; DNREC, 2017; etc.). The average sea level for the 1991-2009 epoch period at Lewes, DE, is 0.0325 m higher than the average sea level for NTDE1992.

2.3 Sea Level Rise Projections

The different components of sea level rise, both local and global, do not necessarily occur at the same rate. Straightforward extrapolation of the observed sea level rise may not be representative of the future rate of sea level rise, especially after 2050. According to Sweet et al. (2022), as the science in SLR has advanced, there is less divergence among the GMSL rise scenarios in the near term (from present to 2050). Based on the updated GMSL scenarios, the median of the 2050 observation-based extrapolations is bounded by the Intermediate-Low and Intermediate scenarios. Many researchers, research institutions, and government agencies have developed projections of sea level rise using different approaches and blends of approaches that incorporate process modeling (*e.g.*, ocean and atmospheric and climate related phenomena), probabilistic modeling (ensembles of models using different assumptions), and empirical and semi-empirical

17 National Tidal Datum Epoch (NTDE): https://tidesandcurrents.noaa.gov/datum-updates/ntde/ . The NTDE Update: https://tidesandcurrents.noaa.gov/datum-updates/assets/pdf/NTDE_fs.pdf

methods (statistical relationships between known or predicted characteristics). It is not the purpose of this report to develop SLR projections. Instead, this report reviews, synthesizes, and utilizes a range of SLR projections from others who have researched and developed local estimates.

A review of the literature from major research institutions yielded a variety of projections of local sea level rise (**Figure 2.3-1**). Three sources of recent sea level rise projections were used to establish a range of future SLR scenarios for planning horizons through the years 2060 and 2100. The projections are for sea level where the Delaware Bay meets the Atlantic Ocean at Lewes, DE. The sources are from DNREC, NJSTAP, and NOAA:

- Delaware Department of Natural Resources and Environmental Control (DNREC) (Callahan, et. al., 2017);
- New Jersey Science and Technical Advisory Panel (NJSTAP) convened by Rutgers University on behalf of the New Jersey Climate Change Alliance (Kopp, et. al., 2019); and

- U.S. Sea Level Rise and Coastal Flood Hazard Scenarios and Tools Interagency Task Force (Sweet, et al., 2022).

All projections are referenced to the baseline of 2000[18]. These projections provide a significant range of severity based on various future greenhouse gas emissions and global sea level rise assumptions. The full set of NJSTAP 2019 projections are not shown; however, the full limits of the range of results are included in the selected projections. Further details on SLR projections by the three different sources are presented in Appendix A. As science and ability to estimate components of sea level rise continues to evolve, sea level rise projections should continue to be revised and evaluated.

2.4 Values of Sea Level Rise Evaluated for this Study

Numerous SLR projections from various sources were consolidated into five (5) selected representative future SLR scenarios relative to baseline 2000 for DRBC model simulation and analysis:

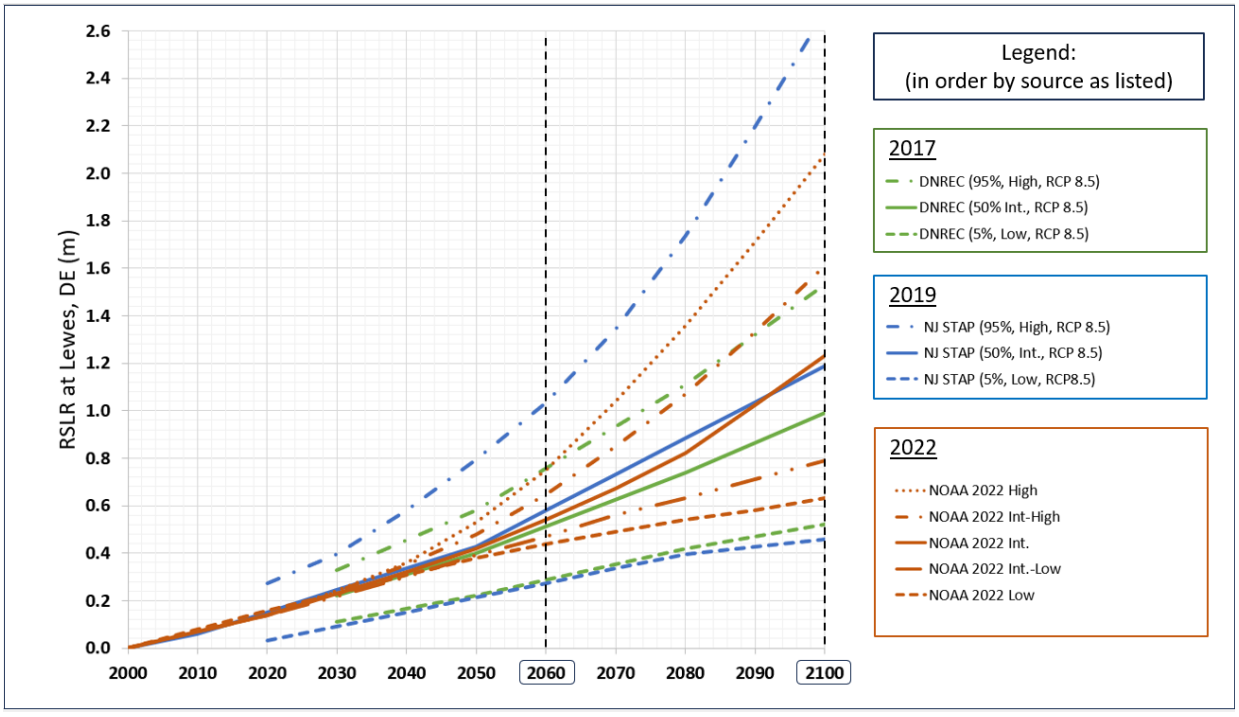

Figure 2.3-1. Relative sea level rise (RSLR) projections relative to baseline of 2000 for Lewes, DE.

Note: Only the median values of each projection are shown in Figure 2.3-1; there are uncertainty bounds associated with each projection. Details of these SLR projections are presented in Appendix A.3.Regional observation extrapolation through 2050 and regional scenarios at NOAA Tide Station 8557380 Lewes, DE, with NOAA 2022 projections and uncertainty bounds (Sweet, et al. 2022) is presented in Appendix Figure A.3-3c, which is referenced from NOAA sea level calculator https://coast.noaa.gov/sealevelcalculator.

- 0.3 m (0.98 ft) SLR;
- 0.5 m (1.64 ft) SLR;
- 0.8 m (2.62 ft) SLR;
- 1.0 m (3.28 ft) SLR; and
- 1.6 m (5.25 ft) SLR.

As shown in **Figure 2.4-1** for the planning years 2060 and 2100, the five selected values represent various levels of the severity range of SLR projections for the targeted years. For the 2100 target year, the maximum DRBC SLR scenario of 1.6 m (5.25 ft) is lower than two of the highest NJSTAP 2019 projections and the "High" NOAA 2022 projection. SLR projections after 2050/2060 increasingly depend upon the pathway of future global greenhouse gas emissions. Based upon current source methods, each of the projections greater than 1.6 m have a low likelihood that they will be realized or exceeded by 2100. SLR projections and modeling scenarios above 1.6 m (5.25 ft) can be re-examined in the future based upon updated data and future emission and global SLR projections as needed.

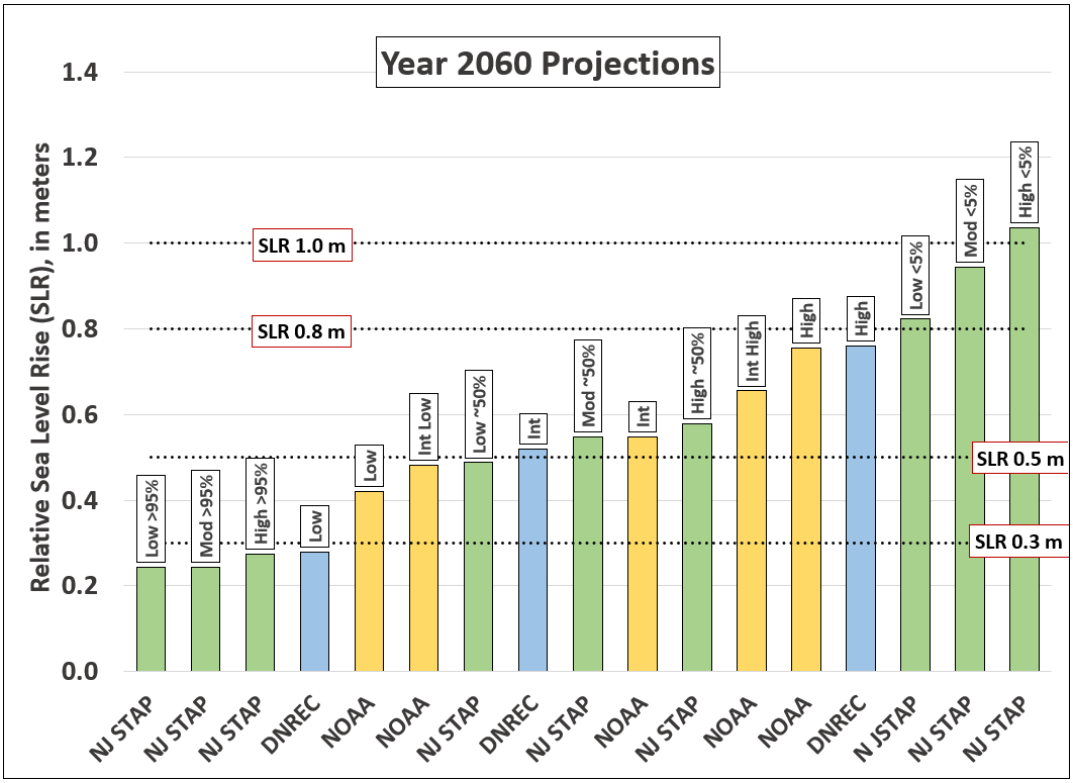

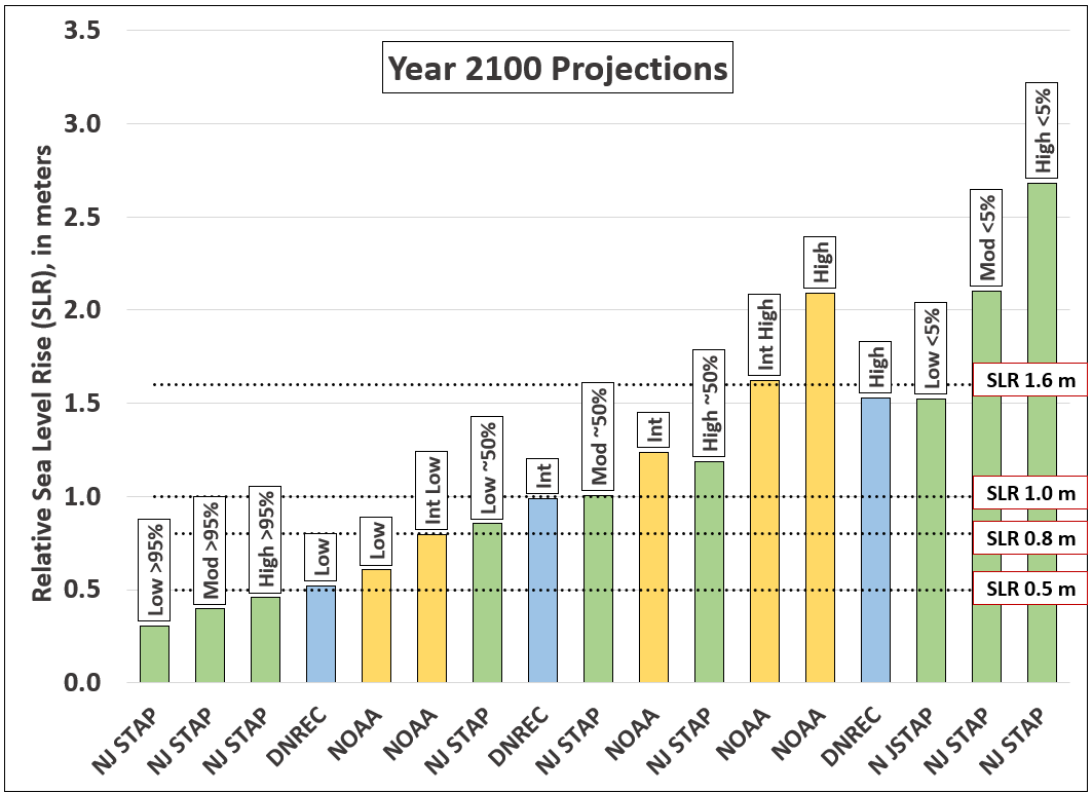

Figure 2.4-1. Sea Level Rise projections for Lewes, DE, for 2060 and 2100.

3. ANALYTICAL APPROACH

Salinity transport is a phenomenon affected by the bathymetry, shape, and hydrodynamic forces of an estuary such as river discharge, tide elevation, and sea level rise. A three-dimensional hydrodynamic model is necessary to simulate the effects of the complex physical processes, such as tidal forcing, density differences related to temperature, buoyancy, surface heat exchange, currents, climatological/meteorological drivers, and wind-wave induced forces, among others. The interplay among these drivers must be captured to determine their relative effects on salinity transport.

For this study, a three-dimensional hydrodynamic salinity model (the "salinity model" or SM3D) was developed by DRBC for the purpose of evaluating the impacts of sea level rise on salinity intrusion. The model development and calibration are documented in a separate report (Chen et al., 2025). SM3D is intended to be a "living" tool to be refined with new information and data as it becomes available so that the model may be used to evaluate current and future issues related to sea level rise, salinity, and hydrodynamics.

The approach used in this study is summarized by the steps listed below.

- A literature review of sea level rise projections for the Delaware Bay was performed.
- Multiple values of sea level rise were chosen to represent a range of planning scenarios, horizons, and probabilities of occurrence.
- Diagnostic simulations were performed to evaluate how the model configuration and assumptions affected the results.
- Hydrologic conditions from multiple years were simulated to estimate the effect of various river and stream flows on salinity intrusion.
- Effects of other conditions resulting from climate change and changes, such as ocean temperature, were simulated.
- A conceptual analysis of management actions for reducing the impacts of sea level rise on salinity was also performed.

Estuary hydrodynamics, including circulation and salinity transport, are three-dimensional and often affected by complex estuary geometry and bathymetry. Near the mouth of the Bay, a typical two-layer current and salinity structure exists (also known as tidal exchange flow structure) as the result of competing forcings from upstream inflows and ocean tidal forcing. Fresher, less dense water from inflows to the Estuary is flushed downstream on the surface layer, and saltier, denser ocean water is pushed upstream along the bottom layer. The phenomenon is known as estuary exchange flow. As a result, a relatively strong vertical stratification of salinity is often observed in

the Lower Bay. Moving upstream from the mouth of the Bay, the vertical stratification becomes weaker. Vertical stratification affects the mixing processes and consequent salinity transport in the Estuary. Near Marcus Hook, PA (RM 79), and upstream, the tidal River becomes well-mixed with a uniform vertical salinity profile.

To simulate the complexity of the vertical structure correctly, a three-dimensional model is necessary to capture the effects of the complex hydrodynamics affecting the vertical salinity structure and transport. Moreover, a full three-dimensional numerical realization allows for the representation of many physical processes, including buoyancy, density differences related to temperature, tidal forcing, climatological/meteorological factors, surface heat exchange, wind forcing (local and remote), wind-wave induced current, and other processes. The interplay among these physical processes makes necessary the use of a three-dimensional model to simulate salinity transport.

3.1 Three-Dimensional Hydrodynamic and Salinity Model (SM3D)

SM3D was developed with the Environmental Fluid Dynamics Code (EFDC), which is maintained by Tetra Tech and supported by the U.S. Environmental Protection Agency (EPA) (USEPA, 2007). EFDC is a general purpose three-dimensional hydrodynamic model code capable of simulating time-variable flow in rivers, lakes, reservoirs, estuaries, and coastal areas (Hamrick, 1992 and 2007). The model solves multiple state equations for the fundamental processes affecting the movement of water in an estuary, including conservation of mass, momentum, transport, and the interplay between temperature and salinity (e.g., density-driven circulation due to spatial and temporal gradients in temperature and salinity). The effects of vertical turbulence on mixing and transport in the water column are also simulated. EFDC has a history of extensive use in the United States and worldwide (Wool et al., 2003; Sucsy and Morris, 2002; SJRWMD, 2012; Ji et al., 2007). A complete description of EFDC is provided in Hamrick (1992).

The tasks involved in the development of SM3D included developing a numerical model grid, processing bathymetric data, assigning initial hydrodynamic conditions in the water column, defining meteorological boundary conditions at the water surface, assigning inflow boundary conditions from rivers and streams, determining the lateral inputs from point sources, and configuring the downstream open boundary condition in Delaware Bay. A summary of the model development is provided herein. Detailed information about the development and calibration of SM3D is available in the model development and calibration report (Chen et al., 2025).

It should be noted that DRBC has developed two hydrodynamic models. Initially, DRBC intended to develop one three-dimensional hydrodynamic model of the Estuary for both a eutrophication study and a salinity study. However, the eutrophication study required the hydrodynamic model to link with a water quality model, USEPA's Water Quality Analysis Simulation Program (WASP).

After testing multiple model configurations, evaluating the requirements for linking EFDC to WASP, and selecting model options and assumptions, it was determined that two separate models were needed. Both hydrodynamic models were developed with EFDC, but their final model domains differ. For the eutrophication study, the model domain extends from the head of tide on the Delaware River at Trenton (RM 133) to the mouth of the Delaware Bay (RM 0). The open boundary was set at the Bay mouth to utilize all the nutrient data collected there; thus, numerous parameters that govern bio-chemical processes can be calibrated in the linked EFDC–WASP model. In contrast, the domain for the salinity model extends into the ocean to minimize the uncertainty in specifying salinity at the ocean open boundary. A summary of major differences between the two models is presented in Appendix A of the calibration report (Chen et al., 2025).

3.1.1 Model Development

3.1.1.1 Model Domain and Numerical Grid

The foundation of a hydrodynamic model is the representation of the water body. A boundary-fitted, curvilinear numerical grid was used to represent the geometry of the Estuary. The geographical extent of the model numerical grid encompasses the entire 218 km (or 133 mi) tidal River and Delaware Bay from the fall line 2 km (1.2 mi) north of Trenton to the mouth of the Bay. The grid also extends from the mouth of the Bay to approximately 68 km (or 42 mi) into the Atlantic Ocean on the continental shelf. The northern and southern boundaries of the modeled coastal zone are located 96 and 100 km (60 and 62 miles) from the mouth of Delaware Bay, respectively. In addition, the Chesapeake and Delaware Canal (C&D Canal) is included in the model from the Estuary to its western end near the NOAA tide gauge station 8573927 at Chesapeake City, MD. The eastern end of the canal is located at RM 58.5. The model domain, numerical grid, and projected bathymetry are shown in **Figure 3.1-1**.

Although the area of interest for this study is the Estuary, the grid includes a portion of the coastal area surrounding the Bay. It is common practice to set hydrodynamic model boundaries in tidal systems away from the area of interest to ensure that the numerical methods used to specify inputs at model boundaries do not influence model predictions within the area of interest. Up to 20 vertical layers were assigned to cells near the ocean boundary, and eight vertical layers were used in most of the cells in the Federal Navigation Channel (FNC) to adequately capture the vertical structures of salinity and current.

3.1.1.2 Bathymetry

The bathymetry of the Estuary was initially developed using data from the Federal Emergency Management Agency (FEMA) Region III Storm Surge Study (Forte, et al., 2011). It was further

revised for the areas in the vicinity of the Delaware Memorial Bridge and the confluence of the C&D Canal with the Delaware River after with the latest 2022–2023 post-dredging bathymetry survey data from U.S. Army Corps of Engineers (USACE), Philadelphia District. The updated

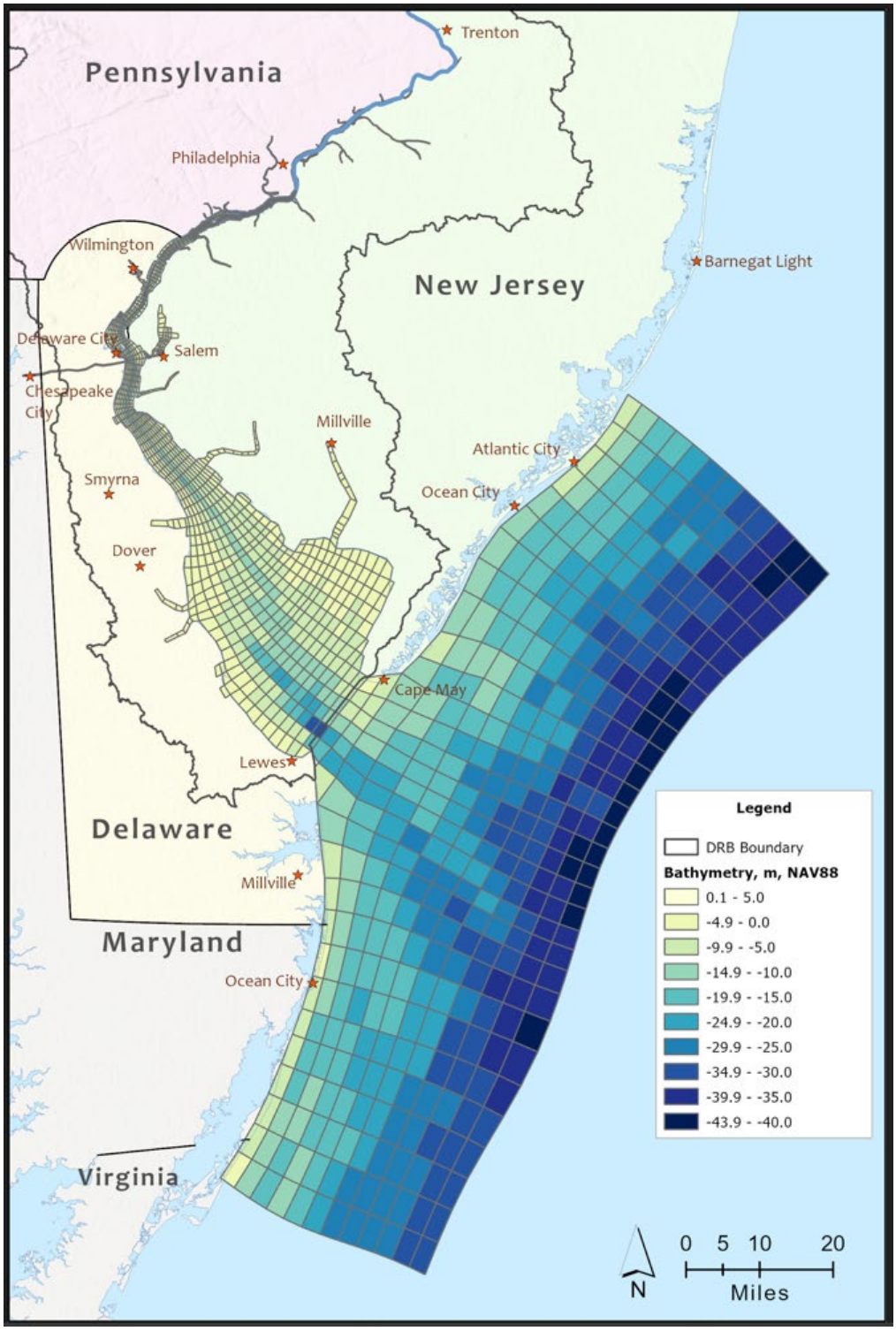

Figure 3.1-1. Model domain, numerical grid, and bathymetry.

bathymetry was applied to the numerical grid representing the FNC, which is 45 ft below mean lower low water (MLLW)[19]. Bathymetry for the C&D Canal, which is 35 ft below MLLW, was developed with NOAA nautical charts (12277, 12304, 12311 to 12314). The final bathymetry projected on the numerical grid is shown in **Figure 3.1-1**.

3.1.2 Model Drivers

Flows and tides are the primary drivers of salinity intrusion, and these drivers are specified at model boundaries, as well as salinity, temperature, and other climatic and meteorological conditions. A detailed discussion of these drivers is provided in the calibration report (Chen, et al. 2025). A summary is provided below. The following model conditions were specified:

- **Freshwater flow**: Inflows into the main stem Delaware River and the 31 major tributaries with measured flow were specified using available USGS data (Chen et al., 2025). Hourly flow data were utilized for the Delaware River at Trenton and Schuylkill River due to their significant contributions to the total freshwater input. Flows for each ungaged portion of tidal streams were estimated based on data from a similar watershed.
- **Withdrawals**: Among the 130 withdrawals in the Estuary, eight major withdrawals account for approximately 90 percent of the total discharge flow. Monthly withdrawal rates for the eight major withdrawals were specified, based on the DRBC Water Use database (withdrawal rates were based on data from DRBC's surface water charging program[20]). These withdrawals were assumed to be the same for the SLR simulations.
- **Point discharges**: Point source wastewater discharges were specified for 71 discharges that were monitored during 2018–19 (DRBC, 2019)[21]. The discharges were specified based on weekly and monthly data. The discharge rates obtained during 2019 were used for the SLR simulations.

19 Mean lower low water is a tidal datum or reference point defined as the average of the lowest tides of each day over a 19-year period, which is the National Tidal Datum Epoch (NTDE). It is used for navigation and charting purposes, establishing the vertical reference for nautical charts in the United States. It is a specific tidal datum used to create a standardized and reliable reference. Other common tidal datums include mean higher high water (MHHW) and mean sea level (MSL). The current NTDE is 1983–2002.

20 18 CFR Part 420. (2019). Basin Regulations - Water Supply Charges. With amendments through July 1, 2019. Delaware River Basin Commission. https://www.nj.gov/drbc/library/documents/water_chargesCFR.pdf

21 In March 2018, DRBC initiated a second round of point-discharge monitoring, a two-year intensive nutrient monitoring program to obtain model input data for the 2018-2019 calibration period based on a Resolution for the Minutes adopted on September 13, 2017. The complete Resolution for the Minutes can be found online at https://www.nj.gov/drbc/library/documents/ResforMinutes091317_nutrient-mon.pdf.

- **Water surface elevations**: Water surface elevations at the ocean open boundary control tidal flows into and out of the Estuary, and these elevations were determined from published tidal databases (Szpilka, et al., 2016). For simulations under future SLR conditions, SLR was added to the water surface elevation at the ocean open boundary and at the western end of the C&D Canal.
- **Water temperature and salinity**: Water temperature and specific conductance data from USGS gaging stations were used to specify the water temperature and salinity boundary conditions for the Delaware River at Trenton and for all tributaries. If specific conductance data were unavailable for the Delaware River at Trenton, the salinity was set to 0.1 psu. For tributaries below Trenton and above the confluence of the Schuylkill River, the continuous salinity from Trenton were scaled by the ratio of the tributary and Trenton concentration of grab samples. Tributaries located downstream of the Schuylkill River were assigned the same salinity as the Schuylkill River. If specific conductance data were unavailable from the Schuylkill River, the salinity was set to 0.2 psu. The salinity from point source discharges were derived from a report by PWD (PWD, 2020).
- **Ocean temperature**: Near-surface water temperature at the ocean open boundary was assumed to be the observed water temperature recorded at NOAA station (8557380) at Lewes, DE. The water column temperatures below the surface layer were specified for different depths based on the World Ocean Atlas 2013 (WOA13) database (Locarnini, R. A. et al., 2013, and Zweng, M. M, et al, 2013) monthly mean data near the mouth of the Delaware Bay. The water temperature and salinity boundary conditions at the C&D Canal boundary were established based on water temperature and conductivity data collected at NOAA Station (8573927) Chesapeake City, MD.
- **Ocean salinity:** Mean monthly salinity at the ocean boundary was based on data for various depths from 2005 to 2012 from the World Ocean Atlas 2013 (Chen et al., 2025). For future SLR simulations, ocean salinity and water temperature boundaries were not altered.
- **Climatological and meteorological forcing:** Spatially variable climatological and meteorological forcing boundary conditions, including air temperature and pressure, dew point, cloud conditions, wind speed, wind direction, precipitation, and solar radiation were determined from meteorological data collected at five NOAA National Climatic Data Center (NCDC) weather stations (Chen et al., 2025). For future SLR simulations, no changes were made to the meteorological forcing boundary conditions. While important, an evaluation of the effect of changes to meteorological parameters due to climate change on model results was outside the scope of this analysis.

Specification of some boundary conditions required additional analysis. The process included estimation of ungaged streamflow and conductivity values, and calculation of model parameters at ocean boundaries, such as density. Details of the development of these boundary conditions are described in Chen et al. (2025).

3.1.3 Model Performance for Historical Conditions

During model calibration, the model performance was assessed by comparing the results with historical conditions. Representative results of model performance evaluations are summarized below along with critical metrics. The major calibration metrics presented are (1) water surface elevation, (2) current velocity, (3) water temperature, and (4) salinity. Detailed calibration results of SM3D are documented in the full model calibration report (Chen et al., 2025).

Guidelines of model acceptance have been recommended by researchers and agencies (e.g., Willmott, 1981; Hess et al., 2003; Zhang et al., 2006; Patchen, 2007; and Bever et al., 2013). NOAA (Hess et al., 2003; and Zhang et al., 2006) proposed acceptable error bounds for predicting water level (15 cm), current velocity (26 cm/s), phase (0.5 hrs.), water temperature (3.0^{o}C), and salinity (3.5 psu). To provide a succinct method to evaluate and report the accuracy of a large number of comparisons, MacWilliams M.L. et al (2015) established a standardized set of cutoff values for skill scores. The guidelines recommended by these researchers and agencies were used in calibrating the model.

3.1.3.1 Water Surface Elevation

Water surface elevation (WSE) fluctuates in response to tidal motion. The tide wave enters the Estuary at the mouth near Cape May, NJ, and Lewes, DE, and progresses upstream to the head of tide at Trenton, NJ. Simulated and measured WSE were compared at several locations to evaluate model performance in simulating WSE. The statistics used to quantify the model performance are summarized in Chen et al. (2025). The predicted WSE has minimal bias (typically less than 12 cm) and low unbiased root mean square difference (ubRMSD), which ranged from 7 to 26 cm). The model skill score ranged from +0.976 to +0.991 (a perfect skill score value is +1). These statistical measures demonstrate that the model accurately predicts tidal water surface elevation throughout the Estuary and can be used to meet the objectives of this study.

3.1.3.2 Current Velocity

Current velocity measurements at three NOAA stations and one Rutgers mooring station during 2012 and 2018–2019 were used for model calibration. Current velocity measurements are not available for each year and years that have data were simulated as part of model calibration exercise. The model skill score for predicted current velocity ranged from +0.938 to +0.991 and

ubRMSE ranged from 8.9 to 16.8 cm/s. Model performance for predicted along-channel depth-averaged current velocity for three PWD buoy stations for 2012 and 2016 Acoustic Doppler Current Profiler (ADCP) survey data shows skill scores are all above 0.96 with root mean square error (RMSE) all less than 20 cm/s. The statistical measures for predicted current velocity at the four station locations are summarized in the model calibration report (Chen et al., 2025). These statistical measures indicate that the hydrodynamic model simulates current velocity with sufficient accuracy to meet the objectives of this study.

3.1.3.3 Temperature

The model over-predicted water temperature near the surface during the summer in the Bay downstream of Reedy Island (RM 54), and it performed reasonably well for stations in the upper portion of the tidal River (i.e., upstream of Chester at RM 83). The model was able to simulate the seasonal variation in temperature at all stations, with average bias from -0.92 to 0.79 ºC for 2016 to 2020. A summary of the statistical measures for temperature is presented in Chen et al.(2025).

3.1.3.4 Salinity

The model was calibrated with salinity data from 2017–2018 and validated using data from other years and multiple sources. The data included continuous salinity (conductivity or specific conductance) measurements from NOAA and USGS monitoring locations, discrete sampling of along-channel salinity profiles from DRBC's Boat Run[22], and a 2011 survey of near-surface and near-bottom salinity performed by Rutgers University (Aristizabal and Chant, 2014).

The long-term average salinity was reproduced with a small bias (-0.18 to 0.13 psu during 2017 to 2018 period) for both locations. The standard deviation of the predicted salinity was similar to that of the data. Overall model performance for predicted salinity is reasonable with skill scores of 0.88 to 0.94 for the 2017–2018 period. At Lewes, DE, near the mouth, the model has less skill in predicting salinity. The grid cell size near Lewes is too large for the salinity to be predicted with a high degree of accuracy because the bathymetry lacks the needed detail for the complex hydrodynamics simulated. However, the areas under investigation are well upstream from the mouth of the Bay, and so the model skill at Lewes, DE, does not limit model adequacy. The results indicate that the model adequately predicted salinity near Ship John Shoal (RM 37) and at the USGS gage at Reedy Island (RM 54). The Delaware Estuary water-quality monitoring program, known as boat run surveys, for the Delaware River main stem and the Delaware Bay have been performed since 1967. Samples were collected monthly during a short 4-to-5-hour time window at 22 locations along the River and provide a "snapshot" of the longitudinal salinity profile. The

22 https://www.nj.gov/drbc/programs/quality/boat-run_explorer-app.html

predicted tidally-averaged salinity longitudinal profile agreed with the boat-run data over a wide range of flow and tidal conditions.

During September 16–17, 2011, Rutgers University collected along-channel salinity and water temperature profile data both near the surface and near the bottom at 23 locations from the Bay mouth (RM 0) to RM 123.6, over a 30-hour time span encompassing two tide cycles. The survey was conducted one week after a high-flow event when the maximum flow at Trenton was over 177,000 cfs on September 9, 2011 (a 10-year flood at Trenton; Schopp and Firda, 2008). The observed salt front was located downstream of RM 50 during the survey. The model successfully reproduced the near-surface and near-bottom salinity as well as the water temperature longitudinal profiles.

3.1.4 Key Findings from SM3D Model Development

The key findings from the hydrodynamic Model SM3D development are:

- The majority of the ocean saltwater is transported in the FNC in the Upper Estuary where the River narrows and vertical mixing results in a relatively consistent salinity throughout the water column and width[23].
- The tidal River[24] becomes relatively well-mixed near Marcus Hook, PA (RM 79), under normal conditions.
- The net inflow from the C&D Canal should be further investigated with more observed data. However, the model assumptions for the net canal inflow and salinity produce results with reasonable accuracy.
- SM3D is suitable for use in evaluating the impacts of sea level rise on salinity intrusion.

3.2 Capabilities and Limitations

SM3D was configured to simulate physical processes that are most important for the prediction of salinity intrusion that persists for more than several days. Processes with only minor short-term effects on the upstream extent of salinity intrusion were not simulated, and this intentional

23 The thalweg of the estuary follows the FNC, and the denser and saltier ocean water transports salinity upstream near the bottom. The maximum width is of the Bay is 45 km, The width narrows to 2 km at Wilmington and to 0.3 km at Trenton. The width of the modern shipping channel is about 150 meters, approximately 25% of the total width near Philadelphia. The width of the shipping channel in the Bay is less than 1 percent of the total width.

24 The section of a river affected by the tides is the tidal reach of the river. The Delaware River downstream of Trenton is tidally affected. The portion of the tidal River upstream of the extent of the salinity intrusion can be defined as the "tidal fresh river".

omission limits the uncertainty associated with estimating the parameters needed to do so. These omitted processes include salinity intrusion into groundwater, groundwater-surface water interaction, groundwater discharges, wave-induced current, wave-current interaction, and sediment transport.

Groundwater related processes were not simulated because the relative net contribution of salinity into the Estuary from groundwater is multiple orders of magnitude smaller than the contribution from the ocean (V. DePaul, USGS, written communication, January 12, 2021). Direct input of groundwater was estimated to be less than one percent of total water volume in the Bay (Masterson et al., 2016).

Impacts from remote ocean waves on estuary hydrodynamics are partially addressed by the water surface elevation boundary conditions, but the wave-current interaction inside the model domain was not simulated. The net contribution of wave-related vortex forces to the momentum budget was modest and an order of magnitude smaller than the other factors such as surface stress, bottom stress, and the wave-induced pressure gradient (Pareja-Roman, L. F., et al. 2019). Impacts due to remote wind waves from offshore on wave significant height and wave energy inside the Bay are limited to areas near to the Bay mouth. For most of the Estuary above the Lower Bay, waves are controlled predominantly by local wind and bathymetry (Chen J.L. et al., 2018). Wave energy dissipates through the water column exponentially, constraining the impact on salinity transport to the uppermost layers of the water column. Most of the salinity is transported upstream through the FNC in the tidal River, and the long-term effect of waves on salinity transport is small. Sediment transport was not simulated because the contribution of salinity from sediment is small compared to that of the ocean.

3.3 Assumptions for Sea Level Rise Simulations

Future conditions in the Delaware Estuary are likely to be affected by multiple stressors; however, estimates of how the stressors will change in the future are unknown or of significant uncertainty. Examples include changes to bathymetry from sedimentation, scour, or dredging, and meteorological parameters (wind, temperature, precipitation), among others. Detailed evaluations of how future changes in these factors, in combination with sea level rise, will affect salinity transport were outside the scope of this study. However, the sensitivity of model results based on model assumptions was tested. The major assumptions used for the sea level rise simulations and discussion of their uncertainties are summarized below.

- Sea levels are represented by applying the SLR projection to the detrended water surface elevation at both the ocean boundary and western end of C&D Canal. Relative local SLR at the western end of C&D Canal is equivalent to the SLR at the mouth of the Bay[25].
- The current post-dredging bathymetry does not change (the elevation of the Estuary bed does not change relative to the year 2000 baseline/datum).
- The bathymetry outside the navigation channel will not significantly change as the result of SLR (e.g., the bathymetry will not be substantially altered by sedimentation).
- The amplitude and phase of tidal harmonics at the model ocean boundary will not change.
- The impacts from wind and wave action on salinity intrusion in the upper tidal River do not persist and do not affect the longer-term movement of salinity.
- The four-month low-flow period of July–October 2002 is representative of a moderately dry condition for diagnostic simulations.
- The effect of changes in point source discharges and withdrawals is likely to be insignificant in comparison with impacts from SLR.
- Observed meteorological drivers associated with the hydrology simulated were used. The compounding effect of SLR with the change in hydrologic conditions, such as, precipitation, air temperature, river discharge, and others that result from climate change were not considered in this study.
- Groundwater-surface water interactions (volume and salinity) are insignificant relative to other forcings.

[25] According to NOAA Sea Level Rise Viewer and 2022 updated projections, the relative SLR at Lewes, DE, is similar to Baltimore, MD. For 2060, SLR at Lewes and Baltimore is 2.13 ft and 2.07 ft with the Intermediate High scenario, respectively. For 2100, SLR at Lewes and Baltimore is 5.28 ft and 5.15 ft with the Intermediate High scenario, respectively. The difference is 2 to 4 centimeters. No information is available about SLR associated with NOAA scenarios for the C&D Canal. Change in water level at the western end of C&D Canal may affect the net flow from the Chesapeake Bay to the Delaware Estuary. Sensitivity to the water surface elevation boundary was conducted and presented in the model calibration report (Chen et al., 2025).

4. IMPACTS OF SEA LEVEL RISE ON SALINITY IN THE DELAWARE ESTUARY

Using the calibrated SM3D model, two sets of simulations were performed to evaluate salinity intrusion over a range of SLR values: one-year diagnostic simulations and multi-year ensemble simulations. The one-year diagnostic simulations represent hypothetical 365-day periods with a representative moderately low-flow condition. For these simulations, the flows of 2002 are used, which includes the low-flow period of June through October 2002. Results of these one-year simulations provide a general understanding of how sea level rise affects tidal water elevations and salinity structure, which are better demonstrated with a relatively "normal" rather than extreme low-flow condition. Results also provide an understanding of how different model configurations and other conditions may affect model results (these results are presented in Sections 5 and 6, respectively). The multi-year ensemble simulations comprise 10 respresentative flow years and include the driest year (1965) in the drought of record. The selected years are 1965, 2001, 2002, 2011, 2012, 2013, 2016, 2017, 2018, and 2019.

It should be noted that the results for the baseline simulations do not match those of historical simulations for the following reasons: The channel bathymetry incorporates the current post-dredge depth of 45 feet in the FNC. The sea level rise value used in simulations is applied to the detrended tide, so the water surface elevation differs from that of the historical condition.

4.1 TIDAL AND STRUCTURAL IMPACTS UNDER A REPRESENTATIVE LOW-FLOW CONDITION

Diagnostic SM3D simulations reflect present-day bathymetry and include a representative low-flow period, based on conditions of July through October 2002. Results with and without sea level rise were compared to determine the relative impact of SLR on tidal constituents and salinity structure. Unless otherwise noted, salinity results are presented as tidally and cross-sectionally averaged. In this report, the term "tidally-averaged" refers to averaging a tidally-influenced parameter (such as WSE or salinity) over a period that is longer than one tidal cycle (from one day up to several months).

4.1.1 Tidal Water Surface Elevation

Simulation results demonstrate that the effects of sea level rise on tidal water surface water elevations extend far upriver. Under normal conditions without SLR, the tidal amplitude increases between the mouth of the Bay (RM 0) and the head of tide at Trenton (RM 133). As the shorelines converge in the upper reaches of the Estuary, the tide is amplified. As simulation results show,

with sea level rise, the relative difference in water surface elevation between RM 0 and RM 133 is further amplified.

The tidal water surface elevation consists of an astronomical tide signal and sub-tidal fluctuations. The simulated water level amplitudes of the major astronomical tide (M2, the principal lunar semidiurnal constituent, a part of the astronomical tide) are presented in **Figure 4.1-1** by RM for 0, 1.0 and 1.6 m of sea level rise. With 1.0 and 1.6 m sea level rise, the difference in M2 amplitude was 0–0.1 m and 0–0.2 m, respectively, below RM 80 (one mile upstream from Marcus Hook, PA) and approximately 0.1 m and 0.2 m, respectively, above RM 80. A table of the predicted change in tidal constituents and figures showing the longitudinal distribution of tidal range, change in tidal range, and surface water elevation with sea level rise are provided in Appendix G.1.

4.1.2 Salinity Structure

Ocean water (salinity 34–35 psu) entering Delaware Bay is diluted by freshwater (salinity <0.5 psu) from upstream, creating a longitudinal salinity profile. Mixing occurs as tides push ocean

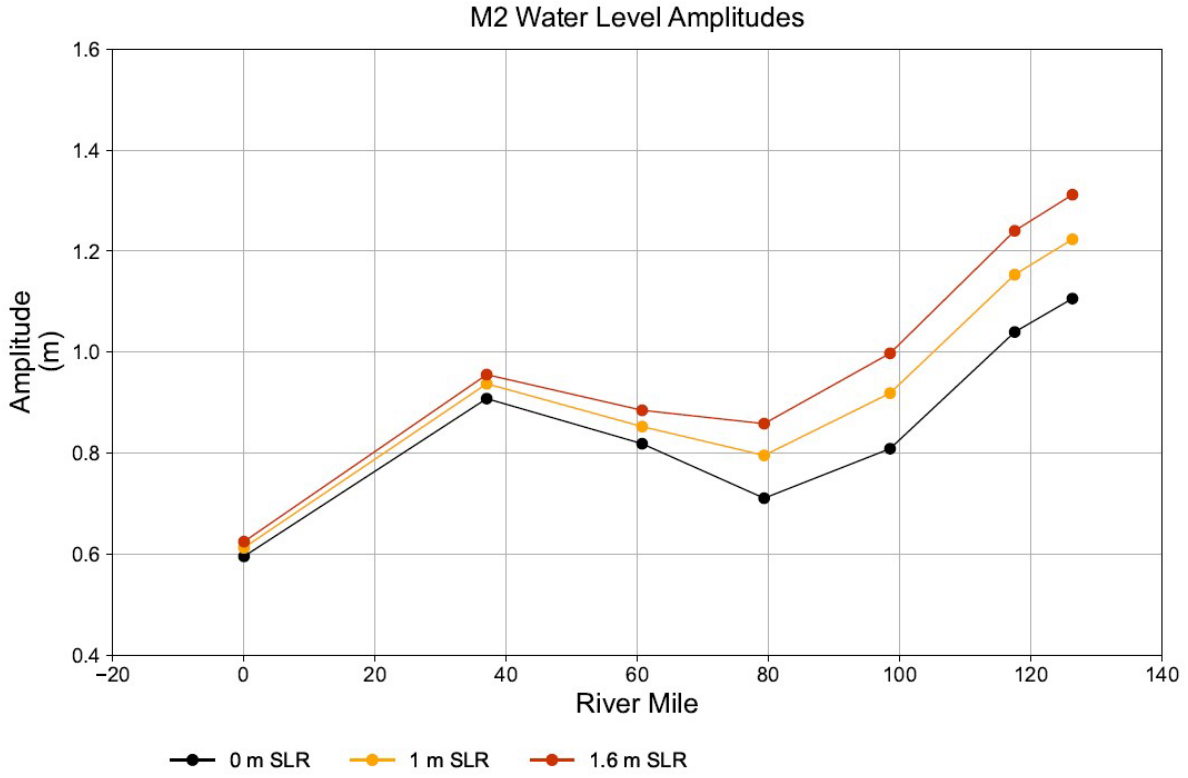

Figure 4.1-1. Simulated longitudinal distribution of M2 water level tidal amplitudes with sea level rise.

water upstream and gravity conveys freshwater toward the ocean. The colder, denser ocean water tends to remain near the bottom of the water column, while less dense, fresher water tends to remain closer to the surface. Vertical stratification is most prominent in the lower portion of the Estuary, and the Estuary is well-mixed upstream of Marcus Hook, PA (RM 79). Sea level rise increases the amount of saltwater entering the Bay and results in greater stratification of salinity in the water column. The simulated instantaneous longitudinal (cross-sectionally averaged) salinity profiles along the navigation channel for 0 m and 1.6 m SLR are depicted in **Figure 4.1-2.** The larger tidal forcing from 1.6 m SLR results in larger differences in salintiy. At RM 20 and 0 m SLR, the salinity is close to 30 psu in the water colum with higher salinity near the bottom. For 1.6 m sea level rise at RM 20, the salinity is greater than 30 psu *throughout* the water column. The extent of salinity intrusion is also evident in the profiles.

Ocean water salinity transport occurs predominantly in the deeper navigation channel, and higher salinity tends to occur in and above the channel. In shallower areas and along the shore, the influence of freshwater runoff is more prominent, and salinity tends to be lower than in areas near the channel. **Figure 4.1-3** presents cross-section views of simulated tidally averaged salinity for spring and neap tides for 0 m, 1.0 m, and 1.6 m sea level rise at Ship John Shoal in the Bay (RM 37). The salinities for both a spring and a neap tide are presented because the difference in the strength of vertical mixing between the spring and neap tides results in different degrees of stratification through the water column. For the spring tide, the salinity at the surface is higher

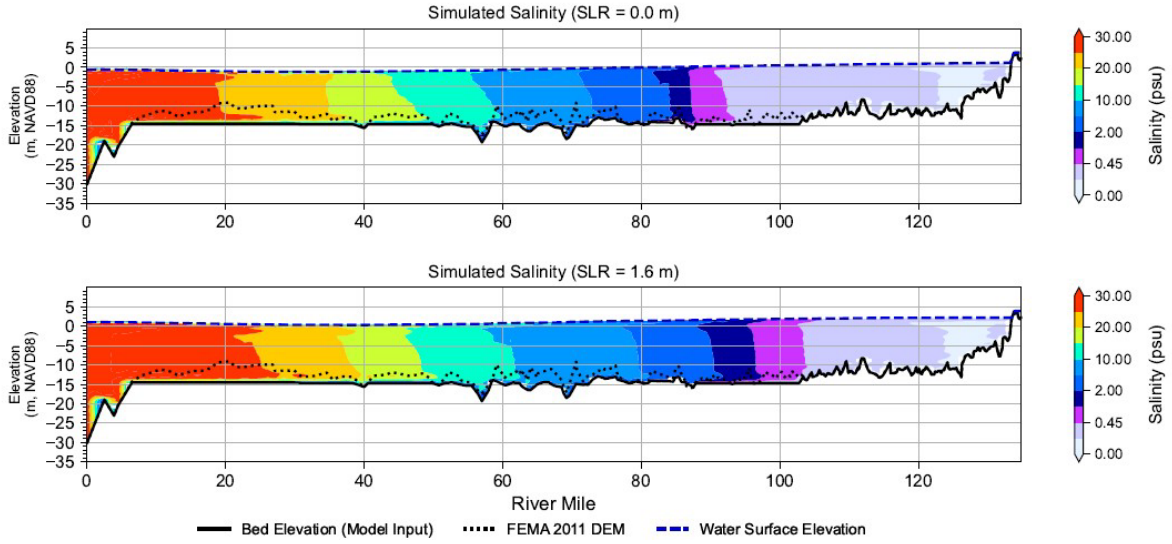

Figure 4.1-2. Longitudinal salinity structure for a representative low-flow condition with 0 m and 1.6 m Sea Level Rise.

Snapshot is for October 6 at 3:00 am of the simulated year. The average flow at Trenton on the corresponding day in 2002 was 3,670 cfs (30%) of average daily flow.

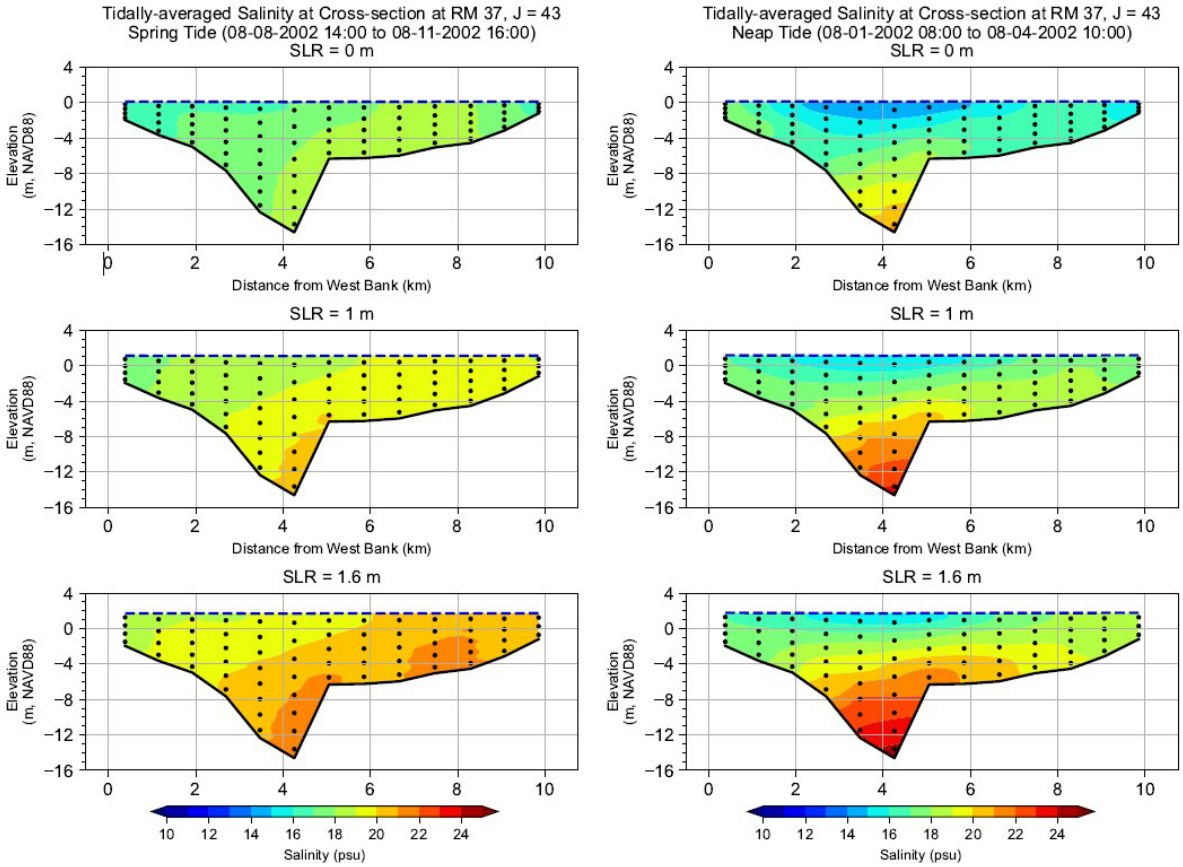

Figure 4.1-3. Simulated tidally averaged salinity gradient at Ship John Shoal (RM 37) for a spring and neap tide during a representative low flow condition with sea level rise.

This snapshot is for August 8 at 14:00 am of the simulated year.

than during a neap tide but lower along the bottom of the channel. Although salinity increases with sea level rise, the relative difference in salinity between the surface and the bottom is similar. During the neap tide, salinity is much more stratified with a larger difference in salinity between the top to the bottom. The spring tide, with a larger tidal range than that of the neap tide, results in stronger vertical mixing and less stratification in both the navigation channel and in shallower areas. During a neap tide, the smaller tidal range results in weak vertical mixing and thus greater stratification (Aristizabal and Chant, 2013). For all values of sea level rise, salinity during spring tide was higher near the western New Jersey coast (right side of the cross section) compared to the eastern Delaware coast (left side of the cross section). The slightly greater lateral transport of salinity is related to the circulation of the estuary exchange flow, which is counterclockwise and pushes saltwater towards the New Jersey coast. This phenomenon indicates that freshwater from

the Delaware and Schuylkill Rivers mixes more readily with salt water on the western side of the FNC, near Delaware.

The spatial distribution of the tidally averaged maximum bottom salinity for the low-flow period is presented in **Figure 4.1-4** for 0 and 1.6 m sea level rise between location (RM 15) and Wilmington, DE (RM 75). The difference in salinity between the New Jersey and Delaware Coasts, albeit small, is evident and more pronounced with 1.6 m sea level rise. For the representative low flow condition simulated, the largest increases in the maximum salinity (1–4 psu) are in the FNC and nearby deep areas as the result of more stratified water occurring farther upstream. While not the primary subject of this study, bottom salinity is an important component of shellfish habitat. and the locations of several commercial oyster beds are present within the area. The salinity of healthy

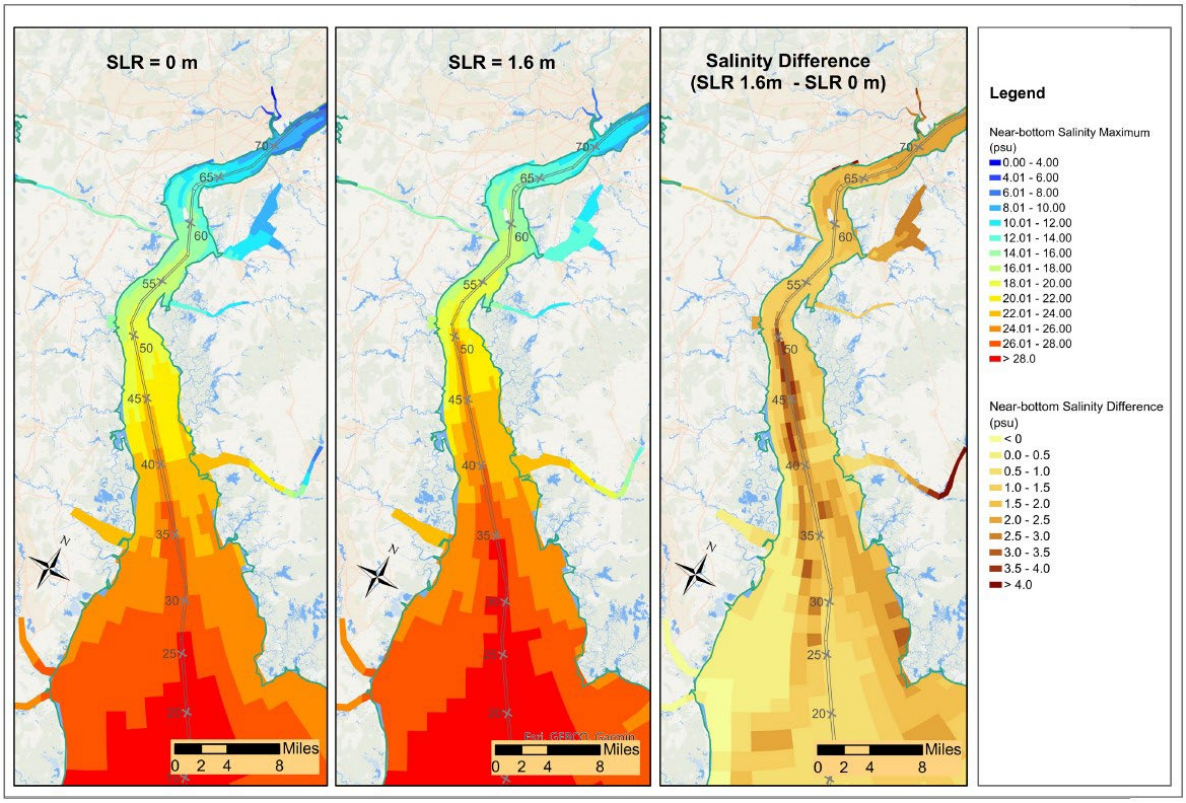

Figure 4.1-4. Maximum tidally averaged near-bottom spatial salinity for a seasonal low flow period with sea level rise.

Note: the seasonal low flow period used in this analysis was represented by using flow conditions from July through October 2002.

habitat for oysters is typically 14-28 psu[26] (Volety, 2008; Gregory, M. K. and M. Hare. 2020). With 1.6 m of sea level rise, the salinity remains within the range of tolerance by oysters, although additonal study may be warranted.

4.2 Impacts under a range of annual Flow Conditions

4.2.1 Simulation Approach

The impacts of sea level rise for multiple consecutive years of different flow regimes and the frequency of salinity intrusion were also evaluated. The impacts of sea level rise over a hypothetical multi-year period were simulated using 10 annual time series representing a range of annual flow conditions. Flow conditions of 1965, 2001 to 2002, 2011 to 2013, and 2016 to 2019 were selected as representative of the period of record. Wet years are represented by conditions observed during 2011, 2018 and 2019. Normal years are represented by conditions observed during 2012, 2013 and 2017. Dry years are represented by conditions observed during 1965 (during the drought of record)[27], 2001, and 2002 (during the third worst drought on record) and 2016 (a recent dry period). Per the flow objective in the DRBC Water Code, the minimum flows at Trenton range from 2,500 to 2,900 cfs during drought conditions[28]. However, for the purposes of this study, the minimum flow objective of 2,500 cfs was used in simulations for simplicity, including for conditions during 1965. The effect of the flow objective on salinity is discussed in more detail in Section 7.1.

An analysis was conducted to demonstrate that the years selected for these simulations are representative of the range of flows during the period of record. **Figure 4.2-1** presents the probability distributions of the daily flow at Trenton, NJ, for the entire period of record versus the flows of the 10 simulated years. The close similarity of the two distributions shows that the ten years used to construct the simulation time series provide a reasonable approximation of low flow and flood conditions in the Basin. Although the flow distributions are similar, the historical record includes some smaller low flows and some larger high flows. Many of the lower flows in the record occurred prior to the establishment of the flow objective at Trenton, NJ. In addition, the

[26] At higher salinities, oysters are more susceptible to disease and certain predators. In addition, the quality of food and the taste of the oysters can also be negatively affected. A detailed discussion about the effects of salinity on oyster habitat is outside the scope of this report.

27 Although the maximum salt front location during the 1960s drought of record occurred during 1964, the tidal record for 1964 is incomplete and is missing verified hourly water level data at the NOAA gage at Lewes, DE from 3/3 through 9/22. Also, data are not sufficient for some other boundary conditions. Consequently, although the simulation of saltwater intrusion during 1964 conditions would be possible, it would not be very accurate.

28 Delaware River Basin Water Code, Section 2.5.3. https://www.nj.gov/drbc/library/documents/watercode.pdf

development of reservoirs in the Basin and their minimum conservation release rates have improved low flow conditions in the Basin. Also, some of the worst flooding in the Basin occurred during and prior to 1955, before the development of several flood control reservoirs which reduce flow rates during flooding events. Thus, the range of years used to construct the time series provides a reasonable approximation of low flow and flood conditions in the Basin.

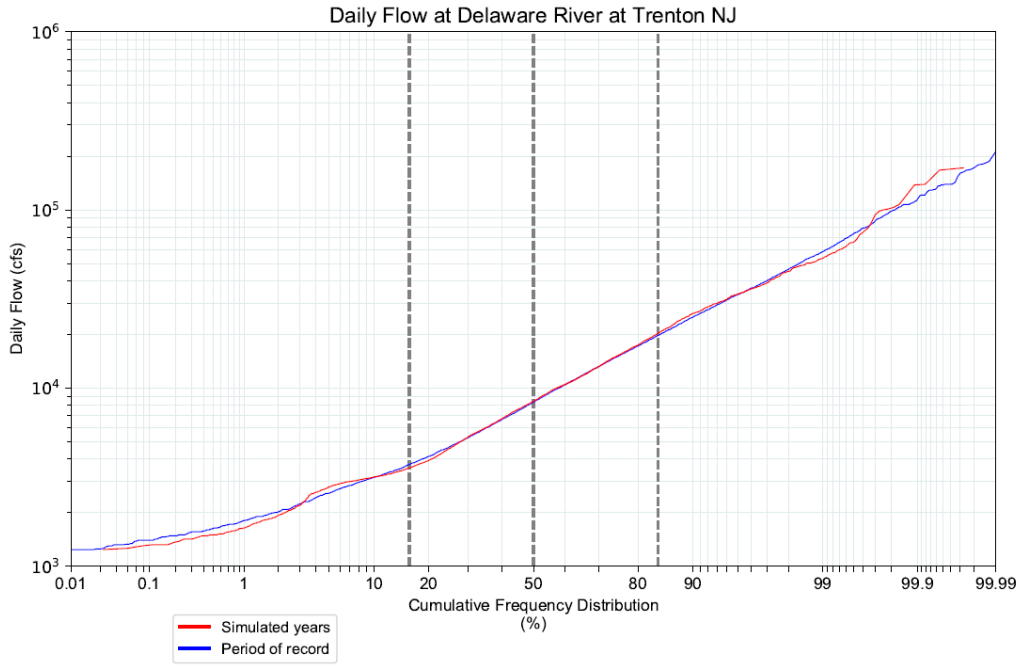

Figure 4.2-1. Comparison of the probability distributions of the daily flow at Trenton, NJ, for the period of record and for the ten years simulated.

Note: daily flows were from USGS Gage 01463599 on the Delaware River at Trenton, period of record 1913–2022.

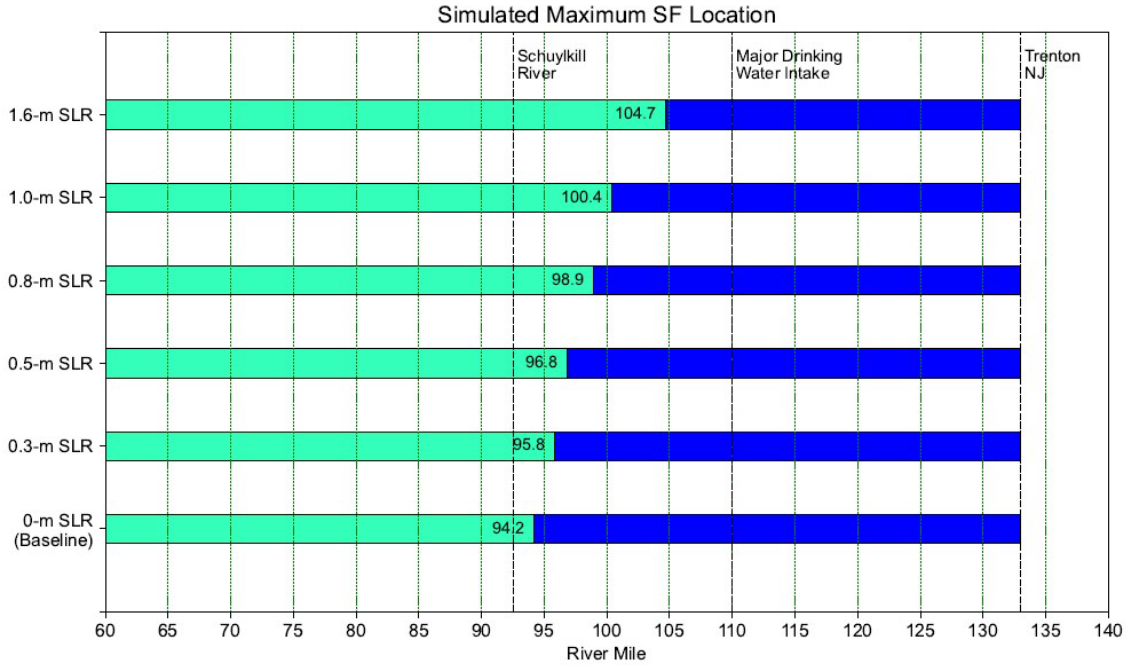

Figure 4.2-2. Simulated maximum location of the salt front with SLR during a hypothetical repeat of 1965 flows with a 2,500 cfs flow objective at Trenton, NJ.

4.2.2 Salt Front

The maximum salt front location simulated during the 10 ensemble simulation years with SLR is shown graphically in **Figure 4.2-2** and summarized in **Table 4.2-1**. For all values of SLR, the maximum salt front location occurred during the simulated 1965 flow conditions (with implementation of a Trenton flow objective of 2,500 cfs). With 1.0 m SLR, the simulated salt front advances above RM 100, the maximum reached during the 1960s drought. With SLR, the maximum salt front location increased from the baseline condition at RM 94.2 to RM 96.8 with 0.5 m SLR, to RM 100.4 with 1.0 m SLR, and to RM 104.7 with 1.6 m SLR (5.3 miles from the major drinking water intakes). The maximum salt front location advances farther upstream from the baseline condition by 2.6, 6.2, and 10.5 miles for 0.5 m, 1.0 m, and 1.6 m SLR, respectively.

Table 4.2-1. Simulated maximum location of the salt front with sea level rise and the normal range of the salt front location from the 10-year ensemble simulations.

Sea Level Rise (m)	Normal Range of Salt Front Location from the 10-year Ensemble (RM)	Maximum Salt Front Location (RM)	Increase in Simulated Maximum Salt Front from Baseline (RM)
0	61.6–76.5	94.2	–
0.3	62.7–77.8	95.8	1.6
0.5	63.4–78.7	96.8	2.6
0.8	64.3–80.1	98.9	4.7
1.0	64.9–81.2	100.4	6.2
1.6	66.8–84.1	104.7	10.5

The maximum location of the salt front occurred during the simulated 1965 conditions with implementation of a constant Trenton flow objective of 2,500 cfs.

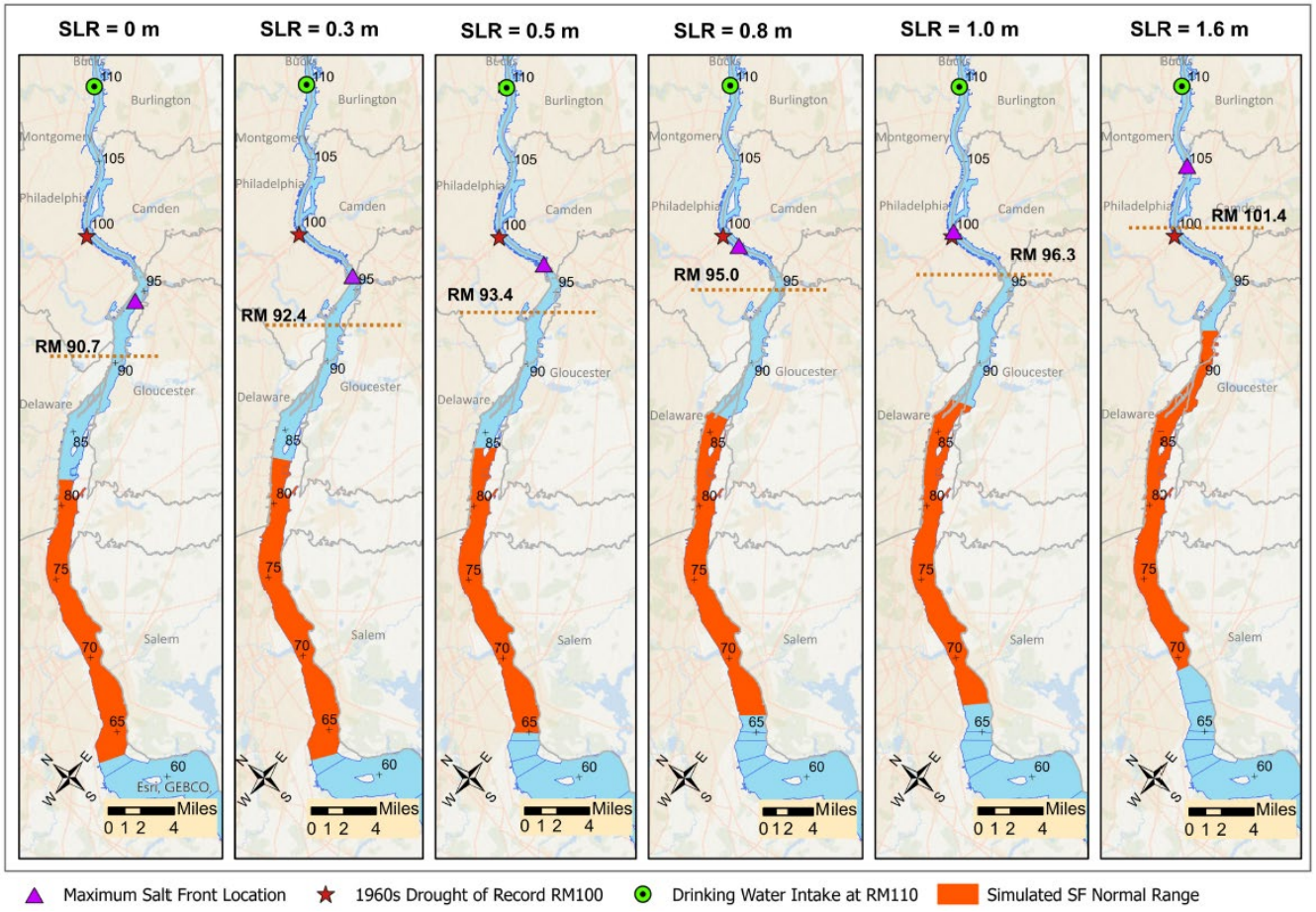

Figure 4.2-3. Maximum and normal range of the salt front location with SLR based on the ten years simulated.

Note: The historical record of the maximum salt front location in the 1960s drought at RM 102 was the commonly reported value calculated from instantaneous measurements reported at RM 100 and RM 106 in November 1964. The actual salt front location (location of the 7-dma chloride concentration was RM 100).

The normal range of the salt front is defined as the area in the Delaware River Estuary where the salt front is located approximately 50 percent of the time (25 percent of the time it is located below the bottom of the range and 25 percent of the time it is located above the top of the range)[29]. **Figure 4.2-3** shows the normal location of the salt front based on simulation of the 10 ensemble years. For the baseline condition, the simulated salt front is typically between RM 61.6, upstream of Pea Patch Island, and RM 76.5 near Grubbs Landing, PA, 2.5 miles downstream from Marcus Hook, PA. With 1.0 m SLR, the normal range increases and shifts upstream by 3 to 5 miles (RM 64.9–81.2). For 1.6 m SLR, the normal range is further increased and shifts 5 to 7 miles farther upstream (RM 66.8–84.1). Additional results from the ensemble simulations are presented in Appendix G.2.

4.2.3 Chloride Concentrations

A maximum 30-dma chloride concentration of 180 mg/L at RM 98 (Camden) is a DRBC water quality criterion for salinity management (DRBC Water Quality Regulations). The simulated 30-dma chloride concentrations with SLR at RM 98 are summarized in **Table 4.2-2** and **Figure 4.2-4**. For the baseline condition (0 m SLR) and with SLR at or below 0.5 m, the water quality standard is met. For simuations with 0.8 m to 1.0 m SLR, all exceedances of the 30-dma 180 mg/L chloride standard occur during the simulated year represented by 1965 flow conditions. For example, with 1.0 m SLR, there were 118 days (3.2 percent of the time) of water quality exceedance during the 10 ensemble years (3652 days) simulated. With 1.6 m SLR, this chloride standard was exceeded in 4 years (2001, 2002, 2016 and 1965). Another standard is a 15-dma chloride concentration of 50 mg/L for water quality Zone 2 (RM 108.4 to RM 133.37), which encompasses the location of major water-supply intakes (RM 110). Additional analyses show that with SLR of 1 and 1.6 m, this standard is exceeded 1 and 4 percent of the time, respectively (see Table G.7 in Appendix G.)

4.2.4 Salinity

The median, maximum, and normal range of daily depth-averaged salinity for the 10 years simulated are presented for eight locations in the Delaware Estuary in **Table 4.2-3**. The simulated median daily depth-averaged salinity at the Schuylkill River and upstream is typically at or below 0.14 psu, regardless of sea level rise. In the area of the Delaware Estuary above the Schuylkill River, the salinity is reflective of the background concentrations in the freshwater inflows. However, the maximum daily depth-average salinity above the Schuylkill River increases with increasing sea level rise. For the baseline condition, the maximum daily depth-averaged salinity

[29] The location of the salt front is reported on DRBC's website on a map with the normal range and other reference landmarks. Graphs and tables summarizing the information, updated daily, are available on hydrosnap.drbc.net. Monthly and annual reports are located on the DRBC website at https://www.nj.gov/drbc/programs/flow/hydrologic-reports.html.

Table 4.2-2. Simulated maximum 30-dma chloride concentration at River Mile 98.

Sea Level Rise (m)	30-dma chloride concentration at Camden, RM 98 (mg/L)	Total number of days 30-dma chloride concentration exceeds 180 mg/L	Percent of time 30-dma chloride concentration exceeds 180 mg/L
0	119	0	0%
0.3	152	0	0%
0.5	178	0	0%
0.8	225	80 *	2.2% *
1.0	263	118 *	3.2% *
1.6	431	273	7.5%

Total number of days simulated = 3652.
* Simulated exceedances only occurred in 1965 with the constant 2,500 cfs flow objective at Trenton. For 1.6 m SLR, exceedances occurred in 4 years (2001, 2002, 2016, and 1965).

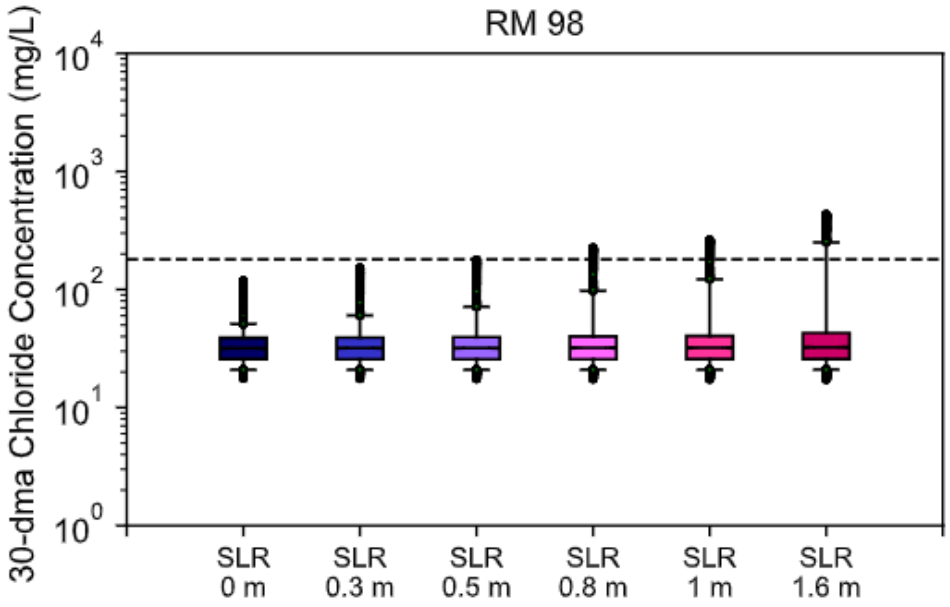

Figure 4.2-4. Simulated maximum 30-day moving average chloride concentration at RM 98 based on 10-year ensemble results.

Note: dashed line indicates the water quality standard of 180 mg/L chloride concentration at RM 98. In these ensemble simulations, a 2,500 cfs minimum flow was set on the Delaware River at Trenton to reflect the flow objective under drought conditions of 1965. Simulated years are 1965, 2001-2002, 2011-2013, and 2016-2019.

Table 4.2-3. Simulated daily depth-averaged salinity with sea level rise at selected River Mile locations in the Delaware River Estuary. All units are psu.

SLR (m)	Value	SHIP JOHN SHOAL RM 37	REEDY ISLAND RM 54	DELAWARE MEMORIAL BRIDGE RM 69	CHESTER RM 83.6	SCHUYLKILL RIVER CONFLUENCE RM 92.5	CAMDEN RM 98	BEN FRANKLIN BRIDGE RM 100	DRINKING WATER INTAKES RM 110
0	median	14.98	4.28	0.53	0.15	0.14	0.12	0.12	0.10
	max	24.90	17.15	7.93	2.13	0.75	0.36	0.30	0.17
	range	11.62–17.88	1.81–7.56	0.17–2.14	0.12–0.22	0.11–0.17	0.09–0.15	0.09–0.14	0.08–0.12
0.3	median	15.41	4.66	0.64	0.15	0.13	0.12	0.12	0.10
	max	24.89	17.16	8.29	2.50	0.89	0.43	0.36	0.17
	range	12.21–18.11	2.15–7.88	0.19–2.49	0.12–0.26	0.11–0.17	0.1–0.15	0.09–0.14	0.08–0.12
0.5	median	15.68	4.92	0.75	0.15	0.13	0.12	0.12	0.10
	max	24.81	17.12	8.54	2.74	0.99	0.49	0.41	0.17
	range	12.64–18.3	2.38–8.08	0.21–2.74	0.12–0.3	0.11–0.17	0.1–0.15	0.09–0.15	0.08–0.12
0.8	median	16.11	5.32	0.92	0.15	0.13	0.12	0.12	0.10
	max	24.71	17.00	8.89	3.12	1.15	0.59	0.50	0.19
	range	13.25–18.63	2.75–8.42	0.25–3.12	0.12–0.36	0.11–0.17	0.1–0.15	0.09–0.15	0.08–0.12
1.0	median	16.44	5.60	1.05	0.16	0.13	0.12	0.12	0.10
	max	24.69	16.94	9.13	3.38	1.27	0.67	0.57	0.22
	range	13.67–18.87	3.04–8.67	0.29–3.39	0.12–0.43	0.11–0.17	0.1–0.15	0.09–0.15	0.08–0.12
1.6	median	17.54	6.63	1.62	0.18	0.14	0.12	0.12	0.10
	max	24.72	16.92	9.95	4.30	1.78	1.00	0.87	0.34
	range	15.03–19.64	4.12–9.56	0.51–4.3	0.12–0.74	0.11–0.21	0.1–0.16	0.09–0.15	0.08–0.13

Note: Simulations with 1965 flow include implementation of the flow objective at Trenton (minimum flow set to 2,500 cfs). Simulations use flows for years 1965, 2001-2002, 2011-2013, and 2016-2019.

is 0.75 psu at the Schuylkill River confluence. With 0.3 m, 0.5 m, 0.8 m, 1.0 m, and 1.6 m of sea level rise, the maximum daily depth-average salinity is 0.89, 0.99, 1.15, 1.27, and 1.78 psu, respectively, at the Schuylkill River confluence. Box plots of the daily depth-averaged salinity at eight locations with sea level rise are shown in **Figure 4.2-5**. With sea level rise, simulated daily depth-averaged salinity is more variable between Chester and Ben Franklin Bridge, as indicated by the larger range of salinity between the 25th and 75th percentiles. The simulated daily maximum salinity by River Mile and simulated increase in the daily maximum salinity with sea level rise are presented in **Figure 4.2-6** and **Figure 4.2-7**, respectively. The largest increases in the maximum salinity occur between the Delaware Memorial Bridge (RM 69) and Chester (RM 83).

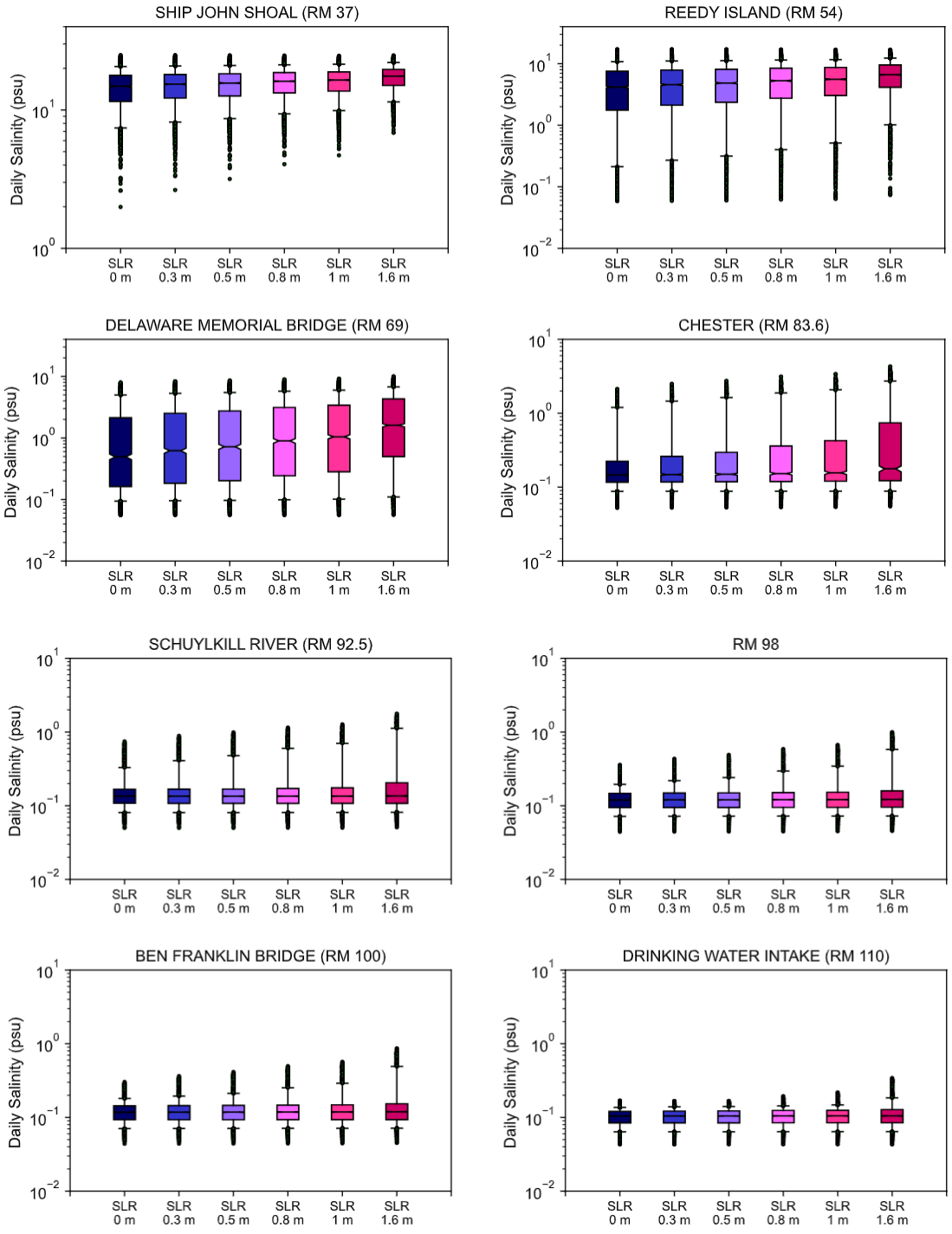

Figure 4.2-5. Simulated daily depth-averaged salinity with sea level rise at selected River Mile locations in the Delaware River Estuary.

Note: Simulations with 1965 flow include implementation of the flow objective at Trenton (minimum flow set to 2,500 cfs). Simulations use flows for 1965, 2001-2002, 2011-2013, and 2016-2019.

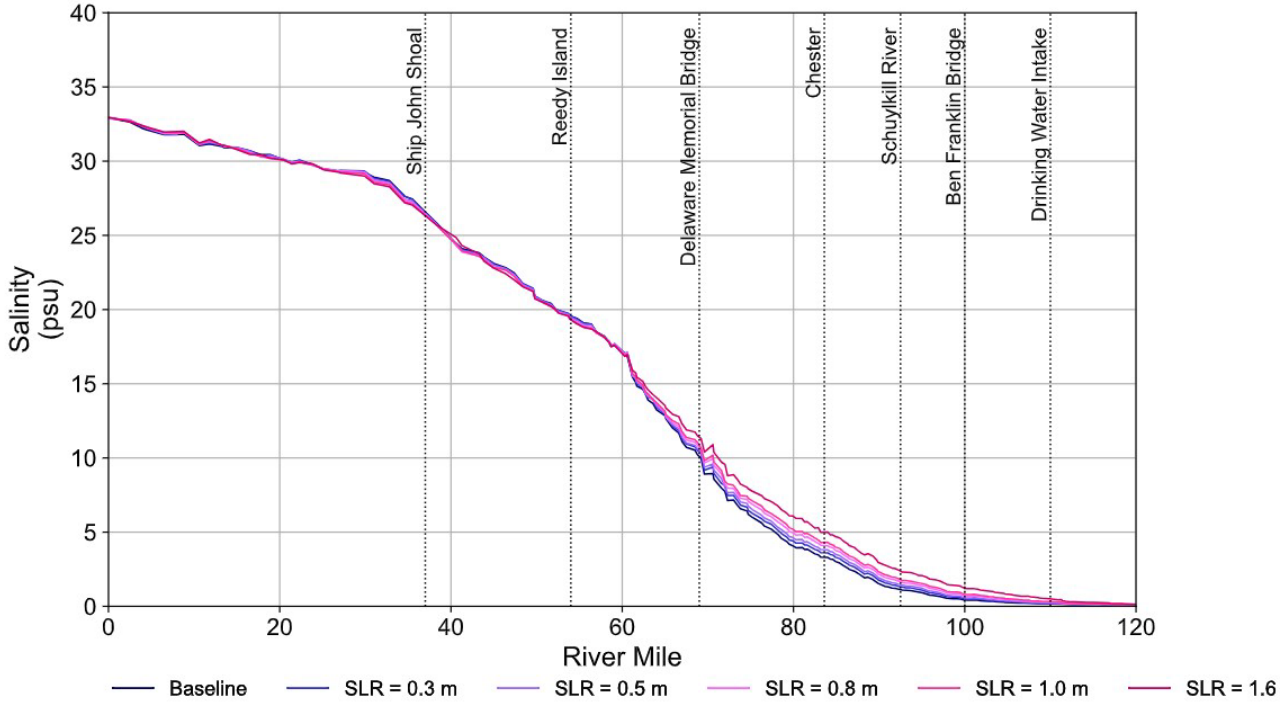

Figure 4.2-6. Simulated daily maximum along-channel salinity profile with sea level rise and 1965 historical flows.

Note: In these ensemble simulations, a 2,500 cfs minimum flow was set on the Delaware River at Trenton to reflect the flow objective under drought conditions of 1965.

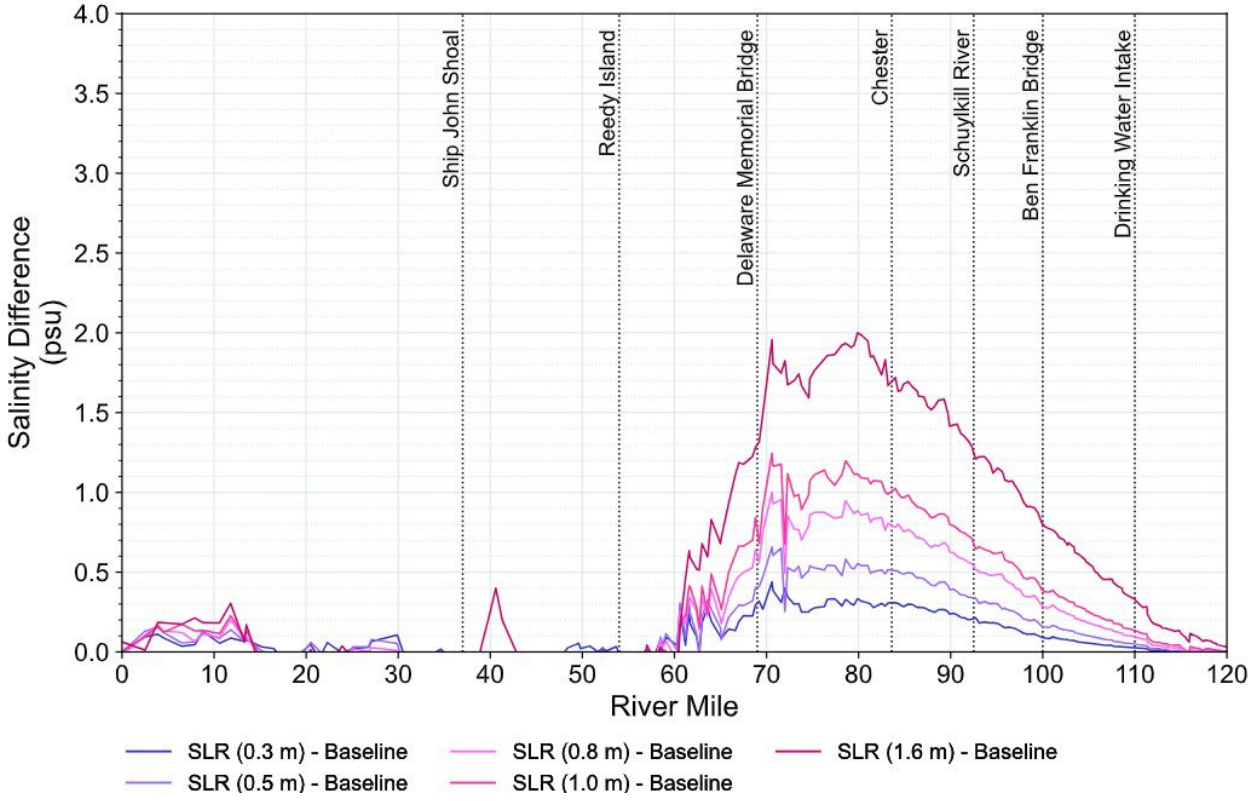

Figure 4.2-7. Increase in simulated daily maximum along-channel salinity from baseline with sea level rise in the Delaware River Estuary.

4.3 Discussion

Results of simulations demonstrate that sea level rise alters the hydrodynamics, salinity structure, and along-channel salinity profile and creates conditions more conducive to salinity intrusion in the Delaware River Estuary. Diagnostic simulations performed for a representative low flow period demonstrate that with SLR, salinity intrusion will be exacerbated. With sea level rise, the amplitude of the tide is larger, increasing the forces pushing salinity into the Delaware Estuary, and the vertical stratification of salinity becomes stronger in the Bay. Salinity is predominantly transported along the channel bottom, and as sea level rises, more salinity is transported within the FNC as well as outside the shallower areas of the Estuary closer to New Jersey. The largest changes in salinity occur in the FNC and deeper areas alongside the channel.

Ensemble simulations that use hydrologic conditions from 10 representative years demonstrate that flow is a critical factor affecting the salt front advancement for a given SLR scenario. The worst salinity intrusion occurs during the simulation with 1965 flows (adjusted to reflect a minimum flow objective of 2,500 cfs at Trenton, New Jersey. For the baseline condition without SLR, the maximum salt front location is RM 94.2. At 0.5 m of SLR, the maximum salt front is at RM 96.8, For 1.0 m SLR, the salt front reaches RM 100.4 near the historical maximum location at the Ben Franklin Bridge. and for 1.6 m, the salt front reaches RM 104.7, 10.5 miles upstream of the baseline and 5.3 miles downstream from the drinking water intakes.

The water quality standard (the maximum 30-dma chloride concentration less than 180 mg/L at RM 98) is exceeded with 1965 hydrology with SLR at and above 0.8 m. The standard is not exceeded with flow conditions from years other than 1965 until SLR reaches 1.6 m. For 1.6 m sea level rise, the standard is exceeded during three of the simulated years and is above the standard for 7.5 percent of the time during the 10 years simulated.

The results from the ensemble simulations indicate that with SLR, salinity in the Estuary between Chester and the Ben Franklin Bridge becomes more variable. Above the Schuylkill River, salinity between the Delaware Memorial Bridge and Chester, where the water column becomes more uniform.is largely reflective of the background freshwater inflow concentrations, and the maximum salinity is less than 2 psu for SLR less than 1.6 m. The largest increases in the maximum salinity occur between the Delaware Memorial Bridge and Chester, where the water column becomes more uniform.

5. EFFECTS OF MODEL CONFIGURATION ON SIMULATION RESULTS

Different aspects of model configuration that relate to potential future conditions can affect salinity intrusion simulations. The effects of specific model features on simulated salinity were examined, and these features included (1) tidal and intertidal marsh areas, which affect the tidal prism[30]; (2) bottom roughness in marshes, which impacts energy loss as the tide moves upstream; (3) extent of permanent marsh inundation resulting from shoreline retreat and bank erosion; and (4) navigation channel bathymetry. The results of sensitivity tests are presented in terms of the salt front location. Additional sensitivity tests examining the effects of vertical grid resolution, net flow and salinity in the C&D Canal, and ocean salinity are documented in the SM3D calibration report (Chen et al., 2025). While the simulations demonstrate the effects of marsh area, bottom roughness, shoreline retreat, and bank erosion on salinity intrusion, the model does not predict how these features will be affected by sea level rise. The simulations presented in this section are one-year simulations that represent a low-flow condition and are based on 2002 hydrologic conditions. It is important to note that the marsh simulations are intended only to determine how the addition of marsh area and related characteristics affect model results relevant to salinity and salinity intrusion.

5.1 Amount of Marsh Area Represented

Low-lying marshes around the Bay affect tidal energy and salinity transport. As the tide comes into the Estuary, the converging shorelines amplify the tidal wave and related energy. As a result of this convergence, the tidal range at Philadelphia, PA, (RM 100) is larger than the tidal range at Lewes, DE, near the mouth of the Bay (RM 0). Marshes counteract this effect by providing additional space for water to spread, which also increases the volume of the tidal prism. With SLR, marsh areas closer to the coast will be inundated more frequently and may affect the amount of tidal energy driving salinity transport. As the tidal prism increases, a wider extent of marsh area is inundated with each tide, which results in 1) reduced tidal amplitude and 2) reduced volume of water moving in and out of the upper reaches of the Estuary. Sensitivity tests were conducted to quantify the magnitude of these effects, and the results of the tests are presented below.

In the test simulations, the model domain of SM3D was modified to incorporate additional marsh area (SM3D+M) to evaluate how the inundation of more marsh area affects salinity transport. This

30 The tidal prism is the total volume of water moving into and out of the estuary, excluding freshwater inflows (Hume 2005).

model configuration represents a scenario in which marshes migrate farther inland, and no net sediment deposition occurs.

The amplitude of the largest tidal constituent (M2) increases with SLR and this is observed in the model results with marshes included (SM3D+M) and without the marshes (SM3D), however, the amount of increase is different with the SM3D+M in the upper tidal River. For instance, with 1.6 m SLR, the increase in the amplitude of the largest tidal constituent (M2) with respect to the baseline (0 m SLR) at RM 126 was 5 cm less with additional marsh area (SM3D+M) than without additional marsh area (SM3D). With 1.6 m SLR, at RM 37 the M2 amplitude was 8 cm less with additional marshes (SM3D+M) than without additional marshes (SM3D). At RM 37, the increase in the M2 tidal amplitude at 1.6 m SLR was slightly smaller than the corresponding baseline, measuring 3.5 cm less with the additional marsh area (SM3D+M). In contrast, there was a 4.8 cm increase compared to the baseline without the additional marsh area (SM3D). The baseline M2 amplitudes for both SM3D and SM3D+M are roughly the same, at 0.91 cm. Results for the simulated M2 tidal constituent at multiple locations in the Estuary are presented in **Table J.1-3** and **Table J.1-4** in Appendix J.1.

Including additional marsh area has a substantial effect on the extent of salinity intrusion. Diagnostic simulations with representative dry hydrologic conditions from July through October 2002 demonstrated that for the baseline (0 m SLR), the predicted maximum salt front location for SM3D+M is 0.2 miles farther downstream than that simulated using SM3D. With 0.8 m SLR, the maximum salt front location is 1.0 miles farther downstream with additional marshes. With 1.6 m SLR, the maximum salt front location is 2.6 miles farther downstream with additional marshes.

These results demonstrate that the model configuration without additional marsh area is more conservative with respect to salinity intrusion and protecting public water supplies. The results also demonstrate that preserving marsh areas is beneficial for reducing tidal amplification and salinity intrusion, particularly in the Upper Delaware River Estuary. Details of simulations used to evaluate the effect of additional marsh area are presented in Appendix J.1.

5.2 Bottom Roughness in Marsh Areas

The shape and characteristics of an estuary bottom can affect the flow of water over it due to friction and is an important factor for simulating wave energy loss. The model parameter used to represent the characteristics of an estuary bottom is the bottom roughness height, which is difficult to define for marsh areas because vegetation-induced friction losses are highly variable and depend on vegetation type, density, height, and submergence. Bottom roughness height may change with SLR as the vegetation type, density, height, and depth of submergence change. Some existing marsh areas may even become permanently inundated. Model sensitivity to bottom roughness height was tested by adjusting this variable in the additional marsh areas in the

SM3D+M model. Results indicate that the modeled salt front location is not sensitive to marsh bottom roughness height over the range tested (from 0.0025 m to 0.05 m). The difference in predicted maximum salt font location across the range of tested bottom roughness heights is 0.01–0.3 miles for 1.0 m SLR and 0.29–0.3 miles for 1.6 m SLR. A time series of simulated salt front location showed that varying bottom roughness height results in relatively minor differences in the salt front location with 1.0 or 1.6 m SLR. These results show that bottom roughness is not an important factor for evaluating the impacts of sea level rise on salinity intrusion. Additional details of this sensitivity analysis are presented in Appendix J.2.

5.3 Shoreline Retreat and Bank Erosion

The wetland and marsh areas surrounding the Estuary provide protection from storms by absorbing energy, reducing wind penetration, and reducing wave strength. These areas are also habitats for many species, including ribbed mussels, fiddler crabs, horseshoe crabs, marsh mud snails, grass shrimp, as well as fishes, turtles, and birds (DNREC, 1999). Storm forces disturb the marsh vegetation, which holds soils and sediments in place, causing erosion and the loss of coastline and bank areas. Sea level rise is likely to result in shoreline erosion and wetlands migration (Kearny et al., 2002; Schieder, et al., 2017), which may impact the storm protection and habitat values of these areas. Shoreline retreat and bank erosion may affect salinity intrusion.

Sensitivity simulations were conducted to evaluate the impact of SLR-induced shoreline retreat and bank erosion[31] on salinity intrusion. In a selected part of the SM3D+M model representing the total marsh area surrounding the Bay, the near-shore bed elevation was lowered by 1.0 m to reflect permanent inundation of those marshes. Given the current estimated marsh loss rate (1.1–1.9 percent per decade; New Jersey Science Advisory Board, 2020), this scenario is unlikely to occur within the next 50 years, and, therefore, the total marsh losses simulated may be overestimated.

The simulated salt front was only marginally affected by the modeled representation of shoreline retreat and bank erosion. With shoreline retreat, the salt front location was slightly farther downstream compared to that of the simulation without shoreline retreat. The difference attributed to shoreline retreat becomes smaller as SLR increases; the maximum salt front location with shoreline retreat was 0.76 miles farther downstream for 1.0 m SLR and 0.16 miles farther downstream for 1.6 m SLR.

31 Shoreline or coastal erosion is a natural process resulting from the loss of shoreline sediments. https://oceanservice.noaa.gov/facts/shoreline-armoring.html

These results show that modeling salinity intrusion without representing shoreline retreat and bank erosion is a conservative approach with respect to the protection of drinking water intakes. The analysis of the sensitivity of model results to near-shore bed elevation helps in further understanding the uncertainty in simulation results.

5.4 Channel Bathymetry

The depth and width of an estuary (bathymetry and morphology) typically change over time as the result of natural processes (sediment accumulation and erosion) and human activity, (dredging), and these changes can affect salinity intrusion. The bathymetry of the Delaware Estuary has remained largely unchanged except in the FNC. The FNC is maintained by the United States Army Corps of Engineers (USACE) and is periodically dredged to remove sediment and maintain an appropriate depth for shipping. According to the USACE, channel deepening along the full length of the Estuary began late in the 19th century and has continued to accommodate the increasing drafts of ships bound for the ports of Wilmington and Philadelphia. In 1848, the natural channel depth near Philadelphia was estimated to be 20 ft. The channel was deepened to 26 ft in 1898, 30 ft in 1910, 35 ft in 1926, 40 ft in 1940, and most recently 45 ft (PhilaPort, 2018).

Simulations were performed to evaluate the relative effect of changes to bathymetry on salinity intrusion in comparison with the effect of SLR on salinity intrusion. Two bathymetries with different channel depths were evaluated: 1) the current channel bathymetry (depth of 45-ft below MLLW, post-dredge) is the baseline SM3D; and 2) 40-ft below MLLW (pre-dredge) bathymetry, based on the 2011 FEMA bathymetry with the depth of the channel cells adjusted to 40 ft. The 45-ft channel bathymetry[32] represents present and future conditions. A series of simulations with both channel depths were performed for SLR values of 0, 0.5, 1.0, and 1.6 m.

Results of these simulations are presented in **Table 5.4-1** to compare the relative and combined differences due to the change in channel depth and the change in sea level rise on the maximum salt front location as follows:

A. Change due to channel depth for each value of sea level rise (e.g., 45-ft channel at 0.5 m minus the 40-ft channel at 0.5 m)

B. Change due to SLR for (e.g., 45-ft channel at 0.5 m minus the 45-ft channel at 0 m) for both depths; and

C. Difference in B for 45-ft channel and B for 40-ft channel.

32 45-ft depth channel refers to the post-dredging bathymetry, and 45-ft depth is referenced to MLLW and 1983-2001 NTDE. 40-ft depth channel refers to the pre-dredging bathymetry, and 40-ft depth is referenced to MLLW and 1983-2001 NTDE.

Table 5.4-1. Sensitivity of salt front location to channel bathymetry and SLR.

SLR (m)	Channel Depth (ft)	Simulated Maximum Salt Front Location (RM)	Change in Salt Front Location Due to Increased Channel Depth (mi) [1] SF45 – SF40	Change in Salt Front Location Due to SLR for 40-ft Channel (mi) [2] SF(SLR) – SF(0m)	Change in Salt Front Location Due to SLR for 45-ft Channel (mi) [3] SF(SLR) – SF(0m)	Total Change in Salt Front Location Due to SLR and Channel Depth (mi) [4]* SF(45ft,SLR) – SF(40ft,0m)
0	40	88.3		–	–	
	45	90.7	2.4	–		2.4
0.5	40	91.3		3.0		
	45	93.4	2.1		2.7	5.1
1.0	40	94.1		5.8	–	
	45	96.3	2.2		5.6	8.0
1.6	40	99.0		10.7	–	
	45	101.4	2.4		10.7	13.1

Note: the analysis was based on the 2002 hydrologic conditions. 2002 is one of the dry years.
* The total change in the salt front location with the channel deepening (45-ft channel) AND SLR compared to the SF for a 40-ft channel and 0 m SLR.

The changes in the maximum salt front location between a 40-ft and a 45-ft navigation channel at the same sea level are 2.4, 2.1, 2.2, and 2.4 miles upstream for SLR of 0 m, 0.5 m, 1.0 m, and 1.6 m, respectively (**Table 5.4-1** Column 1). The model results indicate that the differences in the maximum salt front location due to the change in channel bathymetry (40-ft to 45-ft) by itself are similar, approximately 2 miles, regardless of the value of sea level rise (**Table 5.4-1** Column 1). The change in the maximum salt front location due to sea level rise for the same channel depth, , is similar for both channel depths for each value of SLR (e.g., 3.0 vs 2.7 miles at 0.5 m SLR; and 5.8 vs 5.6 at 1.0 m SLR: Columns 2 and 3). For the conditions simulated, the effect of changing the channel depth by 5 ft is relatively constant (2–2.4 miles) regardless of the sea level when the change in depth occurs. However, the combined effect of the deepening and SLR is nearly additive (Column 4). Comparing the results for the 45-ft channel at different SLR values with the 40-ft channel at 0 m SLR (Column 4 vs Column 3), the maximum salt front is farther upstream by an amount similar to changing the channel depth at any sea level (Column 1). For example, with SLR but no change in the channel depth (Column 2), the salt front is 3 miles farther upstream

(RM 88.3 vs. RM 91.3). However, if the channel depth is then increased, the salt front is 5.1 miles upstream (RM 88.3 vs. RM 93.4) (Column 4). The results indicate that the impacts of channel deepening and SLR are additive for the condition simulated (2002 hydrologic conditions). Additional details about the effects of bathymetry and SLR on salinity and the sensitivity test results conducted for this study are presented in Appendix J.3.

5.5 Discussion

Future conditions of the Estuary relating to marsh area, marsh characteristics, shoreline status and bathymetry are uncertain, and changes in these conditions may influence the impact of SLR on salinity intrusion. The results of simulations using a range of SLR scenarios and model configurations representing these different conditions demonstrate the extent of these potential influences and provide insight to the suitability of the calibrated model configuration.

Including additional marsh areas has a substantial effect on the simulated extent of salinity intrusion. The model configuration without additional marsh area is more conservative with respect to salinity intrusion and is therefore suitable for this analysis.

The characteristics of the estuary bottom are difficult to define in the model and may change with SLR. However, the modeled salt front location was not sensitive to changes in the model parameter used to represent the estuary bottom character.

Although sea level rise is likely to result in shoreline erosion and wetlands migration, the simulated salt front was only marginally affected by the modeled representation of shoreline retreat and bank erosion.

The bathymetry of the FNC was shown to influence salinity intrusion with SLR, and the difference in simulated maximum salt front location with change in depth ranged from 2.1 to 2.4 miles under SLR of 0 to 1.6 m. With SLR, the difference in the maximum salt front location compared to corresponding baseline is similar regardless of the value of SLR. However, the difference in simulated maximum salt front location between the baseline (40-ft channel, 0 m SLR) and a 45-ft channel with SLR appears to be additive. These results indicate that the changes to channel bathymetry are consistent at different values of SLR and nearly additive to the relative effect of sea level rise alone on salinity intrusion.

These results show that with its current marsh area, the SM3D model is conservative and appropriate for use in analyzing the impacts of SLR on salinity intrusion in the Delaware Estuary.

6. ANALYSIS OF OTHER POTENTIAL CONDITIONS

Other conditions and assumptions that may affect the extent of salinity intrusion from sea level rise were also evaluated, including changes in salinity from non-tidal sources[33] and increase of the ocean surface water temperature resulting from global warming along with future sea level rise; increased drought severity resulting from climate change; and increased ocean temperature, which affects density-driven circulation. Simulations were performed to evaluate the effect of changes in these conditions on model results.

6.1 SALINITY FROM NON-TIDAL SOURCES

Future increases in the salinity of freshwater sources will affect salinity and chloride concentrations downstream, primarily in the Upper Estuary, where salinity is lower than that of the ocean. Instream monitoring of the non-tidal River over time has shown an increasing trend in salinity and related chloride concentrations. The trend is not unique to the Delaware River, and it is becoming commonplace in areas of the U.S. with significant roadway de-icing activity (Rumsey C.A., et al., 2023).

Another source of salinity is from point source (PS) wastewater treatment discharges to the main stem Delaware River. PS salinity values reported by PWD (2020) were applied to the 11 major point source discharges considered in the model (Appendix F). Salinity loads from minor discharges were not included due to the insignificant amount of water contributed to the Delaware River[34]. These constant PS salinity values were used in the base case simulations.

Two sets of sensitivity simulations were conducted for the representative low flow period:

- (1) Sensitivity to increases in salinity from non-tidal River and tributary streams; and
- (2) Sensitivity to point source salinity temporal variability.

The low flow period of 2002 was simulated to represent a moderate drought condition. The results were compared with the base case simulation. For the base case simulation, tributary salinity for the Delaware was set based on daily specific conductance data collected at USGS gage 01463500 on the Delaware River at Trenton in 2002; due to lack of data for 2002, Schuylkill River salinity was set to two times the salinity observed from the Delaware River at Trenton.

33 Non-tidal terrestrial salinity sources include natural processes such as rock weathering and saline springs, as well as human activities including agricultural runoff, de-icing salts, wastewater discharge, and mining.

34 Based on analysis of data from 2018-2019, 80 percent of the flow from PS sources into the Delaware Estuary by volume is from the 11 major dischargers.

6.1.1 Sensitivity to Non-tidal and Tributary Salinity Loads

For the Delaware River at Trenton, NJ, trends in observed chloride concentrations indicate an increasing rate of 0.28 mg/L per year as a result of roadway de-icing and other human activities. By 2060, average chloride concentrations are projected to double what they were in 2002, although not consistently throughout the year, from 17.1 mg/L to 34.4 mg/L (equivalent to salinity of 0.09 psu and 0.12 psu, respectively)[35]. To assess how increasing non-tidal chloride loading may contribute to future salinity intrusion events, the time-series chloride concentration input to the model (as salinity) was scaled so that the average seasonal concentration of the input data would be equivalent to the projected concentration in 2060.

Results of simulations show that with increased freshwater tributary salinity, the maximum salt front location is 0.6 to 0.9 miles farther upstream for SLR values simulated, exacerbating the effect of sea level rise. With sea level rise and the increased tributary salinity load, the maximum salt front location is 0.9 miles farther upstream with 1.0 m SLR, which is much less than the effect of SLR by itself (up to RM 96.3, or 5.6 miles farther upstream from the base case). The salt front is not “moved” by the increased salinity, but the combined concentration of ocean and tributary salinity results in the calculated maximum salt front location that is farther upstream. The simulated range of 30-dma chloride concentrations at RM 98 (Camden) also shows that the effect of increased salinity loads from tributaries is smaller than the effect of SLR by itself. The results also indicate that the 180-mg/L water quality standard at RM 98 may occasionally be exceeded with SLR of 1.0 m or more. Details of the sensitivity analysis are presented in Appendix K.1.1.

6.1.2 Sensitivity to Point Source Salinity Load Variability

Limited data are available to specify time-series point source salinity boundary conditions. In simulations including under future SLR conditions, the PS salinity is constant over the course of the year. However, observed salinity loads change seasonally. A sensitivity simulation using variable monthly PS salinity was conducted and compared to the base case using constant PS salinity. Results of the simulations with a constant PS salinity were compared to those of simulations with monthly PS salinities, and the differences were indiscernible. Information regarding point source salinity is included in Appendix F. Details of the sensitivity analysis are presented in Appendix K.1.2.

35 NWQDP site: https://www.waterqualitydata.us/#within=0.5&lat=40.219698&long=-74.778365&sampleMedia=Water&characteristicName=Chloride&mimeType=csv&dataProfile=resultPhysChem&providers=NWIS&providers=STEWARDS&providers=STORET
USGS water quality trend analysis for chloride at Trenton on the Delaware River: https://nrtwq.usgs.gov/nwqn/#/site/cx_USGS-01463500/graphics

6.2 Increased Drought Severity

Another compounding factor related to sea level rise and its impact on salinity is how precipitation, runoff, and streamflow may be altered by climate change. A “stress-testing” scenario using streamflow representing an extreme drought in the future was simulated to evaluate salinity intrusion with both SLR and increased drought severity. Previous analyses of historical drought streamflow and of predicted effects of climate change provided background and guidance for developing such a scenario.

The consensus view of climate researchers is that climate change is most likely to result in increased annual precipitation in the Delaware River Basin. However, a climate with an increase in mean annual precipitation and related runoff and streamflow does not preclude changes to the characteristics of extreme drought events. Global climate models have predicted that drought will likely occur with similar frequency as the climate changes, but with a greater likelihood of rapid onset droughts (Pendergrass, 2020). Hydrologic models of future streamflow have limitations in that the uncertainty associated with their use and predicted future climate (non-stationarity) may lead to physically unrealistic results for extreme events that lack credibility (Serinaldi and Kilsby, 2015). Thus, with concerns about the likelihood of extreme future droughts predicted by climate models, an alternative approach was used to develop “more severe” drought flows for sensitivity testing.

The approach used for representing a more extreme drought (a stressor) was to develop a sequence of the lowest observed monthly average flows from historical data. The lowest average monthly flows at the two major non-tidal freshwater sources (the non-tidal Delaware and Schuylkill Rivers) did not occur consecutively or during the same year. Although the resulting constructed time series of extremely low average monthly flows is unlikely, the individual low monthly flows have occurred in the past and are known to be physically possible. Thus, it seems plausible that in the future they could occur again, perchance in sequence, creating a more extreme drought condition that could exacerbate salinity intrusion with SLR.

The historical combined minimum monthly flows for the Delaware and Schuylkill Rivers were considered in formulating the more extreme drought scenario. The combined minimum monthly flows during January–April and July–December were all less than 95 percent of the respective monthly flows in 1965, and so these flows were used (**Table K.2-1** in Appendix K.2). The low monthly flows during May and June were at least 98 percent of the respective monthly flows in 1965, and so these flows were adjusted to be 95 percent (5 percent less) of the respective combined minimum monthly flows observed during 1965. By making this adjustment, the simulated drought condition is substantially more severe than the 1965 flows during the 1960s drought of record (base case) (Appendix K.2). The time-series of flows for the more extreme drought simulation was constructed with daily historical flows scaled by the ratio of the combined

minimum observed monthly flow to the combined observed monthly flows of 1965. Scaling the 1965 flows was chosen to avoid differences in the salt front related to the timing of low flows within the month, rather than just the lower flow rate. For comparison purposes, a minimum flow of 2,500 cfs at Trenton was used so the base case would be consistent with other simulations. Noted that although the 2,500 cfs minimum flow was used in both the baseline simulation and the simulation of a more extreme drought, the period for which the Trenton flow was maintained at 2,500 cfs was much longer in the extreme drought scenario during October and December[36]. Moreover, every month the flows from the Schuylkill River were lower than those that occurred during 1965, so the condition still reflects a more extreme drought with less freshwater flow entering the Estuary. The average annual flow with the flow objective for the more extreme drought was 83 percent of the flow during 1965. Simulations of the hypothetical more extreme drought flows without the Trenton Flow Objective (i.e., historical observed flows) are also presented in Appendix K.2.

6.2.1 Salt Front

Figure 6.2-1 shows the annual time series of the 1965 flows and the flows representing a more extreme drought along with the simulated time series of the maximum salt front location with 0 m, 0.5 m, 1.0 m, and 1.6 m of SLR. The simulated maximum salt front extends farther upstream under a more extreme drought condition compared with the simulated maximum salt front during 1965. With sea level rise, the effect of the drought is more pronounced, and the salt front extends up to several miles farther upstream. Less flow is available to counteract the force of the tide pushing salinity upstream with SLR.

The salt front begins the year at the same location for each value of SLR. Results of the 1965 simulation show that the higher flows in February push the salt front downstream. Results of the more extreme drought simulations show that the salt moves downstream more gradually, because the lower February flows are less effective in keeping the salt downstream. Results of the 1965 simulation show that the salt front location is relatively constant, remaining within approximately 5 miles of its location in early March until mid-May; the decreasing tidal forces are balanced by the flow forcing. For the more extreme drought conditions, the salt front does not achieve a relatively constant location until mid-April. In both cases the salt front begins to move upstream again in mid-May. The flow in the base case and the more extreme drought scenario were nearly the same from mid-June through late-September. Thus, by July, the salt front locations for the more extreme drought simulations are less than one mile upstream from those of the respective 1965 simulations and are located at nearly the same location through October 1. However, as the

36 The resulting flow record does not include the October 1965 storm event, which resulted in flows strong enough to push the salt front downstream for approximately two weeks. Without that event, salinity intrusion in 1965 would likely have been farther upstream.

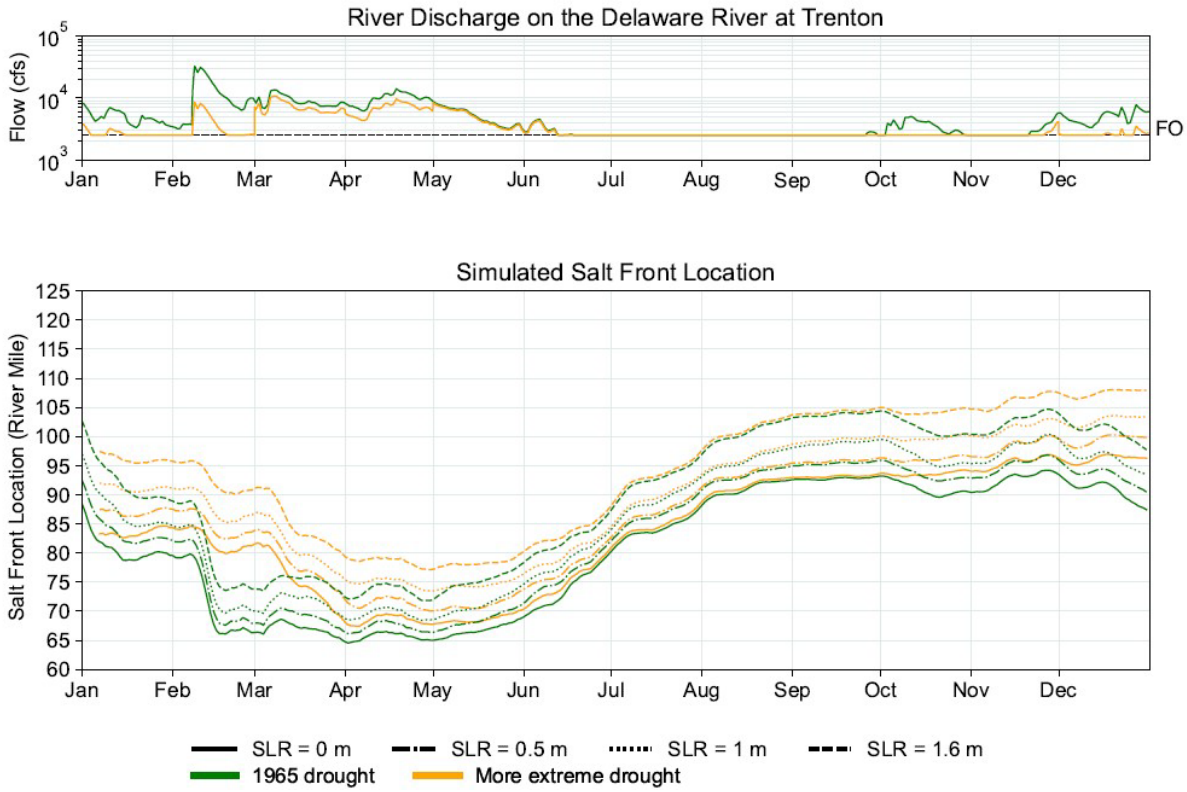

Figure 6.2-1. Inflow conditions and simulated salt front location with sea level rise during a repeat of 1965 flows during the 1960s drought and under a more extreme drought.

The 2,500 cfs Trenton flow objective was used in both simulations.

flows in the 1965 base case simulation increase, flows in the more extreme drought simulation remain lower and the salt front locations diverge. The dominating factor that controls the maximum salt front location is the low flow condition from July through December. In the more severe drought simulation, the Trenton flow remains at 2,500 cfs between June and December except during a few short periods of higher flow. In the base case simulation, higher flows in October and December moved the salt front downstream. The prolonged and persistent low flows in October and November coincide with relatively higher water levels, indicating that both the ocean and low freshwater flows play important roles in saltwater intrusion.

During the critical season for salinity intrusion from September through November (based on historical observations), the simulated salt front under 1965 conditions reached the most upstream location around October 1. With the lower flows used in the extreme drought simulation, the salt front continued to advance farther upstream until it reached its most upstream location in November. In December under 1965 conditions, the salt front began to move downstream with

the increase in flow and seasonal decrease in tidal forces. Under the extreme drought conditions when the flow is lower, the salt front continues to move upstream until late December when it becomes relatively stable.

Simulation results show that during the more extreme drought conditions simulated, sea level rise would increase the susceptibility of the major drinking water intakes to salinity intrusion. With 0 m SRL, the sustained low flow under increased drought severity pushed the maximum salt front to RM 96.9 by late-November. With 1.0 m and 1.6 m SLR, salinity intrusion extended farther upstream to RM 103.6 and RM 108.1 (6.4 and 1.9 miles below the major drinking water intakes) respectively. Compared to the base case with the 1965 inflow, the extreme drought simulation salt front is farther upstream by 2.7–3.5 miles (**Figure 6.2-2** and **Table 6.2-1**). Results from these simulations demonstrate that prolonged sustained low flow, especially in the fall, combined with sea level rise, would exacerbate salinity intrusion and potentially threaten major drinking water intakes.

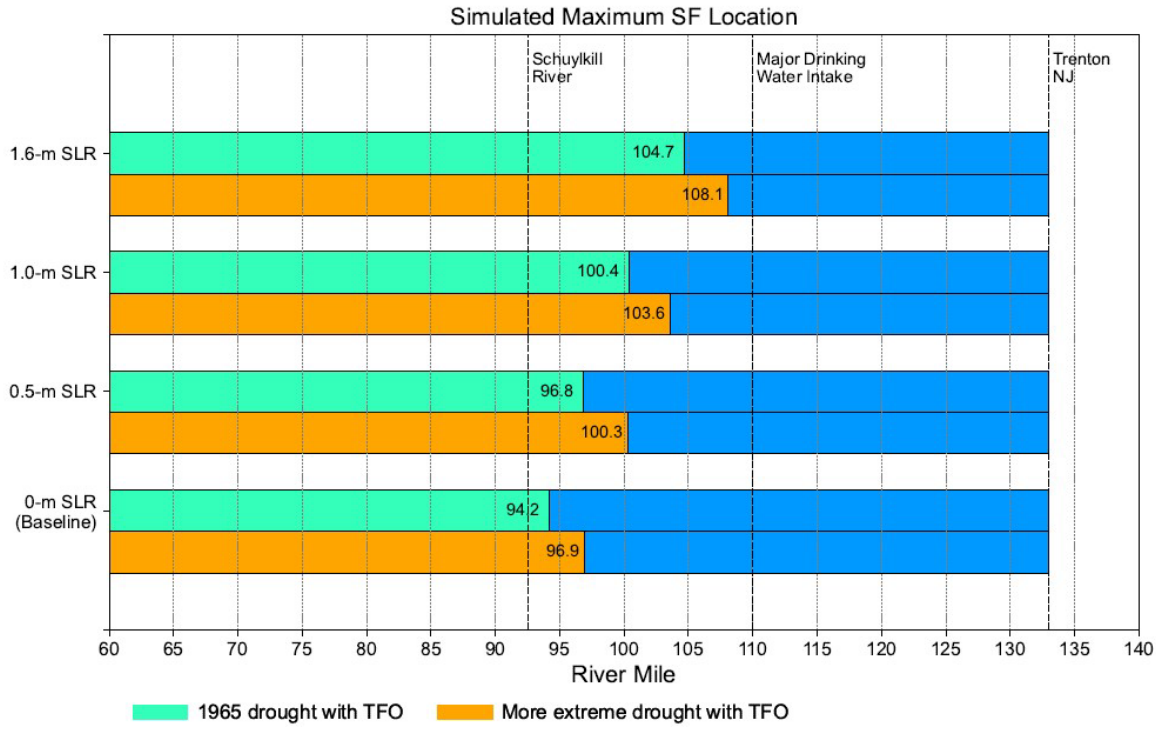

Figure 6.2-2. Simulated maximum location of the salt front with sea level rise during a hypothetical repeat of 1965 flows during the 1960s drought and during a more extreme drought.

Note: TFO = Trenton Flow Objective. The 2,500 cfs Trenton flow objective was maintained in both simulations. The green bars represent the results using 1965 flows with a minimum flow of 2,500 cfs set for Trenton. The orange bars represent the results for simulations of a more extreme drought condition, and the difference in the length between the green and orange bars quantifies the impact from the lower flow conditions.

Table 6.2-1. Simulated maximum salt front locations with sea level rise during a hypothetical repeat of 1965 flows during the 1960s drought and during a more extreme drought condition. A 2,500 cfs Trenton Flow Objective was included in the simulations.

Sea Level Rise (m)	1965 Flow with TEFO (RM)	More Extreme Drought with TEFO (RM)	Difference (mi)
0	94.2	96.9	2.7
0.5	96.8	100.3	3.5
1.0	100.4	103.6	3.2
1.6	104.7	108.1	3.4

It should be noted that the streamflow time series used to represent extreme drought was constructed to approximate a more severe drought than that of the 1960s. The probability of the lower flows occurring in sequence and coincidently in the Delaware and Schuylkill Basins is low but was not calculated. Additional work is needed to develop an alternate streamflow time-series to represent a more severe drought design scenario to evaluate climate change impacts.

6.2.2 Chloride Concentrations

Simulated 30-dma chloride concentrations at RM 98 (Camden) with SLR under the base case 1965 drought condition and under the more extreme drought conditions, respectively, are presented in **Figure 6.2-3** and **Table 6.2-2**. The box plots in **Figure 6.2-3** show that the 30-dma chloride concentrations and the range of concentrations at RM 98 increase with SLR. The simulated 30-dma chloride concentration increases with sea level rise, and the increases are greater during the simulated drought. With 0 m SLR at RM 98, the simulated maximum 30-dma chloride concentration was 119 mg/L during 1965 with Trenton Flow Objective (TFO). Under the more extreme drought conditions with TFO, this simulated concentration increased by 58 percent to 188 mg/L, exceeding the water quality standard of 180 mg/L. For 0.5, 1.0, and 1.6 m SLR in conjunction with the more extreme drought condition and TFO, the respective simulated maximum 30-dma chloride concentrations at RM 98 are 290, 434, and 675 mg/L, which are 63, 65, and 57 percent greater than those simulated under conditions of 1965 during the 1960s drought with TFO.

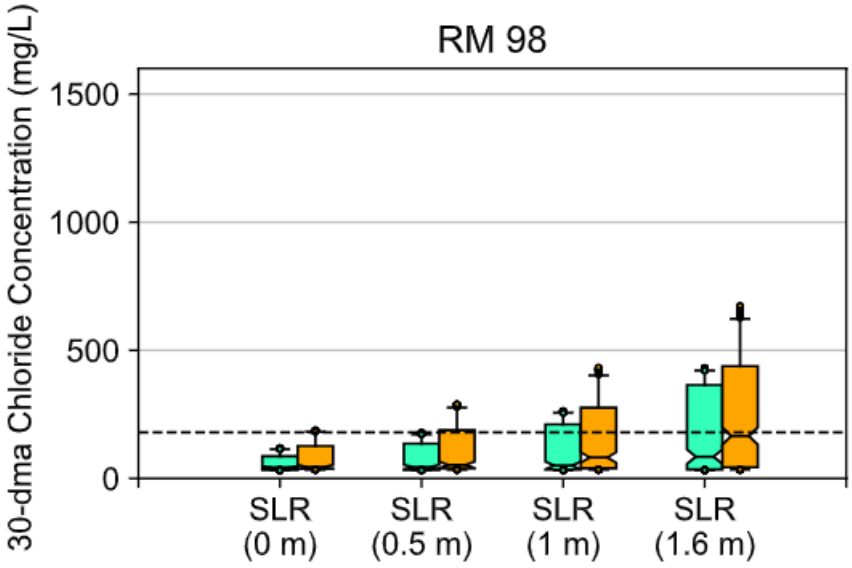

Figure 6.2-3. Range of the 30-dma chloride concentration at RM 98 (Camden) for 1965 hydrology and a more extreme drought, and with and without sea level rise. A 2,500 cfs Trenton Flow Objective was included in all simulations.

Note: dashed line indicates the water quality standard of 180 mg/L chloride concentration at RM 98.

Table 6.2-2. Comparison of simulated maximum 30-dma chloride concentrations at RM 98 (Camden) with sea level rise: 1965 flow with the flow objective and under a more extreme drought condition. A 2,500 cfs Trenton Flow Objective was included in all simulations.

Sea Level Rise (m)	1965 Flow with Flow Objective (mg/L)	More Extreme Drought with Flow Objective (mg/L)	Percent Difference in Maximum 30-dma Chloride Concentration (%)
0	119	188	58
0.5	178	290	63
1	263	434	65
1.6	431	675	57

Table 6.2-3 presents the number of days and the percentage of time that the water quality standard set for RM 98 (Camden) is exceeded during the simulated year. With a more extreme drought and with 0.5 m, 1.0 m and 1.6 m SLR, more than 27, 35 and 44 percent of the time during the simulated year, respectively, the water quality standard was violated.

6.2.3 Salinity

The range of simulated daily depth-averaged salinity with SLR under the base case 1965 conditions and under the more extreme drought conditions are shown in **Figure 6.2-4** and **Figure 6.2-5**, and summarized in **Table 6.2-4**. The ocean salinity remains nearly unchanged with the simulated SLR scenarios, and changes in the depth-averaged salinity in the Lower Bay are minimal as shown in the results at Ship John Shoal, which is 37 miles from the Bay mouth. The impact of extreme drought on salinity intrusion due to SLR becoming more pronounced for locations farther upstream. Depth-averaged salinity increases by 0.6 psu, which is more than a 7 percent increase, at Delaware Memorial Bridge with 0 m SLR for the drought severity scenario in comparison with the 1965 historical drought scenario. The increase in salinity at RM 92.5 is approximately 0.3 psu, a 30 percent increase. Similarly, with 1.0 m SLR, the increase in the depth-averaged salinity is roughly 0.5 psu (6 percent) at Delaware Memorial Bridge and RM 92.5.

Table 6.2-3. Comparison of the number of days (percent of year) the 30-dma chloride concentration at RM 98 (Camden) exceeded the 180 mg/L water quality standard for a more extreme drought and for 1965 flows with sea level rise. A 2,500 cfs Trenton Flow Objective was included in all simulations.

Sea Level Rise (m)	1965 Flow with Flow Objective (days) [percent of year]	More Extreme Drought with Flow Objective (days) [percent of year]	Difference (days)
0	0 [0.0%]	22 [6.1%]	22
0.5	0 [0.0%]	100 [27.6%]	100
1	118 [32.3%]	129 [35.6%]	11
1.6	146 [40.0%]	162 [44.8%]	16

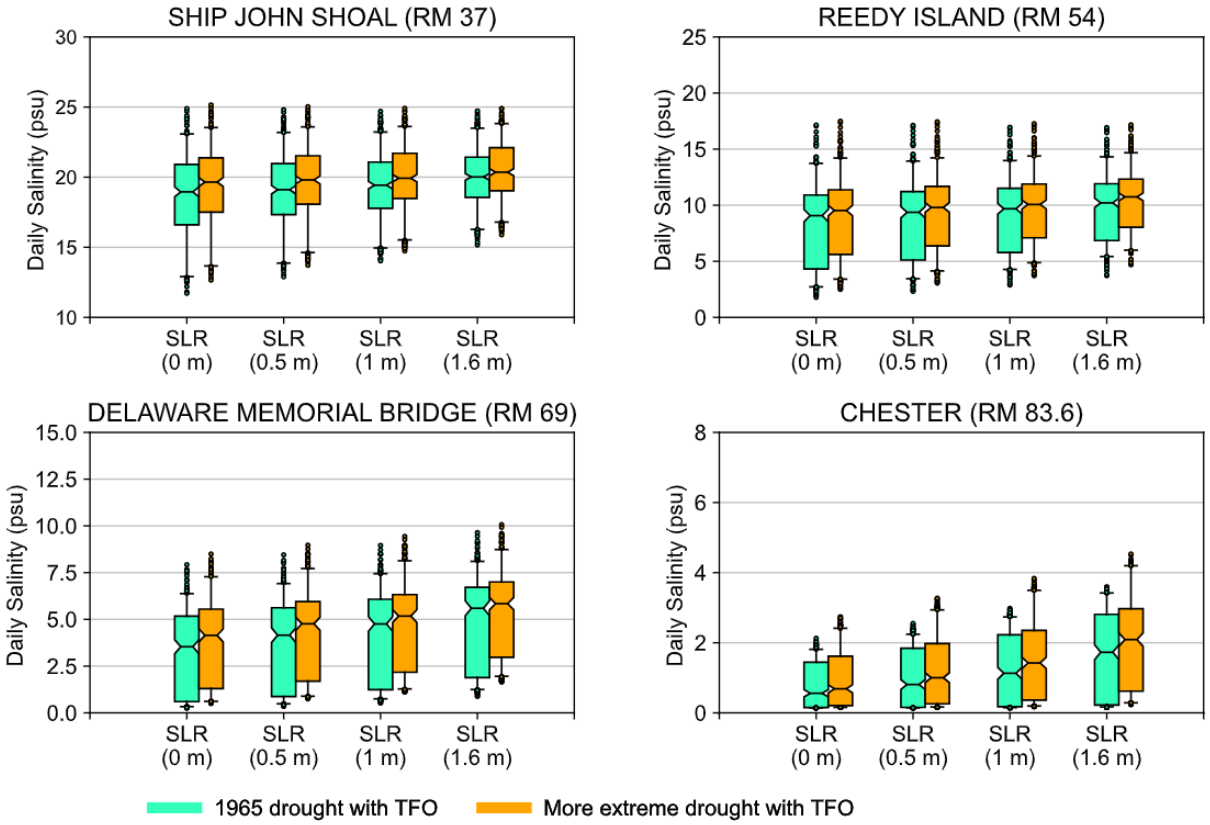

Figure 6.2-4. Range of simulated depth-averaged salinity for a more extreme drought and for 1965 flows during the 1960s drought with and without sea level rise at or downstream stream of Chester. A 2,500 cfs Trenton Flow Objective was included in the simulations.

TFO = Trenton Flow Objective

Simulated along-channel depth-averaged daily maximum salinity profiles comparing results for 1965 conditions and the more extreme drought conditions are presented in **Figure 6.2-6** for three SLR scenarios. Under the more extreme drought conditions, the daily maximum salinity profile shifts farther upstream in comparison with that under the 1965 condition. The differences between the simulated profiles under 1965 conditions and the more extreme drought conditions for two SLR scenarios are shown in **Figure 6.2-7**. The difference resulting from the more extreme drought without SLR is shown as gray dotted lines. The change due to SLR under 1965 flow conditions are shown as dashed lines, and the change resulting from both SLR and more extreme drought are shown as solid lines. It should be noted that the time that maximum salinity was achieved at locations along the Estuary were not the same and varied among different simulation scenarios, and the impact from SLR and extreme drought flow is not additive, nonetheless, the compounding impact from both SLR and the extreme drought appears to be roughly the sum of the individual

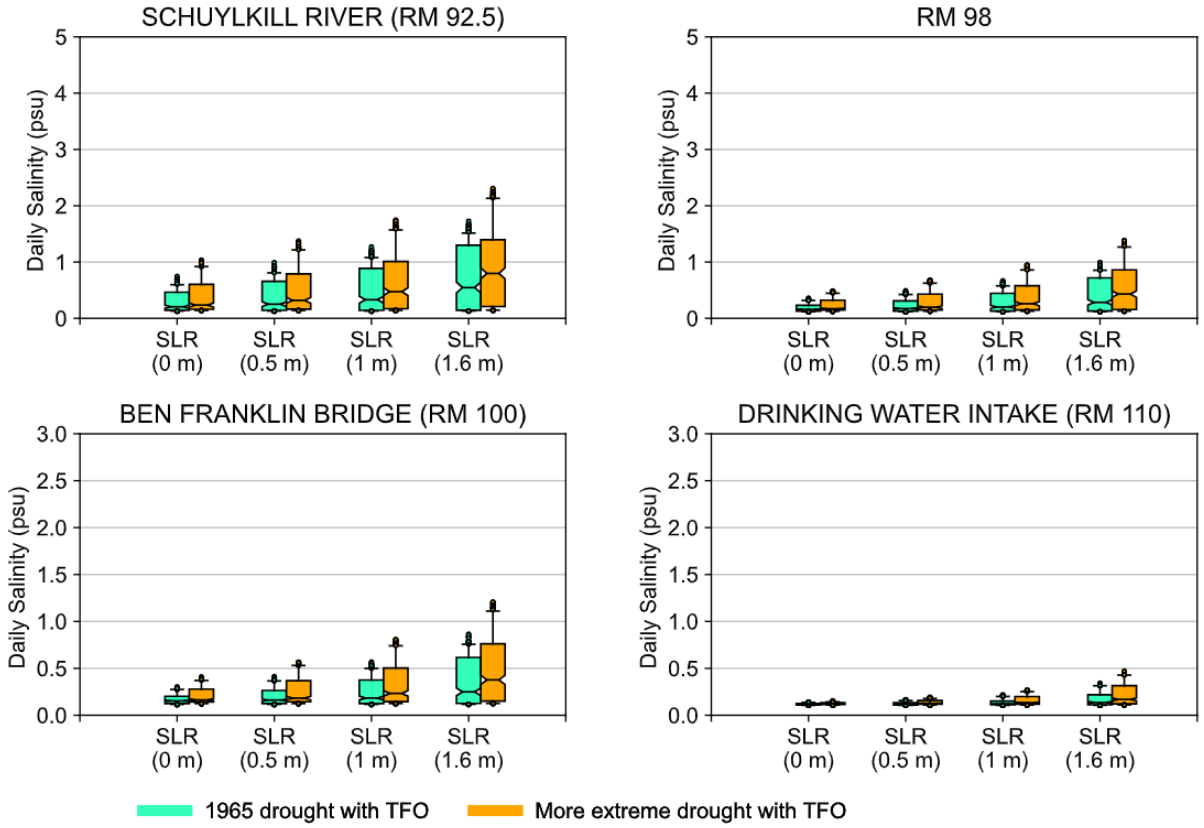

Figure 6.2-5. Range of simulated depth-averaged salinity for a more extreme drought and for 1965 during the 1960s drought, with and without sea level rise at or upstream of Schuylkill River confluence with the Delaware River. A 2,500 cfs Trenton Flow Objective was included in the simulations.

TFO = Trenton Flow Objective

impacts in the upper tidal River above RM 70, where the River width is narrowed and not changed dramatically.

The most significant increase in the maximum depth-averaged salinity occurs between RM 75 and 85 for all cases. The impact to the salinity profile from the more extreme drought flow alone (without SLR) is similar to the impact due to 0.5-m SLR with the 1965 flow conditions and Trenton flow objective applied. In general, SLR in conjunction with extreme drought produced the most significant impact on the salinity in the Delaware Estuary.

Table 6.2-4. Comparison of the maximum daily depth-averaged salinity for a more extreme drought and for 1965 flows during the 1960s drought, with and without sea level rise. A 2,500 cfs Trenton Flow Objective was included in the simulations.

SLR (m)		SHIP JOHN SHOAL RM 37 (psu)	REEDY ISLAND RM 54 (psu)	DELAWARE MEMORIAL BRIDGE RM 69 (psu)	CHESTER RM 83.6 (psu)	SCHUYLKILL RIVER RM 92.5 (psu)	CAMDEN RM 98 (psu)	BEN FRANKLIN BRIDGE RM 100 (psu)	DRINKING WATER INTAKES RM 110 (psu)
0	1965 Conditions	24.9	17.15	7.93	2.13	0.75	0.36	0.3	0.14
	More extreme drought	25.15	17.49	8.5	2.74	1.04	0.49	0.41	0.15
	Percent Diff. (%)	1	2	7	29	39	36	37	7
0.5	1965 Conditions	24.81	17.12	8.46	2.55	0.99	0.49	0.41	0.17
	More extreme drought	25.04	17.44	8.97	3.27	1.37	0.68	0.57	0.2
	Percent Diff. (%)	1	2	6	28	38	39	39	18
1.0	1965 Conditions	24.69	16.94	8.96	2.98	1.27	0.67	0.57	0.22
	More extreme drought	24.91	17.27	9.44	3.83	1.75	0.95	0.81	0.27
	Percent Diff. (%)	1	2	5	29	38	42	42	23
1.6	1965 Conditions	24.72	16.92	9.64	3.59	1.73	1	0.87	0.34
	More extreme drought	24.89	17.17	10.06	4.53	2.31	1.38	1.21	0.47
	Percent Diff. (%)	1	1	4	26	34	38	39	38

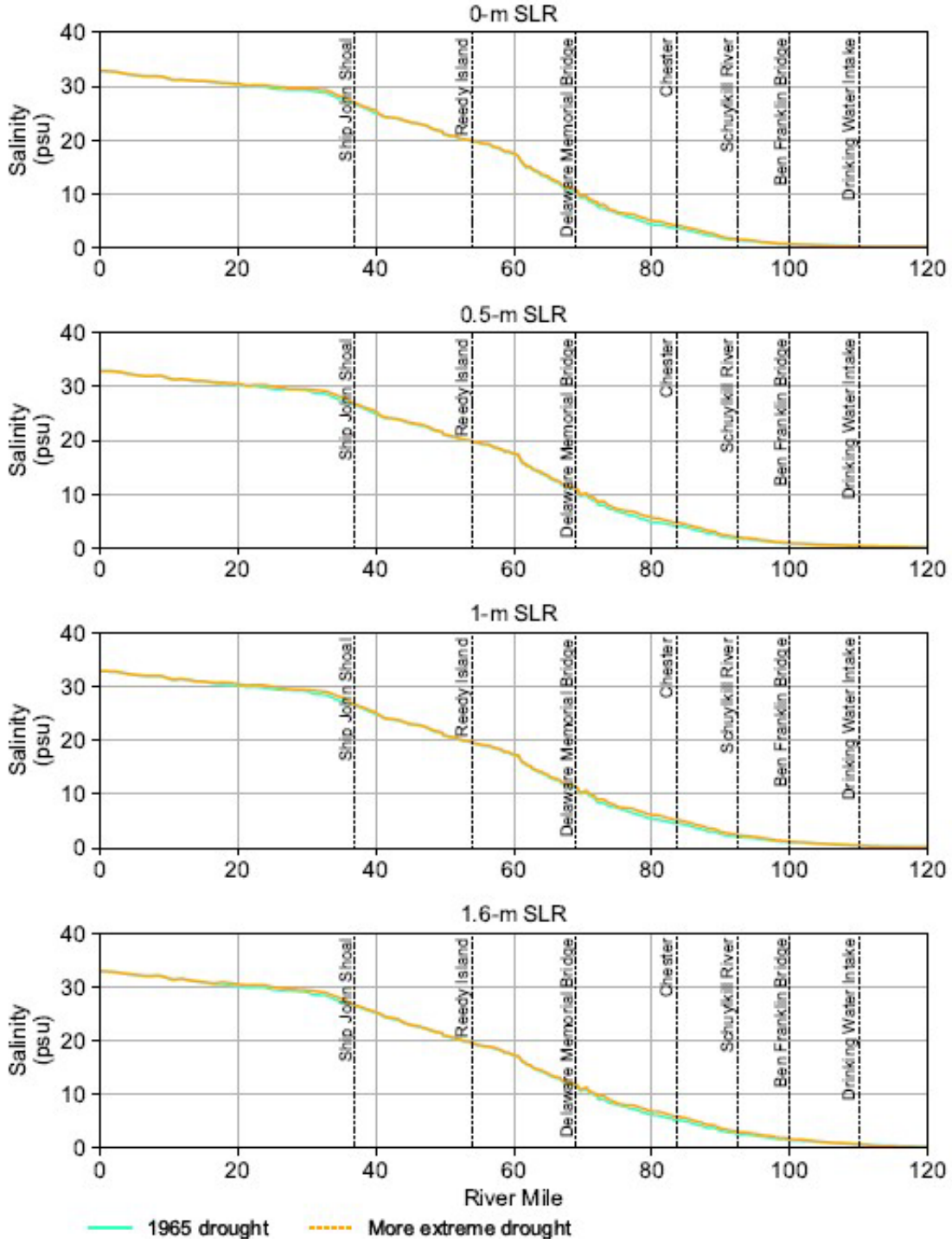

Figure 6.2-6. Simulated daily maximum along-channel salinity from baseline with sea level rise in the Delaware River Estuary: 1965 conditions during the 1960s drought vs. a more extreme drought. A 2,500 cfs Trenton Flow Objective was included in the simulations.

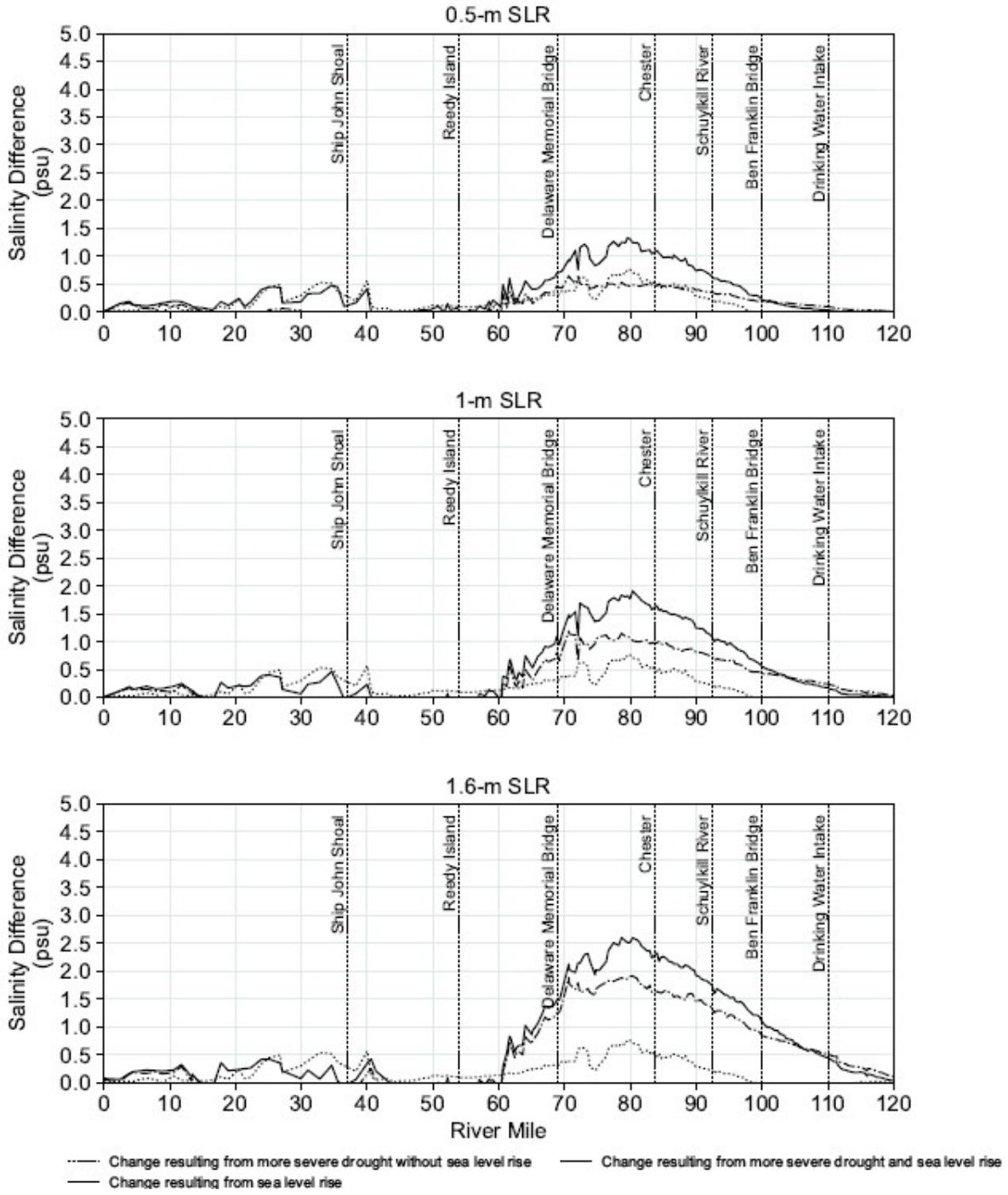

Figure 6.2-7. Increase in simulated maximum along-channel salinity from baseline with sea level rise in the Delaware River Estuary: 1965 conditions during the 1960s drought vs. a more extreme drought. A 2,500 cfs Trenton Flow Objective was included in the simulations.

6.3 Ocean Surface Water Temperature

The density of sea water is a function of the water temperature and the salinity. The density-driven current and exchange flows at the mouth of Delaware Bay are a significant component of salinity transport into the Estuary. One of the boundary conditions in the model is the ocean temperature. Because ocean temperature in the future is uncertain, the sensitivity of model results to the ocean temperature boundary condition was tested. An estimate of the rate of increase in ocean temperature data based on historical data is 0.11°C/decade. For the sensitivity test, the ocean temperature was increased by 1°C, which would be the approximate increase by the end of the century at the current rate of ocean warming and an intermediate value if the rate of temperature increase is accelerated with climate change. The simulations were performed with the moderate low flows of July–October 2002. For all SLR scenarios, increasing ocean temperature by 1°C reduced the maximum salt front location slightly as noted in **Table 6.3-1**. The potential effects of increasing the water temperature of the surface layer in the Estuary on estuarine circulation and salinity intrusion was not evaluated, but these effects may be topics for future investigation.

Table 6.3-1. Predicted salt front location sensitivity to ocean temperature.

SLR (m)	Maximum Salt Front Location (RM)		
	Base	+1°C	Difference
0	90.7	90.4	-0.3
0.5	93.4	93.1	-0.3
1	96.3	95.9	-0.4
1.6	101.4	101.0	-0.4

Note: these simulations used a representative low flow condition from 2002.

6.4 Discussion

Climate change may result in changes in other conditions that could contribute to or exacerbate SLR-driven salinity intrusion. Although ocean temperatures are likely to rise, results of simulations show that an increase in ocean temperature only slightly affects salinity transport in the Estuary. Salinity loads from non-tidal sources including non-tidal tributaries are projected to increase, and point-source salinity loads may also increase in the future. Simulations show that increased salinity loads from these non-tidal sources contribute to higher salinity concentrations in the Estuary and the salt front is farther upstream. However, these loads do not affect the amount of ocean salt entering the Estuary, and the effect of non-tidal sources on the calculated salt front locations is smaller than the effect of SLR by itself. With the changing climate, and despite projections of increased annual precipitation in the Basin, concerns persist about salinity intrusion that might occur with sea level rise in conjunction with a severe drought that is more extreme than the 1960s drought of record. Simulation results show that sea level rise would increase the susceptibility of the major drinking water intakes to salinity intrusion during the more extreme drought conditions simulated. Current measures for drought management may no longer be protective of drinking water intakes from salinity intrusion exacerbated by sea level rise.

The following section presents results of simulations designed to show the effect of flow-augmentation strategies for reducing impacts of sea level rise on salinity intrusion in the Estuary.

.

7. CONCEPTUAL ANALYSIS OF MANAGEMENT ACTIONS FOR REDUCING THE IMPACTS OF SALINITY INTRUSION

Freshwater flowing into the Estuary influences the extent of salinity intrusion, and maintaining or increasing the flow into the Estuary is a means to manage salinity and the salt front. For the development of the Basin-wide drought management program, the Commission engaged the USACE to conduct the "Level B" Study, published in 1981[37], to understand issues related to the conservation and use of water supplies and water-related uses and provide solutions to potential problems. Based on various analyses, using conservative assumptions for consumptive use and accounting for projected sea level rise (unspecified amount), it was determined that a flow on the Delaware River at Trenton of 2,605 cfs could maintain a 30-dma chloride concentration at 180 mg/L at RM 98 to protect the drinking water wells for Camden, NJ, from salinity intrusion during a repeat of the drought of record through the year 2000. Results also indicated that the same flow would limit the maximum instantaneous chloride concentration at the Torresdale Intake of the Philadelphia Water Department to 47 mg/L during such a drought. In addition to the recommended flow rate for salinity repulsion, the report also included other recommendations for maintaining flow in the River, such as water conservation and the acquisition of additional reservoir storage for low flow augmentation. For the drought management program, the flow objective (referred to as the Trenton Flow Objective or TFO) was established to preserve regional storage and repel salinity. The minimum flows TFO range from 2,500 to 2,900 cfs during drought conditions[38]. However, for the purposes of this study, a minimum flow objective of 2,500 cfs was used in simulations for simplicity.

Simulations under future SLR conditions were performed to evaluate three aspects of reservoir releases to repel salinity.

- The first set of simulations was used to demonstrate the effectiveness of the 2,500 cfs Trenton Flow Objective under projected SLR conditions.
- The second set was designed to test the benefit and efficiency of a reservoir pulse release (a temporary sustained increase in flow). For these simulations, the additional water to meet the flow objective or the pulse release is represented as additional flow at Trenton.
- The third set of simulations was performed to determine if the location from where reservoir releases enter the Estuary influences the effectiveness of the additional flow in repelling salinity.

[37] https://www.nj.gov/drbc/library/documents/Level-B-Study_May1981.pdf

[38] Delaware River Basin Water Code, Section 2.5.3. https://www.nj.gov/drbc/library/documents/watercode.pdf

The first two sets of simulations for the flow objective and pulse releases were performed using the historical 1965 inflows. The purpose is to show the effectiveness of the flow objective and pulse releases in repelling salinity driven by sea level rise. The results also provide insight into the vulnerability of the Basin to drought conditions if the storage reserved for making releases is unavailable (due to maintenance, repairs, rehabilitation, or failures). The third analysis regarding the location/source of water for flow augmentation is conceptual and was performed with constant flows from the Delaware and Schuylkill Rivers for simplicity.

7.1 Impact of Flow Objectives

The primary sources of reservoir releases to meet the 2,500 cfs Trenton Flow Objective and repel salinity intrusion during normal and drought conditions are the Beltzville Reservoir in the Lehigh River watershed and the Blue Marsh Reservoir in the Schuylkill River watershed, shown in **Figure 7.1-1**. Although releases from Blue Marsh Reservoir enter the Estuary below Trenton, the additional water released is considered part of the flow needed to meet the Trenton Flow Objective[39]. The Delaware River Basin Commission partially funded construction of the reservoirs and pays for a portion of the operations and maintenance, called joint use maintenance, so that water is available and can be used by the DRBC to meet the Trenton Flow Objective. During drought conditions, additional water from other reservoirs may be used in accordance with the Basin's drought management plan, which is described in the Delaware Basin Water Code (18 CFR Part 410, Sections 2.5.3–2.5.6) and Section 10.4 of the Delaware River Basin Compact. Reservoirs in the Basin that are used for these purposes are shown in **Figure 7.1-1**.

As in prior scenarios with 1965 hydrologic conditions, the flow objective is assumed to be met during the simulation period and is represented by increasing 1965 historical inflows from the Delaware River at Trenton to 2,500 cfs if the value in the flow record was less than 2,500 cfs[40]. The 1965 flows were used, rather than the 2002 low flow period used previously for the sensitivity simulations discussed in Section 5 and 6, because during 2002 the flow objective is already reflected in the historical record and is unrelated to the model configuration. The historical flow used in simulations was adjusted upward for 106 days between June 13 and October 2 and for 21 days in November to meet TFO.

39 The Trenton Flow Objective is also known as the Trenton Equivalent Flow Objective (TEFO) to indicate that water released from Blue Marsh Reservoir, which is located in the Schuylkill River Basin, counts toward meeting the flow objective. For ease of reference, it is called the Trenton Flow Objective.

40 For the purposes of the simulation, the additional water was added to the Delaware inflows.

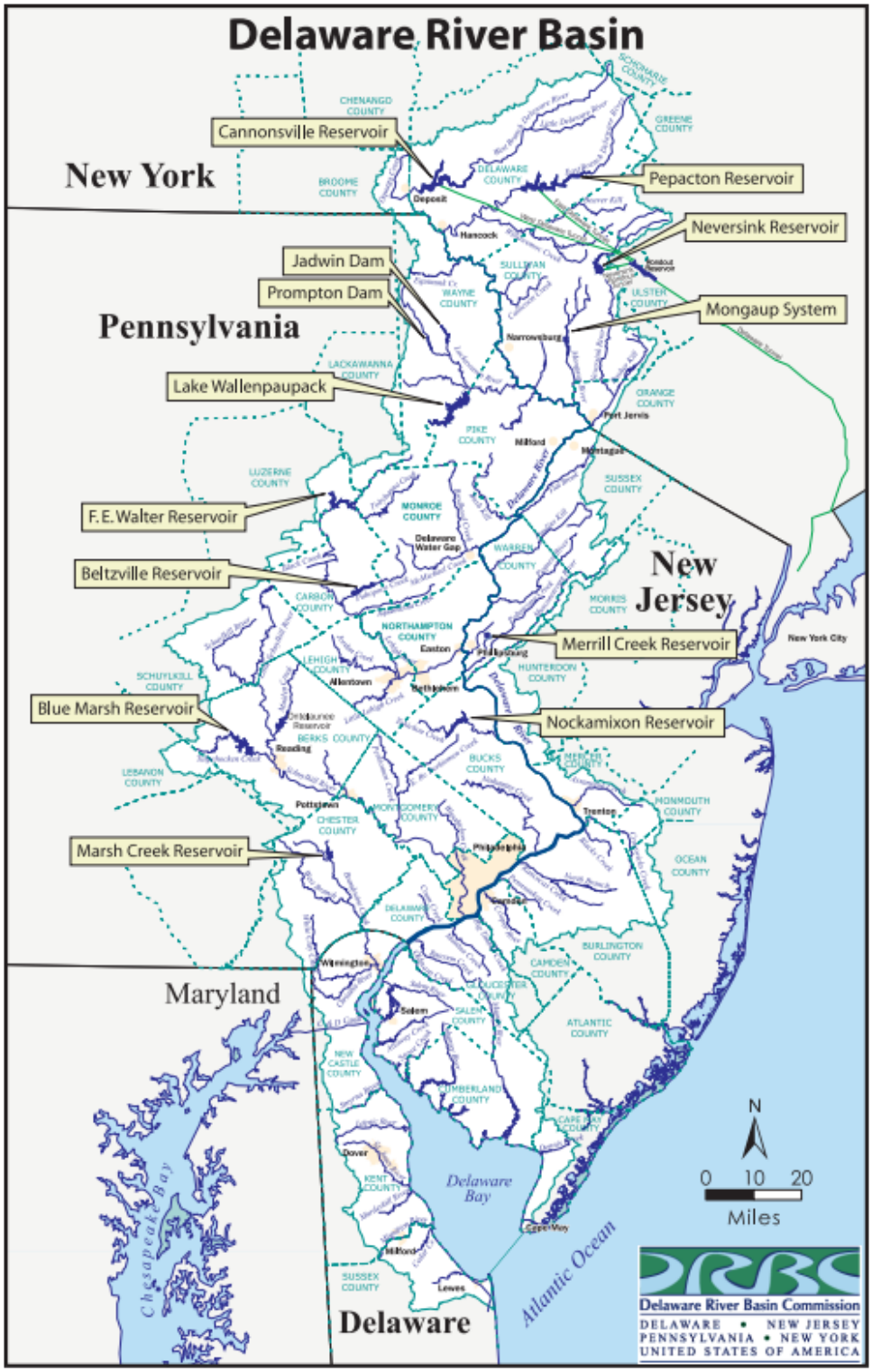

Figure 7.1-1. Reservoirs in the Delaware River Basin

(Available at https://www.nj.gov/drbc/programs/flow/reservoirs.html)

7.1.1 Salt Front

In this section, scenarios are presented to evaluate the influence and benefit of the TFO in countering the impact of sea level rise on salinity intrusion and the maximum salt front location. These analyses also evaluate salinity intrusion that could result due to SLR if TFO could not be maintained during a sustained drought period. Simulation results show that by increasing the flow during 1965 flow conditions to a minimum of 2,500 cfs as needed to reflect the flow objective, the simulated salt front does not advance as far upstream for the selected sea level rise scenarios, as shown in **Figure 7.1-2** and **Table 7.1-1**. For the SLR of 1.6 m without TFO, the maximum salt front location extends as far as RM 109.0, which is 1 mile below the major drinking water intakes. With TFO is met, the maximum salt front location is below RM 105. As shown on **Table 7.1-1**, for the baseline condition (SLR=0 m), the benefit of TFO is to keep the salt front 3.3 miles downstream. With SLR, the benefit of TFO (maintaining flow of at least 2,500 cfs) is to keep the salt front 4.1–4.3 miles downstream. **Figure L.1-1** shows the time series of simulated salt front movement and compares cases with and without the FO for all SLR scenarios in Appendix L.

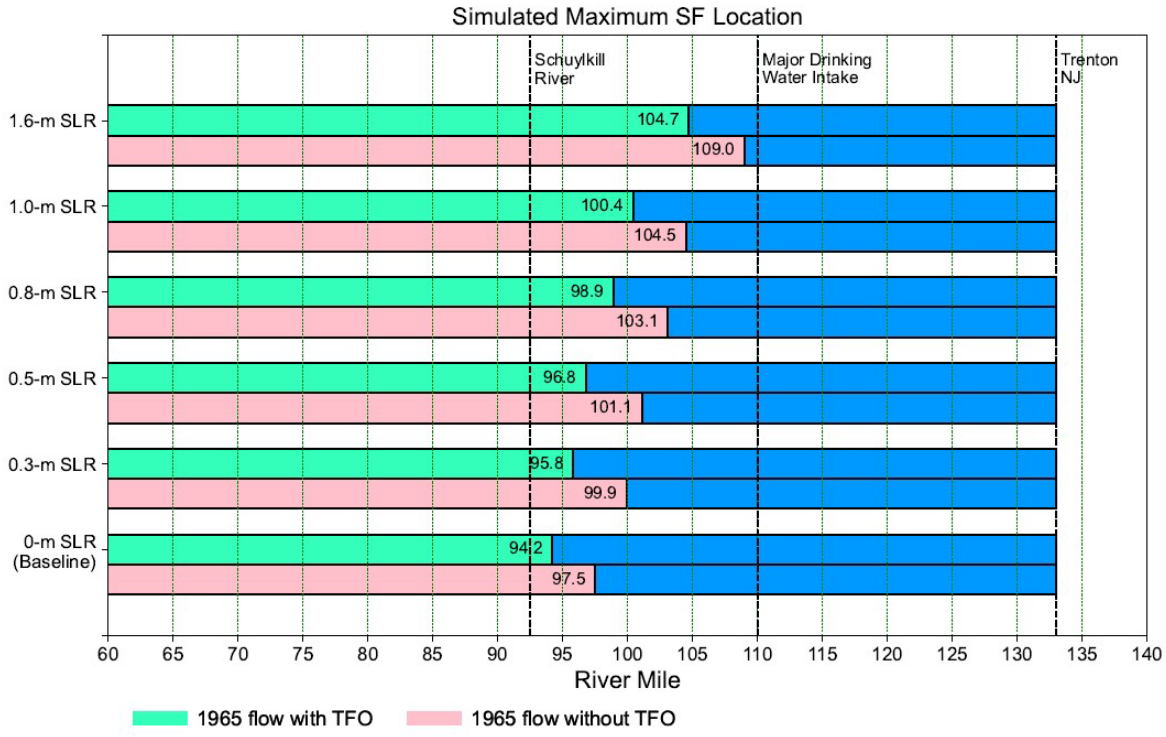

Figure 7.1-2. Simulated maximum salt front location during a repeat of 1965 flows during the 1960s drought with sea level rise: Evaluation of the Trenton Flow Objective.

Note: TFO = Trenton Flow Objective. The edge between blue and green bars is the maximum location of SF with the flow objective; the edge between pink and blue bars is the maximum location of SF without the flow objective.

Table 7.1-1. Simulated maximum salt front location during a repeat of 1965 flows during the 1960s drought with sea level rise: Evaluation of the Trenton Flow Objective.

Sea Level Rise (m)	Maximum Salt Front Location with Historical Flows (River Mile)	Maximum Salt Front Location with Historical Flows plus 2,500 cfs Flow Objective (River Mile)	Change in Simulated Maximum Salt Front Location (mi)
0	97.5	94.2	-3.3
0.3	99.9	95.8	-4.1
0.5	101.1	96.8	-4.3
0.8	103.1	98.9	-4.2
1.0	104.5	100.4	-4.1
1.6	109.0	104.7	-4.3

7.1.2 Chloride Concentrations

The simulated range of the 30-dma chloride concentrations at RM 98 (Camden) for the simulations with 1965 hydrologic conditions and with and without the flow objective is presented in **Figure 7.1-3**. With sea level rise, the chloride concentrations increase because saltwater moves farther upstream.

Figure 7.1-3 presents the maximum 30-dma chloride concentrations at RM 98 and shows that with TFO, the maximum chloride concentration is reduced, and the concentration range is smaller than without TFO. **Table 7.1-2** shows the simulated 30-dma chloride concentration at RM 98 under SLR conditions and with the repeated 1965 flows with and without TFO. The maximum 30-dma chloride concentration at RM 98 without the TFO for the baseline condition is 224 mg/L, and the maximum concentration increases to 322, 489 and 768 mg/L for 0.5 m, 1.0 m and 1.6 m sea level rise, respectively. With the flow objective, the maximum 30-dma chloride concentration at RM 98 is 123, 218, 358, and 607 mg/L for sea level rise of 0 m, 0.5 m, 1.0 m, and 1.6 m, respectively. These concentrations are 45, 32, 27, and 21 percent lower than those resulting with the flow objective, respectively. For 0 m sea level rise with the flow objective, the simulated maximum 30-dma chloride concentration of 123 mg/L at RM 98 is below the water quality standard of 180 mg/L, in concurrence with the design of the standard. However, the results indicate that a

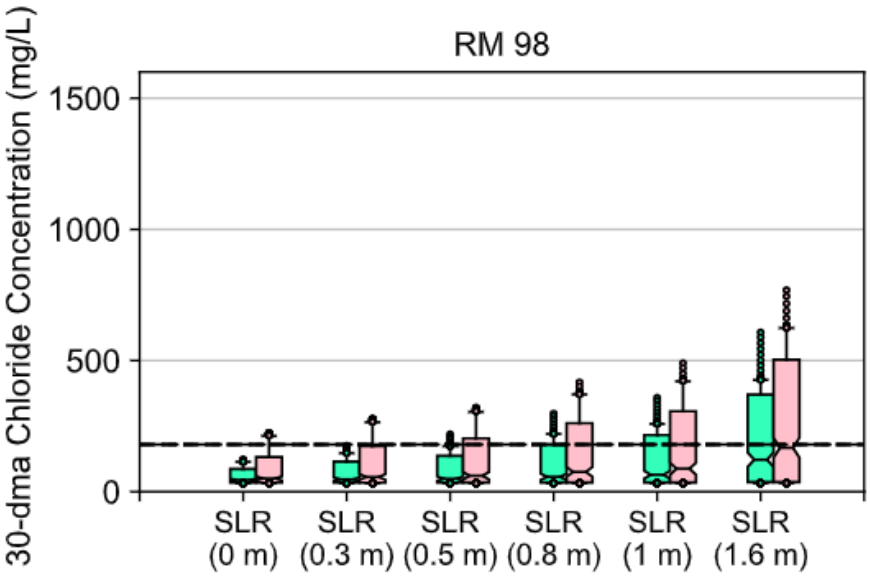

Figure 7.1-3. Range of simulated 30-dma chloride concentrations at RM 98 (Camden) with sea level rise during a repeat of 1965 flows during the 1960s drought: Evaluation of the Trenton Flow Objective.

Note: TFO = Trenton Flow Objective. The horizontal dashed line indicates the water quality standard of 30-dma chloride concentration of 180 mg/L at RM 98.

Table 7.1-2. Simulated maximum 30-dma chloride concentrations at RM 98 (Camden) with sea level rise during a repeat of 1965 flows during the 1960s drought: Evaluation of the Trenton Flow Objective.

Sea Level Rise (m)	Maximum 30-dma Chloride Concentration with Historical Flows (mg/L)	Maximum 30-dma Chloride Concentration with Historical Flows Plus 2,500 cfs Flow Objective (mg/L)	Difference in 30-dma Chloride Concentration (%)
0	224	123	-45%
0.3	278	175	-37%
0.5	322	218	-32%
0.8	417	298	-29%
1.0	489	358	-27%
1.6	768	607	-21%

flow objective of 2,500 cfs may not be adequate for maintaining the water quality standard with a sea level rise of 0.5 m or more, because the simulated maximum 30-dma chloride concentration exceeds the water quality standard 1 percent of the time or more during the drought year simulated (**Table 7.1-3**). Additional modeling would be needed to determine an appropriate flow objective to meet the water quality standard under future sea level rise conditions.

7.1.3 Salinity

Due to the lower salinity of freshwater, the additional flow has a diluting effect in the upper portion of the Estuary. **Figure 7.1-4** and **Figure 7.1-5** present the range of the daily depth-averaged salinity at eight locations for the simulations with and without TFO for 0 m, 0.3 m, 0.5 m, 0.8 m, 1.0 m, and 1.6 m SLR. The differences in the range and maximum salinity with and without TFO and with SLR are evident at all locations.

Table 7.1-3. Simulated days (percent of year) the maximum 30-dma chloride concentration at RM 98 (Camden) exceeds the water quality standard of 180 mg/L with sea level rise during a repeat of 1965 flows during the 1960s drought: Evaluation of the Trenton Flow Objective.

Sea Level Rise (m)	Historical Flows (days) [percent of year]	Historical Flows plus 2,500 cfs Flow Objective (days) [percent of year]	Difference (days)
0	43 [11.8%]	0 [0%]	-43
0.3	84 [23.0%]	0 [0%]	-84
0.5	115 [31.5%]	4 [1.1%]	-111
0.8	150 [41.1%]	91 [24.9%]	-59
1.0	160 [43.8%]	132 [36.2%]	-28
1.6	180 [49.3%]	170 [46.6%]	-10

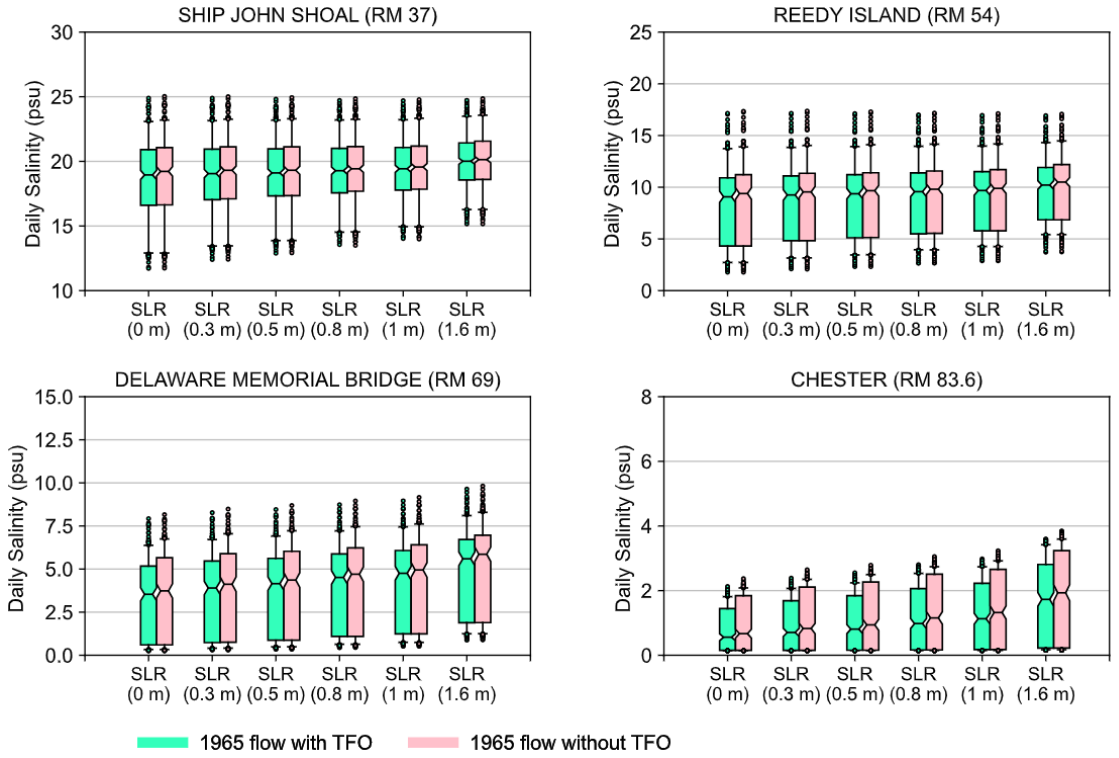

Figure 7.1-4. Simulated daily depth-averaged salinity with sea level rise during a repeat of 1965 flows during the 1960s drought at selected River Mile locations in the Delaware River Estuary at and downstream of the Schuylkill River: Evaluation of the Trenton Flow Objective.

Note: TFO = Trenton Flow Objective.

Table 7.1-4 presents the simulated maximum of the daily depth-averaged salinity. For locations at or below the Delaware Memorial Bridge and regardless of the amount of SLR, the change in salinity is less than 3 percent. At or above Chester, the daily depth-averaged salinity is less than 4 psu for all values of SLR. At Chester, the relative decreases in salinity are 10, 9, 8, and 7 percent for 0 m, 0.5 m, 1.0 m, and 1.6 m of SLR, respectively. At and above Camden (≥ RM 98), and for all values of SLR, the maximum salinity was less than 1.3 psu.

Besides the daily averaged salinity, the instantaneous maximum salinity simulated under SLR conditions is also of interest to assess the risk to water supplies. The simulated hourly salinities at each location along the navigation channel were statistically summarized. The maximum salinity during the simulation period at a given location was used to construct a longitudinal salinity profile representing the instantaneous (hourly) salinity maximum, as shown in **Figure 7.1-6**.The

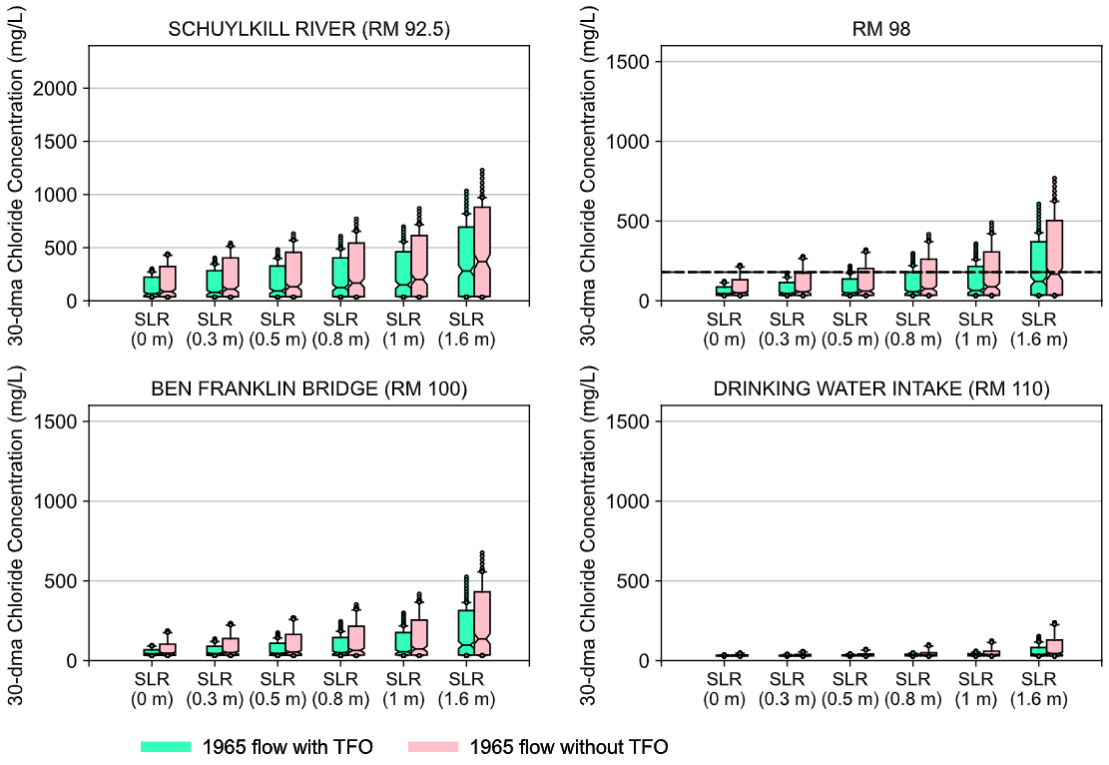

Figure 7.1-5. Simulated daily depth-averaged salinity with sea level rise during a repeat of 1965 flows during the 1960s drought at selected River Mile locations in the Delaware River Estuary at and upstream of the Schuylkill River: Evaluation of the Trenton Flow Objective.

Note: TFO = Trenton Flow Objective.

differences in the simulated maximum salinity longitudinal profile from the baseline with and without TFO for 0.5 m, 1.0 m and 1.6 m of SLR are shown in **Figure 7.1-7**. The difference between values of simulated salinity changes for each SLR increment (the gap between same-colored solid and dotted lines in **Figure 7.1-7**) indicates the relative change in salinity from the base case simulation without the flow objective. For the simulations of 1965 historical flows with and without TFO, the largest differences in the maximum salinity are approximately 1.0–1.2 psu for 1.0 m of SLR and 1.7–1.9 psu for 1.6 m of SLR and occur between the Delaware Memorial Bridge and Chester. With TFO and under 0.5 m, 1.0 m, and 1.6 m of SLR, upstream of Chester (between Chester and RM 110) the maximum salinity is reduced roughly by 0.2 to 0.3 psu. **Figure 7.1-7** show that from the Schuylkill River and upstream, flow augmentation reduces salinity to less than that of the base case without the flow objective at Benjamin Franklin Bridge (RM 100) for SLR of 0.5 m. At the drinking water intakes, the additional water reduces the salinity at 1.6 m SLR by twice as much as for 1.0 m of SLR. Additional discussion is presented in Appendix L.1.

Table 7.1-4. Simulated maximum of daily depth-averaged salinity with sea level rise during a repeat of 1965 flows during the 1960s drought with flow objective, at selected locations in the Delaware Estuary:

SLR (m)		SHIP JOHN SHOAL RM 37	REEDY ISLAND RM 54	DELAWARE MEMORIAL BRIDGE RM 69	CHESTER RM 83.6	SCHUYLKILL RIVER RM 92.5	CAMDEN RM 98	BEN FRANKLIN BRIDGE RM 100	DRINKING WATER INTAKES RM 110
0	1965	25.03	17.34	8.16	2.37	0.91	0.52	0.45	0.19
	1965 with FO	24.9	17.15	7.93	2.13	0.75	0.36	0.3	0.14
	% Diff	-1%	-1%	-3%	-10%	-18%	-31%	-33%	-26%
0.3	1965	25	17.37	8.48	2.65	1.07	0.61	0.53	0.22
	1965 with FO	24.89	17.16	8.27	2.39	0.89	0.43	0.36	0.16
	% Diff	-1%	-1%	-3%	-10%	-18%	-31%	-33%	-26%
0.5	1965	24.94	17.3	8.69	2.79	1.16	0.68	0.59	0.24
	1965 with FO	24.81	17.12	8.46	2.55	0.99	0.49	0.41	0.17
	% Diff	-1%	-1%	-3%	-9%	-15%	-28%	-31%	-29%
0.8	1965	24.84	17.17	8.95	3.05	1.34	0.79	0.7	0.3
	1965 with FO	24.71	17	8.74	2.81	1.15	0.59	0.5	0.19
	% Diff	-1%	-1%	-2%	-8%	-14%	-25%	-29%	-37%
1.0	1965	24.78	17.13	9.16	3.23	1.47	0.88	0.79	0.34
	1965 with FO	24.69	16.94	8.96	2.98	1.27	0.67	0.57	0.22
	% Diff	0%	-1%	-2%	-8%	-14%	-24%	-28%	-35%
1.6	1965	24.85	17.06	9.82	3.84	1.96	1.23	1.11	0.54
	1965 with FO	24.72	16.92	9.64	3.59	1.73	1	0.87	0.34
	% Diff	-1%	-1%	-2%	-7%	-12%	-19%	-22%	-37%

Note: FO = Flow objective; salinity unit is psu. Percent difference is rounded to integers.

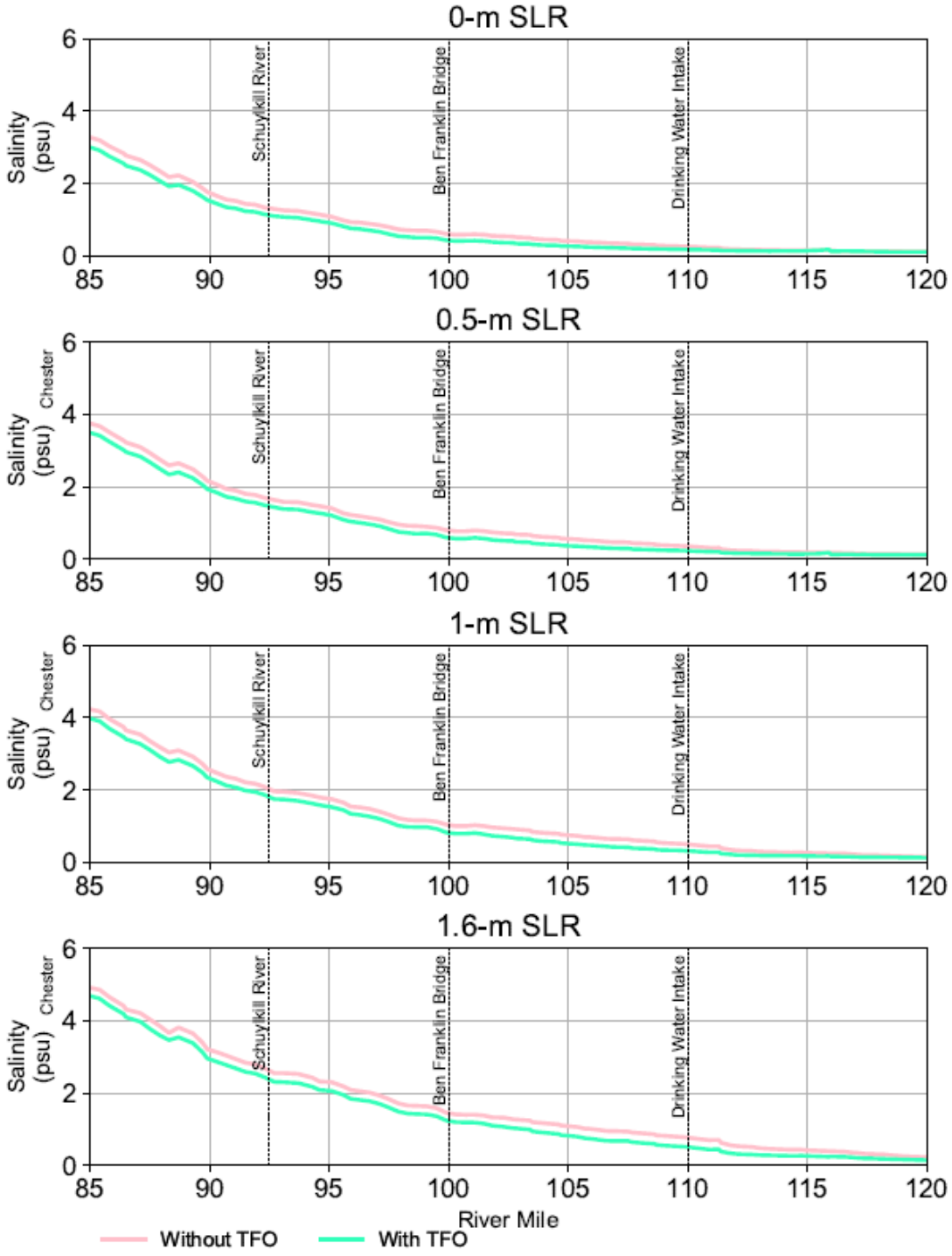

Figure 7.1-6. Simulation maximum along-channel depth-averaged salinity with sea level rise during a repeat of 1965 flows during the 1960s drought in the Delaware Estuary: Evaluation of the Trenton Flow Objective.

Note: TFO= "Trenton Flow Objective". All differences are referenced to the same baseline simulation of 1965 flow without TFO and 0 m SLR.

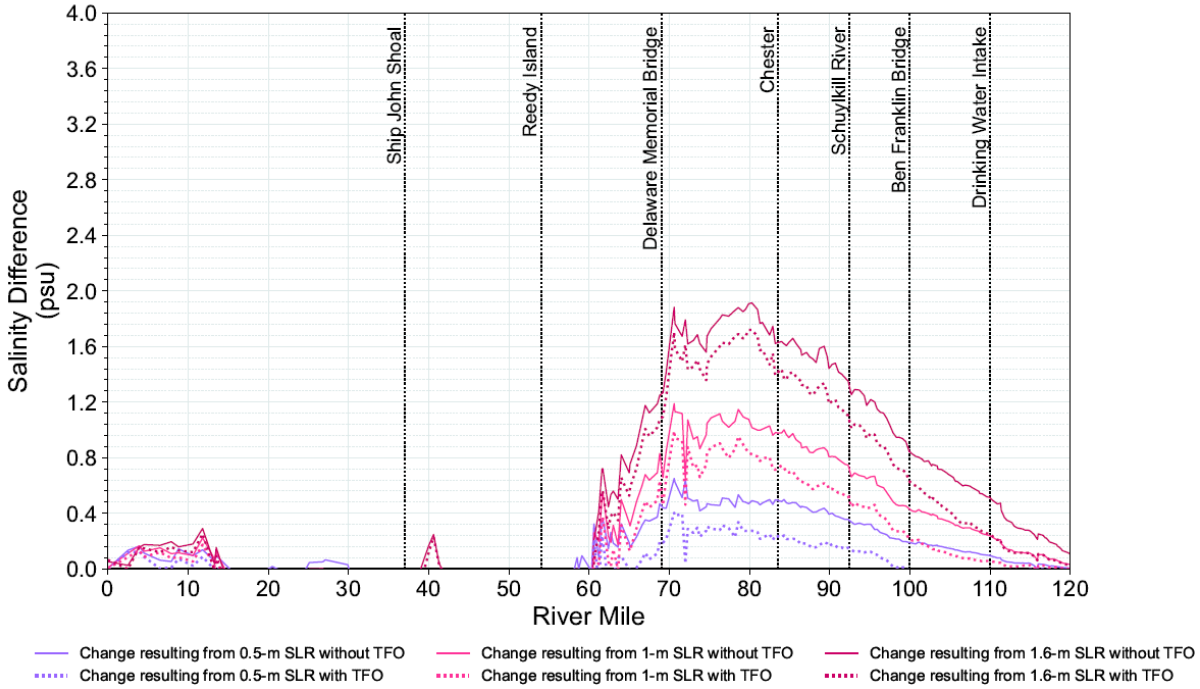

Figure 7.1-7. Simulated change from baseline (0 m SLR without TFO) in the maximum along-channel depth-averaged salinity during 1965 in the Delaware Estuary: Evaluation of the Trenton Flow Objective.

Note: "TFO" = "Trenton Flow Objective". Change is referenced to the same baseline simulation without TFO. The benefit from TFO is shown as the gap between solid and the dotted lines.

7.2 Impact of Pulse Releases on Salinity Intrusion

Results of simulations presented in Section 7.1 previously imply that a minimum flow objective of 2,500 cfs may not be effective in repelling salinity in the future. Another conceptual salinity management option is pulse releases. Simulations were performed to determine if a short-term increase in flow with a pulse of water, rather than a higher flow objective, could be used to reduce the impacts of SLR-driven salinity intrusion. The concept is that a pulse with a trigger, rather than a constant higher flow objective, saves water.

Pulses were simulated by increasing the modified 1965 flows at Trenton from September 1 through September 25 of the simulation year by a constant value (500 or 1,000 cfs) in addition to the 2,500 cfs TFO, as depicted in the top panel of **Figure 7.2-1**. For the baseline case of 0 m SLR, the pulse is initiated when the salt front reaches RM 92.5 on September 1 and discontinued on September 26 because a rainfall event resulted in natural flow of more than 2,500 cfs for four days. For the SLR simulations, the pulse occurs during the same period, even though the salt

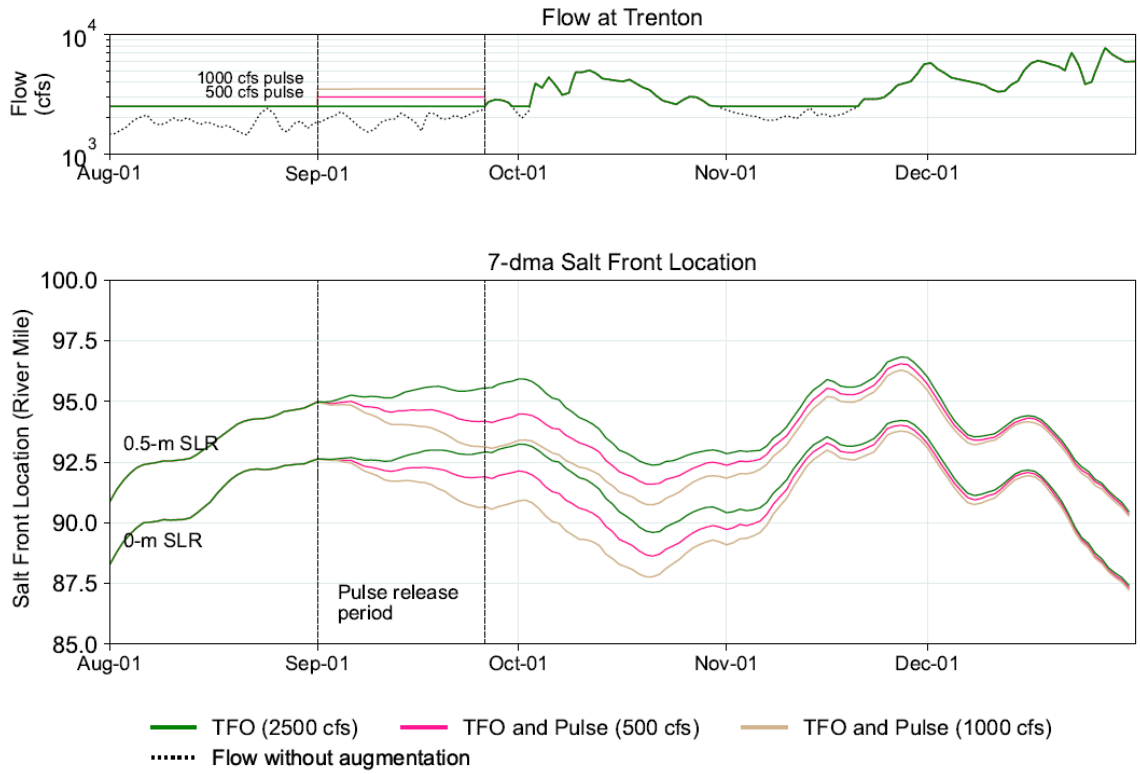

Figure 7.2-1. Inflow conditions and simulated salt front location with sea level rise during a repeat of 1965 flows during the 1960s drought with a 2,500 cfs flow objective at Trenton, NJ: Evaluation of Pulse Releases through the end of December.

Note: the color refers to the flow cases. The pulses were simulated by increasing the 1965 flow at Trenton (with the 2,500 cfs flow objective) from September 1 through September 25 by a constant value 500 or 1,000 cfs.

front is farther upstream, so that the pulse is the only variable altered (e.g., the timing and tide-flow combination can affect results). Post-pulse, two rainfall events occurred, one immediately after the pulse and one in October. It should be noted that the historical flows in 1965 were much lower than 2,500 cfs from June–September, but briefly larger in October after which another low flow period occurred in November.

7.2.1 Salt Front

The pulse simulations were performed for the baseline (0 m SLR) and 0.5 m, 1.0 m, and 1.6 m of SLR. **Figure 7.2-1** presents the simulated flow of the Delaware River at Trenton compared to the flow without TFO (top frame) and the simulated salt front location (bottom frame) with and without pulses from August 1 through December 31For the baseline (0 m SLR) simulations without a pulse and with TFO of 2,500 cfs, the salt front moves steadily (relatively) upstream to RM 93.2

until early October, when it begins to move downstream after the increase in natural flow in October. After 3 weeks, the salt front begins to move upstream again. The rate accelerates after the first week in November, when the flow is back to 2,500 cfs (the minimum TFO). The salt front continues to advance upstream even with flows above 2,500 cfs, until the third week in November, when it reaches its maximum location for the year at RM 94.2. The flow increases again in December, and the salt front moves downstream. The movement of the salt front is similar for all values of SLR but differs in magnitude with the amount of the pulse release. **Table 7.2-1** presents the maximum salt front location for the baseline (0 m) and SLR (0.5 m, 1.0 m, and 1.6 m) with and without pulses between September 25 and October 31 and between January 1 and December 31 to quantify the near-term and longer-term effects of the pulse releases. The distance the pulse moves the maximum salt front location downstream increases with the pulse rate and SLR, except the near-term effect of the 1,000 cfs pulse at 1.6 m (-3.2 miles difference) is slightly less than at 1.0 m (-3.3 miles difference).

Table 7.2-1. Simulated maximum salt front location with sea level rise. Maximum salt front location for September 25 through October 31 (near-term) and the full year are presented.

Additional Pulse Release (cfs)	SLR (m)	Near Term (9/25 through 10/31)			Long Term (1/1 through 12/31)		
		WITHOUT Pulse Release (RM)	WITH Pulse Release (RM)	Diff. (mi)	WITHOUT Pulse Release (RM)	WITH Pulse Release (RM)	Diff. (mi)
500	0	93.2	92.1	-1.1	94.2	94.0	-0.2
	0.5	95.9	94.5	-1.4	96.8	96.5	-0.3
	1.0	99.5	97.6	-1.9	100.4	100.0	-0.4
	1.6	104.4	102.8	-1.6	104.7	104.2	-0.5
1000	0	93.2	90.9	-2.3	94.2	93.8	-0.4
	0.5	95.9	93.4	-2.5	96.8	96.3	-0.5
	1.0	99.5	96.2	-3.3	100.4	99.7	-0.7
	1.6	104.4	101.3	-3.2	104.7	103.8	-0.9

Note: The salt front reaches maximum in late November when the impact from the pulse release has dissipated. Another pulse release would be needed to repel the salt front in early November.

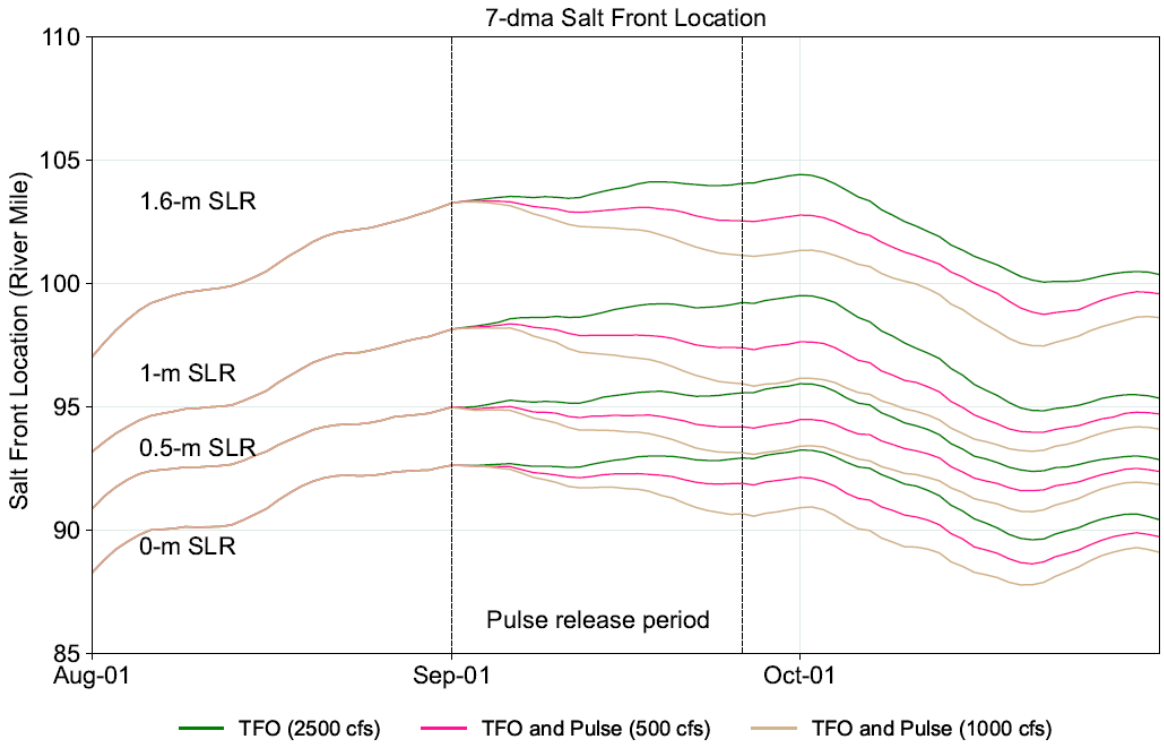

Figure 7.2-2. Simulated location of the salt front with sea level rise during a hypothetical repeat of 1965 flows during the 1960s drought with a 2,500 cfs flow objective at Trenton, NJ during August through October: Evaluation of Pulse Releases through the end of October.

Note: the color code refers to the flow cases. The pulses were simulated by increasing the 1965 flow at Trenton (with the 2,500 cfs flow objective) from September 1 through September 25 by a constant value 500 or 1,000 cfs.

Figure 7.2-2 presents the simulated salt front location with and without pulses from August 1 through October 31 to illustrate the effect of the pulse releases in more detail. The salt front starts at the same location for the no pulse and pulse simulations prior to the pulse. Upon initiation of the pulse, the salt front immediately begins to move downstream becoming increasing farther downstream than the salt front in the no-pulse simulation. The salt front then begins to move back upstream at the same rate until the flow increases in early October, when the salt front moves downstream as expected. While the flows are still higher than the flow objective, the distance between the pulse and no pulse salt front remains roughly the same. Once the flow decreases to 2,500 cfs at the end of October, the salt front begins to move upstream again at a faster rate than the no pulse salt front, decreasing the distance between the pulse and no pulse salt front locations (**Figure 7.2-1**). By the end of November, the salt front has almost returned to the pre-pulse location for the no pulse and pulse simulations, due to the second low flow period beginning in late October. Another pulse would be needed to keep the salt front below the second maximum

location. It is worth noting that the salt front locations in the pulse simulations do reach the no-pulse location before the end of the year. Thus, for this simulation, the effect of the pulse persisted, albeit with diminishing benefit, for almost two months after the termination of the pulse, possibly longer. **Figure 7.2-3** presents the maximum salt front location for the pulse simulations between September 1 and October 31 to isolate the near-term effect of the pulses. Depending on the amount of SLR, when the pulse is terminated on September 26, the distance the pulse moved the salt front downstream is 1.1-1.9 miles for 500 cfs and 2.3-3.3 miles for 1,000 cfs (**Table 7.2-1**).

It should be noted that the pulse simulations were performed as a conceptual sensitivity analysis and do not represent a proposal and/or test of a new flow objective or release program. The assumptions for the timing, duration, and amount of additional flow were not intended to imply, justify, or quantify the need for additional flow augmentation, but rather to inform the scoping of future planned projects. More research is needed to develop an understanding of the balance

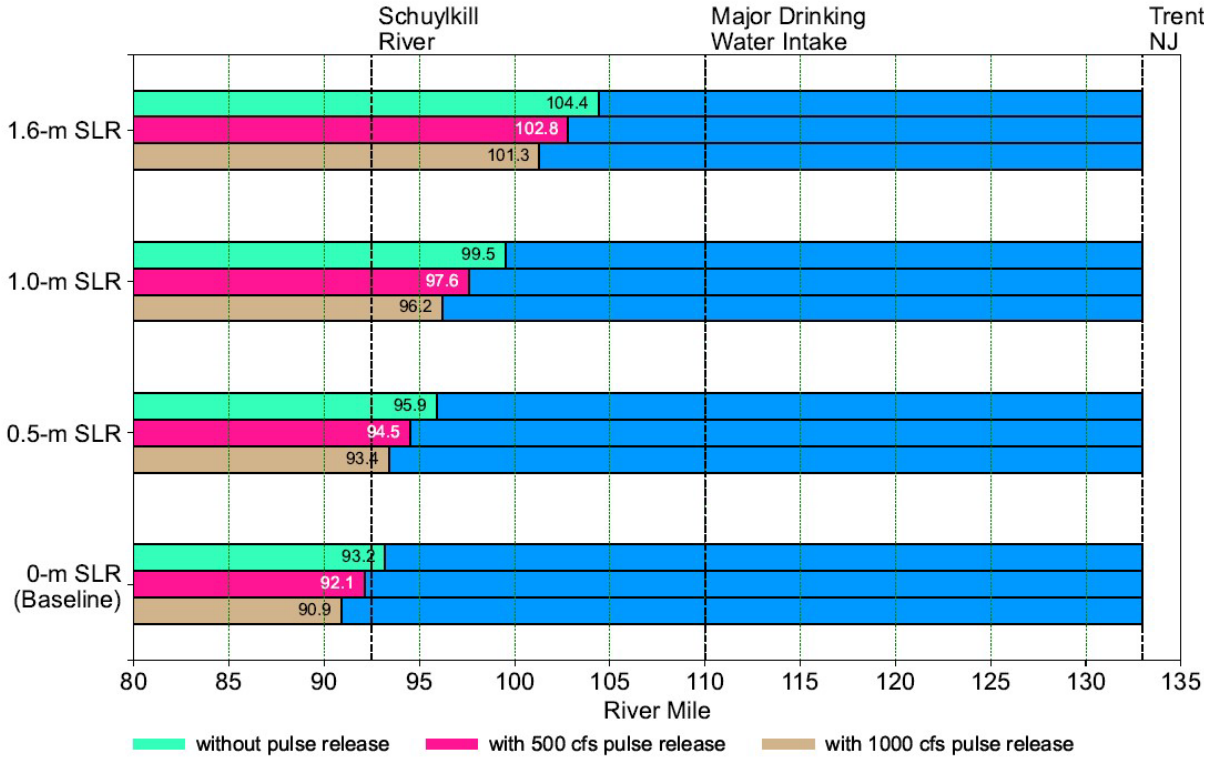

Figure 7.2-3. The effect of flow augmentation and sea level rise on the simulated maximum salt front location (between September 1 and October 31) following a pulse release.

Note: the color code refers to the flow cases. The pulses were simulated by increasing the 1965 flow at Trenton (with the 2,500 cfs flow objective) from September 1 through September 25 by a constant value 500 or 1,000 cfs. Simulated 7-dma SF during 9/25 through 10/31 were used in this analysis.

among SLR (tides and ocean forcing), flow, and salt front location prior to flow augmentation. DRBC studies are underway to examine different methods of flow augmentation (revised flow objectives, pulses), criteria for initiation and discontinuance, and how to best use existing water resources for salinity repulsion.

7.2.2 Chloride Concentrations

The simulated range of 30-dma chloride concentrations at RM 98 (Camden) for simulations with and without pulse releases from September through December (122 days) of the simulated year are presented in **Figure 7.2-4**, and the simulated maximum 30-dma Chloride Concentration at RM 98 (Camden) during September through December are shown in **Table 7.2-2.** The durations of exceedances of the chloride concentration standard are shown in **Table 7.2-3**.

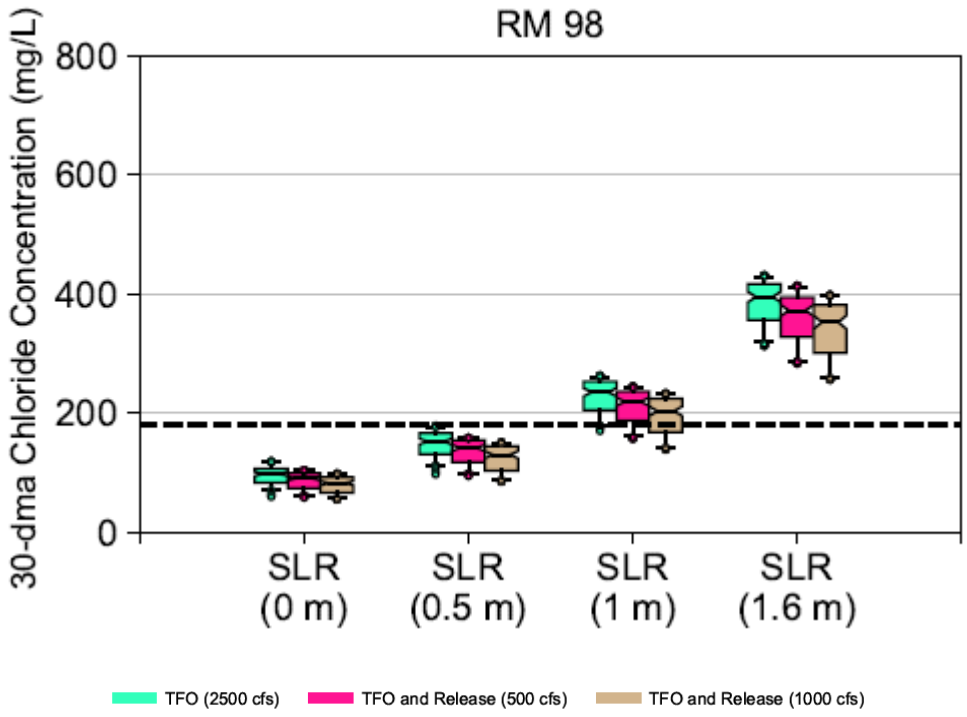

Figure 7.2-4. Simulated 30-dma chloride concentration at RM 98 (Camden) with SLR during September through December: Evaluation of Pulse Releases.

Note: the pulses were simulated by increasing the 1965 flow at Trenton with the 2,500 cfs TFO from September 1 through September 25 by a constant value (500 or 1,000 cfs). The statistical measurements were based on the simulation results from September 1 through December 31. The impact from the pulse release was felt throughout the end of the year. The horizontal dashed line indicates the water quality standard of 30-dma chloride concentration of 180-mg/L at RM 98.

Table 7.2-2. Simulated maximum 30-dma chloride concentration at RM 98 (Camden) during September through December.

Sea Level Rise (m)	With Flow Objective (mg/L)	With Flow Objective and 500 cfs Pulse (mg/L)	Percent Difference (%)	With Flow Objective and 1000 cfs Pulse (mg/L)	Percent Difference (%)
0	119	104	-13	98	-18
0.5	178	158	-11	150	-16
1	263	244	-7	233	-11
1.6	431	414	-4	398	-8

Note: the color code refers to the flow cases. The pulses were simulated by increasing the 1965 flow at Trenton (with the 2,500 cfs flow objective) from September 1 through September 25 by a constant value 500 or 1,000 cfs.

Table 7.2-3. Summary of percent exceedance of the 30-dma-180 mg/L chloride concentration water quality standard at RM 98 (Camden) during September through December.

SLR (m)	Without Pulse Release	With 500 cfs Pulse Release		With 1000 cfs Pulse Release	
	Number of Days Exceeded Water Quality Standard (days) [percent of time]	Number of Days Exceeded Water Quality Standard (days) [percent of time]	Difference (days)	Number of Days Exceeded Water Quality Standard (days) [percent of time]	Difference (days)
0	0 [0%]	0 [0%]	0	0 [0%]	0
0.5	0 [0%]	0 [0%]	0	0 [0%]	0
1.0	113 [92.6%]	98 [80.3%]	-15	80 [65.6%]	-33
1.6	122 [100%]	122 [100%]	0	122 [100%]	0

Note: a time series plot for the simulated 30-dma-180 mg/L chloride concentration is presented in Appendix L.2.

The water quality standard for the 30-dma chloride concentration of 180 mg/L is satisfied under the baseline condition (0 m SLR) and for 0.5 m SLR with or without the pulse release. With 1.0 m SLR, the maximum simulated 30-dma chloride concentration at RM 98 (Camden) is reduced from 263 mg/L to 244 mg/L (-7 percent) and to 233 mg/L (-11 percent) with 500 cfs and 1,000 cfs pulse releases, respectively. With 1.6 m SLR, the maximum simulated 30-dma chloride concentration at RM 98 is reduced from 431 mg/L to 414 mg/L (4 percent) and 398 mg/L (-8 percent) with 500 cfs and 1,000 cfs pulse releases, respectively.

Pulses are not needed during the baseline or 0.5 m SLR simulations to meet the chloride standard. Without pulses, the standard is exceeded 113 days (92.6%) and all of the 122 days, respectively, for 1.0 m and 1.6 m SLR (**Table 7.2-3**). With pulses and 1.0 m SLR, the 30-dma concentration is higher than the standard for 15 fewer days with a 500 cfs pulse and 33 fewer days for a 1,000 cfs pulse. For 1.6 m SLR, the simulated 30-dma chloride during September through December is always exceeded, regardless of the pulse volume.

7.2.3 Salinity

The simulated range of the daily depth-averaged salinity at selected locations in the Delaware Estuary from September 25 through October 31 (total 37 days) of the simulated year are presented in **Figure 7.2-5** and **Figure 7.2-6**to illustrate the effect of pulse releases on salinity. The results are summarized from September 25 to October 31 (total 37 days). The effect of the pulse release builds through September and diminishes after October 31 and is most pronounced during that period. By November, the simulated salinity returns to a level comparable to the simulations without the pulse release. The maximum of the daily depth-averaged salinity at the selected locations during this period is presented in **Table 7.2-4.** The relative decrease in the maximum of the daily depth-averaged salinity ranges from 3 to 26 percent at locations at upstream of Chester (RM 83.6). From the Delaware Memorial Bridge (RM 69) and downstream, the effect of the pulse releases on the maximum daily depth-averaged salinity was less than or equal to 2 percent.

Along-channel profiles for the simulated 37-day period maximum instantaneous depth-averaged salinity based on hourly model output are presented in **Figure 7.2-7**, focused upstream of RM 75. Differences in the maximum salinity resulting from the pulse releases for SLR scenarios are presented in **Figure 7.2-8.** The differences by River Mile are larger upstream of the Delaware Memorial Bridge (RM 69) because the additional fresh water from the pulse is pushing the salt water farther downstream. The difference between scenarios with and without the pulses are in the range of 0 to 0.2 psu compared to the difference in the sea level rise scenarios by up to 1.75 psu. The maximum decrease in the maximum instantaneous depth-averaged salinity is near RM 80 with the 1000 cfs pulse release.

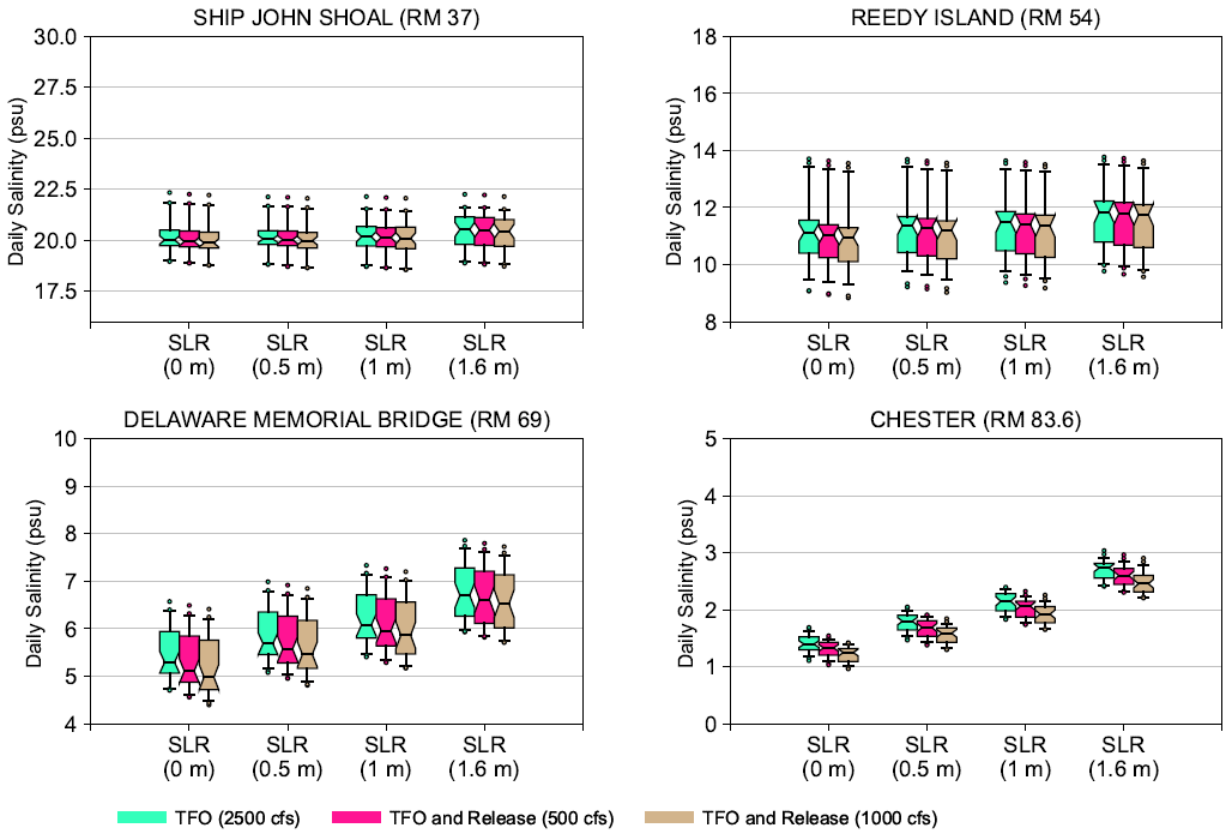

Figure 7.2-5. Simulated maximum of the daily depth-averaged salinity at four selected locations on the Delaware River downstream of the Schuylkill River during September 25 to October 31: Evaluation of pulse releases.

Note: the color code refers to the flow cases. The pulses were simulated by increasing the 1965 flow at Trenton (with the 2,500 cfs flow objective) from September 1 through September 25 by a constant value 500 or 1,000 cfs.

A time series plot of simulated salinity at RM 98 during September 1 through October 31 is presented in **Figure L.2-3** in Appendix L. The maximum instantaneous depth-averaged salinity during this period occurred around October 1. The difference between values of simulated salinity changes for each SLR increment (the gap between same-colored solid and dotted lines in **Figure 7.2-8**) indicates the extent of return to the baseline salinity that results from the pulse flow

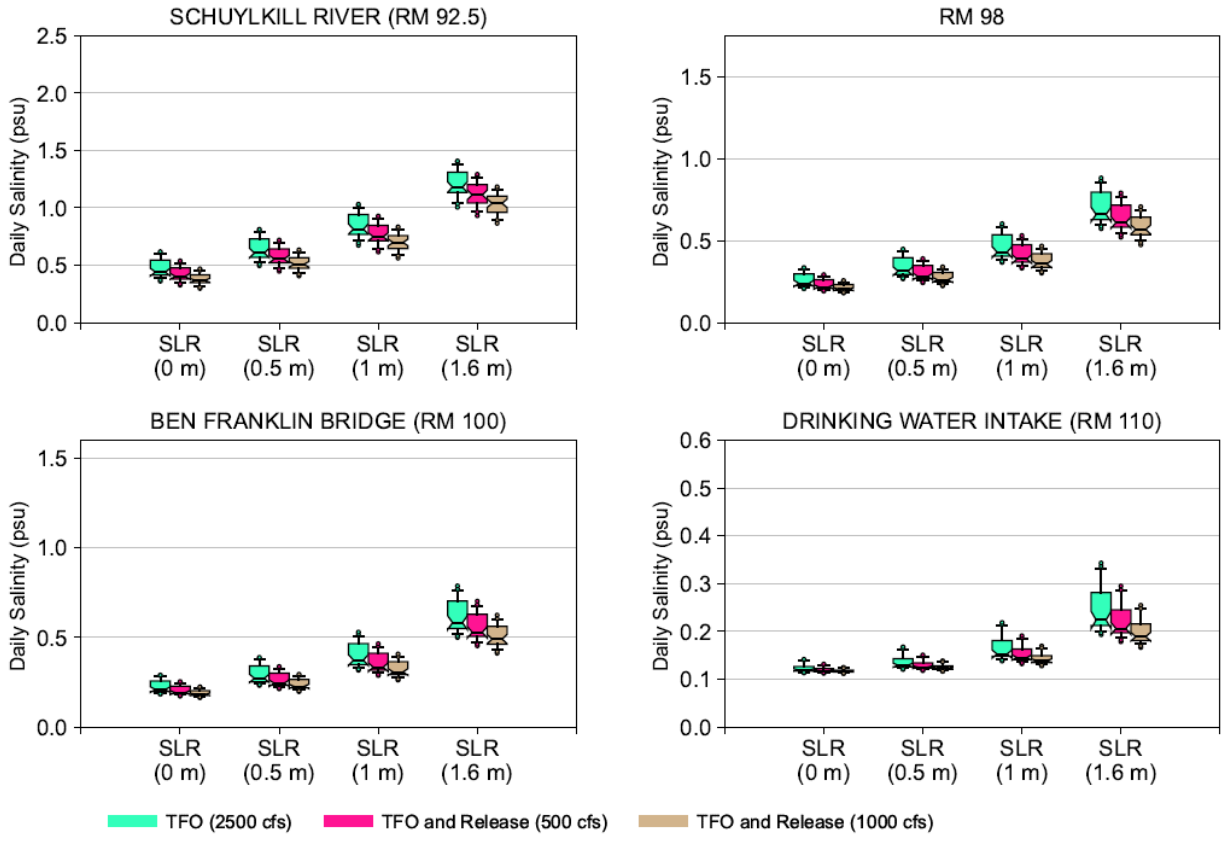

Figure 7.2-6. Simulated maximum of the daily depth-averaged salinity at selected locations on the Delaware River upstream of the Schuylkill River during September 25 to October 31: Evaluation of pulse releases.

Note: the color code refers to the flow cases. The pulses were simulated by increasing the 1965 flow at Trenton (with the 2,500 cfs flow objective) from September 1 through September 25 by a constant value 500 or 1,000 cfs.

augmentation. For the tidal River upstream of Chester (RM 83.6), the maximum salinity occurs when the salinity intrusion reaches its greatest extent. Since the impact of the pulse release is transient and the salinity intrusion returns to the pre-pulse location approximately one month after the release, the gaps between the solid and dotted lines of the same color in **Figure 7.2-8** are small. In the lower part of the Delaware River, between the Delaware Memorial Bridge and Chester, the maximum salinity is lower in the simulations with the pulse release. This suggests that the dilution effect from the pulse persisted longer in this portion of the Estuary.

Table 7.2-4. Simulated period-maximum of the depth-averaged salinity with SLR at selected locations during September 25 through October 31: Evaluation of pulse releases. Salinity units are psu.

SLR (m)		SHIP JOHN SHOAL RM 37	REEDY ISLAND RM 54	DELAWARE MEMORIAL BRIDGE RM 69	CHESTER RM 83.6	SCHUYLKILL RIVER RM 92.5	CAMDEN RM 98	BEN FRANKLIN BRIDGE RM 100	DRINKING WATER INTAKES RM 110
0	No pulse	22.33	13.71	6.57	1.69	0.62	0.34	0.29	0.14
	500 cfs Pulse	22.25	13.63	6.49	1.54	0.54	0.29	0.25	0.13
	% Diff	0	-1	-1	-9	-13	-15	-14	-7
	1000 cfs Pulse	22.21	13.55	6.41	1.42	0.47	0.26	0.22	0.13
	% Diff	-1	-1	-2	-16	-24	-24	-24	-7
0.5	No pulse	22.12	13.69	6.99	2.05	0.81	0.45	0.39	0.17
	500 cfs Pulse	22.1	13.63	6.92	1.91	0.72	0.39	0.34	0.15
	% Diff	0	0	-1	-7	-11	-13	-13	-12
	1000 cfs Pulse	22.05	13.56	6.85	1.84	0.63	0.34	0.3	0.14
	% Diff	0	-1	-2	-10	-22	-24	-23	-18
1.0	No pulse	22.14	13.64	7.33	2.4	1.03	0.6	0.53	0.22
	500 cfs Pulse	22.09	13.58	7.26	2.32	0.93	0.53	0.47	0.19
	% Diff	0	0	-1	-3	-10	-12	-11	-14
	1000 cfs Pulse	22.06	13.51	7.2	2.26	0.83	0.47	0.41	0.17
	% Diff	0	-1	-2	-6	-19	-22	-23	-23
1.6	No pulse	22.25	13.77	7.86	3.04	1.41	0.88	0.79	0.34
	500 cfs Pulse	22.21	13.73	7.8	2.96	1.29	0.79	0.7	0.3
	% Diff	0	0	-1	-3	-9	-10	-11	-12
	1000 cfs Pulse	22.14	13.64	7.73	2.9	1.18	0.71	0.62	0.25
	% Diff	0	-1	-2	-5	-16	-19	-22	-26

Note: the color code refers to the flow cases. The pulses were simulated by increasing the 1965 flow at Trenton (2,500 cfs with the flow objective) from September 1 through September 25 by a constant value 500 or 1,000 cfs.

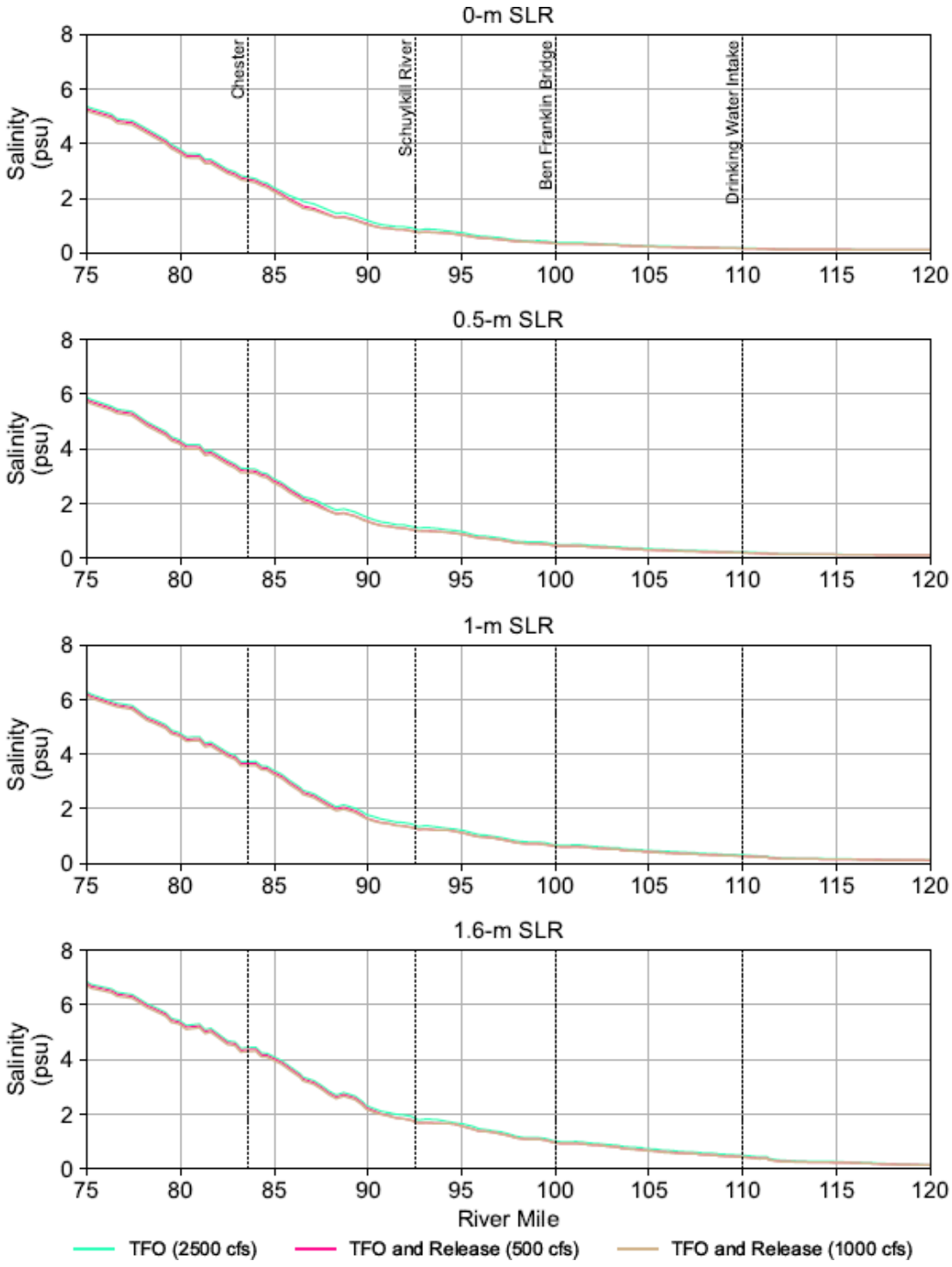

Figure 7.2-7. Simulated along-channel profiles of the maximum depth-averaged salinity during September 25 through October 31: Evaluation of pulse releases.

Note: the color code refers to the flow cases. The pulses were simulated by increasing the 1965 flow at Trenton (with the 2,500 cfs flow objective) from September 1 through September 25 by a constant value 500 or 1,000 cfs.

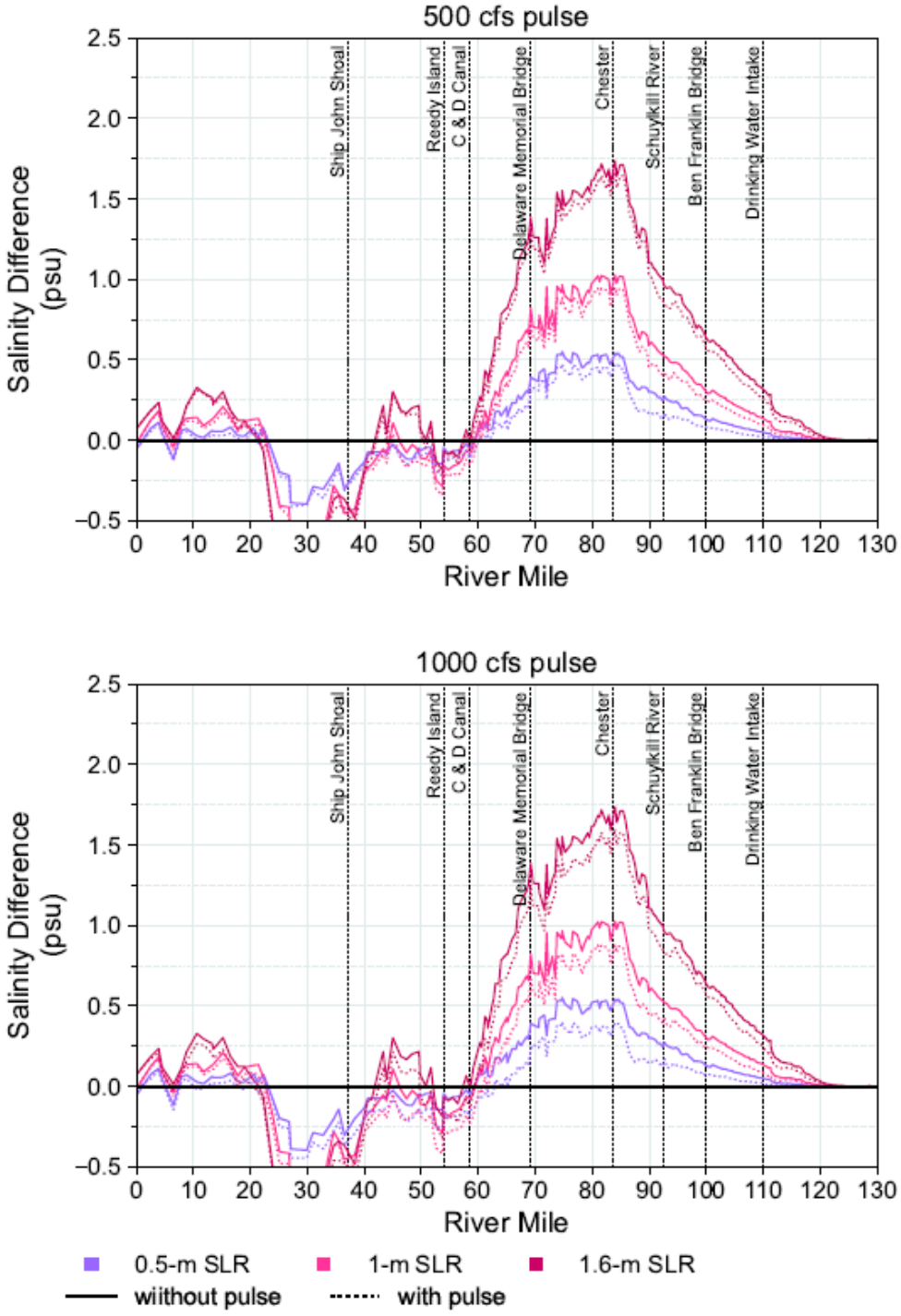

Figure 7.2-8. Simulated changes in along-channel period-maximum depth-averaged salinity profile during September 25 through October 31: Evaluation of pulse releases.

Note: the color code refers to the flow cases. The pulses were simulated by increasing the 1965 flow at Trenton (with the 2,500 cfs flow objective) from September 1 through September 25 by a constant value 500 or 1,000 cfs.

7.3 Comparison of Flow Augmentation from the Delaware and Schuylkill Rivers

Reservoir sources with water that can be used to meet the Trenton flow objective and make pulse releases are located throughout the Basin (Section 7.1). Flow augmentation water is conveyed to the Estuary through either the non-tidal Delaware River at Trenton or the Schuylkill River at Philadelphia. Only a finite amount of storage is available for flow augmentation, and the likelihood of refill is dependent on precipitation, which will be limited in times of drought. In addition, reservoirs are typically constructed for multiple purposes (direct-draw water supply, flow augmentation, flood control, recreation, power generation), and releases for flow augmentation may impact the storage available for the other purposes. Thus, it may be important to consider the effectiveness of the source and location of releases for salinity repulsion when selecting which reservoir to use for those releases.

To evaluate the efficiency of augmenting river flows from different sources (the Delaware River or the Schuylkill River), seven simulation trials were conducted for each of the three SLR increments with historical freshwater flows from a representative dry year (i.e., 2002). For each trial, initial conditions were established at midnight on May 1, prior to when releases are needed for the flow objective. For May 1 through November 30 (seven months), alternate constant flow combinations, representing various augmentation rates and source locations are outlined in **Table 7.3-1**. Comparisons of the simulations span the same seven-month period, beginning with the May 1 initial conditions and ending on November 30. Results are presented for August through November, the period during which the effects of flow augmentation and the resulting system response are evident.

The simulations are intended to show the relative influence of flow augmentation entering the Estuary from the 1) Delaware River, 2) the Schuylkill River, or 3) equal amounts from both. Without augmentation, the flows are 2,500 cfs for the Delaware River (the minimum TFO), and 300 cfs for the Schuylkill River[41], with a total flow of 2,800 cfs from the two Rivers (Trial 1). The were constant May through November, when the salt front is moving upstream. Two sets of simulations were performed with combined flows of 3,300 cfs (Trials 2-4) and 3,700 cfs (Trials 5-7). The results indicate the relative efficiencies of the two sources of augmentation flow.

[41] According to the monthly statistics for the Schuylkill River discharge at USGS gage 01474500 Schuylkill River at Philadelphia, PA, the average flow for June through December 1965 are 261, 289, 254, 210, 439, 231, and 446, respectively. The average flow is 305 cfs for this period. The average flow at USGS 01463500 Delaware River at Trenton NJ is 2,740 cfs during this same period, and if December is excluded, the average flow at Trenton is 2,360 cfs.

Table 7.3-1. Delaware River at Trenton and Schuylkill River flows used in simulations to test the relative efficiency of reservoir releases from the two sources in repelling salinity intrusion.

Trial	Trenton Flow (cfs)	Schuylkill Flow (cfs)	Combined Flow from the Delaware and Schuylkill Rivers (cfs)	Amount of Flow Augmentation (5/1–11/30) (cfs)
Trial 1 (Baseline)	2,500	300	2,800	0
Trial 2	3,000	300	3,300	500
Trial 3	2,500	800		
Trial 4	2,750	550		
Trial 5	3,400	300	3,700	900
Trial 6	2,500	1,200		
Trial 7	2,950	750		

Note: All simulations are of the seven-month period with constant flow conditions from May 1 through November 30. Results from May through July were excluded because the salt front location was in the lower part of the tidal River and not the area of concern. Results presented in the table are for August to November, under the designed constant flow conditions to focus on the period when flow augmentation and the subsequent impact are most evident.

7.3.1 Salt Front

Simulated 7-dma salt front results are presented in **Table 7.3-2** and **Figure 7.3-1** through **Figure 7.3-4** for September 1 through October 31 (the maximum salt front location occurs in October). The time series of simulated salt front locations for Trials 1-7 show the extent to which the addition of water moves the salt front during this time period (**Figure 7.3-1** and **Figure 7.3-2**).

For 0 m sea level rise and the addition of 500 cfs flow augmentation (for a combined flow of 3,300 cfs—Trials 2-4) keeps the salt front 2.6 to 2.8 miles farther downstream from RM 98.9 regardless of the source of the additional flow (**Figure 7.3-3**, **Table 7.3-2**). A marginally larger benefit (-0.1 miles) occurs if all the flow (500 cfs) is applied at the Delaware River at Trenton. With the addition of 900 cfs flow augmentation (for a combined flow of 3,700 cfs—Trials 5-7), the salt front at 0 m SLR is kept between 4.6 and 4.7 miles farther downstream (**Figure 7.3-4**, **Table 7.3-2**). A marginally larger benefit (-0.1 miles) occurs if all the flow is applied at the Schuylkill River for 0 m SLR. However, the difference in maximum location does not vary by more than 0.2 miles among the flow combinations (RM 96.1 to 96.3 for 3,300 cfs and RM 94.2 to 94.3 for 3,700 cfs).

Table 7.3-2. Simulated maximum salt front location, with sea level rise and Delaware River and Schuylkill River flow augmentation.

Total Constant Flow (cfs)		2,800	3,300			3,700		
Pulse (cfs) and Location		No pulse	500 to Delaware	500 to Schuylkill	250 to each	900 to Delaware	900 to Schuylkill	450 to each
Flow (cfs)	Delaware	2,500	3,000	2,500	2,750	3,400	2,500	2,950
	Schuylkill	300	300	800	550	300	1200	750
SLR	Trial	1	2	3	4	5	6	7
0 m	Salt Front	98.9	96.1	96.3	96.2	94.3	94.2	94.3
	Difference		-2.8	-2.6	-2.7	-4.6	-4.7	-4.6
0.5 m	Salt Front	102.3	99.5	100.1	99.9	97.2	97.6	97.5
	Difference		-2.8	-2.2	-2.4	-5.1	-4.7	-4.8
1.0 m	Salt Front	105.8	102.9	103.6	103.3	100.9	101.9	101.4
	Difference		-2.9	-2.2	-2.5	-4.9	-3.9	-4.4
1.6 m	Salt Front	109.5	107.7	108.4	108.0	105.6	107.3	106.5
	Difference		-1.8	-1.1	-1.5	-3.9	-2.2	-3.0

Notes: Constant flow maintained from May through November. The results were summarized for August through November, the most critical period for the salt front.

For 1.0 m of sea level rise, adding the water to the Delaware River is more effective in moving the salt front. For the addition of 500 cfs (for a total flow rate of 3,300 cfs), the salt front is kept 2.9 miles farther downstream (from RM 105.8 to RM 102.9) compared with less than 2.6 miles farther downstream if the flow enters at the Schuylkill River or is split between the sources. The salt front is kept 3.9-4.9 miles farther downstream with the addition of 900 cfs (for a total of 3,700 cfs). If all additional flow is applied to the Delaware River at Trenton, the maximum salt front location is kept 4.9 miles farther downstream (from RM 105.8 to RM 100.9). If the flow enters at the Schuylkill

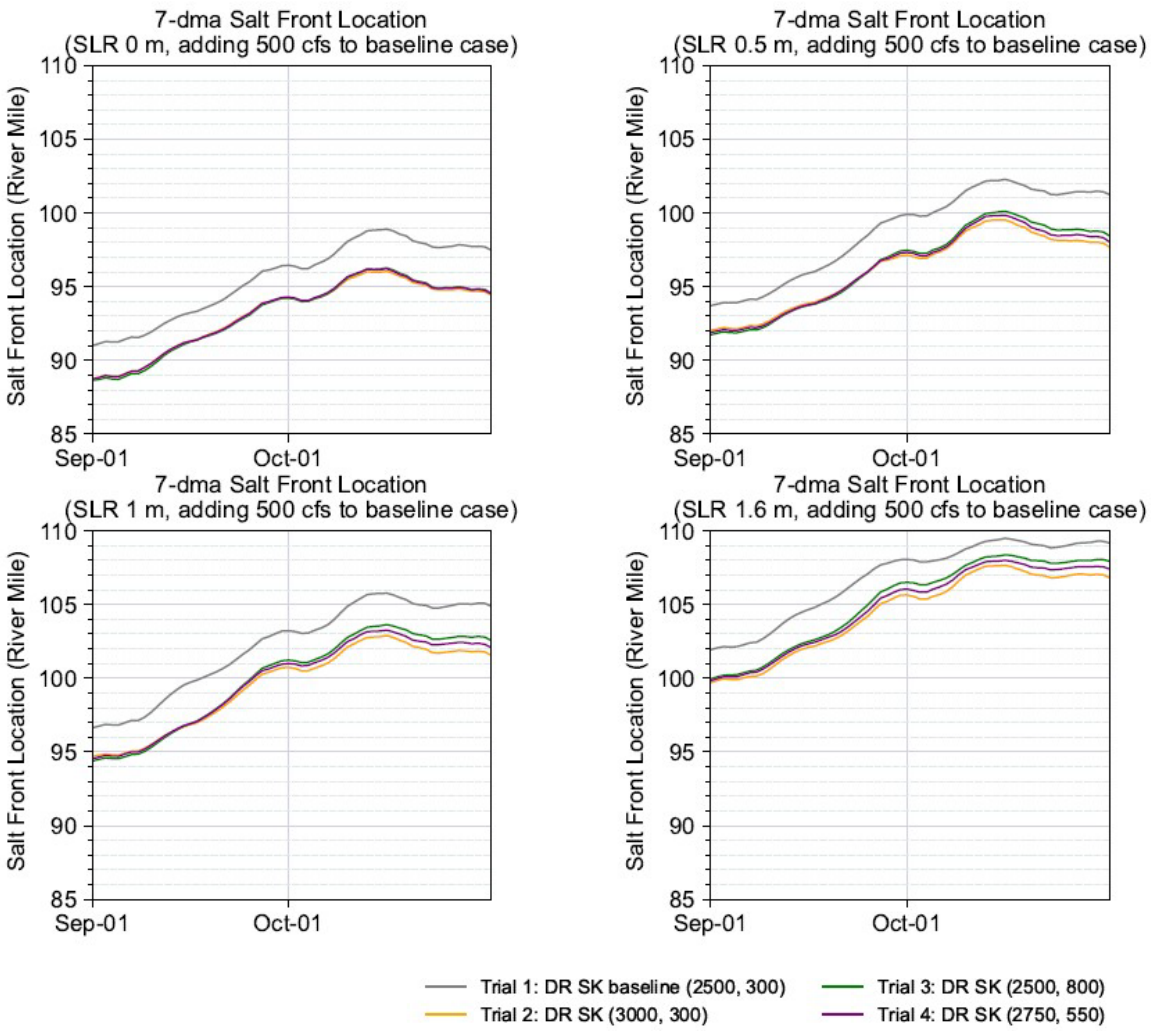

Figure 7.3-1. Time series of simulated salt front location for Trials 1-4, with Delaware and Schuylkill River flow augmentation and SLR. The combined flow of the Delaware River at Trenton and the Schuylkill River is 2,800 cfs for Trial 1 and 3,300 cfs for Trials 2–4.

Notes: The results for the September and October period are shown. DR = Delaware River, SK = Schuylkill River

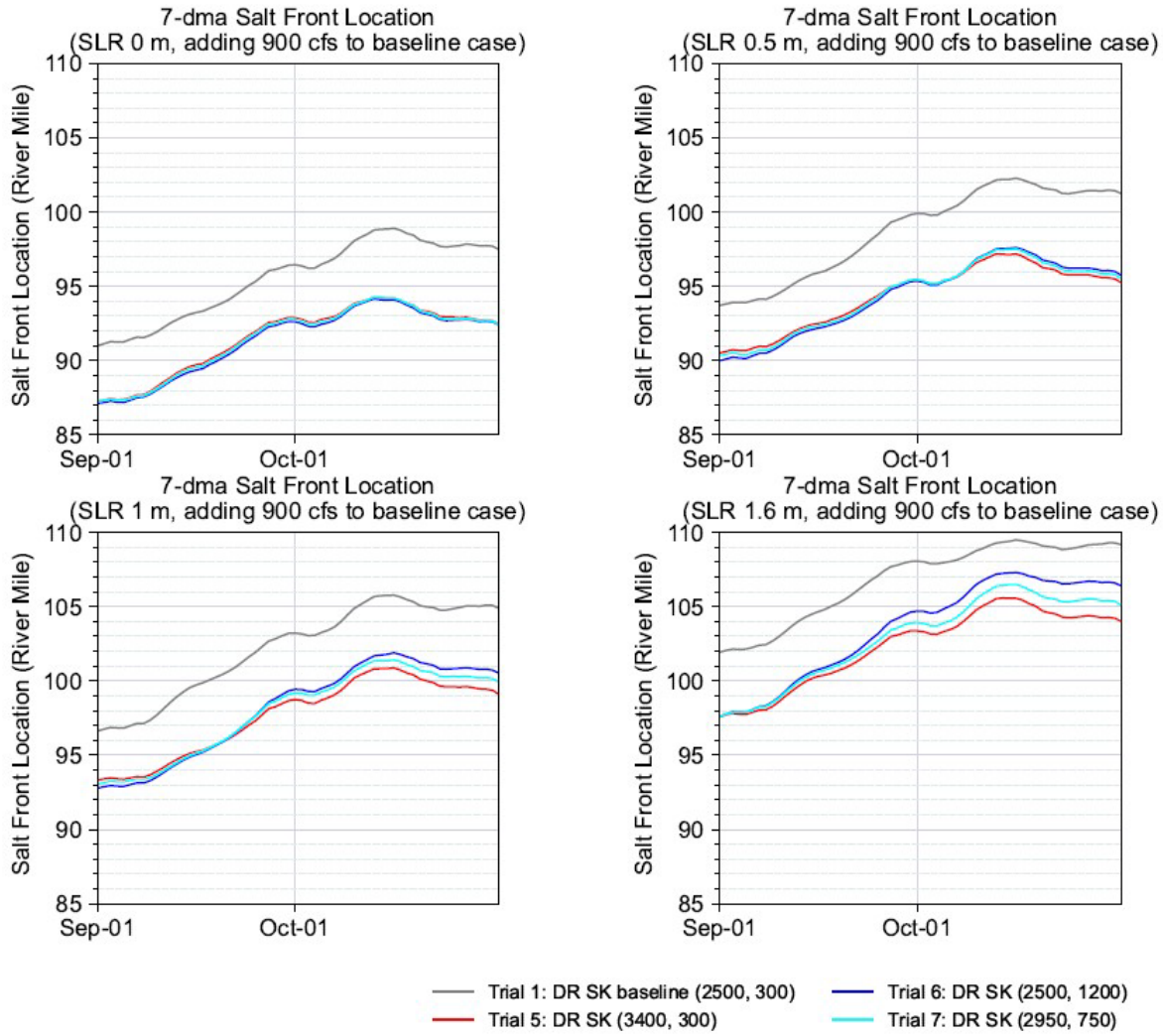

Figure 7.3-2. Time series of simulated salt front location for Trials 1, 5, 6, and 7, with Delaware and Schuylkill River flow augmentation and SLR. The combined flow of the Delaware River at Trenton and the Schuylkill River is 2,800 cfs for Trial 1 and 3,700 cfs for Trial 5–7.

Notes: The results for the September and October period are shown. DR = Delaware River, SK = Schuylkill River

River or is split, the maximum salt front location is 3.9–4.4 miles farther downstream (RM 101.9 and 101.4), respectively. The difference among the combinations is 1 mile or less (0.7 miles for 3,300 cfs and 1 mile for 3,700 cfs). Increasing the flow to the Delaware at Trenton is more effective with 1.0 m SLR because the salt front (higher salinity water) is already above the confluence of

the two Rivers. Augmenting flow from the Schuylkill River was marginally less effective with either amount of flow augmentation under 1.0 m SLR.

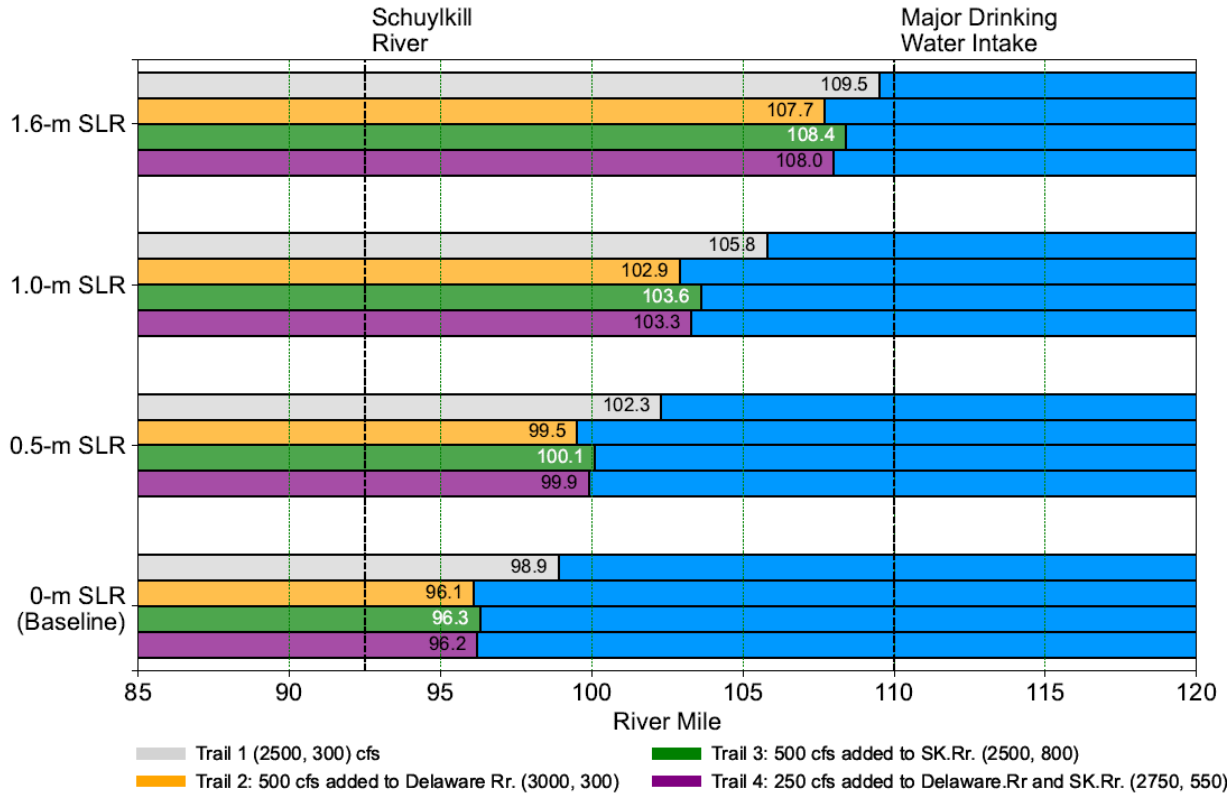

Figure 7.3-3. Simulated maximum salt front location, with sea level rise and Delaware River and Schuylkill River flow augmentation. The combined flow of Delaware River at Trenton and Schuylkill River is 2,800 cfs for Trial 1 and 3,300 cfs for Trial 2–4.

Note: constant flow rate was assigned for the Delaware River and Schuylkill River from May through November. Results were summarized for August through November period.

For 1.6 m sea level rise, the addition of water to the Delaware at Trenton is again more effective in moving the salt front than adding flow to the Schuylkill River. For 500 cfs augmentation, the salt front is kept 1.8, 1.1, and 1.5 miles farther downstream (from RM 109.5 to RM 107.7, 108.4, and 108.0) for water added to the Delaware, Schuylkill, or split, respectively. For 3900 cfs augmentation, the salt front is kept 2.2 to 3.9 miles farther downstream. Regardless of the amount of water added, providing more water via the Delaware River at Trenton was the most effective combination with SLR at 1.6 m. Adding water from the Schuylkill River was the least effective of the flow combinations for 1.0 m and 1.6 m sea level rise. The dilution effect of the freshwater

plume from the Schuylkill River diminishes with the increased volume of brackish water in the River with higher SLR.

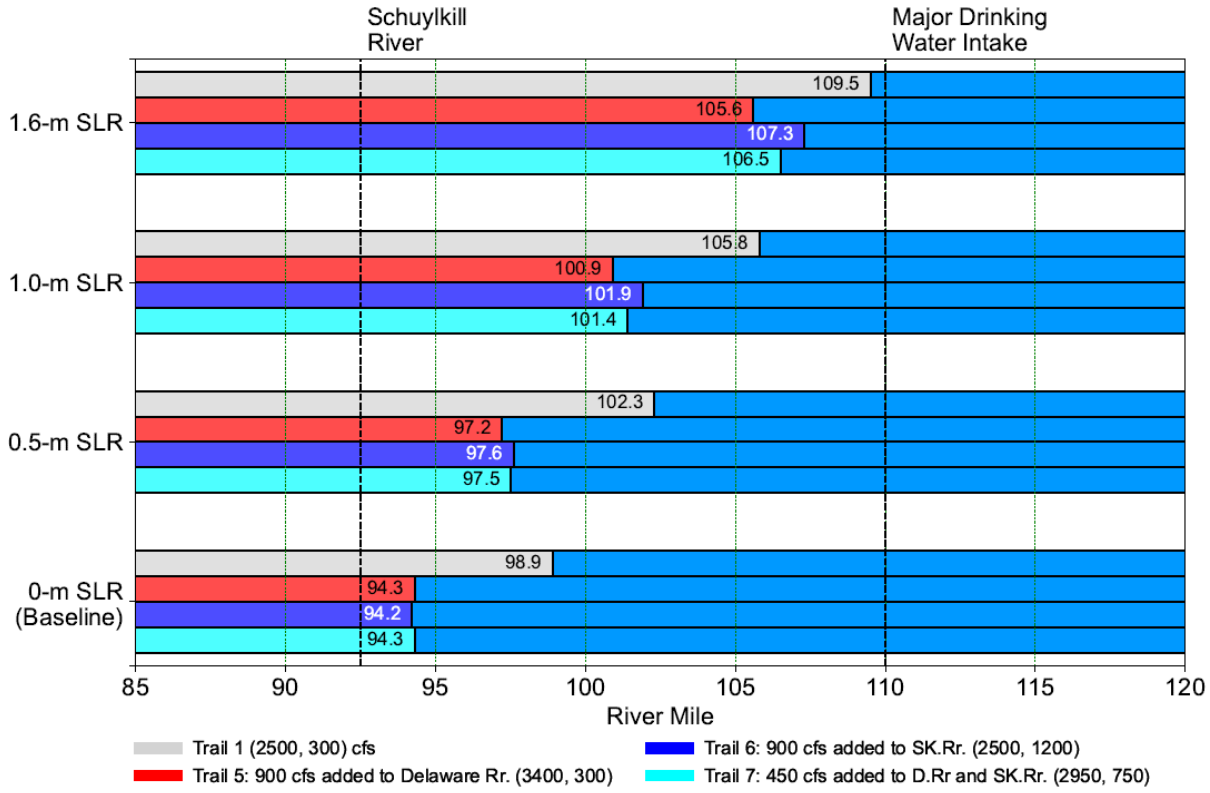

Figure 7.3-4. Simulated maximum salt front location, with sea level rise and Delaware River and Schuylkill River flow augmentation. The combined flow of Delaware River at Trenton and Schuylkill River is 2,800 cfs for Trial 1 and 3,700 cfs for Trial 5–7.

Note: constant flow rate was assigned for the Delaware River and Schuylkill River from May through November. Results were summarized for August through November period.

Although the maximum salt front location is important, the time-series of the salt front's progression upstream indicates that the efficacy of the source may depend on the location of the salt front when flow is augmented. Adding larger amounts of flow to the Schuylkill River is marginally more effective when the baseline salt front is near the Schuylkill River confluence. The plume of additional freshwater dilutes the salinity of water below the Schuylkill River and impedes the upstream movement of salt. The effect is evident in the time series plot of the salt front movement during September and October in **Figure 7.3-2** for Trials 5, 6, and 7, with the combined Delaware and Schuylkill River flow of 3,700 cfs and SLR. The blue line (Trail 6, adding 900 cfs through the Schuylkill River) starts farther downstream with 0 m and 0.5 m SLR on September 1,

when the SF is at RM 87 and 91, respectively, and remains the lowest for the entire month of September until early- to mid-October when the SF locations for all three Trials (5, 6 and 7) converge. Once the SF is a mile or so above the mouth of the Schuylkill River (RM 92.5), the influence of flow augmentation with additional water added to the Delaware River (Trail 5) becomes relatively more effective (i.e., the red line moves from being above to being below the blue line). This phenomenon is also observed with 1.0 m SLR (the lower-left panel of **Figure 7.3-2**). With 1.0 m SLR, the blue line (Trail 6) flips from being the lowest to being above the red line (Trail 5) earlier, around mid-August, when the SF is moving upstream and is passing RM 95, 2.5 miles above the confluence of the Schuylkill River and the Delaware River. The results presented in **Figure 7.3-2** imply that the relative effectiveness of the source of flow augmentation may vary depending on the location of the salt front when the water is released.

To further explore the possibility that the source of flow augmentation water may be more beneficial under certain circumstances, an additional suite of five simulations was designed and conducted in which the baseline total constant flow is higher (3,600 cfs), and additional flow of 500 cfs or 900 cfs is augmented from either the Delaware River or the Schuylkill River. The higher total constant flow situates the maximum salt front closer to the RM 92.5 confluence with the Schuylkill River. The results indicate that for the baseline case the source of water is not significant until the salt front location is above RM 85. Due to the mixing zone effect, once the salt front is above approximately RM 85, and downstream from a few miles above the Delaware-Schuylkill confluence (~RM 92-95), the Schuylkill River augmentation is more effective in repelling the salt front (See **Table L.3-5**, and **Figure L.3-9** and **L.3-10** in Appendix L.3.2). A more thorough study regarding the source of flow augmentation water was outside the scope of this report but may be pursued in the future.

7.3.2 Chloride Concentrations

For the baseline Trail 1 and all flow augmentation trails with 0 m SLR, the baseline maximum 30-dma chloride concentration at RM 98 (Camden) is 238 mg/L (**Table L.4-1**), which is higher than the 180 mg/L water quality standard for salinity control. With 1.0 m and 1.6 m SLR, the maximum 30-dma chloride concentrations at RM 98 for the baseline are 584 mg/L and 900 mg/L, respectively (see **Table L.4-2 and Table L.4-3)**. A statistical summary of simulation results for the period August 1 through November 30, when constant inflow was assigned to the Delaware River at Trenton and Schuylkill River, is presented in Appendix L.3 and Appendix L.4.

With 1.0 m SLR, adding 500 cfs reduces the chloride concentration from the 584 mg/L baseline concentration to a range of 418 to 440 mg/L. With 1.6 m SLR, the 500 cfs augmentation reduced the concentration from a baseline concentration of 900 mg/L to a range of 703 to 725 mg/L.

With 1.0 m SLR, adding 900 cfs reduced the concentration from the baseline concentration of 584 mg/L to a range of 310 to 340 mg/L (**Table L.4-2)**. With 1.6 m SLR and adding 900 cfs, the concentration was reduced from the baseline concentration 900 mg/L to a range of 565 to 598 mg/L (**Table L.4-3)**. Flow augmentation does not lower chloride concentrations to below the 180 mg/L standard in any of the trials with SLR of 1.0 m or 1.6 m. **Figure 7.3-5** shows the range of simulated 30-dma chloride concentrations at RM 98 as an example. More simulation results with other SLR scenarios are presented in Appendix L.3 and Appendix L.4.

7.3.3 Salinity

Simulated maximum daily depth-averaged salinity was calculated for the period August 1 through November 30, when constant inflow was assigned to the Delaware River at Trenton and Schuylkill River. The impact of the additional flow varied and can be seen at individual locations. **Figure 7.3-6** depicts the range of the simulated maximum depth-averaged salinity at four locations on the Delaware River with 1.0 m SLR as an example. Similar to chloride results, the effectiveness of increased flow on daily depth-averaged salinity at a given location also depends on where the contribution is added. If the salt front is below or near the Schuylkill River, adding flow to the

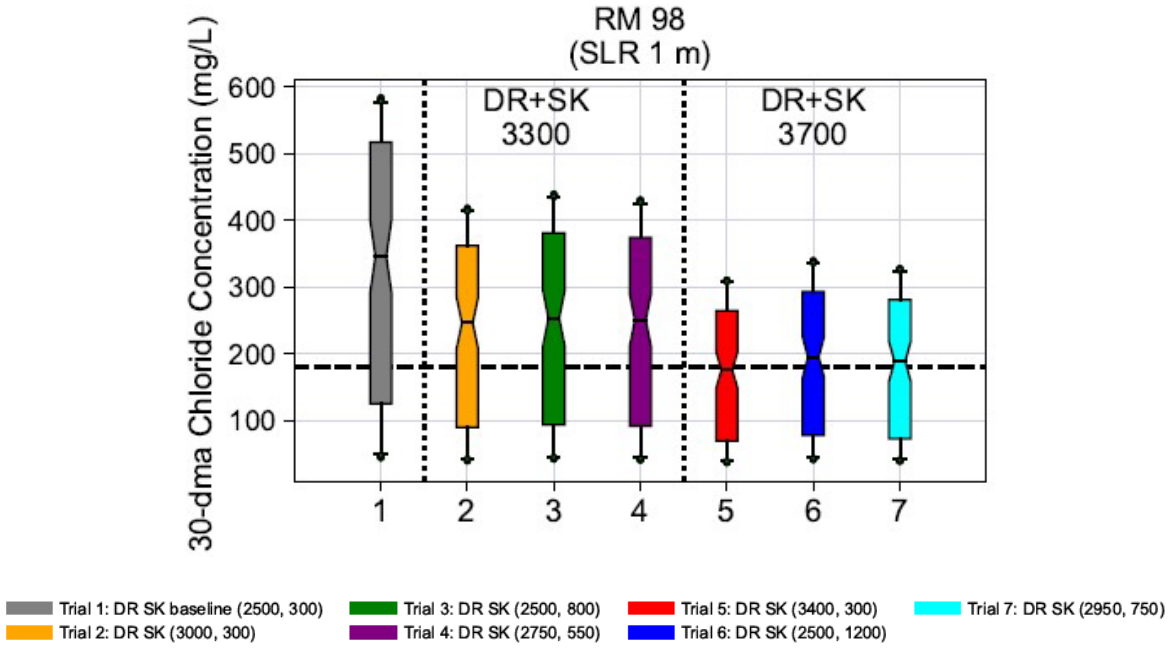

Figure 7.3-5. Comparison of simulated 30-dma chloride concentration at RM 98, with Delaware River at Trenton and Schuylkill River flow augmentation and SLR = 1.0 m.

Notes: Constant flow maintained from May through November. The results were summarized for August through November, the most critical period for the salt front. DR = the Delaware River, SK = Schuylkill River

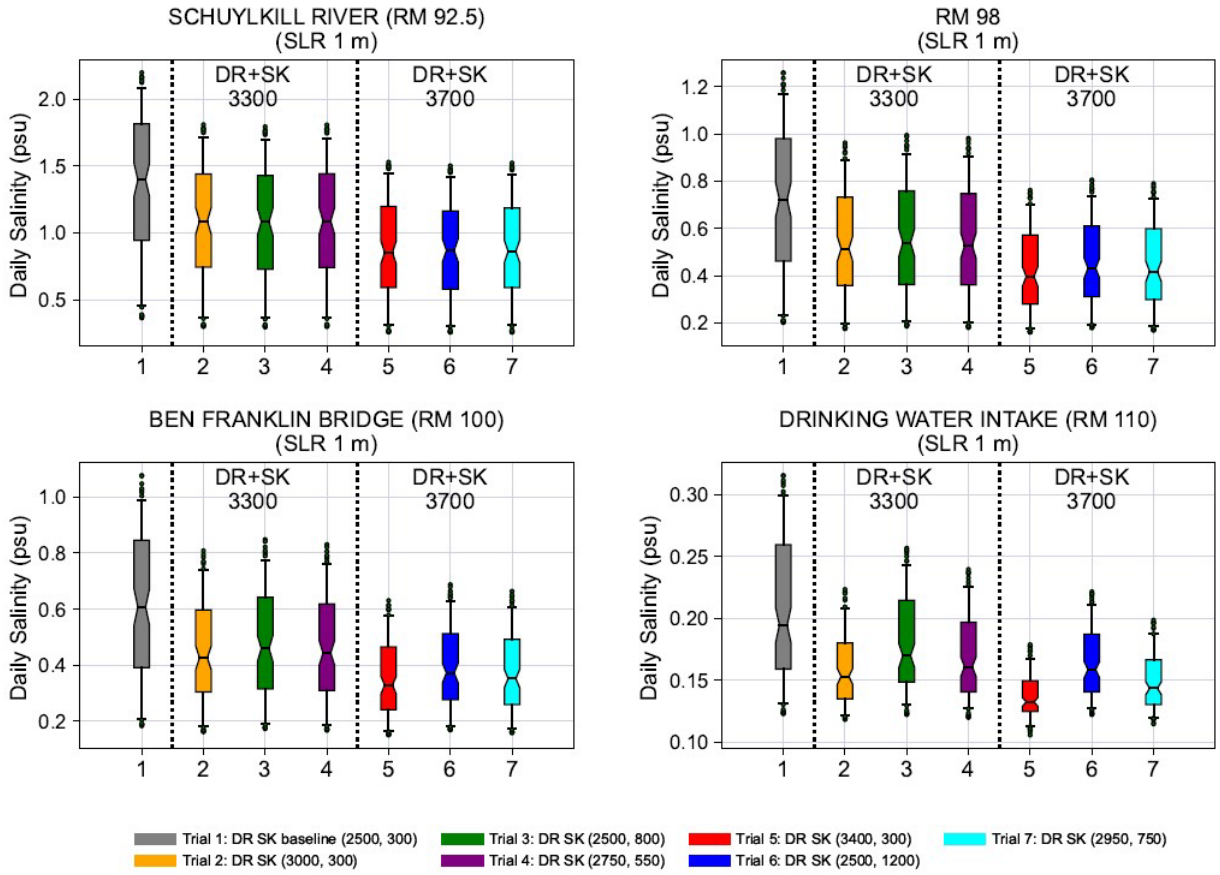

Figure 7.3-6. Comparison of simulated daily depth-averaged salinity ranges at four locations, with Delaware River at Trenton and Schuylkill River flow augmentation and SLR = 1.0 m.

Notes: Constant flow maintained from May through November. The results were summarized for August through November, the most critical period for the salt front. DR = the Delaware River, SK = Schuylkill River

Schuylkill River flow is more effective in reducing the salinity in the vicinity of the Schuylkill River and Delaware River confluence. When the salt front is more than a few miles above the Schuylkill River, adding flow to the Delaware River is more effective in reducing salinity at locations upstream of the Schuylkill River confluence. The results imply that if the salt front is downstream of the Schuylkill River confluence, such as at Chester, then the effect of additional flow from the Schuylkill River is greater than additional flow to the Delaware River at Trenton. If the salt front is above the Schuylkill River confluence, such as at RM 98 (Camden), then flow added at Trenton has a greater effect. Results are presented in **Table L.3-1** through **Table L.3-4** in Appendix L.3. More simulation results are provided with additional discussion in Appendix L.3 and Appendix L.4.

7.4 Discussion

A flow objective for the Delaware River at Trenton (TFO) is an effective means for managing salinity intrusion. For the baseline (0 m SLR), with a repeat of 1965 flow conditions, and with TFO, the simulated maximum salt front (RM 94.2) is 3.3 miles downstream from where it would otherwise be without TFO (RM 97.5), both of which are below the drinking water intakes at RM 110. For the SLR simulations (0.3 m to 1.6 m of SLR), the salt front is between 4.1 and 4.3 miles farther downstream of where it would have been without TFO.[42] At 1.0 m and 1.6 m of sea level rise, the maximum salt front is above RM 100 (the historical maximum), even with a flow objective of 2,500 cfs. For all SLR simulations, the TFO results in less salinity intrusion. As expected, the results for the maximum 30-dma chloride concentration and salinity are consistent with those for the salt front.

In addition to TFO, pulse releases of additional freshwater from upstream sources are effective for salinity repulsion. At 0.5 m of SLR, the simulated pulse releases of 500 cfs and 1000 cfs reduced salinity intrusion, as measured by the initial maximum salt front location (through the end of October), by 1.4 and 2.5 miles, respectively. At 1.0 m of SLR, the simulated pulse releases of 500 cfs and 1000 cfs reduced salinity intrusion, as measured by the initial maximum salt front location (through the end of October), by 1.9 and 3.3 miles, respectively, and SF is downstream of RM 98. In simulations of 1.6 m SLR, the initial maximum salt front locations remain above RM 100 (the historic maximum), even with pulse releases. Only a limited number of pulse release scenarios were simulated to determine the impacts and benefits of these short duration pulses. Additional studies of pulse initiation, duration, flow rate, storage requirements, and operational criteria are needed to further evaluate the utility of pulse releases for salinity repulsion.

Results indicate that the source and location of freshwater flow augmentation into the Estuary may have implications for salinity management. The two sources, the Schuylkill River (RM 92.5) at Philadelphia and the non-tidal Delaware River at Trenton (RM 133) are 40.5 River Miles apart, and their position relative to the salt front location at the time of augmentation is important. For limiting the extent of salinity intrusion, additional water from the Delaware River at Trenton is more efficient in repelling the salt front when the salt front is already a few miles above the Schuylkill River confluence. Augmenting with Schuylkill River flow is more effective than augmenting with Delaware River flow during periods when the salt front is below or near the confluence of the Schuylkill and the Delaware Rivers. The impact of the additional water is influenced by a mixing

42 The difference of 3.3 miles for the baseline simulation and approximately 4 miles with the flow objective is related to where the salt front location (approximately RM 92.5) prior to two storm events in mid-August and September, which raised the flow from the Schuylkill River from less than 100 cfs to greater than greater than 890 and 944 cfs, respectively.

zone created by the freshwater plume near the Schuylkill River, the volume of water in the River, and the location of the salt front in relation to the Delaware-Schuylkill confluence.

8. CONCLUSIONS

A three-dimensional hydrodynamic salinity model (SM3D) was used to assess the effects of SLR on salinity intrusion for a range of historical hydrologic and meteorological conditions. The baseline scenario (0 m SLR) was based on the 19-year tidal datum epoch (1991–2009) that is centered on the year 2000 and is consistent with studies by others. SLR increments of 0.3 m, 0.5 m, 0.8 m, 1.0 m, and 1.6 m were also simulated. The values for SLR were informed by three sets of SLR projections through 2100 by NOAA, DNREC, and NJSTAP. A range of SLR values was simulated because a single value is not appropriate for multiple planning horizons or scenarios with a variety of potential greenhouse emission pathways. For example, the probability of 1.0 m SLR is approximately 1.5 percent by 2060 but may be 50 percent by 2100. In addition, SLR projections are revised as the science of sea level rise continues to evolve. For example, in 2017, NOAA projected 0.9 m SLR by 2060 at Lewes, DE, for the intermediate emission scenario, but in 2022 this projection was revised to 0.66 m. The projection of 1.6 m has a very low probability of being realized or exceeded by 2100.

Diagnostic simulations (Section 4) with a moderately low flow condition, represented with flows measured during June–October 2002, were performed for the range of SLR increments to examine how the salinity structure in the Estuary would be impacted with SLR. The representative low flow condition was also used to test different model assumptions and boundary conditions and their effects on model results (Section 5). Simulations with the flows of 1965, during the drought of record, were used to stress test some of the model assumptions under more severe conditions (Section 6).

The impacts of sea level rise on salinity intrusion were also evaluated for a range of annual flow conditions represented by 10 individual years of historical flows (Section 4). The years simulated were 1965 (the drought of record), 2001 to 2002, 2011 to 2013, and 2016 to 2019 and are representative of the period of record. The years include two drought periods and other dry conditions, normal conditions, and high flow years. In addition, conditions resulting from three severe storms with strong tidal forcings were represented, specifically, tropical storms Irene and Lee (2011) and hurricane Sandy (2012).

Conceptual simulations were then performed to evaluate the different aspects of flow management for low flow augmentation under projected SLR conditions (Section 7). Collectively, the results indicate that as sea level rises, that TFO is likely inadequate to maintain the salt front below RM 92.5.

Key findings from the study are summarized below and are organized as follows: the impacts of sea level rise on salinity, the effects of model configuration (associated with the channel deepening and marsh inundation and migration with SLR), the effects of other potential

conditions, and conceptual flow management actions for salinity repulsion to offset the impacts of sea level rise. Potential next steps are also summarized.

8.1 Impacts of Sea Level Rise on Salinity

To evaluate how SLR will affect salinity in the Estuary, a variety of diagnostic, ensemble, and sensitivity simulations were performed. The impacts of sea level rise on salinity intrusion were also evaluated for a range of annual flow conditions represented by 10 individual years of historical flows (Section 4). The effect of sea level rise on the hydrodynamics and salinity was evaluated using water surface elevation, the salinity structure, the salt front, chloride concentration, and salinity.

8.1.1 Water Surface Elevation

Simulation results demonstrate that the effects of sea level rise on tidal water surface water elevations extend as far upstream as Trenton. Under normal conditions without SLR, the tidal amplitude increases between the mouth of the Bay (RM 0) and the head of tide at Trenton (RM 133). Simulation results show that with sea level rise, the relative difference in water surface elevation between RM 0 and RM 133 is further amplified.

8.1.2 Salinity Structure

Sea level rise increases the amount of salt water entering the Delaware Estuary and results in greater stratification of salinity in the water column and increased salinity near the bottom of the FNC in the Delaware Bay. With a higher water level and increased density-driven forces, more saline water spreads into the area outside the FNC and across the Delaware Bay. Thus, more salt water is transported upstream over the shallower area on the New Jersey side during flood tide, and moves back downstream along the Delaware side during ebb tide.

8.1.3 Salt Front Location, Chloride Concentrations, and Salinity

For a range of annual flow conditions, the maximum salt front location is farther upstream for all SLR values simulated. The simulated maximum salt front location from the 10 representative ensemble years occurs for 1965 flows (the drought of record) with the flow objective. Without sea level rise (0 m), the maximum salt front location is RM 94.2, 15.8 miles below the drinking water intakes (at RM 110). With sea level rise of 0.3, 0.5, 0.8, 1.0, and 1.6 m, the most upstream salt front location reaches RM 95.8, 96.8, 98.9, 100.4, and 104.7, respectively.

The percent of time that the 30-dma chloride concentration equaled or exceeded DRBC's water quality criteria 180 mg/L at RM 98 (Camden), was calculated for the 10 years of representative flows. With 0 SLR and up to 0.5 m SLR, the water quality standard was not exceeded. With 0.8,

1.0 and 1.6 m SLR, the chloride water quality standard is exceeded 2.2 percent, 3.2 percent, and 7.5 percent of the time, respectively. For 0.8 and 1.0 m SLR, the simulated 30-dma chloride concentration exceeds the standard only during the simulation of 1965 conditions. For 1.6 m SLR, the chloride standard is exceeded in four of the 10 years simulated.

Results indicate that the simulated maximum salinity at the Schuylkill River confluence remains below 2 psu for all cases of SLR. The largest increases in the maximum salinity are between the Delaware Memorial Bridge (RM 70) and Chester (RM 83).

8.2 Model Sensitivity Testing

*S*imulations, detailed in Section 5, were conducted to investigate model sensitivity to: (1) inclusion of additional marsh area, (2) bottom roughness in marshes, (3) shoreline retreat and bank erosion, and (4) channel bathymetry. From results of this testing, it was determined that SM3D without modification was appropriately conservative for the sea level rise simulations. While the simulations demonstrate the sensitivity of results due to the amount of marsh area represented in the model domain, bottom roughness shoreline retreat, and bank erosion on salinity intrusion, the model does not predict how these features will be affected by sea level rise.

8.2.1 Additional Marsh Area

To determine how results are affected by the amount of marsh area included in the model domain, a version of SM3D was modified to include additional low-lying marsh areas that may be inundated more often with SLR (SM3D+M). Without SLR, the additional marsh area has a minor effect, with a maximum salt front location 0.2 miles farther downstream. With 0.8 and 1.6 m SLR, the additional marsh area results in a maximum salt front location 1.0 and 2.6 miles downstream, respectively. Overall, the original model domain (without the additional marsh area) produces more conservative results for evaluating salinity intrusion. Unrelated to the model configuration, the results imply that preserving marsh areas is beneficial for reducing tidal amplification and salinity intrusion, particularly in the Upper Delaware River Estuary. However, a more detailed study would be needed to evaluate and quantify the potential mitigating benefits of maintaining low-lying marsh areas.

8.2.2 Marsh Bottom Roughness, Shoreline Retreat, and Bank Erosion

Simulations to test the effect of bottom roughness, shoreline retreat, and bank erosion indicate that predicted salinity intrusion is not sensitive to these model parameters within the ranges evaluated. Differences in the predicted maximum salt front location with different parameter values are less than 0.4 mile.

8.2.3 Channel Bathymetry

Changes in the depth and width of an estuary resulting from natural processes and human activities, such as dredging, can affect salinity intrusion. The FNC is maintained by the United States Army Corps of Engineers (USACE) and was recently dredged by 5 ft to a depth of 45 ft, the majority of which occurred between 2010 and 2016. Simulations were performed to compare the salinity intrusion with SLR for both 40- and 45-ft channel bathymetry. Results of simulations without SLR indicate that the maximum salt front is 2.4 miles farther upstream with the deeper channel. With up to 1.6 m SLR, the simulated salt front is also up to 2.4 miles farther upstream with the deeper channel. Results show that the bathymetry of the FNC influences salinity intrusion. However, the simulated incremental change in salt front location with increasing sea level rise is similar with either the 40-ft or 45-ft channel.

8.3 Other Potential Conditions

Other conditions that may affect salinity intrusion along with sea level rise were also evaluated, including increased salinity from non-tidal and point sources, increased drought severity, and ocean temperature (which affects density-driven circulation). These simulations were performed to assess the effect of model assumptions about boundary conditions for flow, salinity, and ocean temperature (Section 6).

8.3.1 Sensitivity to Non-tidal Sources of Salinity

Simulation results indicate that if the non-tidal tributary salinity is doubled as projected by the year 2060, the maximum salt front location is up to 0.9 miles farther upstream. Model results were not sensitive to the specification of point-source salinity as either variable by month or constant. Sea level rise has a much larger impact on the simulated salt front location and chloride concentrations than increases in salinity from non-tidal sources.

8.3.2 Increased Drought Severity

A hypothetical extreme drought scenario, worse than the 1965 drought of record, was formulated using a series of minimum monthly historical flows with an annual average of 83 percent of the 1965 drought (both simulations used a flow objective of 2,500 cfs). Simulations with flows representing this scenario indicate that during such a formulated event, even with no sea level rise, the maximum salt front is as far upstream as RM 96.9, within 4 miles of its maximum location in the 1960s, when no flow objective was in place. With 0.5 m and 1.0 m SLR, the simulated maximum salt front locations with this severe drought are at RM 100.3 and RM 103.6, respectively. With 1.6 m SLR, the maximum salt front location is at RM 108.1, within 2 miles of the drinking water intakes at RM 110. Although unlikely, this scenario indicates that a more severe

drought than the drought of record would represent a major management concern. At RM 98 (Camden), the maximum 30-dma chloride concentration exceeded the 180 mg/L water quality standard for all values of sea level rise, including the baseline (approximately 6 percent time of exceedance), under this more severe drought condition.

8.3.3 Ocean Surface Water Temperature

As the ocean temperature rises, the absorbed heat lowers the density of the ocean water, which decreases the pressure forcing at the ocean boundary, reducing salinity intrusion. A sensitivity analysis was conducted to determine the effect of increased ocean temperature on salinity intrusion, and this effect is found to be marginal. Results indicate that a 1°C increase in ocean surface water temperature results in slightly less salinity intrusion, with the maximum salt front locations 0.3, 0.4 and 0.4 miles farther downstream for 0 m, 1.0 m, and 1.6 m sea level rise, respectively.

8.4 Conceptual Analysis of Potential Management Actions for Salinity Repulsion

Currently, salinity is managed by maintaining freshwater inflows to the Delaware Estuary with reservoir releases to meet the Trenton Flow Objective. However, with sea level rise, TFO may no longer be sufficient to keep the salt front below RM 92.5. Simulations were performed to show the benefit of TFO and two conceptual flow management options for using the water available for TFO: 1) temporary increase in flow with pulses to preserve water; and 2) choice of source and when it is most effective (Section 7).

8.4.1 Flow Objectives

The flow objective (such as the Trenton Flow Objective) is the current management action used for salinity repulsion in the drought management plan for the Basin[43]. Simulations using the historical flows of 1965, and historical flows of 1965 adjusted so the minimum flow was 2,500 cfs, were used to demonstrate the effectiveness of the flow objective in repelling salinity. The results show that with SLR of 1.6 m and without the Trenton Flow Objective, the maximum salt front location extends as far as RM 109.0, which is 1 mile below the major drinking water intakes. Results of simulations with the flow objective show that the salt front is kept farther downstream

[43] For the purposes of this report, the minimum flow objective in the drought management program is 2,500 cfs. The current flow objective ranges from 2,500–3,000 cfs. The flow objective is 3,000 cfs under normal conditions and reduced based on the drought level. During a drought emergency, the flow objective varies by the location of the salt front and season. Provisions of the drought management program are in the Delaware Basin Water Code: https://www.nj.gov/drbc/library/documents/watercode.pdf

by 3.3, 4.1, and 4.3 miles for 0 m, 1.0 m, and 1.6 m sea level rise, respectively, and it is kept below RM 105 for all SLR scenarios. The evaluation of results with respect to chloride concentrations indicates that a flow objective of 2,500 cfs may not be adequate for maintaining the chloride water quality standard with a sea level rise of 0.5 m or more, because the simulated maximum 30-dma chloride concentration at RM 98 exceeds the water quality standard during the drought year simulated.

8.4.2 Pulse Releases

Simulations were conducted to determine the potential benefits of short-term increases with flow (pulses) to augment TFO in repelling salinity driven by SLR, in lieu of increasing the flow objective. The concept of a pulse release strategy is to use water effectively to repel salinity while preserving water for use during potentially worse conditions. Historical flows of 1965 with a flow objective of 2,500 cfs were simulated, along with additional flow pulses of 500 cfs or 1,000 cfs during September 1 to 25, when the historical flows increase naturally from a rainfall event. The pulse is immediately effective at pushing the salt front downstream, but the benefit diminishes over time after termination of the pulse (although not completely) for the conditions simulated. Compared to the baseline (0 m SLR), the near-term effect of the pulses is to move the salt front between 1.1 and 1.9 miles downstream for the 500 cfs pulse and between 2.3 and 3.3 miles downstream for the 1,000 cfs pulse. However, without additional pulses, the effect diminishes over time, and by the end of the simulation, the differences in the salt front location ranges from 0.2 to 0.5 miles and 0.4 to 0.9 miles downstream for the 500 and 1,000 cfs pulses, respectively. Except for the baseline condition with 0 m SLR, the salt front is not pushed below the Schuylkill River confluence (RM 92.5) or below the baseline maximum salt front location of RM 93.2 without a pulse in addition to TFO. Without a pulse release, SLR of 1.0 m or more raises the maximum 30-dma chloride concentration at RM 98 above the 180 mg/L water quality standard for at least 92 percent of the time from September through December of the simulated year. Pulse releases in addition to TFO lower the concentration at RM 98 to varying degrees, but the chloride concentration remains above the water quality standard for at least part or all of this time period. Simulated pulses only partially reduce the impact of SLR on salinity.

The distance a pulse keeps the salt front downstream and the length of time until it returns to the pre-pulse location are affected by multiple factors, including (1) the base flow to which the pulse is added and (2) the salt front location prior to the pulse (or the timing of the pulse release). Detailed evaluation of the volume, timing, and geographic triggers for pulse releases or other flow augmentation constructs, such as constant, seasonal, or RM-based flow objectives were outside the scope of this study.

8.4.3 Flow Augmentation from the Delaware River at Trenton versus Schuylkill Rivers

Water for salinity repulsion is currently released from reservoirs in the non-tidal Delaware or Schuylkill River watershed. Simulations were performed to determine the relative efficiencies of water releases from either location or a combination thereof. Model results show that the upstream source of freshwater flow augmentation into the Estuary is relevant to salinity management. Once the salt front is a few miles above the mouth of the Schuylkill River, additional water from the Delaware River at Trenton is more efficient in moving the salt front than the additional water entering the Estuary from the Schuylkill River. When the salt front is below the confluence, the plume of freshwater from the Schuylkill River dilutes the ocean salt temporarily, impeding upstream transport. Once saltier water is above the confluence, the dilution from the influx of fresh water has less effect on the maximum salt front location. For chloride concentrations and salinity, the results are similar.

8.5 Potential Future Work

This analysis of the impacts of sea-level rise on salinity intrusion in the Delaware River Estuary considered multiple factors, yielding critical insights into how the system may behave under future environmental conditions and how it might respond to potential management actions. The findings from this work also highlight the need for several additional studies, including:

- The current drought and salinity management program with flow objectives is an effective method for addressing near-term salinity issues related to sea level rise for most flow conditions. However, more detailed analyses are warranted to determine the flow needed to repel salinity as SLR increases. In addition, the availability of water in storage for flow augmentation with SLR should be re-evaluated with consideration of the potential changes to the flow regime (such as changes in seasonality, volume, and distribution), non-tidal chloride inputs, and water demands, under future climate-impacted scenarios.
- Analyses of the SM3D model configuration indicate that it is appropriate for conservative evaluation of sea level rise scenarios and their impact on salinity and salinity management in the Estuary. As more information and data become available the model can be refined if needed. Model assumptions, such as non-tidal salinity, ocean temperature, and other boundary conditions, may also be factors to consider when designing detailed scenarios for future planning efforts. Climate change may alter the distribution and seasonality of inflows to the Estuary, so additional analysis of other climate-impacted flow conditions may be warranted. The DRBC Advisory Committee on Climate Change, along with other stakeholders, will be engaged to determine appropriate scenarios for future planning efforts.

- The results of this study demonstrate the need for consideration of sea level rise for future planning efforts related to flow and drought management as well as water availability and water supply sustainability. Drinking water purveyors and other water users design treatment and processing equipment based on an expected range of salinity, which can affect the taste and odor of drinking water, interfere with production processes, impact products, and damage equipment and infrastructure. Understanding how the Estuary salinity may change with sea level rise is critical for the protection of public health and safety as well as maintaining adequate water quality for the diverse uses of surface water.
- Salinity is one of many factors used to identify suitable habitat for estuarine aquatic life. Evaluating the impacts of sea level rise on habitat and aquatic life is outside the scope of this study. Although SM3D was developed to evaluate the impacts of SLR and salinity intrusion particularly for public water supplies, it may also be useful for initial qualitative assessments of the impact of sea level rise on habitat and the health of aquatic life.
- Periodic refinement of the model based on new data and other information.

9. REFERENCES

Antonov, J.I., Locarnini, R.A., Boyer, T.P., Mishonov, A.V., Garcia, H.E., Levitus, S., (2006). World Ocean Atlas 2005 Volume 2: Salinity, in: Jolley, D.W. et al. (Ed.) (2002). The North Atlantic Igneous Province: stratigraphy, tectonic, volcanic and magmatic processes. Geological Society Special Publication, 197: pp. 253-269. NOAA Atlas NESDIS, 62(2). NOAA[S.l.]. 182 pp.

American Public Health Association. (1995). Standard Methods for the Examination of Water and Wastewater. APHA, Washington, DC.

Aristizabal M. and R. Chant, (2013). A Numerical Study of Salt Fluxes in Delaware Bay Estuary. Journal of Physical Oceanography, American Meteorological Society, Volume 43, 1572-1588.

Aristizabal M. and R. Chant, (2014). Mechanisns driving stratification in Delaware Bay estuary, Ocean Dynamics (2014) 64: 1615-1629. Doi: 10.1007/s10236-014-0770-1

Aristizabal M. F. and R. J. Chant, (2015). An Observational Study of Salt Fluxes in Delaware Bay. Journal of Geophysical Research: Oceans, American Geophysical Union, Volume 120 2751-2768.

Arnoldo Valle-Levinson, (2010). Definition and classification of estuaries. Cambridge University Press, 978-0-521-89967-3 – Contemporary Issues in Estuarine Physics, Edited by A. Valle-Levinson. Contemporary issues in estuarine physics completo (unam.mx)

Bever AJ, MacWilliams ML. (2013). Simulating sediment transport processes in San Pablo Bay using coupled hydrodynamic, wave, and sediment transport models.

Beckley, B.; Zelensky, N.P.; Holmes, S.A.; Lemoine, F.G.; Ray, R.D.; Mitchum, G.T.; Desai, S.; Brown, S.T.. 2022. Integrated Multi-Mission Ocean Altimeter Data for Climate Research Version 5.1. PO.DAAC, CA, USA. Dataset accessed October 26, 2022, at https://doi.org/10.5067/ALTCY-TJA51

Blunden, J. and D. S. Arndt, Eds., 2019: State of the Climate in 2018. Bull. Amer. Meteor. Soc., 100 (9), Si–S305, doi:10.1175/2019BAMSStateoftheClimate.1. Also see NOAA website https://www.ncdc.noaa.gov/bams

Callahan, John A., Benjamin P. Horton, Daria L. Nikitina, Christopher K. Sommerfield, Thomas E. McKenna, and Danielle Swallow, (2017). Recommendation of Sea-Level Rise Planning Scenarios for Delaware: Technical Report, prepared for Delaware Department of Natural Resources and Environmental Control (DNREC) Delaware Coastal Programs. 116 pp. https://www.dgs.udel.edu/sites/default/files/projects-docs/Delaware%20SLR%20Technical%20Report%202017.pdf

Chant, R.J., Sommerfield, C.K. & Talke, S.A. Correction to: Impact of Channel Deepening on Tidal and Gravitational Circulation in a Highly Engineered Estuarine Basin. Estuaries and Coasts 41, 2447 (2018). https://doi.org/10.1007/s12237-018-0462-z

Chen, F., Shallcross, A., and Fogarty, J. (2025). Three-Dimensional Hydrodynamic and Salinity Model for the Delaware Estuary, Model Calibration Report: DRBC Report No 2025-5. West Trenton, New Jersey. Delaware River Basin Commission. https://www.nj.gov/drbc/library/documents/SalinityModelCalibrationDec2025.pdf.

Chen, J.-L., Ralston, D. K., Geyer, W. R., Sommerfield, C. K., & Chant, R. J. (2018). Wave Generation, Dissipation, and Disequilibrium in an Embayment With Complex Bathymetry. Journal of Geophysical Research: Oceans, 123. doi: doi:10.1029/2018JC014381

Christine Szpilka, Kendra Dresback, Randall Kolar, Jesse Feyen and Jindong Wang. (2016). Improvements for the Western North Atlantic, Caribbean and Gulf of Mexico ADCIRC Tidal Database (EC2015). J. Mar. Sci. Eng. 2016, 4(4), 72; https://doi.org/10.3390/jmse4040072

Church, J.A. and White, N.J. 2006: A 20th century acceleration in global sea-level rise, Geophysical Research Letters, vol. 33, pp. n/a-n/a, 2006. http://dx.doi.org/10.1029/2005GL024826

Church, J.A. and White, N.J. 2011: Sea-Level Rise from the Late 19th to the Early 21st Century, Surveys in Geophysics, vol. 32, pp. 585-602, 2011. http://dx.doi.org/10.1007/s10712-011-9119-1

Church, J.A., White, N.J., Konikow, L.F., Domingues, C.M., Cogley, J.G., Rignot, E., Gregory, J.M., van den Broeke, M.R., Monaghan, A.J., Velicogna, I., 2011: Revisiting the Earth's sea-level and energy budgets from 1961 to 2008. Geophys. Res. Lett. 38 (18).

Coen, Loren D. Mark W. Luckenbach and Denise Breitburg 1999: The Role of Oyster Reefs as Essential Fish Habitat:A Review of Current Knowledge and Some New Perspectives. American Fisheries Society Symposium 22:438–454, 1999.

Dangendorf, S., Hay, C., Calafat, F.M., Marcos, M., Piecuch, C.G., Berk K., and Jensen, J. 2019: Persistent acceleration in global sea-level rise since the 1960s, Nature Climate Change, Vol 9, 705–710, www.nature.com/natureclimatechange . https://doi.org/10.1038/s41558-019-0531-8

David L. Meyer,Edward C. Townsend,Gordon W. Thayer 2008: Stabilization and Erosion Control Value of Oyster Cultch for Intertidal Marsh. First published: 28 June 2008 https://doi.org/10.1046/j.1526-100X.1997.09710.x

Davis, J. L., and N. T. Vinogradova (2017), Causes of accelerating sea level on the East Coast of North America, Geophys. Res. Lett., 44, 5133–5141, doi:10.1002/2017GL072845

Dolgopolova, E. N. (2014). Sediment Transport and Saltwater Intrusion into the Weakly Stratified Estuary of the Delaware River. WATER RESOURCES Vol. 41 No. 2 2014.

DNREC, 1999. Delaware National Estuarine Research Reserve: Estuarine Profile. Delaware Department of Natural Resources and Environmental Control, Dover, Delaware. June 1999.

DRBC, 2019. DRBC Surface Water Charging Program: (18 CFR Part 420) Basin Regulations - Water Supply Charges. With amendments through July 1, 2019. https://www.nj.gov/drbc/library/documents/water_chargesCFR.pdf

DRBC, 2003. DYNHYD5 Hydrodynamic Model (version 2.0) and Chloride Water Quality Model for the Delaware Estuary. Delaware River Basin Commission, West Trenton, New Jersey, December 2003.

DRBC, 2022. Delaware River Basin Water Code, Sections 2.5.3 through 2.5.6 (18 CFR Part 410): https://www.nj.gov/drbc/library/documents/watercode.pdf

DRBC, 2022. Modeling Eutrophication Processes in the Delaware River Estuary: Three-Dimensional Water Quality Model. September 2022 Draft. https://www.nj.gov/drbc/library/documents/AnalysisAttainability/WQModelCalibrationRpt_DRAFTsept2022.pdf

DRBC, 2023. Delaware River Basin Commission Salt Front website, https://www.nj.gov/drbc/programs/flow/salt-front.html

Dutton, A., Carlson, A. E., Long, A. J., Milne, G. A., Clark, P. U., DeConto, R., Horton, B. P., S. Rahmstorf, S., and Raymo, M.E., 2015: Sea-level rise due to polar ice-sheet mass loss during past warm periods. Science, 10 JULY 2015, VOL 349 ISSUE 6244.

Melinda K. Ehrich, Lora A. Harris, A review of existing eastern oyster filtration rate models, Ecological Modelling, Volume 297, 2015, Pages 201-212, ISSN 0304-3800, https://doi.org/10.1016/j.ecolmodel.2014.11.023. (https://www.sciencedirect.com/science/article/pii/S0304380014005961)

Engelhart, S.E. and Horton, B.P., 2009: Holocene sea level database for the Atlantic coast of the United States. Quaternary Science Reviews. Volume 54, 26 October 2012, Pages 12-25.

Engelhart, S.E., Peltier, W.R, and Horton, B.P. 2011: Holocene relative sea-level changes and glacial isostatic adjustment of U.S. Atlantic Coast. Geology, July 2011. Doi: 10.1130/G31857.1

England, M.H., McGregor, S., Spence, P., Meehl, G.A., Timmermann, A., Cai, W., Gupta, A.S., McPhaden, M.J., Purich, A., and Santoso, A. 2014: Recent intensification of wind-driven circulation in the Pacific and the ongoing warming hiatus, Nature Climate Change, vol. 4, pp. 222-227, 2014. http://dx.doi.org/10.1038/nclimate2106

Ezer, T., Atkinson, L.P., Corlett, W.B., and Blanco, J.L., 2013: Gulf Stream's induced sea level rise and variability along the U.S. mid-Atlantic coast. J. Geophysical Research: OCEANS, VOL. 118, 685–697, doi:10.1002/jgrc.20091, 2013

Ezer, T., 2015: Detecting changes in the transport of the Gulf Stream and the Atlantic overturning circulation from coastal sea level data: The extreme decline in 2009–2010 and estimated variations for 1935–2012. Global and Planetary Change, Volume 129, June 2015, Pages 23-36. https://doi.org/10.1016/j.gloplacha.2015.03.002

FEMA, 2011. FEMA Region III Storm Surge Study, "Coastal Storm Surge Analysis System Digital Elevation Model. Report 1: Intermediate Submission No. 1.1". Prepared by USACE ERDC in March 2011.

Galloway, D.L., Jones, D.R., and Ingebritsen, S.E., 2000. Land Subsidence in the United States. USGS Fact Sheet 165-00, December 2000. https://water.usgs.gov/ogw/pubs/fs00165/SubsidenceFS.v7.PDF

Galperin B., L. H. Kantha, S. Hassid, and A. Rosati, (1988). A Quasi-equilibrium Turbulent Energy Model for Geophysical Flows. Journal of the Atmospheric Sciences, American Meteorological Society, Volume 45, No. 1 55-62.

Glick, P., J. Clough, and B. Nunley, B. 2008. "Sea-level rise and coastal habitats in the Chesapeake Bay region." https://www.nwf.org/~/media/PDFs/Global-Warming/Reports/SeaLevelRiseandCoastalHabitats_ChesapeakeRegion.ashx

Goddard, P.B., Yin, J., Griffies, S.M., and Zhang, S., 2015. An extreme event of sea-level rise along the Northeast coast of North America in 2009–2010. Nature Communications 6:6346. DOI: 10.1038/ncomms7346

Gregory J, White N, Church J, Bierkens M, Box J, van den Broeke R, Cogley J, Fettweis X, Hanna E, Huybrechts P, Konikow L, Leclercq P, Marzeion B, Orelemans J, Tamisiea M, Wada Y, Wake L, van den Wal R, 2013: Twentieth-century global-mean sea-level rise: is the whole greater than the sum of the parts? J Clim 26:4476–4499. https://doi.org/10.1175/JCLI-D-12-00319.1

Gregory, Jonathan M., Stephen M. Griffies, Chris W. Hughes, Jason A. Lowe, John A. Church, Ichiro Fukimori, Natalya Gomez, Robert E. Kopp, Felix Landerer, Gone´ri Le Cozannet, Rui M. Ponte, Detlef Stammer, Mark E. Tamisiea, Roderik S. W. van de Wal, 2019: Concepts and Terminology for Sea Level: Mean, Variability and Change, Both Local and Global. Surveys in Geophysics (2019) 40:1251–1289, https://doi.org/10.1007/s10712-019-09525-z

Gregory, M. K. and M. Hare. 2020. The Effect of Salinity on Eastern Oyster Reproduction in the Hudson River Estuary. Section IV:1-43 pp. In S.H. Fernald, D.J. Yozzo, and H. Andreyko (eds.), Final Reports of the Tibor T. Polgar Fellowship Program, 2018. Hudson River Foundation.

Forte, M.F., Stillwell, L., Luettich, R., Roberts, H., Atkinson, J., and Miller, J., 2011. Coastal Storm Surge Analysis System Digital Elevation Model. FEMA Region III Storm Surge Study, Report 1: Intermediate Submission No. 1.1. U.S. Army Corps of Engineers, Coastal and Hydraulics Laboratory, ERDC/CHL TR-11-1.
https://erdc-library.erdc.dren.mil/jspui/bitstream/11681/7728/1/CHL-TR-11-1.pdf

Foster, G. and Brown, P.T. 2014: Time and tide: analysis of sea level time series, Climate Dynamics, vol. 45, pp. 291-308, 2014. http://dx.doi.org/10.1007/s00382-014-2224-3

Hall, J.A., S. Gill, J. Obeysekera, W. Sweet, K. Knuuti, and J. Marburger. (2016). Regional Sea Level Scenarios for Coastal Risk Management: Managing the Uncertainty of Future Sea Level Change and Extreme Water Levels for Department of Defense Coastal Sites Worldwide. U.S. Department of Defense, Strategic Environmental Research and Development Program. 224 pp.

Hammond, J.C., and B.J. Fleming. "Evaluating Low Flow Patterns, Drivers and Trends in the Delaware River Basin." *Journal of Hydrology* 598, no. 2021 (March 2021): 13. https://doi.org/10.1016/j.jhydrol.2021.126246.

Hamlington, B. D., S. H. Cheon, P. R. Thompson, M. A. Merrifield, R. S. Nerem, R. R. Leben, and K.-Y. Kim, 2016: An ongoing shift in Pacific Ocean sea level, J. Geophys. Res. Oceans, 121, 5084–5097, doi:10.1002/2016JC011815.

Hamrick, J.M., (1992). A Three-Dimensional Environmental Fluid Dynamics Code: Theoretical and Computational Aspects. Special Report 317 in Applied Marine Science and Ocean Engineering, Virginia Institute of Marine Science, VA.

Hamrick, J.M. (2007a.) "The Environmental Fluid Dynamics Code User Manual: US EPA Version 1.01," Tetra Tech, Inc., Fairfax, VA.

Hamrick, J.M. (2007b.) "The Environmental Fluid Dynamics Code Theory and Computation. Volume 1: Hydrodynamics and Mass Transport," Tetra Tech, Inc., Fairfax, VA.

Hamrick, J.M. (2007c.) "The Environmental Fluid Dynamics Code Theory and Computation. Volume 2: Sediment and Contaminant Transport and Fate," Tetra Tech, Inc., Fairfax, VA.

Hay, Carling C., Eric Morrow, Robert E. Kopp, and Jerry X. Mitrovica1, 2015: Probabilistic reanalysis of twentieth-century sea-level rise. Nature, 2015, vol. 517, pp. 481-484, 2015. doi:10.1038/nature14093. http://dx.doi.org/10.1038/nature14093

Hay, Carling C., Lau, H.C.P., Gomez, N., Amustermann, J., Powell, E., Mitrovica, J. X., Latychev, K, and Wiens D.A., 2017: Sea Level Fingerprints in a Region of Complex Earth Structure: The Case of WAIS. American Meteorological Society, Journal of Climate, Vol. 30, March 2017, pp1881-1892. DOI: 10.1175/JCLI-D-16-0388.1

Hausfather, Zeke 2019: How climate change is accelerating sea level rise, September 2019, from Carbon Brief (CB) website https://www.carbonbrief.org/explainer-how-climate-change-is-accelerating-sea-level-rise

Horton, B.P., Kopp, R.E., Garner, A.J., Hay, C.C., Khan, N.S., Roy, K., and Shaw, T.A., 2018: Mapping Sea-Level Change in Time, Space, and Probability. Annual Review of Environment and Resources. 2018.43:481-521. https://doi.org/10.1146/annurev-environ-102017-025826, Downloaded from www.annualreviews.org

Hume, T.M. (2005). Tidal Prism. In: Schwartz, M.L. (eds) Encyclopedia of Coastal Science. Encyclopedia of Earth Science Series. Springer, Dordrecht. https://doi.org/10.1007/1-4020-3880-1_320 and https://en.wikipedia.org/wiki/Tidal_prism

ICF Incorporated, L.L.C. (2014): Useful Climate Information for Philadelphia: Past and Future, August 2014. https://www.phila.gov/media/20160505145605/Useful-Climate-Science-for-Philadelphia.pdf

IPCC, 2014 (AR5): Climate Change 2014: Synthesis Report. Contribution of Working Groups I, II and III to the Fifth Assessment Report of the Intergovernmental Panel on Climate Change [Core Writing Team, R.K. Pachauri and L.A. Meyer (eds.)]. IPCC, Geneva, Switzerland, 151 pp.

IPCC, 2021 (AR6): IPCC, 2021: Climate Change 2021: The Physical Science Basis. Contribution of Working Group I to the Sixth Assessment Report of the Intergovernmental Panel on Climate Change [Masson-Delmotte, V., P. Zhai, A. Pirani, S.L. Connors, C. Péan, S. Berger, N. Caud, Y. Chen, L. Goldfarb, M.I. Gomis, M. Huang, K. Leitzell, E. Lonnoy, J.B.R. Matthews, T.K. Maycock, T. Waterfield, O. Yelekçi, R. Yu, and B. Zhou (eds.)]. Cambridge University Press, Cambridge, United Kingdom and New York, NY, USA, 2391 pp. doi:10.1017/9781009157896. https://report.ipcc.ch/ar6/wg1/IPCC_AR6_WGI_FullReport.pdf

Jean-François Legeais, Michaël Ablain, Lionel Zawadzki, Hao Zuo, Johnny A. Johannessen, Martin G. Scharffenberg, Luciana Fenoglio-Marc, M. Joana Fernandes, Ole Baltazar Andersen, Sergei Rudenko, Paolo Cipollini, Graham D. Quartly, Marcello Passaro, Anny Cazenave, Jérôme Benveniste, 2017: An Accurate and Homogeneous Altimeter Sea Level Record from the ESA Climate Change Initiative, Earth Syst. Sci. Data Discuss., https://doi.org/10.5194/essd-2017-116

Jean-François Legeais, Michaël Ablain, Lionel Zawadzki, Hao Zuo, Johnny A. Johannessen, Martin G. Scharffenberg, Luciana Fenoglio-Marc, M. Joana Fernandes, Ole Baltazar Andersen, Sergei Rudenko, Paolo Cipollini, Graham D. Quartly, Marcello Passaro, Anny Cazenave, and Jérôme Benveniste, 2018: An improved and homogeneous altimeter sea level record from the ESA Climate Change Initiative, Earth Syst. Sci. Data, 10, 281–301, 2018. https://doi.org/10.5194/essd-10-281-2018

Ji, Z.-G., M.R. Morton, and J.M. Hamrick. (2001). “Wetting and drying simulation of estuarine processes,” Estuarine, Coastal and Shelf Science, 53:683-700.

Ji, Z.-G., G. Hu, J. Shen, and Y. Wan. (2007). "Three-dimensional modeling of hydrodynamic processes in the St. Lucie Estuary," Estuarine, Coastal and Shelf Science, 73:188-200.

John C. Warner, Brandy Armstrong, Ruoying He, and Joseph B. Zambon1 (2010), Development of a Coupled Ocean-Atmosphere-Wave-Sediment Transport (COAWST) Modeling System, Ocean Modelling, 35(2010)230—244

Johnson, B.H., 2010. Application of the Delaware Bay and River 3D Hydrodynamic Model to Assess the Impact of Sea Level Rise on Salinity. USACE-NAD.

Kauffman, G. J., and K. J. Vonck (2011), Frequency and intensity of extreme drought in the Delaware Basin, 1600–2002, Water Resour. Res., 47, W05521, doi:10.1029/2009WR008821.

Kearney, M., J. Rogers, E. Townshend, E. Rizzo, D. Stutzer, J. Stevenson, and K. Sundborg. 2002. "Landsat Imagery Shows Decline of Coastal Marshes in Chesapeake and Delaware Bays." Eos 83(16): 173-178.

Kendall, R. A., Mitrovica, J.X., and Milne, G.A., 2005: On post-glacial sea level – II. Numerical formulation and comparative results on spherically symmetric models, Geophys. J. Int. (2005) 161, 679–706 doi: 10.1111/j.1365-246X.2005.02553.x

Kemp, A.C., Horton, B.P., Donnellyc, J.P., Mannd, M.E., Vermeere, M., and Rahmstorff, S., 2011: Climate related sea-level variations over the past two millennia. Proceedings of National Academy of Sciences of the United States of America (PNAS), July 5, 2011, vol. 108, no. 27. https://www.pnas.org/content/pnas/108/27/11017.full.pdf

Kemp, A.C., Horton, B.P., Vane, C.H., Bernhardt, C.E., D. Corbett, R., Engelhart, S.E., Anisfeld, S.C., Parnell, A.C., and Cahill, N., 2013: Sea-level change during the last 2500 years in New Jersey, USA. Quaternary Science Reviews. 81 (2013) 90-104. http://dx.doi.org/10.1016/j.quascirev.2013.09.024

Kim, K.W. and Johnson, B.H., 2007. Salinity Re-Validation of the Delaware Bay and River 3D Hydrodynamic Model with Applications to Assess the Impact of Channel Deepening, Consumptive Water Use, and Sea Level Change.

Kim, K.W. and Johnson, B. H., 1998. Assessment of Channel Deepening in the Delaware River and Bay: A Three-Dimensional Numerical Model Study, USACE Technical Report CHL-98-29, September 1998).

Kim, Sung-Chan (2012), Evaluation of a Three-Dimensional Hydrodynamic Model Applied to Chesapeake Bay Through Long-term Simulation of Transport Processes, JAWRA, Vol.49, No.5.

Kopp, R. E., R. M. Horton, C. M. Little, J. X. Mitrovica, M. Oppenheimer, D. J. Rasmussen, B. H. Strauss, and C. Tebaldi, 2014: Probabilistic 21st and 22nd century sea-level projections at a global network of tide-gauge sites, Earth's Future, 2, 383–406, doi:10.1002/2014EF000239.

Kopp, R. E., Andrew C. Kemp, Klaus Bittermann, Benjamin P. Horton, Jeffrey P. Donnelly, W. Roland Gehrels, Carling C. Hay, Jerry X. Mitrovica, Eric D. Morrow, and Stefan Rahmstorf, 2016a: Temperature-driven global sea-level variability in the Common Era, Proceedings of the National Academy of Science, USA, 11(13):E1434–E1441, doi:10.1073/pnas.1517056113. https://www.pnas.org/content/113/11/E1434

Kopp, R.E., A. Broccoli, B. Horton, D. Kreeger, R. Leichenko, J.A. Miller, J.K. Miller, P. Orton, A. Parris, D. Robinson, C.P. Weaver, M. Campo, M. Kaplan, M. Buchanan, J. Herb, L. Auermuller, and C. Andrews, 2016. Assessing New Jersey's Exposure to Sea-Level Rise and Coastal Storms: Report of the New Jersey Climate Adaptation Alliance Science and Technical Advisory Panel, Prepared for the New Jersey Climate Adaptation Alliance. New Brunswick, New Jersey, 34 pp.

Kopp, R.E., C. Andrews, A. Broccoli, A. Garner, D. Kreeger, R. Leichenko, N. Lin, C. Little, J.A. Miller, J.K. Miller, K.G. Miller, R. Moss, P. Orton, A. Parris, D. Robinson, W. Sweet, J. Walker, C.P. Weaver, K. White, M. Campo, M. Kaplan, J. Herb, and L. Auermuller (2019). New Jersey's Rising Seas and Changing Coastal Storms: Report of the 2019 Science and Technical Advisory Panel. Rutgers, The State University of New Jersey. Prepared for the New Jersey Department of Environmental Protection. Trenton, New Jersey.
https://climatechange.rutgers.edu/resources/climate-change-and-new-jersey/nj-sea-level-rise-reports

Kopp, R.E., (2020a), "Sea Level Rise in New Jersey", New Jersey Climate Change Resource Center (NJCCRC) webinar, Rutgers University, June 3, 2020.

Kopp, R.E., (2020b), "Sea Level Rise in the Delaware River Basin". Advisory Committee on Climate Change (ACCC) webinar, December 17, 2020.

Lambeck, K., Rouby, H., Purcella, A., Sunc, Y., and Sambridgea, M., 2014: Sea level and global ice volumes from the Last Glacial Maximum to the Holocene. Proceedings of National Academy of Sciences of the United States of America (PNAS), October 28, 2014, vol. 111, no. 43. https://doi.org/10.1073/pnas.1411762111

Leonard B. P., A. P. Lock, and M. K. MacVean, (1996). Conservative Explicit Unrestricted-Time-Step Multidimensional Constancy-Preserving Advection Schemes. Monthly Weather Review, American Meteorological Society, Volume 124, 2588-2606.

Little, C.M., R.M. Horton, R.E. Kopp, M. Oppenheimer, and S. Yip, 2015: Uncertainty in twenty-first-century CMIP5 sea level projections. J. Climate, 28, no. 2, 838-852, doi:10.1175/JCLI-D-14-00453.1.
Locarnini, R. A., A. V. Mishonov, J. I. Antonov, T. P. Boyer, H. E. Garcia, O. K. Baranova, M. M. Zweng, C. R. Paver, J. R. Reagan, D. R. Johnson, M. Hamilton, D. Seidov, (2013). World Ocean

Atlas 2013, Volume 1: Temperature. S. Levitus, Ed.; A. Mishonov, Technical Ed.; NOAA Atlas NESDIS 73, 40 pp. This document is available online at http://www.nodc.noaa.gov/OC5/indprod.html

MacCready and Geyer (2010): Advances in Estuarine Physics, Annu. Rev. Mar. Sci. 2010. 2:35–58. doi: 10.1146/annurev-marine-120308-081015

MacWilliams, Michael L., Bever, Aaron J., Gross, Edward S., Gerard S. Ketefian2, and Wim J. Kimmerer3 (2015). Three-Dimensional Modeling of Hydrodynamics and Salinity in the San Francisco Estuary: An Evaluation of Model Accuracy, X2, and the Low–Salinity Zone. San Francisco Estuary and Watershed Science, 13(1). https://doi.org/10.15447/sfews.2015v13iss1art2

Mar G Willmott CJ. (1981). On the validation of models. PhysGeogr 2:184–194. Available from: http://climate.geog.udel.edu/~climate/publication_html/Pdf/W_Phys_Geog_1981.pdf eol 345:235–253.

Masterson, J.P., Pope, J.P., Fienen, M.N., Monti, Jack, Jr., Nardi, M.R., and Finkelstein, J.S., 2016, Documentation of a groundwater flow model developed to assess groundwater availability in the Northern Atlantic Coastal Plain aquifer system from Long Island, New York, to North Carolina (ver. 1.1, December 2016): U.S. Geological Survey Scientific Investigations Report 2016–5076, 70 p., https://doi.org/10.3133/sir20165076

Martin Horwath et al, Global sea-level budget and ocean-mass budget, with a focus on advanced data products and uncertainty characterization, Earth System Science Data (2022). DOI: 10.5194/essd-14-411-2022 ; https://phys.org/news/2022-02-individual-contributors-global-sea-level.html

McCabe, Gregory, and David Wolock. “Hydro-Climatic Drought in the Delaware River Basin.” Journal of the American Water Resources Association 56, no. 6 (December 2020): 14. https://doi.org/10.1111/1752-1688.12875 .

Mellor G. L. and T. Yamada, 1982. Development of a Turbulence Closure Model for Geophysical Fluid Problems. Reviews of Geophysics and Space Physics, Volume 20, No. 4, 851-875.

Mitrovica, J.X., Hay, C.C., Kopp, R.E., Harig, C., Latychev, K. 2018: Quantifying the Sensitivity of Sea Level Change in Coastal Localities to the Geometry of Polar Ice Mass Flux, American Meteorological Society, Journal of Climate, Vol. 31, May 2018, pp3701-3709. DOI: 10.1175/JCLI-D-17-0465.1.

Mitrovica, J. X., Gomez, N., Morrow, E., Hay, C., Latychev, K., and Tamisiea, M. E. 2011: On the robustness of predictions of sea level fingerprints. Geophys. J. Int. (2011) 187, 729–742. doi: 10.1111/j.1365-246X.2011.05090.x

Murphy, J.C., Shoda, M.E. and Follette, D.D., 2020, Water-quality trends for rivers and streams in the Delaware River Basin using Weighted Regressions on Time, Discharge, and Season (WRTDS) models, Seasonal Kendall Trend (SKT) tests, and multisource data, Water Year 1978-2018: U.S. Geological Survey data release, https://doi.org/10.5066/P9KMWNJ5.

National Research Council 2010. Advancing the Science of Climate Change.Washington, DC: The National Academies Press. https://doi.org/10.17226/12782 See also https://www.nap.edu/read/12782/chapter/1

NJDEP Science Advisory Board, August 2020. "The Status and Future of Tidal Marshes in New Jersey Faced with Sea Level Rise" https://dep.nj.gov/wp-content/uploads/sab/sab-salt-marsh.pdf

Nicholas Dudley Ward, Jeffrey A. Gebert, and J. Richard Weggel. (2009). Hydraulic Study of the Chesapeake and Delaware Canal. Journal of Waterway, Port, Coastal, and Ccean Engineering, ASCE, January/February 2009.

Ning Lina,, Robert E. Koppb,c,d, Benjamin P. Hortond,e,f,g, and Jeffrey P. Donnellyh 2016: Hurricane Sandy's flood frequency increasing from year 1800 to 2100. www.pnas.org/cgi/doi/10.1073/pnas.1604386113

Nikitina, D.L., Kemp, A.C., Horton, B.P., Vane, C.H., Orson van de Plassche, and Engelhart, S.E., 2014: Storm erosion during the past 2000 years along the north shore of Delaware Bay, USA. February 2014 Geomorphology 208:160–172. DOI: 10.1016/j.geomorph.2013.11.022

Nikitina, Daria, Andrew C. Kemp, Simon E. Engelhart, Benjamin P. Horton, David F. Hill, Robert E. Kopp, 2015: Sea-level change and subsidence in the Delaware Estuary during the last ~2200 years, Estuarine, Coastal and Shelf Science, Volume 164, 2015, Pages 506-519, ISSN 0272-7714, https://doi.org/10.1016/j.ecss.2015.08.012

NYCDEP, 2020: Climate Resiliency Design Guidelines, Version 4.0, September 2020. https://www1.nyc.gov/assets/orr/pdf/NYC_Climate_Resiliency_Design_Guidelines_v4-0.pdf

Pareja-Roman, L. F., Chant, R. J., and Ralston, D. K. (2019). Effects of locally generated wind waves on the momentum budget and subtidal exchange in a coastal plain estuary. Journal of Geophysical Research: Oceans, 124, 1005–1028. https://doi.org/10.1029/2018JC014585

Pareja-Roman, L. F. (2019): Delaware Bay: Hydrodynamics and Sediment Transport in the Anthopocene. Ph.D. dissertation, School of Graduate Studies, Rutgers, The State University of New Jersey, Graduate Program in Oceanography, written under the direction of Robert J. Chant. New Brunswick, New Jersey, October 2019.

Parris, A., P. Bromirski, V. Burkett, D. Cayan, M. Culver, J. Hall, R. Horton, K. Knuuti, R. Moss, J. Obeysekera, A. Sallenger, and J. Weiss. 2012: Global Sea Level Rise Scenarios for the US National Climate Assessment. NOAA Tech Memo OAR CPO-1. 37 pp.

Peltier, W.R. 2004: Global glacial isostasy and the surface of the ice-age Earth: the ICE-5G (VM2) model and GRACE. Annual Review of Earth and Planetary Sciences, May 2004, Vol 32, 111-149.

Peltier, W. R., 2009: Closure of the budget of global sea level rise over the GRACE era: the importance and magnitudes of the required corrections for global glacial isostatic adjustment. Quaternary Science Reviews. (2009) 1-7. doi:10.1016/j.quascirev.2009.04.004

Pendergrass, A.G., Meehl, G.A., Pulwarty, R., Hobbins, M., Hoell, A., AghaKouchak, A., Bonfils, C.J.W., Gallant, A.J.E., Hoerling, M., Hoffmann, D., Kaatz, L., Lehner, F., Llewellyn, D., Mote, P., Neale, R.B., Overpeck, J.T., Sheffield, A., Stahl, K., Svoboda, M., Wheeler, M.C., Wood, A.W., Woodhouse, C.A., 2020. Flash droughts present a new challenge for subseasonal-to-seasonal prediction. Nat. Clim. Change 10 (3), 191–199.

PhilaPort, 2018. Delaware River deepening: 30 years and 16 million cubic yards of sand, muck and rock later. PhilaPort The Port of Philadelphia. https://www.philaport.com/delaware-river-deepening-30-years-and-16-million-cubic-later/

PWD (Philadelphia Water Department) 2023. Website (accessed May 23, 2023) https://water.phila.gov/about-pwd/

PWD Climate Change Adaptation Program: website
https://www.phila.gov/water/sustainability/Pages/ClimateChange.aspx

PWD (May, 2020), Delaware Estuary Salinity Model Validation, Philadelphia Water Department, Watershed Protection Program. https://water.phila.gov/wp-content/uploads/files/salinity-model-validation-report-2020-05.pdf

Rahmstorf, Stefan, and Vermeer, Martin, 2011: Discussion of: Houston, J.R. and Dean, R.G., 2011. Sea-Level Acceleration Based on U.S. Tide Gauges and Extensions of Previous Global-Gauge Analyses. Journal of Coastal Research, 27(3), 409–417. Published by Coastal Education and Research Foundation. URL: https://doi.org/10.2112/JCOASTRES-D-11-00082.1

Rahmstorf, Stefan, Perrette, Mahe, and M. Vermeer, 2011: Testing the robustness of semi-empirical sea level projections. Climate Dynamics, vol. 39, pp. 861-875, 2011. http://dx.doi.org/10.1007/s00382-011-1226-7

Rahmstorf, Stefan, Jason E. Box, Georg Feulner, Michael E. Mann, Alexander Robinson, Scott Rutherford, and Erik J. Schaffernicht, 2015: Exceptional twentieth-century slowdown in Atlantic Ocean overturning circulation. Nature Climate Change, March 2015, DOI:10.1038/NCLIMATE2554

Rumsey, C.A., Hammond J.C., Murphy J., Shoda M., Soroka A. (2023): Spatial patterns and seasonal timing of increasing riverine specific conductance from 1998 to 2018 suggest legacy

contamination in the Delaware River Basin. Journal of Science of the Total Environment 858 (2023) 159691. http://dx.doi.org/10.1016/j.scitotenv.2022.159691

Ray, R.D., and Douglas, B.C., 2011: Experiments in reconstructing twentieth-century sea levels. Progress in Oceanography, 91, 496-515, doi:10.1016/j.pocean.2011.07.021. Plain text dataset available at https://www.psmsl.org/products/reconstructions/

Rockwell, Julia (2020): Climate Impacts, Risks and Adaptation, webinar presented by Philadelphia Water Department, Climate Week at Penn, Panel Discussion on Climate Change Impacts in the Delaware River Basin. From New York to Philadelphia: Expert Perspectives on Climate Change Impacts to Water Systems in the Delaware River Basin. September 22, 2020.

Salehi, Mehrdad (2017), Thermal Recirculation Modeling for Power Plants in an Estuarine Environment, J. of Marine Science and Engineering, 2017, Vol.5, No.5, doi: 10.3390/jmse5010005

Schopp, R.D., and Firda, G.D., (2008), Flood magnitude and frequency of the Delaware River in New Jersey, New York, and Pennsylvania: U.S. Geological Survey Open-File Report 2008–1203, 7 p

Schuckmann, K. von, M.D. Palmer, K.E. Trenberth, A. Cazenave, D. Chamber, N. Champollion, J. Hansen, S.A. Josey, N. Loeb, P.P. Mathieu, B. Meyssignac, and M. Wild, 2016: An imperative to monitor Earth's energy imbalance. Nature Climate Change, Vol 6. Pp 138-144. Doi:10.1038/NCLIMATE2876

Sharp, J. H., K. Yoshiyama, A. E. Parker, M. C. Schwartz, S. E. Curless, A. Y. Beauregard, J. E., Ossolinski, and A. R. Davis, (2009). A biogeochemical view of estuarine eutrophication: seasonal and spatial trends and correlations in the Delaware Estuary. Estuaries and Coasts, 32: 1023-1043.

Schieder, N., D. Walters, and M. Kirwan. 2017. "Massive Upland to Wetland Conversion Compensated for Historical Marsh Loss in Chesapeake Bay, USA." Estuaries and Coasts https://doi.org/10.1007/s12237-017-0336-9

Schopp, R.D., and Firda, G.D., 2008, Flood magnitude and frequency of the Delaware River in New Jersey, New York, and Pennsylvania: U.S. Geological Survey Open-File Report 2008–1203.

Spada, G. and Galassi, G. 2016: Spectral analysis of sea level during the altimetry era, and evidence for GIA and glacial melting fingerprints, Global and Planetary Change, Vol 143, (2016) 34-49. http://dx.doi.org/10.1016/j.gloplacha.2016.05.006

Spada, G. and Melini, D., 2019: On Some Properties of the Glacial Isostatic Adjustment Fingerprints. Water 2019, 11, 1844; doi:10.3390/w11091844.

St. Johns River Water Management District (SJRWMD). 2012. “St. Johns River Water Supply Impact Study,” Technical Publication SJ2012-1. St. Johns River Water Management District, Palatka, FL.

Stammer, D., van de Wal, R. S. W., Nicholls, R. J., Church, J. A., Le Cozannet, G., Lowe, J. A., et al. 2019: Framework for high-end estimates of sea level rise for stakeholder applications. Earth's Future, 7, 923–938. https://doi.org/10.1029/2019EF001163

Sucsy, P.V., and F.W. Morris. (2002). “Calibration of a Three-dimensional Circulation and Mixing Model of the Lower St. Johns River,” Technical Memorandum, St. Johns River Water Management District, Palatka, FL.

Susan Love, Tricia Arndt, and Molly Ellwood, 2014: Recommendations for Adapting to Sea Level Rise in Delaware: Final Report of the Delaware Sea Level Rise Advisory Committee. http://www.dnrec.delaware.gov/coastal/Documents/SeaLevelRise/FinalAdaptationPlanasPublished.pdf

Sweet, W.V., B.D. Hamlington, R.E. Kopp, C.P. Weaver, P.L. Barnard, D. Bekaert, W. Brooks, M. Craghan, G. Dusek, T. Frederikse, G. Garner, A.S. Genz, J.P. Krasting, E. Larour, D. Marcy, J.J. Marra, J. Obeysekera, M. Osler, M. Pendleton, D. Roman, L. Schmied, W. Veatch, K.D. White, and C. Zuzak, (2022): Global and Regional Sea Level Rise Scenarios for the United States: Updated Mean Projections and Extreme Water Level Probabilities Along U.S. Coastlines. NOAA Technical Report NOS 01. National Oceanic and Atmospheric Administration, National Ocean Service, Silver Spring, MD, 111 pp. https://oceanservice.noaa.gov/hazards/sealevelrise/noaa-nos-techrpt01-global-regional-SLR-scenarios-US.pdf

Sweet, W.V., R.E. Kopp, C.P. Weaver, J. Obeysekera, R.M. Horton, E.R. Thieler, and C. Zervas, January 2017: Global and Regional Sea Level Rise Scenarios for the United States. NOAA, National Ocean Service, Silver Spring, MD. 75 pp. NOAA Technical Report NOS CO-OPS 083, 2017
https://tidesandcurrents.noaa.gov/publications/techrpt83_Global_and_Regional_SLR_Scenarios_for_the_US_final.pdf

Sweet, W.V., Dusek, G., Obeysekera, J., and Marra, J.J., 2018: Patterns and Projections of High Tide Flooding Along the U.S. Coastline Using a Common Impact Threshold. NOAA, National Ocean Service, Silver Spring, MD. NOAA Technical Report NOS CO-OPS 086. February 2018.

Tebaldi, C., B. H. Strauss and C. E. Zervas (2012). Modelling sea level rise impacts on storm surges along US coasts. Environmental Research Letters, 7(1, Jan-March 2012), 014032. doi: 10.1088/1748-9326/7/1/014032

Tetra Tech, Inc. (2002). User’s Manual for Environmental Fluid Dynamics Code. Hydro Version 1.00 for U.S. Environmental Protection Agency, Region 4, Atlanta, GA. August 1, 2002.

Tetra Tech, Inc. (2006). EFDC Technical Memorandum: Theoretical and Computational Aspects of the Generalized Vertical Coordinate Option in the EFDC Model. Prepared for US Environmental Protection Agency, Region 4, Atlanta, GA. March 2006

USACE (1997): Delaware River Main Channel Deepening Project (Pennsylvania, New Jersey, and Delaware) Supplemental Environmental Impact Statement. Philadelphia District. 1997

USACE (2013): Incorporating Sea Level Change in Civil Works Programs. December 2013. Regulation (ER) No. 1100-2-8162.

USACE (2014): Procedures to Evaluate Sea Level Change Impact, Responses, and Adaptation. June 2014, Technical Letter (ETL) No. 1100-2-1.

USACE (2018), "Oyster and Water Quality Study for the Delaware River Main Channel Deepening Project", prepared for U.S. Army Corps of Engineers, Philadelphia District, 100 Penn Square East Philadelphia, PA 19107-3390. Prepared by David Bushek, Jason Morson, Amanda Bromilow, Patrick Donovan, Max Ruehrmund, Danielle Kreeger, David Velinsky, Roger Thomas.

USEPA, 2007. Environment Fluid Dynamics Code, EPA version 1.01, https://www.epa.gov/ceam/environment-fluid-dynamics-code-efdc-download-page

USGCRP, 2009: Global Climate Change Impacts in the United States, Thomas R. Karl, Jerry M. Melillo, and Thomas C. Peterson, (eds.). Cambridge University Press, 2009. https://downloads.globalchange.gov/usimpacts/pdfs/climate-impacts-report.pdf

USGCRP, 2017: Climate Science Special Report: Fourth National Climate Assessment, Volume I [Wuebbles, D.J., D.W. Fahey, K.A. Hibbard, D.J. Dokken, B.C. Stewart, and T.K. Maycock (eds.)]. U.S. Global Change Research Program, Washington, DC, USA, 470 pp., doi: 10.7930/J0J964J6. https://science2017.globalchange.gov/

USGS, 2000: Land Subsidence in the United States, USGS Fact Sheet-165-00, December 2000. https://water.usgs.gov/ogw/pubs/fs00165/SubsidenceFS.v7.PDF

Vermeer, M. and Rahmstorf, S., 2009: Global sea level linked to global temperature. Proceedings of the National Academy of Science, USA, PNAS, December 22, 2009, vol. 106, no. 51. doi:10.1073/pnas.0907765106.

van Vuuren, D.P., Edmonds, J., Kainuma, M. et al. The representative concentration pathways: an overview. Climatic Change 109, 5 (2011). https://doi.org/10.1007/s10584-011-0148-z

Volety, A.K. 2008. Effects of salinity, heavy metals and pesticides on health and physiology of oysters in the Caloosahatchee Estuary, Florida. Ecotoxicology 17(7).

Wahl, T., and D. P. Chambers, 2015: Evidence for multidecadal variability in US extreme sea level records, J. Geophys. Res. Oceans, 120, 1527–1544, doi:10.1002/2014JC010443.

WCRP Global Sea Level Budget Group (2018). Global Sea Level Budget 1993-Present. Earth System Science Data, 10(3), 1551-1590. https://doi.org/10.5194/essd-10-1551-2018; https://research-information.bris.ac.uk/ws/portalfiles/portal/170642290/Full_text_PDF_final_published_version_.pdf

Wang, H. V., Johnson, B. H. (2002). Validation and Application of the Second Generation Three=Dimensional Hydrodynamic Model of Chesapeake Bay. Water Quality and Ecosystem Modeling.

Weis, J.S., Harman, C., Ravit, B., and Watson, E., 2020: The Status and Future if Tidal Marshes in New Jersey Faced with Sea Level Rise. NJDEP Science Advisory Board (SAB) Final Report.

Williamson, Tanja N., Elizabeth A. Nystrom, and Paul C.D. Milly. “Sensitivity of the Projected Hydroclimatic Environment of the Delaware River Basin to Formulation of Potential Evapotranspiration.” *Climate Change* 139 (2016): 215–28. https://doi.org/10.1007/s10584-016-1782-2

Wool, T.A., S.R. Davie, and H.N. Rodriguez. 2003. “Development of Three-Dimensional Hydrodynamic and Water Quality Models to Support Total Maximum Daily Load Decision Process for the Neuse River Estuary, North Carolina,” Journal of Water Resources Planning and Management, 129(4), 295–306.

Zervas, C. 2009: Sea Level Variations of the United States 1854–2006. NOAA Technical Report NOS CO-OPS 053, 75p, Appendices A–E.

Zervas, C., Gill, S., and Sweet, W., 2013. Estimating vertical land motion from long-term tide gauge records. NOAA Tech. Rep. NOS CO-OPS 65, 22 p. https://tidesandcurrents.noaa.gov/publications/Technical_Report_NOS_CO-OPS_065.pdf

Zweng, M. M, J. R. Reagan, J. I. Antonov, R. A. Locarnini, A. V. Mishonov, T. P. Boyer, H. E. Garcia, O.K. Baranova, D.R. Johnson, D. Seidov, M.M. Biddle, (2013). World Ocean Atlas 2013, Volume 2: Salinity. S. Levitus, Ed.; A. Mishonov, Technical Ed.; NOAA Atlas NESDIS 74, 39 pp. This document is available on line at http://www.nodc.noaa.gov/OC5/indprod.html

Zheng, L., Chen, F., Bransky, J., Panuccio, E., Beganskas, S., Amidon, T., Yagecic, J., Suk, N., & Kavanagh, K.B. (2024). Modeling Eutrophication Processes in the Delaware River Estuary: Three-Dimensional Water Quality Model. (DRBC Report No. 2024-5). Delaware River Basin Commission.

The Impact of Sea Level Rise on Salinity Intrusion in the Delaware River Estuary Appendices

Technical Report No. 2025 - 6

Managing, Protecting and Improving
the Water Resources of the
Delaware River Basin since 1961

Delaware River Basin Commission
DELAWARE • NEW JERSEY
PENNSYLVANIA • NEW YORK
UNITED STATES OF AMERICA

TABLE OF CONTENTS

APPENDIX A. SEA LEVEL RISE LITERATURE REVIEW

A.1 PRIMARY CAUSES OF GLOBAL AND LOCAL SLR

Sea level rise is typically referenced in two ways: global mean sea level rise (GMSLR) is the result of phenomena happening around the globe, and local relative sea level rise (LRSLR) is caused by local or regional phenomena. Relative sea level (RSL) is defined as the difference in elevation between the sea surface and the land. Global mean sea level (GMSL) is defined as the areal mean of either RSL or sea-surface height over the global ocean. It is important to better understand the variability and the causes of global mean sea-level rise (GMSLR) as well as the local relative sea-level rise (LRSLR) in Delaware Bay. The primary causes of SLR and SLR projections for the Delaware estuary are discussed in this section.

A.1.1 Global Mean Sea level Rise

Global mean sea level (GMSL) is an indicator that reflects the response to natural and anthropogenic forcing factors, and is an essential climate variable (ECV) of the Global Climate Observing System (GCOS) (https://gcos.wmo.int/en/essential-climate-variables). During the past several decades, international concerted efforts were undertaken to monitor the sea level change and provided global and regional long-term sea level records, including both satellite-based and tidal gauge-based measurements (Legeais et al. 2017, 2018; Dangendorf et al., 2019, Rahmstorf and Vermeer 2011). Global observations of sea level variations show an increasing trend since 1900s, and the rate of rise in GMSL is expected to accelerate in the near future under various assumptions of greenhouse gas emission scenarios. The rise in sea level is primarily caused by anthropogenic global warming **Figure A.1-1** (IPCC, AR5 2014, AR6 2022).

Scientists have studied the specific mechanisms causing GMSLR over the past several decades. A study of the earth energy imbalance (EEI) by Schuckmann et. al. (2016) indicated that excess heat accumulation is becoming increasingly dominated by the influence of greenhouse gases and is driving global warming. Ninety percent of the excess heat (positive EEI) is absorbed by the ocean and increased ocean heat capacity, and a small percentage of the excess heat contributes to the melting of arctic sea ice in glaciers, Greenland, and Antarctica. Green-house gas emissions over the past several hundred years have resulted in a steady increase in global atmospheric temperature, which results in the primary drivers in GMSLR: (a) thermal expansion due to the heating of the ocean from global warming; and (b) the increase of ocean mass due to the melting of land-based glaciers and ice sheets. Thermal expansion is caused by the absorption of heat from the atmosphere. Factors that have secondary impact on GMSL include changes in the movement of water between ocean and land as a result of human activities, such as groundwater depletion and water impoundment. The magnitude of liquid water storage on land (e.g., lakes, rivers, groundwater), which affects the amount of water mass in the oceans, is considered highly uncertain (Sweet 2022, Horton et al., 2018; WCRP 2018; Gregory et al., 2019; Kopp et al., 2016; Callahan et al., 2017; and

Kopp et al., 2019, among others). NASA explains and summarizes the major causes of GMSLR in its sea level rise story board website.[1]

Quantifying uncertainties and identifying sources of discrepancies among components in the SLR budget are useful for various applications in climate research. Components of the SLR

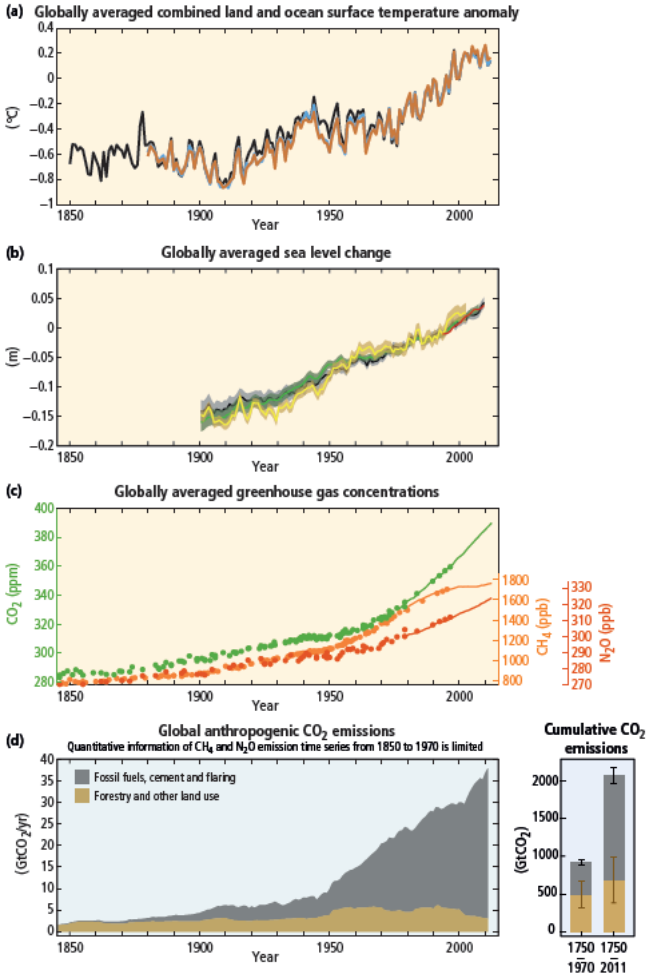

IPCC AR5 (2014) - The complex relationship between the observations (panels a, b, c, yellow background) and the emissions (panel d, light blue background). (a) Annually and globally averaged combined land and ocean surface temperature anomalies relative to the average over the period 1986 to 2005. Colors indicate different data sets. (b) Annually and globally averaged sea level change relative to the average over the period 1986 to 2005 in the longest-running dataset. Colors indicate different data sets. All datasets are aligned to have the same value in 1993, the first year of satellite altimetry data (red). Where assessed, uncertainties are indicated by colored shading. (c) Atmospheric concentrations of the greenhouse gases carbon dioxide (CO2, green), methane (CH4, orange) and nitrous oxide (N2O, red) determined from ice core data (dots) and from direct atmospheric measurements (lines). Indicators: (d) Global anthropogenic CO2 emissions from forestry and other land use as well as from burning of fossil fuel, cement production and flaring. Cumulative emissions of CO2 from these sources and their uncertainties are shown as bars and whiskers, respectively, on the right-hand side.

Figure A.1-1. The complex relationship between observations (panels a, b, c, yellow background) and greenhouse gas emissions (panel d, light blue background) (from IPCC AR5,2014)

budget and its main driving factors were estimated by Hausfather (2019) using data from IPCC AR5 (2014) and shown in **Figure A.1-2**. The estimated rate of SLR in the Church and White dataset (2011) is shown by the black square, and the gap indicates possible missing causes contributing to SLR. For earlier periods, the contributions from each component were not estimated because there is insufficient data. Observations of thermal expansion were not

[1] NASA story board for sea level rise: https://www.nasa.gov/specials/sea-level-rise-2020/

available during the 1901-1990 period in the IPCC AR5 (2014). Large uncertainty seems to exist in estimating the glacial melting (GM) contribution. GM has been estimated to have contributed approximately 1.5 ± 0.5 mm per year to mean sea-level rise during 1993–2010 (Church et al., 2013). This is close to 1.4 mm/year estimated by Mitrovica et al. (2011, 2018). The melting of glaciers and ice caps contributed an estimated 0.7 mm per year, with Greenland and Antarctica contributing about 0.4 mm per year during 1961 to 2008 (Church et al., 2011). The accuracy of estimated ice sheet loss has been improved by satellite gravimetric sensors (GRACE) since the early 2000s.[2]

Melting glaciers and ice sheets contributed roughly two thirds of the total GMSLR between 2005 and 2016, according to the American Meteorological Society (AMS) BAMS report (2018),[3] and one-third of total GMSLR is attributed to thermal expansion between 1993 and

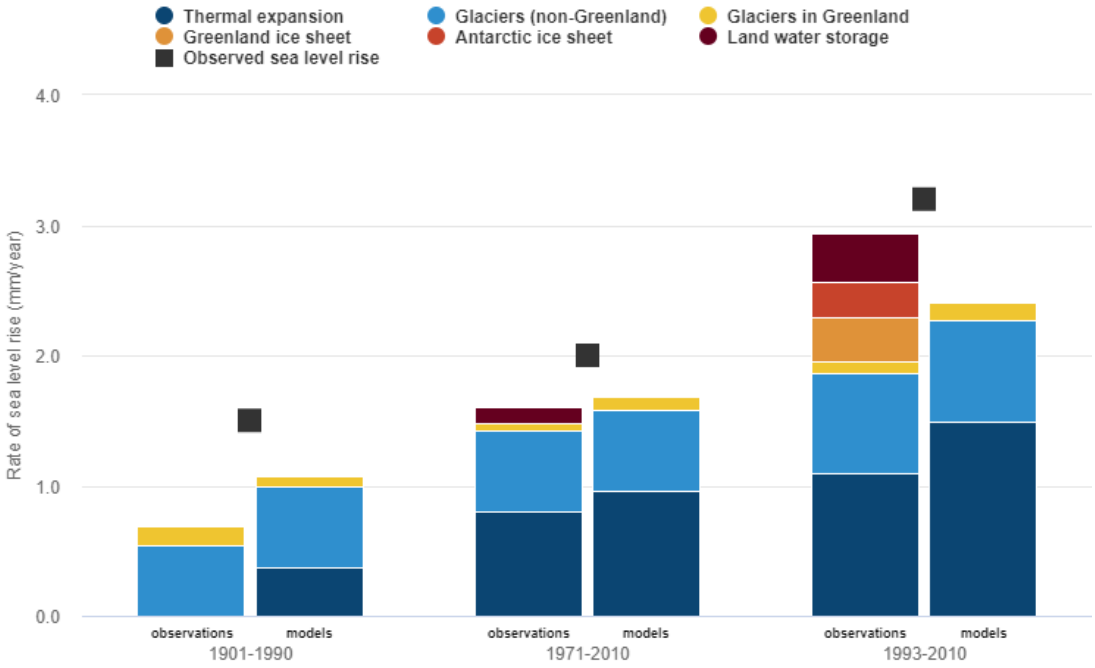

Observed and modelled contributions to the rate of historical sea level rise for the 1901-1990, 1971-2010 and 1993-2010 periods. Overall annual average sea level rise for each period is shown by black squares, based on Church and White 2011. Source: Based on Table 13.1 in Chapter 13 of the IPCC AR5 (pdf). Estimates of ice loss in Greenland comes from two sources that are tracked separately: top-down melting of ice sheets and ice lost from the outflow of glaciers.
Figure from Carbon Brief (CB) website https://www.carbonbrief.org/explainer-how-climate-change-is-accelerating-sea-level-rise

Figure A.1-2. Factors contributing to global sea level rise (from Hausfather, 2019).

[2] https://en.wikipedia.org/wiki/GRACE_and_GRACE-FO

[3] AMS Bulletin of the American Meteorological Society (BAMS) report: https://www.ncei.noaa.gov/bams-state-of-climate

2010, according to Hausfather (2019). The rapid increase in ocean heat content has led to approximately 19 mm of the total 54 mm sea level rise from thermal expansion between 1993 and 2010 (Hausfather, 2019). The World Climate Research Program (WCRP)[4] initiated an international effort involving the sea-level community worldwide to estimate components of the sea-level budget (on a mass-contribution basis) during the altimetry era (1993 to present) (WCRP Global Sea Level Budget Group, 2018). This effort estimated that ocean thermal expansion, melting glaciers, and ice mass loss from Greenland and from Antarctica contribute 42, 21, 15 and 8 percent, respectively, to the global mean sea level rise over the 1993 to present period. The NASA Sea level rise portal provides up-to-date estimates of the rate of change of each component in the global sea level change budget,[5] and it also provides component analysis results for specific future time horizons for specific regions on the earth associated with five global sea level rise scenarios.[6] For example, the analysis for the year 2060 for the contiguous USA is presented in **Figure A.1-3**.

A recent component estimation of SLR by Kopp (2020a, 2020b) showed that contributions from ice melting, thermal expansion of ocean water, and terrestrial water storage are 50, 40, and 10 percent, respectively, for the New Jersey and Delaware coasts. A similar component analysis was presented in NJACC STAP 2019 report (Kopp, et.al., 2019) and is cited in **Table A.1-1.** From this analysis, for the New Jersey coast, vertical downward land motion, including GIA, sediment compaction and other subsidence, is the largest component (47 percent); ocean thermal expansion is the second largest component (27 percent); followed by melting of glaciers and ice sheets (19 percent). This accounting left 7 percent in the overall SLR budget without clear explanation. Recent studies have further closed the uncertainty gaps in the sea level rise budget (Martin Horwath et al., 2022).[7]

[4] WCRP website https://www.wcrp-climate.org/

[5] NASA sea level change portal: https://sealevel.nasa.gov/ and https://sealevel.nasa.gov/understanding-sea-level/by-the-numbers

[6] Earth Data, Interagency sea level rise scenario tool: https://sealevel.nasa.gov/task-force-scenario-tool?type=regional&region=EC

[7] Martin Horwath et al, Global sea-level budget and ocean-mass budget, with a focus on advanced data products and uncertainty characterisation, Earth System Science Data (2022). DOI: 10.5194/essd-14-411-2022;

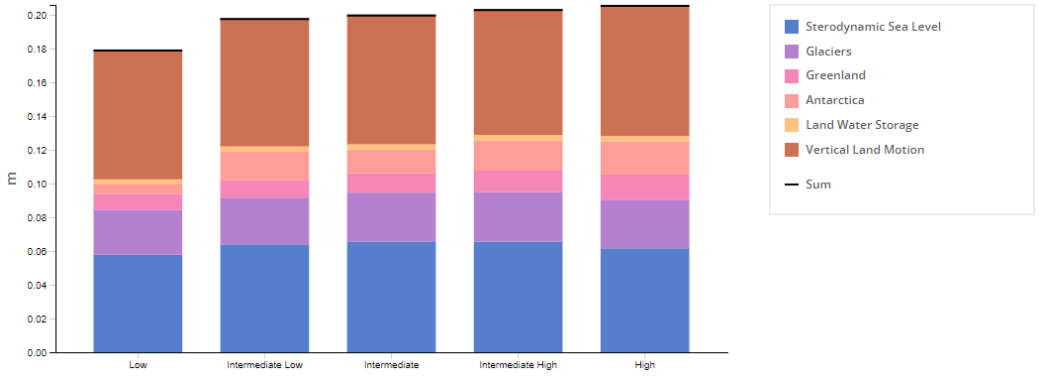

(a) for 2030

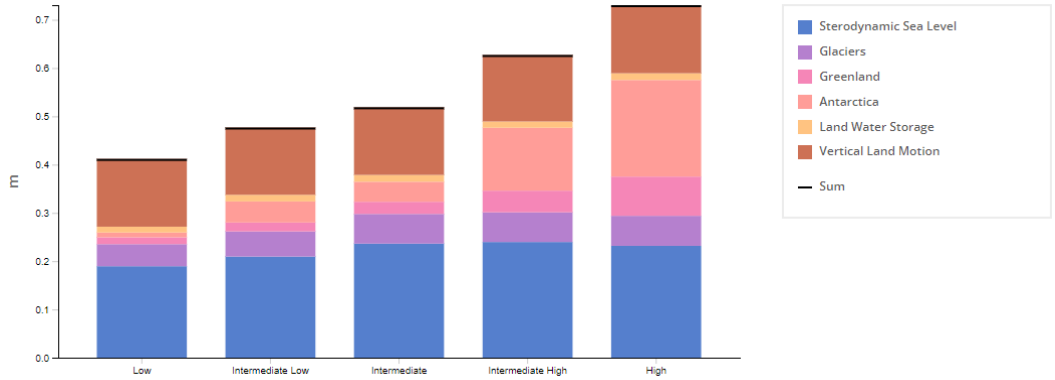

(b) for 2060

Notes: Median sea level projection values from years 2030 to 2150 for individual processes contributing to relative sea level change, relative to a baseline of year 2000. Contributions are shown for the 5 sea level scenarios for the user-selected time period (see at bottom). The sum of the contributions is noted by the black line. In cases where one of the processes has a negative contribution (e.g., uplift), this sum will be lower than the top of the bar.
Source: NASA Earth Data, Interagency Sea Level Rise Scenario Tool.
Link provided from NOAA website: https://sealevel.nasa.gov/task-force-scenario-tool?type=regional&region=EC

Figure A.1-3. Individual process contributions to GMSLR for five sea level rise scenarios for the contiguous USA.

Table A.1-1 Global and New Jersey sea-level budgets, 1993-2017 (in/decade [mm/yr]), from the NJACC STAP 2019 report (Kopp, et.al., 2019)

	Global	New Jersey
Total observed	1.2 ± 0.1 [3.07 ± 0.37]	1.9 ± 0.1 [4.8 ± 0.2]
Global-mean thermal expansion	0.5 ± 0.2 [1.3 ± 0.4]	0.5 ± 0.2 [1.3 ± 0.4]
Glaciers	0.26 ± 0.06 [0.65 ± 0.15]	0.16 ± 0.04 [0.4 ± 0.1]
Greenland ice Sheet	0.19 ± 0.04 [0.48 ± 0.10]	0.09 ± 0.02 [0.23 ± 0.05]
Antarctic Ice sheet	0.10 ± 0.04 [0.25 ± 0.10]	0.12 ± 0.04 [0.3 ± 0.1]
Terrestrial water storage	(poorly constrained)	(poorly constrained)
Dynamic sea level	N/A	(poorly constrained)
GIA and natural sediment compaction	N/A	0.6 ± 0.04 [1.5 ± 0.1]
Other subsidence	N/A	0.3 ± 0.1 [0.7 ± 0.2]
Total of well-characterized components	1.1 ± 0.2 [2.7 ± 0.5]	1.7 ± 0. 2 [4.4 ± 0.5]

Notes: The global budget for 1993-2017 is based on WCRP Global Sea Level Budget Group (2018). The New Jersey budget is based on the GRD fingerprint factors from Kopp et al. (2014) for glacier and ice sheet contributions, GIA and other natural subsidence from geological records (Kopp et al., 2016), and other subsidence from both a comparison of long-term trends and the analysis of Johnson et al. (2018). Uncertainties are one standard error.

A.1.2 Local Sea Level Rise

The change in regional relative sea level is the most important when assessing the impact of climate change and sea level rise. LRSL differs from GMSL in rate and magnitude over different time scales because driving processes for local RSL change are spatially variable (Horton et al., 2018). Processes attributed to LRSL change, in addition to thermal expansion and melting of the glaciers and ice sheet, include:

1) Geologic land subsidence due to the Glacial Isostatic Adjustment (GIA) from the Laurentide ice sheet during the last Ice Age (the ongoing adjustment of the solid Earth to the loss of the North American ice sheet at the end of the last ice age);

2) Land Water Storage (LWS),[8] which results from the Gravitational, Rotational, and Deformational (GRD) effects of Glacial Melting (GM), including the effect of melting ice sheets of Greenland and Antarctica on ocean mass redistribution;

3) Vertical Land Motion (VLM) due to tectonics or coastal plain sediment consolidation and groundwater withdrawal along the coastal areas; and

4) Sterodynamic Variability,[9] which involves the changes in atmosphere-ocean dynamics, such as ocean circulation.

As mentioned in previous sections, the largest contributor to local sea level rise is the combination of all types of vertical land motions (VLM) for the Delaware Bay and coastal area. Land subsidence in the mid-Atlantic region since the Last Glacial Maximum is dominated by GIA (Kopp et al., 2016a). The loss of mass from glacial ice removes the weight pushing the ground into the earth. When that weight is relieved, the elevation of the terrestrial surface previously covered by the glacier rises, while the area not formerly covered sinks. Assuming that the solid Earth response is elastic, numerical models were developed to estimate the impact from GIA and glacial melting (GM). One such model is ICE-5G (VM2) (Peltier, 2004, 2009). These models predict the geographical pattern of static sea level change on a rotating Earth without coupling with ocean dynamics. The static sea level change is gravitationally self-consistent and is simulated by changing the Earth surface loading and redistribution of mass from the melting ice sheets (Peltier 2004, Kendall et al. 2005, Mitrovica et al. 2018).

Local SLR can also result from changes in ocean circulation. Atlantic Meridional Overturning Circulation (AMOC)[10] also exerts some control on North Atlantic sea levels, particularly along the Northeast Coast of North America. The melting of ice sheets on Greenland adds more fresh cold water to the northern part of the current and may cause slowing or weakening of the AMOC. Freshwater has a lower density than saltwater, so the water sinks more slowly than when less freshwater is added (because the salt is diluted) at the poles due to melting. As a result, the slower or weaker rate of sinking due to the density difference causes the current to slow down. Exceptional AMOC weakening during the winter of 2009–10 period has been implicated in a damaging 13 cm sea level rise along the New York coastline (Goddard, 2015). Some scientists believe that the weakening of AMOC may cause a buildup of water along the U.S. mid-Atlantic coast (Rahmstorf et al., 2015; Ezer et al., 2013; Ezer, 2015).

[8] Land Water Storage: Changes associated with the transfer of water between land and ocean. This includes variability in the global water cycle, groundwater withdrawal, and water impoundment. These changes are expressed regionally through gravitational, rotational and deformational (GRD) changes that have a characteristic pattern, or fingerprint. See NASA https://sealevel.nasa.gov/understanding-sea-level/regional-sea-level/overview

[9] Sterodynamic Variability: Sea level change that arises from variability in the ocean's circulation, temperature and saltiness. This includes large-scale climate signals like the seasonal cycle, El Niño-Southern Oscillation, North Atlantic Oscillation, and Pacific Decadal Oscillation. This also includes longer-term changes in ocean circulation that may occur in the future and global sea level rise associated with long-term warming of the ocean and associated expansion. See NASA https://sealevel.nasa.gov/understanding-sea-level/regional-sea-level/overview

[10] AMOC: Atlantic Meridional Overturning Circulation (AMOC) is the north-south circulation of water in the Atlantic Ocean with water on the surface flowing north and deeper water flowing south, resulting in the transport of heat (energy) from the equator towards the pole. Warm water travels north to the artic then cools, sinks and flows south. It warms at the equator and then flows north again. Heat or energy moves from warmer (higher energy) areas to colder (lower energy) areas.

The two largest ice sheets on Earth today, the Greenland ice sheet (GIS) and the Antarctica ice sheet (AIS), cover most of Greenland and Antarctica. During the last ice age, ice sheets also covered much of North America and Scandinavia. These huge ice sheets contain more than 99 percent of the freshwater ice on Earth.[11] The Greenland Ice Sheet (GIS) extends over about 1.7 million square kilometers (660,000 square miles). The Antarctic ice sheet is about 2 kilometers (1.2 miles) thick. It covers more than 14 million square kilometers (5.4 million square miles) and contains about 30 million cubic kilometers (7.2 million cubic miles) of water. Rapid melting of an ice sheet (e.g., the Greenland and Antarctic ice sheets) would lead to a geographically variable sea level change due to weakening of the gravitational force. The huge ice sheet (the GIS weighs on the order of 30,000 trillion tons) attracts (pulls up) the surrounding seawater by the powerful gravitational force. As the ice sheet melts, the gravitational force exerted on the nearby seawater relaxes. As a result of the melting ice sheet, two opposite effects occur: the seawater surface rises as the addition of water mass flows into the ocean; on the other hand, the ocean surface becomes lower near the vicinity of the melting ice sheet because the gravitational influence diminishes (Mitrovica et al., 2011, 2018; Hay et al., 2015). The rate of volume loss of the Greenland Ice Sheet (GIS) from rapid melting is equivalent to a GMSL rise of 1 mm per year. However, the local SLR is spatially variable. Sea level may drop within 1000 miles or 2000 km from the melting GIS; beyond that distance, the contribution from the melting ice sheet to SLR becomes positive and includes the Delaware coast. The predicted sea level change generally increases at greater distance from the ice sheet, with maximum values of ~1.4 mm per year in regions far from the melting ice (Mitrovica et al. 2011 and 2018).

Local vertical land movement (e.g., land subsidence) may be caused by the consolidation and compaction of coastal plain sediments due to groundwater withdrawal from lower aquifers and natural sediment compaction. Observed from the ocean, the land appears to be sinking, whereas from the land, the ocean appears to be rising more quickly than the global rate. Bowers Beach and the Dover area in Delaware may be experiencing possible land subsidence due to this process (USGS Fact Sheet-165-00 December 2000).

Multiple physical processes that influence regional sea level rise are described in the NASA sea level change website.[12]

[11] Ice Sheet: https://education.nationalgeographic.org/resource/ice-sheet

[12] NASA sea level change website: https://sealevel.nasa.gov/understanding-sea-level/regional-sea-level/overview

A.2 Historical SLR Records

Saltmarsh sediments from Delaware Bay preserve the elevation and age of past sea level. Analysis of these sediments indicates that the historic rate of LSLR from 2200 to 150 years BP[13] is 1.25 ± 0.27 mm/yr (Nikitina et al., 2014). Research by Lambeck et al. (2014) documented global sea level change over the past 35,000 years. They found that global ocean volume remained relatively constant from 2500 years until the recent rise beginning about 150 years ago.

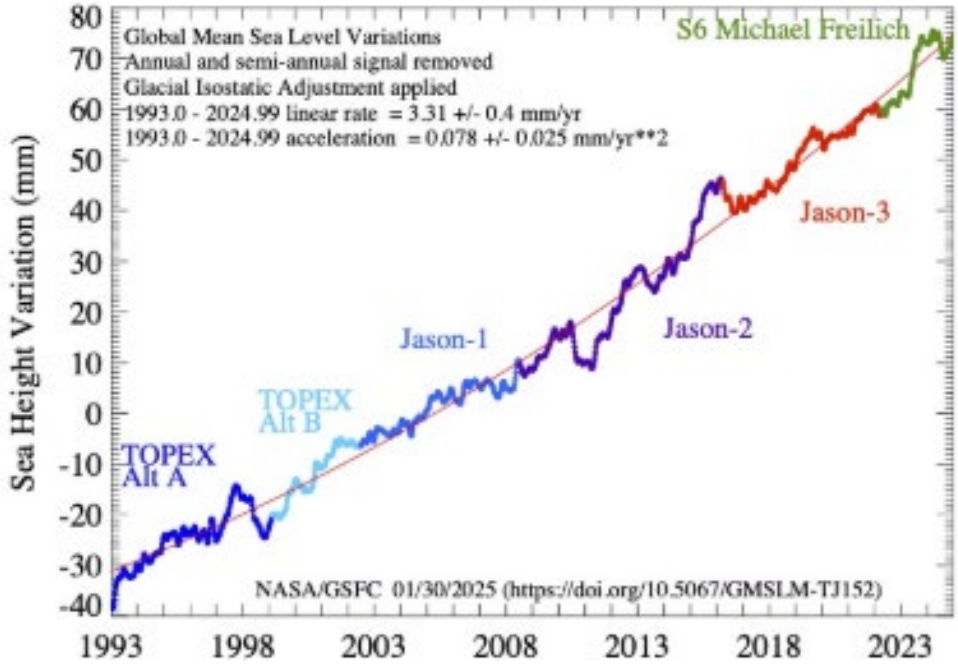

Source NASA (Beckley et al., 2024
https://podaac.jpl.nasa.gov/dataset/MERGED_TP_J1_OSTM_OST_GMSL_ASCII_V52

(1992-Sep-01 to Present)

Figure A.2-1 Trend in global mean sea level change from 1993 to October 2022, based on data collected from satellite altimeters.

Observations of sea levels averaged over the globe, or global mean sea level (GMSL), demonstrate an increasing trend since the 1900s. Based on analyses of satellite observations

[13] BP: kilo annum before present. For example, 150 years BP means 150 years ago.

summarized in NASA's Integrated Multi-Mission Ocean Altimeter Data for Climate Research, GMSL has risen by 104 mm (4.09 inches) since 1993, and the average rate of change was 3.4 (+/- 0.4) mm/year or 1.34 inch/decade (as of October 26, 2022).[14] **Figure A.2-1** presents the two-month running average of GMSL from September 1993 through October 26, 2022. Based on satellite and in-situ tide gauge records, the rate of GMSLR was 1.7 (1.5 to 1.9) mm/year between 1901 and 2010, and 3.2 mm/year between 1993 and 2010 (IPCC AR5, 2014). Satellite data indicates that SLR is not constant around the globe but varies throughout the ocean and along the coasts. The differences are due to local phenomena that also affect SLR. Local sea level rise projections are calculated as the change in sea surface height (SSH), based on climatic causes and vertical land movement (VLM) related to non-climatic causes. Examples of the physical processes that create local sea level rise (LSLR, or also relative local sea level rise–RLSLR) include land subsidence, compaction of sediments, groundwater withdrawals in coastal areas (e.g., VLM) and changes in ocean currents, temperature and salinity, and gravitational, rotational, and deformation effects from the loss of mass from melting ice in Greenland and Antarctica (SSH). Estimates of GMSLR among tide gauge and satellite altimetry studies of large areas over the global oceans, apart from the coastal areas, for the same time period (approximately 1993 to 2019), are in relatively close agreement at Cape May, New Jersey (**Figure A.2-2**).

Hay et al. (2015) revisited estimates of twentieth century GMSLR using probabilistic techniques and calculated a rate of GMSLR from 1901 to 1990 of 1.2 ± 0.2 mm/year (90% confidence interval) and 3.0 ± 0.7 mm/year between 1993 and 2010, which is consistent with prior estimates from tide gauge records. The World Climate Research Program (WCRP) estimated that the average rate of GMSLR during 1993-2017 was 3.1 ± 0.4 mm/year and increased from about 2.1 mm/year at the start of this period to about 4.1 mm/year today (WCRP Global Sea Level Budget Group, 2018).

The SLR footprint varies worldwide. The local sea level changes are displayed in **Figure A.2-3** determined from satellite altimeters during the period from 1993 to 2019 are displayed in **Figure A.2-3**. SLR is much faster than the global average near Australia, as shown in shades of red, while other areas, such as the western coasts of North America, have experienced falling sea levels (shades of blue). Air temperature has been rising in New Jersey (part of the Delaware Estuary) faster than the global average (Kopp 2020a and 2020b). **Table A.2-1** contains a list of the linear trends and confidence intervals for stations in the Delaware Estuary region, calculated from tide gauge monthly MSL records for each station's period of record. The rate at the Lewes station at the mouth of the Delaware Bay is greater than the 20th century GMSLR rate primarily due to vertical land subsidence effects. **Figure A.2-4** shows the monthly variation and long-term trend of sea level at multiple NOAA tidal gage stations from the Lewes, Reedy Point tide gauges to Philadelphia. At the Lewes tide gauge, the linear rate of 3.53 mm/year equates to about 0.353 m of sea-level rise since 1919 using available data up to 2019[15]. At the NOAA tide gauge at Philadelphia, the relative sea level trend is 3.02 mm/year

[14] NASA Sea Level Change website https://sealevel.nasa.gov/

[15] Noted that these figures have been updated by NOAA every year, at the time of this modeling study, the information as of 2019 was used

with a 95 percent confidence interval of +/- 0.19 mm/year, based on monthly mean sea level data from for 1900 to 2020, which is equivalent to a change of 0.36 m or 1.2 ft in 120 years.

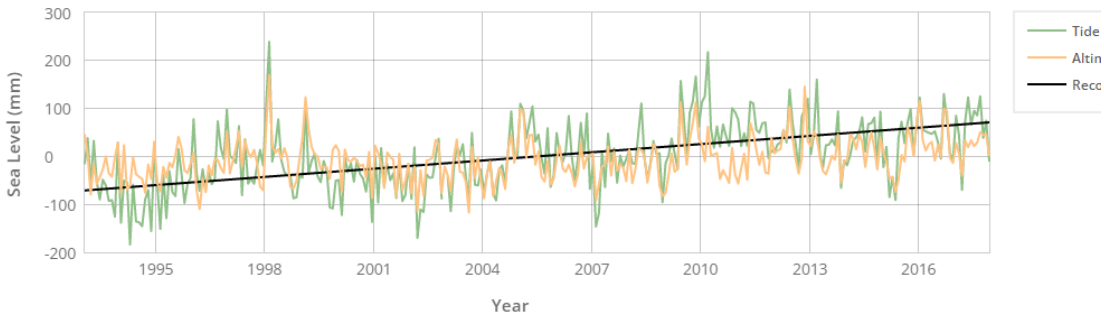

Source: NASA: https://sealevel.nasa.gov/sea-level-evaluation-tool?psmsl_id=1153

Notes: Comparison of tide gauge data and satellite altimetry data measured at nearest point to tide gauge location. Note, satellite altimetry does not provide measurements right at the coast, potentially leading to disagreements with the tide gauge data. The contribution from subsidence ('land') at the tide gauge location can be toggled on and off. For direct comparison to satellite altimetry data, the trend contribution from subsidence to the tide gauge should be turned off. This figure includes the land subsidence.

Figure A.2-2 Comparison of sea levels measured using altimetry and tide gauge data at Cape May, New Jersey.

Table A.2-1. Observed local SLR rates and confidence intervals for selected NOAA tide stations.

NOAA Tide Station	Station Name	Period of Record	Number of Years of Record	Linear Trend and 95% Confidence Interval (mm/year)
8534720	Atlantic City, NJ	1911-2019	108	4.12 +/1 0.15
8536110	Cape May, NJ	1965-2019	54	4.73 +/- 0.49
8557380	Lewes, DE	1919-2019	100	3.53 +/- 0.23
8545240	Philadelphia, PA	1900-2019	119	3.02 +/- 0.19
8551910	Reedy Point, DE	1956-2019	63	3.69 +/- 0.46
8573927	Chesapeake City, MD	1972-2019	47	4.07 +/- 0.67

Source: NOAA Tides and Currents Sea Level Trends website, https://tidesandcurrents.noaa.gov/sltrends/sltrends.html

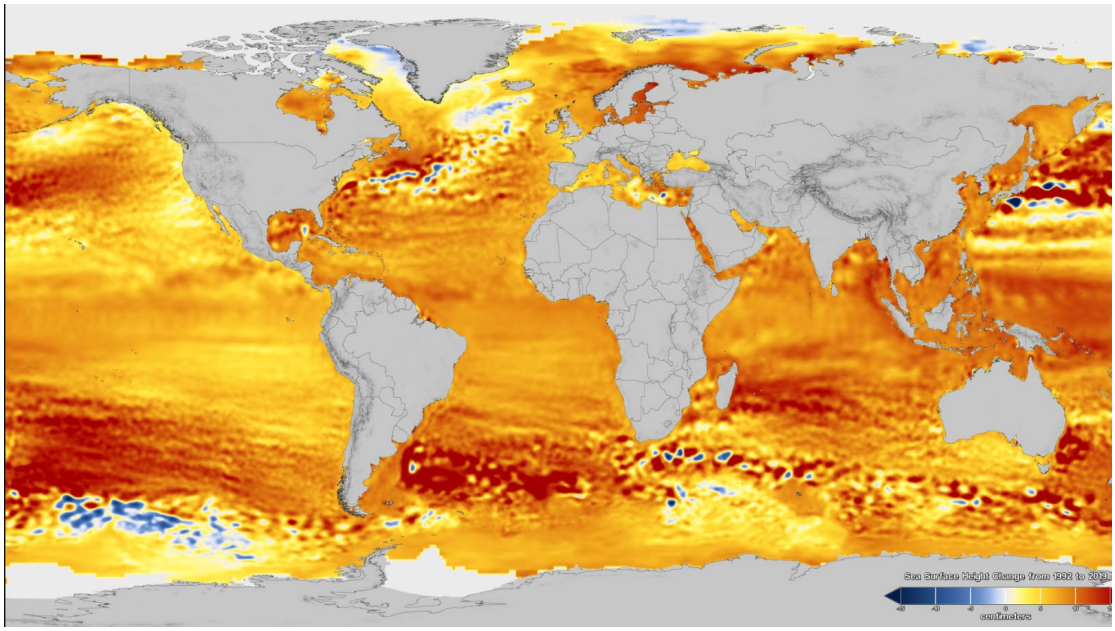

Figure from the NASA Scientific Visualization web site: https://sealevel.nasa.gov/internal_resources/443

Figure A.2-3 Global mean sea level change from 1992-2019, based on data collected from satellite altimeters.

NOAA uses a 19-year tidal cycle, called an epoch, to calculate tidal datums. The present National Tidal Datum Epoch (NTDE) is 1983 through 2001 (centered on 1992), known as the 1983-2001 epoch. In this study, the baseline datum was set to be centered in the year 2000 (i.e.,1991-2009 epoch) to be consistent with other studies (Sweet et al. 2017; Sweet et al, 2022; STAP 2019; DRNEC 2017.). This is defined as the **baseline of 2000.**[16] The offset from current MSL datum centered on 1992 (1983-2001 epoch) is 0.0325 m or 1.28 inch.

[16] **Baseline of 2000 (also used as "2000 Baseline")**: this study adopts the same concept that has been used by others such as NOAA and NJSTAP. Scientists in the U.S. measure sea-level with respect to a geodetic datum named the North American Vertical Datum of 1988 (NAVD88). NOAA measures tidal datum levels such as Mean Sea-level (MSL) in relation to the NAVD88 geodetic datum over a 19-year tidal cycle referred to as a tidal datum epoch. For example, the current National Tidal Datum Epoch is 1983 – 2001 centered in 1992 (also called NTDE 1992). The 19-year period is necessary to accurately determine the complete 37 harmonic constituents of the astronomic tide. Based on data collected from NOAA station 8557380 at Lewes DE, the average sea level for the 1991-2009 period (centered on 2000) is 0.0325 meter or 1.28 inch above the mean sea level for NTDE 1992. Therefore, there is a datum adjustment with the baseline of 2000 as well as simulated SLR scenarios.

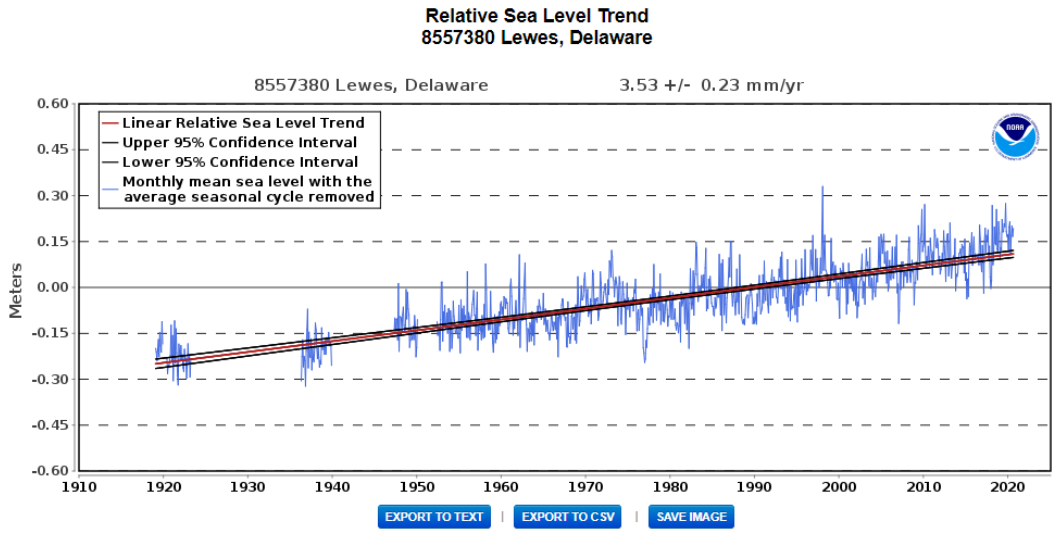

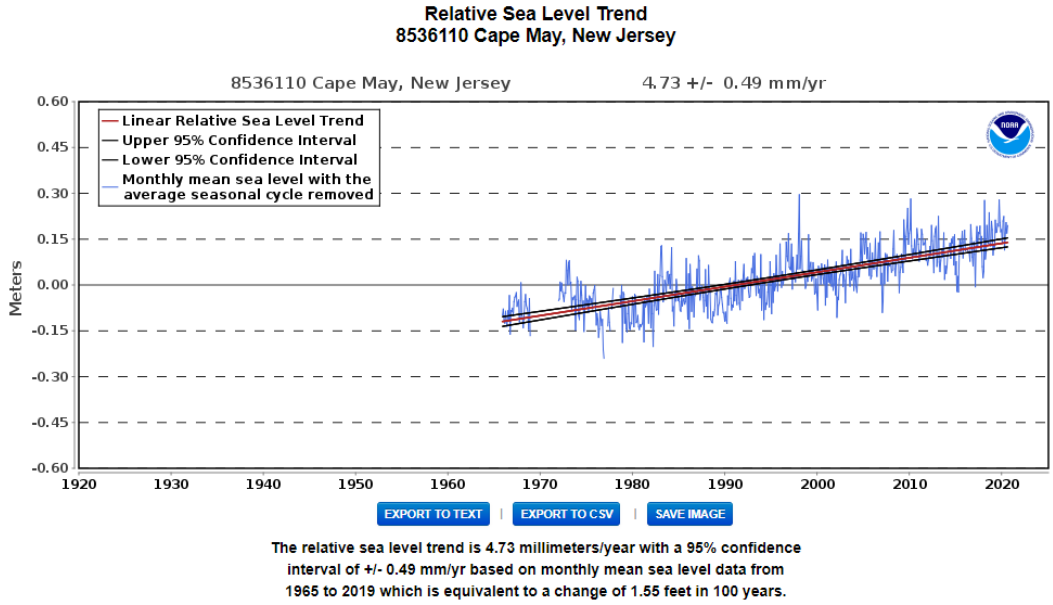

Linear MSL trend and 95% confidence interval shown in red and black, respectively. Data referenced to NTDE 1983-2001 MSL. Source: NOAA CO-OPS Tides and Currents SLR Trends. Figure was last updated in 2019. website, https://tidesandcurrents.noaa.gov/sltrends/sltrends.html;

Figure A.2-4 (a) Relative sea level trend for selected NOAA stations.

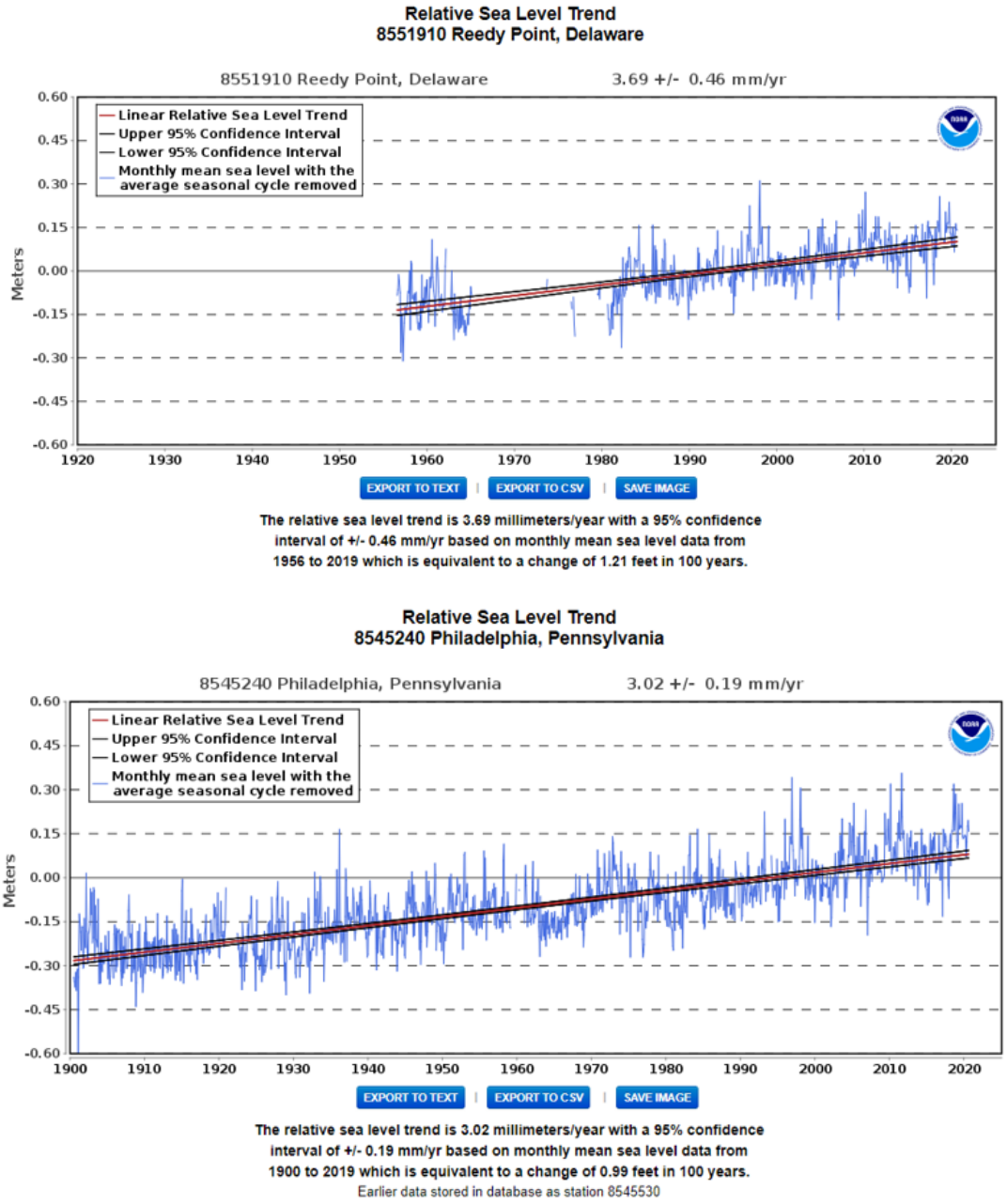

Linear MSL trend and 95% confidence interval shown in red and black, respectively. Data referenced to NTDE 1983-2001 MSL. Source: NOAA CO-OPS Tides and Currents SLR Trends. Figure was last updated in 2019. website, https://tidesandcurrents.noaa.gov/sltrends/sltrends.html

Figure A.2-4 (b) Relative sea level trend for selected NOAA stations.

A.3 SLR PROJECTIONS

A.3.1 Understanding the Relative Sea Level for the Delaware Coast

Relative sea level (RSL) is defined as the height of the sea surface at a specific location, measured with respect to the height of the surface of the solid Earth. To determine the LRSLR for analyses for future conditions, the NOAA 2017 report (Sweet et al., 2017) approach was used and represented by the following equation.

$$\Delta RSL = \Delta SSH - VLM \quad (2.3\text{-}1)$$

where ΔRSL = the Local Relative Sea Level change (positive for rising sea level);

ΔSSH = Local change in Sea Surface Height (related to climatic causes); and

VLM = Local Vertical Land Motion (related to non-climatic causes)

In general, ΔRSL could be negative if the sea surface height SSH decreases. A negative VLM (downward sinking) contributes to a positive local sea level rise. According to the NOAA 2017 report (Sweet et al., 2017), local SSH addresses the variation of mass or volume of oceans as a result of climate change. VLM is the contribution from the changes of the land with respect to the sea surface. The SSH and VLM in equation (2.3-1) can be differentiated into separate processes of climatic and non-climatic causes. Changes in local SSH are the result of the global-warming induced changes in GMSL caused by 1) melting glaciers and ice sheets; 2) thermal expansion of ocean water; and 3) the amount of freshwater storage on land, etc.; and 4) VLM. VLM includes longer-time-scaled processes such as 1) GIA, tectonics and sediment compaction (ongoing since the end of the last ice age at a quasi-steady rate and not-related to current and future climate change); and 2) land subsidence from shorter-time-scale processes such as the pumping of groundwater and extraction of fossil fuels. NOAA estimated the vertical land motion (VLM) in the Delaware Bay area to be -1.66 mm/year according to NOAA Technical Report NOS CO-OPS 065 (Zervas, et al., 2013).[17]

The relative sea level rise as a result of climate change relative to the baseline of 2000, ΔRSL or RSL, was projected by NOAA and is available through the NOAA website (details are provided in the following sections) at tide gauge stations along the coasts of the United States. For the Delaware coast, the area most relevant to this study, the projections at NOAA station 8557380 at Lewes, DE were used. Information from nearby stations such as Atlantic City NJ was also reviewed and compared with the projections for the Delaware Estuary.

Since the RSL projections for future SLR already include the VLM, the land movement as well as sediment transport processes were not considered in this study. The local relative sea level

[17] The current SLR rate at Lewes is 3.53mm/yr based on historical data up to 2019. The contribution of land subsidence is 1.66/3.53 = 47 percent or approximately half of the total LSLR.

rise at the mouth of Delaware Bay was used to represent the tidal forcing for existing boundary conditions.

Using the NOAA SLR viewer (https://coast.noaa.gov/slr/#/layer/slr) estimates of RSL at Reedy Point (eastern end of the C&D Cannel) and a station at Baltimore MD, the estimated magnitude of SLR is comparable between the upper Chesapeake Bay and the eastern end of the C&D Cannel. In this study, the same magnitude of SLR was assigned at the mouth of the bay and at the western end of the C&D Canal. Further investigation might be needed to account for water surface elevation change in the C&D Canal under future conditions.

A.3.2 GMSLR Projections

The first term on the right-hand side of equation (2.3-1) is a function of GMSL change. Probability projections provided by IPCC AR5 (2014) are summarized in **Table A.3-1** and **Figure A.3-1**. The report (IPCC AR5 2014) includes the following conclusions:

- "Surface temperature is projected to rise over the 21st century under all assessed emission scenarios. It is very likely that heat waves will occur more often and last longer, and that extreme precipitation events will become more intense and frequent in many regions. The ocean will continue to warm and acidify, and global mean sea level to rise".

- "The increase of global mean surface temperature by the end of the 21st century (2081–2100) relative to 1986–2005 is likely to be 0.3°C to 1.7°C under RCP2.6, 1.1°C to 2.6°C under RCP4.5, 1.4°C to 3.1°C under RCP6.0 and 2.6°C to 4.8°C under RCP8.59. The Arctic region will continue to warm more rapidly than the global mean. The global ocean will continue to warm during the 21st century, with the strongest warming projected for the surface in tropical and Northern Hemisphere subtropical regions".

- "Ocean warming dominates the increase in energy stored in the climate system, accounting for more than 90 percent of the energy accumulated between 1971 and 2010 (high confidence), with only about 1 percent stored in the atmosphere. On a global scale, the ocean warming is largest near the surface, and the upper 75 m warmed by 0.11 [0.09 to 0.13] °C per decade over the period 1971 to 2010. It is virtually certain that the upper ocean (0−700 m) warmed from 1971 to 2010, and it likely warmed between the 1870s and 1971"

- "Global mean sea level rise will continue during the 21st century, very likely at a faster rate than observed from 1971 to 2010. For the period 2081–2100 relative to 1986–2005, the rise will likely be in the ranges of 0.26 to 0.55 m for RCP2.6, and of 0.45 to 0.82 m for RCP8.5 (medium confidence). Sea level rise will not be uniform across regions. By the end of the 21st century, it is very likely that sea level will rise in more than about 95 percent of the ocean area.

About 70 percent of the coastlines worldwide are projected to experience a sea level change within ±20 percent of the global mean".

In AR5, the RCP 8.5 pathway represents the high-end, business-as-usual emissions scenario, whereas RCP 4.5 pathway represents a moderate global emissions scenario and RCP 2.6 represents intense mitigation scenario. The likely temperature and GMSLR ranges for each scenario for mid- and late- 21 century are presented in **Table A.3-1**.

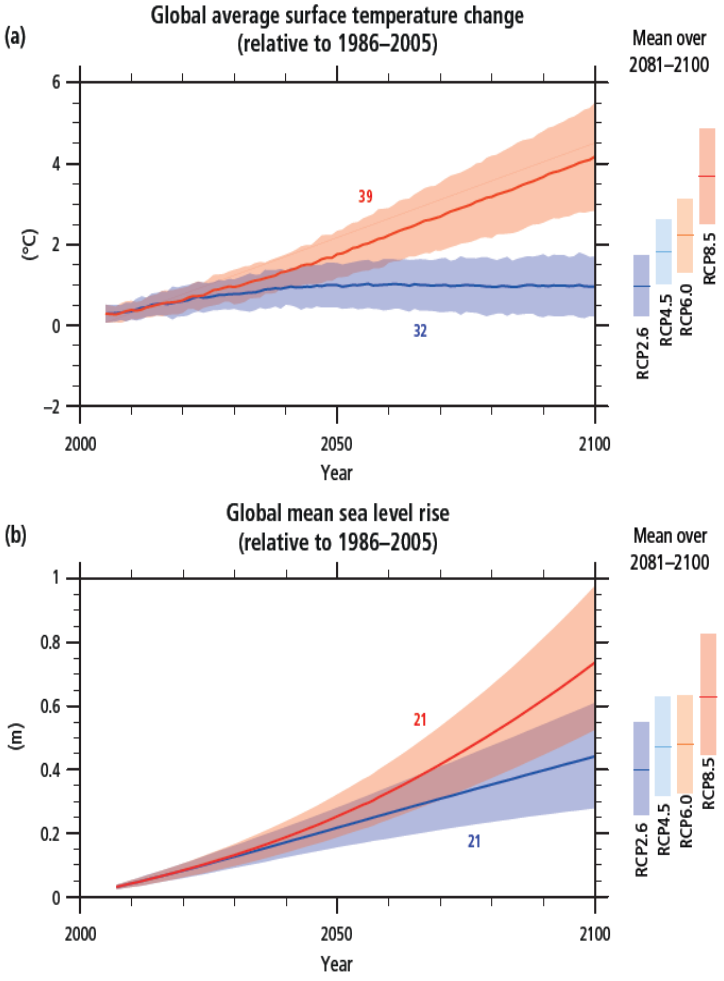

Global average surface temperature change (a) and global mean sea level rise10 (b) from 2006 to 2100 as determined by multi-model simulations. All changes are relative to 1986–2005. Time series of projections and a measure of uncertainty (shading) are shown for scenarios RCP2.6 (blue) and RCP8.5 (red). The mean and associated uncertainties averaged over 2081–2100 are given for all RCP scenarios as colored vertical bars at the right hand side of each panel. The number of Coupled Model Intercomparison Project Phase 5 (CMIP5) models used to calculate the multi-model mean is indicated.

Figure A.3-1. Global average surface temperature and sea level change projections over the 21st century (from IPCC, AR5 (2014).

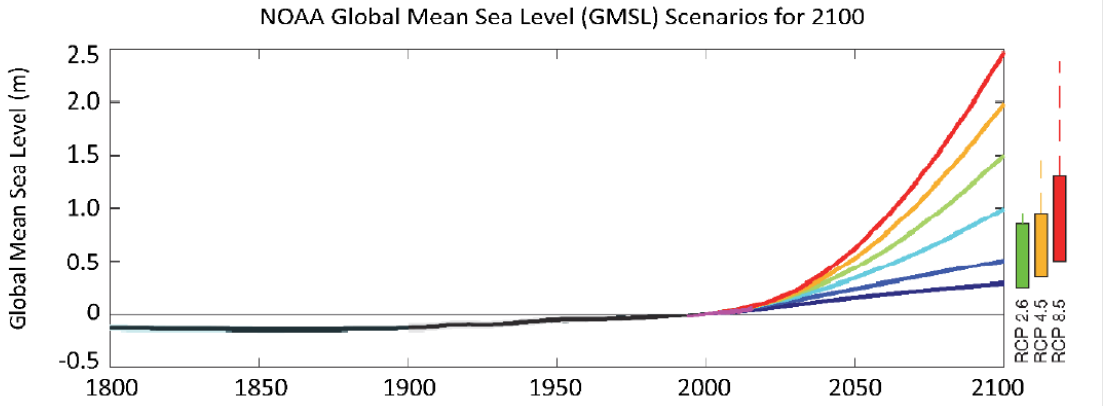

GMSL rise Scenario	RCP2.6	RCP4.5	RCP8.5
Low (0.3 m)	94%	98%	100%
Intermediate-Low (0.5 m)	49%	73%	96%
Intermediate (1.0 m)	2%	3%	17%
Intermediate-High (1.5 m)	0.4%	0.5%	1.3%
High (2.0 m)	0.1%	0.1%	0.3%
Extreme (2.5 m)	0.05%	0.05%	0.1%

GMSL Scenario (meters)	2010	2020	2030	2040	2050	2060	2070	2080	2090	2100	2120	2150	2200
Low	0.03	0.06	0.09	0.13	0.16	0.19	0.22	0.25	0.28	0.30	0.34	0.37	0.39
Intermediate-Low	0.04	0.08	0.13	0.18	0.24	0.29	0.35	0.4	0.45	0.50	0.60	0.73	0.95
Intermediate	0.04	0.10	0.16	0.25	0.34	0.45	0.57	0.71	0.85	1.0	1.3	1.8	2.8
Intermediate-High	0.05	0.10	0.19	0.30	0.44	0.60	0.79	1.0	1.2	1.5	2.0	3.1	5.1
High	0.05	0.11	0.21	0.36	0.54	0.77	1.0	1.3	1.7	2.0	2.8	4.3	7.5
Extreme	0.04	0.11	0.24	0.41	0.63	0.90	1.2	1.6	2.0	2.5	3.6	5.5	9.7

NOAA (2017): This study's six representative GMSL rise scenarios for 2100 (6 colored lines) relative to historical geological, tide gauge and satellite altimeter GMSL reconstructions from 1800–2015 (black and magenta lines; as in Figure 3a) and central 90% conditional probability ranges (colored boxes) of RCP-based GMSL projections of recent studies (Church et al., 2013a; Kopp et al., 2014; 2016a; Slangen et al., 2014; Grinsted et al., 2015; Mengel et al., 2016). These central 90% probability ranges are augmented (dashed lines) by the difference between the median Antarctic contribution of the Kopp et al. (2014) probabilistic GMSL/RSL study and the median Antarctic projections of DeConto and Pollard (2016), which have not yet been incorporated into a probabilistic assessment of future GMSL. (A labeling error in the x-axis was corrected on January 30, 2017).
The six GMSL rise scenarios (colored coded curves) are shown in the table relative to the probability of exceedance in 2100, as assessed by the RCP-based probabilistic projections of Kopp et al. (2014).

Figure A.3-2 NOAA GMSL scenarios and probability of exceedance in 2100 (from the NOAA 2017 report by Sweet et al., 2017).

The NOAA 2017 report *Global and Regional Sea Level Rise Scenarios for the United States* (Sweet et al., 2017) contains probabilistic GMSL rise projections from Parris et al. (2012) and Hall et al. (2016) in addition to those from IPCC AR5 (Church et al., 2013). Scenarios in Parris et al. (2012) provide a range of possible future GMSL rise values by 2100, bounded by a low- (0.2 m) and a high-end (2.0 m) member with two intermediate members (0.5 m and 1.2 m). Each of these four scenarios exemplifies a specific set of scientific assumptions about 21st century GMSL. More recently, Hall et al. (2016) provided a set of five discrete GMSL rise scenarios for 2100 (0.2, 0.5, 1.0, 1.5 and 2 m), including lower and upper bounds to provide a plausible range of GMSL-rise related risks of concern for DoD installation managers. Intermediate scenarios were simply discretized by 0.5-m increments and aligned with emissions-based, conditional probabilistic storylines and global model projections. **Table A.3-2** summarizes the five global scenarios and their associated rationales provided by Hall et al. (2016).

Table A.3-1 Projected change in global mean surface temperature and global mean sea level rise for the mid- and late 21st century, relative to the 1986–2005 period (reproduced from IPCC AR5, 2014).

		2046–2065		2081–2100	
	Scenario	Mean	Likely range [c]	Mean	Likely range [c]
Global Mean Surface Temperature Change (°C) [a]	RCP2.6	1.0	0.4 to 1.6	1.0	0.3 to 1.7
	RCP4.5	1.4	0.9 to 2.0	1.8	1.1 to 2.6
	RCP6.0	1.3	0.8 to 1.8	2.2	1.4 to 3.1
	RCP8.5	2.0	1.4 to 2.6	3.7	2.6 to 4.8
	Scenario	Mean	Likely range [d]	Mean	Likely range [d]
Global Mean Sea Level Rise (m) [b]	RCP2.6	0.24	0.17 to 0.32	0.40	0.26 to 0.55
	RCP4.5	0.26	0.19 to 0.33	0.47	0.32 to 0.63
	RCP6.0	0.25	0.18 to 0.32	0.48	0.33 to 0.63
	RCP8.5	0.30	0.22 to 0.38	0.63	0.45 to 0.82

Notes: This table and notes are from IPCC AR5 2014.
a. Based on the Coupled Model Intercomparison Project Phase 5 (CMIP5) ensemble; changes calculated with respect to the 1986–2005 period. Using Hadley Centre Climatic Research Unit Gridded Surface Temperature Data Set 4 (HadCRUT4) and its uncertainty estimate (5 to 95% confidence interval), the observed warming from 1850–1900 to the reference period 1986–2005 is 0.61 [0.55 to 0.67] °C. Likely ranges have not been assessed here with respect to earlier reference periods because methods are not generally available in the literature for combining the uncertainties in models and observations. Adding projected and observed changes does not account for potential effects of model biases compared to observations, and for natural internal variability during the observational reference period.
b. Based on 21 CMIP5 models; changes calculated with respect to the 1986–2005 period. Based on current understanding (from observations, physical understanding and modelling), only the collapse of marine-based sectors of the Antarctic ice sheet, if initiated, could cause global mean sea level to rise substantially above the likely range during the 21st century. There is medium confidence that this additional contribution would not exceed several tenths of a meter of sea level rise during the 21st century.
c. Calculated from projections as 5 to 95% model ranges. These ranges are then assessed to be likely ranges after accounting for additional uncertainties or different levels of confidence in models. For projections of global mean surface temperature change in 2046–2065, confidence is medium, because the relative importance of natural internal variability, and uncertainty in non-greenhouse gas forcing and response, are larger than for the 2081–2100 period. The likely ranges for 2046–2065 do not take into account the possible influence of factors that lead to the assessed range for near term (2016–2035) change in global mean surface temperature that is lower than the 5 to 95% model range, because the influence of these factors on longer term projections has not been quantified due to insufficient scientific understanding.
d. Calculated from projections as 5 to 95% model ranges. These ranges are then assessed to be likely ranges after accounting for additional uncertainties or different levels of confidence in models. For projections of global mean sea level rise confidence is medium for both time horizons.

Table A.3-2 Rationale and/or correspondences for the five global SLR scenarios (from Hall et al. 2016).

Global SLR Scenario by 2100	Rationale/Correspondences to RCP-Based SLR Simulations
0.2 m (0.7 ft)	▪ Linear extrapolation of the long-term (since 1900) global tide gauge record (Church and White 2011) ▪ Within the 99% probability range of Kopp et al. (2014) for RCP 2.6 (relative to 2000) ▪ Meehl et al. (2012) derived an ensemble mean value of 0.25 m for RCP 2.6 using one coupled atmosphere-ocean global climate model in the middle of the range of climate sensitivities (relative to 1986 to 2005) ▪ Church et al. (2013a) identified 0.26 m as the 5th percentile of the range of projections from process-based models for RCP 2.6 considered "likely" (2/3 probability)
0.5 m (1.6 ft)	▪ Approximate upper bound (95th percentile) for the RCP 2.6 likely range of Church et al. (2013a) ▪ Approximate median value for the RCP 4.5 likely range of Church et al. (2013a) ▪ Approximate lower bound (5th percentile) for the RCP 8.5 likely range of Church et al. (2013a)
1.0 m (3.3 ft)	▪ Approximate upper bound (95th percentile) for the RCP 8.5 likely range of Church et al. (2013a)
1.5 m (4.9 ft)	▪ Approximate value using semi-empirical approaches (Jevrejeva et al. [2014], Meehl et al. [2012]), with the latter estimate explicitly tied to RCP 8.5)
2.0 m (6.6 ft)	▪ Physically plausible glacier and ice-sheet loss by the end of the century and estimated ocean warming (Pfeffer et al. 2008) ▪ Approximately equal to low probability but plausible estimates of Jevrejeva et al. (2014) and Kopp et al. (2014) associated with RCP 8.5

After a review of the literature, the NOAA 2017 report (Sweet et al., 2017) recommended six GMSL scenarios ranging from 0.3 m (low-end) to 2.5 m (extreme) for 2100 (Sweet et al., 2017). These scenarios included information on rapid ice melt in Greenland and Antarctica based on observational data and model results at the time. The six GMSL rise scenarios and the likelihood of exceedance are:

- **Low**, GMSL rise of 0.3 m by 2100, with 94-100 percent likelihood to be exceeded.
- **Intermediate-Low**, GMSL rise of 0.5 m by 2100, with a 49-96 percent likelihood to be exceeded;
- **Intermediate**, GMSL rise of 1.0 m by 2100, with a 2-17 percent likelihood to be exceeded.
- **Intermediate-High**, GMSL rise of 1.5 m by 2100, with a 0.4-1.3 percent likelihood to be exceeded.
- **High**, GMSL rise of 2.0 m by 2100, with a 0.1-0.3 percent likelihood to be exceeded.
- ***Extreme***, GMSL rise of 2.5 m by 2100, with a 0.05-0.1 percent likelihood to be exceeded.

These GMSL rise scenarios form the basis of the regional RSL rise and are related to the baseline of 2000. The GMSL values listed above are the estimated median and the likelihood of exceeding the median values.

NOAA updated its SLR study and modified these projections in 2022 (Sweet et al., 2022) while keeping the names and definition of these GMSL rise categories unchanged. Those findings are summarized in section A.3.2.1.

Compared to other studies, the set of projections encompass a larger range of GMSL rise by 2100 (0.3–2.5 m), see Table A.3-3 and **Figure A.3-2**. GMSL projection for 2060 are shown in Figure A.3-2 along each of the six scenario curves. By 2060, the GMSL is mostly likely to be in the range of 0.19 to 0.45 m. On the Intermediate-High, High and Extreme scenario curves, GMSLR is projected to be 0.60, 0.77 and 0.90 m by 2060, respectively, with low probabilities less than 1.3 percent (0.05 to 1.3 percent).

Table A.3-3 Representative GMSL rise scenarios probability of exceedance for 2100 (see Table 4 in Sweet, et al. 2017)

GMSL	RCP2.6	RCP4.5	RCP8.5
Low (0.3 m)	94%	98%	100%
Intermediate-Low (0.5 m)	49%	73%	96%
Intermediate (1.0 m)	2%	3%	17%
Intermediate-High (1.5 m)	0.40%	0.50%	1.30%
High (2.0 m)	0.10%	0.10%	0.30%
Extreme (2.5 m)	0.05%	0.05%	0.10%

A.3.2.1 NOAA 2022 Updated Projections

NOAA updated its sea level rise projections in early 2022 (Sweet et al., 2022).

The names for the GMSL categories (defined by the GMSL rise value in 2100 relative to the year 2000 baseline) given in the NOAA 2022 report are the same as those used in the NOAA 2017 report, except the omission of the extreme high scenario of 2.5 m GMSL rise in 2100. The five NOAA GMSL rise categories given in the NOAA 2022 report are:

- **Low**: GMSL rise in 2100 is 0.3 m relative to the 2000 baseline.
- **Intermediate-low**: GMSL rise in 2100 is 0.5 m relative to the 2000 baseline.
- **Intermediate**: GMSL rise in 2100 is 1 m relative to the 2000 baseline.
- **Intermediate-high**: GMSL rise in 2100 is 1.5 m relative to the 2000 baseline.
- **High**: GMSL rise in 2100 is 2 m relative to the 2000 baseline.

The set of GMSL rise scenarios from the NOAA 2017 report were updated based on the latest generation of GCMs and the IPCC AR6 (AR6; IPCC, 2021) through the efforts of the NASA Sea Level Change Team. Major changes are summarized below.

- Used the latest generation of GCMs and the IPCC AR6 methodology;
- The principal difference between the NOAA 2022 report and the NOAA 2017 report is the update of temporal trajectories and exceedance probabilities, which was based on global warming levels rather than emissions scenarios. The benefit of this update is that it provides a straightforward physical link for the GMSL scenarios

and establishes a connection to global temperature monitoring efforts. This is demonstrated in **Table A.3-4**.

- The major sources of future sea level rise is the melting of icesheets and glaciers, and it is also the biggest source of uncertainty in projecting the timing and magnitude of future possible rise. The updated projections incorporated multiple improved methods of projecting future ice-sheet changes. The time path of the higher GMSL scenarios is more realistic in 2022 projections than in those of Sweet et al. (2017).

- An important change from the Sweet et al. (2017) report is the exclusion of the Extreme (2.5 m) scenario in the NOAA 2022 report (Sweet et al., 2022). “Based on the most recent scientific understanding and as discussed in the IPCC AR6, the uncertain physical processes such as ice-sheet loss that could lead to much higher increases in sea level are now viewed as less plausible in the coming decades before potentially becoming a factor toward the end of the 21st century and beyond. A GMSL increase of 2.5 m by 2100 is thus viewed as less plausible” (Sweet et al., 2022).

The probability information is presented partly in **Table A.3-4** and is associated with the level of global warming. The updated projections in the NOAA 2022 sea level rise report (Sweet, et al., 2022) are summarized in **Table A.3-5** and **A.3-6** for the near-term (present to 2050) and long-term (2050-2150) periods, respectively. No likelihood or probability associated with these five categories are explicitly provided in these tables.

For the near-term (**Table A.3-5**), the ranges between the median values of the Low and High GMSL rise scenarios in 2020, 2030, 2040, and 2050 were 0.05 m, 0.12 m, 0.23 m, and 0.38 m, respectively (Table 5 in Sweet et al., 2017). With the improvement in the 2022 report, the uncertainty in the near-term projection was significantly reduced, and as a result, the range between the Low and High scenarios in 2020, 2030, 2040, and 2050 was updated to 0.02 m, 0.06 m, 0.15 m, and 0.28 m, respectively. There is less divergence between the GMSL scenarios in this near-term time period up to 2050. This range reduction reflects a downward shift in the higher scenarios, while the projection with the Low scenario is about the same. For example, the projected value in 2050 for the High scenario in the NOAA 2022 report (0.43 m) is roughly the same as that for the Intermediate-High projected value (0.44 m) for 2050 reported by Sweet et al. (2017). This also means that the paths to get to these target values have changed in the updated projections.

Table A.3-6 presents the updated long-term GMSL rise values in 2050, 2100, and 2150 relative to a 2000 baseline for each of the five scenarios in the NOAA 2022 report. After 2050, the differences between sea level scenarios become increasingly large and the differences are closely associated with potential greenhouse gas emissions and global warming. Compared with the NOAA 2017 report, reductions were seen in the Intermediate-High and High scenarios and resulted in a narrower range for the 2050 to 2150 period.

Table A.3-4 provides information about the likelihood or probability for the five NOAA GMSL rise categories to be realized in 2100, and the probability is related to the level of global warming and the Shared Socioeconomic Pathways (SSP).[18]

Table A.3-4 Representative GMSL rise scenarios probability of exceedance for 2050 and 2100 (from Sweet, et al. 2022).

Table 2.4: IPCC warming level–based global mean sea level projections. Global mean surface air temperature anomalies are projected for years 2081–2100 relative to the 1850–1900 climatology. Sea level anomalies are relative to a 2005 baseline (adapted from Fox-Kemper et al., 2021). The probabilities are *imprecise probabilities*, representing a consensus among all projection methods applied. For imprecise probabilities >50%, all methods agree that the probability of the outcome stated is at least that value; for imprecise probabilities <50%, all methods agree that the probability of the outcome stated is *less than or equal to* the value stated.

Global Mean Surface Air Temperature 2081–2100	1.5°C	2.0°C	3.0°C	4.0°C	5.0°C	Unknown Likelihood, High Impact – Low Emissions	Unknown Likelihood, High Impact – Very High Emissions
Closest Emissions Scenario–Based GMSL Projection	Low (SSP1-2.6)	Low (SSP1-2.6) to Intermediate (SSP2-4.5)	Intermediate (SSP2-4.5) to High (SSP3-7.0)	High (SSP3-7.0)	Very High (SSP5-8.5)	Low (SSP1-2.6), *Low Confidence* processes	Very High (SSP5-8.5), *Low Confidence* processes
Total (2050)	0.18 (0.16–0.24)	0.20 (0.17–0.26)	0.21 (0.18–0.27)	0.22 (0.19–0.28)	0.25 (0.22–0.31)	0.20 (0.16–0.31)	0.24 (0.20–0.40)
Total (2100)	0.44 (0.34–0.59)	0.51 (0.40–0.69)	0.61 (0.50–0.81)	0.70 (0.58–0.92)	0.81 (0.69–1.05)	0.45 (0.32–0.79)	0.88 (0.63–1.60)
Bounding Median Scenarios in 2100	Low to Intermediate-Low	Intermediate-Low to Intermediate	Intermediate-Low to Intermediate	Intermediate-Low to Intermediate	Intermediate-Low to Intermediate	Low to Intermediate-Low	Intermediate-Low to Intermediate
Probability > Low (0.3 m) in 2100	92%	98%	>99%	>99%	>99%	89%	>99%
Probability > Int.-Low (0.5 m) in 2100	37%	50%	82%	97%	>99%	49%	96%
Probability > Int. (1.0 m) in 2100	<1%	2%	5%	10%	23%	7%	49%
Probability > Int.-High (1.5 m) in 2100	<1%	<1%	<1%	1%	2%	1%	20%
Probability > High (2.0 m) in 2100	<1%	<1%	<1%	<1%	< %	<1%	8%

Note: the GMSL rise values referenced in this table are relative to the 2005 baseline, not the 2000 baseline. IPCC AR6 (2021) presented five illustrative scenarios and are referred to as SSPx-y, where 'SSPx' refers to the Shared Socio-economic Pathway or 'SSP' describing the socio-economic trends underlying the scenario, and 'y' refers to the approximate level of radiative forcing (in W m–2) resulting from the scenario in the year 2100, which is known as RCP.

Based on **Table A.3-4**, the median GMSL projection for 2100 for a world with global mean surface air temperature in 2081–2100 averaging 2.0°C above 1850–1900 levels is 0.5 m (likely range of 0.4–0.7 m). The median GMSL projection for a world with global mean surface air temperature in 2081–2100 averaging 4.0°C higher is 0.7 m (likely range of 0.6–0.9 m). It should be noted that the largest contributions to long-term GMSL rise come from ice-sheet

[18] SSP: Shared Socioeconomic Pathways. Introduced in in IPCC AR6 (2021). Increasing the amount of greenhouse gases (GHGs) in the atmosphere will trap more heat in the earth system. The amount of GHGs in the atmosphere determines the "forcing" of climate change and its effects, such as changes in temperature and sea level rise. Various forcing scenarios describe possible GHG emissions pathways, which range from quick emissions to reduction to unmitigated future emissions. In the IPCC AR6 (2021), these possible future pathways are referred to as Shared Socioeconomic Pathways (SSPs).

processes with low confidence described in Box 9.4 in IPCC AR6 (2021). Large uncertainty in modeling the ice-sheet processes under the higher emissions scenario resulted in GMSL rise values beyond the likely range.

The exceedance probability for **0.5 m** GMSL rise by 2100 (***Intermediate-low***) is **50%** if various SSPs lead to 2.0°C global warming above 1850–1900 levels. The exceedance probability is 97% if global warming is 4.0°C (SSP3-7 or with RCP 7), and it is greater than 99% if global warming is 5.0°C (SSP5-8.5 or with RCP 8.5).

The exceedance probability for **1 m** GMSL rise by 2100 (***Intermediate***) is **2%** if various SSPs lead to 2.0°C global warming above 1850–1900 levels, and it is 10% and 23% if global warming is 4.0°C and 5.0°C, respectively.

The exceedance probability for **1.5 m** GMSL rise by 2100 (***Intermediate-high***) is **less than 1%** if various SSPs lead up to 3.0°C global warming above 1850–1900 levels, and it is **1% and 2%** if global warming is 4.0°C and 5.0°C, respectively.

The exceedance probability for **2.0 m** GMSL rise by 2100 (***high***) is **less than 1%** under all global warming scenarios considered. The probability becomes greater than 1% if the GHG emission rate is very high (with SSP5-8.5, or with the RCP8.5 pathway). This scenario is very unlikely because the processes that lead to this amount of sea level rise are very unlikely.

Projections of GMSL rise for time horizons beyond the year 2100 are not provided in the NOAA 2022 report.

Detailed local relative sea level rise (LRLSR) projections provided by NOAA and other agencies for the Delaware coast are reviewed in the following section.

Table A.3-5 Near-term sea level rise projections for five scenarios for 2020 to 2050 (from Sweet, et al., 2022).

Table 2.1: Observation-based extrapolations and five scenarios, in meters, for global mean sea level and relative sea level for the contiguous United States from 2020 to 2050 relative to a baseline of 2000. Median [likely ranges] are shown.

Global Mean Sea Level				
	2020	2030	2040	2050
Obs. Extrapolation	0.07 [0.06, 0.08]	0.12 [0.11, 0.13]	0.18 [0.16, 0.19]	0.24 [0.19, 0.29]
Low	0.06 [0.05, 0.07]	0.09 [0.08, 0.10]	0.12 [0.11, 0.13]	0.15 [0.14, 0.17]
Intermediate-Low	0.07 [0.06, 0.07]	0.11 [0.09, 0.12]	0.15 [0.13, 0.17]	0.20 [0.18, 0.23]
Intermediate	0.07 [0.07, 0.09]	0.13 [0.11, 0.15]	0.19 [0.16, 0.23]	0.28 [0.22, 0.32]
Intermediate-High	0.08 [0.07, 0.10]	0.14 [0.11, 0.20]	0.23 [0.18, 0.32]	0.37 [0.27, 0.46]
High	0.08 [0.07, 0.10]	0.15 [0.11, 0.22]	0.27 [0.18, 0.39]	0.43 [0.31, 0.57]
Contiguous United States				
	2020	2030	2040	2050
Obs. Extrapolation	0.11 [0.09, 0.13]	0.19 [0.16, 0.21]	0.28 [0.23, 0.32]	0.38 [0.32, 0.45]
Low	0.12 [0.09, 0.15]	0.18 [0.14, 0.23]	0.25 [0.19, 0.31]	0.31 [0.24, 0.39]
Intermediate-Low	0.13 [0.10, 0.16]	0.20 [0.15, 0.25]	0.28 [0.22, 0.34]	0.36 [0.28, 0.44]
Intermediate	0.13 [0.10, 0.16]	0.21 [0.16, 0.26]	0.30 [0.23, 0.37]	0.40 [0.31, 0.49]
Intermediate-High	0.13 [0.10, 0.16]	0.22 [0.16, 0.28]	0.33 [0.24, 0.43]	0.46 [0.35, 0.61]
High	0.13 [0.10, 0.16]	0.22 [0.17, 0.29]	0.35 [0.26, 0.47]	0.52 [0.39, 0.68]

Note: likely range means 17th–83rd percentile values.

Table A.3-6 Long-term sea level rise projections for five scenarios for 2050 to 2150 (from Sweet, et al., 2022).

Table 2.3: Global mean sea level and contiguous United States scenarios, in meters, relative to a 2000 baseline.

Global Mean Sea Level				Contiguous United States			
	2050	2100	2150		2050	2100	2150
Low	0.15	0.3	0.4	Low	0.31	0.6	0.8
Intermediate-Low	0.20	0.5	0.8	Intermediate-Low	0.36	0.7	1.2
Intermediate	0.28	1.0	1.9	Intermediate	0.40	1.2	2.2
Intermediate-High	0.37	1.5	2.7	Intermediate-High	0.46	1.7	2.8
High	0.43	2.0	3.7	High	0.52	2.2	3.9

Note: the likely range for GMSL in 2050 and 2100 as well as the associated global warming information can be found in **Table A.3-4**.

A.3.3 LRSLR Projections for DRB

Four sources of local sea level rise projections for the Delaware Estuary were examined by DRBC in more detail:

- U.S. Army Corps of Engineers (USACE 2013 and 2014);
- National Ocean and Atmospheric Administration 2017 and 2022 (Sweet et al. 2017, 2022), known as the NOAA 2017 and 2022 reports;
- New Jersey Climate Adaptation Alliance/Rutgers University (Kopp, R.E, et al. 2016 and 2019), known as the NJSTAP 2019 report;
- Delaware Department of Natural Resources and Environmental Control (Callahan, J. A. et al. 2017), known as the DNREC 2017 report;

Although some of the studies listed above are relatively dated in comparison with others, and although SLR projections are changing as the SLR science evolves, the information from the more dated studies is still relevant and is reviewed in this study. More dated information has been used in many projects that have already been designed or are being planned with that information as their guidance, and construction of these projects has been underway for years. The latest SLR projections are based on the NOAA 2022 SLR study (Sweet et al. 2022) and are considered more accurate.

USACE Projections

USACE (2013 and 2014) developed three options for projecting sea level rise, representing low, intermediate and high rates of rise. The low rate is based on an extrapolation of historic tide gauge rate and is considered representative of near future local sea level rise. Intermediate and high rates account for future acceleration of GMSL. **Table A.3-7** presents the estimated sea level rise for Lewes, Delaware, from the year 2000 through 2100. The projected SLR values from the USACE SLR calculator do not have associated exceedance probabilities.

Table A.3-7. USACE (2013) sea level change curve at Lewes, DE Station 8557380, (m).

	USACE Low	USACE Int	USACE High
2000	0	0	0
2010	0.03	0.04	0.06
2020	0.06	0.08	0.15
2030	0.09	0.13	0.26
2040	0.12	0.19	0.38
2050	0.16	0.25	0.54
2060	0.19	0.31	0.71
2070	0.22	0.38	0.91
2080	0.25	0.46	1.13
2090	0.28	0.54	1.37
2100	0.32	0.63	1.63

Notes: data source: http://corpsmapu.usace.army.mil/rccinfo/slc/slcc_calc.html.
Calculations assume VLM=0.53mm/yr. Published estimates were centered on 1992. Values are relative to the year 2000.

NOAA Projections

The NOAA 2017 report (Sweet et al., 2017) recommended six probability projections up to year 2100, conditioned on the GMSL scenarios similar to Hall et al. (2016). As described in the NOAA 2017 report, gridded responses of the spatial SSH as well as the background rate of change (related to equation 2.3-1) were projected by the CMIP5 GCMs and a spatiotemporal statistical model, respectively. Following the basic approach outlined by Kopp et al. (2014), 20,000 Monte Carlo[19]-sampled time series of GMSL and regional RSL projections were generated for each of RCP2.6, RCP4.5 and RCP8.5 to tie the regional probabilistic projections to the GMSL rise scenarios. These projections were then stratified into the six categories to form subsets listed in **Table A.3-2**. Only the GMSL (and corresponding RSL) Monte Carlo estimates that fell within the prescribed range per scenario (e.g., 50 ± 2 cm for the 0.5 m scenario) were utilized. The median of the stratified subset of

[19] Monte Carlo simulation is a mathematical technique using random combinations of assumptions in models to generate a range of possible outcomes and then determine the probability of specific outcomes. The process is used to quantify the risk associated with different estimates for decision makers in professions related to finance, engineering, research and development, energy, manufacturing, insurance, and the environment, among others.

projections was used to determine the time-evolution of GMSL for each scenario and the associated projections of RSL change.

In the Northeast Atlantic region (Virginia coast and northward), RSL rise is projected to be greater than the global average for almost all future GMSL rise scenarios (e.g., 0.3-0.5 m more RSL rise by the year 2100 than GMSL rise under the *Intermediate* scenario) according to the NOAA 2017 report (Sweet, et al., 2017). The projections from six SLR scenarios provided by NOAA for the Delaware coast are shown in **Table A.3-8** and **Figure A.3-3a**. The NOAA updated projection is shown in **Figure A.3-3b**. SLR projections at Lewes and Philadelphia, with the approach used in the NOAA 2017 and 2022 reports, are given in **Table A.3-9** and **A.3-10**, respectively. In comparison, NOAA 2022 SLR projections at the bay mouth and at Philadelphia decreased for all three scenarios from the scenario *Intermediate* to *High.* The projection for the *Intermediate Low* increased from 0.4 m to 0.47 m at Lewes. The discrepancies between the NOAA 2022 and 2017 projections are discussed in Section A.3.2.1, and in short, they can be attributed to the following factors: **a)** More weight is given to the near-term observed SLR rates and their extrapolation to 2050; **b)** SLR probabilities are base global warming levels, not emissions scenarios (end point temperature, not how emissions change over time). The GMSLR scenario of 2.5 m by 2100 is now considered less plausible, and therefore this extreme scenario was eliminated from 2022 projections; **c)** Ice sheet change models have improved, and the timing of near-term ice sheet change does not diverge among scenarios until 2050.

The projected local SLR at NOAA Lewes, DE tide gage at the mouth of the Delaware Bay is listed in **Table A.3-11** with 66% confidence bands, based on NOAA 2022 projections.

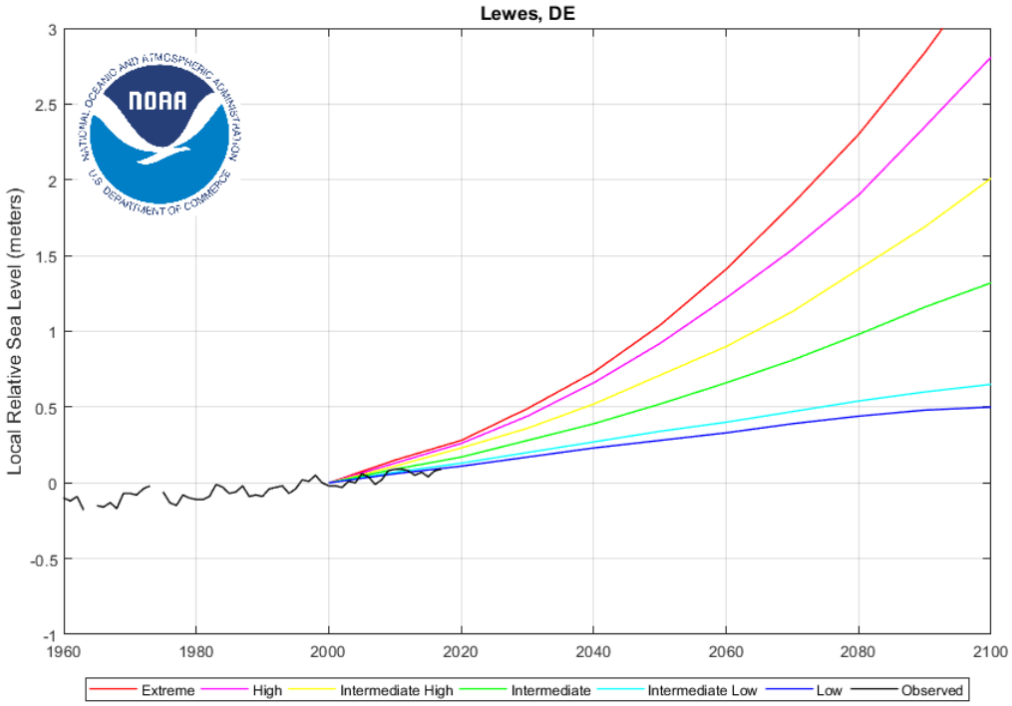

The figure shows the station's annual mean relative sea level with its six regionalized sea level rise scenarios plotted relative to a 1991-2009 baseline period (i.e., year 2000 is the 'zero' for the figure) as described in the report on Global and Regional Sea Level Rise Scenarios for the United States (NOAA, 2017).

Figure A.3-3a Annual mean relative sea level since 1960 and regional scenarios at NOAA Tide Station 8557380 Lewes, Delaware with NOAA 2017 Projections (Sweet, et al., 2017).

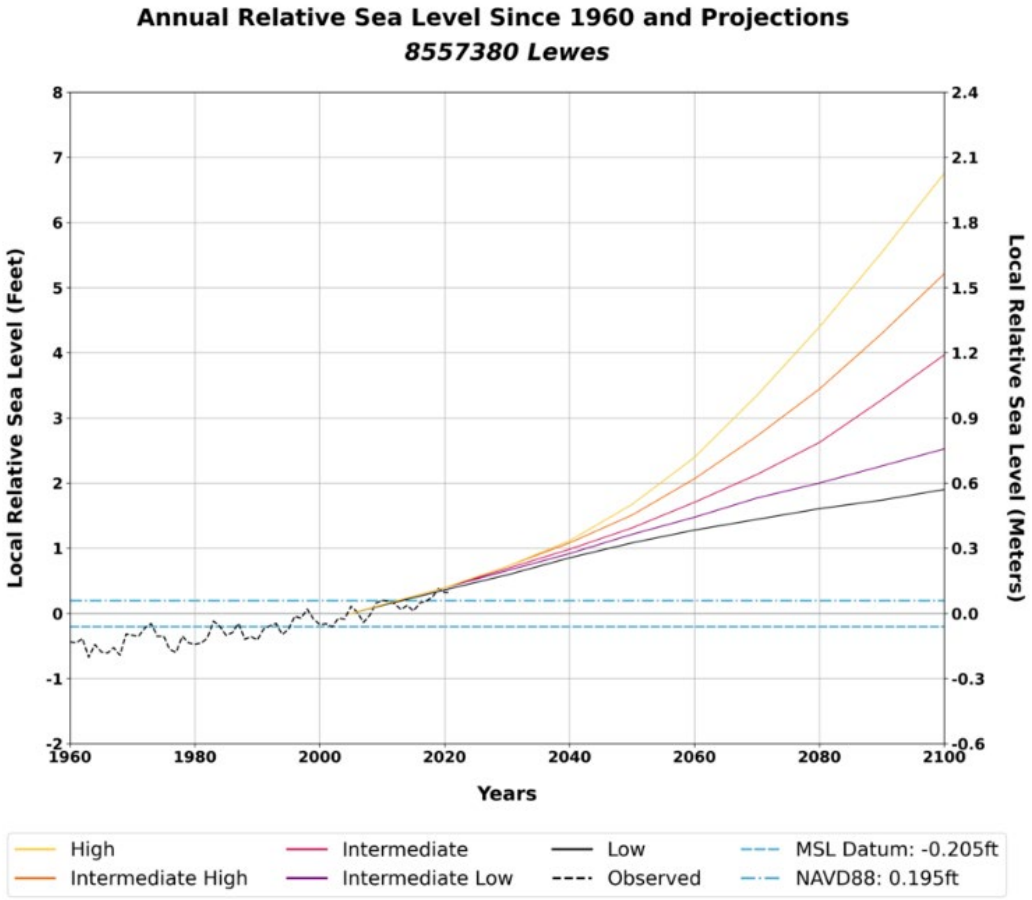

The projection of future sea levels that are shown below were released in 2022 by a U.S. interagency task force in preparation for the Fifth National Climate Assessment. The projections for 5 sea level change scenarios are expected to assist decision makers in responding to local relative sea level rise. The 2022 Sea Level Rise Technical Report provides further detailed information on the projections.

Source: NOAA https://tidesandcurrents.noaa.gov/sltrends/sltrends_station.shtml?id=8557380

Figure A.3-3b Annual mean relative sea level since 1960 and regional scenarios at NOAA Tide Station 8557380 Lewes, Delaware with NOAA 2022 Projections (Sweet, et al. 2022).

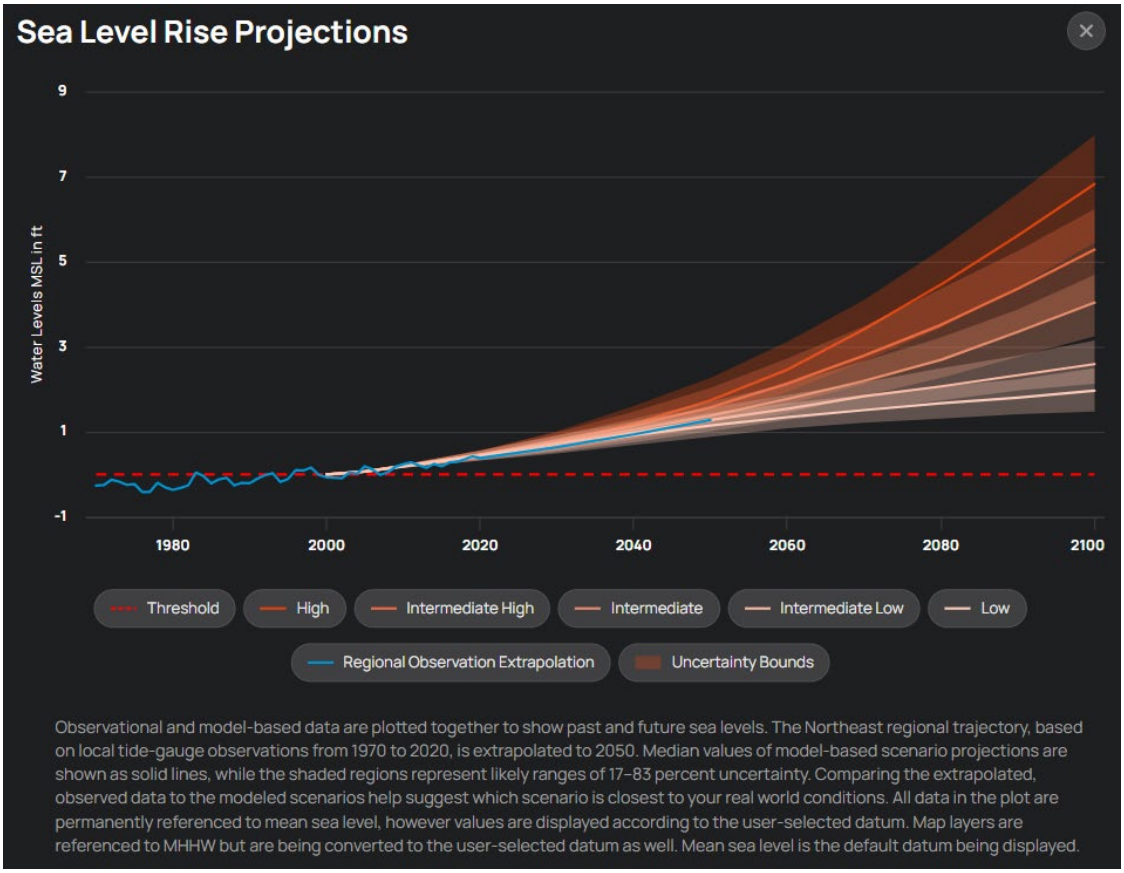

Source: NOAA, https://coast.noaa.gov/sealevelcalculator

Notes: observational and model-based data are plotted together to show past and future sea levels. The Northeast regional trajectory, based on local tide-gauge observations from 1970 to 2020, is extrapolated to 2050. Median values of model-based scenario projections are shown as solid lines, while the shaded regions represent likely ranges of 17–83 percent uncertainty. Comparing the extrapolated, observed data to the modeled scenarios helps suggest which scenario is closest to real-world conditions. All data in the plot are permanently referenced to mean sea level, however values are displayed according to the user-selected datum. Map layers are referenced to MHHW but are being converted to the user-selected datum as well. Mean sea level is the default datum being displayed.

Figure A.3-3c Regional observation extrapolations through 2050 and regional scenarios at NOAA Tide Station 8557380 Lewes, Delaware with NOAA 2022 Projections and uncertainty bounds (Sweet, et al. 2022).

Table A.3-8. NOAA (2017) Sea level rise projection for Lewes, DE, Station 8557380, (m).

Year	NOAA Low	NOAA Intermediate-Low	NOAA Intermediate	NOAA Intermediate-High	NOAA High	NOAA Extreme
2000	0	0	0	0	0	0
2010	0.06	0.07	0.09	0.11	0.13	0.15
2020	0.11	0.13	0.17	0.23	0.26	0.28
2030	0.17	0.2	0.28	0.36	0.44	0.49
2040	0.23	0.27	0.39	0.52	0.66	0.73
2050	0.28	0.34	0.52	0.71	0.92	1.04
2060	0.33	0.4	0.66	0.9	1.22	1.41
2070	0.39	0.47	0.81	1.13	1.54	1.84
2080	0.44	0.54	0.98	1.41	1.9	2.3
2090	0.48	0.6	1.16	1.69	2.35	2.84
2100	0.5	0.65	1.32	2.01	2.81	3.44

Note: the values were obtained using the USACE SLR calculator from the website: https://cwbi-app.sec.usace.army.mil/rccslc/slcc_calc.html . The values in this table are slightly different from those in Table A.3-6b. One reason could be that the VLM in the SLR calculator and the NOAA SLR viewer was considered differently. The USACE SLR calculator allows the user to specify vertical land motion (VLM). The VLM rate of 0.00173 m/year for Lewes was set in the calculator. Different SLR values may result from different local VLM rates. Since NOAA has updated its SLR report in 2022, it recommends using the latest projections based on the report by Sweet et al. (2022).

Table A.3-9 NOAA SLR projection for the year 2060 (2017 Projection).

	Lewes		Philadelphia		Relative Diff. (RM100-RM0)	
	ft	m	ft	m	ft	m
Extreme	4.63	1.41	4.56	1.39	-0.07	-0.02
High	4	1.22	3.94	1.2	-0.06	-0.02
Intermediate High	2.95	0.9	2.89	0.88	-0.06	-0.02
Intermediate	2.17	0.66	2.07	0.63	-0.10	-0.03
Intermediate Low	1.31	0.4	1.21	0.37	-0.10	-0.03

Source: NOAA SLR viewer website: https://coast.noaa.gov/slr/#/layer/sce/0/-8475990.829707442/4857918.579163033/8/satellite/6/0.8/2050/high/midAccretion
NOAA updated its SLR report in 2022, and it recommends using the latest projections based on report Sweet et al. (2022).

Table A.3-10 NOAA SLR projection for the year 2060 (2022 Projection).

	Lewes		Philadelphia		Relative Diff. (RM100-RM0)	
	ft	m	ft	m	ft	m
High	2.46	0.75	2.33	0.71	-0.13	-0.04
Intermediate High	2.13	0.65	2.03	0.62	-0.10	-0.03
Intermediate	1.77	0.54	1.67	0.51	-0.10	-0.03
Intermediate Low	1.54	0.47	1.44	0.44	-0.10	-0.03

Note: the extreme scenario was considered not plausible and was removed from 2022 projections. Projections at Lewes, DE for years from 2020 through 2100 based on NOAA 2022 study are presented in Table A.3-11.
Source: NOAA SLR viewer website: https://coast.noaa.gov/slr/#/layer/sce/0/-8475990.829707442/4857918.579163033/8/satellite/6/0.8/2050/high/midAccretion

In **Table A.3-11**, the uncertainty in various potential GHG emissions is estimated by the 66% confidence bands in addition to median values for given NOAA scenarios. The confidence bands overlap among different categories. The information from this table can be used to answer this question: "***What is a likely range of SLR for the Delaware Estuary in year XX?***". In order to have a "likely" range (17-83 percentile exceedance probability) of SLR in a given year, there is a need to assemble all time-series of projections of all 5 categories with all possible SSP pathways together and determine the SLR range that corresponds to the 17-83 percentile exceedance probability for that year. Based on **Table A.3-11** (NOAA 2022 study), that "likely" range would be inferred and bounded by combined *Intermediate-low* and *Intermediate* categories. For example, for a 2060 time horizon, the likely range is bounded in the **0.39-to-0.65 m** range, and it is bounded in the **0.65-to-1.43 m** range for the year 2100, considering all potential possible GHG emission pathways. All SLR amounts are relative to the baseline of the year 2000.

For planners developing a feasibility study and who want to perform a risk analysis, they may want to look at a local SLR scenario outside the likely range, for example, one with an exceedance probability of 1 percent. Based on the NOAA 2022 study, **the 1-percent**

exceedance probability of SLR at Lewes, DE is in the category of *Intermediate-high*. The median value and confidence bounds of the *Intermediate-high* scenario is **0.65 [0.50 – 0.83] m** and **1.6 [1.23 – 1.90] m** for the years 2060 and 2100, respectively.

This question has been investigated by NJSTAP2019 or DNREC2017 with specific GHG emission assumptions (i.e., RCP2.6 or 8.5) with information and approach similar to those of the NOAA2017 SLR study that was available at the time of their studies. See details in the following sections.

Table A.3-11. Local sea level rise projection with uncertainty range for Lewes, DE (8557380), according to the NOAA 2022 study.

	NOAA GMSL Rise Category	Low			Intermediate-Low			Intermediate			Intermediate-high			High		
	NOAA GMSL rise in 2100 relative to 2000 baseline	0.3 m (92% to >99%)			0.5 m (37% to > 99%)			1 m (<1% to 23%)			1.5 m (<1% to 2%)			2.0 m (<1% to 0%)		
Year	Linear Trend	17th percen-tile	Median	83rd percen-tile	17th percen-tile	Median	83rd percen-tile	17th percen-tile	Median	83rd percen-tile	17th percen-tile	Median	83rd percen-tile	17th percen-tile	Median	83rd percen-tile
2020	0.0845	0.098	0.128	0.148	0.098	0.138	0.168	0.108	0.138	0.168	0.108	0.138	0.168	0.108	0.138	0.168
2025	0.1035	0.123	0.163	0.203	0.128	0.178	0.223	0.138	0.183	0.223	0.138	0.188	0.233	0.143	0.188	0.238
2030	0.1215	0.148	0.198	0.258	0.158	0.218	0.278	0.168	0.228	0.278	0.168	0.238	0.298	0.178	0.238	0.308
2035	0.1405	0.178	0.238	0.303	0.193	0.258	0.328	0.208	0.273	0.338	0.213	0.293	0.373	0.223	0.298	0.398
2040	0.1585	0.208	0.278	0.348	0.228	0.298	0.378	0.248	0.318	0.398	0.258	0.348	0.448	0.268	0.358	0.488
2045	0.1775	0.238	0.313	0.393	0.268	0.343	0.428	0.293	0.368	0.458	0.313	0.413	0.533	0.338	0.443	0.588
2050	0.1955	0.268	0.348	0.438	0.308	0.388	0.478	0.338	0.418	0.518	0.368	0.478	0.618	0.408	0.528	0.688
2055	0.2145	0.298	0.378	0.473	0.348	0.428	0.523	0.388	0.478	0.583	0.433	0.563	0.723	0.498	0.638	0.818
2060	**0.2325**	**0.328**	**0.408**	**0.508**	**0.388**	**0.468**	**0.568**	**0.438**	**0.538**	**0.648**	**0.498**	**0.648**	**0.828**	**0.588**	**0.748**	**0.948**
2065	0.2505	0.348	0.433	0.538	0.423	0.513	0.613	0.498	0.603	0.728	0.573	0.748	0.943	0.698	0.893	1.098
2070	0.2695	0.368	0.458	0.568	0.458	0.558	0.658	0.558	0.668	0.808	0.648	0.848	1.058	0.808	1.038	1.248
2075	0.2875	0.383	0.483	0.598	0.493	0.593	0.708	0.623	0.743	0.893	0.733	0.958	1.193	0.928	1.198	1.428
2080	0.3065	0.398	0.508	0.628	0.528	0.628	0.758	0.688	0.818	0.978	0.818	1.068	1.328	1.048	1.358	1.608
2085	0.3245	0.413	0.528	0.653	0.563	0.668	0.803	0.763	0.918	1.078	0.923	1.198	1.463	1.193	1.533	1.808
2090	0.3435	0.428	0.548	0.678	0.598	0.708	0.848	0.838	1.018	1.178	1.028	1.328	1.598	1.338	1.708	2.008
2095	0.3615	0.438	0.573	0.718	0.623	0.748	0.903	0.913	1.123	1.303	1.128	1.468	1.748	1.498	1.893	2.218
2100	**0.3805**	**0.448**	**0.598**	**0.758**	**0.648**	**0.788**	**0.958**	**0.988**	**1.228**	**1.428**	**1.228**	**1.608**	**1.898**	**1.658**	**2.078**	**2.428**

Source: https://climate.sec.usace.army.mil/slr_app/, also from https://climate.sec.usace.army.mil/slat/ using NOAA 2022 projections.

Units: Meters above Mean Sea Level Datum (1991-2009 epoch) centered in 2000. *The offset from current MSL datum centered in 1992 (1983-2001 epoch) is 0.0325 m or 1.28 inch.*

The percentage range in the header row represents the range of exceedance probability for the GMSL rise to happen in 2100 under global warming level from 1.5 °C to 5 °C relative to the 1850–1900 climatology following various SSPs. The linear trend projection is based on historical sea level rise rate of 0.00353m/year using data up to 2019. The probability associated with the five NOAA GMSL rise scenarios under different GHG emission pathways and global warming conditions can be found in Table 2.4 in the NOAA 2022 report.

The exceedance probability of a given SLR in a year other than 2100 is not provided in the NOAA 2022 report.

The range (17^{th}-83^{rd} percentile) represents the 66% confidence band for the projection.

Delaware Sea-Level Rise Technical Committee

The Delaware Sea-Level Rise Technical Committee coordinated by the Delaware Geological Survey (DGS) prepared a SLR study report for Delaware Department of Natural Resources and Environmental Control (DNREC) Coastal Programs in 2017 (Callahan et al 2017). The framework, described in Kopp et al. (2014), was used as the scientific basis for incorporating sea-level rise into Delaware coastal planning activities. The methodology described by Kopp et al. (2014) is a comprehensive probabilistic approach, conditioned upon selection of the RCP scenario of greenhouse gas emissions and more complete information for the time period leading up to the year 2100. Probabilities are determined for the projection for use by planners to select estimates appropriate for their purposes. The recommendation by the Delaware SLR Technical Committee is to use the 5, 50, and 95 percent probability levels of sea-level rise in Delaware as the *Low, Intermediate*, and *High* SLR planning scenarios, respectively, as determined by the Kopp et al. (2014) methodology under the IPCC AR5 RCP 8.5 emission scenario. These levels equate to 0.52 m, 0.99 m, and 1.53 m of SLR, respectively, by 2100, relative to year 2000 baseline MSL (Callahan et al 2017). The projections are summarized in Table A.3-7 through A.3-9, also shown on **Figure A.3-4**. The mid-term projections are 0.29 m (*Low, the 5th percentile*), 0.51 m (*Intermediate, the 50th percentile*) and 0.76 m (*High, the 95th percentile*).

Table A.3-7. 2017 Delaware SLR planning scenarios for selected years under IPCC AR5 RCP 8.5 Emission Scenario.

Year	Low	Intermediate	High
2030	0.11 m / 0.36 ft	0.22 m / 0.72 ft	0.33 m / 1.08 ft
2050	0.22 m / 0.72 ft	0.40 m / 1.31 ft	0.58 m / 1.90 ft
2080	0.42 m / 1.38 ft	0.74 m / 2.43 ft	1.11 m / 3.64 ft
2100	0.52 m / 1.71 ft	0.99 m / 3.25 ft	1.53 m / 5.02 ft

Notes: Data are in meters and feet relative to 2000 MSL. All three of the Delaware SLR planning scenarios use the Kopp et al.(2014) results under the RCP 8.5 “business as usual” future greenhouse gas emission assumption.

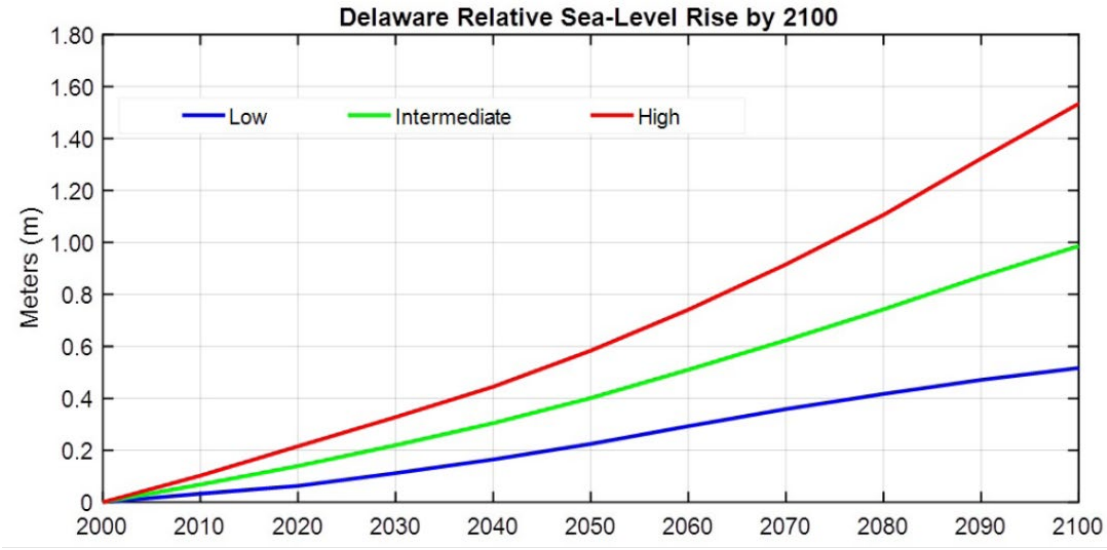

SLR Planning Scenario	SLR by 2100	
Low Scenario (5%)	**0.52 m**	**1.71 ft**
Intermediate Scenario (50%)	**0.99 m**	**3.25 ft**
High Scenario (95%)	**1.53 m**	**5.02 ft**

The Low, Intermediate and High planning scenarios correspond to 5%, 50%, and 95% probability levels. It is the recommendation of the SLR Technical Committee to use the 5, 50, and 95 percent probability levels of sea-level rise in Delaware, determined by the Kopp et al. (2014) methodology under the IPCC AR5 RCP 8.5 emission scenario, as the Low, Intermediate, and High SLR planning scenarios, respectively. These equate to 0.52 m, 0.99 m, and 1.53 m of SLR by 2100, respectively, relative to year 2000 MSL. Depending on time horizon and sensitivity to coastal flooding, projects also may benefit by planning for SLR scenarios greater than the High (95%) planning scenario.

Figure A.3-4 The 2017 Delaware SLR planning scenario curves to the year 2100 (Delaware Sea-Level Rise Technical Committee report for DRNEC (Callahan, et. al., 2017).

Table A.3-8. Probability of SLR in Delaware for selected magnitudes and years under IPCC AR5 RCP 8.5 Emission Scenario (DNREC-DGS, 2017).

Year	1.0 ft	2.0 ft	3.0 ft	4.0 ft	5.0 ft	6.0 ft	7.0 ft	8.0 ft	9.0 ft	10.0 ft
	0.30 m	0.61 m	0.91 m	1.22 m	1.52 m	1.83 m	2.13 m	2.44 m	2.74 m	3.05m
2020	0.10%									
2030	12%									
2040	51%	0.40%								
2050	80%	5.50%	0.20%							
2060	92%	25%	1.70%	0.20%	0.10%					
2070	96%	52%	8.20%	1.10%	0.20%	0.10%				
2080	98%	71%	24%	4.10%	1.00%	0.30%	0.10%	0.10%		
2090	98%	82%	43%	13%	3.20%	1.10%	0.40%	0.20%	0.10%	0.10%
2100	98%	87%	58%	25%	8.50%	2.70%	1.20%	0.50%	0.30%	0.20%

Notes: Values are the probability that SLR in Delaware will meet or exceed the column heading value for the stated year in the row heading. Based on the methodology of Kopp et al. (2014) under RCP 8.5 greenhouse gas emission scenario, relative to 2000 MSL. Gray shaded areas have less than 0.1% chance of occurrence for the stated year in the row heading.

Table A.3-9 SLR Projections with different probability levels under RCP8.5 for Delaware (from DNREC-DGS, 2017).

	Low End		At least a 66% chance between						High End	
Year	Greater than a 95% chance SLR exceeds		Greater than an 83% chance SLR exceeds		~50% chance SLR exceeds		Less than a 17% chance SLR exceeds		Less than a 5% chance SLR exceeds	
	m	ft	m	ft	m	ft	m	ft	m	ft
2000	0.00	0.00	0.00	0.00	0.00	0.00	0.00	0.00	0.00	0.00
2010	0.04	0.12	0.05	0.17	0.07	0.24	0.09	0.31	0.11	0.36
2020	0.07	0.24	0.11	0.35	0.15	0.48	0.19	0.61	0.22	0.72
2030	0.11	0.36	0.16	0.52	0.22	0.72	0.28	0.92	0.33	1.08
2040	0.17	0.54	0.23	0.75	0.31	1.02	0.39	1.28	0.46	1.49
2050	0.22	0.72	0.30	0.98	0.40	1.31	0.50	1.64	0.58	1.90
2060	0.29	0.94	**0.38**	1.26	0.51	1.68	**0.65**	2.13	0.76	2.48
2070	0.35	1.16	0.47	1.53	0.63	2.06	0.80	2.62	0.93	3.06
2080	0.42	1.38	0.55	1.80	0.74	2.43	0.95	3.12	1.11	3.64
2090	0.47	1.54	0.63	2.05	0.87	2.84	1.12	3.67	1.32	4.33
2100	0.52	1.71	**0.70**	2.30	0.99	3.25	**1.29**	4.23	1.53	5.02

According to **Table A.3-9**, the "likely" range (17-83 percent chance of exceedance) **conditioned to a high GHG emissions scenario (RCP8.5)** for the Delaware Estuary in 2060 is **0.38-to-0.65 m**, and the "likely" range is **0.70-to-1.29 m** for year 2100. All SLR values are related to the baseline of 2000. Although these ranges are "likely" given high GHG emissions, they are, in fact, unlikely because the high GHG emissions scenario is unlikely. These projection ranges are considered for planning purposes in feasibility studies because the probability associated with RCP8.5 is now believed to be very low.

New Jersey Climate Adaptation Alliance

The New Jersey Science and Technical Advisory Panel (STAP) on Sea-Level Rise and Coastal Storms, on behalf of the NJ Climate Change Alliance (NJCCA), provided an update of earlier local SLR projections for the coast of New Jersey in 2019 (Kopp et al. 2019), and it is cited here in **Table A.3-10** through **A.3-12**, including Atlantic City, near the mouth of the Delaware Bay.

Kopp adopted a similar approach used by Horton et al. (2018) named the composite projection methodology to develop new projections for STAP 2019, which is a refinement of STAP2016. The report not only provided most-likely outcome as the projected SLR with at least a 66 percent chance (between 17th and 83rd percentiles of the probability distribution of all the SLR projections) to occur, but it also the projected SLR with low (5 percent) and end (95 percent) probabilities for a given time horizon from 2030 to 2150. The STAP 2019 SLR projections through 2050 represent a combination of low- and high-emissions scenario

projections because SLR projections of the scenarios differ by approximately 0.1 feet through 2050. For years beyond 2050, the projections diverge with different emission assumptions.

It should be noted that the local SLR rate for the New Jersey coast is higher than the SLR rate near the Delaware coast. Based on data collected at NOAA tide gauge stations, the current SLR rate at Atlantic City NJ is 4.12 mm/yr, which is higher than the SLR rate observed at Lewes DE (3.53 mm/yr), and this translates to a 6 cm difference over the 100-year period (from 2000 to 2100 if a constant rate is assumed). Under future conditions, the SLR may be accelerated, and the difference between NJ and DE might be more significant.[20]

According to **Table A.3-10** and **Table A.3-11**, the "likely" range (17-83 percent chance of exceedance) with a wide range of emissions (RCP2.6 to 8.5) for the Delaware Estuary in 2060 is **0.34-to-0.85 m**, and the "likely" range is **0.52-to-1.91 m** for year 2100. It should be noted that the rate of SLR on the New Jersey coast is slightly higher than that along the Delaware coast.

Table A.3-10 New Jersey sea-level rise above the year 2000 (1991-2009 average) baseline (ft).

		2030	2050	2070			2100			2150		
				Emissions								
	Chance SLR Exceeds			Low	Mod.	High	Low	Mod.	High	Low	Mod.	High
Low End	95%	0.3	0.7	0.9	1	1.1	1	1.3	1.5	1.3	2.1	2.9
Likely Range	83%	0.5	0.9	1.3	1.4	1.5	1.7	2	2.3	2.4	3.1	3.8
	50%	0.8	1.4	1.9	2.2	2.4	2.8	3.3	3.9	4.2	5.2	6.2
	17%	1.1	2.1	2.7	3.1	3.5	3.9	5.1	6.3	6.3	8.3	10.3
High End	5%	1.3	2.6	3.2	3.8	4.4	5	6.9	8.8	8	13.8	19.6

Notes (from STAP report: Kopp et al. 2019): All values are 19-year means of sea-level measured with respect to a 1991-2009 baseline centered on the year indicated in the top row of the table. Projections are based on Kopp et al. (2014), Rasmussen et al. (2018), and Bamber et al. (2019). Near-term projections (through 2050) exhibit only minor sensitivity to different emissions scenarios (<0.1 feet). Low and high emissions scenarios correspond to global-mean warming by 2100 of 2°C and 5°C above early Industrial (1850-1900) levels, respectively, or equivalently, about 1°C and 4°C above the current global mean temperature. Moderate (Mod.) emissions are interpolated as the midpoint between the high- and low emissions scenarios and approximately correspond to the warming expected under current global policies. Rows correspond to different projection probabilities. There is at least a 95% chance of SLR exceeding the values in the 'Low End' row, while there is less than a 5% chance of exceeding the values in the 'High End' row. There is at least a 66% chance that SLR will fall within the values in the 'Likely Range'. Note that alternative methods may yield higher or lower estimates of the chance of low-end and high-end outcomes.

[20] Source: NOAA sea level trend at Lewes, DE. https://tidesandcurrents.noaa.gov/sltrends/sltrends_station.shtml?id=8557380

Table A.3-11 SLR projections with different probability levels under low-emission RCP 2.6 for New Jersey (STAP report: Kopp et al. 2019).

	Low End		At least a 66% chance between						High End	
Year	Greater than a 95% chance SLR exceeds		Greater than an 83% chance SLR exceeds		~50% chance SLR exceeds		Less than a 17% chance SLR exceeds		Less than a 5% chance SLR exceeds	
	m	ft	m	ft	m	ft	m	ft	m	ft
2000					0.00	0.00				
2010					0.06	0.20				
2020	0.03	0.10	0.09	0.30	0.15	0.50	0.21	0.70	0.27	0.90
2030	0.09	0.30	0.15	0.50	0.24	0.80	0.34	1.10	0.40	1.30
2040	0.15	0.50	0.21	0.70	0.34	1.10	0.46	1.50	0.58	1.90
2050	0.21	0.70	0.27	0.90	0.43	1.40	0.64	2.10	0.79	2.60
2060	0.24	0.80	**0.34**	1.10	0.49	1.60	**0.67**	2.20	0.82	2.70
2070	0.27	0.90	0.40	1.30	0.58	1.90	0.82	2.70	0.98	3.20
2080	0.30	1.00	0.43	1.40	0.67	2.20	0.94	3.10	1.16	3.80
2090	0.30	1.00	0.46	1.50	0.76	2.50	1.07	3.50	1.34	4.40
2100	0.30	1.00	**0.52**	1.70	0.85	2.80	**1.19**	3.90	1.52	5.00

Table A.3-12 SLR Projections with different probability levels under high-emission RCP 8.5 for New Jersey (STAP report: Kopp et al. 2019).

	Low End		At least a 66% chance between						High End	
Year	Greater than a 95% chance SLR exceeds		Greater than an 83% chance SLR exceeds		~50% chance SLR exceeds		Less than a 17% chance SLR exceeds		Less than a 5% chance SLR exceeds	
	m	ft	m	ft	m	ft	m	ft	m	ft
2000					0.00	0.00				
2010					0.06	0.20				
2020	0.03	0.10	0.09	0.30	0.15	0.50	0.21	0.70	0.27	0.90
2030	0.09	0.30	0.15	0.50	0.24	0.80	0.33	1.10	0.39	1.30
2040	0.15	0.50	0.21	0.70	0.33	1.10	0.45	1.50	0.58	1.90
2050	0.21	0.70	0.27	0.90	0.42	1.40	0.64	2.10	0.79	2.60
2060	0.27	0.90	**0.34**	1.20	0.58	1.90	**0.85**	2.80	1.03	3.40
2070	0.33	1.10	0.40	1.50	0.73	2.40	1.06	3.50	1.33	4.40
2080	0.39	1.30	0.43	1.80	0.88	2.90	1.33	4.40	1.73	5.70
2090	0.42	1.40	0.46	2.10	1.03	3.40	1.60	5.30	2.18	7.20
2100	0.45	1.50	**0.52**	2.30	1.18	3.90	**1.91**	6.30	2.66	8.80

Notes: This information is from Table A1. in STAP 2019, page 40. There is no clear differentiation in SLR probability projections before 2060 among all emission scenarios in STAP (2019).

A.4 Selected Local SLR Scenarios for DRBC SLR Modeling Study

Five SLR scenarios were selected for the DRBC SLR study using a 3-D hydrodynamic Model. Based on the information provided in Table 4 of the NJSTAP 2019 report, cited here in **Table A.4-1**, the probabilities of the selected SLR scenarios are presented in **Table A.4-2**, and **Table A.4-3**. The SLR projections have been updated by NOAA (2022), and the probabilities associated with these scenarios have also changed. Values presented in this section should be used with caution. The temperatures associated with the emission scenario given in these tables are the temperatures projected by 2100 with respect to early industrial (1850-1900) levels.

Table A.4-1. Range of probabilities the local SLR will exceed stated values in stated years (ft above 2000 baseline (from Table 4 in STAP report: Kopp et al. 2019).

High-emissions (5°C)

	1 ft	2 ft	3 ft	4 ft	5 ft	6 ft	7 ft	8 ft	9 ft	10 ft
2030	23-29%									
2040	57-68%	1-4%								
2050	83-90%	10-22%	0-2%							
2060	92-97%	34-57%	3-11%	0-2%						
2070	96-99%	59-80%	13-35%	2-9%	0-3%	0-1%				
2080	98-99%	76-91%	30-60%	7-26%	1-9%	0-4%	0-2%	0-1%		
2090	98-100%	85-95%	50-77%	18-47%	5-22%	1-10%	1-6%	0-3%	0-2%	0-1%
2100	98-100%	89-97%	64-85%	32-63%	12-38%	4-20%	1-11%	1-7%	0-5%	0-3%
2110	100%	97-99%	77-94%	40-75%	15-49%	5-28%	2-16%	1-11%	1-8%	0-6%
2120	100%	98-100%	83-96%	52-83%	23-60%	9-38%	4-23%	2-15%	1-11%	1-9%
2130	100%	99-100%	88-98%	63-89%	36-71%	16-50%	7-33%	4-21%	2-15%	1-12%
2140	100%	99-100%	92-98%	72-93%	47-79%	25-60%	12-42%	6-28%	3-20%	2-15%
2150	100%	99-100%	94-99%	79-95%	57-85%	35-69%	19-52%	10-36%	5-25%	3-18%

Low-emissions (2°C)

	1 ft	2 ft	3 ft	4 ft	5 ft	6 ft	7 ft	8 ft	9 ft	10 ft
2030	5-9%									
2040	47-58%	0-1%								
2050	74-83%	3-8%								
2060	88-93%	16-27%	1-2%							
2070	93-96%	38-53%	4-8%	1%						
2080	95-97%	54-69%	11-20%	2-4%	1%					
2090	95-98%	64-78%	22-33%	5-9%	1-2%	1%				
2100	95-98%	73-85%	34-48%	10-16%	3-5%	1-2%	1%			
2110	96-98%	78-87%	47-61%	20-30%	7-11%	3-4%	1-2%	1%		
2120	97-98%	82-89%	55-68%	28-40%	11-18%	5-8%	2-3%	1%	1%	
2130	97-98%	83-91%	60-74%	36-49%	18-26%	8-12%	4-6%	2-3%	1%	0-1%
2140	97-99%	86-93%	66-80%	42-57%	23-33%	11-17%	6-8%	3-4%	2%	1%
2150	97-99%	89-94%	70-83%	46-62%	26-39%	13-21%	6-11%	4-5%	2-3%	1%

Table A.4-2. Exceedance probability for five local SLR scenarios based on SLR projections and Table 4 in NJSTAP (2019) with Low Emission (2 degree C).

LSLR Scenarios (m)	LSLR Scenarios (ft)	2060	2100
0.3	1.0	88-93%	95-98%
0.5	1.6	45-53%	82-90%
0.8	2.6	7-12%	50-63%
1	3.3	0.7-1.4%	27-38%
1.6	5.2	0%	3-4%

Table A.4-3. Exceedance probability for five local SLR scenarios based on SLR projections and Table 4 in NJSTAP (2019) with high emission (5 degree C).

SM3D LSLR Scenarios (m)	SM3D LSLR Scenarios (ft)	2060	2100
0.3	1.0	92-97%	98-100%
0.5	1.6	57-73%	93-98%
0.8	2.6	15-29%	74-89%
1	3.3	2-8%	54-78%
1.6	5.2	0%	10-34%

Appendix B. Estuary Exchange Flow

Estuarine circulation known as “estuary exchange flow” is mainly the result of three competing factors: river flow moving seaward, denser saltier ocean water moving towards the land, and tidal currents providing turbulent mixing. A diagram of the tidally averaged circulation is shown in Figure B-1 (from MacCready and Geyer, 2010). Despite the net seaward flow through any cross-section, ocean water typically moves upstream in the deeper areas near the entrance of the bay. Near-bottom ocean inflow gradually warms and rises in the water column, mixing with freshwater from the river flowing seaward in the upper half of the water column. This dynamic results in an overall pattern called the estuary exchange flow (depicted as Q1 and Q2 in **Figure B-1.a**). The volume flux of the exchange flow is often many times greater than that of the river alone. The corresponding salinity field as shown in **Figure B-1.b** (from MacCready and Geyer, 2010) has a gradual along-channel salinity gradient, from salty to fresh (right to left in the figure). Deep incoming ocean water is continually diluted by the fresh water above due to the vertical turbulent mixing driven by tides. During low-flow periods water becomes weakly stratified due to a relatively stronger tidal forcing against the river inflows, while during high-flow periods a stronger vertical stratification is observed. Vertical stratification and intensity of vertical mixing also vary from spring to neap tidal cycles.

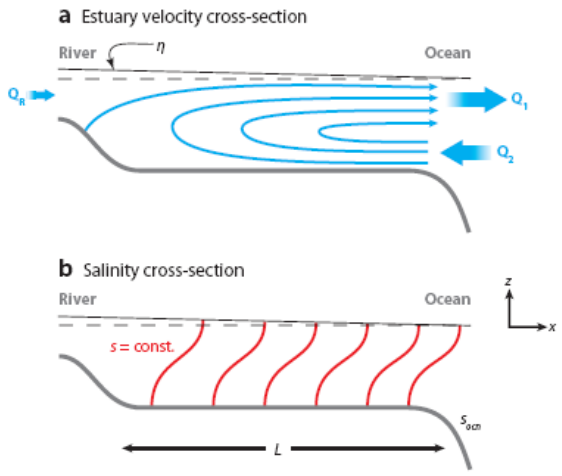

Figure B-1 Diagram of an idealized partially mixed estuary, showing (a) the tidally averaged circulation highlighting the exchange flow and (b) isoahalines. From MacCready and Geyer, 2010.

Appendix C. Salinity and Salt Front

C.1. Methods for Determining Salinity

Three of the most commonly used methods to determine salinity are 1) gravimetric (from dry residue), 2) volumetric (from chlorinity), and 3) conductometric (from electrical conductivity). Each method is briefly described below to explain why salinity is discussed as both salinity and chlorides.

Gravimetric determinization involves weighing a sample from which all the water was evaporated, and volatile compounds were vaporized. The process is tedious because multiple iterations of drying and weighing must occur until a constant mass is obtained to ensure all water is evaporated. Volumetric determination involves a measurement of the chlorinity, which is defined as the mass of silver needed to precipitate all halides (chlorides, bromides, and iodides), converted to an equivalent weight as chloride.[21] The salinity is then calculated using a relationship, where salinity = 0.03 + 1.805 * Chlorinity (S=0.03+1.805Cl).[22] Chlorinity and chlorides are used interchangeably. Salinity is reported in parts per thousand (ppt) using the gravimetric and volumetric methods. In 1978, oceanographers developed and agreed upon a new method to report salinity using the ratio of the electrical conductivity of seawater at 15°C to that of a standard potassium chloride solution (KCl). The ratio is expressed as practical salinity units (psu)[23], based on the Practical Salinity Scale (PSS-78), which equates the ratio to a physical quantity (e.g., 35 psu is approximately 35 ppt). The empirical relationship between chlorinity and salinity is strong for seawater and brackish water estuaries, where salinity is up to 35 psu, but it is not appropriate for salinity lower than 2 psu, which is higher than the salinity of freshwater (**Table C.1-1**). In high salinity areas, such as the lower Estuary or Bay, salinity is often used, but in the upper Estuary, chlorides are typically used as a surrogate for salinity.

[21] Chlorides represent approximately 55 percent of the total dissolved solids in sea water.

[22] The empirical relationship between salinity and chlorinity (chlorides): Salinity=0.03+1.805*Chlorinity (g/kg sea water) devised by Knudsen (1889). In 1962 the Joint Panel for Oceanographic Tables and Standards (JPOTS) established a new proportionality constant in Knudsen's formula: salinity (ppt)=0.00180655 (mg/l).
https://www.ldeo.columbia.edu/edu/k12/snapshotday/activities/2011/Classroom%20HS%20activity/chloride%20conversion/Chloride%20and%20Salinity.pdf
See also Chlorinity and salinity of seawater - EniG. Periodic Table of the Elements (periodni.com)

[23] In this report, salinity unit is Practical Salinity Unity [psu]. The numeric difference between psu and ppt is small; both indicate salinity. The difference has been discussed by scientists, e.g. https://blog.seabird.com/ufaqs/what-are-the-differences-between-salinity-expressions-in-ppt-psu-practical-salinity-and-absolute-salinity/

Table C-1 Salinity ranges for different classifications of water.

Fresh water	< 0.5 psu
Brackish water	0.5 to 30 psu
Saline water	30 to 50 psu
Brine	50 to 280 psu max

Note: the break between brackish and freshwater may vary. For example, the freshwater limit for agricultural irrigation is 0.2 psu.

C.2. CALCULATING SALINITY AND CHLORINITY

Salinity time-series at NOAA and USGS gages, calculated from raw conductivity or specific conductance (SC) and temperature data, were used to determine model salinity boundary conditions and to evaluate model performance. However, chlorinity is used to determine the extent of saltwater intrusion (represented by the salt front location) and whether water quality standards are met. Observed chlorinity data were derived from measured SC at USGS gages using a relationship between SC and chlorinity developed by USGS in the 1970s (Paulson, 1970).

To estimate simulated chlorinity based on simulated salinity, the following empirical equation can be used:

$$\text{Chlorinity (mg/L)} = 553.5260 * \text{Salinity (ppt)} \quad \text{(C-1)}$$

However, this empirical relationship between chloride and salinity breaks down when salinity is lower than 2 ppt (American Public Health Association, 1995). The salt front is defined as the location where the 7-day average chlorinity equals 250 ppm. This concentration is equivalent to a salinity of 0.45 psu using the empirical relationship; however, at this low level the empirical equation no longer be valid. For example, a value of 0.52 psu was suggested for the salt front in the Delaware Estuary in a USGS study by Cook et al. (2023). PWD developed salinity conversion method based on combined PWD and DRBC boat-run samples, and with that conversion 250 mg/L chloride concentration corresponding to 0.50 psu salinity (PWD, 2020)[24]. DRBC investigated the relationship between salinity and chlorinity using boat-

[24] PWD (2020): https://water.phila.gov/pool/files/salinity-model-validation-report-2020-05.pdf

run data and developed a Delaware Estuary–specific relationship between salinity and chloride. To develop this equation, 2,637 boat-run samples collected during 2000–2018 were used for a "two-slope" piecewise-linear regression analysis, with an R^2 score of 0.976 for salinity greater than 0.2 psu. In this report, Equations C-2 and C-3 were thus combined to a piecewise "two-slope" equation, which tends to better characterize the background level salinity in the upper tidal river.

$$Chlorinity\ (mg/L) = 582.8 * Salinity\ (psu) - 63, \quad for\ Salinity \geq 0.2\ psu \tag{C-2}$$

$$Chlorinity\ (mg/L) = 267.6 * Salinity\ (psu), \quad for\ Salinity < 0.2\ psu \tag{C-3}$$

Using this function, the break point at 0.2 psu salinity is approximately corresponding to 54 mg/L chloride concentration. With this relationship (Equations C-2), 250 mg/L chloride concentration is equivalent to salinity of 0.54 psu, this is consistent with what has been estimated using salinity conversion methods by others as discussed earlier.

C.3. The Location of the Salt Front

The location of the salt front is calculated using real-time specific conductance measurements from USGS water quality monitors, a regression equation developed by USGS in the 1970s relating specific conductance and chlorides, and linear-logarithmic interpolation of the location between the water-quality monitoring stations. **Table C-2** presents the gages used to calculate the location of the salt front.

Table C-2 Real-time USGS water quality monitoring stations used to calculate the historical salt front location.

Gage ID	Name	River Mile (RM)	Channel Depth	Channel Width	Location	Sensor Depth
01482800	Reedy Island	54.1	Up to about 50 feet in the shipping channel	12,000 feet	4,500 feet from the right bank on the shore-ward side of Jetty	Approximately 15 feet below the water-surface at low tide
01477050	Chester	83.6	Up to about 40-50 feet in the shipping channel	7,000 feet	Directly along the right bank.	Approximately 10 feet below the water-surface at low tide
01474703	Fort Mifflin	91.9	Up to 50 ft in the shipping channel.	5,300 feet	450 feet from the right bank.	Approximately 5 feet below the water-surface at low tide.
01467200	Ben Franklin Bridge RM 100.1	100.1	Up to 50 feet in the shipping channel.	2,800 feet	500 ft from right bank on downstream side of municipal pier #12	Approximately 10 feet below the water-surface at low tide
	Notes: Specific conductance data are collected at other locations in the Estuary, but the data were not available and/or in range for calculating the salt front for much of the historical record. Data from these locations will be useful for improving model performance and estimating the salt front location. Additional locations include: USGS014670261, Delaware River at Pennypack Woods PA (established February 2011). USGS01482100, Delaware Memorial Bridge at Wilmington, DE (established August 26, 2020). USGS01482695, C and D Canal near Delaware City, DE (established May 26, 2020). USGS01412350, Delaware Bay at Ship John Shoal Lighthouse NJ (established March 10, 2021).					

Information about the history of observed salt front data can be found at the DRBC website:
https://www.nj.gov/drbc/programs/flow/salt-front.html

Appendix D. Variability of Inflow and Salt Front Location

River flow and has a large effect on salinity intrusion in the Delaware Estuary. To account for variability in hydrologic conditions, a multiple-year approach was used in the salinity modeling study. The information provided in this section demonstrates that approach, in which a wide range of flow conditions were considered.

In this study, an ensemble simulation approach was used to cover a wide range of hydrologic and flow conditions in combination with SLR (Section 4 of this report). Ten selected years were considered that include dry years and normal to wet years in terms of flow conditions. The proportion of "dry" years in the 10 simulated years is relatively high compared with that of the historical data, which may lead to a distorted probability distribution of the salt front.

Downstream of Trenton the Delaware River is tidally influenced. The water upstream from Trenton does not flush out of the estuary quickly but rather moves back and forth in the system with the flood and ebb tide cycle. The total cumulative freshwater volume in the system varies slowly. The impact of a rapid change in flow of the Delaware at Trenton (133 miles from the bay mouth) in the lower bay may be delayed by up to two weeks due to the tidal influence. The total amount of upland freshwater in the tidal river plays a key role in controlling salinity movement. A severe salinity intrusion event occurs when a prolonged low flow persists for 2 to 3 months, and the severe salinity intrusion event may also persist for 2 to 3 months. Therefore, both daily and relatively long-term trends should be considered in the flow analysis.

The historical record of flows of the main stem Delaware River at Trenton were ranked and are shown in **Figure D-1**. The simulated years are highlighted in red. USGS daily flow data for gage 01463500 were used, and ranking was performed based on daily, 30-dma, 60-dma, and 90-dma flow rates (**Figure D-1** through **D-4**). The cumulative frequency plot (**Figure D-5**) demonstrates the distribution of daily flow on the Delaware River at Trenton for simulated years and compares this distribution with that of the historical record. In these figures, the 10 selected years are highlighted in red. As only 10 years were simulated, the number of "dry" years among the 10 simulated years are not proportional to the dry years in the full record and reflect conditions that result in more upstream salt front locations (**Figure D-6**).

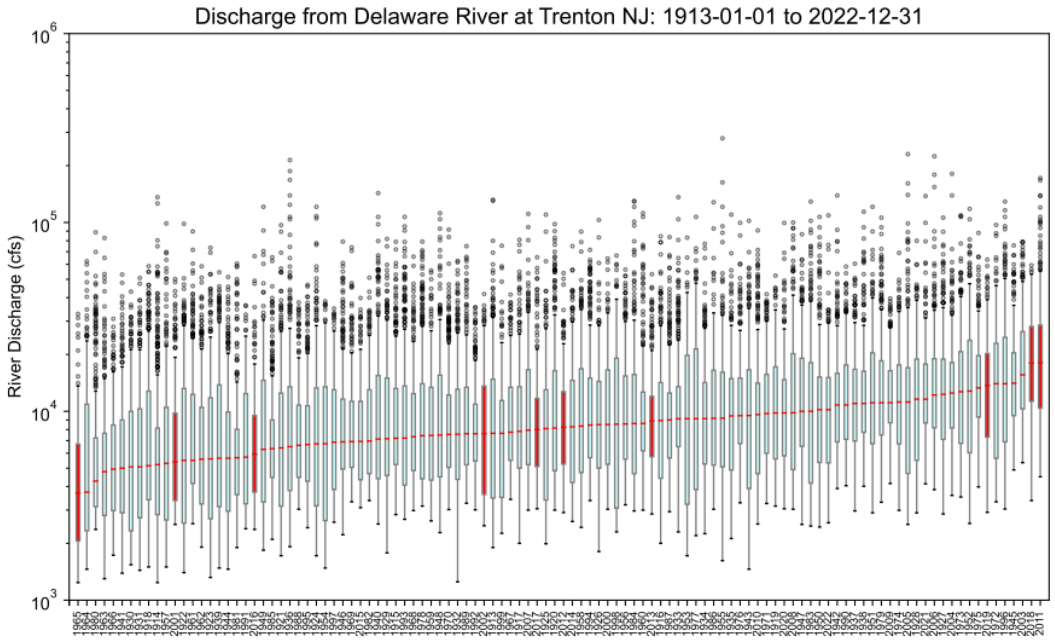

Notes: Analysis was based on calendar year and sorted by annual median value. USGS gauge 01463500, 1913-01-01 to 2022-12-31. Flow from ten years (in red) were used in 3-D model simulations: 1965, 2001-2002, 2011-2013, 2016-2019.

Figure D. 1. Ranking annual median flow for the Delaware River at Trenton, based on the daily flow record from 1913 through 2022.

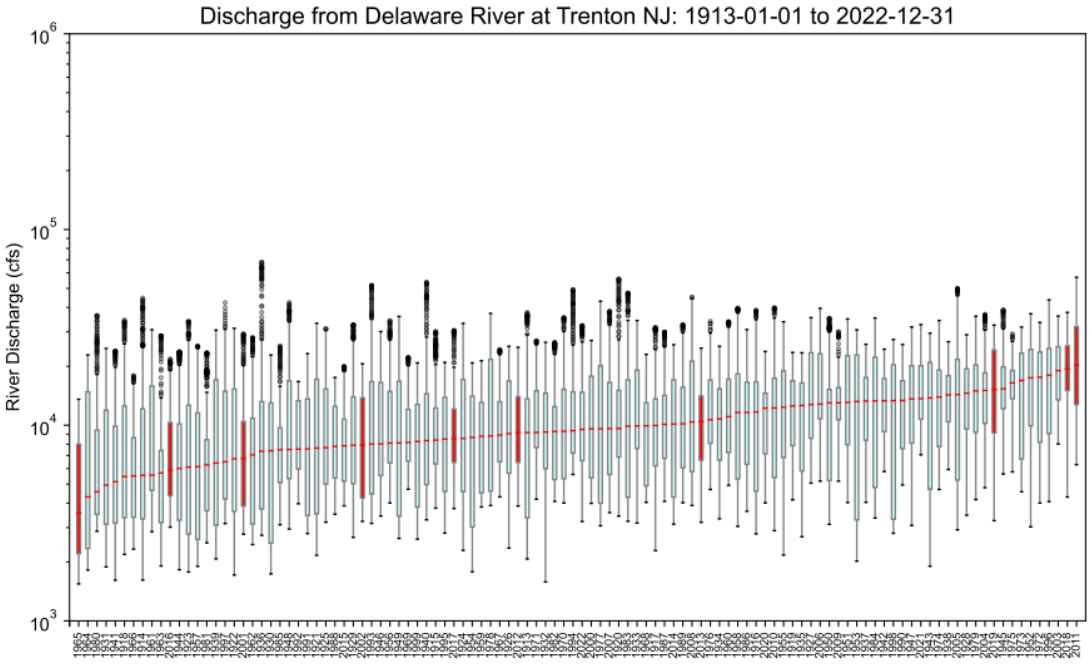

Notes: Analysis was based on calendar year and sorted by annual median value. USGS gauge #: 01463500, 1913-01-01 to 2022-12-31. Flow from ten years (in red) were used in 3-D model simulations: 1965, 2001-2002, 2011-2013, 2016-2019.

Figure D. 2. Ranking annual median 30-dma flow for the Delaware River at Trenton, based on the daily flow record from 1913 through 2022.

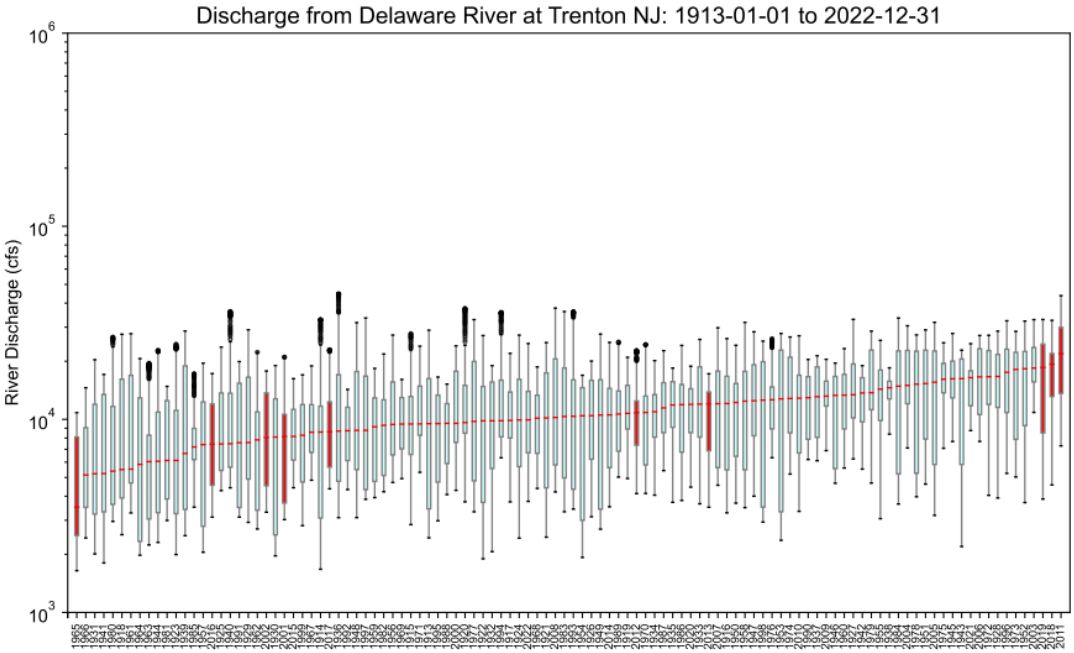

Notes: Analysis was based on calendar year and sorted by annual median value. USGS gauge #: 01463500, 1913-01-01 to 2022-12-31. Flow from ten years (in red) were used in 3-D model simulations: 1965, 2001-2002, 2011-2013, 2016-2019.

Figure D. 3. Ranking annual median 60-dma flow for Delaware River at Trenton, based on the daily flow record from 1913 through 2022.

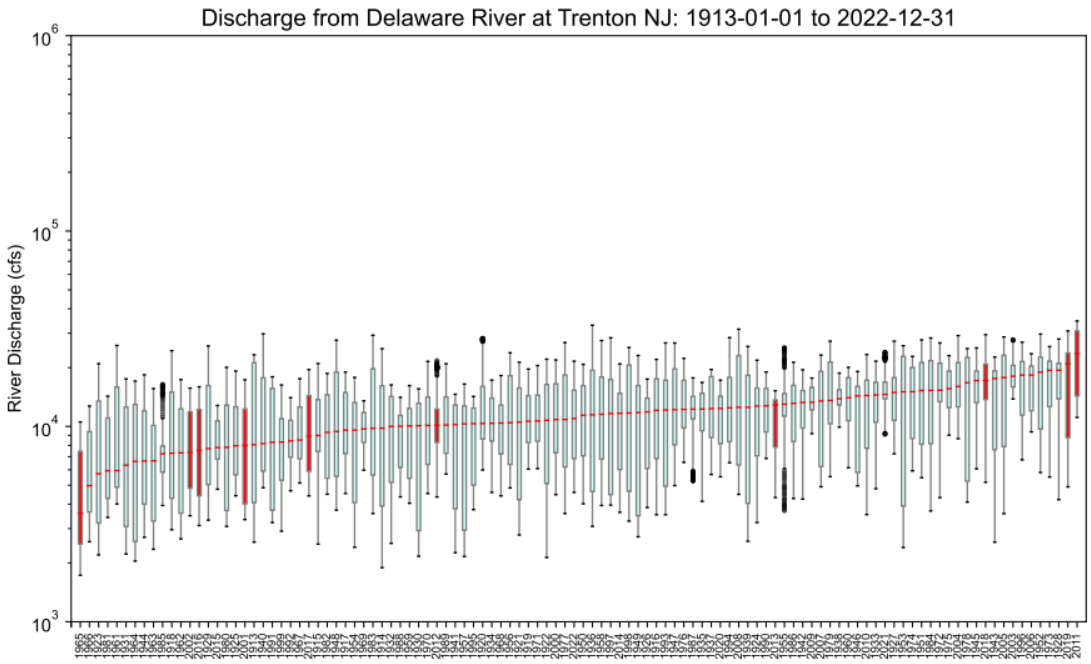

Notes: Analysis was based on calendar year and sorted by annual median value. USGS gauge #: 01463500, 1913-01-01 to 2022-12-31. Flow from ten years (in red) were used in 3-D model simulations: 1965, 2001-2002, 2011-2013, 2016-2019.

Figure D. 4. Ranking annual median 90-dma flow for the Delaware River at Trenton, based on the daily flow record from 1913 through 2022.

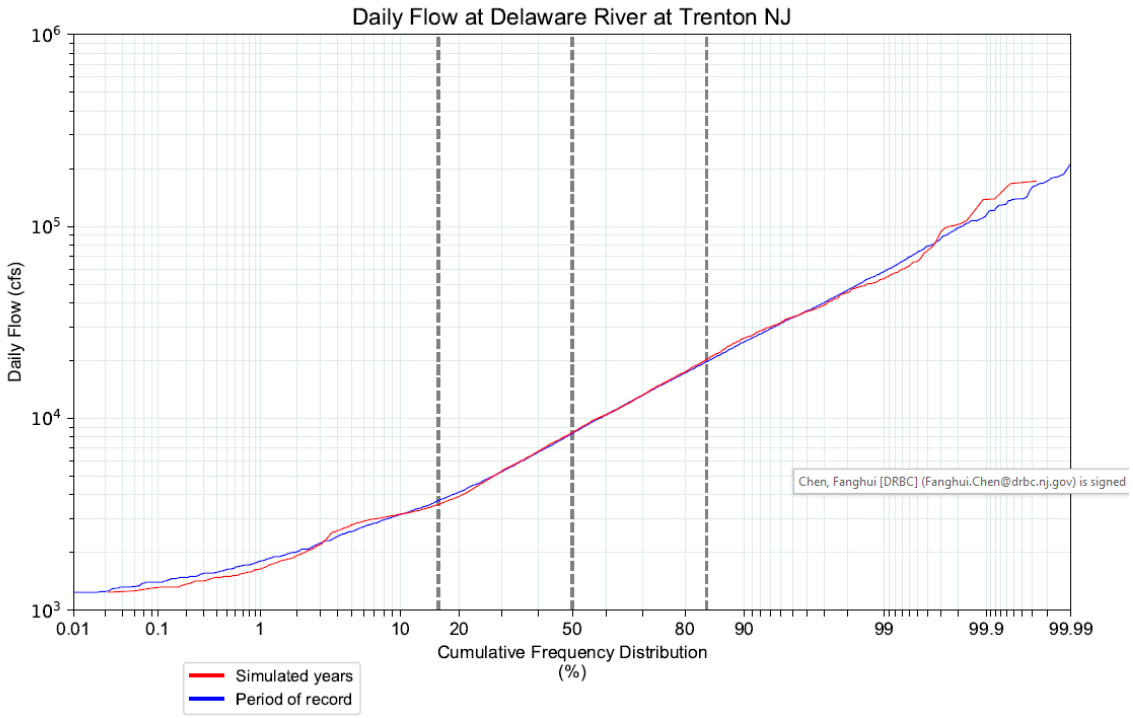

Notes: USGS gauge #: 01463500. Daily flows from 1913 to 2022 were used. Simulated years are:1965,2001,2002,2011,2012,2013,2016,2017,2018,2019.

Figure D. 5. Cumulative frequency distributions of observed and simulated daily flows of the Delaware River at Trenton.

Figure D-6 compares the cumulative frequency distribution, or cumulative distribution function (CDF) of the salt front location for the period of record and for the selected ten years. The CDF of the simulated salt front is farther upstream than the CDF of the observed salt front. The results indicate that the conditions simulated,10 years of flows and tides, were not sufficient for determining the probability of the salt front location under all conditions. The frequency or probability of the salt front reaching different locations should not be interpreted from this limited ensemble of model results.

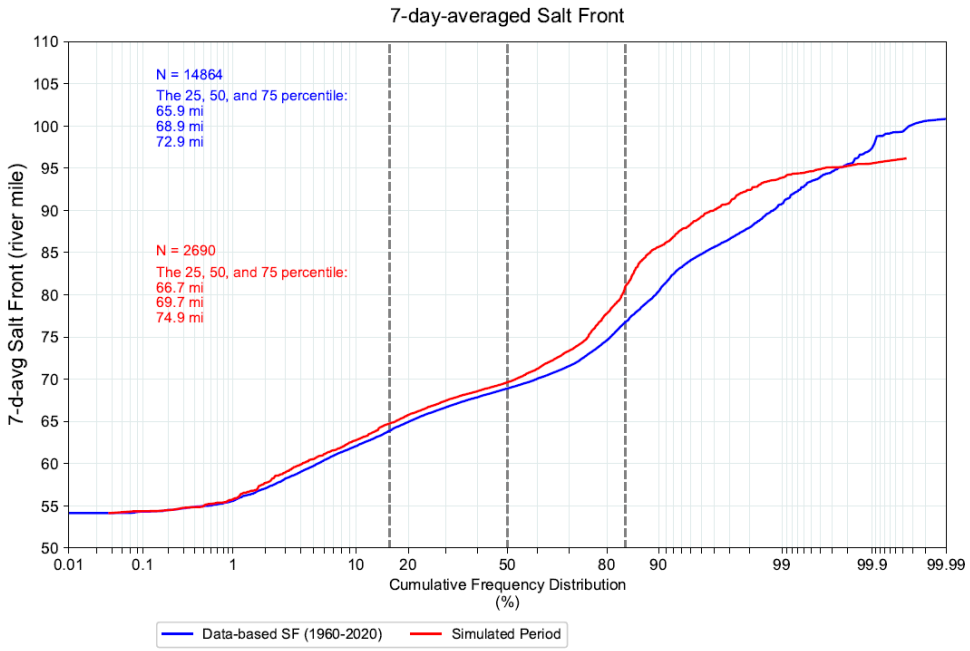

Note: salt front locations lower than RM 54 (Reedy Island) were excluded from this analysis. Data collected from 1963 to 2021 were used. Salt front data for the ten selected years (1965, 2001-2002, 2011-2013, 2016-2019) are shown in red.

Figure D-6. Cumulative frequency distribution of observed salt front location for simulated years and for the entire period of record (1963 to 2021).

Appendix E. Freshwater Inflow Budget Estimated for Year 2002

This appendix provides additional information about the freshwater inflow budget for the selected representative moderate low flow year 2002, which was used in simulations designed to aid in understanding the mechanisms driving salinity transport in the Delaware Estuary.

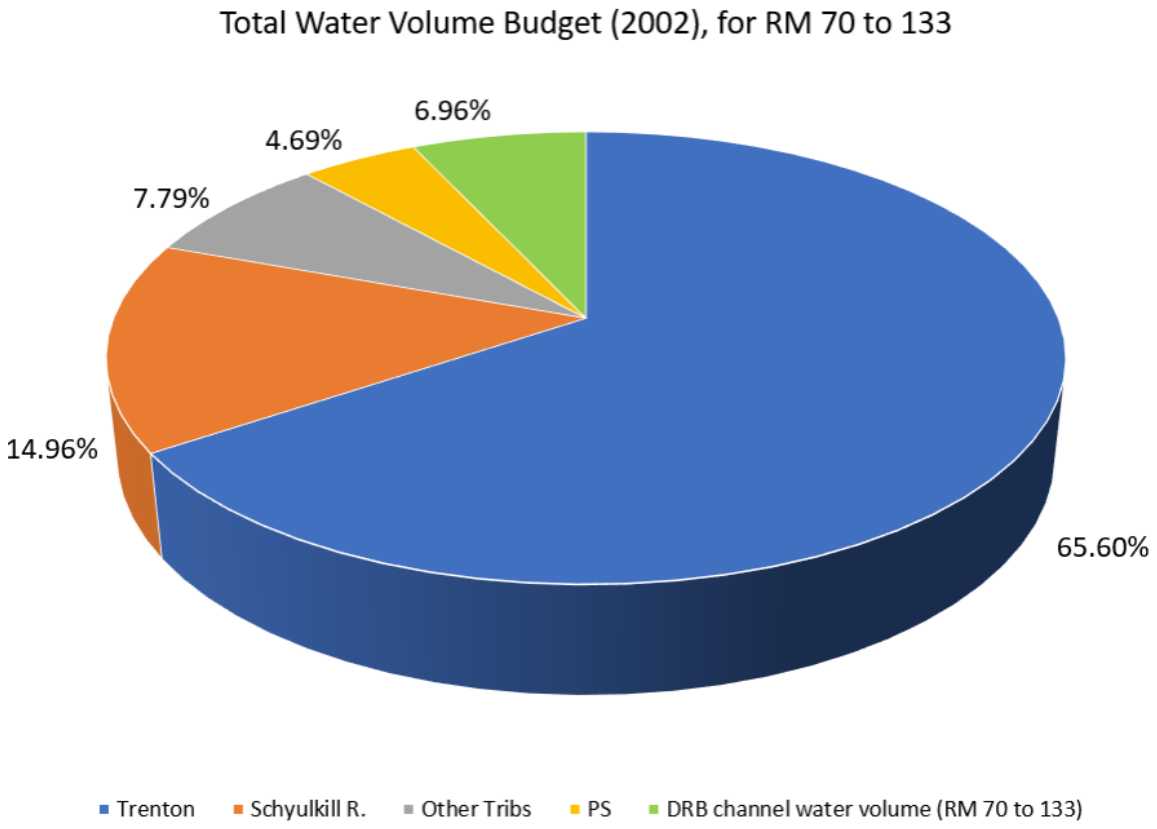

Figure E. 1. Total volumetric water budget for RM 70 to 133 for a representative low flow year (2002). PS=Point source discharges.

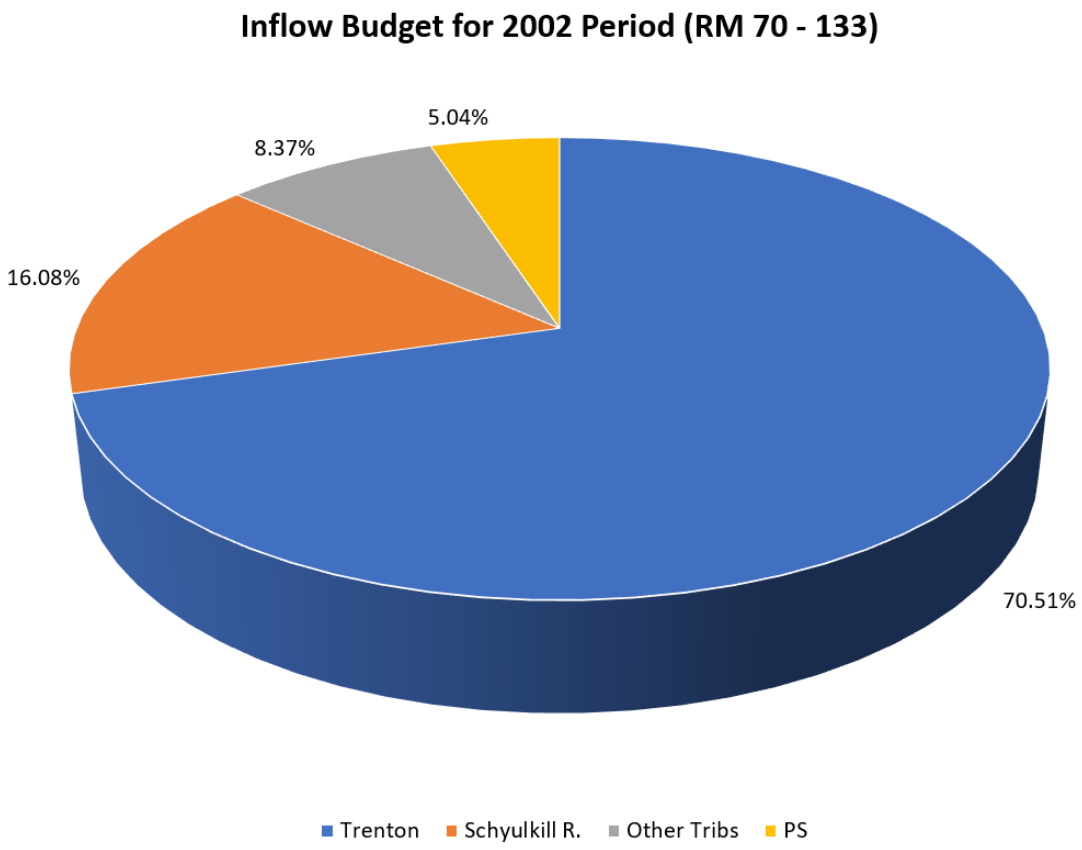

Figure E. 2. Freshwater Inflow budget for RM 70 to 133 for a representative low flow Year (2002).

Table E. 1. Summary of the water budget for RM 70 to 133 for a representative low flow year (2002).

Source	Annual Average Flow (cfs)	Annual Cumulative Flow (million cubic meters)	Contribution to Inflow Budget	Contribution to Total Volumetric Water Budget
Delaware River at Trenton	9873.32	8816.9	70.51%	65.60%
Schuylkill River	2250.91	2010.1	16.08%	14.96%
Other Tributaries	1172.07	1046.7	8.37%	7.79%
Point Source Discharges	706.08	630.5	5.04%	4.69%
Total Inflows	14002.38	12504.1	100%	93.04%
Estimated channel water volume (RM 70 to 133)		935.5		6.96%
Total water volume		13439.7		100%

Notes: flow from CSOs were not considered in the model. Due to the lack of information for 2002, PS discharges were assumed to be the same as they were in 2012.

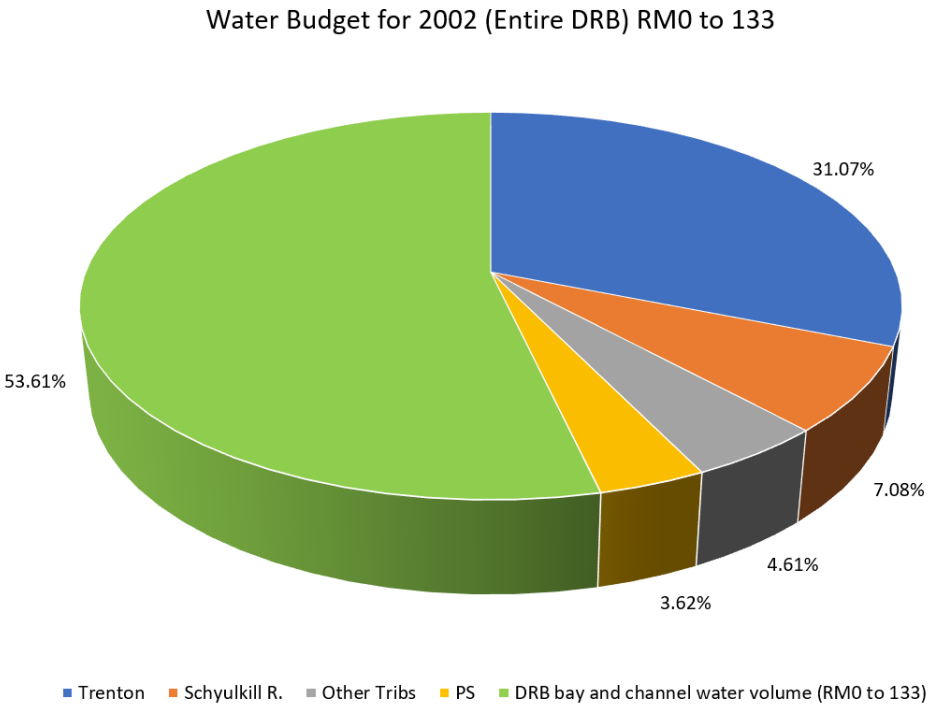

Figure E. 3. Estimated total volumetric water budget for a representative low flow year (2002).

Appendix F. Point Source Salinity

To evaluate the sensitivity of the model to the salinity of point source discharges, a test was conducted using point sources with realistic salinity values. Results of the analysis are presented in section 6.1.2 and in Appendix K.1.2. This appendix explains how the salinity values for point sources were determined.

The salinity of point source (PS) discharges used in the sensitivity analysis were derived from a modeling study conducted by the Philadelphia Water Department (PWD, 2020[25]). For the purpose of their study, 52 facilities classified as discharge only (the majority of discharge only facilities identified) are municipal wastewater treatment plants. Available information for 2014 discharge flow rates, total dissolved solids (TDS) concentrations, conductivity, and chloride was collected. Missing salinity values for 2014 were estimated using information from other databases. Many facilities did not have salinity data (including TDS, chloride, or conductance).

Salinity values for the 12 major tier-1 discharges that were simulated in this study are listed in **Table F.1**. The average salinity value for discharges from the three PWD wastewater treatment plants and Delcora is 0.48 psu. A salinity value of 0.48 psu was assigned to the discharge of facilities without any salinity information.

Seasonal variability in point source discharge salinity is summarized in **Table F.2**.

[25] PWD salinity validation report (May, 2020): https://water.phila.gov/wp-content/uploads/files/salinity-model-validation-report-2020-05.pdf

Table F.1. Salinity values assigned to major point source discharges (data source: PWD, 2020)[26]

State	Facility Name	NPDES Number	Outfall Code	2014 Avg. Flow	2014 Avg. Salinity
				[MGD]	[PSU]
PA	PWD - Southeast WPCP	PA0026662	SEOUT	*	0.43
PA	PWD - Southwest WPCP	PA0026671	SW123E	*	0.48
PA	PPWD - Northeast WPCP	PA0026689	NEOUT	*	0.45
PA	Delcora	PA0027103	1	31.27	0.55
PA	Lower Bucks County JMA	PA0026468	1	7.49	0.31
PA	Morrisville Boro Mun. Auth-STP	PA0026701	1	5.24	0.51
NJ	Camden County MUA	NJ0026182	001A	55.4	0.39
NJ	Gloucester County Utility Authority	NJ0024686	001A	18.45	0.67
NJ	Hamilton Twp WPCF	NJ0026301	001A	8.12	0.36
NJ	Trenton DPW Sewerage Authority	NJ0020923	001A	11.38	0.19
NJ	Willingboro Twp MUA	NJ0023361	001A	3.82	0.25
DE	Wilmington WWTP	DE0020320	1	73.71	0.46

Note: these 12 tier-1 point source discharges contribute approximately 79% of the total point source discharges from all 72 PS simulated by the 3-D model. The discharges from Tier-2 and Tier-3 PS are small, and salinity in those discharges was assigned a common value of 0.48 psu in the 3-D model.

[26] PWD (2020): Philadelphia Water Department Watershed Protection Program, Delaware Estuary Salinity Model Validation, May 2020. Values are from Table 2-9 of the PWD report. https://water.phila.gov/pool/files/salinity-model-validation-report-2020-05.pdf

Table F.2. Seasonal Variability in Point Source Salinity

Month	Camden County Municipal Utilities Authority	City of Wilmington, Department of Public Works	DELCORA	Gloucester County Utilities Authority	Hamilton Township Wastewater Utility	Lower Bucks County Joint Municipal Authority	Morrisville Borough Municipal Authority	Philadelphia Water Department Northeast	Philadelphia Water Department Southeast	Philadelphia Water Department Southwest	Trenton Sewer Utility	Willingboro Municipal Utilities Authority	Mean of the Month
Jan	0.43	0.50	0.61	0.74	0.47	0.38	0.49	0.40	0.39	0.46	0.32	0.29	0.49
Feb	0.52	0.59	0.64	0.83	0.50	0.35	0.52	0.60	0.51	0.69	0.33	0.31	0.54
Mar	0.49	0.53	0.61	0.78	0.50	0.41	0.51	0.55	0.56	0.56	0.32	0.25	0.53
Apr	0.44	0.48	0.58	0.85	0.48	0.42	0.54	0.47	0.42	0.51	0.22	0.30	0.51
May	0.41	0.46	0.57	0.73	0.45	0.44	0.55	0.43	0.42	0.50	0.28	0.30	0.50
Jun	0.40	0.46	0.57	0.75	0.47	0.41	0.55	0.44	0.39	0.46	0.33	0.30	0.49
Jul	0.40	0.47	0.64	0.72	0.49	0.43	0.58	0.44	0.42	0.46	0.30	0.31	0.52
Aug	0.39	0.45	0.64	0.65	0.50	0.45	0.62	0.46	0.38	0.46	0.35	0.32	0.53
Sep	0.38	0.49	0.62	0.68	0.49	0.45	0.67	0.41	0.39	0.44	0.30	0.32	0.55
Oct	0.40	0.48	0.54	0.83	0.50	0.44	0.57	0.41	0.40	0.45	0.36	0.33	0.51
Nov	0.42	0.40	0.48	0.73	0.47	0.43	0.52	0.40	0.37	0.45	0.39	0.31	0.47
Dec	0.37	0.45	0.56	0.68	0.48	0.41	0.49	0.37	0.39	0.42	0.36	0.30	0.47
Annual Mean	0.42	0.48	0.59	0.75	0.48	0.42	0.55	0.44	0.42	0.48	0.32	0.30	0.51
Annual min	0.37	0.40	0.48	0.65	0.45	0.35	0.49	0.37	0.37	0.42	0.22	0.25	0.47
Annual max	0.52	0.59	0.64	0.85	0.50	0.45	0.67	0.60	0.56	0.69	0.39	0.33	0.55

source: DRBC,
unit is psu

Appendix G. Additional Diagnostic Simulation Results from the 3D Model

This appendix provides additional results for the simulations presented in Section 4.

G.1. Effect of SLR on Tidal Water Surface Elevation

A table of the simulated change in tidal constituent M2 with sea level rise are provided in **Table G.1**.

The simulated mean and maximum tidal water surface elevations are shown in **Figures G.1** and **G.2**. Simulated tidal water level ranges and diurnal ranges are presented longitudinally in **Figure G.3a** and **G3b**, and the diurnal range of water level was calculated as the mean higher-high water level (MHHW) minus the mean lower-low water level (MLLW) during the period of interest. The difference in simulated maximum water level is presented in **Figure G.4**. The differences in simulated water level range and diurnal range are presented in **Figure G.5a** and **G.5b**. **Table G.1** presents the simulated M2 amplitude and phase with SLR. As expected, the increase in simulated tidally averaged mean water level is close to SLR below RM 10 (e.g., MWL increases 0.3 m with 0.3 m SLR), and increases moving upstream (e.g., increases ~0.4 m with 0.3 m SLR at RM 130). With 0.3 m SLR, mean and maximum water surface elevations increase by a similar magnitude (e.g., both increase by approximately 0.5 m at RM 130). However, with 1.6 m SLR, maximum water levels increase somewhat more than mean water levels: at RM 130, the mean water level increases by ~1.6 m, while the maximum water level increases by ~1.8 m.

Similar to the increase in M2 amplitude, the tidal range and the diurnal range increase more above RM 80. With a 1.6 m sea level rise (SLR), the tidal range at RM 130 increases from approximately 3.4 m to 3.8 m, while the diurnal range increases from about 2.6 m to 3.1 m. The increase in tidal water level range in the upper portion of the river may result in more frequent tidal flooding, even in the absence of severe weather. For example, at RM 100 (near Ben Franklin Bridge), the predicted mean water level increases approximately the same amount as the SLR specified at the mouth of the Bay. As expected, increased tidal forcing with SLR magnifies the tidal range, even though flow forcing remains unchanged.

Table G. 1. Simulated M2 amplitude and phase with SLR

SLR (m)	Station	Station ID	RM	Modeled M2 Amplitude (m)	Modeled Baseline M2 Amplitude (m)	Difference in Amplitude (cm)	Modeled Phase (hour)	Modeled Baseline Phase (hour)	Difference in Phase (hour)
0	LEWES	8557380	0	0.596	0.596	0.00	7.34	7.34	0.00
1	LEWES	8557380	0	0.613	0.596	1.73	7.28	7.34	-0.05
1.6	LEWES	8557380	0	0.625	0.596	2.92	7.24	7.34	-0.10
0	CAPE MAY	8536110	2	0.720	0.720	0.00	7.40	7.40	0.00
1	CAPE MAY	8536110	2	0.739	0.720	1.89	7.30	7.40	-0.10
1.6	CAPE MAY	8536110	2	0.750	0.720	3.00	7.23	7.40	-0.17
0	SHIP JOHN SHOAL	8537121	37	0.908	0.908	0.00	8.58	8.58	0.00
1	SHIP JOHN SHOAL	8537121	37	0.937	0.908	2.94	8.33	8.58	-0.26
1.6	SHIP JOHN SHOAL	8537121	37	0.956	0.908	4.75	8.17	8.58	-0.41
0	REEDY POINT	8551910	58.5	0.783	0.783	0.00	9.76	9.76	0.00
1	REEDY POINT	8551910	58.5	0.807	0.783	2.42	9.51	9.76	-0.26
1.6	REEDY POINT	8551910	58.5	0.831	0.783	4.85	9.35	9.76	-0.42
0	DELAWARE CITY	8551762	60.7	0.819	0.819	0.00	9.92	9.92	0.00
1	DELAWARE CITY	8551762	60.7	0.853	0.819	3.39	9.65	9.92	-0.26
1.6	DELAWARE CITY	8551762	60.7	0.885	0.819	6.62	9.49	9.92	-0.43
0	MARCUS HOOK	8540433	79.3	0.711	0.711	0.00	11.34	11.34	0.00
1	MARCUS HOOK	8540433	79.3	0.796	0.711	8.48	11.01	11.34	-0.33
1.6	MARCUS HOOK	8540433	79.3	0.858	0.711	14.76	10.79	11.34	-0.55
0	PHILADELPHIA	8545240	98.5	0.809	0.809	0.00	0.42	0.42	0.00
1	PHILADELPHIA	8545240	98.5	0.919	0.809	10.99	12.36	0.42	-0.48
1.6	PHILADELPHIA	8545240	98.5	0.998	0.809	18.88	12.07	0.42	-0.77
0	BURLINGTON	8539094	117.5	1.040	1.040	0.00	1.05	1.05	0.00
1	BURLINGTON	8539094	117.5	1.153	1.040	11.36	0.51	1.05	-0.54
1.6	BURLINGTON	8539094	117.5	1.240	1.040	20.04	0.19	1.05	-0.86
0	NEWBOLD	8548989	126.3	1.106	1.106	0.00	1.16	1.16	0.00
1	NEWBOLD	8548989	126.3	1.223	1.106	11.73	0.61	1.16	-0.55
1.6	NEWBOLD	8548989	126.3	1.312	1.106	20.56	0.28	1.16	-0.89

Note: the analysis is based on one year (2002 hydrologic conditions).

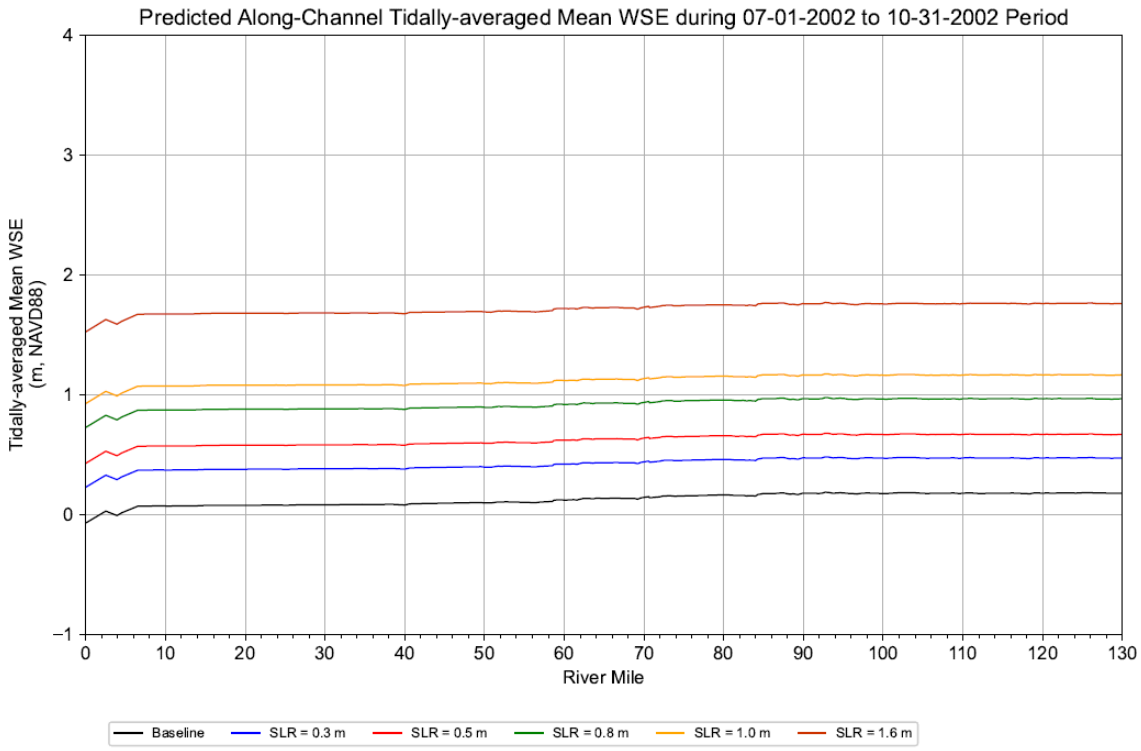

Figure G.1. Simulated tidally averaged water levels with SLR in the Delaware Estuary during a representative low flow period (2002 conditions).

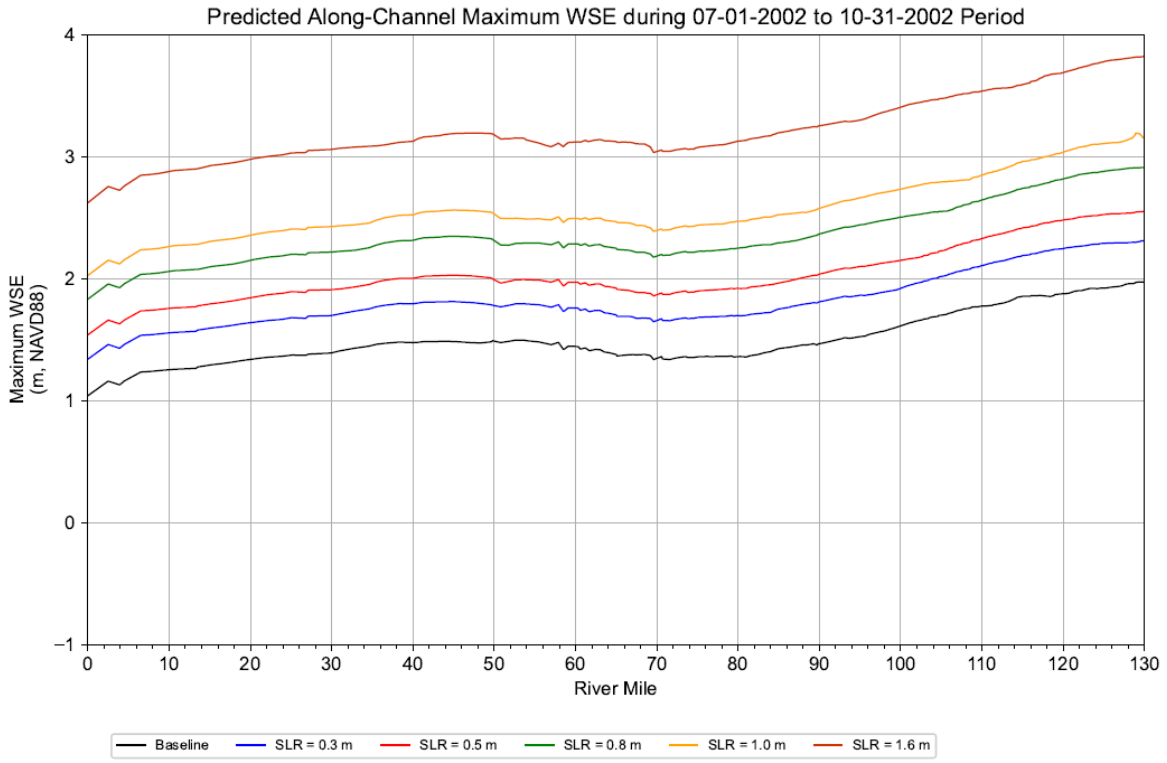

Figure G.2. Simulated maximum water levels under SLR conditions in the Delaware Estuary during a representative low flow period (2002 conditions).

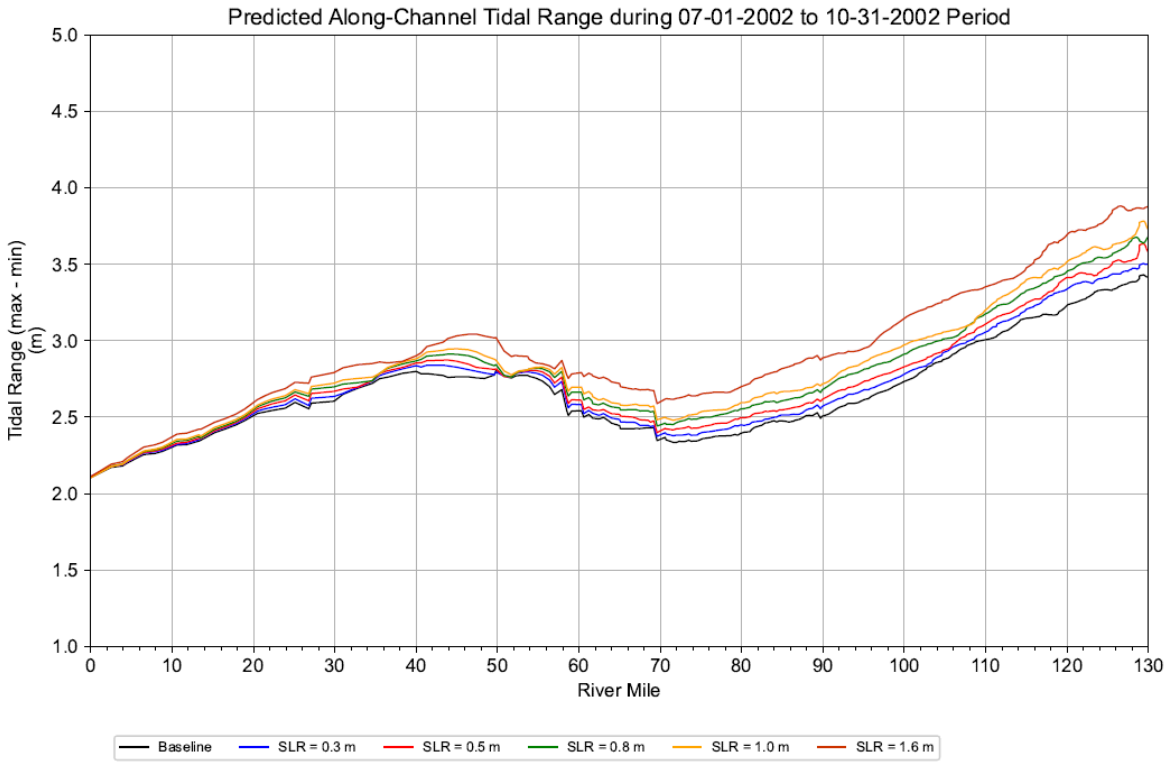

Figure G.3a. Simulated range of water Levels under SLR conditions in the Delaware Estuary during a representative low flow period (2002 conditions). The range was calculated as the maximum water level minus the minimum water level.

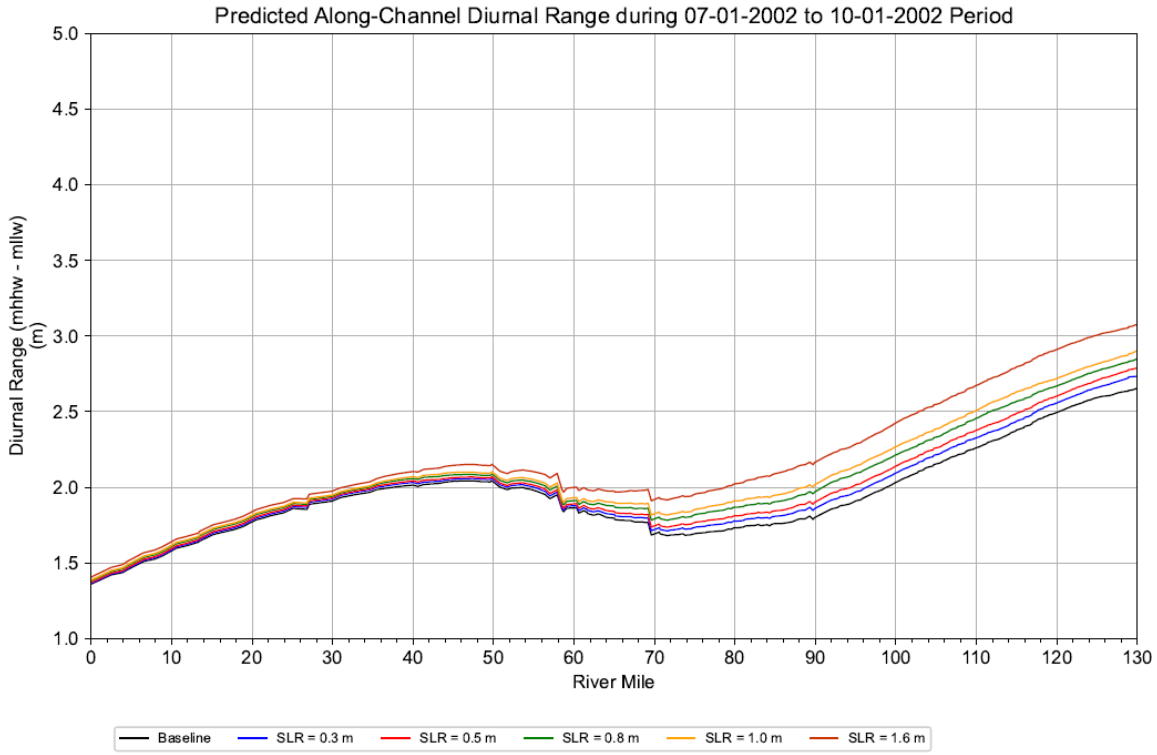

Figure G.3b. Simulated diurnal range of water Levels under SLR conditions in the Delaware Estuary during a representative low flow period (2002 conditions). The diurnal range of water level was calculated as the mean higher-high water level (MHHW) minus the mean lower-low water level (MLLW) during this period.

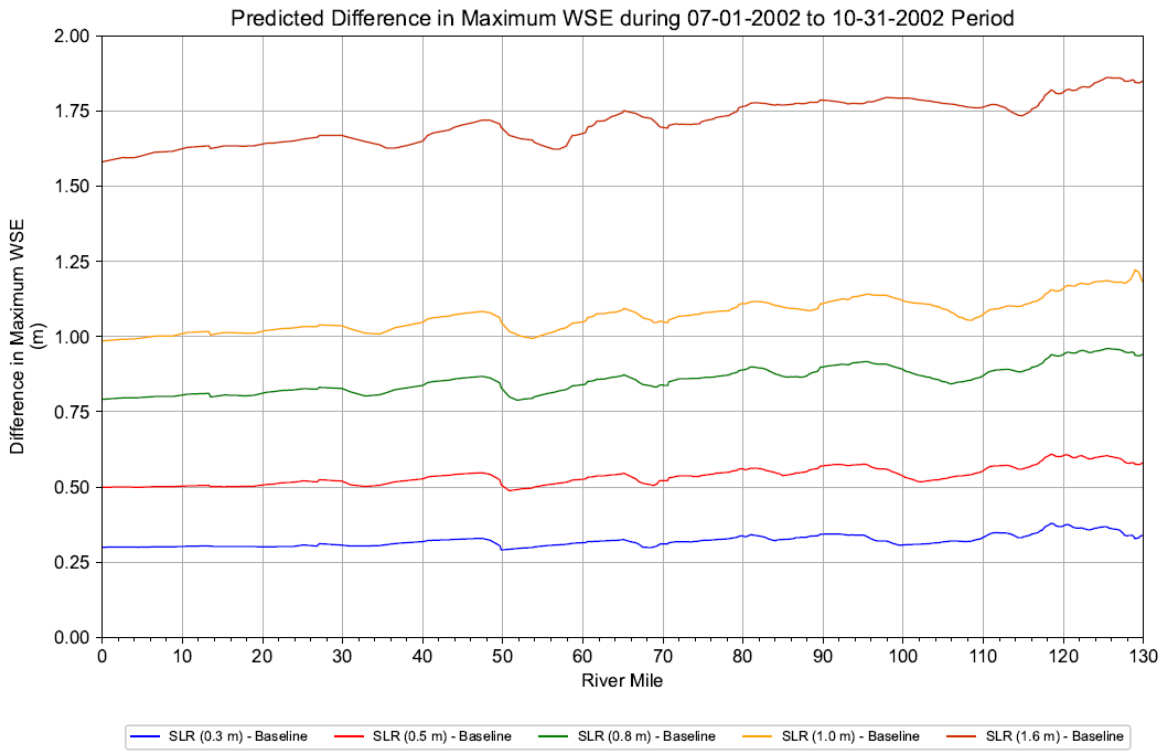

Figure G.4. Difference in simulated maximum water level for six SLR scenarios during a representative low flow period (2002 conditions).

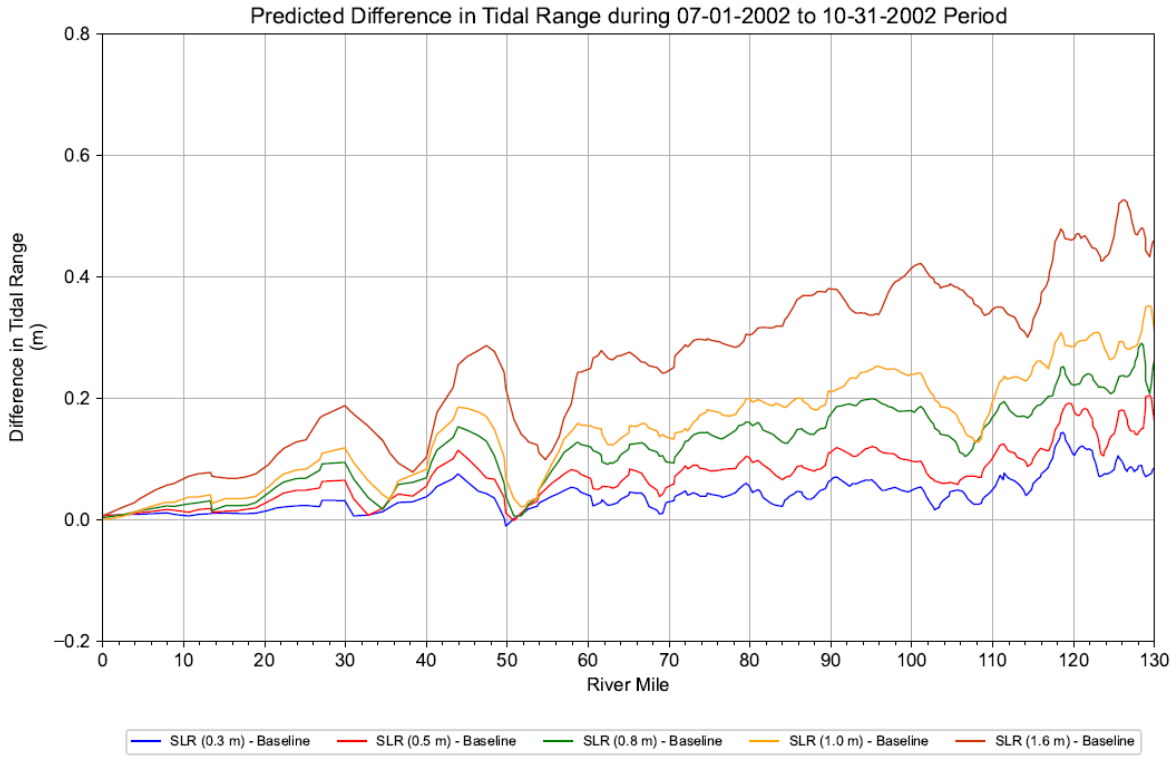

Figure G.5a. Difference in simulated water level range for six SLR scenarios during a representative low flow period (2002 conditions). The range was calculated as the maximum water level minus the minimum water level.

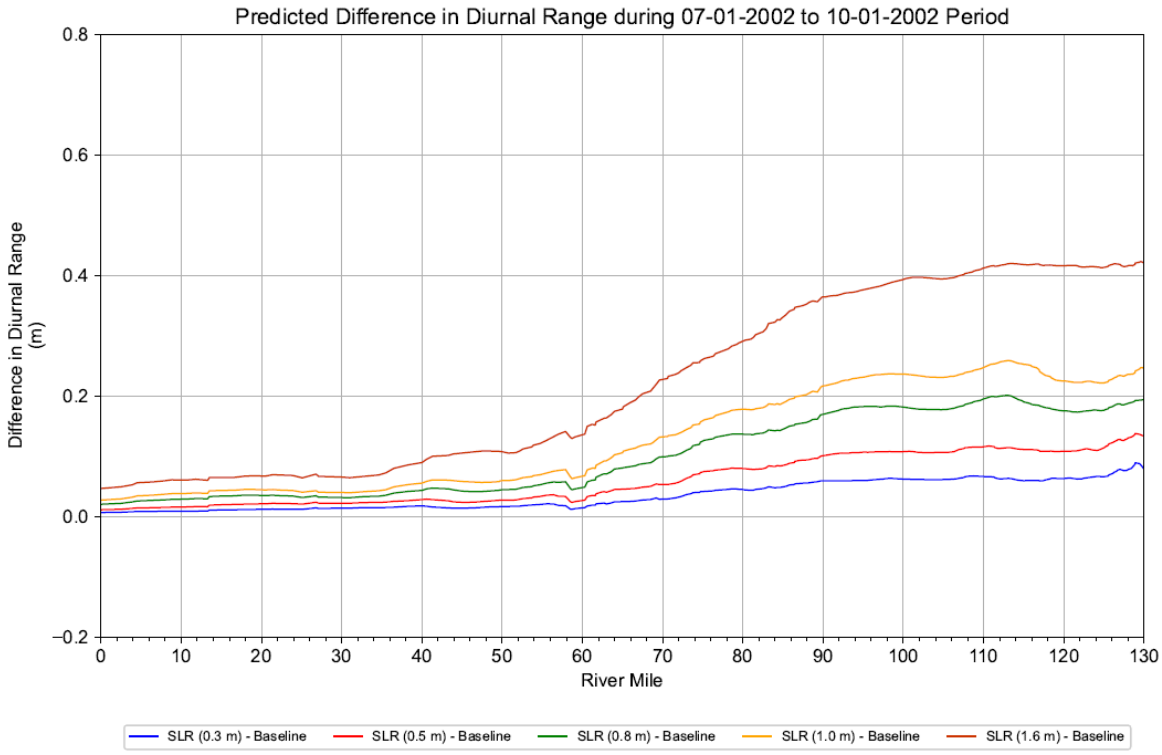

Figure G.5b. Difference in simulated diurnal water level range for six SLR scenarios during a representative low flow period (2002 conditions). The diurnal range of water level was calculated as the mean higher-high water level minus the mean lower-low water level during this period.

Table G. 2. Projected mean water level for 2060 at Lewes, DE and Philadelphia, PA, according to a NOAA 2022 SLR projection.

	Lewes		Philadelphia		Relative Difference (RM100-RM0)	
	ft	m	ft	m	ft	m
High	2.46	0.75	2.33	0.71	-0.13	-0.04
Intermediate High	2.13	0.65	2.03	0.62	-0.10	-0.03
Intermediate	1.77	0.54	1.67	0.51	-0.10	-0.03
Intermediate Low	1.54	0.47	1.44	0.44	-0.10	-0.03

Source: https://coast.noaa.gov/digitalcoast/tools/slr.html and NOAA (2022 Sea Level Rise Technical Report[27]).

[27] 2022 Sea Level Rise Technical Report https://oceanservice.noaa.gov/hazards/sealevelrise/sealevelrise-tech-report.html

Table G. 3. Simulated mean water level change under SLR conditions at Lewes, DE and Philadelphia, PA.

Local SLR at Lewes, DE		Local SLR at Ben Franklin Br. RM 100		Relative Difference (RM100-RM0)	
ft	m	ft	m	ft	m
0	0	0.06	0.02	0.06	0.02
0.98	0.3	1.03	0.31	0.04	0.01
1.64	0.5	1.67	0.51	0.03	0.01
2.62	0.8	2.64	0.80	0.01	0.00
3.28	1	3.28	1.00	0.00	0.00
5.25	1.6	5.23	1.59	-0.02	-0.01

Note: 3D hydrodynamic model results were based on the four-month low-flow period of 07-01-2002 to 10-31-2002. Flow at Trenton for this period was relatively stable at 3000 cfs. The salt front location reached RM 89 at the end of September 2002.

Table G.2 and **G.3** indicate that the simulated relative differences in the water level change between Philadelphia at RM 100 and the mouth of the estuary (RM 0) under various SLR conditions are similar to those suggested by NOAA 2022 projections.

G.2. Ensemble Simulation Results

This section provides additional detailed results from the 10-year ensemble simulations discussed in Section 4.2, including the simulated range of the salt front for each simulated flow year (**Table G.4** and **Figures G.6** and **G.7**), the seasonal variation of the salt front during the simulated flow year (**Figure G.8**), as well as the percentage of time the salt front is above landmark location RM 92.5, which is the Schuylkill River confluence (**Table G.5** and **Figure G.9**).

The ten years simulated include 1965, 2001 to 2002, 2011 to 2013, and 2016 to 2019. There was no flow objective applied at Trenton during 1960s, and the flow at Trenton during the 1965 drought period was much lower than the lowest drought management flow objective of 2,500 cfs, a key requirement of the current drought management plan (Section 2.5.3 Delaware River Water Code). The Trenton Flow Objective (TFO) was established to ensure freshwater inflow to the Delaware River Estuary for salinity management. The simulation results presented in the Section 4.2 reflect a minimum flow of 2500 cfs set for 1965 to represent implementation of TFO. It also should be noted that for these simulations, salinity loads from tributaries reflect the loads observed for the year and do not consider potential increases in

the future. Model sensitivity to point source salinity loads is discussed in Section 6 and Appendix K.

G.2.1 Salt Front Analysis

The proportion of "dry" years among the 10 simulated years is relatively high compared to that of the entire period of record, which may lead to a distorted probability distribution of the salt front (**Figure C-1**). As only 10 years were simulated, for any given day of a year there are only 10 model data points available, which are insufficient for determining the exceedance probability or the likelihood of the salt front location for future conditions. Salt front frequency or probability should be interpreted from model results with caution.

In **Table G.4**, the normal range represents the difference between the 25 to 75 percentiles of the probability distribution of the 7 day-average SF location for the 10 years simulated. The simulated 7-day-averaged salt front is presented in **Figure G.6**. For the predicted salinity intrusion with wet-year hydrology (using inflows from 2018 and 2011) the maximum SF location is below RM 92.5 under all SLR scenarios. Reduced inflows during a dry-year result in a simulated SF location farther upstream. For example, under 1.6 m SLR and with 2002 and 2016 inflows, the predicted maximum 7-day-average SF location advances to RM 101.4 and RM 99.8, respectively. The simulated maximum SF location under all scenarios is below RM 102, excepting the simulation with 1965 flow conditions without TFO and with 1.6 m SLR, in which the SF reaches RM 109. With TFO included, the maximum SF location was roughly 4 miles farther downstream (to RM 104.7 from RM108.9). The effectiveness of TFO is discussed in more detail in Section 7.1. In general, as SLR rises, simulated salinity intrusion increases, and as the inflow increases, the salinity intrusion decreases. An overview of salinity intrusion with all inflow conditions is summarized in **Figure G.7**, in terms of predicted 7-day-averaged SF location.

Simulated seasonal variation of salinity intrusion for all SLR scenarios is presented in Figure G.8. With SLR, the salinity intrusion increases while maintaining the seasonal pattern, in which the critical months are September through December. For example, in October, the normal range went farther upstream from a baseline range of (RM 72.4 to RM 83.8) to a range of (RM 76.5 to RM 89.5) with 1 m SLR and to a range of (RM 79.1 to 93.6) with 1.6 m SLR. Monthly statistics of simulated salt front locations are presented in **Table G.5**.

The percentage of time that the simulated SF location exceeds RM 92.5 was calculated based on an ensemble of 10-year simulation results. The number of days that the simulated SF location is above this location were counted and the percentage of time of this exceedance (as a fraction of the total number of days simulated) was calculated. These results are summarized by various inflow conditions and presented in **Figure G.9** and **Table G.6**. The simulated 7-dma SF location passes above the Schuylkill River confluence at RM 92.5 over 7 and 11 percent of the time with 1m and 1.6 m SLR, respectively, over the 10-year simulation period.

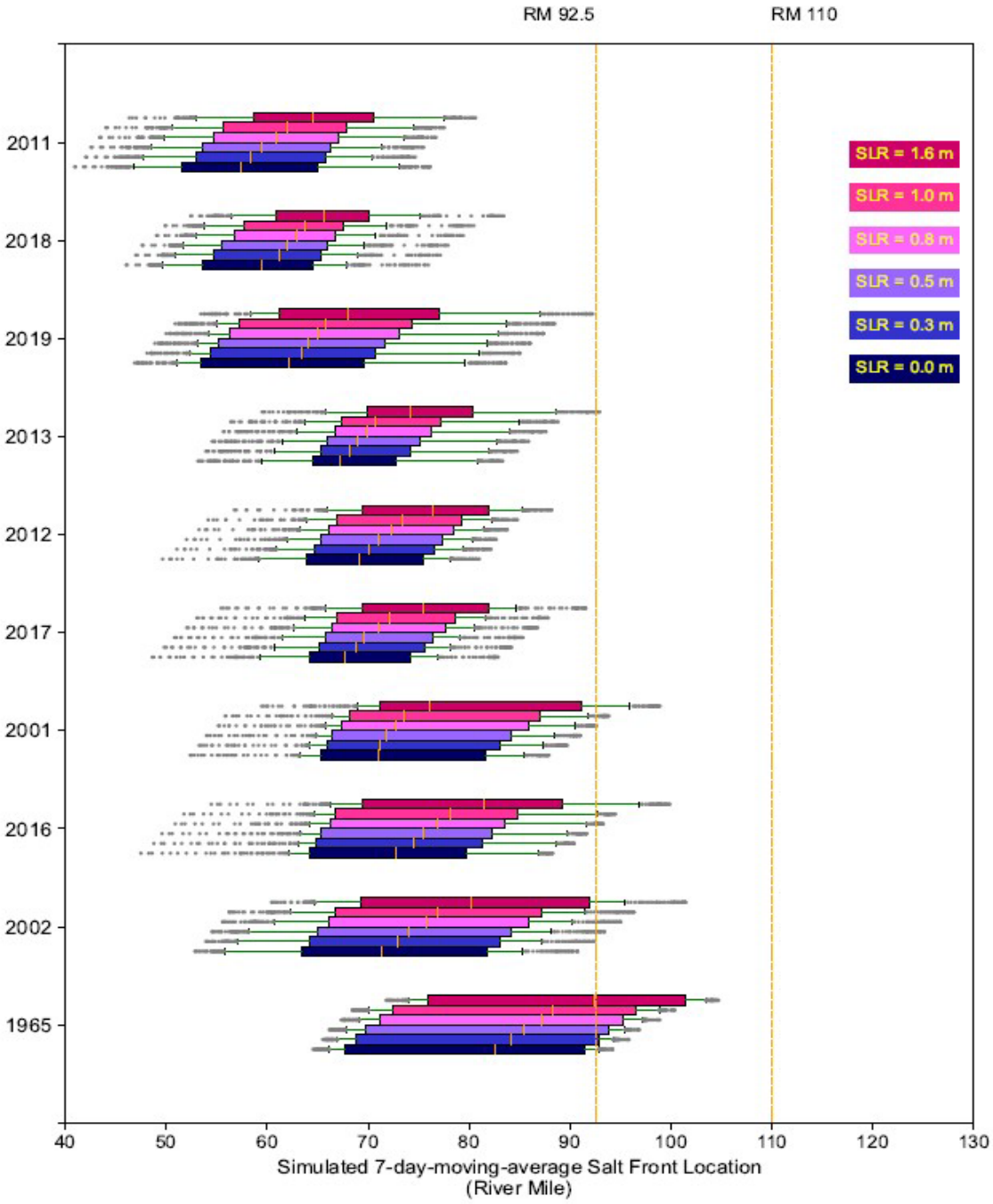

Note: Middle orange line = median; Edge = 25, 75 percentiles; Whiskers = the 10 and 90 percentile, and the farthest dots represent the min and max locations (range). Historical flow was used for all simulated years, except 1965 in which a minimum flow of 2500 cfs was specified for the Delaware River at Trenton to reflect the Trenton Flow Objective, a requirement under the current drought management program.

Figure G.6. Annual statistics of the simulated salt front location with SLR for ten representative years.

Table G. 4. Normal range, median, and maximum location of the predicted salt front with SLR for ten representative years.

Inflow Condition	years	SF Location Statistic	0 m SLR	0.3 m SLR	0.5 m SLR	0.8 m SLR	1 m SLR	1.6 m SLR
Wet	2019	Maximum	83.62	85.03	86.03	87.35	88.43	92.21
	2019	Median	62.07	63.38	64.07	65.01	65.72	68.00
	2019	Normal Range	53.4 - 69.59	54.4 - 70.77	55.11 - 71.65	56.3 - 73.14	57.29 - 74.3	61.14 - 77.04
	2018	Maximum	75.95	77.14	77.91	79.40	80.46	83.42
	2018	Median	59.49	61.12	61.97	62.91	63.65	65.69
	2018	Normal Range	53.66 - 64.52	54.76 - 65.39	55.45 - 65.95	56.68 - 66.79	57.7 - 67.52	60.83 - 70.14
	2011	Maximum	76.14	74.65	75.49	76.71	77.53	80.63
	2011	Median	57.34	58.31	59.41	60.90	62.01	64.54
	2011	Normal Range	51.56 - 64.92	52.89 - 65.84	53.57 - 66.2	54.71 - 67.05	55.58 - 67.83	58.72 - 70.54
Normal	2017	Maximum	82.86	84.17	85.33	86.77	87.79	91.52
	2017	Median	67.63	68.81	69.61	70.95	72.11	75.38
	2017	Normal Range	64.25 - 74.12	65.16 - 75.58	65.72 - 76.44	66.42 - 77.73	66.95 - 78.68	69.42 - 81.94
	2013	Maximum	83.31	84.76	85.87	87.59	88.77	92.89
	2013	Median	67.16	68.24	68.93	69.85	70.71	74.17
	2013	Normal Range	64.53 - 72.73	65.32 - 74.15	65.98 - 75.11	66.74 - 76.31	67.4 - 77.25	69.88 - 80.39
	2012	Maximum	81.00	82.13	82.67	83.76	84.76	88.17
	2012	Median	69.04	70.08	71.03	72.36	73.42	76.34
	2012	Normal Range	63.92 - 75.52	64.73 - 76.6	65.29 - 77.28	66.14 - 78.4	66.82 - 79.28	69.48 - 81.98
Dry	2001	Maximum	87.89	89.72	91.03	92.60	93.81	98.89
	2001	Median	70.96	71.10	71.82	72.79	73.60	76.10
	2001	Normal Range	65.28 - 81.67	65.92 - 83.07	66.47 - 84.1	67.43 - 85.86	68.16 - 87.06	71.16 - 91.12
	2016	Maximum	88.25	90.40	91.64	93.28	94.46	99.84
	2016	Median	72.69	74.56	75.47	76.93	78.09	81.44
	2016	Normal Range	64.27 - 79.8	64.83 - 81.3	65.35 - 82.24	66.21 - 83.59	66.8 - 84.73	69.37 - 89.18
	2002	Maximum	90.74	92.37	93.39	95.01	96.31	101.42
	2002	Median	71.37	72.88	74.04	75.81	76.92	80.17
	2002	Normal Range	63.4 - 81.72	64.23 - 83.08	64.95 - 84.1	66.06 - 85.94	66.79 - 87.19	69.34 - 91.93
	1965 (w/o FO)	Maximum	97.53	99.87	101.09	103.07	104.52	108.98
	1965 (w/o FO)	Median	83.99	85.76	86.96	88.83	90.06	93.97

Inflow Condition	years	SF Location Statistic	0 m SLR	0.3 m SLR	0.5 m SLR	0.8 m SLR	1 m SLR	1.6 m SLR
	1965 (w/o FO)	Normal Range	67.97 - 93.2	69.04 - 94.7	69.91 - 95.69	71.4 - 97.61	72.57 - 99.17	75.98 - 103.93
Min Q 2500 cfs	1965 (with FO)	Maximum	94.21	95.82	96.83	98.86	100.36	104.68
	1965 (with FO)	Median	82.52	84.16	85.41	87.14	88.21	92.36
	1965 (with FO)	Normal Range	67.74 - 91.49	68.87 - 92.85	69.8 - 93.81	71.16 - 95.31	72.49 - 96.56	75.92 - 101.43

Note: Normal range = 25 - 75 percentile range. Also, for comparison, results for the simulation with historical flow from 1965 without TFO are also included in this table (shown in gray-shaded rows).

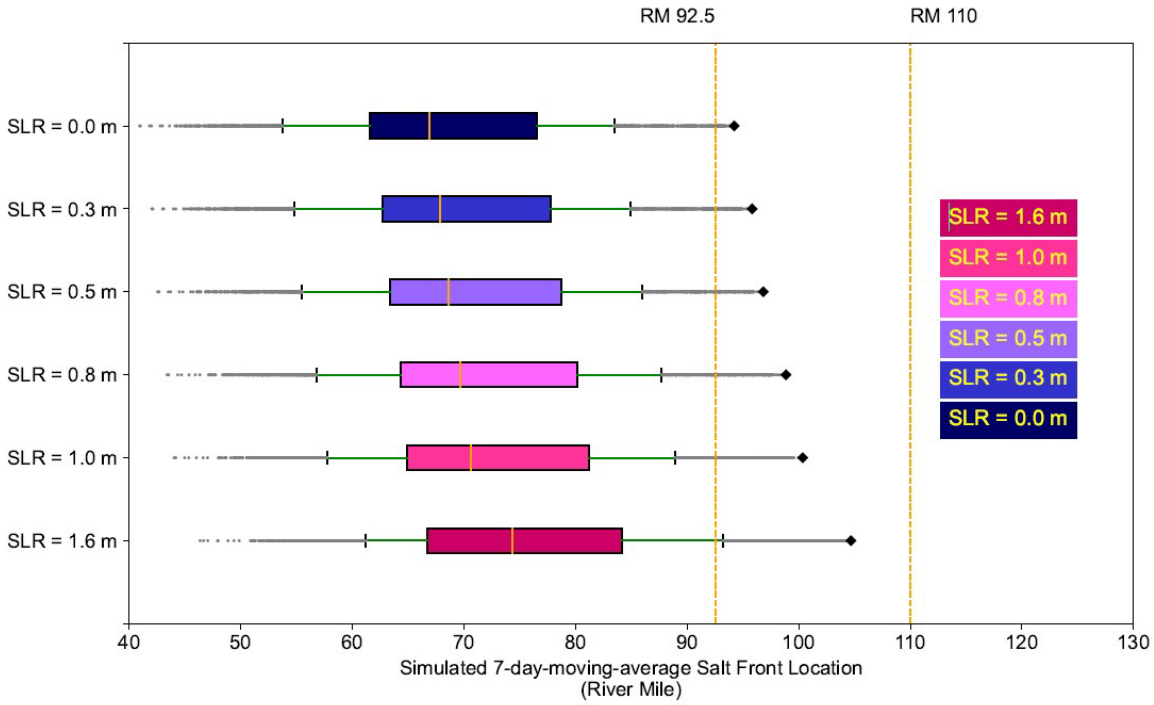

Note: Middle orange line = median; Edge = 25, 75 percentiles; Whiskers = the 10 and 90 percentile, and the farthest dots (diamond shape) represent the min and max locations (range). Historical flow was used for all simulated years, except 1965, in which a minimum flow of 2500 cfs was specified for the Delaware River at Trenton to reflect the Trenton Flow Objective a requirement under the current drought management program.

Figure G.7. Simulated salt front location with SLR for ten representative years.

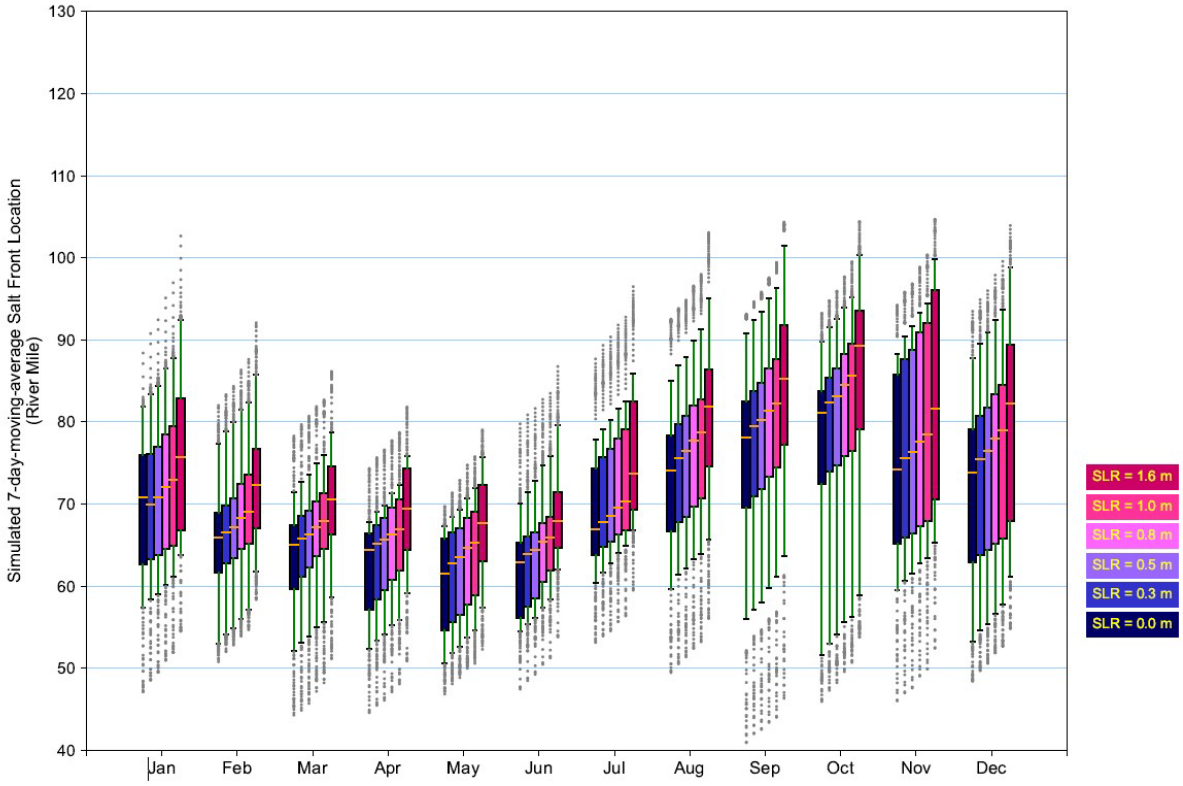

Notes: Model: 3M3D. Hydrological and meteorological conditions were based on these 10 years: 1965, 2001-2002, 2011-2013, 2016, 2017-2019. Historical flow was used for all simulated years, except 1965 in which a minimum flow of 2500 cfs was specified for the Delaware River at Trenton to reflect the Trenton Flow Objective, a requirement under the current drought management program.
Middle orange line = median; Edge = 25, 75 percentiles; Whiskers = the 10 and 90 percentiles

Figure G.8. Monthly statistics for the 7-day-moving-average salt front location of the 10-year ensemble simulations.

Table G.5. Monthly statistics of the simulated 7-dma salt front River Mile based on 10-year ensemble simulations. The Trenton Flow Objective was applied in the simulation of 1965 conditions.

parameter	month	SLR (m)					
		0	0.3	0.5	0.8	1	1.6
maximum	1	88.4	90.8	92.4	95.1	97.0	102.7
maximum	2	82.0	83.3	84.3	86.3	87.6	92.1
maximum	3	78.3	79.7	80.7	81.9	82.7	86.2
maximum	4	74.3	75.7	76.6	77.7	78.7	81.8
maximum	5	69.7	71.4	72.9	74.7	75.8	79.0
maximum	6	79.8	80.9	81.6	82.7	83.5	86.8
maximum	7	87.7	89.3	90.4	91.8	92.8	96.5
maximum	8	92.5	93.8	94.8	96.6	98.0	103.1
maximum	9	93.2	94.6	95.8	97.6	99.4	104.4
maximum	10	93.2	94.8	95.9	97.7	99.5	104.4
maximum	11	94.2	95.8	96.8	98.9	100.4	104.7
maximum	12	93.5	94.9	96.0	97.9	99.6	103.9
median	1	70.9	69.9	70.9	72.1	72.9	75.7
median	2	65.9	66.6	67.2	68.3	69.1	72.4
median	3	65.1	65.8	66.3	67.2	67.9	70.6
median	4	64.4	65.2	65.7	66.3	66.9	69.5
median	5	61.6	62.8	63.6	64.6	65.3	67.7
median	6	62.9	63.9	64.5	65.4	65.9	67.9
median	7	67.0	67.9	68.6	69.6	70.3	73.7
median	8	74.1	75.6	76.4	77.7	78.8	81.9
median	9	78.2	79.5	80.3	81.4	82.3	85.3
median	10	81.1	82.3	83.2	84.5	85.7	89.3
median	11	74.2	75.6	76.4	77.6	78.5	81.6
median	12	73.9	75.4	76.5	78.0	79.0	82.3
25 - 75 percentile range	1	62.64 - 75.95	63.32 - 76.09	63.76 - 76.92	64.52 - 78.46	64.98 - 79.52	66.79 - 82.83
25 - 75 percentile range	2	61.62 - 68.91	62.74 - 69.85	63.45 - 70.74	64.51 - 72.47	65.2 - 73.59	67.11 - 76.73
25 - 75 percentile range	3	59.7 - 67.42	61.11 - 68.5	62.3 - 69.2	63.71 - 70.36	64.5 - 71.35	66.29 - 74.62
25 - 75 percentile range	4	57.11 - 66.43	58.39 - 67.48	59.5 - 68.28	60.76 - 69.55	61.94 - 70.51	64.45 - 74.38
25 - 75 percentile range	5	54.59 - 65.76	55.63 - 66.5	56.48 - 67.08	57.72 - 68.28	58.9 - 69.08	63.09 - 72.39
25 - 75 percentile range	6	56.17 - 65.27	57.48 - 66.07	58.52 - 66.6	60.56 - 67.64	61.9 - 68.43	64.72 - 71.48
25 - 75 percentile range	7	63.73 - 74.35	64.76 - 75.76	65.45 - 76.66	66.3 - 78.0	66.86 - 79.14	69.34 - 82.49
25 - 75 percentile range	8	66.64 - 78.31	67.78 - 79.69	68.5 - 80.69	69.75 - 81.96	70.72 - 82.76	74.59 - 86.34
25 - 75 percentile range	9	69.54 - 82.49	70.91 - 83.72	71.85 - 84.78	73.39 - 86.53	74.43 - 87.7	77.21 - 91.81

parameter	month	SLR (m)					
		0	0.3	0.5	0.8	1	1.6
25 - 75 percentile range	10	72.41 - 83.77	73.9 - 85.4	74.77 - 86.53	75.82 - 88.26	76.51 - 89.54	79.09 - 93.58
25 - 75 percentile range	11	65.11 - 85.74	65.97 - 87.71	66.44 - 88.82	67.34 - 90.89	67.93 - 92.04	70.53 - 96.02
25 - 75 percentile range	12	62.91 - 79.11	63.74 - 80.77	64.4 - 81.78	65.23 - 83.35	65.81 - 84.53	67.91 - 89.38
10 - 90 percentile range	1	57.4 - 81.93	58.32 - 83.33	59.06 - 84.43	60.12 - 86.52	61.15 - 87.83	63.78 - 92.47
10 - 90 percentile range	2	53.01 - 77.54	54.11 - 78.89	54.83 - 80.0	55.94 - 81.5	57.11 - 82.41	61.78 - 85.77
10 - 90 percentile range	3	52.07 - 71.51	53.01 - 72.74	53.77 - 73.63	55.01 - 75.07	55.6 - 76.06	58.64 - 78.75
10 - 90 percentile range	4	52.36 - 67.85	53.31 - 69.05	54.09 - 69.87	55.24 - 71.32	55.92 - 72.36	59.18 - 75.85
10 - 90 percentile range	5	50.53 - 67.28	51.88 - 68.42	52.58 - 69.29	53.8 - 70.67	54.58 - 71.97	57.42 - 75.77
10 - 90 percentile range	6	54.47 - 70.09	55.42 - 71.5	56.07 - 72.82	57.41 - 74.77	58.37 - 75.81	62.06 - 79.59
10 - 90 percentile range	7	60.33 - 78.1	61.59 - 79.3	62.71 - 80.45	64.05 - 81.76	64.88 - 82.71	66.83 - 86.04
10 - 90 percentile range	8	59.67 - 85.4	61.32 - 87.19	62.16 - 88.23	63.23 - 90.12	63.82 - 91.45	65.67 - 95.28
10 - 90 percentile range	9	55.66 - 90.92	56.82 - 92.53	57.66 - 93.55	59.34 - 95.18	60.69 - 96.5	63.41 - 101.6
10 - 90 percentile range	10	51.54 - 89.83	53.02 - 91.55	54.04 - 92.54	55.52 - 93.89	56.17 - 95.16	58.82 - 100.39
10 - 90 percentile range	11	59.55 - 88.47	60.58 - 90.56	61.46 - 91.76	62.66 - 93.36	63.32 - 94.55	65.23 - 99.88
10 - 90 percentile range	12	53.2 - 87.73	54.51 - 89.65	55.23 - 90.94	56.58 - 92.6	57.66 - 93.81	60.98 - 98.81

Note: historical flow was used for all simulated years, except 1965 in which a minimum flow of 2500 cfs was specified for the Delaware River at Trenton to reflect the Trenton Flow Objective, a requirement under the current drought management program.

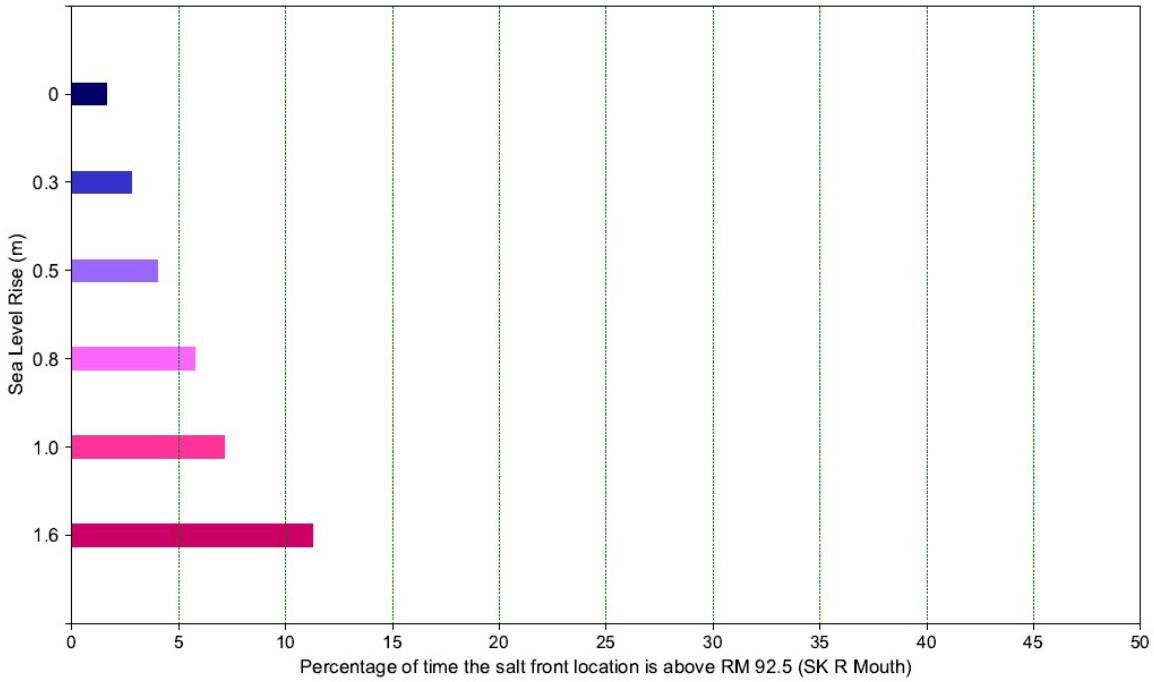

Notes: Model: 3M3D. Hydrological and meteorological conditions were based on these 10 years: 1965, 2001-2002, 2011-2013, 2016, 2017-2019. Historical flow was used for all simulated years, except 1965, in which a minimum flow of 2500 cfs was specified for the Delaware River at Trenton to reflect the Trenton Flow Objective, a requirement under the current drought management program.

Figure G.9. Percentage of time the simulated salt front is upstream from RM 92.5, based on results of the 10-year ensemble simulations of six SLR scenarios.

Table G. 6. The percentage of time during the 10 simulated years that the salt front location is above RM 92.5.

0 m SLR	0.3 m SLR	0.5 m SLR	0.8 m SLR	1 m SLR	1.6 m SLR
1.6	2.8	4.0	5.8	7.1	11.3

Notes: Model: SM3D. Hydrological and meteorological conditions were based on these 10 years: 1965, 2001-2002, 2011-2013, 2016, 2017-2019. Historical flow was used for all simulated years, except 1965, in which a minimum flow of 2500 cfs was specified for the Delaware River at Trenton to reflect the Trenton Flow Objective, a requirement under the current drought management program.

G.2.2 Chloride Analysis

Another standard is a 15-dma chloride concentration of 50 mg/L for water quality Zone 2 (RM 108.4 to RM 133.37), which encompasses the location of major water-supply intakes. Additional model analyses show that at or above SLR of 1 m or more, with the implementation of the flow objective at Trenton, this standard is exceeded up to 4 percent of the time during the 10 simulated years (See **Figure G. 10** and **Tables G. 7**. And **G .8**.)

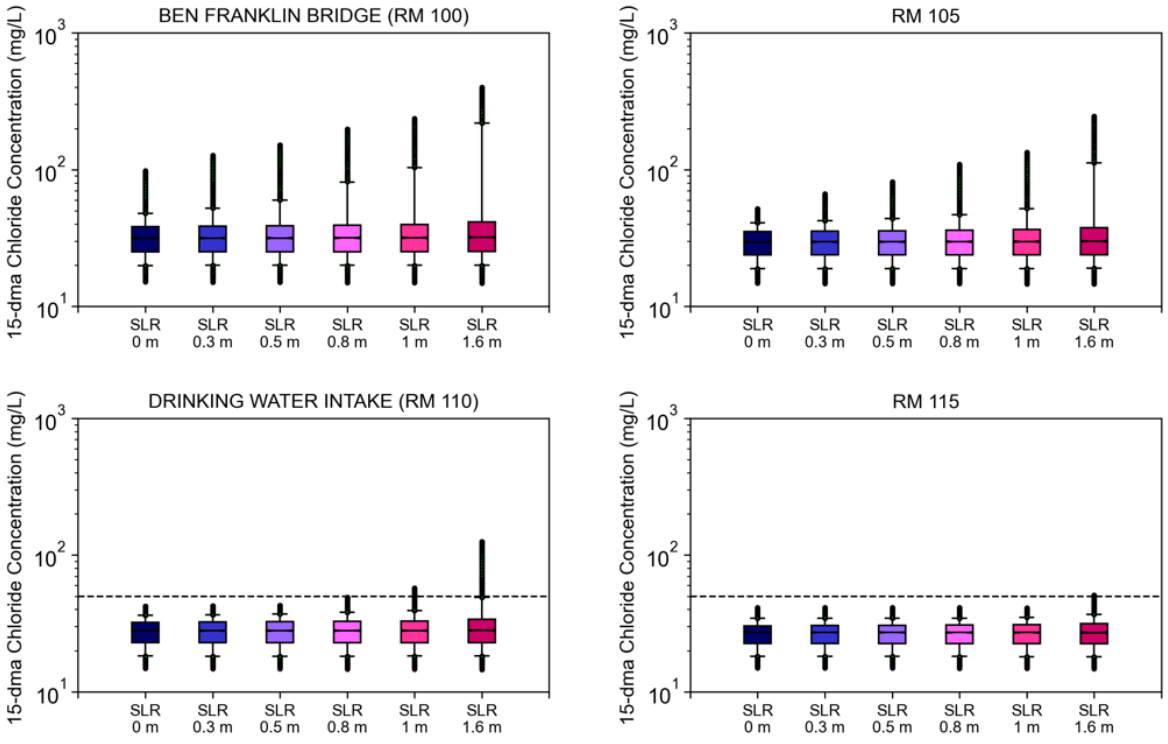

Notes: Model: 3M3D. Hydrological and meteorological conditions were based on these 10 years: 1965, 2001-2002, 2011-2013, 2016, 2017-2019. Historical flow was used for all simulated years, except 1965, in which a minimum flow of 2500 cfs was specified for the Delaware River at Trenton to reflect the Trenton Flow Objective, a requirement under the current drought management program.

Figure G.10. Simulated 15-dma chloride concentration at selected locations during the 10 simulated years.

Table G. 7. Simulated maximum 15-day moving average chloride concentration at River Mile 110 and the percentage of time the simulated concentration exceeds the 15-day moving average of 50 mg/l.

Sea Level Rise	15-dma chloride concentration at RM 110 (Drinking water intake)	Total number of days the 15-dma chloride concentration exceeds 50 mg/l	Percent of time the 15-dma chloride concentration exceeds 50 mg/l
(meters)	(mg/l)	(days)	
0	37	0	0
0.3	40	0	0
0.5	43	0	0
0.8	49	0	0
1	57	39*	1.1% *
1.6	125	155	4.2%

Results are based on 10-year ensemble simulations and a minimum flow of 2500 cfs was applied at Trenton on the Delaware River during the 1965 period.
Total number of days simulated = 3652.
* Exceedances only occurred in the 1965 simulation with the flow objective.
For 1 m SLR, exceedances occur during 1965 simulation. For 1.6 m SLR, exceedances occur during three years (1965, 2002, 2016) of the years simulated.

Table G. 8. Simulated number of days the 15-day moving average chloride concentration exceeds the 15-day moving average of 50 mg/l water quality standard at RM 110. Total number of days is 3652.

	SLR 0 m	SLR 0.3 m	SLR 0.5 m	SLR 0.8 m	SLR 1.0 m	SLR 1.6 m
2001	0	0	0	0	0	0
2002	0	0	0	0	0	**5**
2011	0	0	0	0	0	0
2012	0	0	0	0	0	0
2013	0	0	0	0	0	0
2016	0	0	0	0	0	0
2017	0	0	0	0	0	0
2018	0	0	0	0	0	0
2019	0	0	0	0	0	0
1965	0	38	48	78	102	155
1965 (with FO)	0	0	0	0	39	142
Percentage of time the 15dma Chloride concentration exceeds WQ standard of 50 mg/L.						
10-yr ensemble (without FO)	0.0%	1.0%	1.3%	2.1%	2.8%	4.4%
10-yr ensemble (with FO)	0.0%	0.0%	0.0%	0.0%	1.1%	4.0%

APPENDIX H. SEA LEVEL RISE IMPACT ON SALT FLUXES

As sea level rises, the depth of the flank areas gets deeper. The purpose of this appendix is to answer this question: to what extent do the temporal and spatial distributions of the salt flux components (due to river flow, estuary exchange flow, and tides) change with an increase in sea-level? The goal is to quantify the response to SLR using salt flux decomposition techniques following Geyer et al. (2020) and Lerczak et al. (2006) to understand in greater detail why the increase in sea-level changes the salt intrusion length.

H.1. Salt Flux Decomposition

Estuaries can be classified as salt wedge, strongly stratified, weakly stratified or vertically mixed according to water column stratification or salinity vertical structure. The Delaware Estuary is classified as weakly stratified or partially mixed, considering the competition between a relatively weak buoyancy forcing from upland river discharge and mixing induced by tide and wind. Mixing from tidal forcing (including both astronomical and subtidal fluctuation) is proportional to the volume of oceanic water entering the estuary during every tidal cycle. This volume is also known as the tidal prism. Under future SLR conditions, the potential expansion of the tidal prism results in stronger tidal forcing compared to the river discharge. However, a strong stratification may still occur following a large flood event due to the large volume of freshwater added to the Estuary. A subtle change in the balance of the two major competing forcings may affect the underlying mechanism for salinity intrusion in the estuary.

The mechanisms that control estuary salinity transport through interplay of multiple processes, including stratification and vertical mixing demonstrated by estuarine dynamics, has been the focus of research in the Delaware Estuary for many years (Lerczak, et al. (2006); Aristizábal and Chant (2013, 2015); Geyer et al. (2020); and Pareja-Roman . et al. (2020)). According to these studies, stratification in the system is weakened (or strengthened) with changes in tide and wind-induced vertical mixing (or the freshwater buoyancy forcing). As a result, along-channel vertical salinity and density gradients are established. The structure of a subtidal estuarine exchange flow is relatively stable and varies, driven by the mixing strength during the spring-neap cycle. A short-term tidal variability in the background is also observed in the stratification. In this section, a diagnostic analysis method utilized by Aristizábal and Chant (2015), also known as salt flux decomposition, was used to gain insight to the transport mechanism that may be impacted by SLR. The total area-averaged and tidal-averaged salt flux was decomposed into three different contributions:

- the advective salt flux that represents the flux caused by river input and meteorological-induced flows;
- the steady shear dispersion that is the salt flux driven by estuarine exchange flow;

- the tidal oscillatory salt flux that is induced by tidal currents.

According to Aristizábal and Chant (2015), the advective salt flux is the dominant component of salinity transport because it is influenced by flow and driven by changes in sea surface height associated with wind-driven setup and set down. The steady shear dispersion was always positive and presented a spring/neap variability that was consistent with a two-layer exchange flow. The tidal oscillatory salt flux fluctuated between positive and negative values, and its magnitude may increase around a strong neap tide and decrease on the following spring tide. Their conclusions were based on the analysis of a period of a relatively steady river discharge. Details of the salt flux decomposition method are described below.

The instantaneous total salt flux at a cross section was calculated as:

$$FFs(\mathrm{t}) = \sum_{ij=0}^{n} \sum_{k=KB}^{KC} \left(V_{ij,k}(t) S_{ij,k}(t) A_{ij,k}(t)\right) \tag{7-1}$$

where Vij,k, Sij,k, and Aij,k are the along-channel velocity, salinity, and area of each 3-D model grid cell i,j in the horizontal plane and at vertical layer k (KB is the bottom layer and KC is the surface layer). The total net tidally-averaged salt flux was obtained as:

$$Fs(t) = \langle FFs(t) \rangle \tag{7-2}$$

where the brackets ⟨ ⟩ represent a low-pass filter to remove tidal oscillations. A Lanczos low-pass filter with a cutoff period of 32 and 70 hour half-window was used, as in Aristizábal and Chant (2015). Following Lerczak et al. (2006), the velocity and salinity field were decomposed as follows:

$$V_{ij,k}(t) = V_0(t) + V_{e,ij,k}(t) + V_{t,ij,k}(t) \tag{7-3}$$

$$V_0(t) = \frac{\left\langle \sum_{ij=0}^{n} \sum_{k=KB}^{KC} \left(V_{ij,k}(t) A_{ij,k}(t)\right) \right\rangle}{\left\langle \sum_{ij=0}^{n} \sum_{k=KB}^{KC} \left(A_{ij,k}(t)\right) \right\rangle} = \frac{\langle Q \rangle}{\langle A \rangle} = \frac{Q_0}{A_0} \tag{7-4}$$

$$V_{e,ij,k}(t) = \frac{\langle V_{ij,k}(t) A_{ij,k}(t) \rangle}{\langle A_{ij,k}(t) \rangle} - V_0(t) \tag{7-5}$$

$$V_{t,ij,k}(t) = V_{ij,k}(t) - V_{e,ij,k}(t) - V_0(t) \tag{7-6}$$

where Q and Q0 in equation (7-4) are the instantaneous and tidal-averaged volume flux, and A and A0 are the instantaneous and tidal-averaged total cross-sectional areas, respectively. V0 is an area-averaged, tidal-averaged velocity, and is associated with the river discharge, but includes other contributions, such as meteorological forced flows. Ve is a space-

dependent, tidal-averaged flow and corresponds to the exchange flow, and Vt is a space-dependent and tidally dependent contribution and represents the tidal flows.

There is a corresponding set of equations for salinity by replacing V with S for equation (7-3) through (7-6).

The net total salt flux can be calculated using equation (7-2) and can also be estimated as the sum of three components with simplification (Aristizábal and Chant, 2015):

$$F_s(t) = F_0(t) + F_e(t) + F_t(t) + \ Others \ \approx \ Q_0 S_0 + F_e(t) + F_t(t) \tag{7-7}$$

$$F_e(t) \ = \sum_{ij=0}^{n} \sum_{k=KB}^{KC} \left(V_{e,ij,k}(t) S_{e,ij,k}(t) \langle A_{ij,k}(t) \rangle \right) \tag{7-8}$$

$$F_t(t) \ = \sum_{ij=0}^{n} \sum_{k=KB}^{KC} \left(\langle V_{t,ij,k}(t) S_{t,ij,k}(t) A_{ij,k}(t) \rangle \right) \tag{7-9}$$

From equation (7-2), and ignoring the unaccounted processes, the tidal oscillatory salt flux $F_t(t)$ can be expressed as:

$$F_t(t) \ = \ \langle FFs(t) \rangle \ - \ F_0(t) \ - \ F_e(t) \tag{7-10}$$

Under this decomposition, F0 is the advective salt flux and represents the flux due to river discharge or meteorological-induced flows. Fe is called the steady shear dispersion and is the salt flux driven by the estuarine exchange flow. Ft is known as tidal oscillatory salt flux and is driven by the tidal flows. Aristizábal and Chant (2015) suggest that the tidal oscillatory salt flux can be expressed as a Fickian diffusion process: $F_t = K_t \frac{\partial S}{\partial y}$, where Kt is the along channel dispersion coefficient and $\frac{\partial S}{\partial y}$ is the along-channel salinity gradient.

H.2. Results

Simulations under SLR conditions with 2002 hydrological conditions were the primary diagnostic scenarios discussed in Section 4 of the report. The same simulations were used for the salt flux decomposition analysis for the baseline case (0 m SLR) and compared with the 1.0 m SLR case. The analysis focused on a two-month period from August to September 2002, when the flow from Trenton was relatively low and steady, ranging from 2950 to 3760 cfs in August and from 2600 to 6580 cfs (or 73.6 to 186.3 m^3/s) in September. The mean flows at Trenton and the Schuylkill River at Philadelphia, PA over the two-month period were 3441 cfs (or 97.4 m^3/s) and 484 cfs (or 13.7 m^3/s), respectively. The observed flow at Trenton and water surface elevation (WSE) at Lewes, DE are presented in **Figure H-1**. The observed sea level at Lewes from September through October included three complete spring/neap cycles: the first cycle is from August 10 to 24, the second cycle is from August 24 to September 8, and the third cycle is from September 8 to 23. The first and the third cycles presented a more

pronounced fortnight modulation, while the second cycle included an ocean setup during the neap tide. The historical WSE was adjusted for baseline and 1 m SLR simulations by considering the SLR rate of 3.53 mm/year at NOAA station at Lewes[28], DE, and is referenced to the year 2000 mean sea level.

Salt fluxes were calculated at a cross-section at RM 32 (**Figure H-2**), which involved a total of 14 grid cells with an average lateral length of 1122 meters. The water depth in the navigation channel is 15 meters, with eight active vertical layers, and the mean depth of the flank areas is 5 meters on the west and east sides of the channel. The number of active vertical layers varies from 3 to 6 for the shallow flanks. Simulated current velocity was projected to along-channel and cross-channel directions at the center of the grid cell and the mid-vertical layer depth along with the salinity being reported by the 3-D model at the same location. In the data analysis by Aristizábal and Chant (2015), the spatial resolution was increased for the salt flux calculation, and an interpolation technique was necessary to obtain salinity and current velocity profiles due to coarse spatial resolution of the data. The velocity profiles were also extrapolated to the surface and to the bottom using a logarithmic profile. Salinity was interpolated to reflect the spatial salinity structure of the site according to their current understanding. However, it was noted that the interpolation of salinity required more fine tuning and may have introduced inaccurate estimates of the salt field. In this effort, the horizontal and vertical spatial resolution of our numerical grid was considered adequate for the calculation of the salt flux at the selected cross section for this analysis. No further effort was made to increase the spatial resolution in calculating the salt flux. With the grid configuration, the vertical side at the selected cross section comprised a total of 67 quadrilateral segments or sub-regions.

Simulated two-month-averaged along-channel subtidal current velocity and subtidal salinity are presented in **Figure H-3** and **H-4** for the 0 meter and 1 meter SLR cases, respectively. Unlike in other figures, in these figures a positive velocity indicates a seaward direction. The black dots represent the 67 segments in which model-simulated current velocity and salinity are extracted for salt flux calculation. These two figures clearly reveal the two-layer, two-directional estuary exchange-flow pattern, as well as the vertical and lateral salinity gradients at this location. Under the sea level rise conditions, the majority of the saltwater is still being transported through the navigational channel; with 1 meter SLR, the salinity level increases and more saline water is spread into the shallow flanks where the water tends to be fresher on the Delaware side in comparison with the water on the New Jersey side.

The 32-hour LPF flow at RM 32.5 is depicted by the volumetric flux of Q_0 and is shown in **Figure H-5**, along with the Trenton flow and the subtidal signals observed in the water surface elevation at Lewes, DE. The mean value of Q_0 over the two-month period is 4803 cfs (or 136 m^3/s), which is 23 percent higher than the combined mean flow of the Trenton and Schuylkill Rivers of 3925 cfs (or 111 m^3/s). Similarly, this was also observed in the 1 meter SLR case

[28] The rate was based on NOAA tide gage data from 1919 to 2019. The rate has been updated to 3.71 mm/year with data through 2023.

(as expected) because the freshwater must find its way out of the bay. It is noticeable that the Q0 did not mirror the pattern of the flow from Trenton, and several peaks in Q0 coincided with the peaks of the subtidal fluctuation in water surface elevation at the entrance of the bay. Thus, both the freshwater from the upland as well as the ocean water surface elevation are the driving force for the Q0.

The simulated time series of the area-integrated, tidal-averaged salt fluxes at the RM 32.5 cross-section during 8-01-2002 to 9-30-2002, with 0 m and 1 m SLR, are shown in **Figure H-6** and **H-7**, respectively. The decomposition analysis shows that the advective salt flux F0 is the dominant component. The steady shear dispersion (Fe) and tidal oscillatory salt flux (Ft) are smaller than F0 by one order of magnitude. The steady shear dispersion (Fe) shows positive values most of the time with a clear spring/neap variability, while tidal oscillatory salt flux (Ft) usually oscillates near zero, and the spring/neap variability is not clear. The steady shear dispersion (Fe) also reflects the pattern shown in the sub-tidal water surface fluctuations at the mouth of the bay, which indicates that the change in sea surface elevation is also the main driving force for the Fe component.

Figure H-8 and **H-9** compare salt fluxes between the baseline and 1 m SLR conditions and the distribution over the two-month period. The absolute value of the overall net salt flux increases as SLR rises by 1 meter, and the magnitude of both the positive and the negative values increase for the 1 meter SLR case in comparison with the base case. The same was observed in the F0 component of the salt flux, because the tidally-averaged and cross-sectionally-averaged salinity was higher under SLR conditions. From the distribution perspective, the highest increase occurred within the tails of the percentile ranges, (higher than the top 15th or lower than the lower 15th percentile values). With increased sea surface elevation, the steady shear dispersion (Fe) also increased and remained positive all the time. Fe, which is driven by and is proportional to the vertical gradient of the salinity $\frac{\partial S}{\partial z}$, also known as the vertical stratification, is enhanced during neap tide and reduced during spring tide. This variability is explained by a two-layers vertically-sheared exchange flow that transports relatively fresh water at the surface oceanward and saltier water at depth landward (Aristizábal Chant, 2015). This salt-flux mechanism is enhanced when the vertical stratification increases during neap tide and is restrained when vertical stratification decreases during spring tide. This is more pronounced in the first and third spring/neap cycles, which occurrs outside the stronger subtidal fluctuation period. With SLR, the largest Fe increase occurs during the top 20 percentile values. Under 1 meter SLR conditions, the top 20 percentile Fe values increase by 18 percent. In contrast to F0 and Fe, the area-integrated tidal oscillatory salt flux (Ft), which can be either an oceanward or a landward salt flux, remains relatively unchanged between the base case and 1 m SLR case for the 20th to 80th percentile values. A clear trend in Ft with the SLR is not observed at this location. Detailed analysis for each segment over the spring/neap cycles may illustrate more subtidal variability. Since Fe and Ft are not the dominant components of the salt flux, further investigation of how SLR may affect the detailed change in the subtidal variability was not pursued as part of this study.

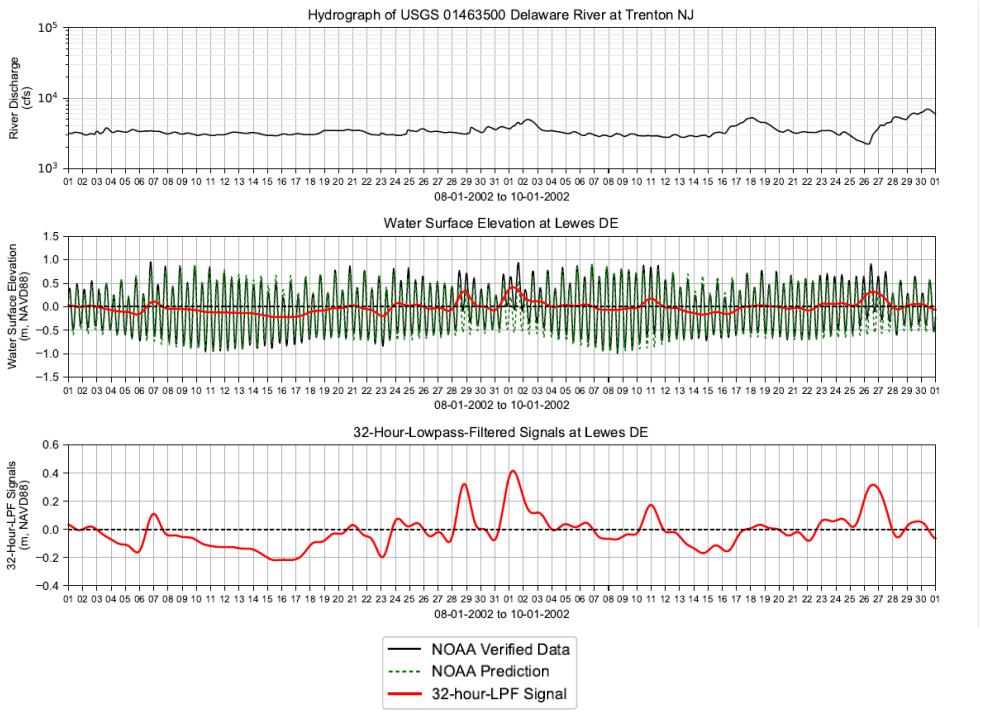

Figure H-1. River flow at Trenton and observed tide at Lewes, DE during 08-01-2002 to 10-01-2002.

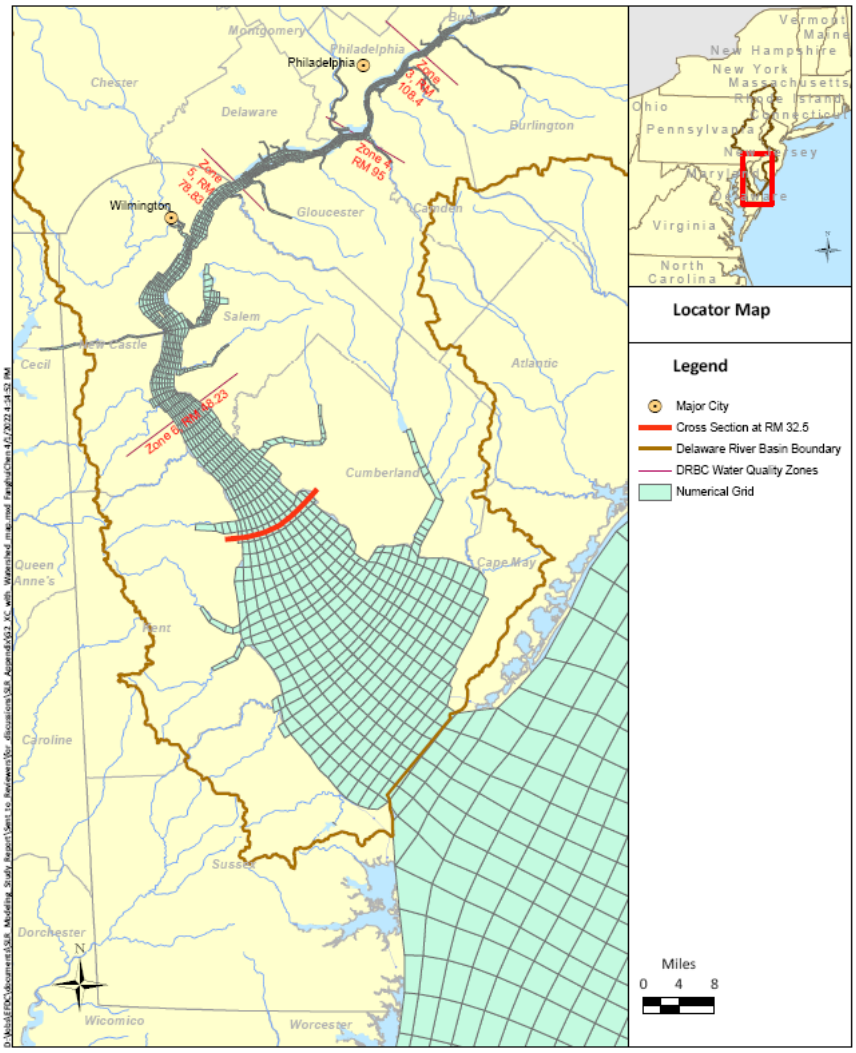

Figure H-2. Selected cross section at RM 32.5 for salt flux analysis.

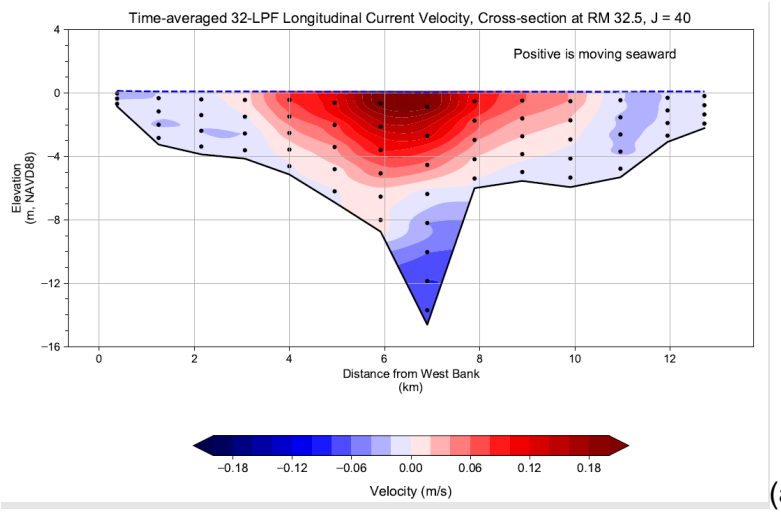

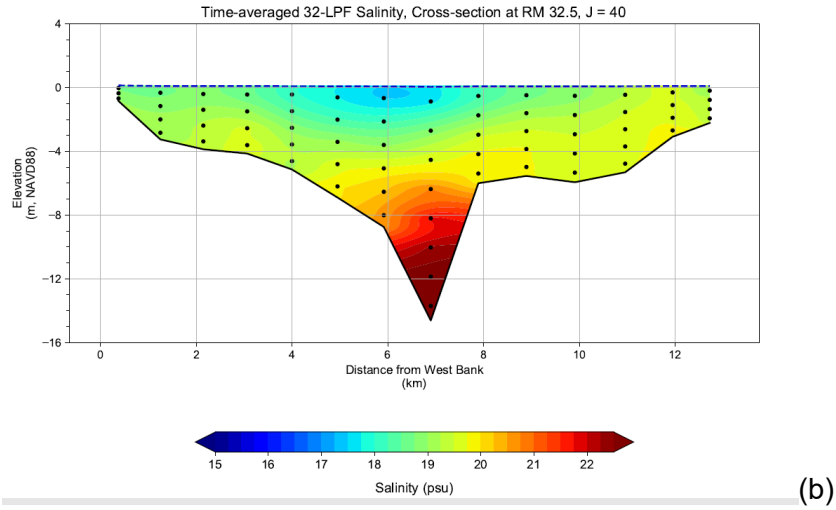

Notes: in this figure, a positive velocity indicates seaward direction. The black dots represent the 67 segments where model simulated current velocity and salinity are extracted for salt flux calculation.

Figure H-3. Simulated 32-LPF along-channel current velocity (a) and salinity (b) at the cross-section at RM 32.5, J = 40 during August and September 2002 under a baseline 0 meter SLR condition.

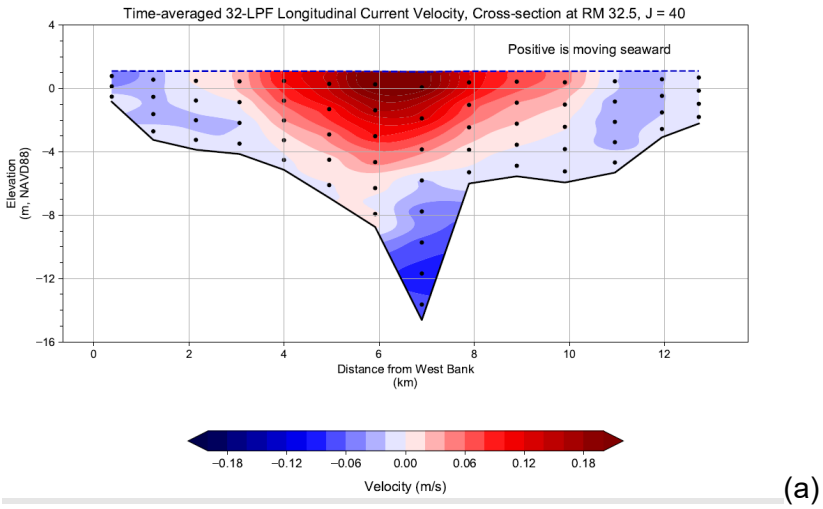

(a)

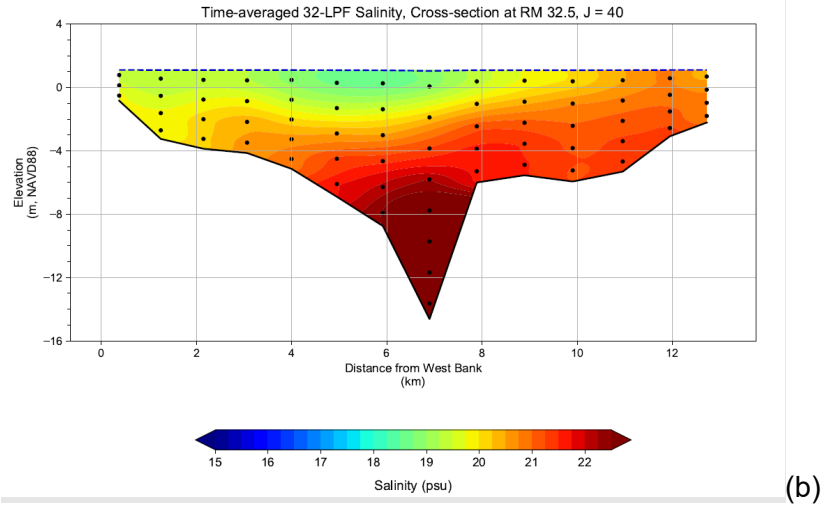

(b)

Notes: in this figure, a positive velocity indicates seaward direction. The black dots represent the 67 segments where model simulated current velocity and salinity are extracted for salt flux calculation.

Figure H-4. Simulated 32-LPF along-channel current velocity (a) and salinity (b) at cross-section at RM 32.5, J = 40 during August and September 2002 under a 1 meter SLR condition.

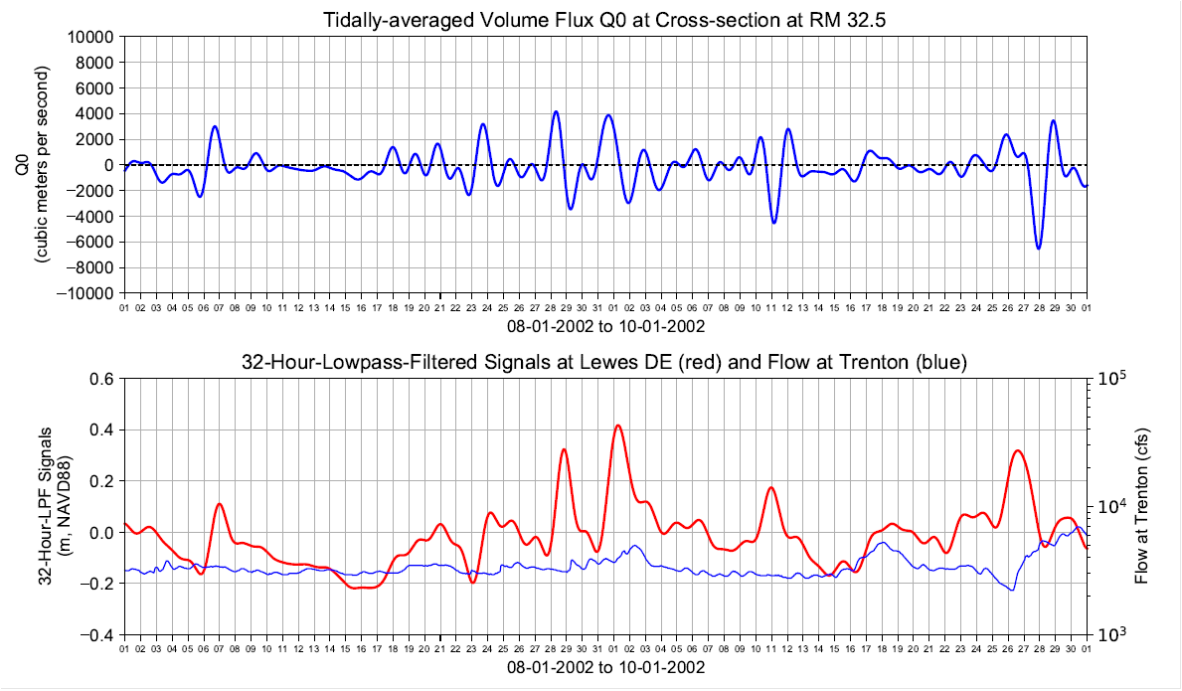

Figure H-5. Simulated time series of tidally-averaged volume flux Q0 at the RM 32.5 cross-section and subtidal fluctuation in water surface elevation at Lewes, DE during 08-01-2002 to 10-01-2002 with 0 meter SLR.

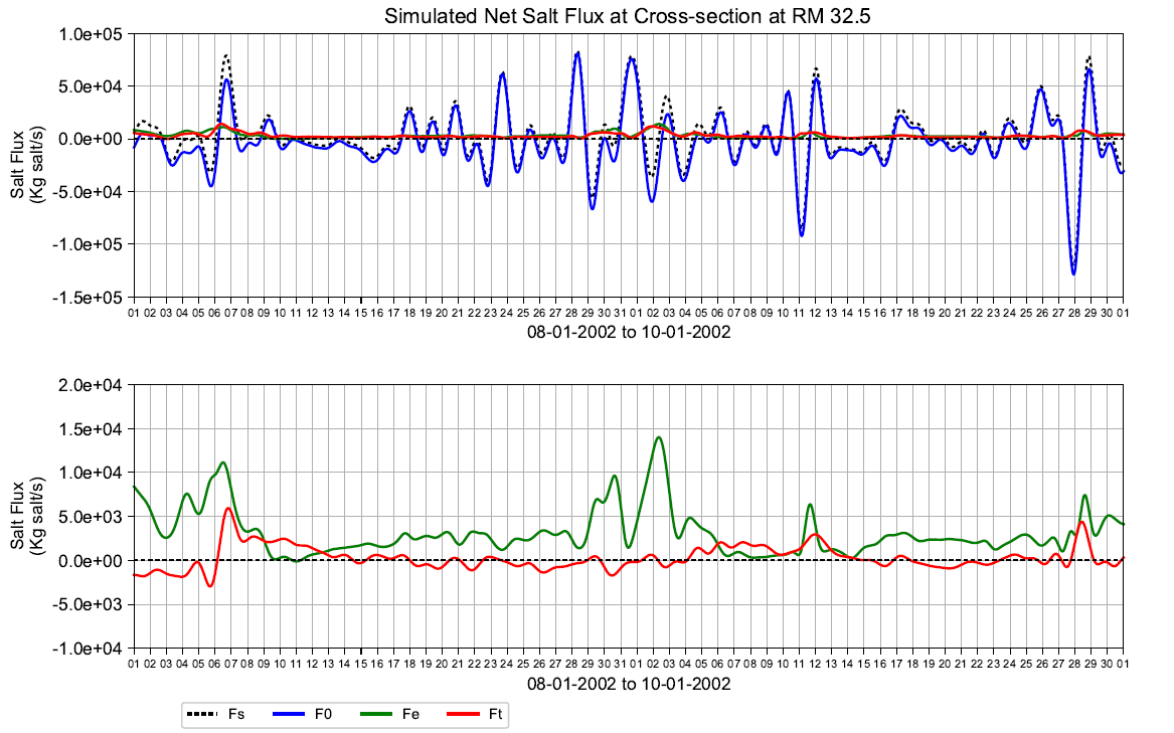

Fs, F0, Fe, and Ft represent the total net salt flux, the advective salt flux, the steady shear dispersion, and the tidal oscillatory salt flux, respectively. Positive values of velocity indicate a landward direction.

Figure H-6. Simulated time series of area-integrated, tidally-averaged salt flux at the RM 32.5 cross-section during 8-01-2002 to 9-30-2002 with 0 m SLR.

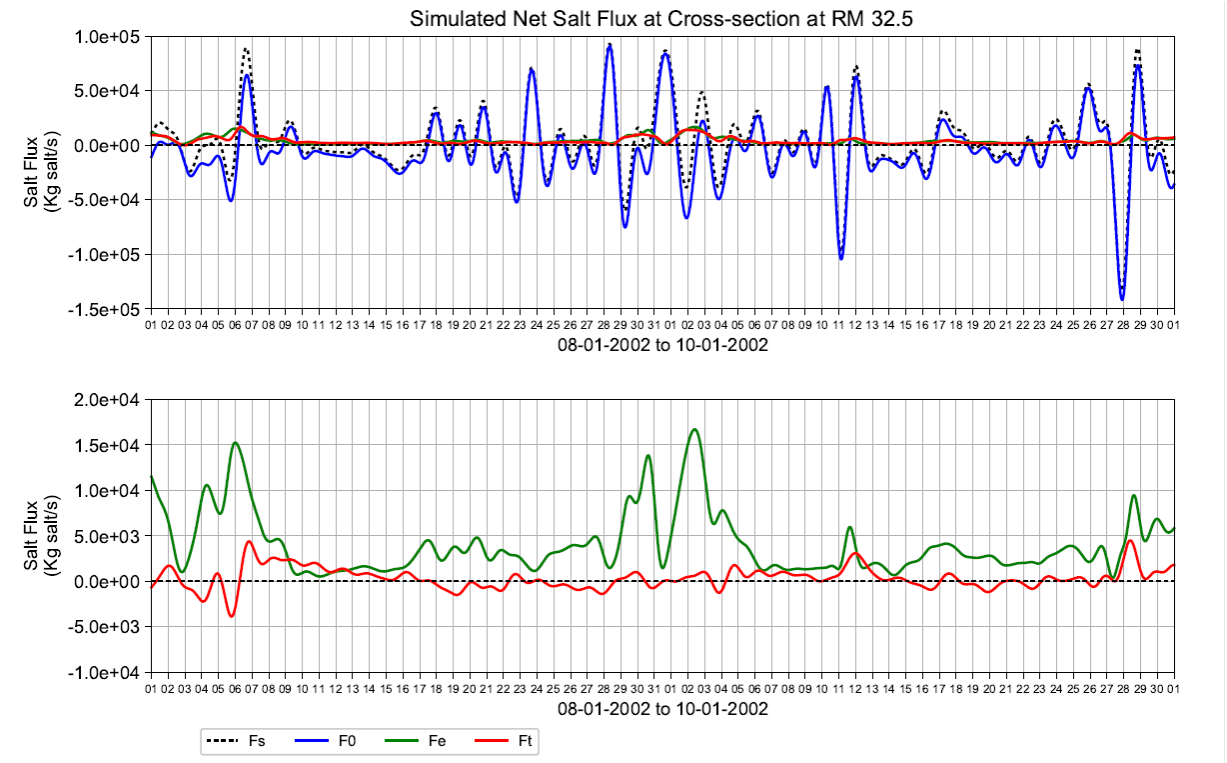

Fs, F0, Fe, and Ft represent the total net salt flux, the advective salt flux, the steady shear dispersion, and the tidal oscillatory salt flux, respectively. Positive values of velocity indicate a landward direction.

Figure H-7. Simulated time series of area-integrated, tidally-average salt flux at the RM 32.5 cross-section during 8-1-2002 to 9-30-2002 with 1 m SLR.

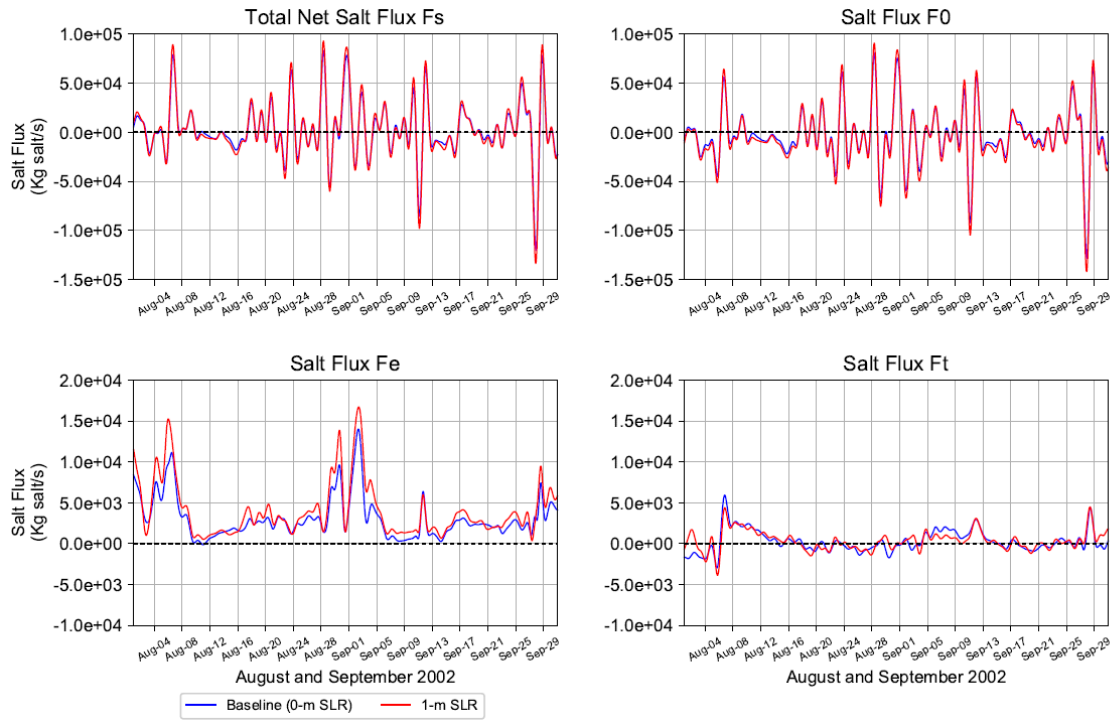

Fs, F0, Fe, and Ft represent the total net salt flux, the advective salt flux, the steady shear dispersion, and the tidal oscillatory salt flux, respectively. Positive values of velocity indicate a landward direction.

Figure H-8. Simulated time series of the area-integrated, tidally-averaged salt flux at the RM 32.5 cross-section during 8-1-2002 to 9-30-2002: comparison of baseline and 1 m SLR cases.

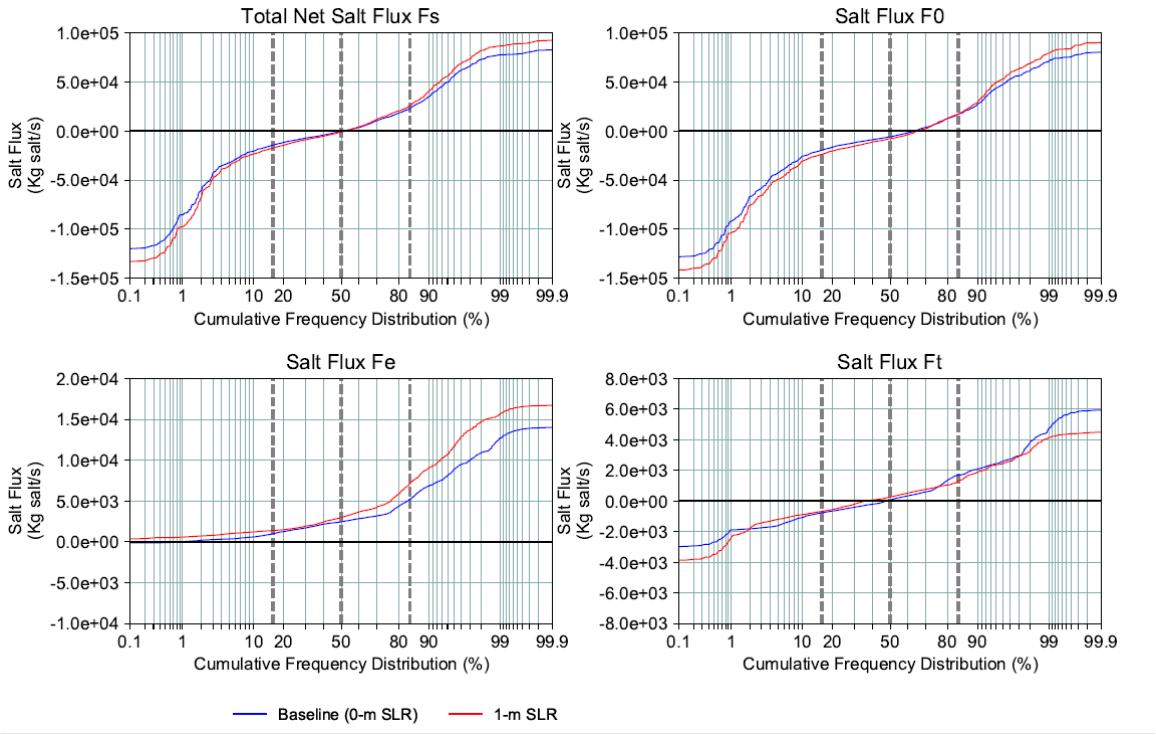

Fs, F0, Fe, and Ft represent the total net salt flux, the advective salt flux, the steady shear dispersion, and the tidal oscillatory salt flux, respectively. Positive values of velocity indicate a landward direction.

Figure H-9. Distribution of the simulated time series of the area-integrated, tidally-averaged salt fluxes at the RM 32.5 Cross-section during 8-1-2002 to 9-30-2002: comparison of baseline and 1 m SLR Cases.

APPENDIX I. VERTICAL STRATIFICATION UNDER SLR

This appendix demonstrates the change in vertical stratification under future SLR conditions in more detail. A straightforward visualization of model-predicted vertical profiles of salinity and current velocity were examined at a location in the middle of the bay at RM 37, near the NOAA Station at Ship John Shoal. First, the tidal signals from the time series of along-channel current velocity and salinity at all vertical layers were filtered using a 32-hour low-pass filter so that the remaining signals are tidally averaged values. Then, the tidally-averaged values were averaged over selected short time periods during a spring tide and neap tide. The selected spring tide period was August 19 to 21, 2012, and the selected neap period was August 10 to 12, 2012 (**Figure I-1**). A relatively steady flow at Trenton of approximately 4000 cfs was specified during these periods.

Simulated mean filtered salinity profiles during 08-10-2012 to 08-12-2012 (Neap Tide) and 08-19-2012 to 08-21-2012 (Spring Tide) Period at RM 37 in the Navigation Channel are shown in **Figure I-2**. Results from three SLR scenarios, base case, 1 meter, and 1.6 meter SLR, are shown. These results demonstrate that sea level rise may cause not only an increase in depth-averaged salinity, but it may also enhance vertical stratification, in which the bottom layer salinity increases more in comparison with the increase in salinity near the surface. The salinity stratification is stronger during the neap tide than the spring tide. Similarly, the mean of the tidally averaged along-channel current velocity profile is shown in **Figure I-3**. A clear, two-layer and two-directional estuary exchange flow pattern can be derived from vertical profiles, with the upper relatively fresh water moving seaward and the saltier water at the lower depth moving landward. With SLR, the turning point (where the flow switches direction) moves upward at this location. The increase in the bottom layer thickness indicates that more volumetric flux of saltwater is moving into the estuary. The two-layer structure is more pronounced during the neap tide period. These results show that the estuary circulation pattern is altered under SLR conditions and results in a stronger vertical stratification, especially in the bay area. The impact of SLR on the change of vertical stratification is discussed more in a qualitative way. Additional research on this topic may become necessary in the future.

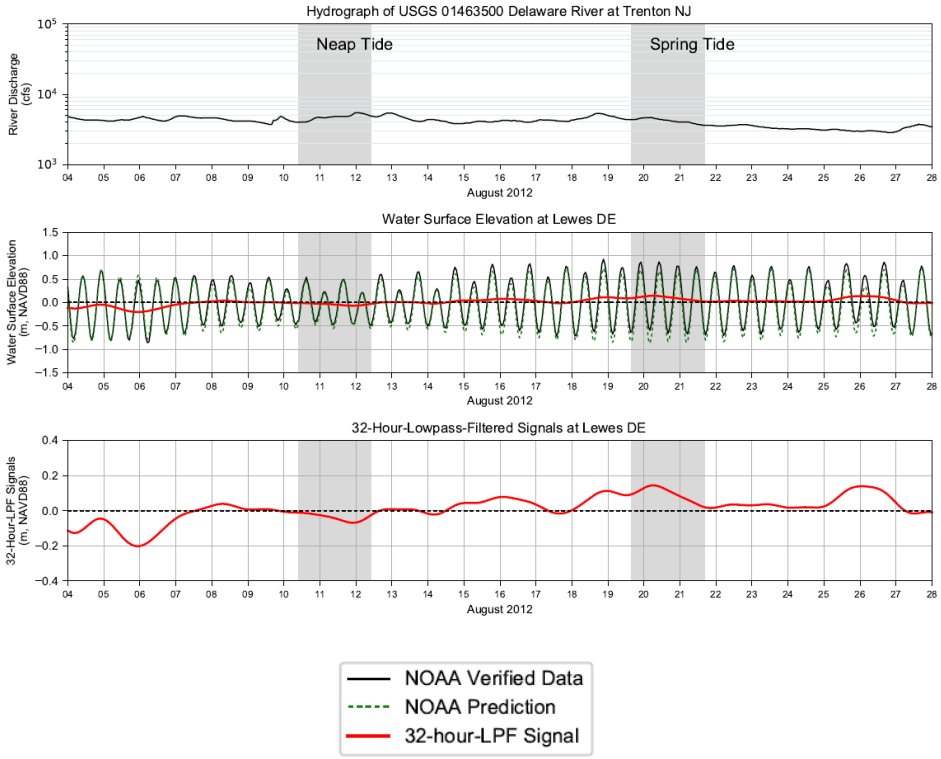

Selected time window for neap tide: 08-10-2012 10:00 to 08-12-2012 10:00
Selected time window for spring tide: 08-19-2012 16:00 to 08-21-2012 16:00

Figure I-1 River flow at Trenton and observed tide at Lewes, DE during August 2012.

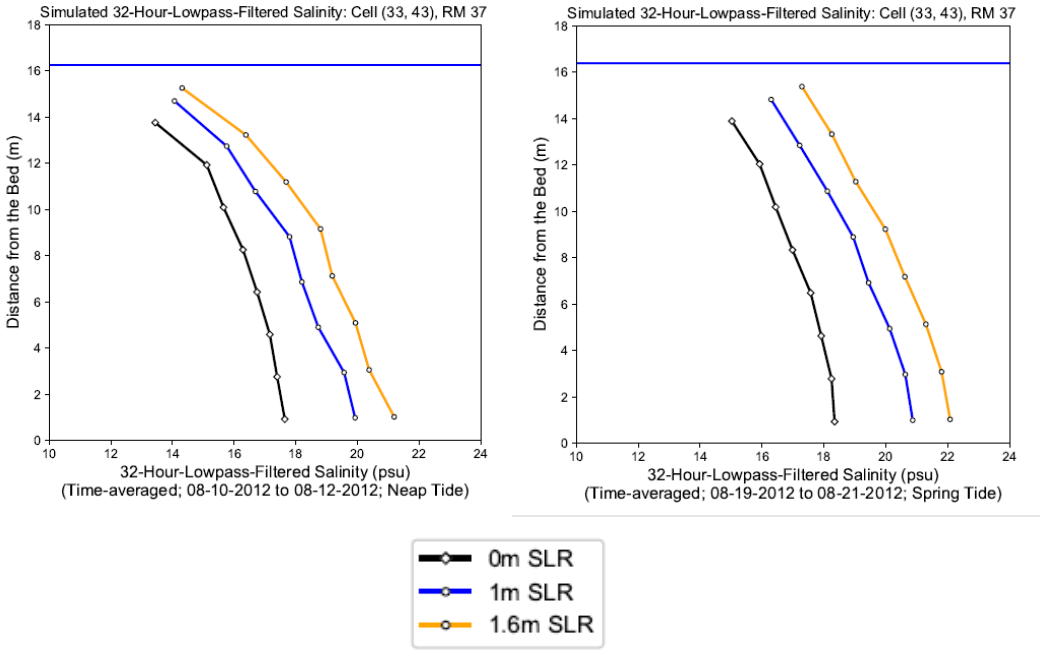

Notes: 32-hr-LPFed results were calculated first, and then averaged over the time period to represent the mean vertical structure for a selected spring and neap tide period.

Figure I-2 Simulated 32-hour-lowpass-filtered salinity profile during the 08-10-2012 to 08-12-2012 neap tide and the 08-19-2012 to 08-21-2012 spring tide at RM 37 in the navigation channel. Results from three SLR scenarios are shown.

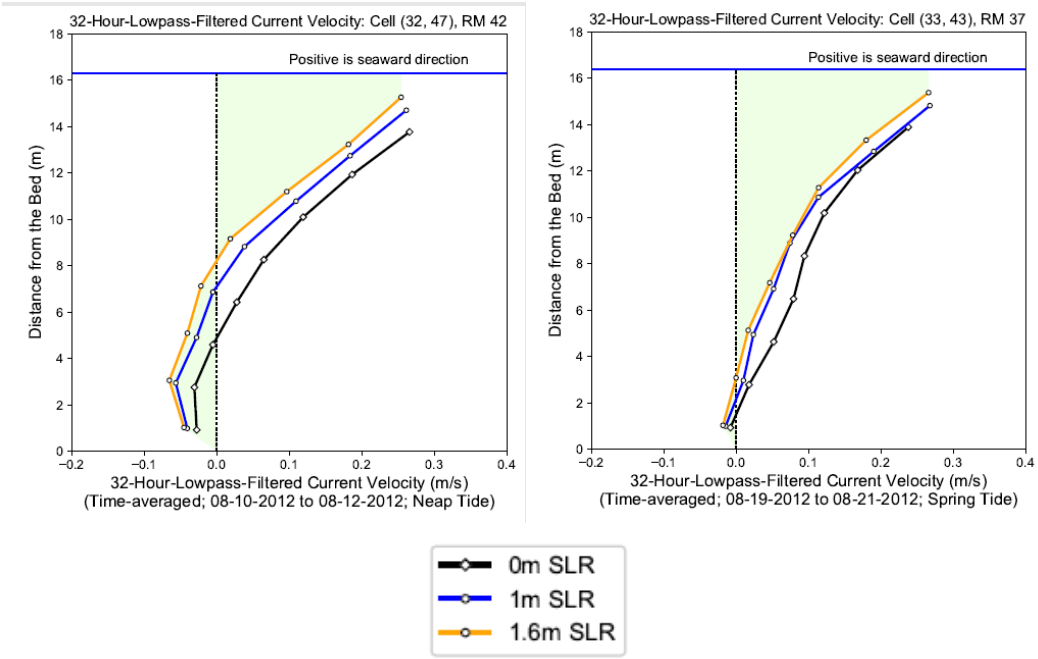

Notes: 32-hr-LPFed results were calculated first, and then averaged over the time period to represent the mean vertical structure for a selected spring and neap tide period.

Figure I-3 Simulated 32-hour-lowpass-filtered along-channel current velocity profile during the 08-10-2012 to 08-12-2012 neap tide and the 08-19-2012 to 08-21-2012 spring tide period at RM 37 in the navigation channel. Results from three SLR scenarios are shown.

Table I-1. Simulated 32-hour-lowpass-filtered salinity profile during the 08-10-2012 to 08-12-2012 neap tide at RM 37 in the navigation channel.

	0 m SLR		1 m SLR		1.6 m SLR	
Vertical Layer	Depth (m)	32-hour-LPF Salinity (psu)	Depth (m)	32-hour-LPF Salinity (psu)	Depth (m)	32-hour-LPF Salinity (psu)
1	0.92	17.64	0.98	19.92	1.02	21.19
2	2.75	17.39	2.94	19.56	3.05	20.38
3	4.59	17.15	4.90	18.73	5.09	19.93
4	6.42	16.74	6.86	18.20	7.12	19.18
5	8.26	16.28	8.82	17.79	9.16	18.80
6	10.09	15.65	10.78	16.69	11.19	17.68
7	11.93	15.11	12.74	15.76	13.22	16.38
8	13.76	13.44	14.70	14.06	15.26	14.31

Table I-2. Simulated 32-hour-lowpass-filtered salinity profile during the 08-19-2012 to 08-21-2012 spring tide at RM 37 in the navigation channel.

	0 m SLR		1 m SLR		1.6 m SLR	
Vertical Layer	Depth (m)	32-hour-LPF Salinity (psu)	Depth (m)	32-hour-LPF Salinity (psu)	Depth (m)	32-hour-LPF Salinity (psu)
1	0.93	18.34	0.99	20.86	1.03	22.07
2	2.78	18.24	2.96	20.62	3.08	21.80
3	4.63	17.91	4.94	20.12	5.13	21.29
4	6.48	17.57	6.92	19.44	7.18	20.61
5	8.33	16.98	8.89	18.94	9.23	19.98
6	10.19	16.44	10.87	18.11	11.28	19.02
7	12.04	15.92	12.84	17.21	13.33	18.25
8	13.89	15.02	14.82	16.29	15.38	17.28

Table I. 3. Simulated 32-hour-lowpass-filtered current velocity profile during the 08-10-2012 to 08-12-2012 neap tide at RM 37 in the navigation channel.

	0 m SLR		1 m SLR		1.6 m SLR	
Vertical Layer	Depth (m)	32-hour-LPF Velocity (m/s)	Depth (m)	32-hour-LPF Velocity (m/s)	Depth (m)	32-hour-LPF Velocity (m/s)
1	0.92	-0.028	0.98	-0.041	1.02	-0.045
2	2.75	-0.031	2.94	-0.057	3.05	-0.065
3	4.59	-0.005	4.90	-0.028	5.09	-0.041
4	6.43	0.028	6.86	-0.005	7.12	-0.022
5	8.26	0.065	8.82	0.038	9.16	0.019
6	10.10	0.119	10.78	0.109	11.20	0.096
7	11.93	0.187	12.74	0.184	13.23	0.182
8	13.77	0.266	14.70	0.261	15.27	0.254

Table I. 4. Simulated 32-hour-lowpass-filtered current velocity profile during the 08-19-2012 to 08-21-2012 spring tide at RM 37 in the navigation channel.

	0 m SLR		1 m SLR		1.6 m SLR	
Vertical Layer	Depth (m)	32-hour-LPF Velocity (m/s)	Depth (m)	32-hour-LPF Velocity (m/s)	Depth (m)	32-hour-LPF Velocity (m/s)
1	0.93	-0.001	0.99	-0.010	1.03	-0.013
2	2.78	0.015	2.97	0.001	3.08	-0.001
3	4.63	0.037	4.94	0.031	5.13	0.035
4	6.49	0.080	6.92	0.067	7.18	0.059
5	8.34	0.112	8.90	0.098	9.24	0.088
6	10.19	0.152	10.88	0.139	11.29	0.119
7	12.05	0.209	12.86	0.196	13.34	0.177
8	13.90	0.294	14.83	0.311	15.39	0.298

APPENDIX J. EFFECTS OF MODEL CONFIGURATION ON RESULTS

Different aspects of model configuration that relate to potential future conditions can affect salinity intrusion simulations. The effects of specific model features on simulated salinity were examined, and these features included (1) marsh area, which affects the volume of water moving in and out of the estuary; (2) bottom roughness in marshes, which impacts energy loss as the tide moves upstream; (3) Navigation channel bathymetry; and (4) shoreline retreat and bank erosion; The results from the sensitivity tests are presented in terms of the salt front location. Additional sensitivity tests examining the effects of vertical grid resolution, net flow and salinity in the C&D Canal, and ocean salinity, are documented in the SM3D calibration report. Details of the effects of model configuration are presented below.

J.1 Amount of Marsh Area Represented

Low-lying, intertidal marshes around the bay affect tidal energy and salinity transport. As the tide moves into the Estuary, the converging shoreline amplifies the tidal wave and related energy. As water moves upstream with the rising tide, the converging shoreline amplifies the tidal wave. As a result of this convergence, the tidal range at Philadelphia, PA (RM 100) is larger than the tidal range at Lewes, DE near the mouth of the Bay (RM 0). Marshes counteract this effect by providing additional space for water to spread out, which also increases the volume of the tidal prism.[29] With SLR, marsh areas closer to the coast will be inundated more frequently and may affect the amount of tidal energy driving salinity transport. As the tidal prism increases, a wider extent of marsh area is inundated with each tide, which results in: 1) reduced tidal amplitude; 2) reduced volume of water moving in and out of the upper reaches of the Estuary; and 3) reduced salinity in the bay (in comparison with effects of SLR without a wider extent of marsh area). Simulation tests were conducted to quantify the magnitude of these effects, and the results of the tests are presented below.

The model domain of SM3D was modified to incorporate additional marsh area (SM3D+M) to evaluate how the inundation of more marsh area affects salinity transport. This model configuration represents a scenario in which marshes migrate farther inland and no net sediment deposition occurs.

With 1.6 m SLR, the increase in the amplitude of the largest tidal constituent (M2) at RM 126 was 5 cm less with marshes (SM3D+M) than without additional marshes (SM3D), With 1.6 m SLR, at

[29] The tidal prism is the total volume of water moving into and out of the estuary, excluding freshwater inflows (Hume 2005).

RM 37 the M2 amplitude was 8 cm less with additional marshes (SM3D+M) than without additional marshes (SM3D).

Including additional marsh area has a substantial effect on the extent of salinity intrusion. For the baseline (0 m SLR), the predicted maximum salt front locations for SM3D+M is 0.2 miles farther downstream than that simulated using SM3D; with 1.6 m SLR, the maximum salt front location is 2.6 miles farther downstream with additional marshes.

These results demonstrate that the model configuration without additional marsh area is more conservative with respect to protecting public water supplies. The results also demonstrate that preserving marsh areas is effective in reducing tidal amplification, particularly in the upper Delaware River.

J.1.1 Updated Model Domain and Historical Salt Front Simulation

Estuary models typically do not include inland marshes, because simulating marsh wetting and drying with each tidal cycle is computationally expensive. SM3D's domain (Grid 2.1) includes only the marsh areas that are currently inundated most of the time. Limiting the marsh area is known as the "bathtub approach" and representative of a scenario in which the coastline is protected from advancing inundation with gray infrastructure, such as sea walls and levees.

The model domain of SM3D was modified to incorporate additional marsh area (SM3D+M) to evaluate how the inundation of more marsh area affects salinity transport. This model configuration represents a scenario in which marshes migrate farther inland, and no net sediment deposition occurs. **Figure J.1-1** shows the model domains of SM3D and SM3D+M; the same bathymetry (45-ft-deep navigation channel) and model parameters were used for common features in both models. **Figure J.1-2** shows the additional marsh area in SM3D+M. The addition of marsh area increased the volume of the tidal prism by 2.4, 3.3, and 4.6 percent for 0 m, 1.0 m, and 1.6 m sea level rise, respectively (see **Table J.1-1** and **Table J.1-2**).

SM3D and SM3D+M both predicted the salt front well for the simulation of January–December 2002 conditions. SM3D predicted the salt front locations slightly farther upstream (0.3 mile) than those predicted by SM3D+M (**Figure J.1-3**). These results are similar because under historical conditions, the additional marsh area would rarely be inundated. During 7/1 through 10/31 of the simulated period, the range of the 7-day-moving average salt front river mile location is 53.4 – 88.3 with marsh excluded and is 53.7 – 87.9 with marsh included). No further calibration effort was made for Grid v4.1 because the simulation for the 2001-2002 period produced only a minor difference in salinity intrusion. In this study, the simulations with Grid v4.1 are considered sensitivity simulations. Ideally, and as time and resources allow, the model with marsh included (Grid v4.1) would be calibrated using the same process as that used for the model without the marsh (Grid v2.1). Parameters, such as bottom roughness height, could be adjusted if hydrodynamics data collected in marsh areas are available. In this study, a universal bottom roughness height of 0.025 meter was used in the model, and the marsh bottom elevation was based on FEMA 2011 survey data and on the NAVD88 datum (FEMA 2011), and it incorporated

the NOAA navigational chart as well as 2022-2023 post-dredging survey data from the USACE. A discussion of model sensitivity to bottom friction is presented in Section J.2.

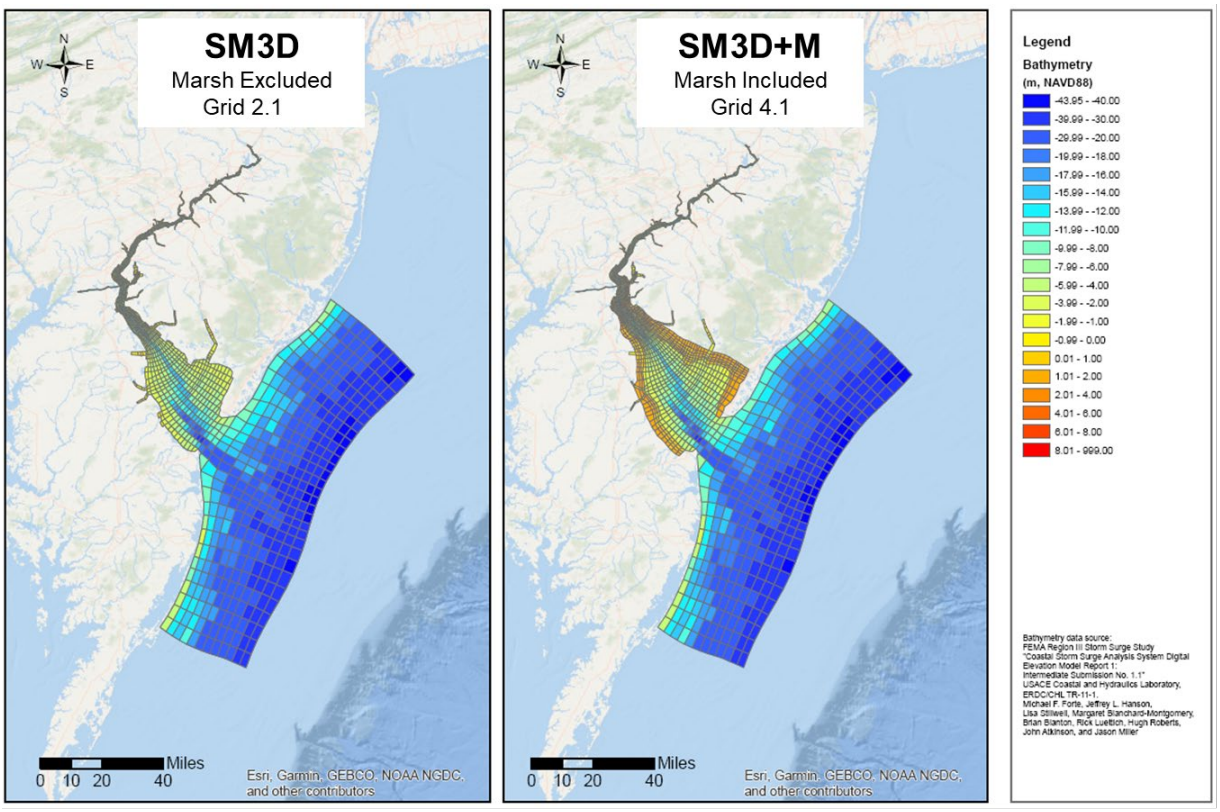

Grid 2.1 (marsh excluded) is the numerical grid for the salinity model, SM3D. Grid 2.1 includes marsh area that is inundated at least once daily. For discussion purposes, it is referenced as "marsh excluded" model. Grid 2.1 contains 2510 grid cells. Grid 4.1 (marsh included) is the numerical grid for testing the impact of low-lying marsh area and is used for SM3D+M. Grid 4.1 includes marsh area that is infrequently inundated under current conditions but may become inundated regularly with SRL. Grid 4.1 contains 2976 grid cells.

Figure J. 1-1. Numerical grids for calibrated model (SM3D, Grid 2.1, with additional marsh excluded) and an alternative model (SM3D+M, Grid 4.1, with additional marsh included).

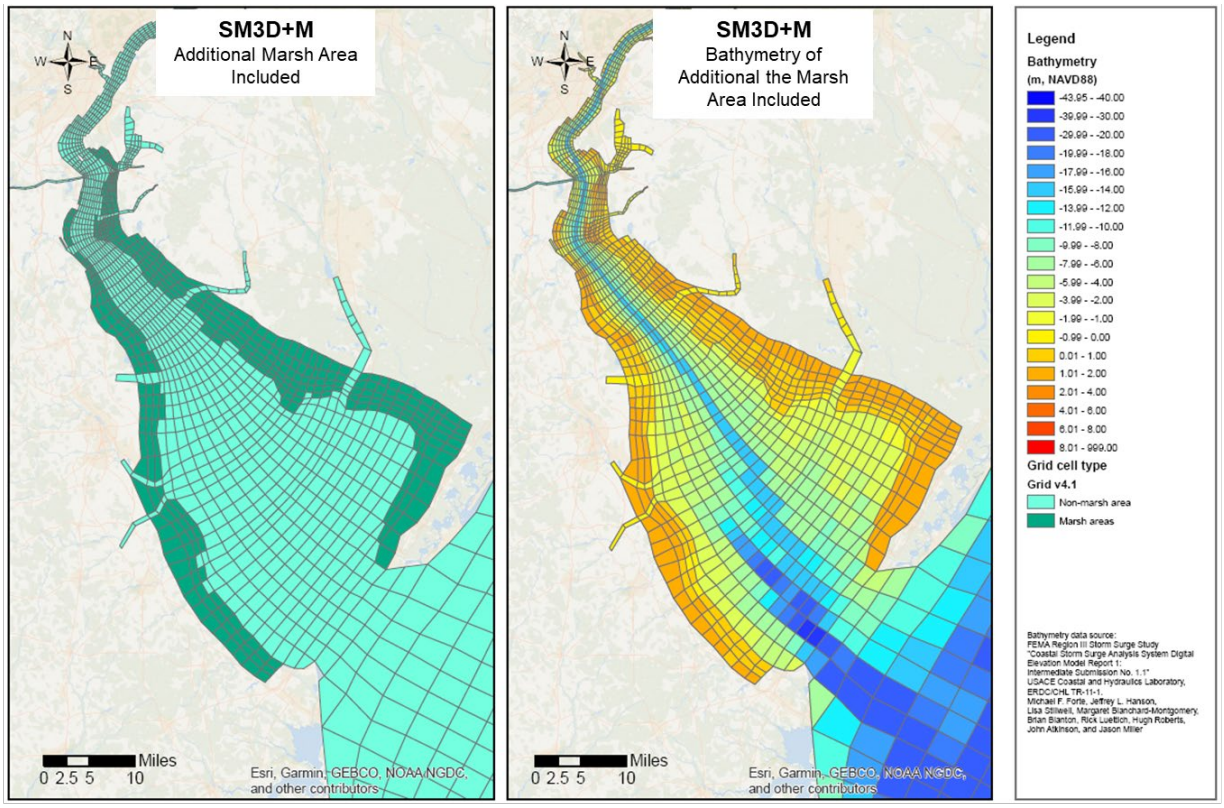

Left panel: Full domain of Grid v4.1. The additional marsh area added Grid v2.1 to form Grid v4.1 is indicated in dark green. Right panel: Bathymetry of Grid v4.1. The volume of water in the tidal prism increased by approximately 2 percent with 0 m SLR and 4 percent for 1.6 m SLR.

Figure J. 1-2. SM3D+M (Grid 4.1) with additional marsh area.

Table J. 1-1. Average water volume in the Delaware Estuary during July 1st - September 30, 2002.

SLR [m]	Grid 2.1	Grid 4.1	Difference	% Diff
0	1.52139E+04	1.55779E+04	364	2.39%
0.3	1.58313E+04	1.62344E+04	403	2.55%
0.5	1.62442E+04	1.66839E+04	440	2.71%
0.8	1.68642e+04	1.73786e+04	514	3.05%
1	1.72779E+04	1.78537E+04	576	3.33%
1.6	1.85197E+04	1.93773E+04	858	4.63%

Notes: volume is in units of million cubic meters; water in C&D canal and tributaries are excluded.

Table J. 1-2. Average water volume in the Delaware Estuary Zone 6 during July 1st - September 30, 2002.

SLR [m]	Grid 4.1 (open water)	Grid 4.1 (marsh)	Volume in marsh/ Volume in open water area
0	1.34770E+04	2.59053E+02	1.92%
0.3	1.40327E+04	2.79101E+02	1.99%
0.5	1.44037E+04	3.02752E+02	2.10%
0.8	1.49647E+04	3.47302E+02	2.32%
1	1.53381E+04	3.89435E+02	2.54%
1.6	1.64577E+04	6.13957E+02	3.73%

Notes: volume is in units of million cubic meters; water in C&D canal and tributaries are excluded.

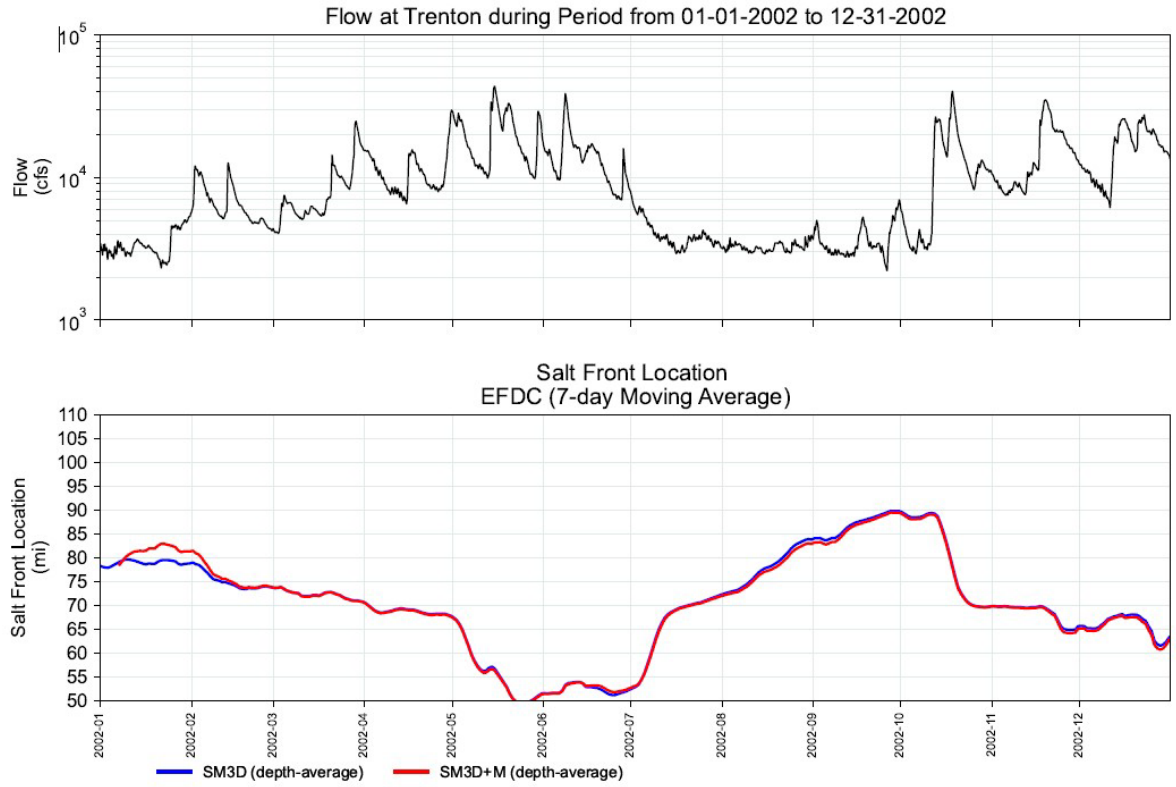

Note: The simulations were performed using historical flows and conditions that were observed during January 2001–December 2002. The navigation channel depth used in simulations is 40 ft. The ranges of the simulated salt front location are: RM 58.3–85.6 (SM3D) and RM 59.0–85.1 (SM3D+M).

Figure J. 1-3. Flow at Trenton during a 1-year simulation and corresponding simulated salt front location without extended marsh area (SM3D) and with extended marsh area (SM3D+Marsh).

J.1.2 SLR Simulations with Marsh Areas Included

Tidal Amplitude

The additional marsh areas resulted in dissipated tidal and wave energy, reducing tidal range, especially in the upper portion of the river. Under current tidal and hydrologic conditions, and with the current geometry and bathymetry (45' deep navigation channel), most of the low-lying wetland and marsh areas in zone 6 (the bay area) of the DRB are intertidal. They may become inundated permanently should sea level rises above a certain threshold in the future. The change in water depth affects the propagation of the tidal wave in the estuary. Spatial distribution of predicted M2 tide amplitude (which carries most of the tidal energy) is presented in **Figure J.1-4**. **Table J.1-3** and **J.1-4** summarize the amplitude and phase of the M2 tide predicted by using Grid 2.1 (additional marsh excluded) and Grid 4.1 (additional marsh included), respectively. For example, under 1.6m SLR, the M2 tide amplitude predicted at Newbold (RM126) increases by 19 percent

compared with the baseline when marshes are excluded, while the amplitude of the M2 increases by 14 percent when marshes are included. Downstream from RM60, the amplitude of the M2 tide slightly decreases, allowing water to inundate the marshes. For example, at Ship John Shoal (RM 37), the amplitude of the M2 tide increases by 5 percent from the baseline when marshes are excluded, while the amplitude decreases by 4 percent from the baseline when marshes are included. All these observations indicate that significant tidal and wave energy is dissipated through marsh areas and reduces the tidal range in the upper portion of the river. The change in the phase indicates that the position at the time of high tide or low tide also changes as sea level rises. This result implies that if low-lying marsh areas are allowed to be inundated and no shoreline protection measures are implemented, higher sea levels will reduce both the tides and tidal amplification, particularly in the upper portion of the Delaware River. These simulation results demonstrate that the model configuration without additional marsh area is more conservative with respect to protecting public water supplies. These results further demonstrate that preserving marsh areas is effective in reducing tidal amplification, particularly in the upper Delaware River.

Table J. 1-3. Predicted M2 tide amplitude using Grid v2.1 with marsh areas excluded.

SLR	Station	Station ID	RM	Modeled M2 Amplitude	Modeled Baseline M2 Amplitude	Difference in Amplitude	Modeled Phase	Modeled Baseline Phase	Difference in Phase
				(m)	(m)	(cm)	(hour)	(hour)	(hour)
0	LEWES	8557380	0	0.596	0.596	0.00	7.34	7.34	0.00
1	LEWES	8557380	0	0.613	0.596	1.73	7.28	7.34	-0.05
1.6	LEWES	8557380	0	0.625	0.596	2.92	7.24	7.34	-0.10
0	CAPE MAY	8536110	2	0.720	0.720	0.00	7.40	7.40	0.00
1	CAPE MAY	8536110	2	0.739	0.720	1.89	7.30	7.40	-0.10
1.6	CAPE MAY	8536110	2	0.750	0.720	3.00	7.23	7.40	-0.17
0	SHIP JOHN SHOAL	8537121	37	0.908	0.908	0.00	8.58	8.58	0.00
1	SHIP JOHN SHOAL	8537121	37	0.937	0.908	2.94	8.33	8.58	-0.26
1.6	SHIP JOHN SHOAL	8537121	37	0.956	0.908	4.75	8.17	8.58	-0.41
0	REEDY POINT	8551910	58.5	0.783	0.783	0.00	9.76	9.76	0.00
1	REEDY POINT	8551910	58.5	0.807	0.783	2.42	9.51	9.76	-0.26
1.6	REEDY POINT	8551910	58.5	0.831	0.783	4.85	9.35	9.76	-0.42
0	DELAWARE CITY	8551762	60.7	0.819	0.819	0.00	9.92	9.92	0.00
1	DELAWARE CITY	8551762	60.7	0.853	0.819	3.39	9.65	9.92	-0.26
1.6	DELAWARE CITY	8551762	60.7	0.885	0.819	6.62	9.49	9.92	-0.43
0	MARCUS HOOK	8540433	79.3	0.711	0.711	0.00	11.34	11.34	0.00
1	MARCUS HOOK	8540433	79.3	0.796	0.711	8.48	11.01	11.34	-0.33
1.6	MARCUS HOOK	8540433	79.3	0.858	0.711	14.76	10.79	11.34	-0.55
0	PHILADELPHIA	8545240	98.5	0.809	0.809	0.00	0.42	0.42	0.00
1	PHILADELPHIA	8545240	98.5	0.919	0.809	10.99	12.36	0.42	-0.48
1.6	PHILADELPHIA	8545240	98.5	0.998	0.809	18.88	12.07	0.42	-0.77
0	BURLINGTON	8539094	117.5	1.040	1.040	0.00	1.05	1.05	0.00
1	BURLINGTON	8539094	117.5	1.153	1.040	11.36	0.51	1.05	-0.54
1.6	BURLINGTON	8539094	117.5	1.240	1.040	20.04	0.19	1.05	-0.86
0	NEWBOLD	8548989	126.3	1.106	1.106	0.00	1.16	1.16	0.00
1	NEWBOLD	8548989	126.3	1.223	1.106	11.73	0.61	1.16	-0.55
1.6	NEWBOLD	8548989	126.3	1.312	1.106	20.56	0.28	1.16	-0.89

Note: the analysis is based on one year (2002 hydrologic conditions).

Table J. 1-4. Predicted M2 tide amplitude using Grid v4.1 with marsh areas included.

SLR	Station	Station ID	RM	Modeled M2 Amplitude	Modeled Baseline M2 Amplitude	Difference in Amplitude	Modeled Phase	Modeled Baseline Phase	Difference in Phase
				(m)	(m)	(cm)	(hour)	(hour)	(hour)
0	LEWES	8557380	0	0.596	0.596	0.00	7.35	7.35	0.00
1	LEWES	8557380	0	0.584	0.596	-1.17	7.38	7.35	0.03
1.6	LEWES	8557380	0	0.559	0.596	-3.65	7.46	7.35	0.11
0	CAPE MAY	8536110	2	0.721	0.721	0.00	7.40	7.40	0.00
1	CAPE MAY	8536110	2	0.714	0.721	-0.73	7.40	7.40	0.00
1.6	CAPE MAY	8536110	2	0.694	0.721	-2.76	7.49	7.40	0.09
0	SHIP JOHN SHOAL	8537121	37	0.907	0.907	0.00	8.60	8.60	0.00
1	SHIP JOHN SHOAL	8537121	37	0.893	0.907	-1.31	8.61	8.60	0.01
1.6	SHIP JOHN SHOAL	8537121	37	0.872	0.907	-3.45	8.80	8.60	0.20
0	REEDY POINT	8551910	58.5	0.775	0.775	0.00	9.79	9.79	0.00
1	REEDY POINT	8551910	58.5	0.770	0.775	-0.54	9.89	9.79	0.10
1.6	REEDY POINT	8551910	58.5	0.778	0.775	0.33	10.13	9.79	0.33
0	DELAWARE CITY	8551762	60.7	0.815	0.815	0.00	9.95	9.95	0.00
1	DELAWARE CITY	8551762	60.7	0.810	0.815	-0.49	10.08	9.95	0.13
1.6	DELAWARE CITY	8551762	60.7	0.822	0.815	0.65	10.34	9.95	0.39
0	MARCUS HOOK	8540433	79.3	0.708	0.708	0.00	11.38	11.38	0.00
1	MARCUS HOOK	8540433	79.3	0.763	0.708	5.52	11.45	11.38	0.07
1.6	MARCUS HOOK	8540433	79.3	0.809	0.708	10.07	11.64	11.38	0.26
0	PHILADELPHIA	8545240	98.5	0.809	0.809	0.00	0.46	0.46	0.00
1	PHILADELPHIA	8545240	98.5	0.895	0.809	8.60	0.37	0.46	-0.08
1.6	PHILADELPHIA	8545240	98.5	0.957	0.809	14.82	0.47	0.46	0.01
0	BURLINGTON	8539094	117.5	1.041	1.041	0.00	1.08	1.08	0.00
1	BURLINGTON	8539094	117.5	1.127	1.041	8.61	0.93	1.08	-0.16
1.6	BURLINGTON	8539094	117.5	1.196	1.041	15.52	0.98	1.08	-0.10
0	NEWBOLD	8548989	126.3	1.105	1.105	0.00	1.21	1.21	0.00
1	NEWBOLD	8548989	126.3	1.194	1.105	8.89	1.03	1.21	-0.18
1.6	NEWBOLD	8548989	126.3	1.265	1.105	15.98	1.07	1.21	-0.13

Note: the analysis is based on one year (2002 hydrologic conditions).

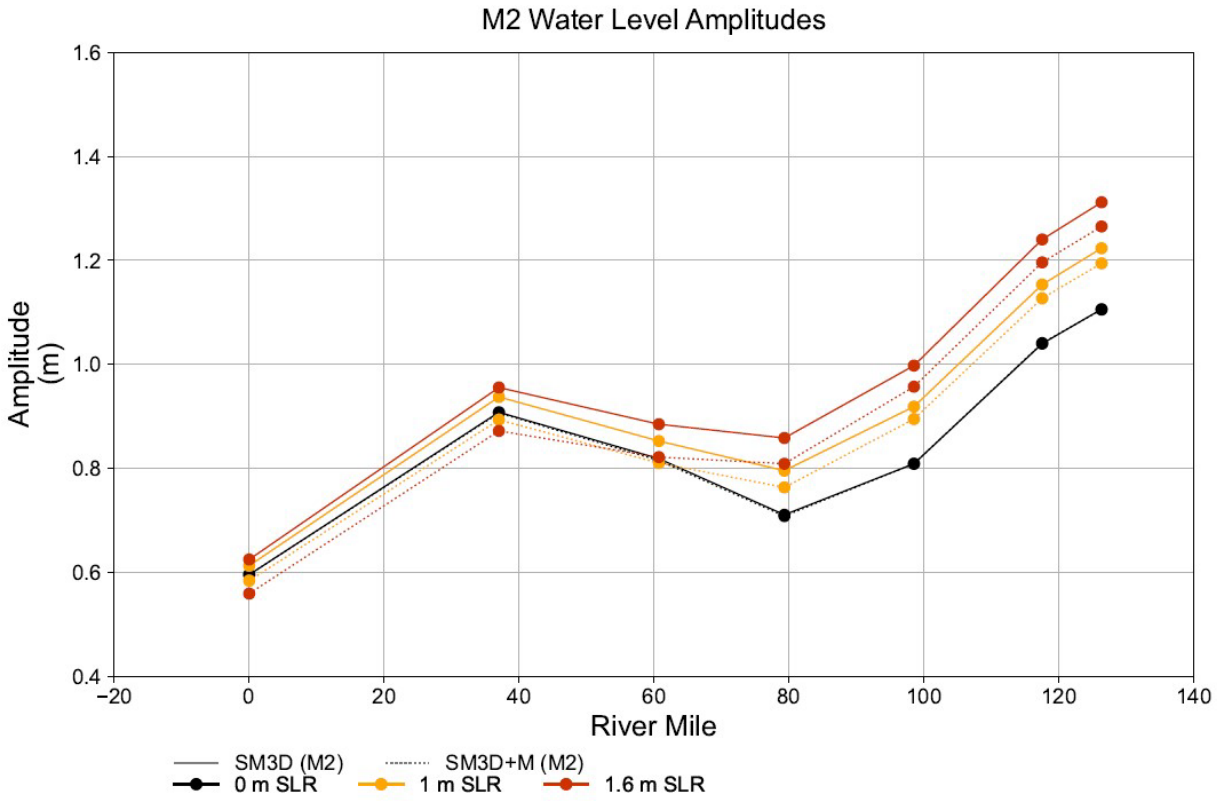

Figure J. 1-4. Simulated spatial distribution of M2 tidal water level amplitude with sea level rise; without extended marsh area (SM3D) and with extended marsh area (SM3D+Marsh).

Salinity Intrusion and the Salt Front

The simulated maximum locations of the salt front with SLR are provided in **Table J.1-5**. The additional marsh area has little effect on salinity or chloride in the baseline scenario, but it has a substantial effect on salinity or chloride with SLR. The maximum salt front location is shown in **Figure J. 1-5** for 0.0-, 1.0-, and 1.6 m SLR. For the baseline (0 m SLR), the predicted maximum salt front location for SM3D+M is 0.2 miles farther downstream than that simulated using SM3D; with 1.6 m SLR and additional marshes, the maximum salt front location is 2.6 miles farther downstream. The impact of marsh on salinity intrusion becomes more significant with SLR greater than 0.8 m.

These results show that modeling salinity intrusion without extending the marsh area is a more conservative approach with respect to the protection of drinking water supplies. The analysis of the model sensitivity to the marsh area extent helps in further understanding the uncertainty in simulation results.

Table J. 1-5. Comparison of the predicted maximum salt front location with (SM3D+M) and without (SM3D) additional marsh area.

SLR (m)	SM3D (RM)	SM3D+M (RM)	Difference (Miles)
0	90.7	90.5	-0.2
0.3	92.4	92.2	-0.2
0.5	93.4	93.0	-0.4
0.8	95.0	94.0	-1.0
1	96.3	94.8	-1.5
1.6	101.4	98.8	-2.6

Note: Simulated flows of July-October 2002.

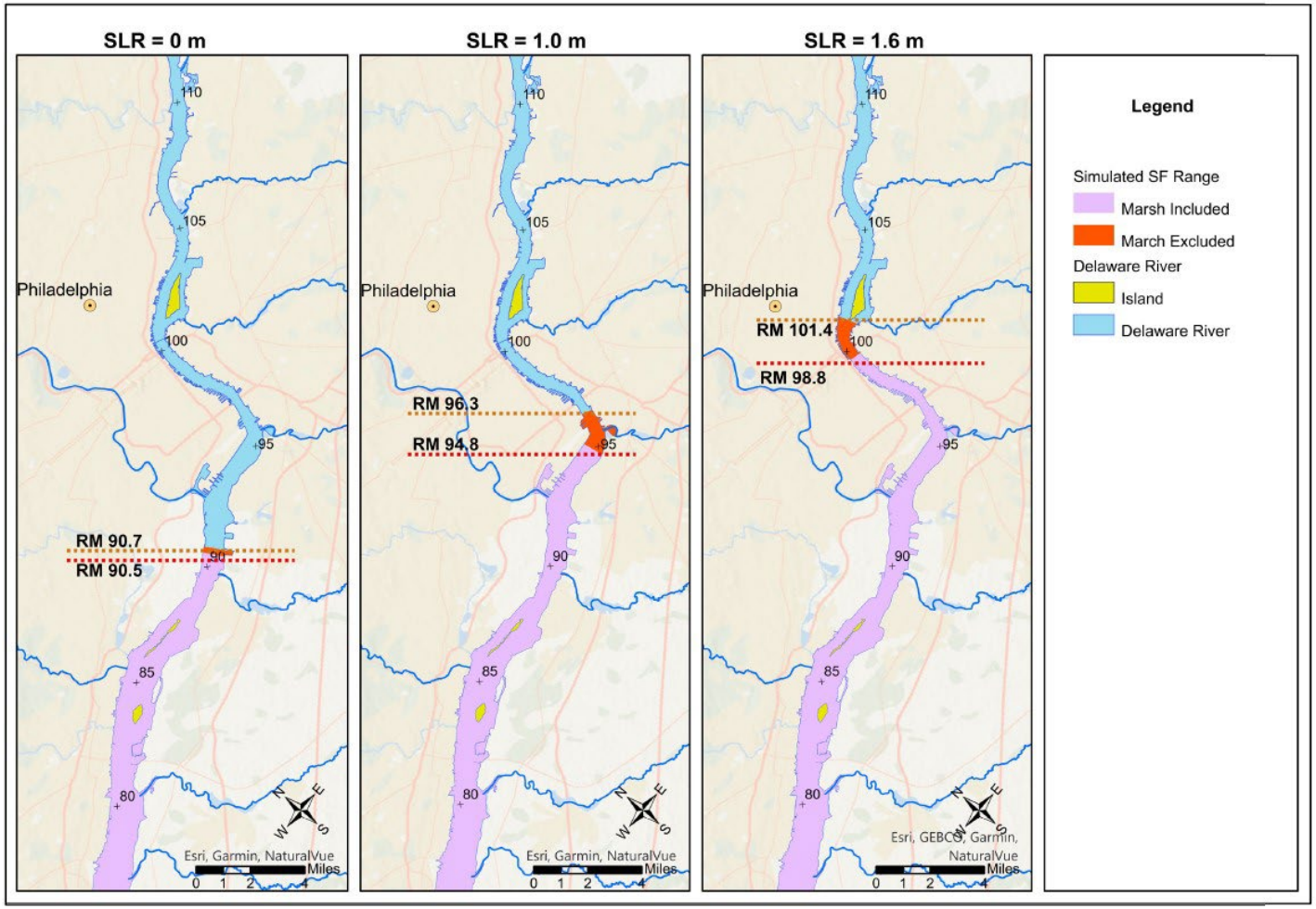

Model: SM3D and SM3D+M. Simulated using flows of July – October 2002. Channel Depth = 45 ft

Figure J. 1-5. Sensitivity of simulated maximum salt front location to marsh extent.

J.2 Bottom Roughness in Marsh Areas

The character of the estuary bottom can affect the flow of water across it because of friction, and it is an important factor in simulating wave energy loss. The model parameter that represents the character of the estuary bottom is the bottom roughness height (designated as z_0). However, z_0 is difficult to define for marsh areas because vegetation-induced friction losses are highly variable and depend on vegetation type, density, height, and submergence. A consensus method for estimating z_0 for marsh areas has not yet been established. SM3D was calibrated with spatially variable z_0. Marsh z_0 was set to a constant value across all simulated SLR scenarios. However, marsh z_0 may change with SLR, as the vegetation type, density, height, and depth of submergence changes. Some existing marsh areas may even become permanently inundated. An understanding of the model sensitivity to z_0, therefore, is needed, and sensitivity testing for marsh z_0 was performed for the additional marsh areas in SM3D+M. The z_0 values tested for the additional marsh areas were 0.0025, 0.025 and 0.05 m. These values are an order of magnitude higher than those specified in the Bay (0.004 m) and ocean (0.001 m), because the effects of z_0 are weaker in deeper water where other hydrodynamic forces are relatively stronger.

The simulated salt front location was not sensitive to marsh z_0 across the range tested. The difference in predicted maximum salt font location across the three tested bottom roughness heights is 0.01 – 0.3 miles for 1.0 m SLR and 0.29 – 0.3 miles for 1.6 m SLR. A time series of predicted salt front location shows that varying bottom roughness height causes no discernable difference in the salt front location with 1.0 m or 1.6 m SLR. These results show that bottom roughness in the marsh areas is not an important factor for evaluating the impacts of sea level rise on salinity intrusion.

J.3 Channel Bathymetry

The depth and width of an estuary (bathymetry and morphology) typically change over time as a result of natural processes (sediment accumulation, and erosion) and human impacts (dredging). However, the bathymetry of the Delaware Estuary has remained largely unchanged, except in the Federal Navigation Channel (FNC). The navigation channel is maintained by the United States Army Corps of Engineers (USACE) and is periodically dredged to remove sediment and maintain an appropriate depth for shipping. According to the USACE, channel deepening and dredging along the full length of the estuary began late in the 19th century and has continued to accommodate increasing drafts of ships bound for the ports of Wilmington and Philadelphia. In 1848, the natural channel depth near Philadelphia was estimated to be 20 ft. The channel was deepened to 26 ft in 1898, 30 ft in 1910, 35 ft in 1926, 40 ft in 1940, and most recently 45 ft (PhilaPort, 2018). Between 2010 and 2017, seven channel segments, totaling 61.5 miles, were dredged by removing 12 million tons of sediment from the estuary and 4 million tons from the Bay.

J.3.1 Previous analyses

USACE used CH3D, a three-dimensional hydrodynamic model, to evaluate the impact of the most recent deepening project on salinity and chloride concentrations. The simulations were performed with 1965 flows (with minimum flows at Trenton adjusted to 2,500 cfs, as in the present-day drought management plan). At RM 98, the predicted maximum chloride concentrations were 175 ppm for the 40 ft channel and 225 ppm for the 45 ft channel, and the 30-dma 180 mg/l isochlor remained below RM 98 (Kim and Johnson, 1998). The maximum salt front location from the study was RM 92.2 with a 40 ft channel and 96.2 with a 45 ft channel, as reported in the July 1997 Final Supplemental Environmental Impact Statement (USACE, 1997).

The impacts of channel bathymetry or channel depth on hydrodynamics, salinity intrusion and sediment transport were also evaluated by Rutgers University (Pareja-Roman, 2019) with the Regional Ocean Modeling System, ROMS (Haidvogel et al., 2008). Simulations with historical (1898, 26-ft deep) and more recent (2014, 45-ft deep) bathymetry were performed with the median flow rate for the Delaware River at Trenton (350 m^3/s or 12,360 cfs) and with no tributary inflow. Results show that channel deepening from 1898–2014 doubled the tidal range, shifted the high water arrival time, and changed the elevation–velocity phase. The simulated extent of salinity intrusion (defined in the study as the 2 psu isohaline in the thalweg) was RM 46.6 in 1848 and RM 62.1 in 2014.

J.3.2 Effects of channel deepening on salinity intrusion from SLR

Simulations were performed to compare pre-dredging bathymetry (40-ft depth referenced to MLLW and 1983-2001 NTDE) and post-dredging bathymetry (45-ft depth referenced to MLLW and 1983-2001 NTDE) with SLR. Results of baseline simulations of salinity intrusion, simulations with SLR, and simulations with SLR and channel deepening were compared. **Table J.3-1** presents the differences in the salt front location among these simulations. Results show that under SLR scenarios, the maximum salt front location advances 2.1-2.4 miles farther upstream as a result of channel deepening. At 0.5 m SLR, the effect of channel deepening is similar to the effect of 0.5 m SLR. With greater SLR, the effect of channel deepening is surpassed by the effect of SLR. The maximum simulated salt front location in any of these SLR scenarios is RM 101.4, which is 8.6 miles downstream from the major public water intakes at RM 110.

These results (Section J.1 and J.3) show that the effects of SLR on salinity intrusion are increased with channel deepening and decreased with additional marsh area. In all simulations with representative (2002) low flow conditions, the maximum salt front location remained below RM 110.

Table J. 3-1 Sensitivity of Salt Front Location to Channel Bathymetry (SM3D)

SLR	Channel depth reference to current MLLW	Maximum Salt Front Location	Difference in Maximum from 0 m SLR Baseline	Difference in Maximum from 40-ft to 45-ft
(m)	(ft)	(River Mile)	(mi)	(mi)
0	40	88.3	–	–
	45	90.7	–	2.4
0.5	40	91.3	3.0	
	45	93.4	2.7	2.1
1	40	94.1	5.8	–
	45	96.3	5.6	2.2
1.6	40	99.00	10.7	–
	45	101.4	10.7	2.4

Model: SM3D. Simulated using flows of July – October 2002.

J.4 Shoreline Retreat and Bank Erosion

The wetland and marsh areas surrounding the Estuary provide protection from storms by absorbing energy, reducing wind penetration, and reducing wave strength. These areas are also habitat for many species, including ribbed mussels, fiddler crabs, horseshoe crabs, marsh mud snails, grass shrimp, as well as fishes, turtles, and birds. Storm forces disturb the marsh vegetation, which holds soils and sediments in place, causing erosion and the loss of coastline and bank areas. Sea level rise is likely to result in shoreline erosion and wetlands migration (Kearny et al., 2002; Schieder, et al., 2017), which may impact the storm protection and habitat values of these areas. Shoreline retreat and bank erosion, in turn, could affect salinity intrusion.

The loss of marshes due to SLR is difficult to quantify. Sensitivity simulations were conducted to evaluate the potential impact of SLR-induced shoreline retreat and bank erosion[30] on salinity intrusion. In a selected part of the total marsh area surrounding the bay in the SM3D+M model, near-shore bed elevation was lowered by 1 m to reflect permanent inundation of those marshes. The current estimated marsh loss rate is1.1–1.9% per decade (New Jersey Science Advisory Board, 2020). The low rate is largely due to marsh area being gained through migration upland into low-lying maritime forests. Field observations indicate that the sediment deposition rate in marshes along the New Jersey side of Delaware Bay is approximately the same rate as current SLR (NJDEP SEB, 2020). The rate of net bed elevation changes in some marsh areas ranged from 1.19 to 6.89 mm/year, and a rough estimate of the mean elevation change rate is 4.0 mm/year, which is nearly the same or slightly greater than the current local SLR rate at the mouth of the Delaware bay (3.53 mm/year for 1919-2019 and 3.71 mm/year for 1919-2024[31]). It should be noted that this scenario of shoreline retreat is unlikely to occur within the next 50 years, and, therefore, the total marsh losses may be over-estimated. Although this hypothetical future shoreline may exaggerate shoreline retreat and bank erosion, the exploration of the impact of marsh loss and SLR on salinity intrusion is worthwhile.

The salt front is only marginally affected by simulated shoreline retreat and bank erosion. With shoreline retreat, the simulated salt front location is slightly farther downstream in comparison with the location simulated without shoreline retreat. The difference attributed to shoreline retreat becomes smaller as SLR increases; with representative (2002) low flow conditions, the maximum salt front location with shoreline retreat was 0.8 miles farther downstream with 1.0 m SLR and 0.2 miles farther downstream with 1.6 m SLR.

These results show that modeling salinity intrusion without representing shoreline retreat and bank erosion is a slightly more conservative approach with respect to the protection of drinking

[30] Shoreline or coastal erosion is a natural process of loss of shoreline sediments. https://oceanservice.noaa.gov/facts/shoreline-armoring.html

[31] The rate of SLR was based on NOAA tide gage data at Lewes DE from 1919 to 2019. The rate has been updated to 3.71 mm/year in 2024 with data up to 2023.

water supplies. The analysis of the sensitivity of model results to near-shore bed elevation helps in further understanding the uncertainty in simulation results.

With shoreline retreat and inland migration of marshes, salinity intrusion distance decreases. The sensitivity simulation results indicate that the impact on salinity intrusion is not significant, and that the maximum SF location is not sensitive to the extent and magnitude of shoreline retreat and bank erosion. Sea level rise is likely to result in shoreline erosion and wetlands migration (Kearny et al., 2002; Schieder et al., 2017). Researchers have used models such as SLAMM (Sea Level Affecting Marches Model) to simulate the dominant processes involved in wetland conversions and shoreline modifications during long-term sea level rise (Grid, et al., 2008).

J.5 Implications of Model Configuration Analysis

Future conditions of the estuary relating to marsh area, marsh characteristics, bathymetry, and shoreline status are uncertain, and such future conditions could influence the impact of SLR on salinity intrusion. The results of simulations using a range of SLR scenarios and model configurations representing these different conditions demonstrate the extent of this influence and, moreover, show that the SW3D model documented by Chen and Shallcross (2025) is appropriately conservative with respect to the protection of public drinking water supplies and that the model can be used for analyzing the impacts of SLR on salinity intrusion in the Delaware Estuary.

APPENDIX K. ANALYSIS OF OTHER POTENTIAL CONDITIONS

Other conditions and assumptions that may affect salinity intrusion along with sea level rise were also evaluated. Examples include changes in salinity from non-tidal sources and the ocean, increased drought severity as a result of climate change, and increased ocean temperature (which affects density-driven circulation). Simulations were performed to assess the effect of these conditions on model results. Supplemental materials are presented in this appendix to support the discussion in Section 6 of the report.

K.1 Salinity from Non-tidal Sources

Future increases in the salinity of freshwater sources will affect salinity and chloride concentrations downstream, primarily in the upper Estuary, where salinity is lower than that of the ocean. Instream monitoring of the non-tidal river over time has shown an increasing trend in salinity and related chloride concentrations. The trend is not unique to the Delaware River, and it is becoming commonplace in areas of the U.S. with significant roadway de-icing activity.

For the Delaware River at Trenton, N.J., chloride measurements are plotted as a time series along with the associate trendline in **Figure K.1-1**. Samples were collected from the Delaware River at the Calhoun Street Bridge in Trenton, NJ, and data were obtained from the National Water Quality Data Portal (NWQDP).[32] Based on the linear regression analysis that was used to calculate the trendline, chloride concentrations are expected to increase by 0.28 mg/l/year. An analysis by the USGS (Murphy, J.C. et al. (2020) demonstrated a similar trend, and the rate of change was 0.27 mg/L/year with data collected from 1944 to 2018.[33]

[32] NWQDP site: https://www.waterqualitydata.us/#within=0.5&lat=40.219698&long=-74.778365&sampleMedia=Water&characteristicName=Chloride&mimeType=csv&dataProfile=resultPhysChem&providers=NWIS&providers=STEWARDS&providers=STORET

[33] USGS water quality trend analysis for chloride at Trenton on the Delaware River: https://nrtwq.usgs.gov/nwqn/#/site/cx_USGS-01463500/graphics

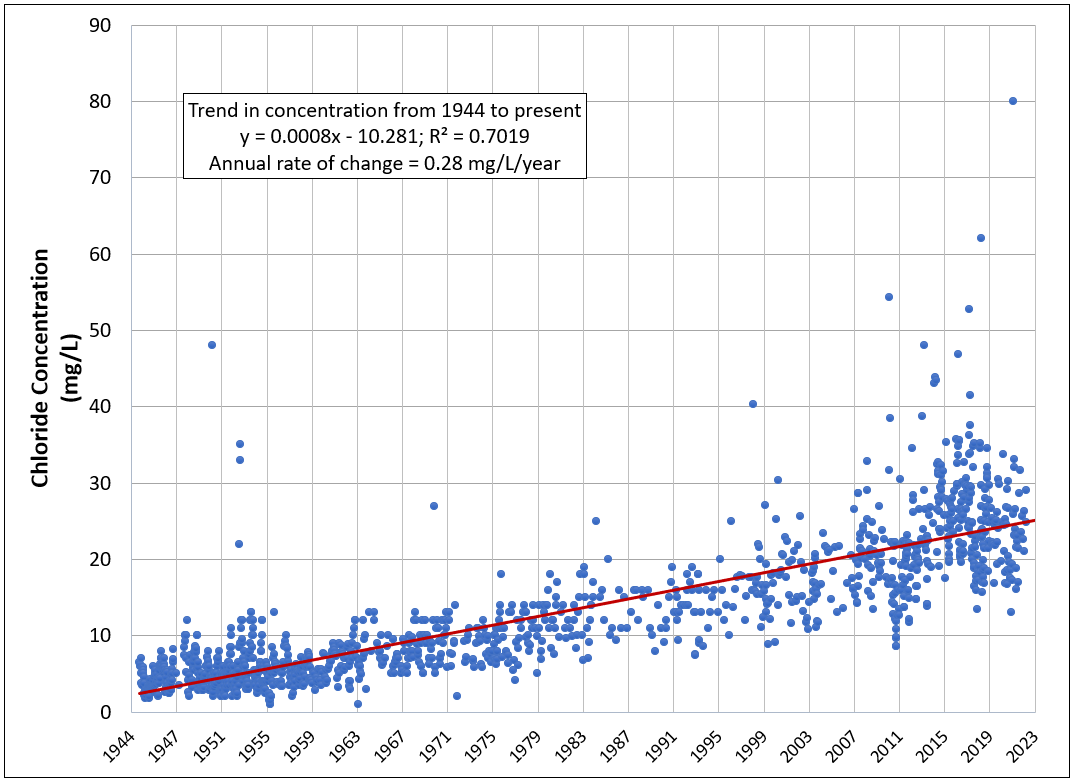

Figure K.1-1. A Chloride concentrations and trend for the Delaware River at Trenton from 1944 through 2022.

Table K.1-1 presents the annual and seasonal trends (as rate of change) in chloride concentrations for the Delaware River.

The year 2060 is the planning horizon for a water availability study under development by DRBC. By 2060, average chloride concentrations are projected to double what they were in 2002. On a seasonal basis, the change is projected to range from 17.1 mg/l to 34.4 mg/l (equivalent to salinity roughly from 0.09 psu to 0.12 psu, respectively). During winter and spring, the chloride concentrations may increase to 2.3 to 2.2 times those of 2002, respectively, whereas the increases during summer and fall are projected to be 1.9 and 1.5 mg/l, respectively. The larger increases earlier in the year are likely the result of de-icing chemicals and flushing in runoff that flows to water bodies after snowfall and rain events. During summer and fall, the increases in chloride concentrations are likely to be the result of other human activities. To assess how increasing non-tidal chloride loading may contribute to future salinity intrusion events, the time-series of chloride concentrations that were used as input to the model (as salinity) was scaled so that the average seasonal concentration of the input data was equivalent to the projected average concentration in 2060.

Table K.1-1. Annual and seasonal trends in chloride concentrations for the Delaware River at Trenton, based on data from 1944-2022, with projection to 2060.

	Rate of Change (mg/L per year)	Chloride Concentration in 2002 (mg/L)	Projected Chloride Concentration in 2060 (mg/L)	Factor of increase
Annual	0.28	17.1	34.4	2.0
Winter	0.34	18.7	40.7	2.2
Spring	0.31	15.5	35.4	2.3
Summer	0.26	17.2	32.9	1.9
Fall	0.25	21.0	32.3	1.5

Another source of salinity is from point sources (PS) discharging to the main stem Delaware River. Values suggested in a report by the Philadelphia Water Department (2020) were applied to the 11 major point source discharges represented in the model (Appendix F, **Table F.1**). Salinity from minor discharges were assigned a constant value of 0.48 psu, and the uncertainty in salinity from these PS discharges has minimal impact on salinity intrusion on the Delaware River mainstem due to the insignificant rates of water discharged to the Delaware River[34].

Two sets of sensitivity simulations were conducted for the representative low flow period:

(1) Sensitivity to increased tributary salinity loads; and

(2) Sensitivity to the temporal variability of point source salinity loads

A representative low flow period of 2002 was selected for these sensitivity tests. During the low-flow period from July to October 2002, the salt front continuously progressed upstream, and the maximum 7-dma salt front location reached RM 89. Simulation results for chloride and salinity are summarized for this low flow period. The year 2002 was one of the drought years during the past century, and the 2002 annual average 90-dma flow ranked in the lowest 12 percent of a 110-year period from 1913 to 2020 (**Figure D.2**).

Results from sensitivity simulations were compared with results of baseline simulation. For the baseline simulation, tributary salinity for the Delaware was set based on daily specific conductance data collected at USGS gage 01463500 on the Delaware River at Trenton in 2002; due to lack of data for 2002, Schuylkill River salinity was set to two times of the salinity observed from the Delaware River at Trenton[35], so that the annual average salinity at the Schuylkill River inflow boundary was specified to be 0.17 psu. PS salinity loads were included.

[34] Based on analysis of data from 2018-2019, 80 percent of the flow from point sources by volume is from the 11 major dischargers.

[35] See scale factor used in specification of the tributary salinity boundary conditions in Section 3, Table 3.3-8 in the SM3D model calibration report (Chen and Shallcross, 2025).

K.1.1 Sensitivity to Tributary Salinity Loads

Salt Front

During the representative low flow period of one year, the simulated salt front progresses upstream to a maximum in late September, as shown in **Figure K.1-2**. The two solid lines at the bottom of the graph show the effect of increasing tributary salinity loads without sea level rise. By increasing the tributary salinity in the simulations, the maximum salt front is roughly 1 mile farther upstream (RM 91.52 vs RM 90.7). The top four lines on the graph in **Figure K.1-2** show that with sea level rise, the effect of increasing tributary salinity loads is to move the maximum salt front as much as 0.9 miles farther upstream, which is much less than the effect of SLR by itself. The simulated maximum salt front locations are presented in **Figure K.1-3**, which show a consistent increase in the salt front location with sea level rise. The maximum salt front locations for these results are presented in **Table K.1-2**. These results indicate that sea level rise has a much larger impact on the salt front than the projected increase in salinity from non-tidal sources.

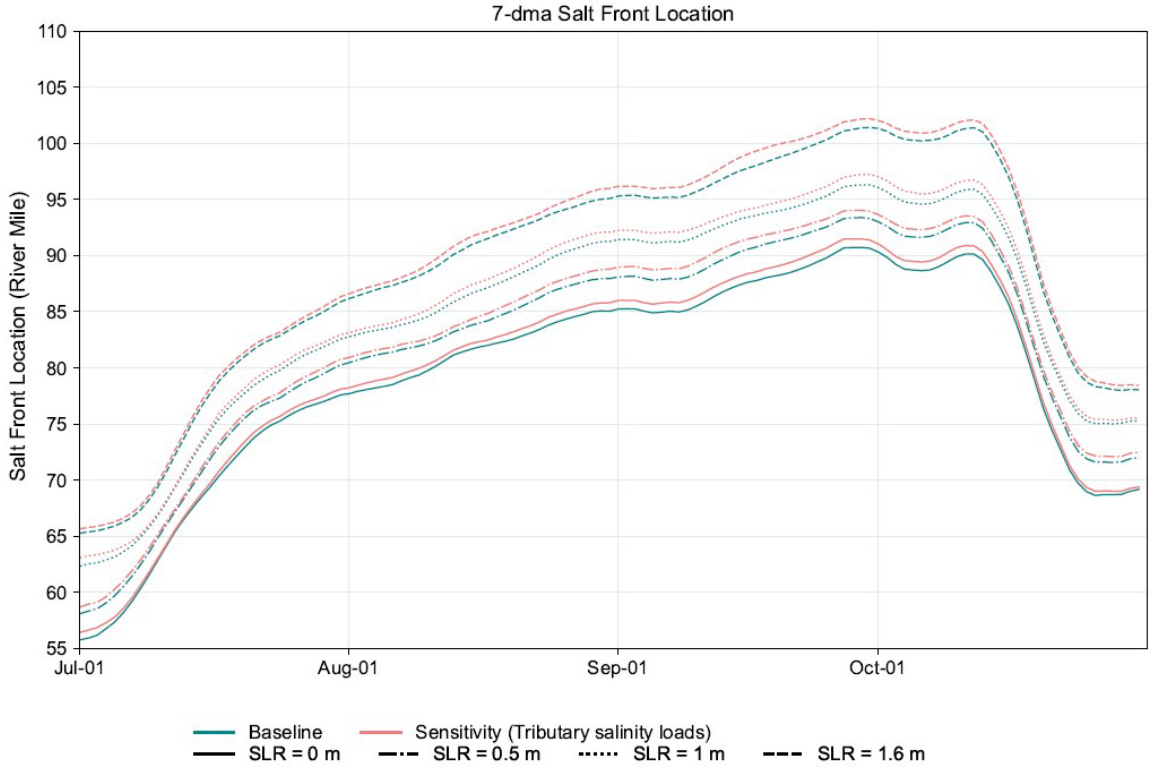

Figure K. 1-2. Simulated time series of salt front locations during a representative low flow condition for three increments of SLR, with and without increased tributary salinity loads.

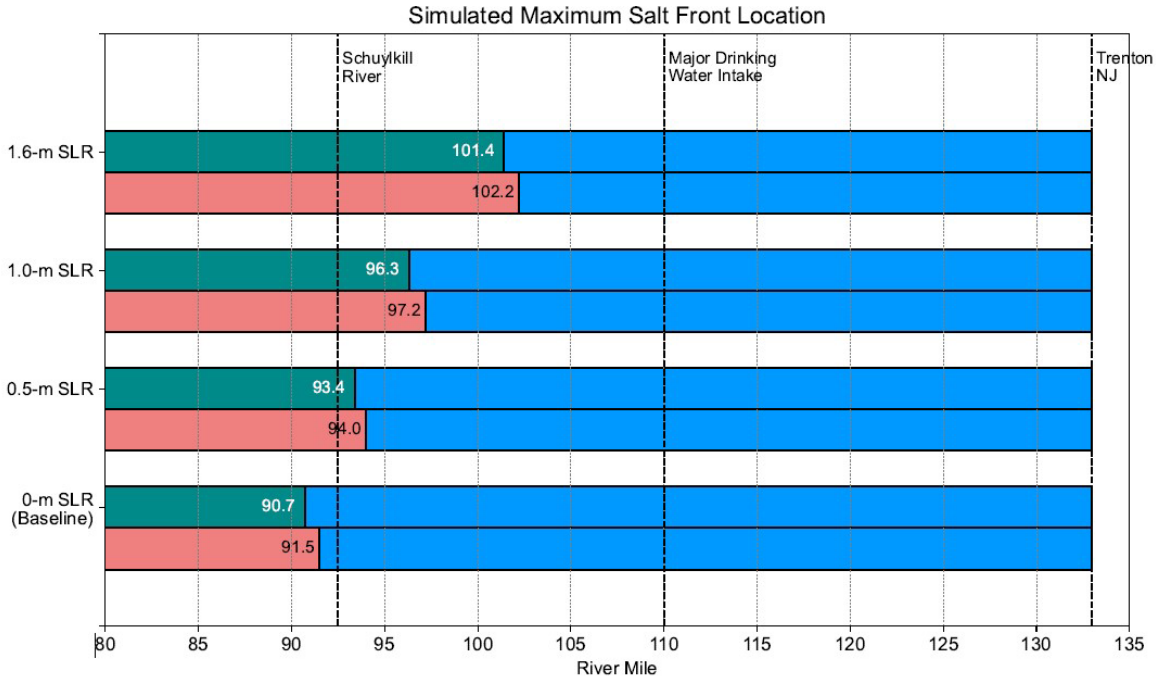

Note: The green bars show results of simulations using 2002 flows that represent a representative low flow condition. The orange bars represent the results from the simulations with increased tributary salinity loads, and the differences in the lengths of the green and orange bars quantify the impact of the increased tributary salinity loads on salinity intrusion.

Figure K. 1-3. Simulated maximum salt front locations during a representative low flow condition for three increments of SLR, with and without increased tributary salinity loads.

Table K.1-2. Simulated maximum salt front location during a representative low-flow condition for three increments of SLR, with and without increased tributary salinity loads.

Sea Level Rise	Maximum Salt Front Location Under Baseline Representative Low Flow Condition (River Mile)	Maximum Salt Front Location with Increased Tributary Salinity Loads (River Mile)	Difference (Miles)
0 m	90.7	91.5	0.8
0.5 m	93.4	94.0	0.6
1.0 m	96.3	97.2	0.9
1.6 m	101.4	102.2	0.8

Chloride Concentrations

The range of simulated 30-dma chloride concentrations at four locations are presented in **Figure K.1-4**, which shows that the effect of increased salinity loads from tributaries is smaller than the effect of SLR. The simulated maximum 30-dma chloride concentrations at RM 98 are presented in **Table K.1-3**. With the increased tributary salinity loads, the maximum 30-dma chloride concentration at RM 98 reached 83, 189, and 363 mg/L with SLR of 0-, 1.0-, and 1.6 m, respectively. These results indicate that the 180 mg/L water quality standard at this location would likely be exceeded at least occasionally with SLR of 1.0 m or more.

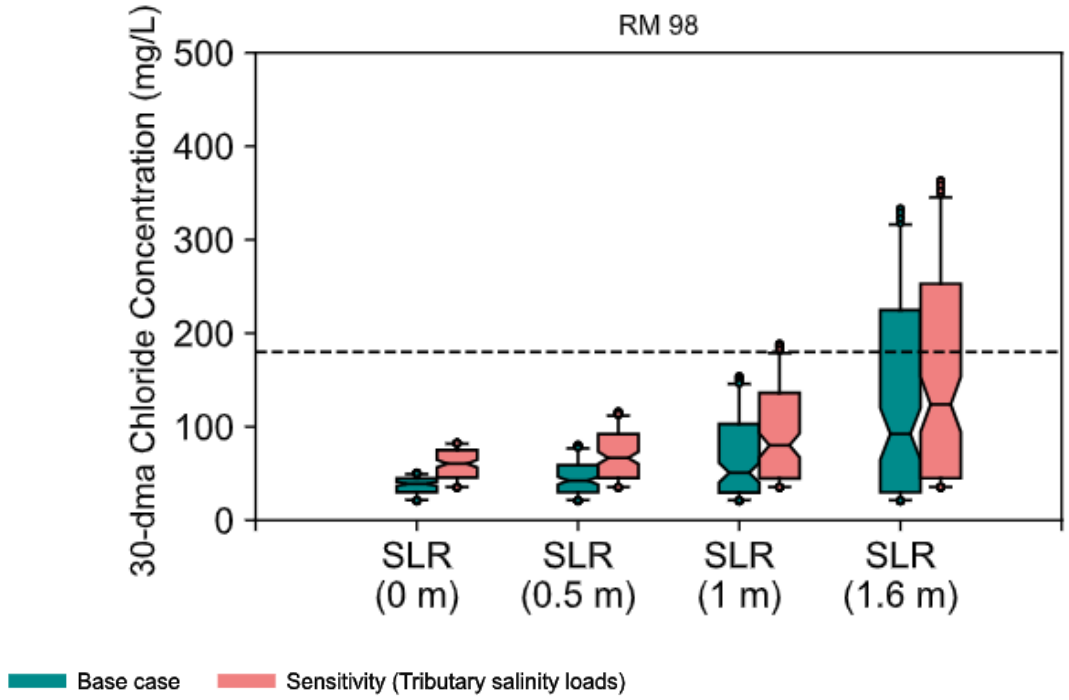

Note: Simulations used flows of a representative four-month low-flow period (July through October 2002).

Figure K.1-4. Range of the maximum 30-dma chloride concentration at RM 98 during a representative low-flow condition for three increments of SLR, with and without increased tributary salinity loads.

Table K.1-3. Simulated maximum 30-dma chloride concentration at RM 98, during a representative low flow condition for three increments of SLR, with and without increased tributary salinity loads.

	Location	Camden
	River Mile	98
SLR = 0 m	Original Loads (mg/L)	51
	Increased Tributary Loads (mg/L)	83
	Percent Difference (%)	63
SLR = 0.5 m	Original Loads (mg/L)	81
	Increased Tributary Loads (mg/L)	116
	Percent Difference (%)	43
SLR = 1 m	Original Loads (mg/L)	154
	Increased Tributary Loads (mg/L)	189
	Percent Difference (%)	23
SLR = 1.6 m	Original Loads (mg/L)	333
	Increased Tributary Loads (mg/L)	363
	Percent Difference (%)	9

Salinity

The simulated range of daily depth-averaged salinity at eight selected locations during a representative low flow condition is presented in this section (**Figures K.1-5, K.1-6**). **Table K.1-4** presents simulated maximum daily-maximum salinity at selected locations during a representative low flow condition for four increments of SLR, with and without increased tributary salinity loads. Salinity increase with SLR is evident at each location. Noticeable increases in simulated salinity due to increased tributary salinity loads are found at locations located farther upstream, where the background salinity level is slightly elevated. Minimum change due to increased tributary salinity loads is evident at locations downstream from Chester, where the ocean saltwater makes a larger contribution to the overall salinity. With 0 m SLR, the maximum salt front location is at RM 91.5 with the increased tributary loads. The maximum daily depth-averaged salinity at the Ben Franklin Bridge (RM 100) increases by 37% from 0.19 to 0.26 psu. The increase in maximum salinity at this location reflects the elevated background level of the salinity caused by increasing the tributary loads. Similarly, at RM 110, the background level of the salinity increase from 0.12 to 0.21 psu. With SLR, the relative percent increase in maximum salinity decreases. For example, with a 1 meter sea-level rise (SLR), the maximum salinity at RM 100 increases from 0.4 to 0.46 psu, representing a 15% rise. This increase is attributed to higher salinity loads from tributaries, though the effect was partly offset by the greater water volume in the upper tidal river, which resulted from the sea-level rise. At and above RM 98 (Camden), and for all values of SLR, the simulated maximum salinity is less than 1 psu.

The maximum depth-averaged salinity by RM with the original and increased tributary salinity loads are presented in **Figure K.1-7** for 0 m, 0.5 m, 1.0 m and 1.6 m SLR. The differences from the baseline for 0.5 m, 1.0 m and 1.6 m SLR-are shown in **Figure K.1-8**. The maximum salinity differences for all cases are with reference to the same base case, which uses the original tributary salinity loads and 0 m SLR. Impacts due to SLR are evident in the increase of the salinity maximum, and the most impacted area is between RM 75 and RM 85. The maximum increase in the maximum salinity ranges from 0.8 to 2.5 psu for the 0.5 m to 1.6 m SLR scenarios, respectively. A noticeable increase in the salinity maximum with 0.5 m SLR along the river is indicated by a gap of about 0.1 psu between the solid and dotted purple lines. As SLR increases to 1 meter and above, the differences caused by the increased tributary salinity loads become negligible downstream from the Delaware Memorial Bridge, and are less than 0.1 psu for the upper portion of the Estuary upstream from Chester. With 1 m SLR and above, the maximum depth-averaged salinity in the lower estuary downstream from the Delaware Memorial Bridge with the increased tributary salinity loads is slightly lower than the base case, which indicates that some change occurs in the vertical salinity stratification that alters the depth-averaged values.

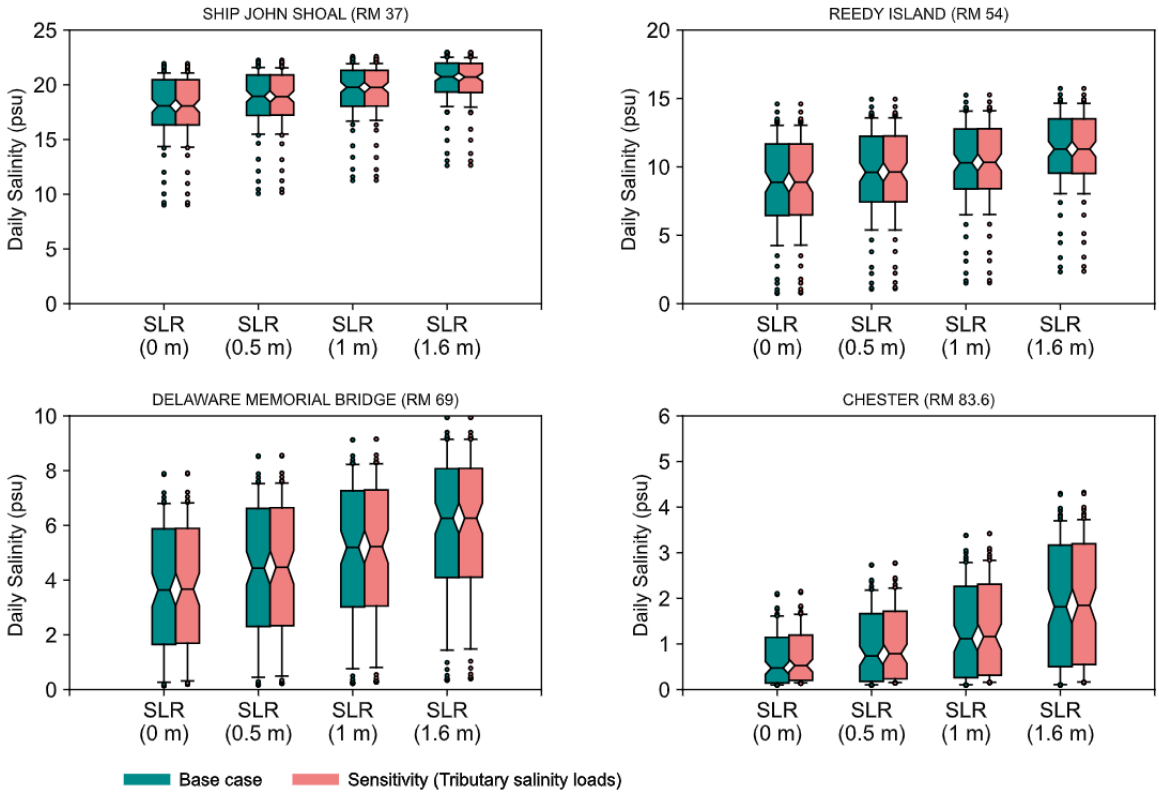

Note: Simulations used flows of a representative four-month low-flow period (July through October 2002).

Figure K.1-5. Range of the simulated seasonal daily-maximum salinity during a representative low-flow condition for three increments of SLR, with and without increased tributary salinity loads at four locations downstream from the Schuylkill River confluence with the Delaware River.

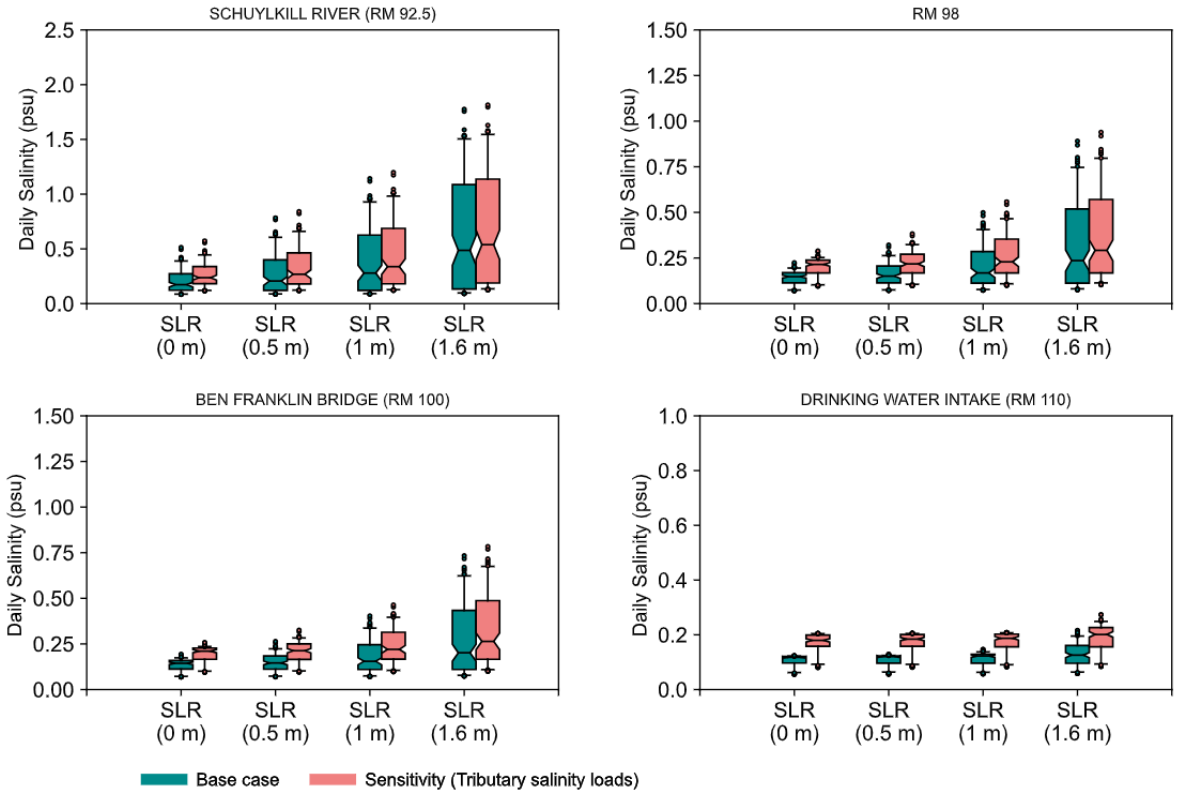

Note: Simulations used flows of a representative four-month low-flow period (July through October 2002).

Figure K.1-6. Range of the simulated seasonal daily-maximum salinity during a representative low-flow condition for three increments of SLR, with and without increased tributary salinity loads at four locations upstream from the Schuylkill River Confluence with the Delaware River.

Table K.1-4. Simulated maximum daily-maximum salinity at selected locations, during a representative low flow condition for four increments of SLR, with and without increased tributary salinity loads.

Location		SHIP JOHN SHOAL	REEDY ISLAND	DELA-WARE MEMO-RIAL BRIDGE	CHESTER	SCHUYL-KILL RIVER	Camden	BEN FRANKLIN BRIDGE	DRINKING WATER INTAKE
River Mile		**37**	**54**	**69**	**83.6**	**92.5**	**98**	**100**	**110**
SLR = 0 m	Original Loads (mg/L)	21.94	14.6	7.9	2.11	0.51	0.22	0.19	0.12
	Increased Tributary Loads (mg/L)	21.94	14.6	7.91	2.15	0.57	0.29	0.26	0.21
	Percent Diff. (%)	0	0	0	2	12	32	37	75
SLR = 0.5 m	Original Loads (mg/L)	22.25	14.94	8.54	2.74	0.78	0.32	0.26	0.13
	Increased Tributary Loads (mg/L)	22.25	14.95	8.56	2.78	0.84	0.38	0.33	0.21
	Percent Diff. (%)	0	0	0	1	8	19	27	62
SLR = 1 m	Original Loads (mg/L)	22.59	15.24	9.13	3.38	1.14	0.5	0.4	0.15
	Increased Tributary Loads (mg/L)	22.6	15.27	9.15	3.43	1.2	0.56	0.46	0.21
	Percent Diff. (%)	0	0	0	1	5	12	15	40
SLR = 1.6 m	Original Loads (mg/L)	22.97	15.73	9.95	4.3	1.78	0.89	0.73	0.22
	Increased Tributary Loads (mg/L)	22.96	15.73	9.95	4.33	1.82	0.94	0.78	0.27
	Percent Diff. (%)	0	0	0	1	2	6	7	23

Note: Simulations used flows of a representative four-month low-flow period (July through October 2002).

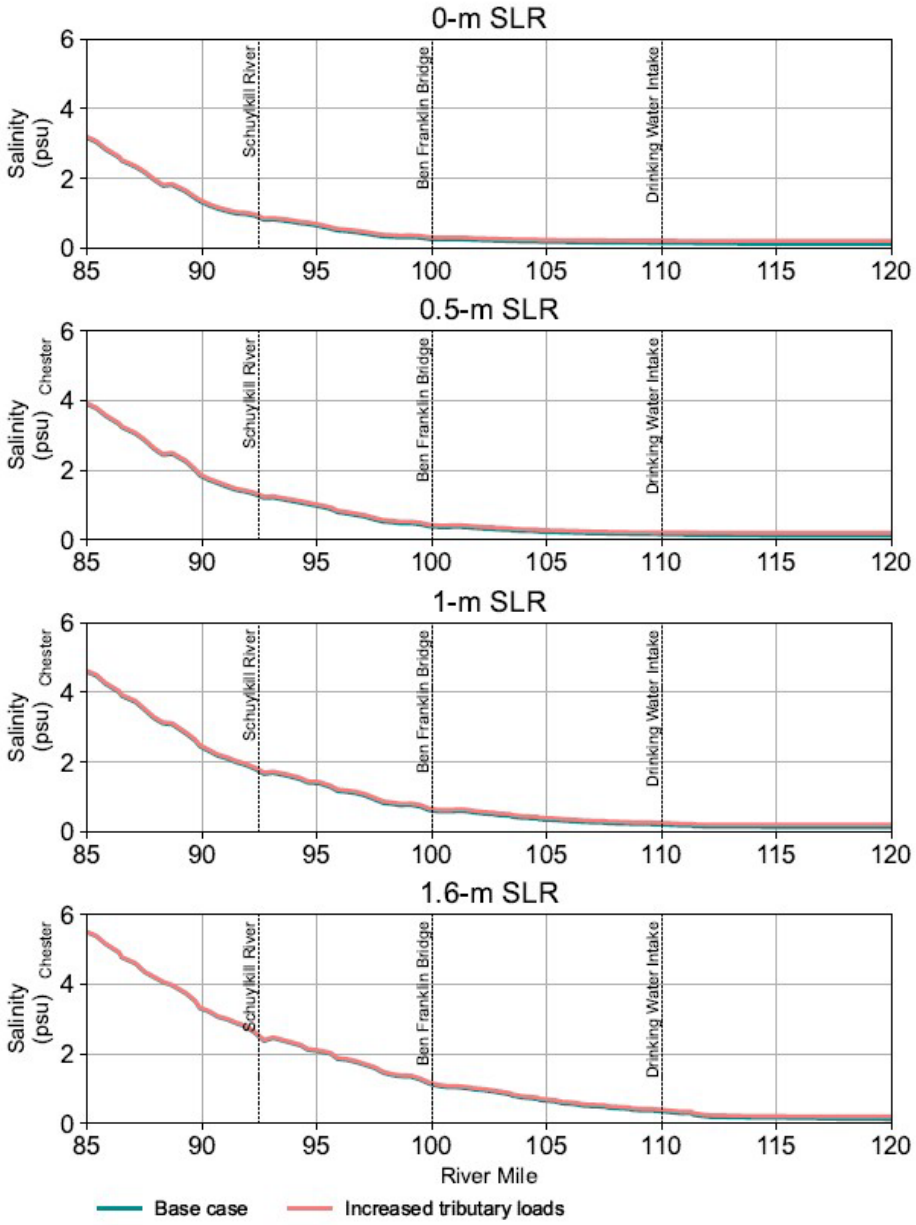

Note: Simulations used flows of a representative four-month low-flow period (July through October 2002).

Figure K.1-7. Simulated along-channel maximum depth-averaged salinity with and without increased tributary salinity loads.

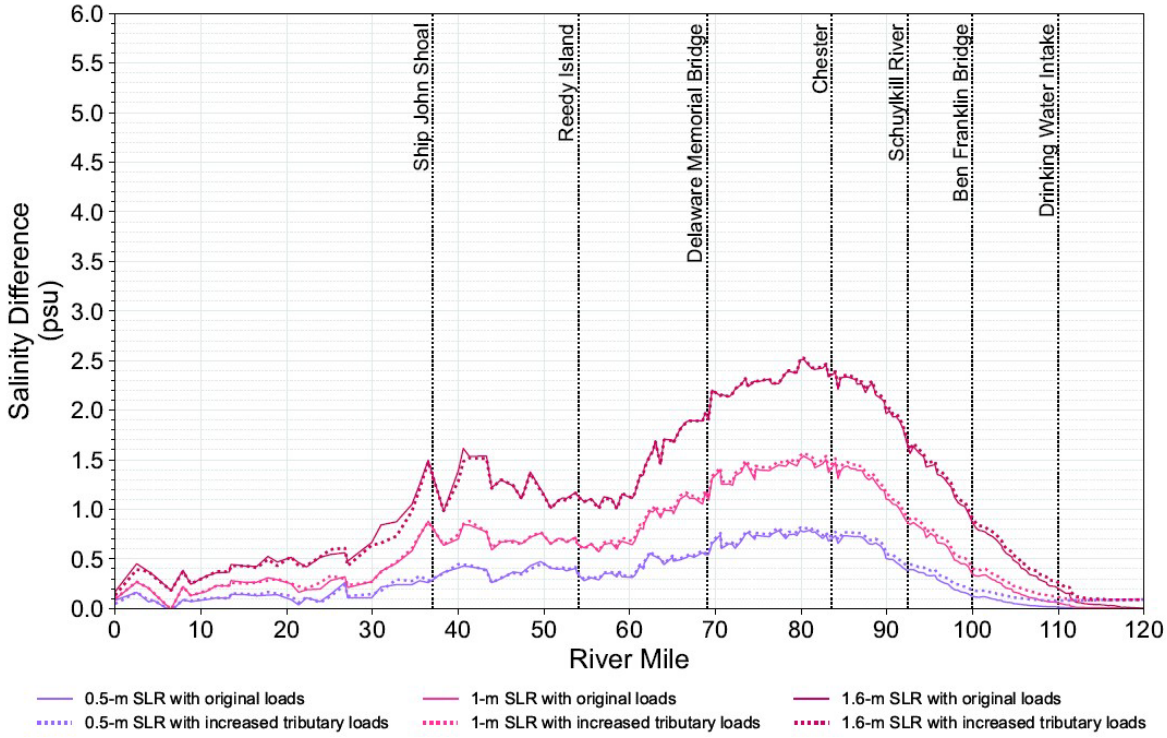

Note: Simulations used flows of a representative four-month low-flow period (July through October 2002).

Figure K.1-8. Simulated change in along-channel maximum depth-averaged salinity with SLR, with and without increased tributary salinity loads.

K.1.2 Sensitivity to Point Source Salinity Loads

Salt Front

Limited data are available to specify the point source salinity boundary conditions, and in all simulations performed for this study, the PS salinity loads are represented as constant over the course of the year. The PS salinity loads are known to vary with changing conditions, and so an analysis was conducted to determine the sensitivity of simulated saltwater intrusion to this variability. The tributary salinity loads are kept as the original loads in these simulations, so that the effect of PS salinity load variability alone can be examined. The basis for representing PS salinity load variability is explained in Appendix F.

Simulated salt front locations for SLR simulations in which point source (PS) salinity loads are represented as either constant or variable on a monthly basis are presented in **Figure K.1-9**, **K.1-10**, and **Table K.1-5**. The figures show that variability of PS salinity loads has essentially no effect on the simulated SF location through the simulated year.

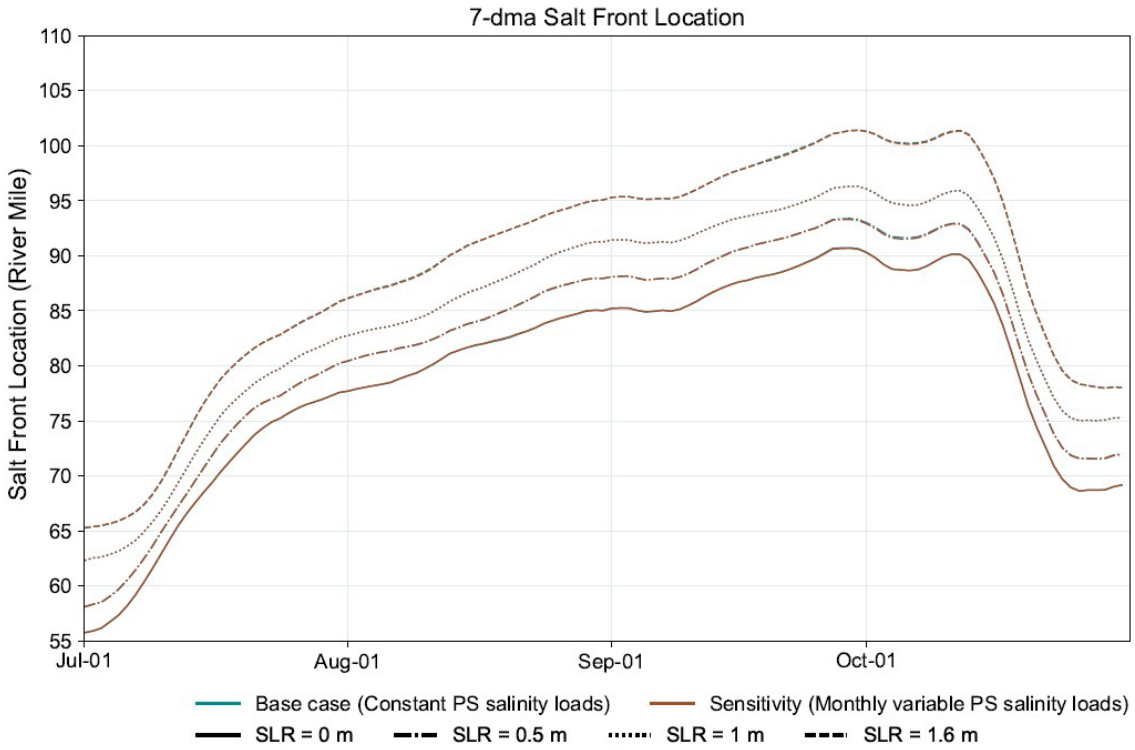

Figure K.1-9 Simulated time series of salt front locations during a representative low flow condition, for three increments of SLR, with and without point source salinity load variability.

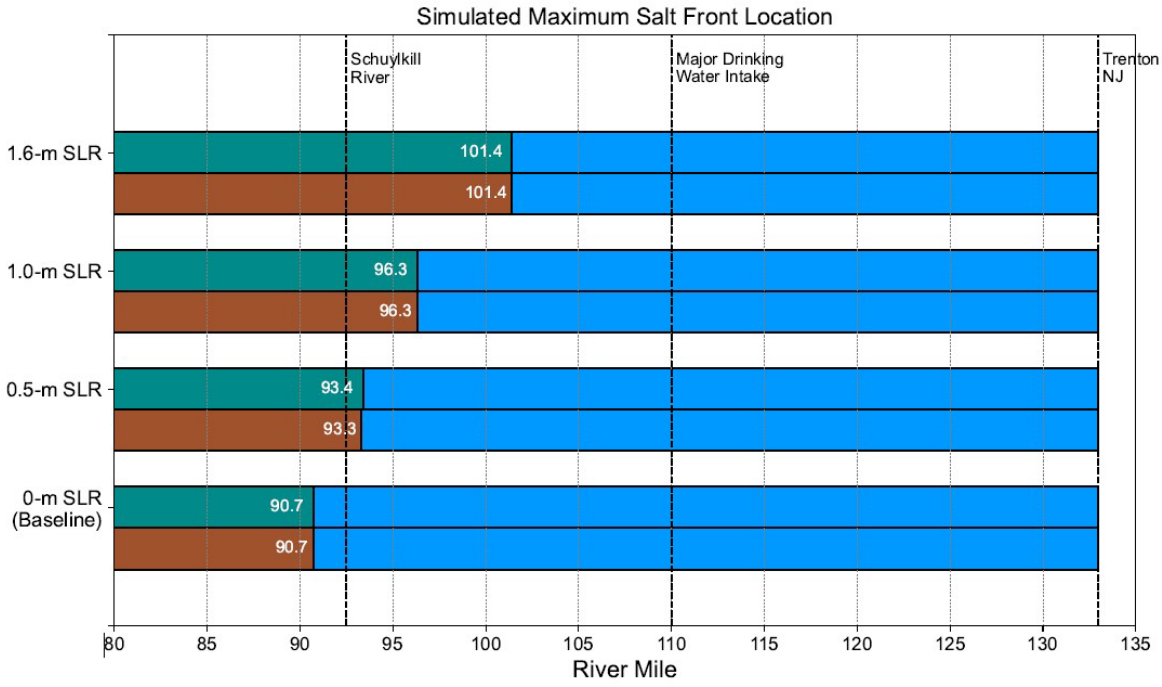

Note: The green bars represent the results using 2002 flows that represent a representative low flow condition and with constant PS salinity loads. The dark brown bars represent the results from the simulations with PS salinity load variability included. The difference in the length of the green and brown bars quantifies the impact of PS salinity load variability.

Figure K. 1-10 Simulated maximum salt front locations during a representative low flow condition for three increments of SLR, with and without point source salinity load variability.

Table K. 1-5. Simulated maximum salt front locations during a representative low-flow condition for three increments of SLR, with and without point source salinity load variability.

Sea Level Rise (m)	Maximum Salt Front Location Under a Representative Low Flow Condition and Constant Point Source Salinity Loads (River Mile)	Maximum Salt Front Location with Monthly-vairable Point Source Salinity Loads (River Mile)	Difference (River Miles)
0	90.7	90.7	0.0
0.5	93.4	93.3	-0.1
1	96.3	96.3	0.0
1.6	101.4	101.4	0.0

Chloride Concentrations

Simulated 30-dma chloride concentrations for the simulations described above are presented in **Figure K.1-11** and **Table K. 1-6**. The 30-dma chloride concentrations at RM 98 for the representative low flow condition with constant and variable PS salinity loads are nearly identical. These results indicate that sea level rise has a much greater impact on the 30-dma 180mg/L chloride concentration than point source salinity variability.

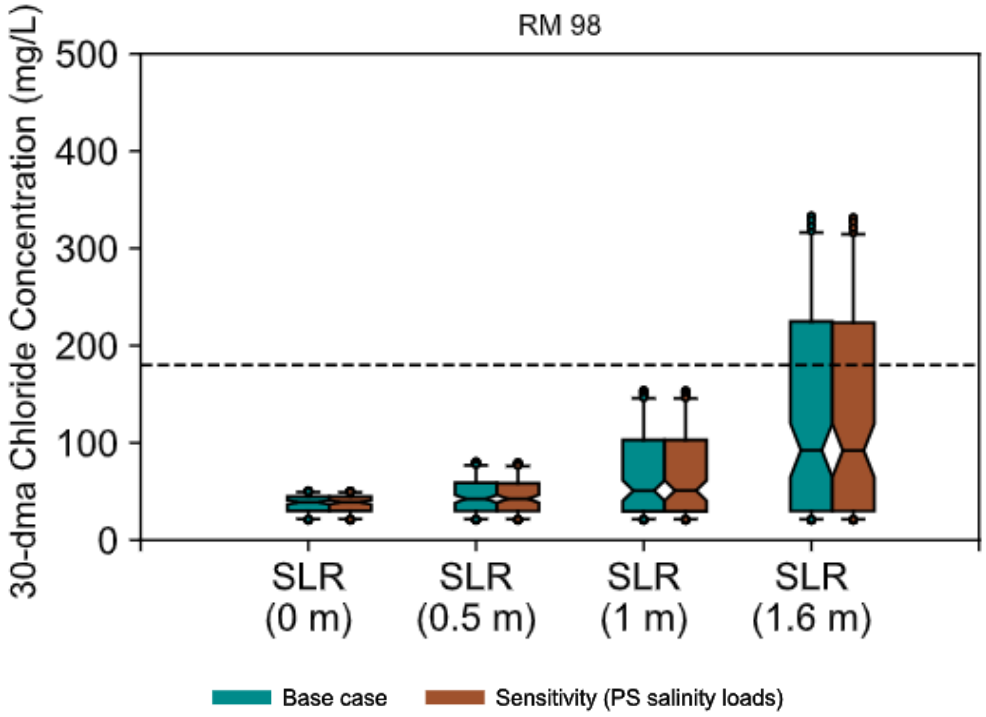

Note: Simulations used flows of a representative four-month low-flow period (July through October 2002).

Figure K. 1-10. Range of the simulated 30-dma chloride concentration during a representative low flow condition for three increments of SLR, with and without point source salinity load variability.

Table K.1-6. Simulated maximum 30-dma chloride concentrations at selected locations during a representative low flow condition for three increments of SLR, with and without point source salinity load variability.

	Location	Camden
	River Mile	98
SLR = 0 m	Original Loads (mg/L)	51
	Point Source Loads Included (mg/L)	50
	Percent Difference (%)	-2
SLR = 0.5 m	Original Loads (mg/L)	81
	Point Source Loads Included (mg/L)	80
	Percent Difference (%)	-1
SLR = 1 m	Original Loads (mg/L)	154
	Point Source Loads Included (mg/L)	154
	Percent Difference (%)	0
SLR = 1.6 m	Original Loads (mg/L)	333
	Point Source Loads Included (mg/L)	331
	Percent Difference (%)	-1

Salinity

Simulated salinity at eight selected locations during a representative low flow condition for the simulations described above are presented in this section (**Figure K.1-12**, **K.1-13**, and **Table K.1-7**). As for the salt front locations and chloride concentrations, the salinity at the 8 locations with and without PS salinity variability are nearly identical.

The maximum depth-averaged salinities by RM with and without PS salinity load variability are presented in **Figure K.1-14** for 0 m, 0.5 m, 1.0 m, and 1.6 m-SLR. The differences from the base-case for 0.5 m, 1.0 m and 1.6 m SLR are shown in **Figure K.1-15**. The maximum salinity differences for all cases are referenced to the same base case with 0 m SLR and constant PS salinity loads. Impacts due to SLR are evident in the increase in the maximum salinity, and the most impacted area is between RM 75 and 85. A slight decrease in the maximum salinity with 0.5 m SLR occurs along the river between RM 38 and 40 and is indicated by a gap of 0.1 psu between the solid and dotted purple lines in **Figure K.1-15**. As SLR increases to 1 meter and above, the differences resulting from PS salinity load variability are slight downstream from Reedy Island, and the differences are negligible for the portion of the estuary upstream from Reedy Island.

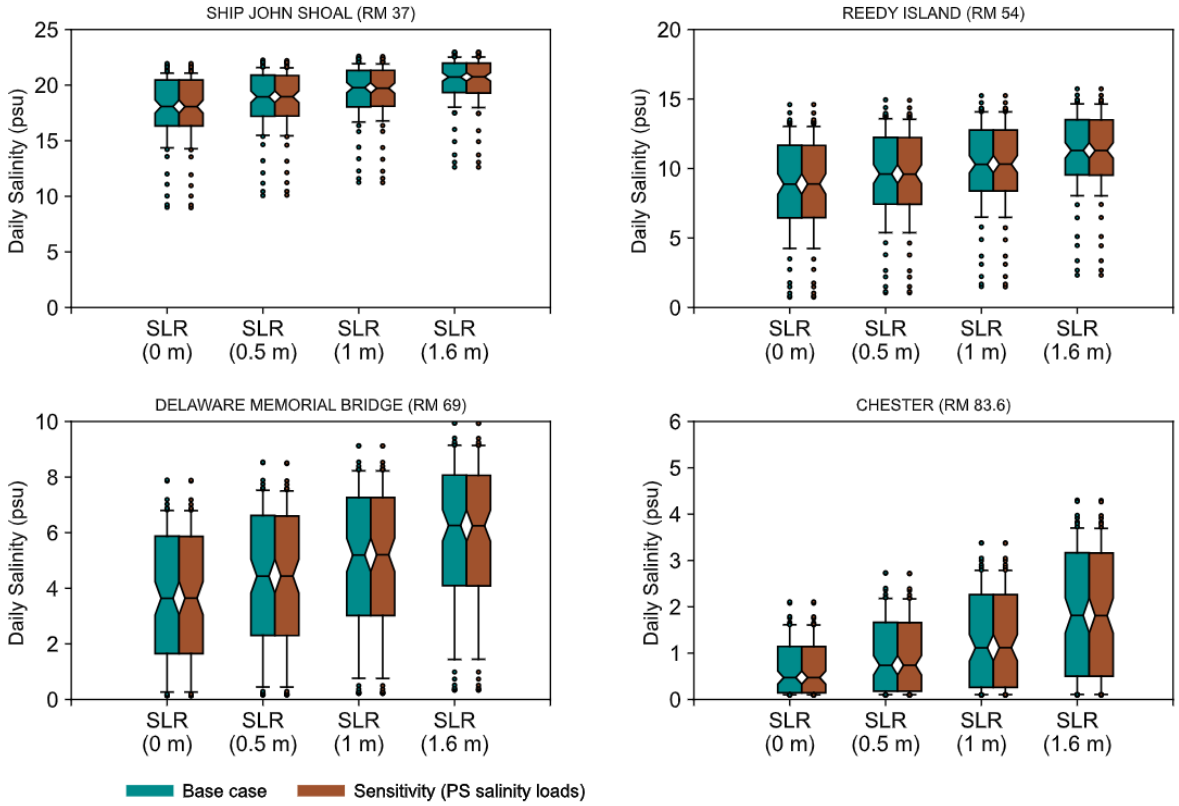

Note: Simulations used flows of a representative four-month low-flow period (July through October 2002).

Figure K.1-12. Range of simulated seasonal daily-maximum salinity during a representative low-flow condition for three increments of SLR, with and without point source salinity load variability at four locations downstream from Chester.

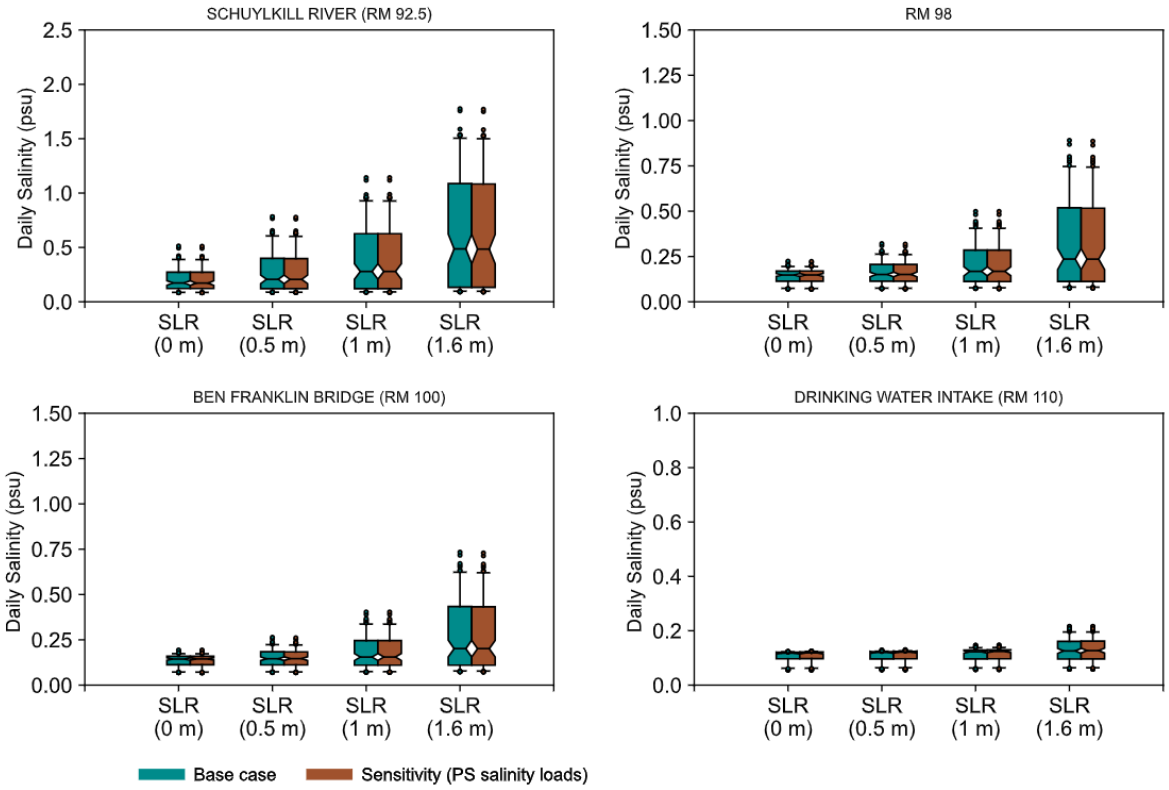

Note: Simulations used flows of a representative four-month low-flow period (July through October 2002).

Figure K.1-13. Range of simulated seasonal daily-maximum salinity during a representative low-flow condition for three increments of SLR, with and without point source salinity load variability at four locations upstream from the Schuylkill River confluence.

Table K. 1-7. Simulated seasonal maximum daily-maximum salinity at selected locations, during a representative low flow condition for three increments of SLR, with and without point source salinity load variability.

Location		SHIP JOHN SHOAL	REEDY ISLAND	DELAWARE MEMORIAL BRIDGE	CHESTER	SCHUYL-KILL RIVER	Camden	BEN FRANKLIN BRIDGE	DRINKING WATER INTAKE
River Mile		**37**	**54**	**69**	**83.6**	**92.5**	**98**	**100**	**110**
SLR = 0 m	Original Loads (mg/L)	21.94	14.6	7.9	2.11	0.51	0.22	0.19	0.12
	Monthly variable Loads (mg/L)	21.94	14.61	7.89	2.11	0.51	0.22	0.19	0.13
	Percent Diff. (%)	0.0	0.1	-0.1	0.0	0.0	0.0	0.0	8.3
SLR = 0.5 m	Original Loads (mg/L)	22.25	14.94	8.54	2.74	0.78	0.32	0.26	0.13
	Monthly variable Loads (mg/L)	22.22	14.92	8.51	2.72	0.78	0.32	0.26	0.13
	Percent Diff. (%)	-0.1	-0.1	-0.4	-0.7	0.0	0.0	0.0	0.0
SLR = 1 m	Original Loads (mg/L)	22.59	15.24	9.13	3.38	1.14	0.5	0.4	0.15
	Monthly variable Loads (mg/L)	22.58	15.25	9.12	3.38	1.14	0.5	0.4	0.15
	Percent Diff. (%)	0.0	0.1	-0.1	0.0	0.0	0.0	0.0	0.0
SLR = 1.6 m	Original Loads (mg/L)	22.97	15.73	9.95	4.3	1.78	0.89	0.73	0.22
	Monthly variable Loads (mg/L)	22.96	15.73	9.94	4.3	1.77	0.89	0.73	0.22
	Percent Diff. (%)	0.0	0.0	-0.1	0.0	-0.6	0.0	0.0	0.0

Note: Simulations used flows of a representative four-month low-flow period (July through October 2002).

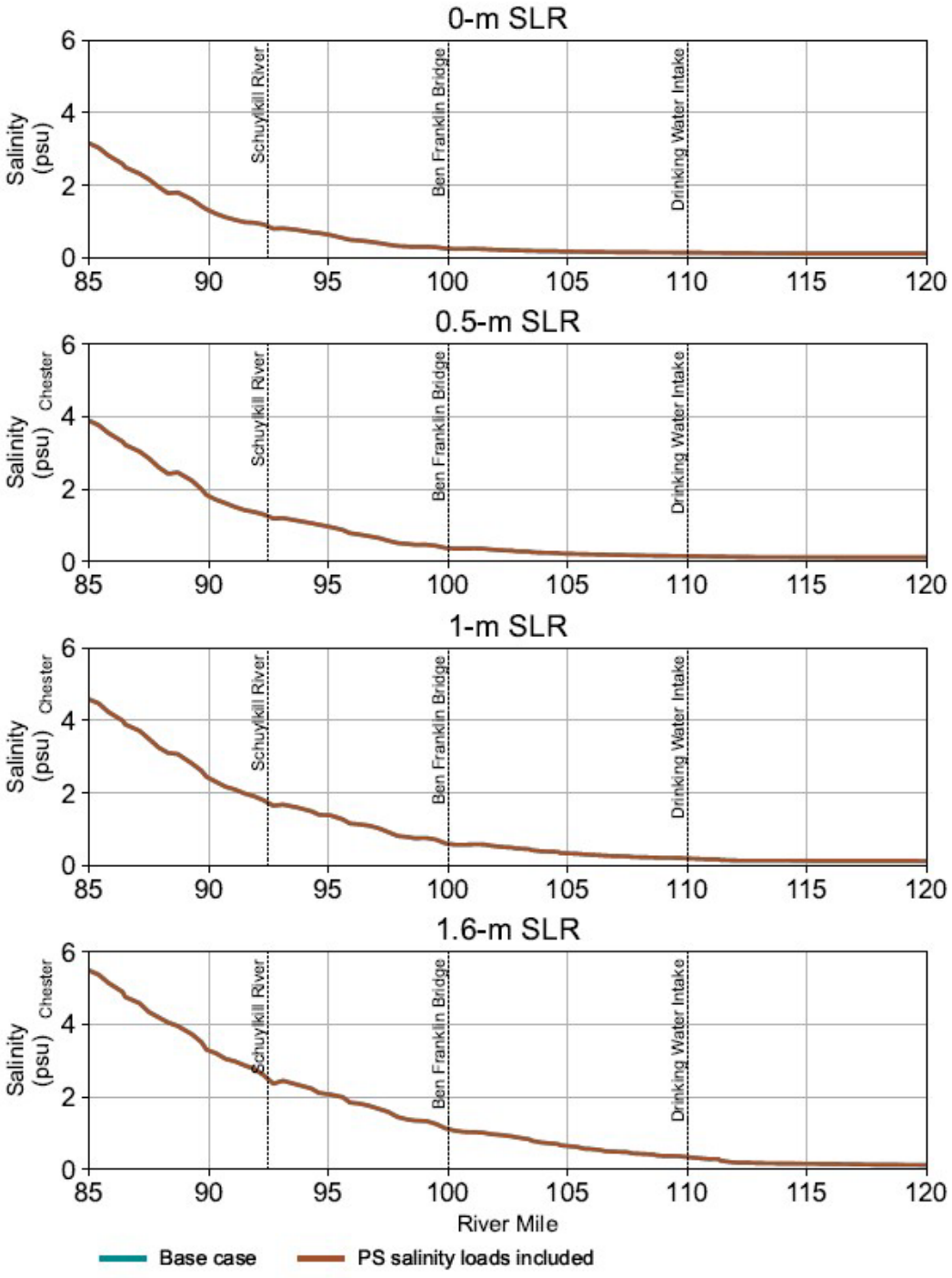

Note: Simulations used flows of a representative four-month low-flow period (July through October 2002).

Figure K.1-14. Simulated along-channel maximum depth-averaged salinity with and without PS salinity load variability.

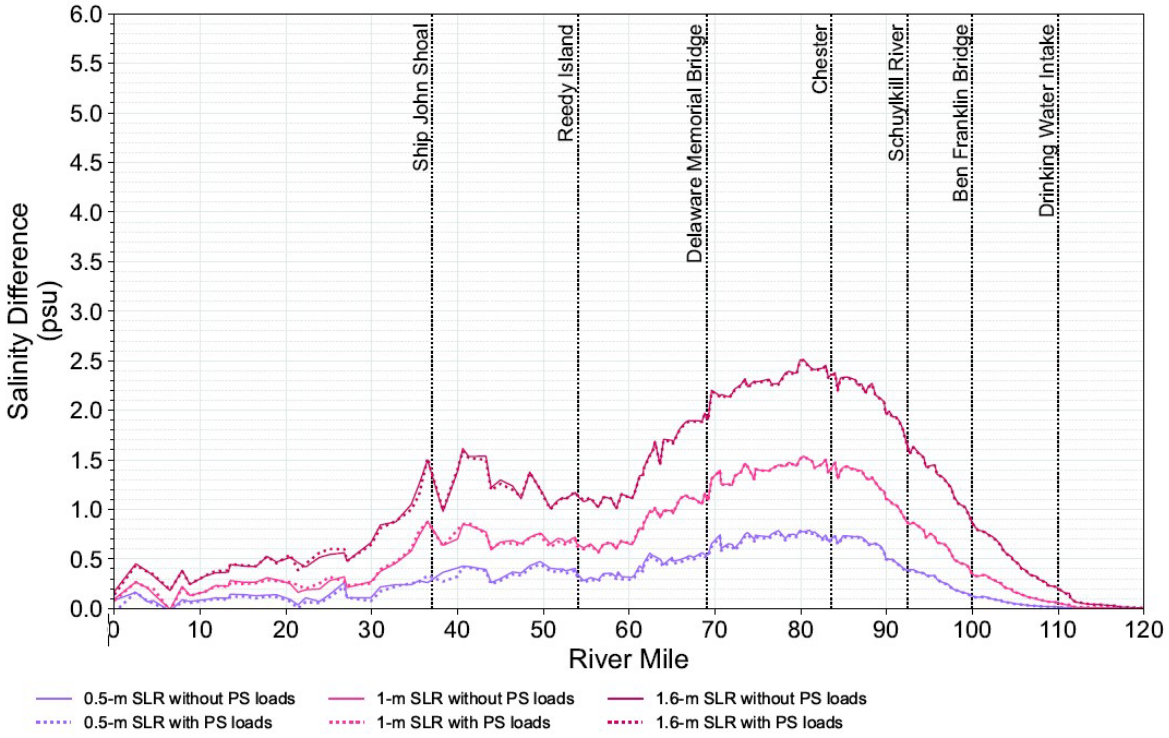

Note: Simulations used flows of a representative four-month low-flow period (July through October 2002).

Figure K.1-15. Simulated change in along-channel maximum depth-averaged salinity with SLR, with and without PS salinity loads.

K.2 Increased Drought Severity

This section provides supplemental information for Section 6.2 of the report.

Table K.1-8 contains the historical minimum monthly flows for the Delaware and Schuylkill Rivers and the year in which they occurred. For eight months, the minimum monthly flow for both rivers did not occur during the same year. During the 1960s drought, the only year and month in which the minimum monthly flow for both rivers was coincidence was June of 1965. Except for May and June, the combined minimum Delaware and Schuylkill River flows were at least six (6) percent lower than flow measured in 1965. Using the minimum monthly flow for each river to approximate a more severe drought condition, the accumulated combined flows from the Delaware and Schuylkill Rivers are lower than those leading up to previous salinity intrusion events. Based on the values in **Table K.2-1**, the combined inflows to the estuary are 62 percent lower than those measured in 1965. The flows for May and June are at least 98 percent of the flows in 1965, so these flows were adjusted to be 95 percent of (5 percent less than) the lowest observed flow, so that the drought condition would be more severe. With this adjustment, the alternative flow record was considered acceptable for a sensitivity simulation of a more severe drought condition. Specification of inflow setup is discussed the Section 6.2.

Table K.2-1. Freshwater inflows used to approximate a more severe drought in comparison with 1965 flows. Flows for the blue-highlighted months are further adjusted to increase the drought severity.

	Constructed Combined Flows for Drought Severity Simulation													
	Minimum Observed Average Monthly Flow and Year by River													
Month	Year of Minimum Delaware Flow	Minimum Delaware Flow (cfs)	Year of Minimum Schuylkill Flow	Minimum Schuylkill Flow (cfs)	Combined Minimum Delaware and Minimum Schuylkill Flows (cfs)	Combined Delaware and Schuylkill River Flows in 1965 (cfs)	Drought Severity Flows as a Percentage of 1965 Flows (cfs)	Monthly Scaled Trenton Flow with FO (cfs)	Monthly Scaled Trenton Flow without FO (cfs)	Monthly Scaled Sk.R. Flow (cfs)	Monthly Sum of Scaled Total Flow without FO (cfs)	Monthly Sum of Scaled Total Flow with FO (cfs)	Drought Severity Flows without FO as aPercentage of 1965 Flows (cfs)	Drought Severity Flows with FO as a Percentage of 1965 Flows (cfs)
(1)	(2)	(3)	(4)	(5)	(6)	(7)	(8)	(9)	(10)	(11)	(12)	(13)	(14)	(15)
January	1981	2,539	1981	340	2,879	6,232	46%	2,651	2,274	590	2,864	3,241	46%	52%
February	1920	3,500	1934	647	4,147	16,048	26%	3,654	3,148	1,013	4,161	4,668	26%	29%
March	1981	7,715	2009	1305	9,020	11,439	79%	7,140	7,140	1,886	9,026	9,026	79%	79%
April	2012	6,597	1985	1237	7,834	11,435	69%	6,784	6,784	1,099	7,883	7,883	69%	69%
May*	1995	5,074	1965	693	5,767	5,902	98%	4,954	4,954	654	5,608	5,608	95%	95%
June*	1965	2,572	1965	261	2,833	2,833	100%	2,810	2,446	247	2,693	3,057	95%	108%
July	1965	1,548	1966	116	1,664	1,837	91%	2,500	1,409	261	1,670	2,761	91%	150%
August	1965	1,808	1966	140	1,948	2,062	94%	2,500	1,700	237	1,937	2,737	94%	133%
September	1932	1,762	1932	117	1,879	2,298	82%	2,500	1,711	171	1,882	2,671	82%	116%
October	1941	1,632	1941	89	1,721	3,917	44%	2,500	1,531	192	1,722	2,692	44%	69%
November	1914	1,868	1931	223	2,091	2,889	72%	2,612	1,912	166	2,077	2,778	72%	96%
December	1922	2,037	1980	444	2,481	5,488	45%	2,612	2,268	200	2,468	2,811	45%	51%
Annual Average					3,685	5,962	62%	3,601	3,106	557	3,666	4,161	70%	87%

(*) For May and June, the combined historical minimum monthly flows were greater than 95 percent of the monthly flow from 1965. To increase the drought severity for these months, the combined monthly inflows were adjusted to be 95% of the historical combined minimum monthly flow.

K.2.1. Simulations with 1965 Flow and without Flow Objective

Simulation results for a more severe drought with the Trenton Flow Objective (TFO or FO), are discussed in Section 6.2 of the report. Additional simulations of the 1965 flows and the more extreme drought flows without the FO are presented in this section. This scenario is implemented for contingency planning or resilience analysis and represents a drought emergency, in which insufficient water is available from the reservoirs to meet the Trenton Flow Objective.

Salt Front

Figure K.2-1 shows annual time series of the 1965 historical flows and the flows representing a more extreme drought without the FO, along with the simulated time series of the maximum salt front location with 0 m, 0.5 m, 1.0 m, and 1.6 m of SLR. The simulated maximum salt front extends 5 to 7 miles farther upstream under a more extreme drought condition in comparison with the simulated maximum salt front for the 1965 drought (**Table K.2-2**). Without the 2500 cfs FO set for the Delaware River at Trenton, the salt front is farther upstream in comparison with the simulations discussed in Section 6.2. With the more severe drought, and without FO, and with SLR greater than or equal to 1 m, the maximum salt front extends to or above the major drinking water intakes at RM 110 (**Figure K.2-2** and **Table K.2-2**). With 0.5 m SLR, the maximum salt front was 2 miles below RM 110. With 1 m SLR, it was at RM 110, and at 1.6 m SLR it was 5 miles above RM 110. The day of the maximum intrusion occurs approximately mid-September to October 1st for the simulations with 1965 flow and without FO, and it occurs in late-November for the simulations with the more severe drought conditions and without FO, because flow is kept low in October and November, and less flow is available to counteract the increased pressure forcing due to SLR and the force of the tide pushing salinity upstream.

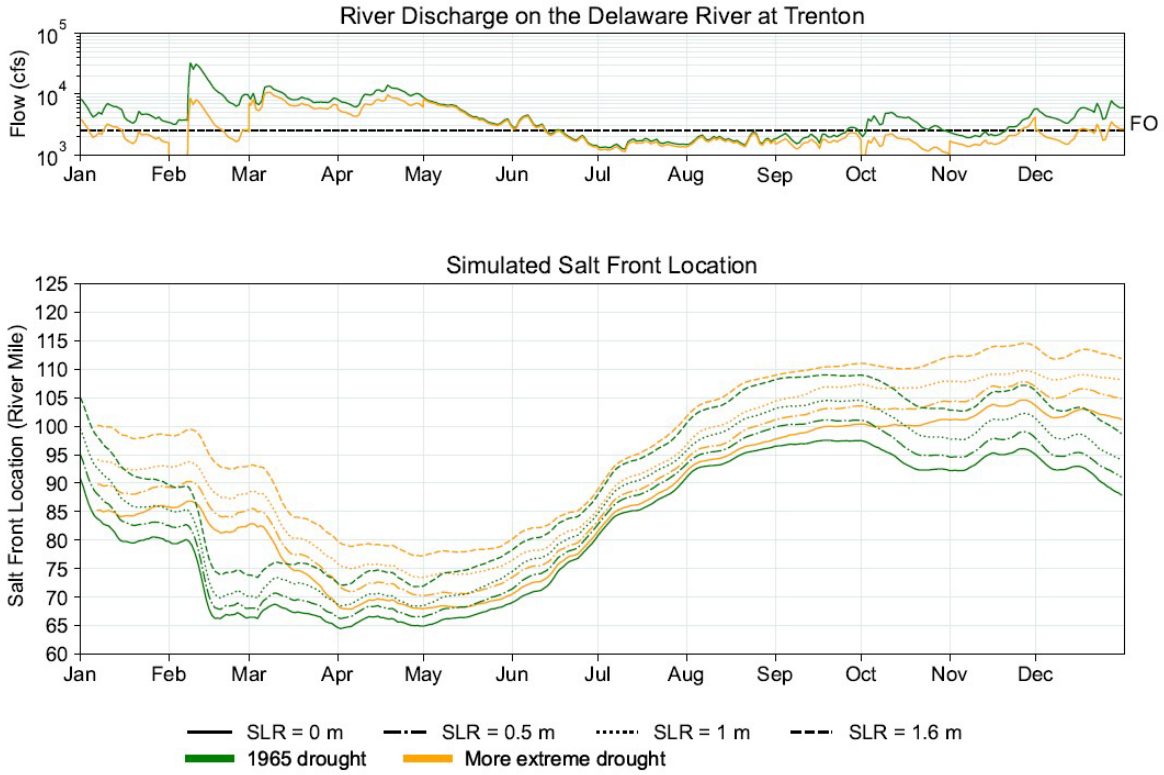

Figure K.2-1. Inflow conditions and time series of simulated salt front location with more severe drought flows in comparison with 1965 flows. The Trenton Flow Objective was not represented in these simulations.

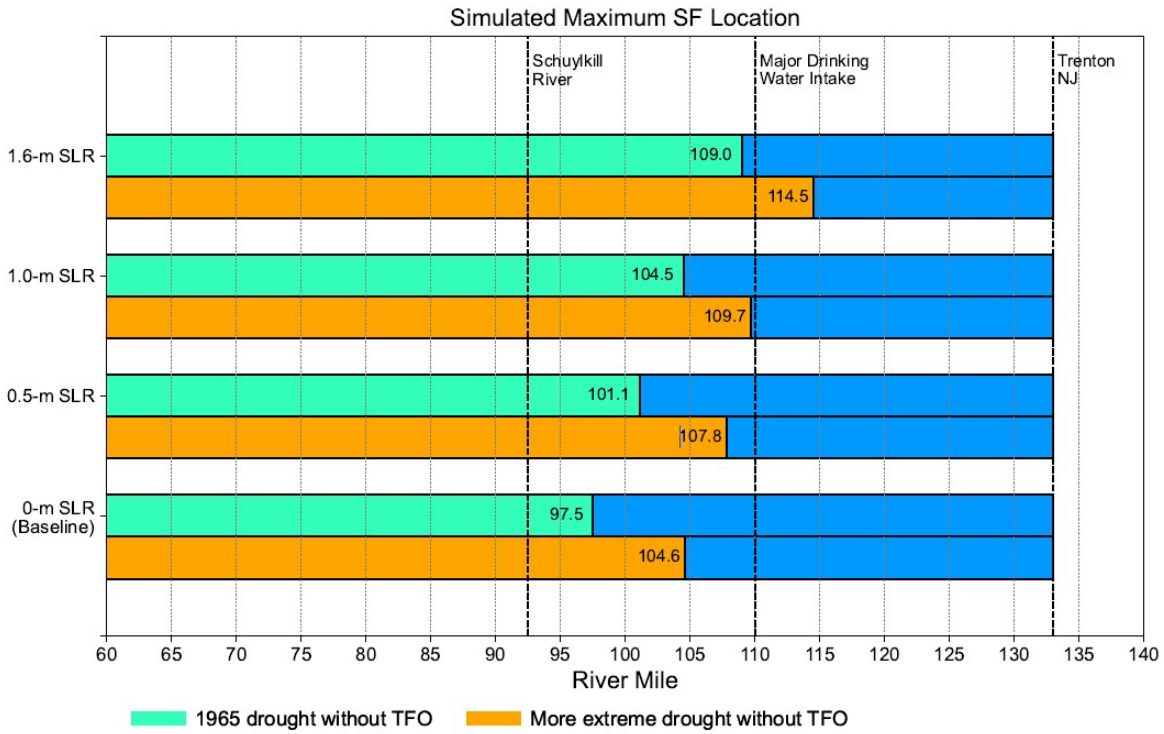

Note: The green bars represent simulation results using 1965 drought flow condition without the Trenton Flow Objective. The orange bars represent the results of simulations of a more severe drought; the differences between the lengths of the green and orange bars quantify the impact of the more severe drought flow conditions on salinity intrusion.

Figure K.2-2. Simulated maximum salt front location with more extreme drought flows in comparison with the simulated location with 1965 Flows. The Trenton Flow Objective was not represented in these simulations.

Table K.2-2. Comparison of the simulated maximum salt front locations with sea level rise under the 1965 flow condition and under a more severe drought condition. The Trenton Flow Objective was not considered in these simulations.

Sea Level Rise	Maximum Salt Front Location with 1965 Flows	Maximum Salt Front Location with More Severe Drought Flows	Difference
	(River Mile)	(River Mile)	(Miles)
0 m	97.5	104.6	7.0
0.5 m	101.1	107.8	6.7
1.0 m	104.5	109.7	5.2
1.6 m	109.0	114.5	5.5

Chloride Concentrations

Simulated depth-averaged 30-dma chloride concentrations at RM 98 with SLR under the base-case 1965 condition and under the more extreme drought conditions are presented in **Figure K.2-3** and **Table K.2-3**. The box plots in **Figure K.2-3** show that the 30-dma chloride concentrations and the range of concentrations increase with SLR. At RM 98, the simulated 30-dma chloride concentration increases with sea level rise, and the increases are greater during the simulated drought. With 0 m SLR at RM 98, the simulated maximum depth-averaged 30-dma chloride concentration is 224 mg/L. The concentration increases by 96% to 438 mg/L under the more extreme drought conditions. For 0.5-, 1.0-, and 1.6 m SLR, the differences in the maximum depth-averaged 30-dma chloride concentration at RM 98 are 583, 748, and 1021 mg/l, respectively, which are 85%, 74%, and 62% greater, respectively, than those for the 1965 drought simulation with the corresponding SLR. Without the FO, the maximum depth-averaged 30-dma chloride concentrations exceed the water quality standard of 180 mg/L for all scenarios.

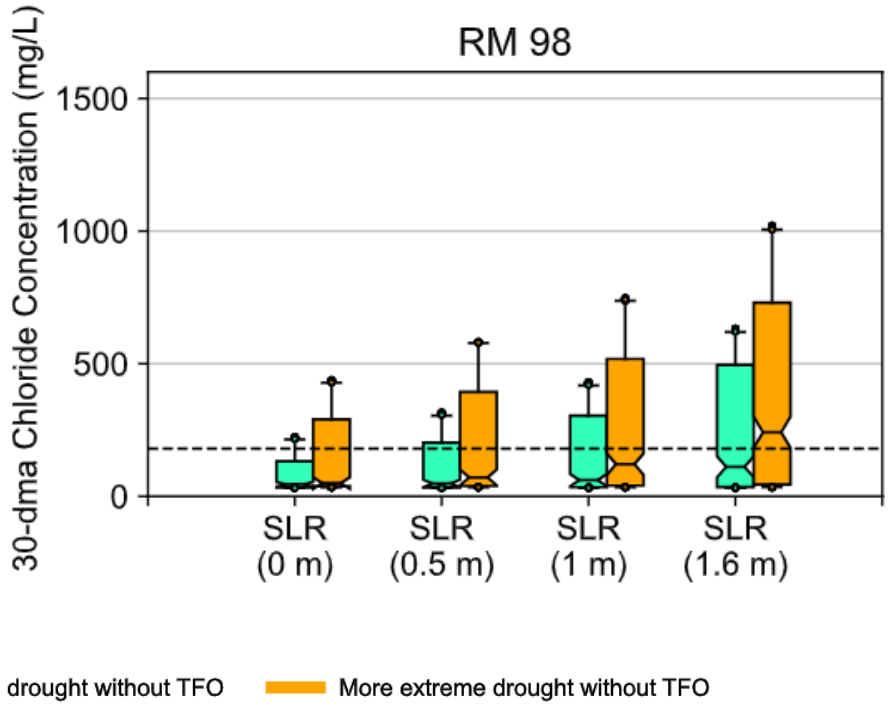

Note: The dashed line indicates the water quality standard of 180 mg/L chloride concentration at RM 98.

Figure K.2-3. Range of simulated 30-dma chloride concentrations at RM 98 during more extreme drought conditions and during 1965 drought conditions, with and without sea Level Rise. The Trenton Flow Objective was not represented in these simulations.

Table K.2-3. Comparison of the simulated maximum 30-dma chloride concentration at RM 98 with and without sea level rise: 1965 flows vs. a more extreme drought condition. The Trenton Flow Objective was not represented in these simulations.

Sea Level Rise	1965 Flows without Flow Objective	More Extreme Drought without Flow Objective	Percent Difference in Maximum 30-dma Chloride Concentration
(meters)	(mg/l)	(mg/l)	(%)
0	224	438	96
0.5	316	583	85
1	431	748	74
1.6	632	1021	62

Table K.2-4 summarizes the percentage of time that the water quality standard set for RM 98 is exceeded during the simulated year. With a more extreme drought and with 0.5 m, 1 m and 1.6 m SLR, roughly 37, 40, and 52 percent of time (respectively) the water quality standard is exceeded during the simulated year.

Table K.2-4. Comparison of the number of days (percentage of the year) that the 30-dma chloride concentration at RM 98 exceeds the 180 mg/l Water Quality Standard for more severe drought conditions and for 1965 flows, with sea level rise. The Trenton Flow Objective was not represented in these Simulations.

Sea Level Rise	Exceedance of the Water Quality Standard Under 1965 Flow Conditions	Exceedance of the Water Quality Standard Under Conditions of a More Extreme Drought	Difference
(meters)	(days [percentage of the year])	(days [percentage of the year])	(days)
0	41 [11.2%]	123 [33.7%]	82
0.5	104 [28.5%]	135 [37.0%]	31
1	141 [38.6%]	145 [39.7%]	4
1.6	154 [42.2%]	188 [51.5%]	34

Salinity

Without the FO, the range of simulated daily depth-averaged salinity with SLR, under the baseline 1965 conditions and under the more extreme drought conditions, are shown in **Figures K.2-4, K.2-5** and are summarized in **Table K.2-5**. The ocean salinity remains nearly unchanged with the simulated SLR scenarios, and changes in the daily depth-averaged salinity in the lower bay are minimal, as shown in the results at Ship John Shoal, which is 37 miles from the bay mouth. The impact of extreme drought on salinity intrusion due to SLR becomes more pronounced for locations farther upstream. At the Delaware Memorial Bridge, the maximum daily depth-averaged salinity increases by 1.1 psu, which is a 13% increase, with 0 meter SLR for the drought severity scenario, in comparison with that of the 1965 historical drought simulation. The increase in maximum daily depth-averaged salinity at RM 92.5 is approximately 0.8 psu, which is a near 87% increase at that location in comparison with that of the 1965 drought simulation. Similarly, with 1 meter SLR, the increase in the maximum daily depth-averaged salinity is roughly 0.9 and 1.0 psu at the Delaware Memorial Bridge and at RM 92.5, respectively.

The simulated along-channel depth-averaged maximum salinity profiles, which compare results for simulations of the 1965 drought and for the more extreme drought conditions without the FO, are presented in **Figure K.2-6** for the three SLR scenarios. With the more extreme drought conditions, the maximum simulated salinity profile shifts farther upstream in comparison with that of the 1965 drought simulation. The differences between the simulated profiles under 1965 conditions and under the more extreme drought conditions for four SLR scenarios are shown in **Figure K.2-7**. The changes resulting from the more extreme drought conditions without SLR are shown as gray dotted lines. The changes due to SLR under 1965 flow conditions are shown as black dashed lines, and the change resulting from both SLR and more extreme drought are shown as black solid lines.

It should be noted that the time of maximum salinity at locations along the Estuary are different. Similar to the results presented in Section 6.2, the compounding impact from both SLR and the extreme drought seems roughly to be the sum of the individual impacts in the upper tidal river above RM 75. The most significant increase in the maximum depth-averaged salinity occurs between RM 70 and RM 85 for all cases. The impact from the more extreme drought flow alone (without SLR) is similar to the impact due to 1 m SLR with 1965 flow conditions and without the FO. In general, the compounding effect of SLR and extreme drought produced the most significant impact on the salinity in the Delaware Estuary.

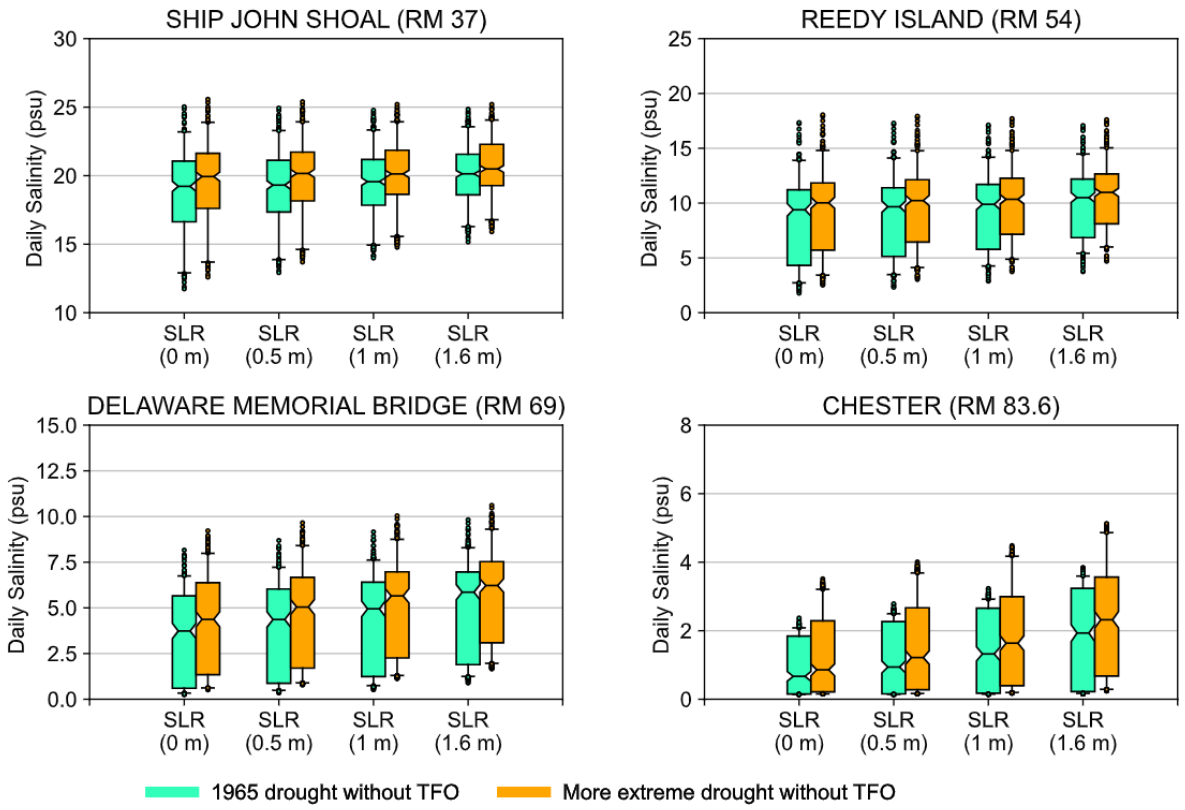

Figure K.2-4. Range of simulated daily depth-averaged salinity downstream from the Schuylkill River during more severe drought conditions and during 1965 drought conditions, with and without sea level rise. The Trenton Flow Objective was not included in these simulations.

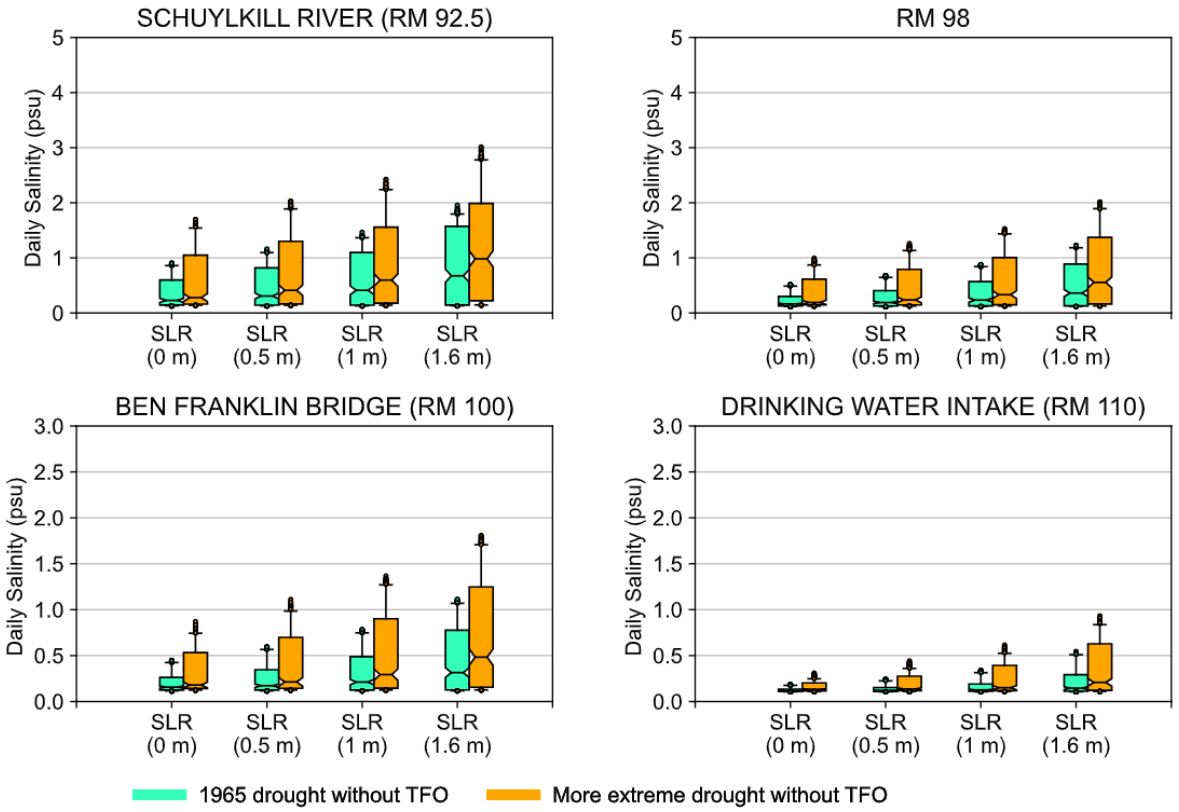

Figure K.2-5. Range of simulated daily depth-averaged salinity at and upstream from the Schuylkill River during more severe drought conditions and during 1965 drought conditions, with and without sea level rise. The Trenton Flow Objective was not considered in the simulations.

Table K.2-5. Comparison of the maximum simulated daily depth-averaged salinity during more severe drought conditions and during 1965 drought conditions, with and without sea level rise. The Trenton Flow Objective was not represented in the Simulations.

		SHIP JOHN SHOAL	REEDY ISLAND	DELAWARE MEMORIAL BRIDGE	CHESTER	SCHUYLKILL RIVER	CHAMDEN	BEN FRANKLIN BRIDGE	DRINKING WATER INTAKE
		(RM 37)	(RM 54)	(RM 69)	(RM 83.6)	(RM 92.5)	(RM 98)	(RM 100)	(RM 110)
		(psu)	(psu)	(psu)	(psu)	(psu)	(psu)	(psu)	(psu)
SLR = 0 m	1965 drought	25.03	17.34	8.16	2.37	0.91	0.52	0.45	0.19
	More extreme drought	25.57	18.06	9.22	3.51	1.7	1	0.87	0.31
	Percent Diff. (%)	2.16	4.15	12.99	48.1	86.81	92.31	93.33	63.16
SLR = 0.5 m	1965 drought	24.94	17.3	8.69	2.79	1.16	0.68	0.59	0.24
	More extreme drought	25.39	17.94	9.65	4.01	2.03	1.26	1.11	0.44
	Percent Diff. (%)	1.8	3.7	11.05	43.73	75	85.29	88.14	83.33
SLR = 1 m	1965 drought	24.78	17.13	9.16	3.23	1.47	0.88	0.79	0.34
	More extreme drought	25.2	17.71	10.04	4.48	2.43	1.53	1.37	0.62
	Percent Diff. (%)	1.69	3.39	9.61	38.7	65.31	73.86	73.42	82.35
SLR = 1.6 m	1965 drought	24.85	17.06	9.82	3.84	1.96	1.23	1.11	0.54
	More extreme drought	25.2	17.6	10.61	5.13	3.02	2.01	1.81	0.93
	Percent Diff. (%)	1.41	3.17	8.04	33.59	54.08	63.41	63.06	72.22

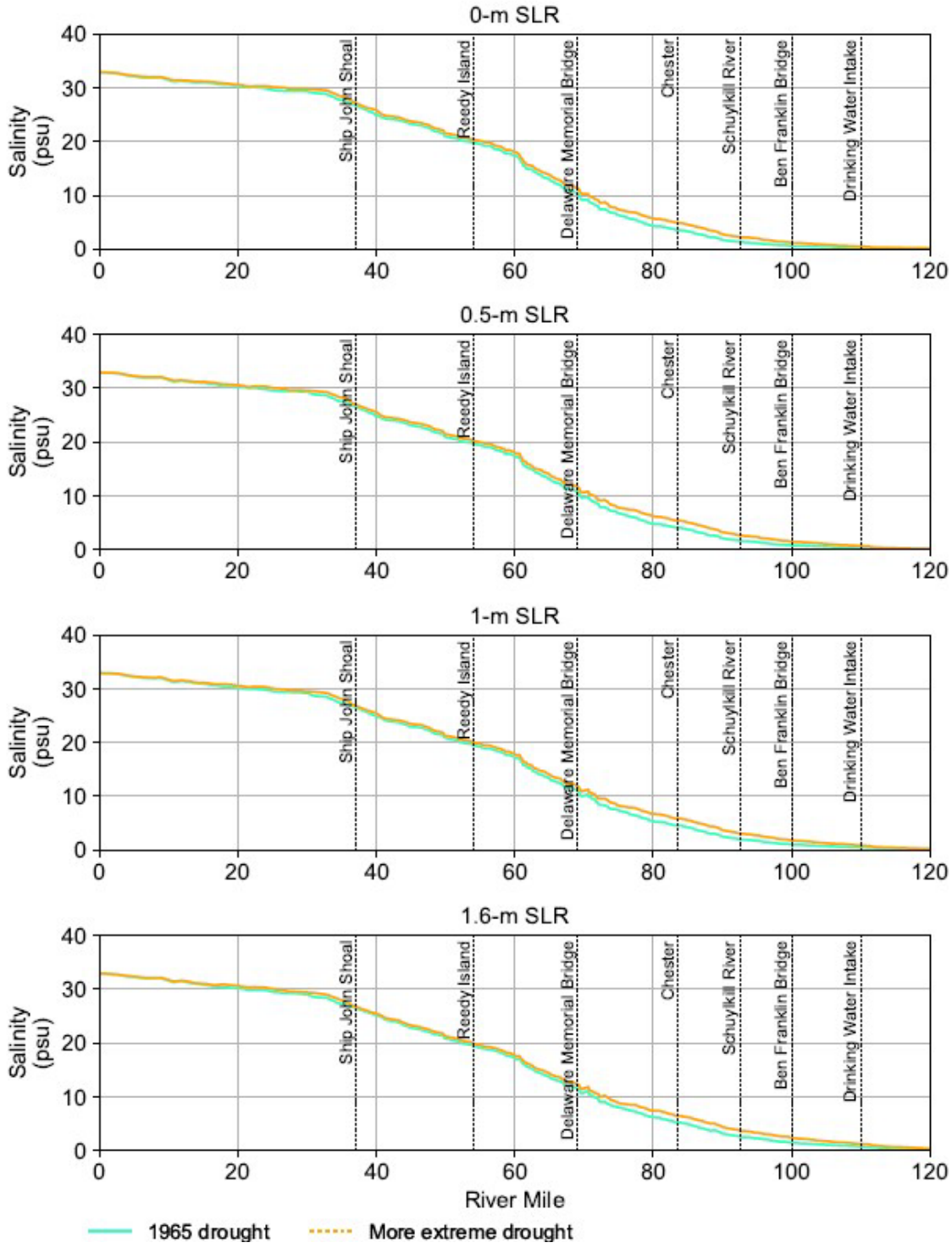

Figure K.2-6. Simulated daily maximum along-channel salinity with sea level rise in the Delaware River Estuary: 1965 drought conditions vs. more extreme drought conditions. The Trenton Flow Objective was not included in these simulations.

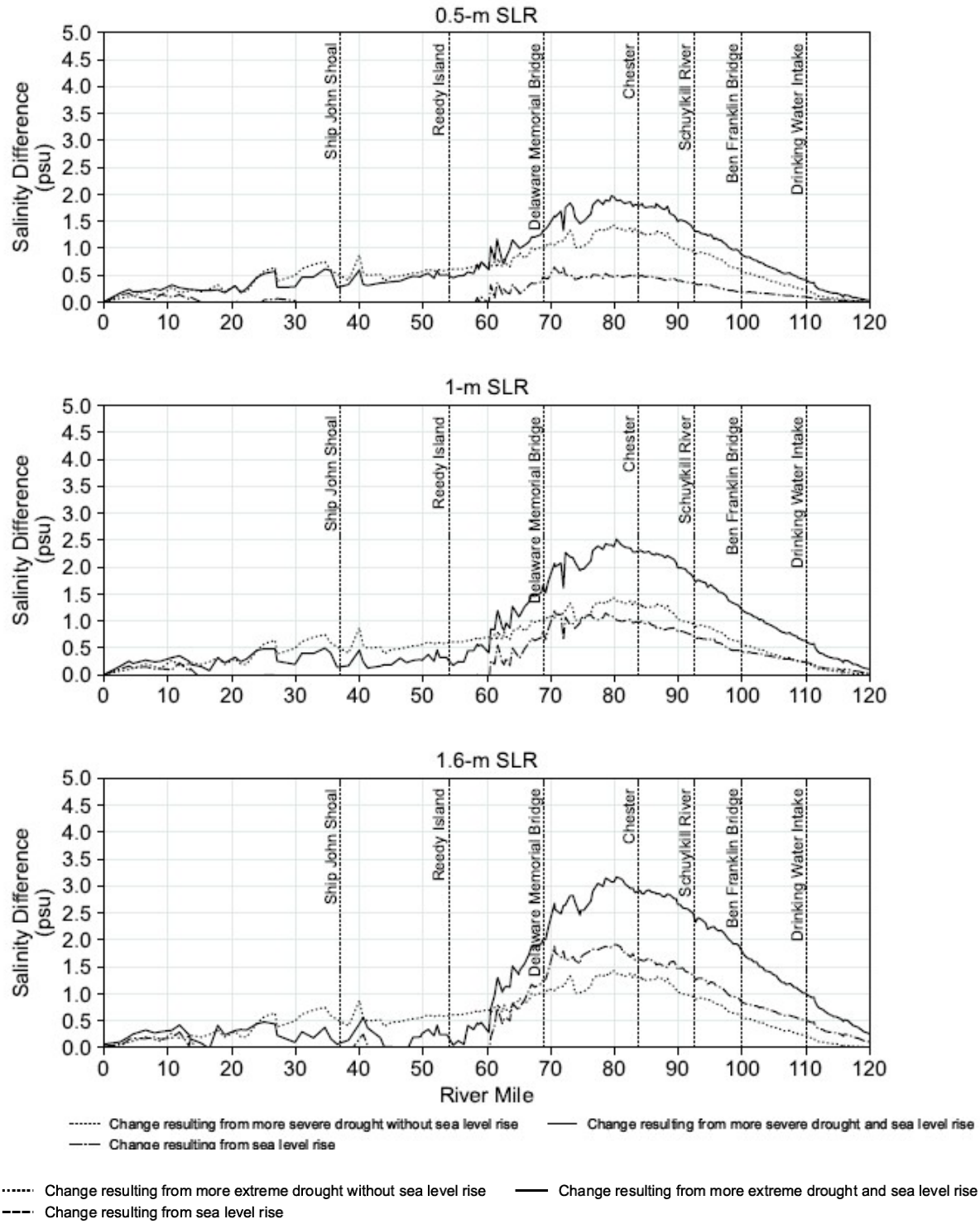

Figure K.2-7. Increase in the simulated maximum along-channel salinity from baseline with sea level rise in the Delaware River Estuary: 1965 drought conditions vs. more extreme drought conditions. The Trenton Flow Objective was not represented in these simulations.

Appendix L. Additional Simulation Results for Flow Management

L.1 Effect of the Trenton Flow Objective on Salinity

Section 7.1 discusses the impact of the Trenton Flow Objective (TFO or FO) on the salinity intrusion in the Delaware Estuary. In a set of simulations, the flow objective is assumed to be met during the simulation period and is simulated by increasing 1965 historical inflows from the Delaware River at Trenton to 2,500 cfs if the value in the flow record is less than 2,500 cfs. The simulated along-channel profiles for maximum depth-averaged salinity with 0.5 m, 1.0 m, and 1.6 m SLR are presented in **Figure 7.1-6**, and the difference in the maximum salinity is presented in **Figure 7.1-1**.

The difference due to SLR between values of simulated salinity changes for each SLR increment (the gap between same-colored solid and dotted lines in **Figure 7.1-7**) indicates the extent of return to the baseline condition that results from the flow augmentation. All differences are referenced to the same baseline simulation of 1965 flow without the FO and with 0 m SLR. The benefit from the FO is shown as the gap between the solid and dotted lines.

Figure L.1-1 shows the time series of simulated salt front movement and compares cases with and without the FO for all SLR scenarios. With the 2,500 cfs FO during the July through September low flow season, and with SLR 1.6 m, the salt front remains below RM 105, which is roughly 4 miles farther downstream in comparison with results for the simulation without the FO, for which the maximum location of the salt front is at RM 109 at the end of September.

Figure L.1-2 shows the effect of the FO as the percentage return to the baseline condition of the simulated maximum salinity for the river segment between RM 80 to RM 115. The greatest relative salinity recovery occurs upstream from Chester. **Figure L.1-2** shows that near the Ben Franklin Bridge at RM 100 with 0.5 SLR, the augmentation results in a complete (100 percent) return to the baseline, as the change in salinity becomes close to zero. Above the Ben Franklin Bridge, the salinity with the FO is lower than the salinity simulated using 1965 drought conditions without the FO, and results in greater than 100 percent return to baseline. With 1.0 m and 1.6 m SLR, the reduction in salinity impact upstream from Chester to RM 110 is about 25-75 percent and 10-50 percent, respectively.

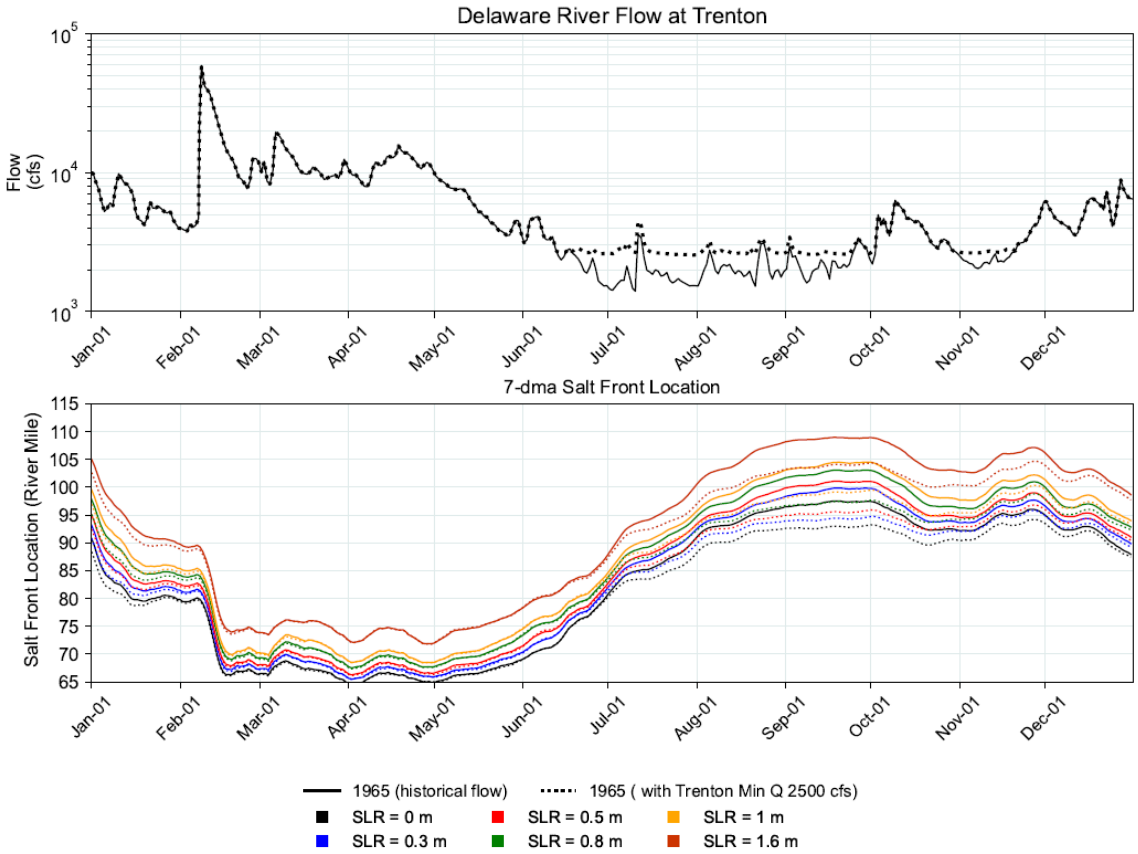

Figure L.1-1. Simulated Salt Front Location with SLR and with 1965 Drought Condition with and without Treton Flow Objective. "FO" = "Trenton Flow Objective"

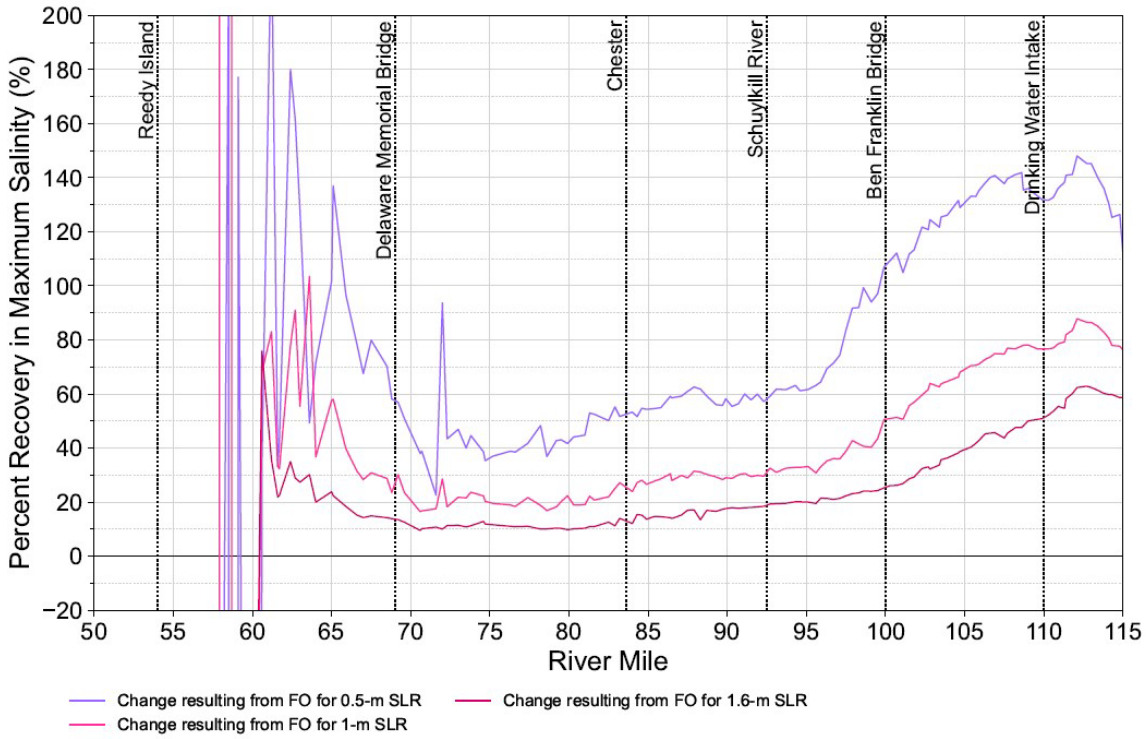

Figure L.1-2. Percent recovery (return to baseline) in simulated along-channel maximum depth-averaged salinity in the Delaware Estuary under 1965 flow conditions: Evaluation of the Trenton Flow Objective. "FO" = "Trenton Flow Objective"

L.2 Effect of Pulse Releases on Salinity

Section 7.2 of the report discusses another conceptual management option utilizing a pulse of water in addition to the Trenton Flow Objective that is currently implemented. The pulses are simulated by increasing the 1965 flow at Trenton from September 1st through September 25th of the simulation year by a constant value (500 or 1,000 cfs), as depicted in the top panel of **Figure 7.2-1**. The pulse is discontinued on September 26 because a rainfall event increased the natural flow to more than the flow objective of 2,500 cfs, ending the low-flow condition.

In Section 7.2, a summary of simulated exceedances of the 30-dma-180 mg/L chloride concentration water quality standard at RM 98 (Camden, NJ) during September 1st through December 31st is presented in **Table 7.2-3**. The time series plots of the simulated 30-dma-180 mg/L chloride concentration for different scenarios are presented in **Figure L.2-1**, in which the water quality standard at RM 98 is shown as the horizontal orange line. This figure demonstrates that the 30-dma-180 mg/L chloride concentration water quality standard at RM 98 (Camden, NJ) is violated for scenarios with 1 m and 1.6 m SLR. With 1.6 meter SLR, the simulated 30-dma-180 mg/L chloride concentration exceeds the water quality standard 100% of the time during this period.

In Section 7.2, along-channel profiles for the simulated three-month maximum depth-averaged salinity are presented in **Figure 7.2-7**, focusing on the portion upstream from RM 75. The differences in the maximum salinity due to 0.5 m, 1 m, and 1.6 m SLR are presented in **Figure 7.2-8**. The analysis was based on the simulation results from August 1st through October the 31st. The differences between values of simulated salinity change for each SLR increment (the gap between same-colored solid and dotted lines in **Figure 7.2-8**) indicates the extent to which salinity returns to the baseline condition as a result of the pulse-flow augmentation, and these differences are presented in **Figure L.2-2**.

Figure L.2-3 depicts the time history of simulated depth-averaged salinity at RM 98 during September through October. During this two-month period, the depth-averaged salinity at RM 98 peaks around October 1st and then decreases. The impact from the pulse release is demonstrated by the separation between the results of the baseline and flow augmentation simulations. The impact fades by the end of October.

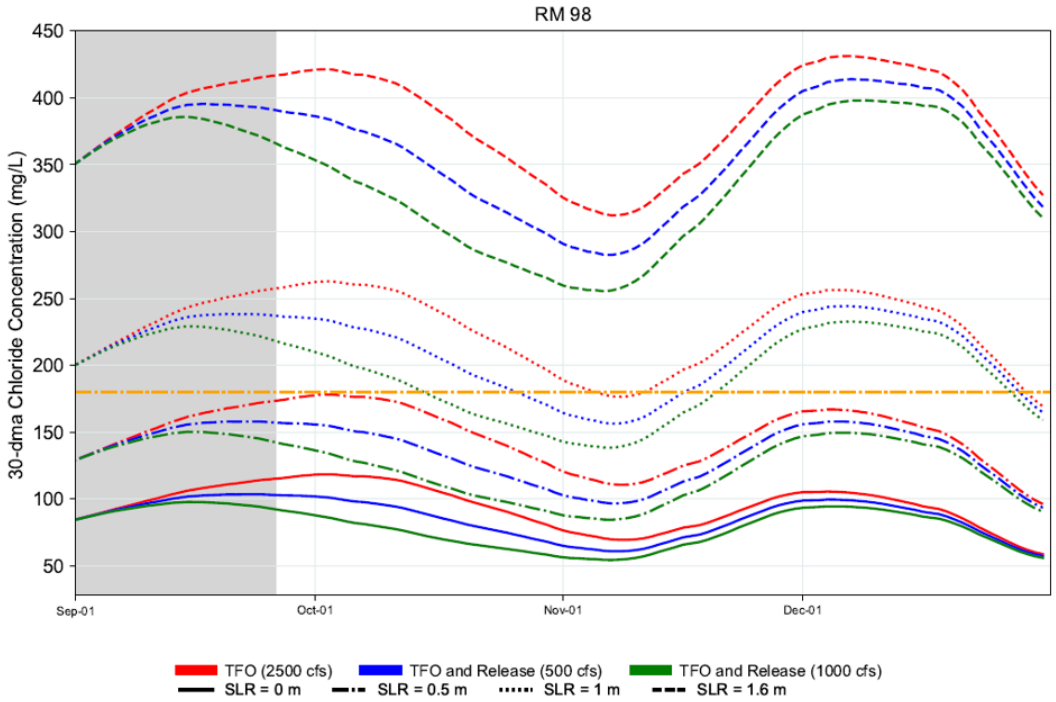

Figure L.2-1 Simulated 30-dma Chloride Concentration at RM 98 during September 1st through December 31: evaluation of pulse releases. The horizontal orange dashed line indicates the water quality standard.

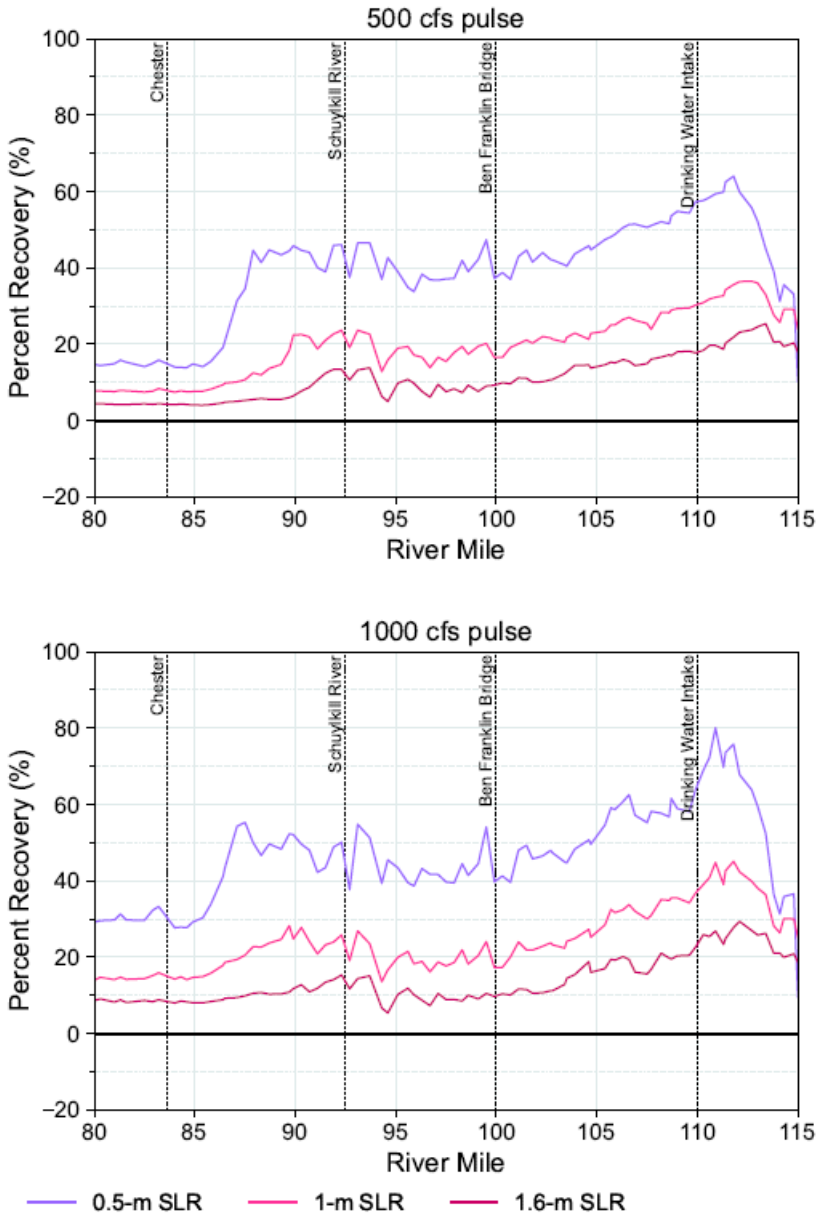

Figure L.2-2. Percent recovery (return to baseline) in simulated along-channel maximum depth-averaged salinity under 1965 flow conditions during September 25 through December 31 in the Delaware Estuary: Evaluation of pulse releases.

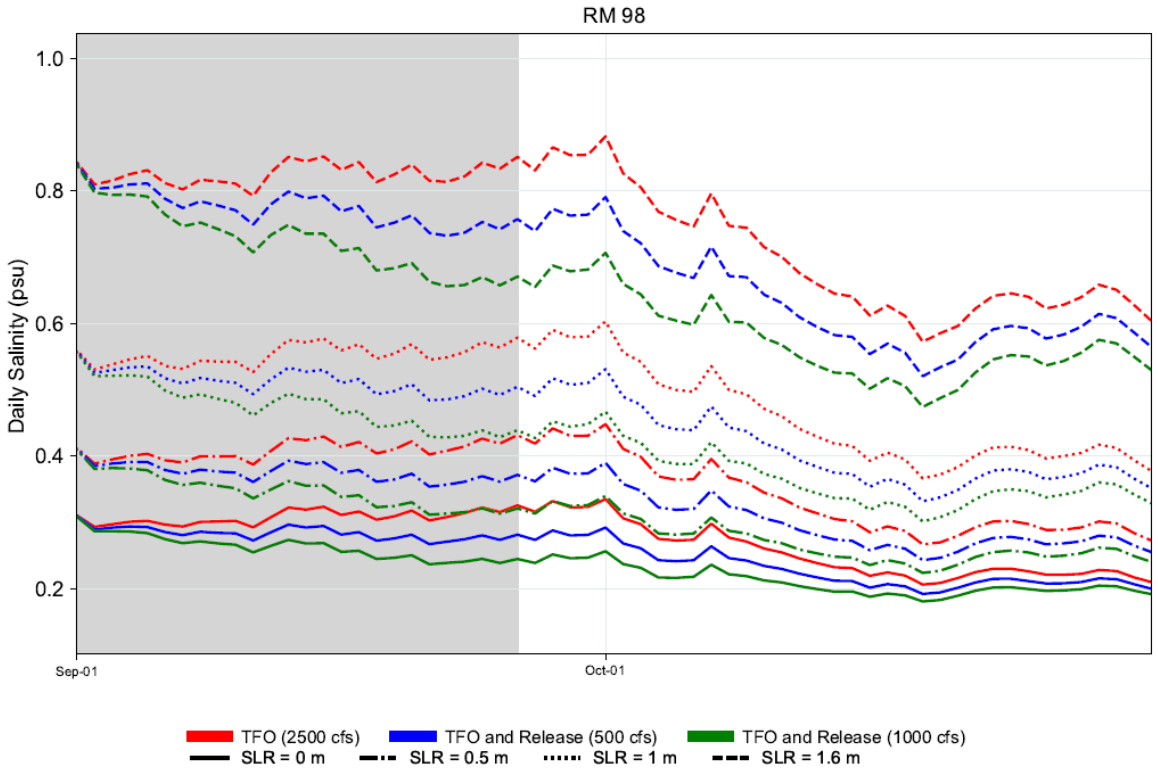

Figure L.2-3. Time history of simulated depth-averaged salinity at RM 98 under 1965 flow conditions during September 1st through December 31 in the Delaware Estuary: Evaluation of pulse releases.

L.3 Comparative Evaluation of Flow Augmentation from the Delaware and Schuylkill Rivers – Additional results and Figures

This section provides additional model results and some insights to the sensitivity simulations described in Section 7.

L.3.1 Additional model results for Section 7.3

Discussion of the Schuylkill River Mixing Zone

A rain event in July of the simulation year adds approximately 684 cfs to the river (153 cfs from the Delaware River and 531 from the Schuylkill River). During the simulation with historical flows (with no flow objective) and sea level rise of less than 1.0 m, the rate of upstream movement of the salt front is paused by the influx of additional water, as indicated by the relatively constant location for approximately one week. With 1.6 m of sea level rise, the upstream movement of the salt front is negligible. The increase in flow from the Schuylkill River creates a plume of fresh water through which the higher salinity water mixes before continuing upstream. However, with 1.6 m sea level rise, the higher salinity water is already above the confluence and unaffected by the addition of fresh water from the Schuylkill River downstream.

With the flow objective, the additional water is applied to the Delaware River flows, and the salt front movement with 1.6 m-sea level rise is markedly affected. The water upstream from the confluence is then also diluted and thus more mixing of water from downstream is needed to raise the salinity of the water and move the salt upstream. The location of the salt front prior to the influx of water, along with the location of the source of additional water, affects the rate of upstream salinity movement. The relative effect of adding flow from either the Delaware or Schuylkill Rivers, or both, is discussed in more detail in Section 7.3.

Chloride Concentrations

Additional flow from the water release lowers the 30-dma chloride concentrations in comparison with baseline concentrations for all simulations (see **Figure L.3-1** through **Figure L.3-4**). In Section 7.3, only the box plot of 30-dma chloride concentration for the 1 m SLR simulation is presented. The baseline maximum 30-dma chloride concentration at RM 98 was 238 mg/L, above the 180 mg/L water quality standard for salinity control for the baseline, and for all simulation trials with 0 m SLR. With 1 m and 1.6 m SLR, the maximum 30-dma chloride concentrations at RM 98 for the baseline is greater than 584 mg/L and 900 mg/L, respectively, exceeding the 180 mg/L standard. See related discussion in the report Section 7.3.

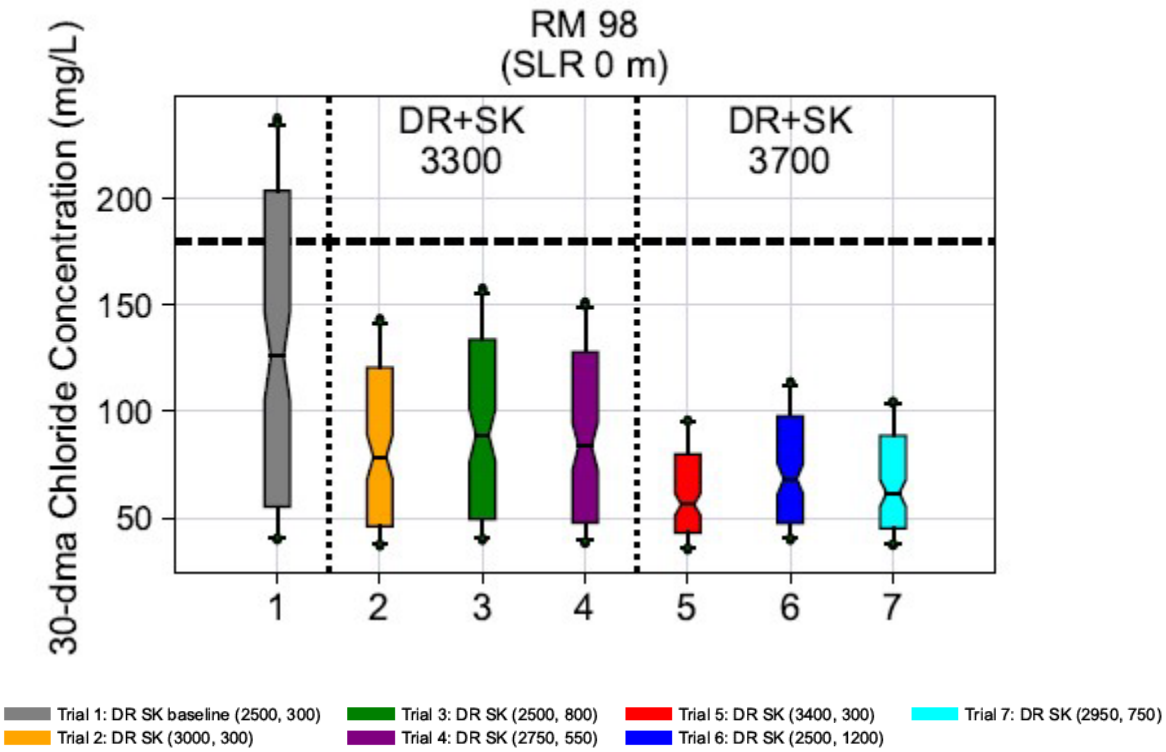

Notes: Constant flow is maintained from May through December. The results are summarized for August through November, the most critical period for the salt front. DR = the Delaware River, SK = Schuylkill River.

Figure L.3-1. Comparison of simulated 30-dma chloride concentration ranges at RM 98, with Delaware and Schuylkill River flow augmentation and SLR = 0 m.

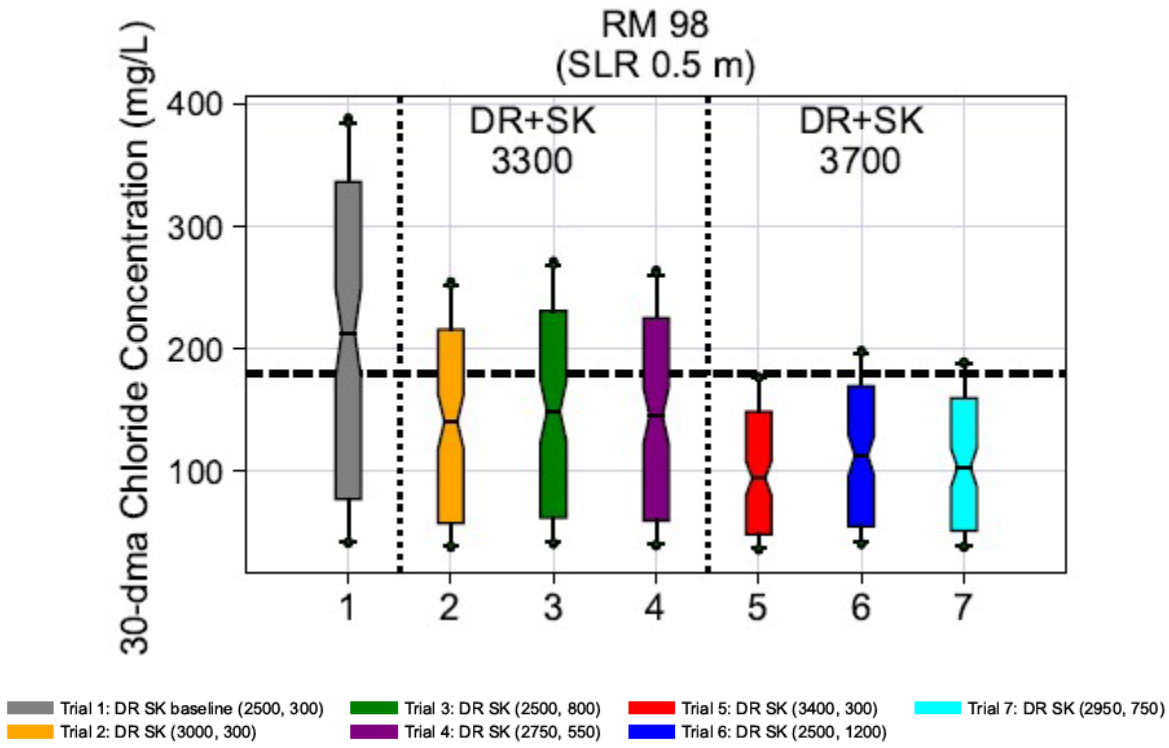

Notes: Constant flow is maintained from May through December. The results are summarized for August through November, the most critical period for the salt front. DR = the Delaware River, SK = Schuylkill River.

Figure L.3-2. Comparison of simulated 30-dma chloride concentration at RM 98, with Delaware and Schuylkill River flow augmentation and SLR = 0.5 m.

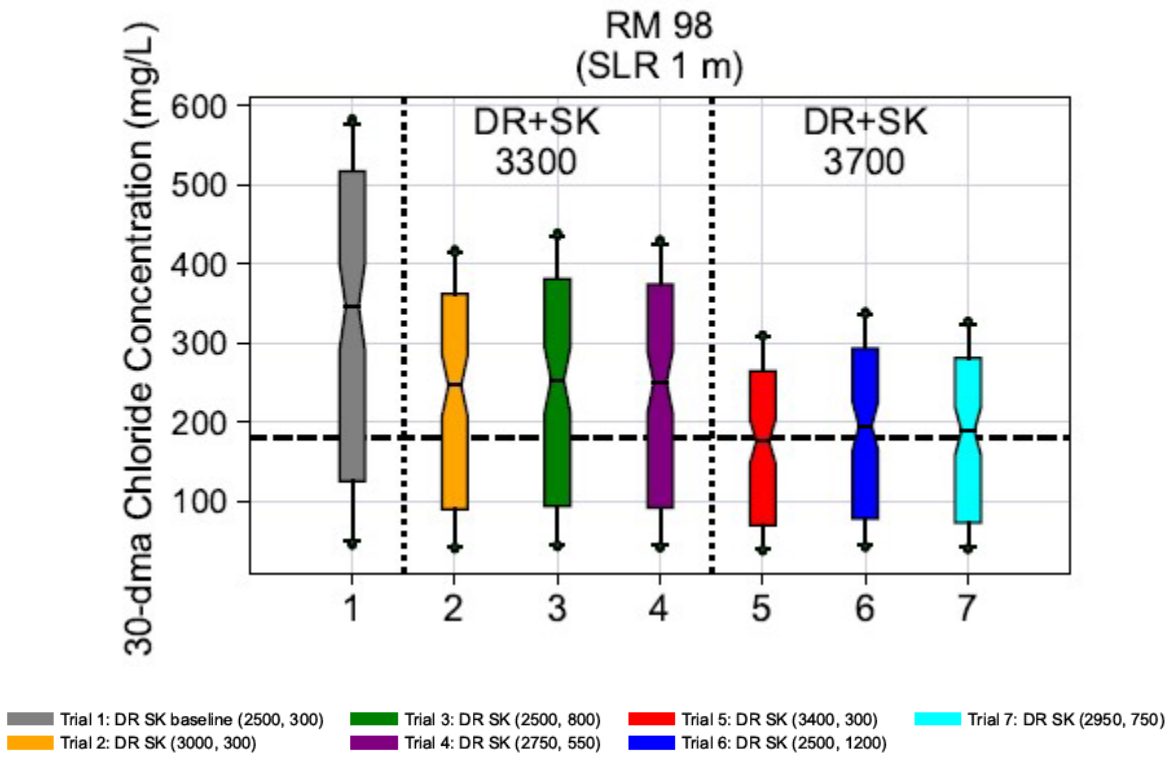

Notes: Constant flow is maintained from May through December. The results are summarized for August through November, the most critical period for the salt front. DR = the Delaware River, SK = Schuylkill River.

Figure L.3-3. Comparison of simulated 30-dma chloride concentration at RM 98, with Delaware and Schuylkill River flow augmentation and SLR = 1 m.

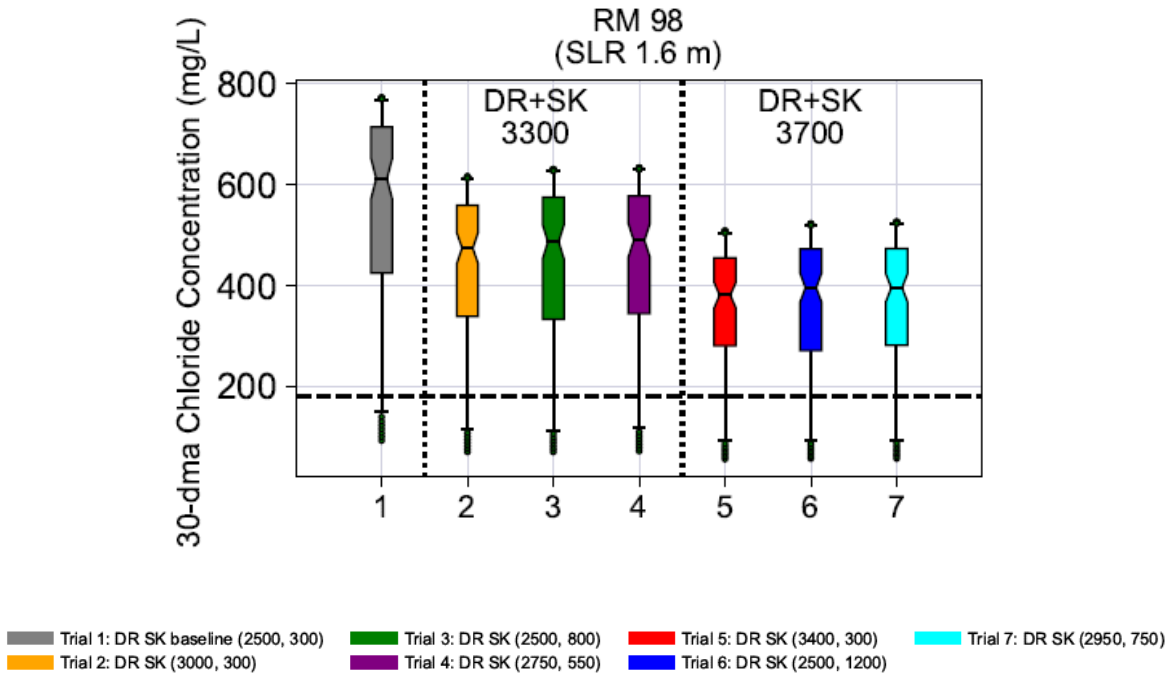

Notes: Constant flow is maintained from May through December. The results are summarized for August through November, the most critical period for the salt front. DR = the Delaware River, SK = Schuylkill River.

Figure L.3-4. Comparison of simulated 30-dma chloride concentration at RM 98, with Delaware and Schuylkill River flow augmentation and SLR = 1.6 m.

Salinity

Simulated maximum daily depth-averaged salinity is summarized over the period August 1st through November 30th (which is the critical period for the salt front). During this period, constant inflows are assigned to the Delaware River at Trenton and Schuylkill River (**Table L.3-1** through **Table L.3-4**). The impact of the additional flow varies and is presented for individual locations. **Figure L.3-5** through **Figure L.3-8** depict the range of the simulated maximum daily depth-averaged salinity at eight locations on the Delaware River with 0 m, 0.5 m, 1 m, and 1.6 m SLR, respectively. As these and other simulations demonstrate, and as is the case for the chloride results, the effectiveness of increased flow on daily depth-averaged salinity at a given location depends on where the flow contribution is added. If the salt front is below or near the Schuylkill River confluence, adding the water to the Schuylkill River flow is more effective in reducing salinity in the vicinity of the confluence. If the salt front is a few miles above the Schuylkill River (RM 92.5), adding the flow to the Delaware River is more effective. In general, if the salt front location is downstream from RM 92.5, and close to the Schuylkill River, such as at Chester, then the additional water from the Schuylkill River has a greater effect in diluting the water at that location. In contrast, if the salt front location is above the Schuylkill River, such as at RM 98, then the water added to the Delaware River at Trenton has a greater effect.

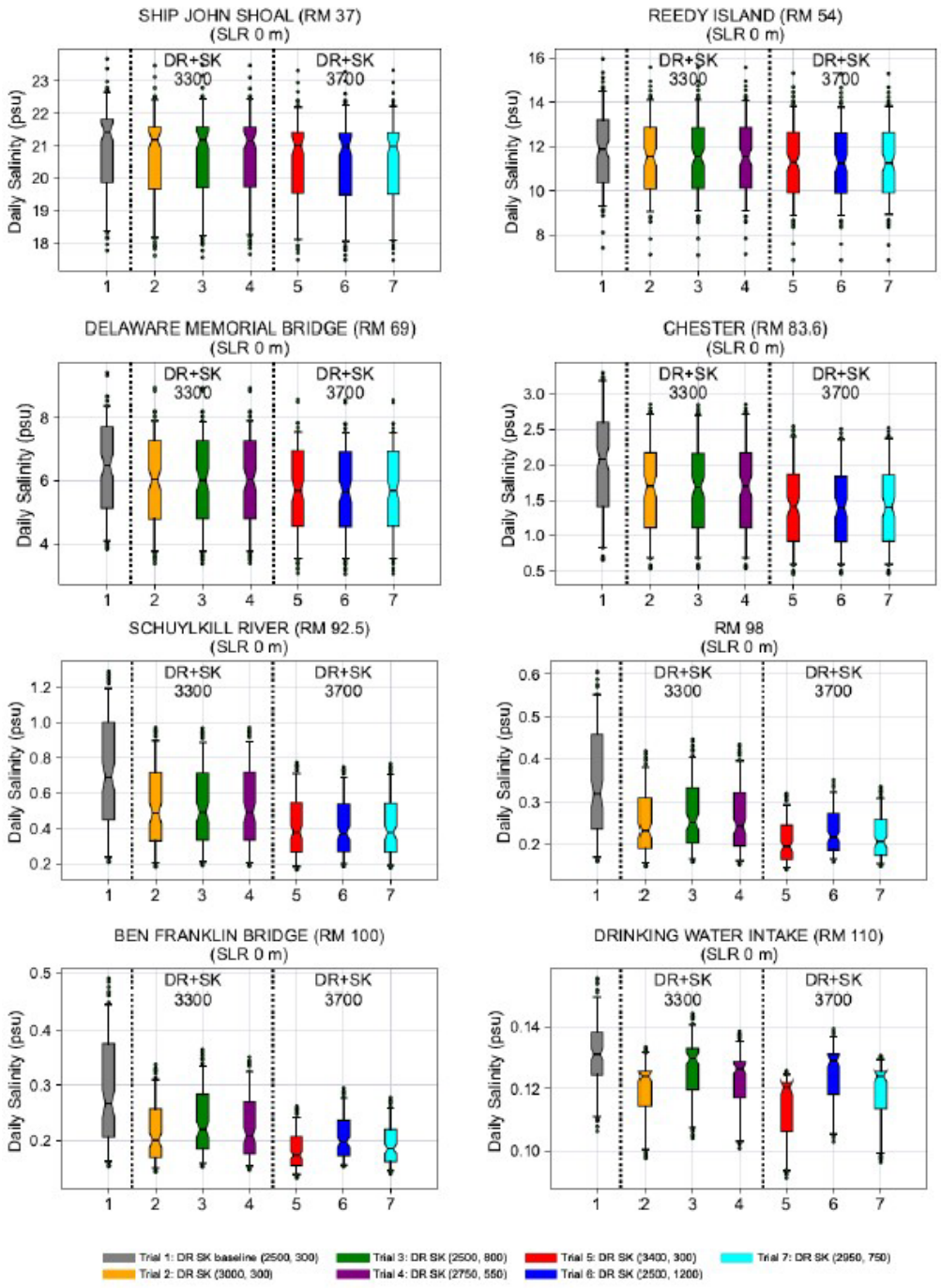

Note: The results are summarized for August through November.

Figure L.3-5. Comparison of daily depth-averaged salinity ranges at eight locations, for simulations with Delaware and Schuylkill River flow augmentation and SLR = 0 m.

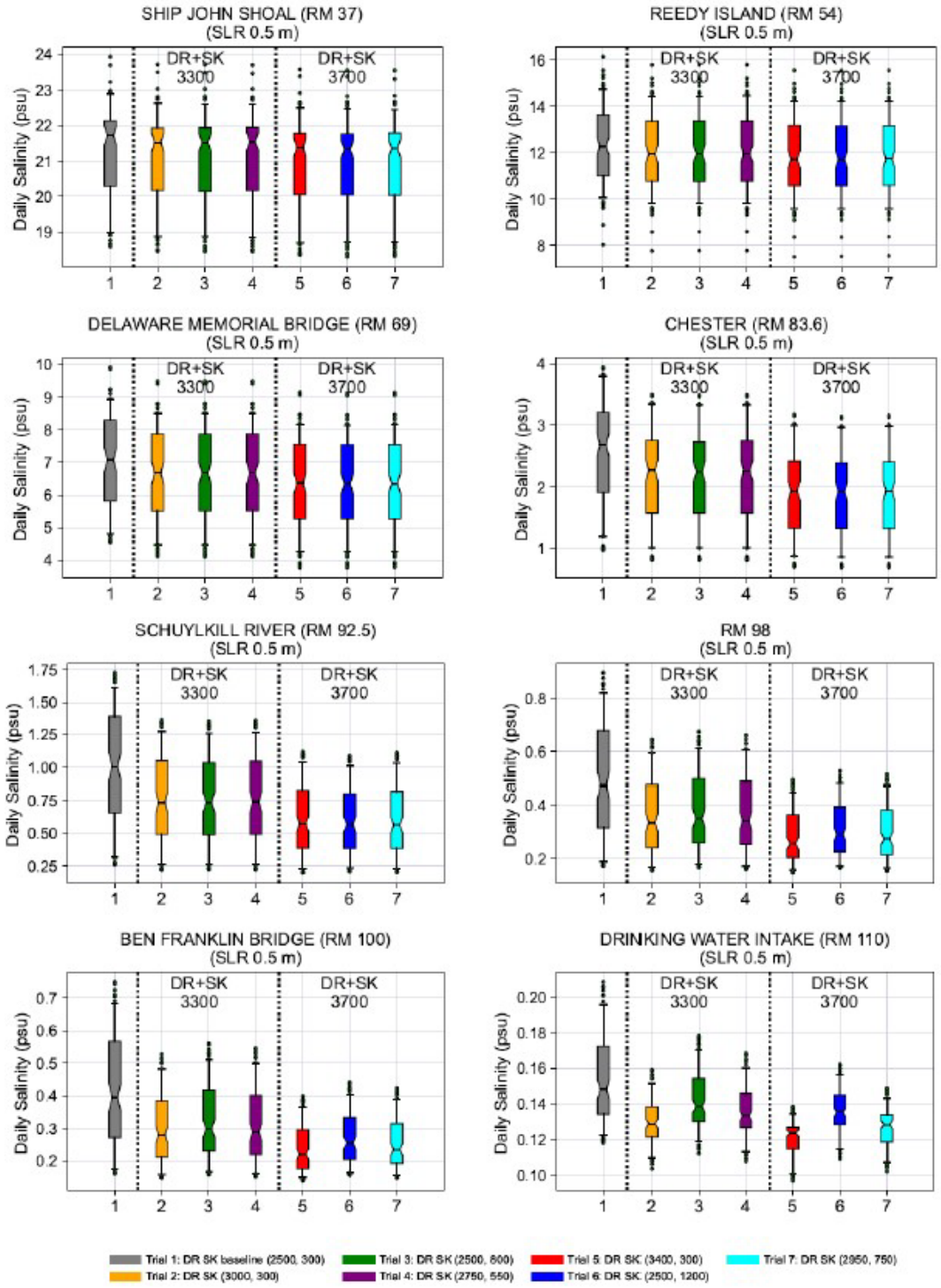

Note: The results are summarized for August through November.

Figure L.3-6. Comparison of daily depth-averaged salinity ranges at eight locations, for simulations with Delaware and Schuylkill River flow augmentation and SLR = 0.5 m.

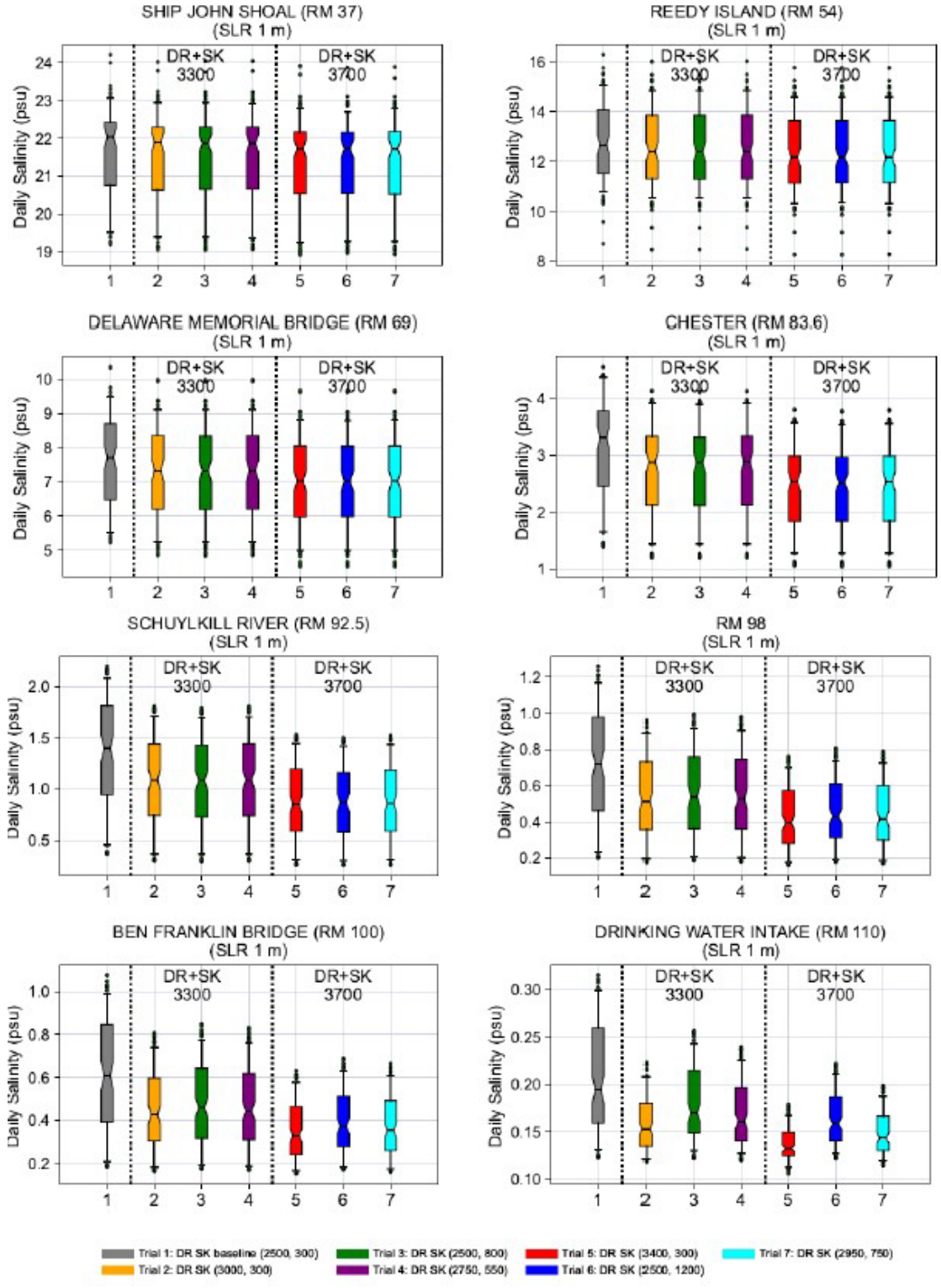

Note: The results are summarized for August through November.

Figure L.3-7. Comparison of daily depth-averaged salinity ranges eight locations, for simulations with Delaware and Schuylkill River flow augmentation and SLR = 1.0 m.

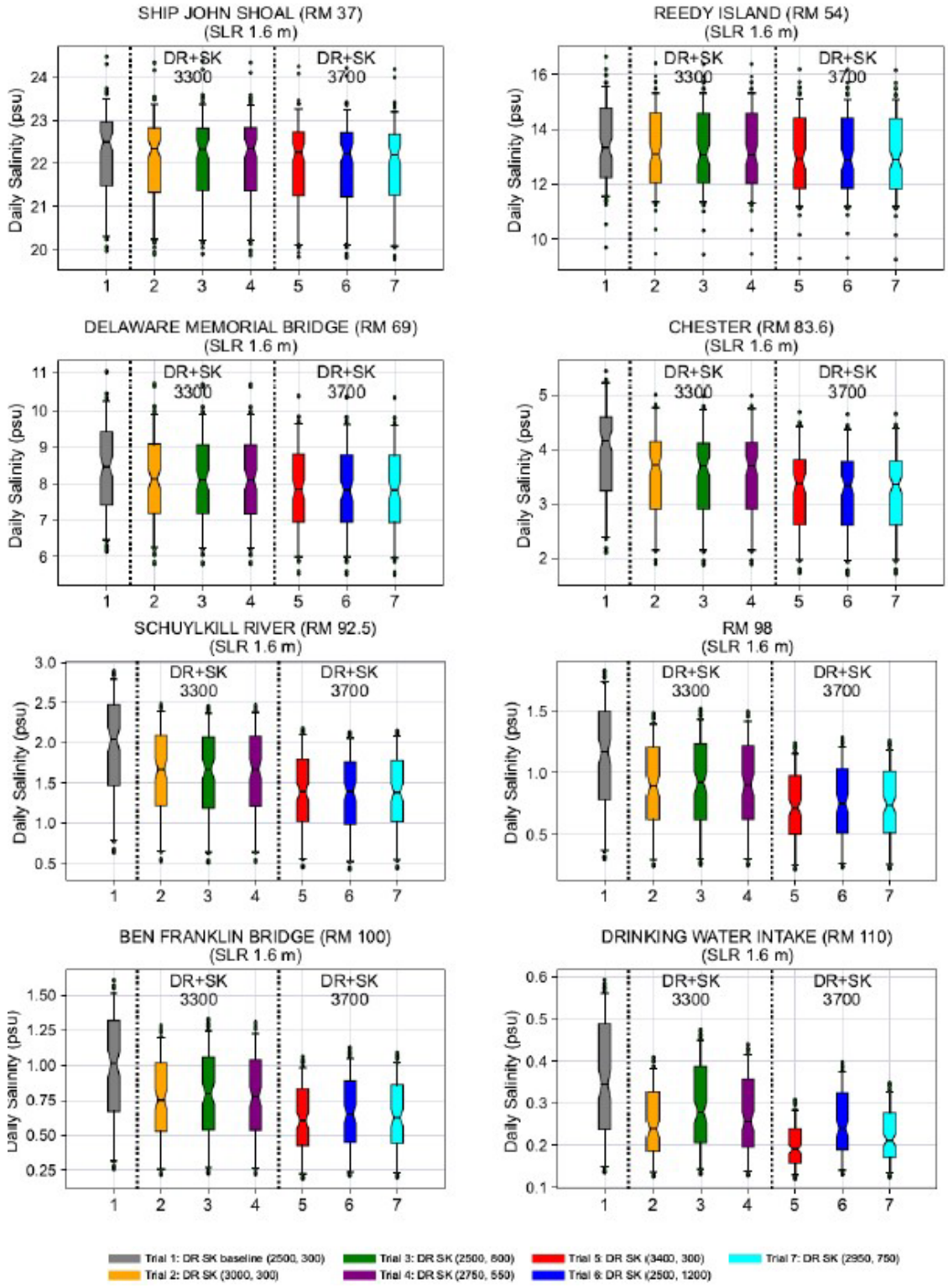

Note: The results are summarized for August through November.

Figure L.3-8. Comparison of daily depth-averaged salinity ranges eight locations, for simulations with Delaware and Schuylkill River flow augmentation and SLR = 1.6 m.

Table L.3-1. Simulated maximum daily depth-averaged salinity at selected location in the Delaware Estuary: sensitivity to Delaware and Schuylkill River flow augmentation with 0 m SLR.

		SLR 0 m						
	Combined DR and SK Flow	Baseline 2,800 cfs	3,300 cfs (adding 500 cfs)			3,700 cfs (adding 900 cfs)		
	Delaware	2500	3000	2500	2750	3400	2500	2950
	Schuylkill	300	300	800	550	300	1200	750
Location	RM	psu	psu	psu	psu	psu	psu	psu
SHIP JOHN SHOAL	37	23.68	23.47	23.49	23.48	23.32	23.29	23.33
REEDY ISLAND	54	15.96	15.58	15.57	15.57	15.32	15.28	15.29
DELAWARE MEMORIAL BRIDGE	69	9.42	8.93	8.93	8.93	8.58	8.55	8.56
CHESTER	83.6	3.31	2.86	2.85	2.86	2.54	2.51	2.52
RM 92.5	92.5	1.29	0.97	0.97	0.97	0.77	0.75	0.77
RM 98	98	0.61	0.42	0.45	0.44	0.32	0.35	0.34
BEN FRANKLIN BRIDGE	100	0.49	0.34	0.36	0.35	0.26	0.29	0.28
RM 110	110	0.16	0.13	0.14	0.14	0.13	0.14	0.13

Table L.3-2. Simulated maximum daily depth-averaged salinity at selected location in the Delaware Estuary: sensitivity to Delaware and Schuylkill River flow augmentation with 0.5 m SLR.

		SLR 0.5 m						
	Combined DR and SK Flow	Baseline 2,800 cfs	3,300 cfs			3,700 cfs		
			(adding 500 cfs)			(adding 900 cfs)		
	Delaware	2500	3000	2500	2750	3400	2500	2950
	Schuylkill	300	300	800	550	300	1200	750
Location	RM	psu	psu	psu	psu	psu	psu	psu
SHIP JOHN SHOAL	37	23.92	23.71	23.71	23.69	23.57	23.54	23.54
REEDY ISLAND	54	16.14	15.8	15.81	15.81	15.56	15.55	15.56
DELAWARE MEMORIAL BRIDGE	69	9.92	9.48	9.48	9.48	9.15	9.13	9.14
CHESTER	83.6	3.94	3.5	3.49	3.49	3.17	3.14	3.16
RM 92.5	92.5	1.73	1.37	1.35	1.36	1.12	1.09	1.11
RM 98	98	0.9	0.65	0.67	0.66	0.49	0.53	0.51
BEN FRANKLIN BRIDGE	100	0.75	0.53	0.56	0.55	0.4	0.44	0.42
RM 110	110	0.21	0.16	0.18	0.17	0.14	0.16	0.15

Table L.3-3. Simulated maximum daily depth-averaged salinity at selected location in the Delaware Estuary: sensitivity to Delaware and Schuylkill River flow augmentation with 1 m SLR.

		SLR 1.0 m						
	Combined DR and SK Flow	Baseline 2,800 cfs	3,300 cfs (adding 500 cfs)			3,700 cfs (adding 900 cfs)		
	Delaware	2500	3000	2500	2750	3400	2500	2950
	Schuylkill	300	300	800	550	300	1200	750
Location	RM	psu	psu	psu	psu	psu	psu	psu
SHIP JOHN SHOAL	37	24.21	24.01	24.04	24.04	23.90	23.87	23.88
REEDY ISLAND	54	16.30	16.01	16.01	16.03	15.78	15.77	15.77
DELAWARE MEMORIAL BRIDGE	69	10.38	9.99	9.98	9.99	9.67	9.67	9.67
CHESTER	83.6	4.56	4.13	4.11	4.12	3.80	3.78	3.79
RM 92.5	92.5	2.20	1.81	1.79	1.81	1.53	1.50	1.52
RM 98	98	1.26	0.96	0.99	0.98	0.76	0.81	0.79
BEN FRANKLIN BRIDGE	100	1.08	0.81	0.85	0.83	0.63	0.69	0.66
RM 110	110	0.32	0.22	0.26	0.24	0.18	0.22	0.20

Table L.3-4. Simulated maximum daily depth-averaged salinity at selected location in the Delaware Estuary: sensitivity to Delaware and Schuylkill River flow augmentation with 1.6 m SLR.

		SLR 1.6 m						
	Combined DR and SK Flow	Baseline 2,800 cfs	3,300 cfs			3,700 cfs		
			(adding 500 cfs)			(adding 900 cfs)		
	Delaware	2500	3000	2500	2750	3400	2500	2950
	Schuylkill	300	300	800	550	300	1200	750
Location	RM	psu	psu	psu	psu	psu	psu	psu
SHIP JOHN SHOAL	37	24.49	24.34	24.39	24.35	24.26	24.23	24.20
REEDY ISLAND	54	16.63	16.39	16.37	16.37	16.17	16.16	16.13
DELAWARE MEMORIAL BRIDGE	69	11.05	10.70	10.69	10.69	10.42	10.40	10.39
CHESTER	83.6	5.41	5.01	4.98	4.99	4.69	4.65	4.65
RM 92.5	92.5	2.90	2.49	2.46	2.48	2.18	2.14	2.16
RM 98	98	1.83	1.48	1.52	1.50	1.24	1.29	1.26
BEN FRANKLIN BRIDGE	100	1.61	1.29	1.33	1.31	1.06	1.13	1.09
RM 110	110	0.59	0.41	0.48	0.44	0.31	0.40	0.35

L.3.2 Additional Simulations

An additional suite of five simulations was conducted in which the baseline total constant flow is higher (3600 cfs), and additional flow of 500 cfs or 900 cfs is augmented from either the Delaware River or the Schuylkill River (**Table L. 3-5**.) The higher total constant flow situated the maximum salt front closer to the RM 92.5 confluence with the Schuylkill River. Results of these simulations demonstrate that if the salt front location remains near or below this confluence, Schuylkill River augmentation is more efficient in repelling the salt front.

Table L.3-5. Simulated maximum salt front location, with 0 meter sea level rise and Delaware and Schuylkill River flow augmentation, Trials 8 through 12.

Flow Source Analysis	Total Constant Flow	3600 cfs	4100 cfs		4500 cfs	
	Location	No pulse	add 500 cfs via Delaware	add 500 cfs via Schuylkill	add 900 cfs via Delaware	add 900 cfs via Schuylkill
Flow Spilt	Delaware Flow	3000	3500	3000	3900	3000
	Schuylkill Flow	600	600	1100	600	1500
Trial No.		**8**	**9**	**10**	**11**	**12**
0 m SLR	Salt Front	94.7	92.8	92.7	91.5	91.3
	Difference with pulse		-1.9	-2.0	-3.2	-3.4

In this set of simulations, the SF max reaches RM 94.7 with DR flow at Trenton set to 3000 cfs and SK R flow set to 600 cfs (Trial 8, **Figure L.3-9**.)

Note that the tidal forcing is the same for all of these simulations. The added flow (500 cfs or 900 cfs) is introduced on May 1st when the SF is near RM 67, much lower than RM 92.5. After May 1st, the flow is basically at steady state, and the ultimate location of the SF is dictated by the total amount of water in the system.

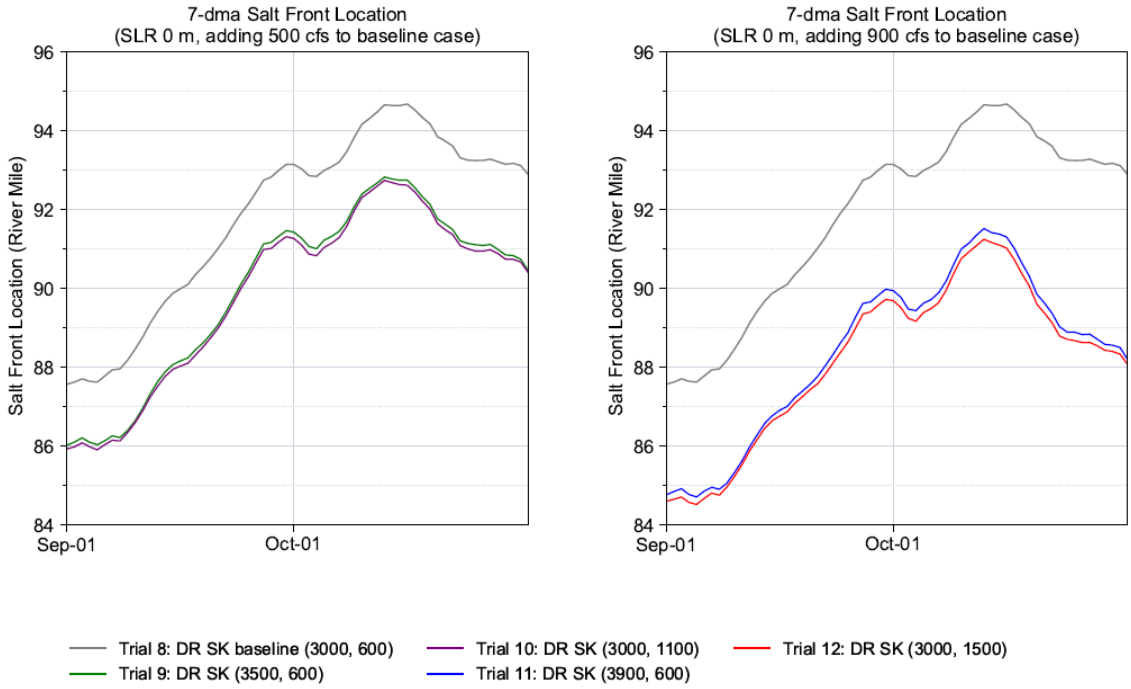

Figure L.3-9. SF locations during Delaware River and Schuylkill River flow augmentation simulations, September 1-October 31, trials 8-12.

The time series plot for SF movement from May 1st to August 31 is shown in Figure L. 3-10. Results show the difference between SF locations for Trial 9 and 10, and between SF locations for Trial 11 and 12, were not significant until early September. On September 1st, the SF was near RM 87~88 for Trial 8. Differences between the simulated SF locations begin in September and October.

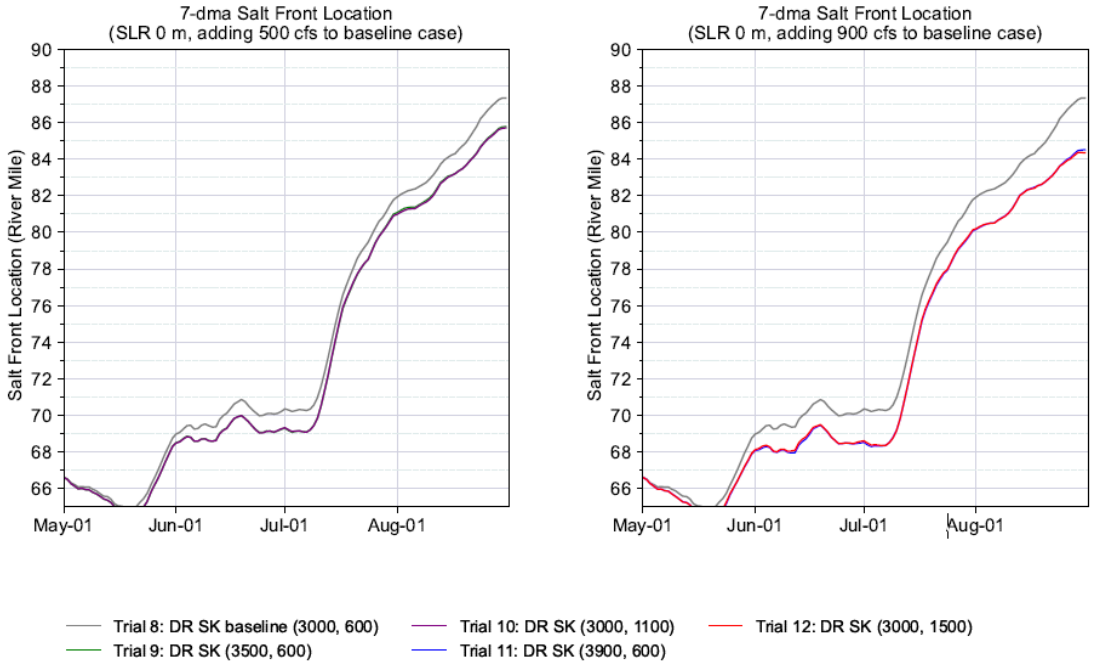

Figure L. 3-10. SF locations during Delaware River and Schuylkill River flow augmentation simulations, May 1- August 31, trials 8-12.

L.4 Discussion of the Balance of the Salinity Transport Processes

In general, the distribution of salt water in an estuary is controlled by the balance of various processes related to tidal flows and subtidal processes. There is no unified understanding of the sensitivity of salt intrusion and stratification in estuaries to various physical forcings, including river discharge, tides, and other meteorological forcings such as wind, etc, because the responses of salinity stratification, the along-channel gradient, and the extent of salinity intrusion show great variability in response to the combined effects of all these factors. For example, the salinity transport mechanism in the bay area may be much different from that in the upper tidal river tens of miles away from the ocean. The upper portion of the Delaware Estuary upstream from the Delaware Memorial Bridge (DMB) at RM 69 is usually a well-mixed and weakly stratified environment, and the underlying salinity transport mechanism is dominated primarily by the balance of two processes: river flushing caused by river discharge and horizontal tidal dispersion during flood and ebb tide periods. In the vicinity of the DMB and downstream from the upper bay area, the salinity transport regime may be characterized by a balance between vertical shear dispersion due to gravitational circulation (also known as estuary exchange flow) and river flushing, where salinity stratification is relatively strong close to the mouth of the bay. Moreover, the water volume distribution decreases exponentially with distance from the mouth of the estuary. Channel bathymetry and geometry further complicate the balance of these processes.

For a given river reach during a flood tide, tidal flow (which imports the salinity to the reach) mixes with upland freshwater discharge and results in powerful mixing and dilution. The relative strengths of the river discharge and the tidal flow determine the effect of the dilution. A new along-channel salinity gradient may be re-established over time if the river discharges change and are sustained for a long time, and the maximum salinity intrusion length will change accordingly. In the sensitivity simulations discussed in Section 7, a constant flow is applied to the Delaware at Trenton or Schuylkill River over several months, and the water volume distribution along the river may reach a new dynamic quasi-equilibrium state. With added flow, the simulated difference between the maximum chloride concentration at the Delaware Memorial Bridge (DMB) and the baseline concentration become insignificant (less than 5 percent) due to a large increase in the water volume moving downstream. At the DMB, the order of magnitude estimate of the instantaneous tidal flow may be approximately 13,500 cubic meters per second (477,000 cfs, or roughly 500,000 cfs) by using a depth-averaged tidal current velocity of 1 meter per second and the cross-sectional area of 13,500 square meters. This is roughly 170 times greater than the combined simulated discharge of the Delaware River at Trenton and the Schuylkill River (2800 cfs). The average water volume for a roughly 24-mile reach between the DMB and the Schuylkill River mouth (RM 92.5) is approximately 577 million cubic meters. The water volume of the 24-mile reach upstream from RM 92.5 is approximately 331 million cubic meters. In comparison, the applied additional flows of 500 cfs and 900 cfs for four months is equivalent to respective totals of 147 and 264 million cubic meters being released into the estuary.

The dilution effect due to the additional flow may be demonstrated by calculating the percent change using the simulated chloride concentration along the river.

Spatial distribution of the percent change as a function of River Mile, based on the simulated maximum 30-dma chloride concentrations, are presented in **Figures L.4-1** through **Figure L.4-6**. The maximum 30-dma chloride concentration simulated during a four-month period (August through November) was used in this analysis, and the results are given in **Table L.4-1** through **Table L.4-3**.

With 0 meter SLR and additional flow of 500 cfs (**Figure L.4-1**), the maximum simulated SF location for the baseline case is RM 94.2 (very close to the Schuylkill River confluence). The dilution effectiveness (represented by percent change) in the river reach upstream from RM 92.5 is greater with more flow added to the Delaware River mainstem at Trenton, while the dilution effect in the river reach downstream from RM 92.5 is greater with more flow added to the Schuylkill River. At RM 93, the percent change is -31 percent whether the additional flow is added to the Delaware River at Trenton or to the Schuylkill River. This is indicated by the crossing of the blue and red lines at RM 93 in **Figure L.4-1**. By increasing its relative flow from 500 cfs to 900 cfs, the Schuylkill River flow becomes the dominating factor for the reach downstream from RM 93 and produces greater influence (**Figure L.4-2**). The maximum chloride concentration is reduced by roughly by one-half from the baseline concentration at RM 98, and the percent change is equal to -54 percent. The largest relative difference in chloride concentrations is between RM 95 to RM 105, where the additional water is most effective in reducing the chloride concentration. The percent change curve is not symmetric, and a greater effect is from the Delaware River upstream from the Schuylkill River confluence because the total water volume from the river reach upstream from RM 92.5 is much smaller than the water volume downstream from RM 92.5.

The two percent change curves represent dilution effect of the additional flow released from the Delaware River at Trenton and from the Schuylkill River cross at some location upstream from RM 92.5. However, with 1 m and 1.6 m SLR, the most affected locations are farther upstream as SLR increases. Pressure forcing from the ocean downstream breaks the balance between the upland freshwater inflow and tidal dispersion and reduces the effect of the additional flow. For SLR of 1.6 m, the percent change is dominated by the additional flow at Trenton on the Delaware River mainstem. The SF reaches its most upstream location at RM 104 and RM 109 with 1 m, and 1.6 m SLR, respectively, without adding flow. In both cases, adding flow to the Delaware River at Trenton is more effective in repelling the SF, and a more pronounced effect was observed in the river reach upstream from the Schuylkill River confluence.

Simulations indicate that adding more flow to the Schuylkill River always shows greater influence downstream from RM 92.5. However, this does not mean it is always more effective in SF repulsion. With 1 m or 1.6 m SLR, the curve changes near RM 92.5 and becomes less steep and flattens and shows much weaker influence in comparison with greater additional flow added to the Delaware River at Trenton (see **Figure L.4-3** to **Figure L.4-6**).

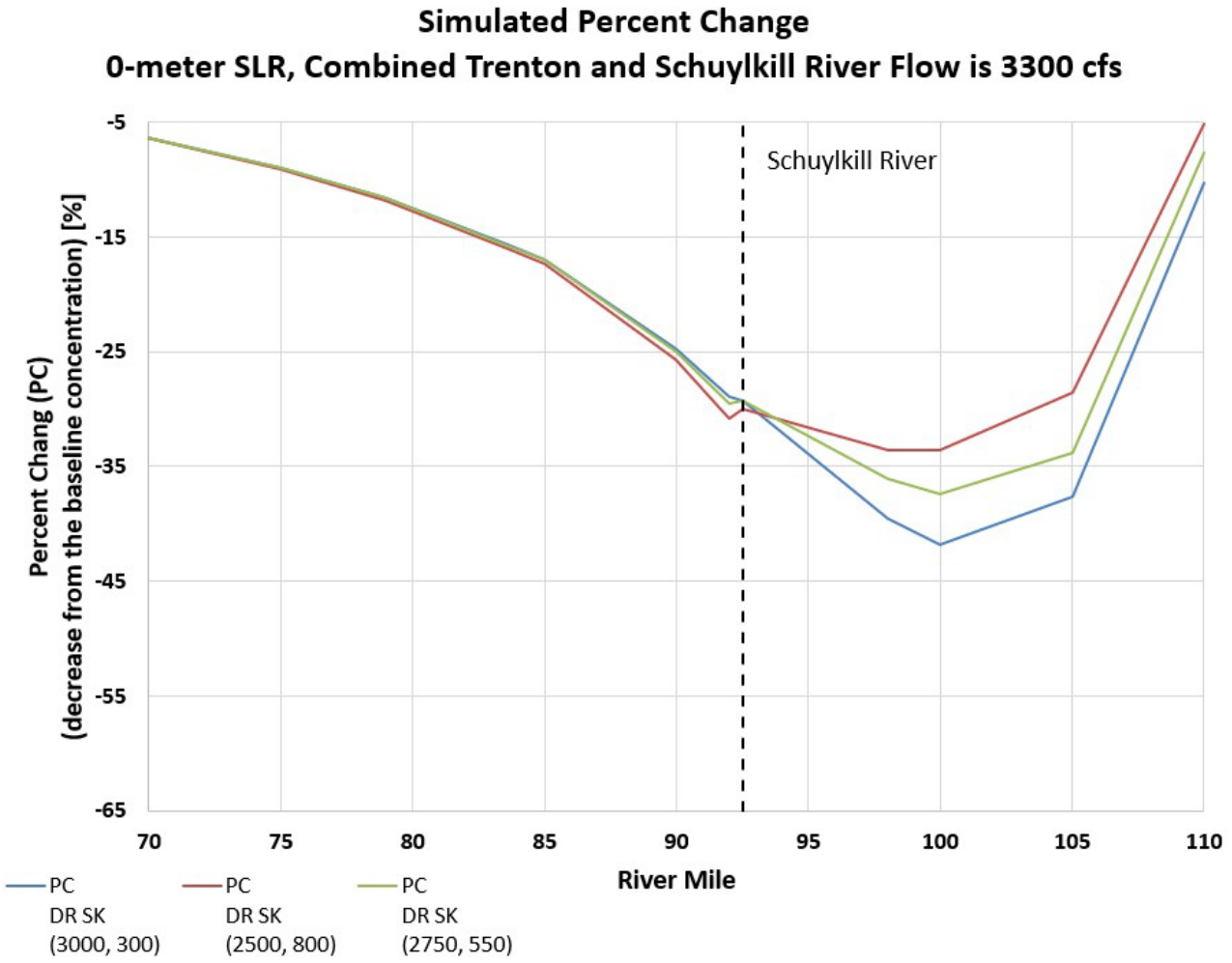

Note: the discharge from the Schuylkill River causes some discontinuity immediately downstream from the Schuylkill River confluence. DR = the Delaware River, SK = Schuylkill River. PC = percent change (%)

Figure L.4-1. Percent Change in simulated 30-dma chloride concentration with combined Delaware River at Trenton and Schuylkill River flow of 3300 cfs and with 0 meter SLR.

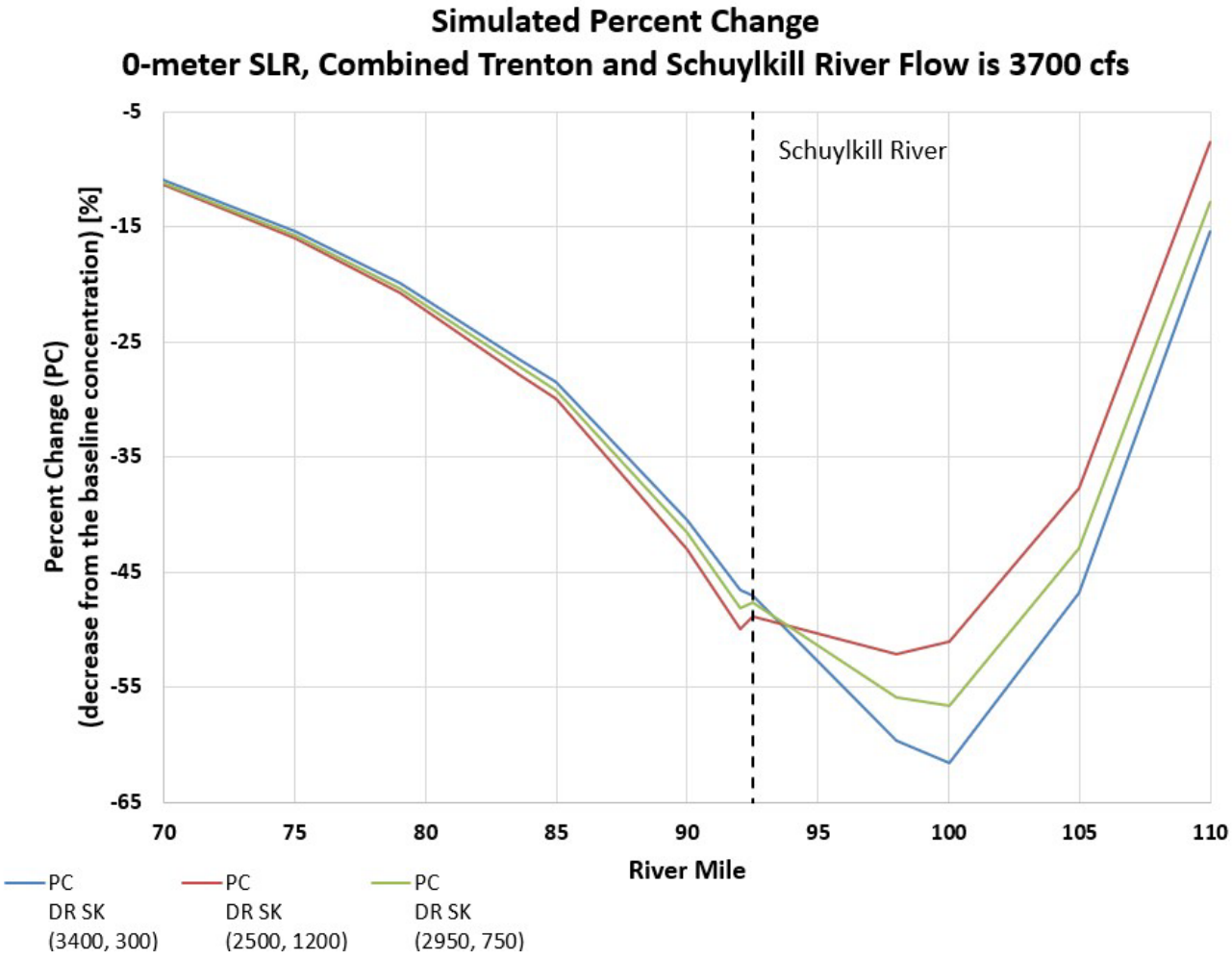

Note: the discharge from the Schuylkill River caused some discontinuity immediately downstream from the Schuylkill River mouth. DR = the Delaware River, SK = Schuylkill River. PC = percent change (%).

Figure L.4-2. Percent Change in simulated 30-dma chloride concentration with combined Delaware River at Trenton and Schuylkill River flow of 3700 cfs and with 0 meter SLR.

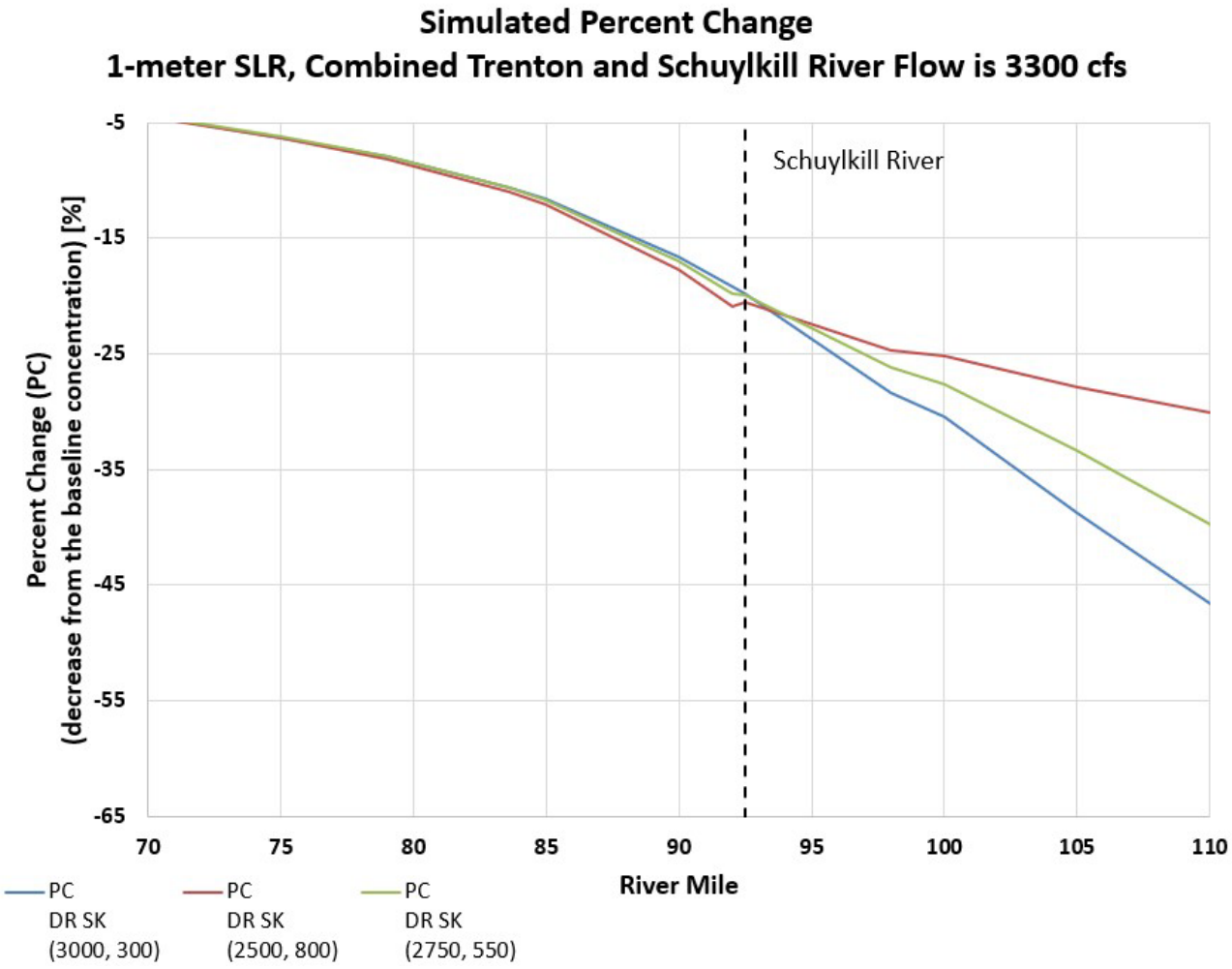

Note: the discharge from the Schuylkill River caused some discontinuity immediately downstream from the Schuylkill River confluence. DR = the Delaware River, SK = Schuylkill River. PC = percent change (%).

Figure L.4-3. Percent Change in simulated 30-dma chloride concentration with combined Delaware River at Trenton and Schuylkill River flow of 3300 cfs and with 1 meter SLR.

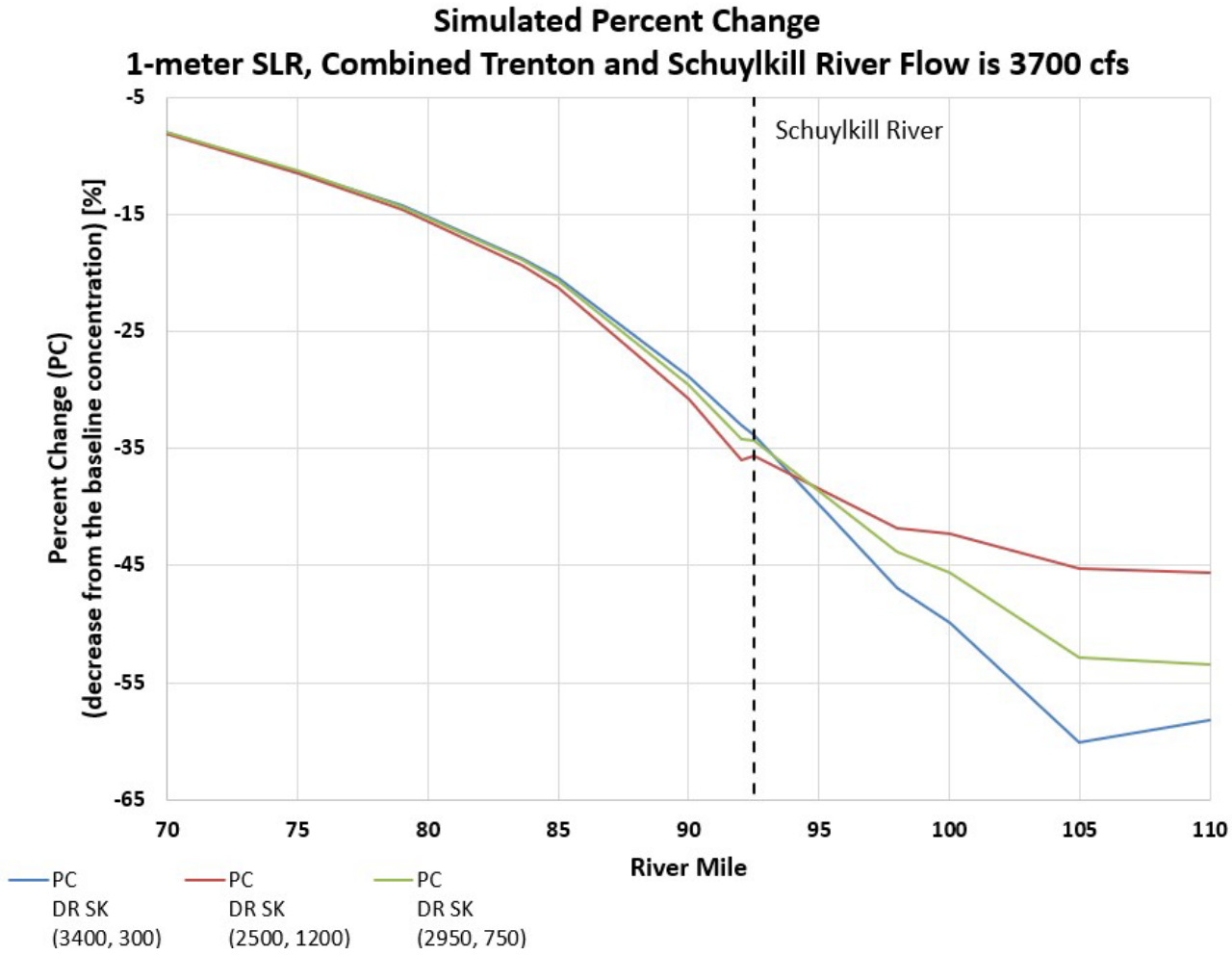

Note: the discharge from the Schuylkill River caused some discontinuity immediately downstream from the Schuylkill River confluence. DR = the Delaware River, SK = Schuylkill River. PC = percent change (%).

Figure L.4-4. Percent Change in simulated 30-dma chloride concentration with combined Delaware River at Trenton and Schuylkill River flow of 3700 cfs and with 1 meter SLR.

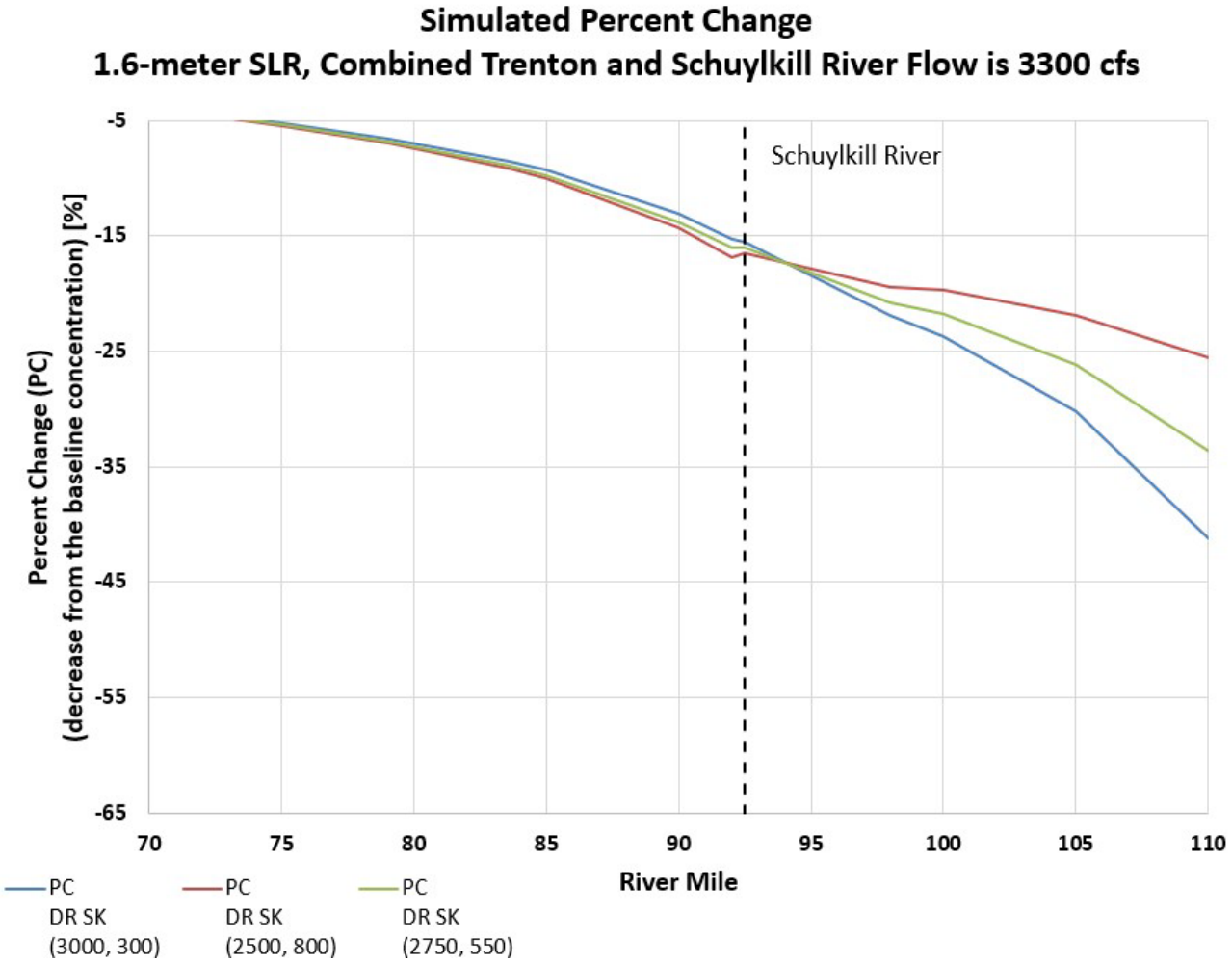

Note: the discharge from the Schuylkill River caused some discontinuity immediately downstream from the Schuylkill River confluence. DR = the Delaware River, SK = Schuylkill River. PC = percent change (%).

Figure L.4-5. Percent Change in simulated 30-dma chloride concentration with combined Delaware River at Trenton and Schuylkill River flow of 3300 cfs and with 1.6 meter SLR.

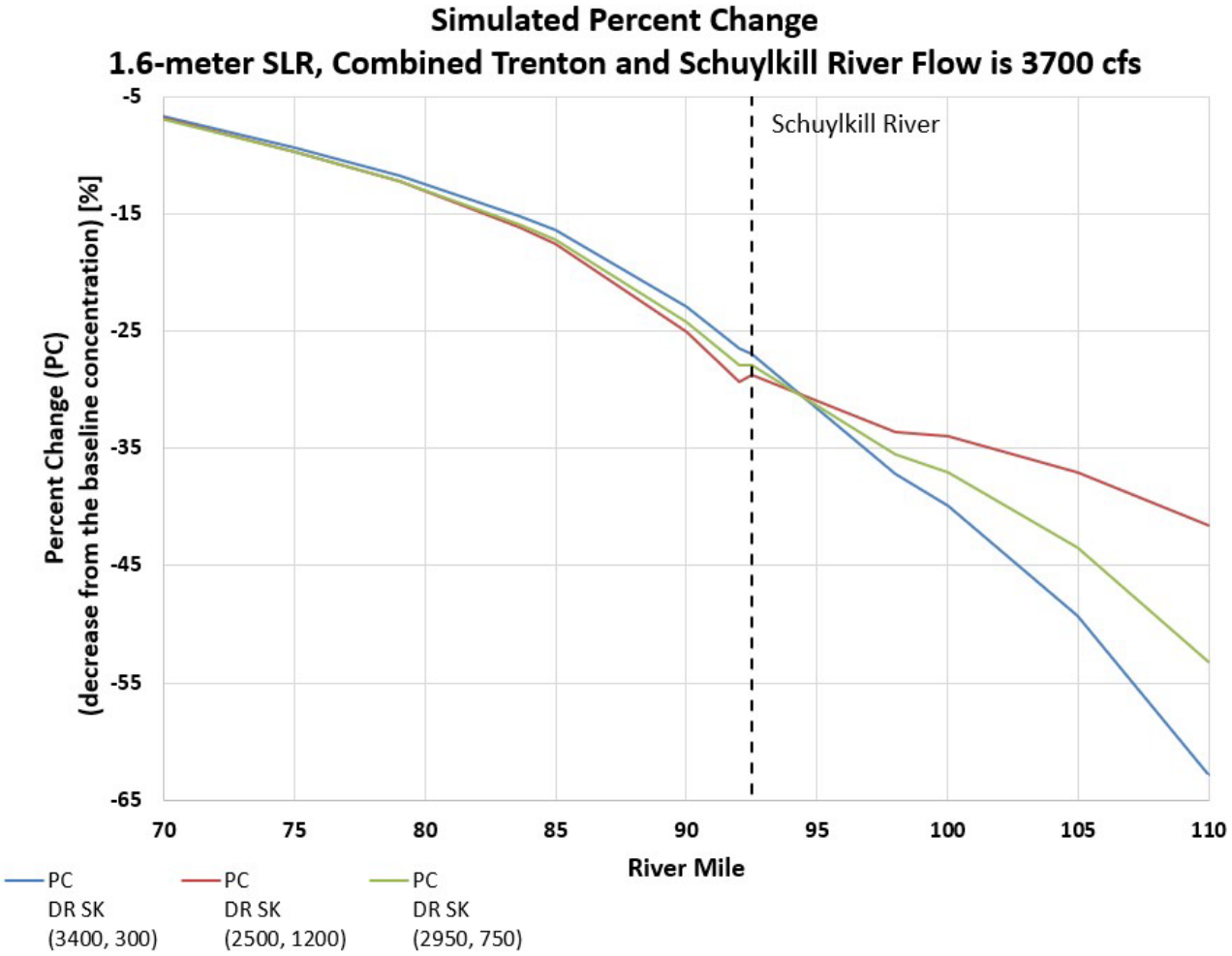

Note: the discharge from the Schuylkill River caused some discontinuity immediately downstream from the Schuylkill River confluence. DR = the Delaware River, SK = Schuylkill River. PC = percent change (%).

Figure L.4-6. Percent Change in simulated 30-dma chloride concentration with combined Trenton and Schuylkill River flow of 3700 cfs and with 1.6 meter SLR.

Table L.4-1 Simulated maximum 30-dma chloride concentration and percent change due to additional flow at selected locations in the Delaware Estuary: SLR = 0 meter.

		SLR 0 m											
		Baseline	DR+SK = 3300						DR+SK = 3700					
	RM	DR SK baseline (2500, 300)	DR SK (3000, 300)	PC DR SK (3000, 300)	DR SK (2500, 800)	PC DR SK (2500, 800)	DR SK (2750, 550)	PC DR SK (2750, 550)	DR SK (3400, 300)	PC DR SK (3400, 300)	DR SK (2500, 1200)	PC DR SK (2500, 1200)	DR SK (2950, 750)	PC DR SK (2950, 750)
BAY MOUTH	0	17,945	17,950	0.03	17,939	-0.03	17,965	0.11	17,940	-0.03	17,946	0.01	17,954	0.05
BRANDYWINE	10	16,371	16,346	-0.15	16,352	-0.12	16,395	0.15	16,332	-0.24	16,321	-0.31	16,370	-0.01
SHIP JOHN SHOAL	37	11,204	11,119	-0.76	11,097	-0.96	11,155	-0.44	11,033	-1.53	11,026	-1.59	11,067	-1.22
REEDY ISLAND	54	8,188	7,979	-2.55	7,979	-2.55	7,976	-2.59	7,835	-4.31	7,815	-4.56	7,820	-4.49
D/S Pea Patch Island RM 60	60	6,953	6,723	-3.31	6,720	-3.35	6,719	-3.37	6,555	-5.72	6,535	-6.01	6,542	-5.91
RM 65	65	5,590	5,335	-4.56	5,332	-4.62	5,331	-4.63	5,146	-7.94	5,127	-8.28	5,134	-8.16
DELAWARE MEMORIAL BRIDGE	69	4,703	4,429	-5.83	4,427	-5.87	4,427	-5.87	4,229	-10.08	4,211	-10.46	4,218	-10.31
RM 75	75	3,216	2,926	-9.02	2,923	-9.11	2,928	-8.96	2,720	-15.42	2,701	-16.01	2,710	-15.73
Marcus Hook RM 79	79	2,487	2,197	-11.66	2,193	-11.82	2,198	-11.62	1,992	-19.90	1,970	-20.79	1,981	-20.35
CHESTER	83.6	1,655	1,395	-15.71	1,389	-16.07	1,394	-15.77	1,215	-26.59	1,194	-27.85	1,205	-27.19
RM 85	85	1,489	1,237	-16.92	1,230	-17.39	1,236	-16.99	1,065	-28.48	1,043	-29.95	1,054	-29.21
RM 90	90	825	621	-24.73	613	-25.70	619	-24.97	491	-40.48	470	-43.03	482	-41.58
Ft. MIFFLIN	92	604	429	-28.97	418	-30.79	426	-29.47	323	-46.52	302	-50.00	313	-48.18
RM 92.5	92.5	583	412	-29.33	408	-30.02	412	-29.33	309	-47.00	298	-48.89	305	-47.68
RM 98	98	238	144	-39.50	158	-33.61	152	-36.13	96	-59.66	114	-52.10	105	-55.88
BEN FRANKLIN BRIDGE	100	182	106	-41.76	121	-33.52	114	-37.36	70	-61.54	89	-51.10	79	-56.59
RM 105	105	77	48	-37.66	55	-28.57	51	-33.77	41	-46.75	48	-37.66	44	-42.86
RM 110	110	39	35	-10.26	37	-5.13	36	-7.69	33	-15.38	36	-7.69	34	-12.82

Note: constant flow was assigned at DR and SK after May 1, 2002; and results from 8/1 - 11/30 were used in this analysis.
DR = the Delaware River, SK = Schuylkill River. PC = percent change (%).

Table L.4-2 Simulated maximum 30-dma chloride concentration and percent change due to additional flow at selected locations in the Delaware Estuary: SLR = 1 meter.

		SLR 1 m												
		Baseline	DR+SK = 3300						DR+SK = 3700					
	RM	DR SK baseline (2500, 300)	DR SK (3000, 300)	PC DR SK (3000, 300)	DR SK (2500, 800)	PC DR SK (2500, 800)	DR SK (2750, 550)	PC DR SK (2750, 550)	DR SK (3400, 300)	PC DR SK (3400, 300)	DR SK (2500, 1200)	PC DR SK (2500, 1200)	DR SK (2950, 750)	PC DR SK (2950, 750)
BAY MOUTH	0	18,148	18,126	-0.12	18,132	-0.09	18,150	0.01	18,122	-0.14	18,128	-0.11	18,125	-0.13
BRANDYWINE	10	16,619	16,588	-0.19	16,599	-0.12	16,640	0.13	16,582	-0.22	16,585	-0.20	16,616	-0.02
SHIP JOHN SHOAL	37	12,168	12,103	-0.53	12,101	-0.55	12,160	-0.07	12,040	-1.05	12,037	-1.08	12,080	-0.72
REEDY ISLAND	54	8,559	8,409	-1.75	8,405	-1.80	8,410	-1.74	8,280	-3.26	8,276	-3.31	8,282	-3.24
D/S Pea Patch Island RM 60	60	7,425	7,253	-2.32	7,248	-2.38	7,254	-2.30	7,106	-4.30	7,103	-4.34	7,109	-4.26
RM 65	65	6,182	5,986	-3.17	5,980	-3.27	5,986	-3.17	5,822	-5.82	5,818	-5.89	5,824	-5.79
DELAWARE MEMORIAL BRIDGE	69	5,340	5,124	-4.04	5,118	-4.16	5,124	-4.04	4,945	-7.40	4,941	-7.47	4,945	-7.40
RM 75	75	3,916	3,670	-6.28	3,666	-6.38	3,672	-6.23	3,472	-11.34	3,467	-11.47	3,473	-11.31
Marcus Hook RM 79	79	3,196	2,941	-7.98	2,935	-8.17	2,942	-7.95	2,740	-14.27	2,731	-14.55	2,739	-14.30
CHESTER	83.6	2,368	2,117	-10.60	2,107	-11.02	2,116	-10.64	1,924	-18.75	1,909	-19.38	1,920	-18.92
RM 85	85	2,160	1,910	-11.57	1,898	-12.13	1,907	-11.71	1,719	-20.42	1,701	-21.25	1,713	-20.69
RM 90	90	1,401	1,168	-16.63	1,152	-17.77	1,163	-16.99	997	-28.84	970	-30.76	987	-29.55
Ft. MIFFLIN	92	1,107	894	-19.24	875	-20.96	888	-19.78	741	-33.06	709	-35.95	729	-34.15
RM 92.5	92.5	1,084	870	-19.74	861	-20.57	868	-19.93	717	-33.86	698	-35.61	712	-34.32
RM 98	98	584	418	-28.42	440	-24.66	431	-26.20	310	-46.92	340	-41.78	328	-43.84
BEN FRANKLIN BRIDGE	100	489	340	-30.47	366	-25.15	354	-27.61	245	-49.90	282	-42.33	266	-45.60
RM 105	105	276	169	-38.77	199	-27.90	184	-33.33	110	-60.14	151	-45.29	130	-52.90
RM 110	110	103	55	-46.60	72	-30.10	62	-39.81	43	-58.25	56	-45.63	48	-53.40

Note: constant flow was assigned at DR and SK after May 1, 2002; results from 8/1 - 11/30 were used in this analysis.
DR = the Delaware River, SK = Schuylkill River. PC = percent change (%).

Table L.4-3 SM3D Simulated maximum 30-dma chloride concentration and percent change due to additional flow at selected locations in the Delaware Estuary: SLR = 1.6 meter.

		SLR 1.6 m											
		Baseline	DR+SK = 3300						DR+SK = 3700					
	RM	DR SK baseline (2500, 300)	DR SK (3000, 300)	PC DR SK (3000, 300)	DR SK (2500, 800)	PC DR SK (2500, 800)	DR SK (2750, 550)	PC DR SK (2750, 550)	DR SK (3400, 300)	PC DR SK (3400, 300)	DR SK (2500, 1200)	PC DR SK (2500, 1200)	DR SK (2950, 750)	PC DR SK (2950, 750)
BAY MOUTH	0	18,254	18,239	-0.08	18,242	-0.07	18,260	0.03	18,239	-0.08	18,242	-0.07	18,235	-0.10
BRANDYWINE	10	16,752	16,729	-0.14	16,737	-0.09	16,776	0.14	16,711	-0.24	16,724	-0.17	16,763	0.07
SHIP JOHN SHOAL	37	12,778	12,715	-0.49	12,693	-0.67	12,781	0.02	12,685	-0.73	12,691	-0.68	12,704	-0.58
REEDY ISLAND	54	8,865	8,736	-1.46	8,729	-1.53	8,728	-1.55	8,628	-2.67	8,619	-2.77	8,603	-2.96
D/S Pea Patch Island RM 60	60	7,798	7,650	-1.90	7,644	-1.97	7,642	-2.00	7,528	-3.46	7,520	-3.57	7,505	-3.76
RM 65	65	6,604	6,430	-2.63	6,423	-2.74	6,422	-2.76	6,287	-4.80	6,278	-4.94	6,267	-5.10
DELAWARE MEMORIAL BRIDGE	69	5,782	5,587	-3.37	5,579	-3.51	5,579	-3.51	5,428	-6.12	5,418	-6.30	5,410	-6.43
RM 75	75	4,393	4,166	-5.17	4,154	-5.44	4,157	-5.37	3,984	-9.31	3,968	-9.67	3,965	-9.74
Marcus Hook RM 79	79	3,684	3,444	-6.51	3,430	-6.89	3,434	-6.79	3,253	-11.70	3,233	-12.24	3,233	-12.24
CHESTER	83.6	2,866	2,622	-8.51	2,605	-9.11	2,610	-8.93	2,431	-15.18	2,405	-16.09	2,411	-15.88
RM 85	85	2,643	2,398	-9.27	2,380	-9.95	2,386	-9.72	2,209	-16.42	2,179	-17.56	2,187	-17.25
RM 90	90	1,847	1,606	-13.05	1,583	-14.29	1,593	-13.75	1,423	-22.96	1,384	-25.07	1,400	-24.20
Ft. MIFFLIN	92	1,513	1,282	-15.27	1,258	-16.85	1,271	-15.99	1,113	-26.44	1,069	-29.35	1,090	-27.96
RM 92.5	92.5	1,489	1,258	-15.51	1,243	-16.52	1,250	-16.05	1,088	-26.93	1,061	-28.74	1,073	-27.94
RM 98	98	900	703	-21.89	725	-19.44	713	-20.78	565	-37.22	598	-33.56	580	-35.56
BEN FRANKLIN BRIDGE	100	782	597	-23.66	628	-19.69	612	-21.74	470	-39.90	516	-34.02	492	-37.08
RM 105	105	513	358	-30.21	401	-21.83	379	-26.12	260	-49.32	323	-37.04	290	-43.47
RM 110	110	250	147	-41.20	186	-25.60	166	-33.60	93	-62.80	146	-41.60	117	-53.20

Note: constant flow was assigned at DR and SK after May 1, 2002; results from 8/1 - 11/30 were used in this analysis.
DR = the Delaware River, SK = Schuylkill River. PC = percent change (%).

END